PRESENT STATUS OF J-PARC

F. Naito#, KEK, Tsukuba, Japan

Abstract

Japan Proton Accelerator Research Complex (J-PARC) is the scientific facility with the high-intensity proton accelerator aiming to realize 1 MW class of the beam power. J-PARC is the joint project between High Energy Accelerator Research Organization (KEK) and Japan Atomic Energy Agency (JAEA). The accelerator of J-PARC consists of a 181-MeV linac, a 3-GeV Rapid-Cycle Synchrotron (RCS) and a 50-GeV Main Ring synchrotron (MR). The beam energy of the linac will be extended to 400 MeV from 181 MeV in the near future. As all components of the linac were aligned on the beam line, the beam commissioning has been started in November 2006. Furthermore the excitation test of the aligned magnets in the RCS has also been started. The RCS beam commissioning is scheduled to start in September 2007. Finally the beam commissioning for the 50-GeV synchrotron will be started in May 2008.

INTRODUCTION

Japan Proton Accelerator Research Complex (J-PARC) is the high-intensity proton accelerator facility which was formed by joining together the Neutron Science Project (NSP) of Japan Atomic Energy Agency (JAEA) and the Japan Hadron Facility (JHF) Project of High Energy Accelerator Research Organization (KEK). J-PARC is aiming to realize 1 MW class of the beam power, which was the target value of NSP and JHF. J-PARC has three main purposes; (1) the study of the material science using the strong neutron beam; (2) the nuclear/particle physics using several secondary particle beams which include the neutrino; (3) the experiment of the Accelerator-Driven transmutation System (ADS) for the nuclear waste.

The construction of J-PARC has been started at Tokai campus of JAEA, where is about 130 km north-east of Tokyo. At the present stage, J-PARC consists of the following accelerators:

- a 181-MeV normal-conducting linac (H^- beam: Peak;30mA, Width;500μs, Repetition;25Hz),
- a 3-GeV rapid cycle synchrotron ring (RCS), which provides proton beams at 333μA (1MW), and
- a 50-GeV main synchrotron ring (MR), which provides proton beams of 15μA (0.75MW).

The schematic layout of the facility is shown in figure 1. The design energy of the normal-conducting linac is 400-MeV. However it is limited by the budget problem [1]. The energy recovery of the linac from 181 to 400 MeV is the essential subject to be carried out before the second phase
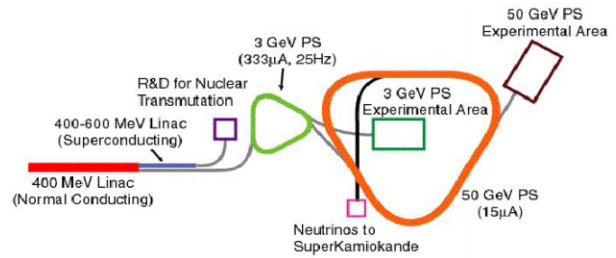
Figure 1: Configuration of J-PARC.

of the project which includes a super-conducting (SC) linac and the ADS. In the second phase the repetition rate of the linac beam is doubled from 25 to 50 Hz. Then one half of the 400-MeV beam from the linac is injected into the RCS, while the other half is further accelerated up to 600 MeV by the SC linac. The 600-MeV beam is transported to the experimental area for the ADS.

The 3-GeV beam from the RCS is mainly used to produce pulsed spallation neutrons and μ-ons for the study of the material and the life sciences.

A part of the beam from the RCS is injected into the 50-GeV synchrotron. The 50-GeV beam is slowly extracted in order to produce the secondary particles for the nuclear/particle physics experiment. It is also fast extracted for the production of the neutrinos, which are sent to the SUPER-KAMIOKANDE detector located 300 km from J-PARC.

The installation of linac has been completed. Thus the linac beam commissioning has been started in November 2006. For the RCS the installation of the components is in progress. In particular, the main magnets have been aligned in the ring. Thus the excitation test of the magnet has been started in December 2006. The linac commissioning and the RCS magnet test are being carried out alternatively. The start time of the beam commissioning of the RCS is scheduled in September 2007. Finally the beam commissioning of the MR will be started in May 2008. The schedule of the J-PARC is shown in figure 2.

LINAC

The linac uses normal-conducting cavities up to 400 MeV, while it uses superconducting cavities (SCC) from 400 to 600 MeV, as shown in figure 3 [1]. The linac is composed of an H^- ion source, an RFQ, a Drift-Tube Linac (DTL), a Separated DTL (SDTL), an Annular Coupled Structure (ACS) linac, an SCC linac and several beam transport lines. All components, except for the ACS and the SCC have been installed in the tunnel. Total number

COMMISSIONING EXPERIENCE OF SNS*

M.A. Plum representing the beam commissioning team, Spallation Neutron Source,
Oak Ridge National Laboratory, Oak Ridge, TN, U.S.A.

Abstract

The Spallation Neutron Source accelerator complex consists of a 2.5 MeV H⁻ front-end injector system, a 186 MeV normal-conducting linear accelerator, a 1 GeV superconducting linear accelerator, an accumulator ring, and associated beam transport lines. The linac was commissioned in five discrete runs, starting in 2002 and completed in 2005. The accumulator ring and associated beam transport lines were commissioned in two runs in January-February and April 2006. With the completed commissioning of the SNS accelerator, the facility has begun initial low-power operations. In the course of beam commissioning, most beam performance parameters and beam intensity goals have been achieved at low duty factor. A number of beam dynamics measurements have been performed, including emittance evolution, transverse coupling in the ring, beam instability thresholds, and beam distributions on the target. The commissioning results, achieved beam performance and initial operating experience of the SNS linac will be presented.

INTRODUCTION

The Spallation Neutron Source (SNS) is a short pulse neutron scattering facility located on the campus of the Oak Ridge National Laboratory in Oak Ridge, TN, USA. The construction project was a partnership of six US DOE national laboratories, each of which had responsibility for designing and manufacturing a portion of the facility. At 1.4 MW of proton beam power on target, the SNS will operate at beam powers a factor of eight beyond that which has been previously achieved [1]. The SNS baseline parameters are summarized in Table 1.

Table 1: SNS Design Parameters

Beam Power on Target	1.4 MW
Beam Energy	1.0 GeV
Linac Beam Macropulse Duty Factor	6.0%
Beam Pulse Length	1.0 msec
Repetition Rate	60 Hz
Chopper Beam-On Duty Factor	68%
Peak macropulse H⁻ current	38 mA
Average Linac H⁻ current	1.6 mA
Ring accumulation time	1060 turns
Ring bunch intensity	1.5×10^{14}
Ring Space-Charge Tune Spread	0.15
Beam Pulse Length on Target	695 nsec

The SNS accelerator complex [2] consists of a 2.5 MeV H⁻ injector [3], a 1 GeV linear accelerator [4], an

accumulator ring, and associated beam transport lines [5]. The injector (also called the Front-End Systems) consists of an H⁻ volume ion-source with 50 mA peak current capability [6], a Radio-Frequency Quadrupole and a Medium Energy Beam Transport line for chopping and matching the 2.5 MeV beam to the linac. The linear accelerator consists of a Drift Tube Linac (DTL) with 87 MeV output energy, a Coupled-Cavity Linac (CCL) with 186 MeV output energy, and a Superconducting RF Linac (SCL) with 1 GeV output energy [7]. At full design capability the linac will produce a 1 msec long, 38 mA peak, chopped beam pulse at 60 Hz for accumulation in the ring. The linac beam is transported via the High Energy Beam Transport (HEBT) line to the injection point in the accumulator ring where it is multi-turn charge-exchange injected over 1060 turns and compressed to less than 1 microsecond, reaching an intensity of 1.5×10^{14} protons per pulse. When accumulation is complete the extraction kicker fires during the 250 nsec gap to remove the accumulated beam in a single turn and direct it into the Ring to Target Beam Transport (RTBT) line, which takes the beam to a liquid mercury target. Staged commissioning of the accelerator complex, completed May 2006, was performed in seven discrete beam commissioning runs (shown in Figure 1) which were devoted to commissioning the i) Front-End, ii) Drift Tube Linac Tank 1, iii) Drift Tube Linac Tanks 1-3, iv) Coupled Cavity Linac, v) Superconducting Linac, vi) High-Energy Beam Transport Line and Accumulator Ring, and vii) Ring to Target Beam Transport Line and the mercury target. Table 2 summarizes the main beam commissioning results, comparing beam measurements with design goals. Ramp up to high power operation is now in progress.

LINAC COMMISSIONING

Linac commissioning results have been presented before [8], but for completeness we will provide a brief summary here.

The linac was successfully commissioned in five discrete runs from December 2002 to August 2005. The warm linac commissioning progressed smoothly and measured beam parameters are in good agreement with expectations [3]. RF phase and amplitude set points were determined using two methods (energy degrader / Faraday Cup acceptance scan and phase scan signature matching) that gave consistent results. We now use the phase scan signature matching method exclusively.

The superconducting linac commissioning proceeded much faster than expected. Before commissioning began there was some uncertainty in the algorithms to set the phases of the rf cavities due to concerns with beam loading, but the simple procedure of fitting the time of flight vs. cavity phase with a sinusoidal curve, for 10 mA

04 Hadron Accelerators
A04 - Circular Accelerators

OVERVIEW OF ENERGY-RECOVERY LINACS

R. Hajima# JAEA-ERL, Tokai, Ibaraki 319-1195, Japan

Abstract

Energy-recovery linacs (ERL), which is able to produce a high-power electron beam with high brightness, has been developed for high-power free-electron lasers. Now, ERL is also considered as a future X-ray light source, where coherent X-ray and ultrashort X-ray pulses are realized. In this paper, we overview current R&D status of ERLs in the world, and give a detail description of the ERL light source project in Japan.

INTRODUCTION

An energy-recovery linac (ERL), which is able to generate a high-brightness electron beam with high-average current, has been developed for a driver of high-power free-electron laser. Now, the ERL is expanding its role and contribution to various fields: next-generation X-ray light sources, high-flux gamma-ray sources, colliders for high-energy physics, an electron-cooler for ion beams, etc. World-wide efforts of R&Ds are launching towards such future ERLs.

For an example of ERL, figure 1 shows a 17-MeV ERL-FEL at Japan Atomic Energy Agency (JAEA). The ERL consists of an injector, a merger, a main linac and a return loop. An electron bunch generated by injector is further accelerated by main linac and delivered to the FEL undulator. If we assume a typical conversion efficiency of 1% from the electron energy to the laser energy, the electrons energy of 99% remains unused after the FEL undulator. The energy-recovery is a technique to recycle this unused electron energy to improve the total efficiency of the FEL from the electricity power to the laser power. This recycling of the unused electron energy is possible by decelerating the electrons at the main linac as seen in fig.1. The decelerated electron beam goes to a beam dump. As a result, the energy-recovery technique enable one to accelerate high-power electron beams with small capacity of RF sources.

In the ERL, a fresh electron bunch is injected to a main linac for acceleration at any time, and we can keep an electron beam of small emittance and/or ultrashort pulse duration. This flexible manipulation of transverse and longitudinal dimension of electron bunch is a common feature to linear accelerators, and generation of high-power CW beams is a strong point of storage rings. Thus, the ERL has advantages of linear accelerators and advantages of storage rings simultaneously. Due to these excellent advantages, the energy-recovery linac is now considered as one of the important topics in accelerator science and technology, and a session for ERL has been regularly organized in xPAC

—————————
hajima.ryoichi@jaea.go.jp

since PAC-2003. In this paper, we overview current status of ERLs in the world, and give a detail description of the ERL light source project in Japan.

HIGH-POWER FELS

From a historical point view, concept of energy-recovery linac was first proposed for an electron collider in 1965, in which electrons are decelerated for energy recovery after passing an interaction point[1]. However, the ERL technology has been developed for high-power free-electron lasers. In 1980s, experimental attempts for increasing FEL power by energy-recovery linacs were conducted at Los Alamos National Laboratory[2] and Stanford University[3]. These early experiments indeed had a certain impact on ERL development, but they revealed the fact at the same time that the ERL requires sophisticated technology of superconducting accelerator. An energy-recovery linac for practical use was first demonstrated at JLAB IR-demo FEL (Thomas Jefferson National Accelerator Facility) [4], which employed CEBAF-type superconducting cavities. Following this first demonstration of ERL-FEL, two ERL-FELs were built in JAERI (Japan Atomic Energy Research Institute) and BINP (Budker Institute of Nuclear Physics).

In JAERI, a research program towards a high-power free-electron laser started in 1987. In the research program, a 17-MeV superconducting linac was developed and a high-power FEL lasing was demonstrated with the linac[5]. For the further enhancement of the FEL power, the linac was modified into an energy-recovery configuration. Design of the ERL started in 1999, and after a construction period, demonstration of ERL was completed in 2002[6]. In order to make best use of energy-recovery, the injector current has been enlarged with keeping the same RF sources for the main linac. The original injector equipped with two 6 kW solid-state amplifiers have been replaced by two 50 kW IOTs, and the repetition rate of the gun pulser has also been doubled from 10 MHz to 20 MHz. The injector beam current of 10 mA is now available (originally 5 mA) [7]. The FEL power has reached to 0.75 kW with an electron beam of 136 kW (17 MeV, 8 mA). The FEL power is now restricted by energy acceptance of the return loop [8].

The ERL at BINP is a unique facility based on a normal conducting accelerator of 12 MeV operating at 180 MHz. An FEL for high-power THz radiation was developed utilizing this ERL. The first lasing of the FEL was achieved in 2003 and laser power of 20 W has been obtained in THz region[9]. They are also constructing the second FEL with a 40-MeV electron beam, which will be the first multi-turn

RESULTS FROM THE FREE-ELECTRON LASER FLASH

S. Schreiber, DESY, Hamburg

Abstract

Since summer 2005 FLASH at DESY is a user facility providing laser like FEL radiation using the SASE principle in the VUV and soft X-ray range. In the last year, we have continuously extended the wavelength range and improved the overall performance of FLASH. The run time is organized in blocks of runs for user experiments alternating with machine study weeks to improve the beam quality. FLASH now covers the wavelength range between 13 and 45 nm. So far, we reached saturation at 13.7 and 32 nm. Also, to a certain extend flexible bunch pattern have been deliverd to experiments, such as intra train repetition rates of 1 MHz, 250 kHz or 100 kHz with various numbers of bunches train. An upgrade in the energy reach to 1 GeV is scheduled early 2007. This will allow lasing down to 6 nm.

PAPER NOT YET RECEIVED

02 Synchrotron Light Sources and FELs

A06 - Free Electron Lasers

STATUS AND PERSPECTIVE OF XFEL PROJECTS IN THE WORLD

T. Shintake, RIKEN Spring-8 Harima, Hyogo

Abstract

Free Electron laser at X-ray wavelength is not any more a story of science fiction. Projects at SLAC and RIKEN/SPring-8 are now under construction aiming at generating first laser X-ray radiation in a few years. Two VUV FELs are already in operation at FLASH/DESY and SCSS/RIKEN. These FELs provide new type of experimental tool with unique features: high intensity, short pulse format and coherent. It is believed that XFEL will open new science cases, that why, there are many other similar projects proposed. The talk will cover, XFEL basic, key technology, and brief status of running and proposed projects.

PAPER NOT YET RECEIVED

REPORT ON ILC

B.C. Barish, CALTECH, Pasadena, California;
K. Yokoya, KEK, Ibaraki

Abstract

Report on ILC

PAPER NOT YET RECEIVED

ILC PARAMETERS RATIONALE AND CHALLENGES

K. Yokoya, KEK, Ibaraki

Abstract

Since the publication of the BCD (Baseline Configuration Document) in December 2005, the main target of the GDE (Global Design Effort) has benn the RDR (Reference Design Report), which contains the first estimation of the cost of the collider system. Through the three meetings at Bangalore in March 2005, at Vancouver in July, and at Valencia in Novemver, the first estimation has been completed and various efforts of cost reduction have been tried. The outline of the resulting design will be presented in the present talk together with the remaining design issues and required R&D items.

PAPER NOT YET RECEIVED

STATUS OF FFAG DEVELOPMENTS

S. Machida, ASTeC, CCLRC Rutherford Appleton Laboratory
Chilton, Didcot, Oxfordshire, OX11 0QX, U.K.

Abstract

Since its revival at KEK in late 1990s, FFAG accelerator draws increasing attentions in many fields including physics experiments, medical, energy, and industrial applications. Construction of prototype machine is going on in Japan and in Europe. We will show status of those activities and accelerator physics issues after some basic of a FFAG accelerator.

INTRODUCTION

What is FFAG?

FFAG stands for Fixed Field Alternating Gradient. Strictly speaking, it only specifies a way of transverse focusing. People, however, usually refer to FFAG focusing accelerator as "FFAG".

A modern synchrotron has Alternating Gradient (AG) focusing. It is sometimes called strong focusing by contrast with weak focusing which uses a magnet with small gradient. Therefore, the primary difference between FFAG and a synchrotron comes from whether magnet field is fixed or ramped.

A synchrotron consists of a dipole to bend a beam and a quadrupole to focus a beam. Bending angle θ and focusing length f of them are,

$$\theta = \frac{BL}{p/e} \quad , \quad (1) \quad \text{and} \quad \frac{1}{f} = \frac{(dB/dx)L}{p/e} \quad , \quad (2)$$

respectively, where L is magnet length and fixed. p is momentum and e is an unit charge. B and (dB/dx) have to be ramped to keep θ and f constant when momentum increases. If they are not ramped, bending radius becomes large to keep the same bending angle and to make an orbit close. In addition, focusing length becomes larger and betatron tune becomes lower.

Fixed field magnets cannot keep bending radius constant for different momenta, but we can make use of the orbit shift to keep betatron tune constant through acceleration. Orbit moves outward and focusing strength is $(dB/dx)L$ so that a magnet with steeper gradient and longer path length outward in principle can keep the betatron tune constant. In terms of bending field profile, it is presented as

$$B_z = B_0 \left(\frac{r}{r_0} \right)^k F(\phi) \quad , \quad (3)$$

where r is radial, ϕ is azimuthal and z is vertical coordinates. F is a function which introduces azimuthal variation. k is called field index. Positive and large k means stronger bending field as the orbit moves outer, which sustain small orbit shift. At the same time, local gradient at the outer orbit is larger so that focusing is stronger.

That type of magnets can focus a beam only in one plane, but not in the other. In order to make an alternating gradient focusing, there are two ways. One is to flip the polarity of magnets alternatively. That changes bending direction as well as sign of focusing. This is called radial sector type FFAG. Another way to make it alternating gradient is to introduce edge focusing for vertical direction in addition to the focusing in the magnet body for horizontal direction. A sharp entrance angle for the all orbits makes the magnet shape spiral. This is called spiral sector type FFAG. Radial sector FFAG tends to be a larger machine compared with spiral one because of reverse bending magnets. It can have higher field index and therefore smaller orbit shift because focusing force comes from magnet body for both directions and can be strong as much as possible. On the other hand, vertical focusing of spiral sector FFAG is limited and that imposes a limit of field index.

What is advantage?

There are several advantages in FFAG compared with other type of machines. Firstly, machine repetition rate can be higher because there is no need to ramp the magnets. Secondly, particles per bunch can be the same or even higher than that of synchrotron because the similar strength of focusing in transverse as well as longitudinal direction is maintained. The larger aperture in horizontal plane even gives more space for particles. Thirdly, output energy can be higher compared with cyclotron because magnet size is smaller.

Beam power of an accelerator is the product of repetition rate, particles per bunch, and output energy. Therefore, compared with a synchrotron and a cyclotron, FFAG can have the potential to be the most powerful accelerator.

There are other advantages. FFAG is not only to be the most powerful accelerator, but with high energy efficiency in terms of beam power out of AC electric power. For example, FFAG with superconducting magnets needs only a power to a beam and the overall efficiency could be very high, which could be well above that of the present accelerators. As an accelerator for accelerator driven transmutation and energy breeder, FFAG has advantage over linac in that respect.

On more technical sides, rf frequency does not have to track magnetic field and horizontal orbit. That eliminates one feedback loop and makes machine operation easier. Also, FFAG has vacuum chamber covering injection to extraction orbits. Although that means physical cross section of the vacuum chamber is larger than that of

CHALLENGES IN ILC SCRF TECHNOLOGY[*]

Detlef Reschke[#], DESY, D-22603 Hamburg, Germany

Abstract

With a baseline operating gradient of 31,5 MV/m at a Q-value of 10^{10} the superconducting nine-cell cavities of the ILC are a challenging milestone for SRF technology. Worldwide intensive ILC R&D programs are underway or in the planning stage in all three regions of America, Asia and Europe. This paper will give an overview of the main activities in the field of superconducting RF (SCRF) technology.

INTRODUCTION

In 2004 the International Technology Recommendation Panel (ITRP) recommended the choice of superconducting rf technology for a future linear collider. This choice was accepted by ICFA [1], and the first workshop on the International Linear Collider (ILC) was held at KEK in November 2004. During the 2nd ILC Workshop at Snowmass in August 2005 the goal was set to define a baseline configuration, which was published after intense discussions at the GDE (Global Design Effort) meeting at Frascati end of 2005. The Baseline Configuration Document (BCD) is a living document and will evolve following developments in design, costing and successful R&D improvements [2, 3]. In addition to the BCD the Alternative Configuration Document (ACD) describes a number of promising future options in order to gain in performance, cost or risk reduction.

Table 1: Main ILC cavity parameters

ILC parameters:		BCD (baseline)	ACD (alternative)
Cavity shape		TESLA	Low Loss or Reentrant
Cavity Acceptance Performance	Eacc [MV/m]	35	40
	Q_0	$0,8 \cdot 10^{10}$	$0,8 \cdot 10^{10}$
Cavity Operation Performance	Eacc [MV/m]	31,5	36
	Q_0	$1,0 \cdot 10^{10}$	$1,0 \cdot 10^{10}$
Coupler		„TTF type III"	
Cryomodule		„Type IV"	
		8(9) cav. /module	8(9) cav. /module

The ILC is based on 1.3 GHz nine-cell structures of ultrapure Niobium (Fig.1). Table 1 shows some important parameters related to cavity and cryomodule design.

Figure 1: 1.3 GHz 9-cell Niobium cavity of TESLA shape.

CAVITY FUNDAMENTALS

The Q-value of a superconducting cavity is related to the surface resistance R_s by $Q_0 = G / R_s$ with the geometry factor G given only by the geometry of the cavity. For accelerator cavities G is about 270 Ω. As explained in detail in [4], the experimentally observed surface resistance can be described by the BCS-component $R_{BCS}(T, \omega)$, the residual resistance R_{res} determined by preparation and experimental conditions as well as a gradient dependant component $R_s(H)$. One example of the latter is the so-called "Q-slope without field emission", which appears in electropolished cavities. In order to cure this effect a special bake procedure is applied [5].

At an operating temperature of 2K a well prepared cavity shows a typical Q-value of $2 \cdot 10^{10}$ at low gradient. The Q-value of 10^{10} at the baseline operating gradient requires excellent preparation and experimental conditions resulting in cavities free of additional loss mechanisms like enhanced field emission (see below).

An intensively discussed topic of the last years is the rf critical magnetic field [4] of Niobium. Experimental results indicate a maximum magnetic surface field of (180 – 190) mT at 2 K.

Cavity shape

The shape of the cavity cells determines important characteristics of the accelerator structure as well as fundamental properties of the accelerator (Figure 2, 3) [6]. Here only some cavity related aspects will be discussed. The well-proven TESLA shape used in more than 120 nine-cell structures is the baseline ILC design. It is optimised with respect to cell-to-cell coupling k_{cc} and a low ratio of surface electric field to gradient E_{peak}/E_{acc}. The cell-to cell-coupling of 1.9 % ensures robust tuning properties, good HOM-damping and avoids trapped modes. E_{peak}/E_{acc} of 2.0 is favourable in order to reduce field emission loading. The tilted iris areas allow good wet cleaning and rinsing. The Low-Loss (LL) shape is optimized with respect to a comparable low magnetic surface field to gradient ratio H_p/E_{acc}. This allows about 15% higher gradient for the same magnetic field value.

OVERVIEW OF REGIONAL INFRASTRUCTURES FOR SCRF DEVELOPMENT

Carlo Pagani, University of Milano and INFN Milano - LASA, Italy

Abstract

The perspective of building the International Linear Collider, ILC, as a global project based on the SCRF technology, which has been pushed in the last decades mainly in Europe by the TESLA Collaboration, imposed to the other two Regions, America and Asia, the investment of consistent resources to locally develop with industry the capability of handling the "cold" technology. Following the success of TTF at DESY, and before of LEP II at CERN and CEBAF at TJNAF, large dedicated infrastructures are being created at Fermilab and KEK. The new regional infrastructures, together with the existing ones, will form the basis for the realization of a global machine, with a single design and distributed production of the key components. In this paper the importance of the SCRF infrastructures is discussed, and their status and plans are outlined.

INTRODUCTION

Since the early 70s, Superconducting RF, SCRF, has been introduced in the particle accelerator community as a promising technology to efficiently transmit energy to a variety of particle beams.

When a superconductor is exposed to a time varying electromagnetic field the electrons which are not coupled as Cooper pairs lead to energy dissipation in the shallow London penetration depth. Nonetheless it was soon realized that in the practical frequency range of RF accelerators the theoretical surface resistance is order of magnitude lower than in a normal conductor, widely compensating for the required cryogenics and leading to an increase of the overall plug to beam power conversion efficiency [1].

A few laboratories and universities started fundamental investigations and experiments to demonstrate the technical feasibility of SCRF acceleration. Very rapidly the results reached severe technological limitations, mainly due to the modest purity of the superconducting material being used to produce the cavities prototypes. Moreover, to approach the theoretical limits, it also turned out that all the cavity fabrication process and handling were not adequate to preserve the purity of the few tenths of nanometres layer at the cavity surface.

In spite of these limitations, in the middle 80s two major laboratories, TJNAF in US and CERN in Europe, planned to build large accelerators based on SCRF technology. To overcome the limitations faced so far by this technology, an impressive effort was performed in setting up large dedicated infrastructures to define and control the production parameters at the basis of the modest performances.

The construction and operation, in strict collaboration with industry, of hundreds of moderate gradient (5-8 MV/m) cavities at TJNAF for CEBAF [2] and at CERN for LEP II [3] has been the basis for setting a new level of quality control and industrialization. In particular the successful technology transfer was possible because of the large effort dedicated in defining reproducible production parameters making use of the large dedicated infrastructures set up for this specific purpose.

A deeper understanding of the limiting factors contributed then to revise the SCRF technology further, in order to be compatible with the new challenging demands emerging from the High Energy Physics community.

The TESLA challenge to use SCRF as the basic technology for the future TeV e+e- Linear Collider impressed the momentum to move SCRF Technology to a new frontier, opening a new era

- Accelerating fields exceeding 35 MV/m
- Quality factor higher then 10^{10}

As for the past experience, the great success of the TESLA Collaboration was mainly determined by the consistent investment, in term of both resources and experienced persons, in setting up at DESY, the host laboratory, a dedicated infrastructure that was designed to include all the past experience. This infrastructure - called TESLA Test facility, TTF - combined most of the existing know-how and has been the "school" were most of the new SCRF scientists have been formed.

The success of TTF opened the way for a consistent proposal of the TESLA Liner Collider, presented to the International Community in March 2001 [4]. To perform a realistic costing of TESLA, industry has been included in the process, initiating the technology transfer in view of a large scale production. Process parameters defined in the TTF infrastructure went through a deep analysis made by industry for cost estimation and a few suggestions became part of the baseline design.

In August 2004, the ITRP (International Technology Recommendation Panel) unanimous recommendation of basing the next International Linear Collider, ILC, on the TESLA "cold" technology has been the successful end of the TESLA experience, while opening a new era where the SCRF technology is considered the right choice for most of the new accelerator projects.

The TESLA Collaboration achievements, together with the experience on large existing cryogenic infrastructures, brought most of the accelerator community to be confident that SCRF Technology can be reliably applied for a cost effective accelerator design. In fact, at the present technology level, the SCRF is respecting the original promise of being competitive in term of investment cost, while giving better conversion efficiency and lower operating costs.

Since the decision for the TESLA technology, the Global Design Effort, GDE - which was established for

TECHNOLOGICAL CHALLANGES OF ERLS

L. Merminga, Jefferson Lab, Newport News, Virginia

Abstract

Technological challanges in ERL and THz Sources

PAPER NOT YET RECEIVED

CRAB CAVITY DEVELOPMENT

Y. Morita[#], K. Akai, K. Ebihara, T. Furuya, K. Hara, T. Honma, K. Hosoyama, A. Kabe, Y. Kojima,
S. Mitsunobu, H. Nakai, K. Nakanishi, M. Ono, Md. M. Rahman* and Y. Yamamoto, KEK,
Tsukuba, Ibaraki, Japan
T. Kanekiyo, Hitachi, Ltd., Tsukuba, Ibaraki, Japan
K. Okubo and K. Sennyu, MHI Kobe Shipyard, Japan

Abstract

Two superconducting crab cavities were installed in the KEKB accelerator. The KEKB (KEK B-factory) is a double-ring, asymmetric-energy, high luminosity electron-positron colliding accelerator with a finite angle beam crossing. A purpose of the crab cavities is to deflect the beam-bunches with time-varying RF fields, and to provide the head-on collision at the interaction point (crab crossing scheme). The head-on collision will drastically increase the luminosity. The crab cavity is required to have high RF fields (kick voltage) to provide beam-bunch deflection. The operating mode (crab mode, 509 MHz) is not the lowest order mode (LOM) of the cavity. In order to sufficiently damp the LOM as well as the HOMs for high beam currents in KEKB, a coaxial coupler is attached along the beam pipe. Two crab cavities have been fabricated and tested in a vertical cryostat. The cavities were recently tested with high RF power in cryostats. We have achieved required kick voltage.

INTRODUCTION

The crab crossing was first proposed by R. B. Palmer for linear colliders to increase the luminosity [1]. K. Oide and K. Yokoya suggested that this crossing scheme is applicable for ring colliders such as KEKB [2]. KEKB is a B-meson factory which consists of two storage rings with a finite angle beam crossing at the collision point. One ring is a 3.5 GeV low energy positron ring (LER) and the other is an 8 GeV high energy electron ring (HER) [3]. Main parameters of KEKB are summarized in Table 1. The crab crossing needs an RF deflector which provides transverse kicks for the beam bunches. Consequently, the beam bunches tilt at the interaction point and collide head-on. After the collision, the beam bunches are kicked back by compensating RF deflectors. Fig. 1 shows the crab crossing scheme.

K. Akai invented a beam deflecting RF cavity (Crab Cavity) [4]. His design is the base of the crab cavity for KEKB. This cavity has several unique characteristics. One is a coaxial coupler to damp the lowest order mode (LOM). Another is a not-round cavity cell (squashed cell) for separating unwanted higher order modes (HOMs). The required RF fields are high for KEKB accelerator. The kick voltage is 1.4 MV corresponding to the surface peak electric field of 21 MV/m.

Superconducting cavity is suitable for the high field requirement. To develop superconducting crab cavity,

_____
[#]Yoshiyuki.morita@kek.jp
*present address: Chittagong Univ., Chittagong, Bangladesh

R&D program started in 1994. Using 1/3-scale Nb model cavities, fabrication methods and surface treatments were studied. In 1996 a full-scale Nb prototype cavity was fabricated and tested intensively. We achieved the required kick voltage after several tests. The second prototype cavity was fabricated for a reproducibility check. The cavity exceeded the required voltage and reached almost 3 MV. This cavity was installed in a prototype cryostat for a cool-down test.

In 2003 K. Ohmi suggested the crab crossing would improve the luminosity [5]. Using a beam-beam simulation method, he concluded that the luminosity would increase two times as much as the present one. Two crab cavities were decided to be installed in both KEKB rings. In this scheme there are no compensating crab cavities. The beam bunches wiggle in the ring. The location of crab cavities was chosen at the straight section 1 km away from the collision point, where superconducting accelerating cavities and a large He refrigerator already exist. This scheme helped to reduce the construction costs. Fabrication of two crab cavities started in 2005.

Table 1: Main parameters of KEKB

	LER	HER
Beam Energy (GeV)	3.5	8.0
Beam Current (A)	1.7	1.3
Crossing angle (mrad)	11 x 2	
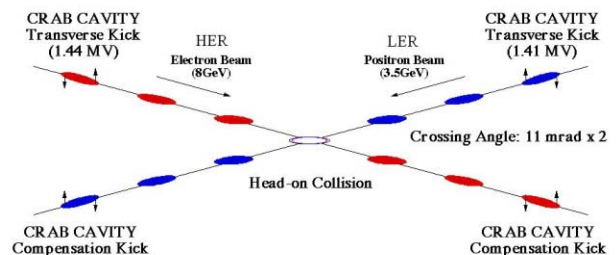
Figure 1: Crab crossing scheme.

CONCEPTUAL DESIGN

The crab cavity is excited with the TM110-like mode (Crab mode, 509 MHz) to kick the beam bunches since this mode has a large R/Q value. However, this mode is not the lowest order mode (LOM). For high current operation, it is important to sufficiently damp the LOM as well as higher order modes (HOMs).

R&D ON VACUUM COMPONENTS
FOR HIGH-CURRENT ACCELERATORS

Y. Suetsugu[#], K. Shibata, H. Hisamatsu, M. Shirai and K. Kanazawa,

KEK, Tsukuba, Japan

Abstract

R&D on various vacuum components adaptable to future high-current accelerators has been continuously progressing at KEK. Copper beam ducts with one or two ante-chambers were designed to dilute the synchrotron radiation (SR) power density, and also to suppress photoelectrons around beams. Inner surfaces with a low secondary electron yield (SEY) were investigated to mitigate electron-cloud formation. Bellows chambers and gate valves with high thermal strength and low beam impedance were developed. A special flange with no gap at the connection point was designed. A novel movable mask (collimator) with low beam impedance was recently proposed. These components have been installed at the KEK B-factory (KEKB), and the performances have been investigated using an intense beam of up to 1.7 A.

INTRODUCTION

In future high-current accelerators, such as Super B-factories, a stored beam current of several amperes and a bunch length of a few mm are required to achieve a luminosity on the order of 1×10^{36} cm^{-2}s^{-1} [1, 2]. These parameters impose very severe challenges to the vacuum system [3, 4]. The beam duct has to manage the synchrotron radiation (SR) power density up to several tens Wmm^{-2}. The vacuum components should have low beam impedance, and be able to stand up against the intense higher order modes (HOM) at the same time. Suppression of the electron cloud instability (ECI) [5] is also a serious problem in a positron ring. These are common key issues not only for a high-current factory machine, but also for the dumping ring (DR) and the collimators of the international linear collider (ILC), and the next generation of SR rings, where a very low emittance is required [6, 7].

R&D on various vacuum components to meet these demands has been progressing at KEK [8-17]. Copper beam ducts with antechambers were designed and manufactured [8, 9]. The antechamber scheme was adopted to deal with the intense SR power and to suppress photoelectrons at the same time. The effects of the inner coatings of NEG materials (Ti, Zr, V) and TiN were studied, which were said to have low secondary electron yields (SEY) [10, 11]. Bellows chambers and gate valves with a comb-type RF-shield were newly developed [12-14]. A special connection flange was designed and examined, which has a small step, or gap, inside, even for a beam duct with antechambers [15]. A movable mask (collimator) with low impedance was recently proposed

[#]yusuke.suetsugu@kek.jp

and the study has just begun [16].

These components have been installed for testing at the KEK B-factory (KEKB) [18, 19]. KEKB is an electron-positron collider with asymmetric energies, and consists of two rings, that is, a 3.5 GeV positron ring (Low Energy Ring, LER) and an 8.0 GeV electron ring (High Energy Ring, HER). The maximum stored beam currents of LER and HER are 1.7 A and 1.4 A at 1389 bunches, respectively. At present, KEKB is the most suitable machine for R&D about future accelerators with high intensities. The R&D is progressing based on various experiences in the vacuum system of KEKB [20, 21]. The concepts of these newly-developed vacuum components and the results of recent studies are reviewed here.

BEAM DUCT

The R&D of vacuum components began with a beam duct with an ante-chamber in 2003 [8, 9]. The beam duct consists of two channels, i.e. a beam channel where a beam circulates, and an SR channel (ante-chamber) aside where synchrotron radiation (SR) passes through. By using the ante-chamber scheme, the maximum power density of SR can be diluted at the side wall. Photoelectrons inside the beam channel, furthermore, are small compared to that of a simple circular duct, which is a big merit for a positron ring to suppress the ECI.

Several kinds of copper beam ducts with ante-chambers have been manufactured, and installed into the KEKB LER. Copper (Oxygen Free Copper, OFC) was adopted for its high thermal strength and good radiation shielding property [20, 21]. The electron beam was used to weld copper to copper. The inner diameter of the beam channel was 94 mm, and the thickness was 6 mm. The depth and the height of the ante-chamber were 65 mm and 15 mm, respectively. The ducts were manufactured using two methods, that is, pressing and forming (cold drawing). A copper beam duct with two ante-chambers is presented in Fig. 1, for example. Two NEG-pump channels were placed at the top and bottom of the ante-chambers.

Beam ducts with one ante-chamber were installed in an arc section of LER. The SR power and the photon density was 3 kW m^{-1} and 8.5×10^{18} photons s^{-1} m^{-1}, respectively, at a beam current of 1 A. The critical energy of SR was 5.8 keV. Beam ducts with two ante-chambers, on the other hand, were installed at a wiggler section, where the SR hits the duct at both sides. The maximum power density and the direct photon density were about 227 Wm^{-1} and 7.5×10^{17} photons m^{-1} s^{-1} at a beam current of 1 A, respectively.

LHC STATUS

Lyndon Evans, CERN, Geneva, Switzerland

Abstract

The installation of the Large Hadron Collider at CERN is now approaching completion. Almost 1100 of the 1232 main bending magnets are installed and the whole ring will be installed by the end of March 2007. Emphasis is now moving from installation to commissioning, with the cool down of the first of the 8 sectors to liquid helium temperature well underway. In the other sectors, interconnect work is proceeding at a satisfactory pace and will be finished by the end of August. It is foreseen to inject the first beam into the LHC in November with the objective of having first collisions at the injection energy (450 GeV/c) in order to debug the machine and detectors before stopping for the annual winter shutdown. During this time, the detector installation will be finished and the machine will be pushed to full current ready for the first physics run at 7 TeV per beam in 2008.

MACHINE LAYOUT

The LHC is a two-ring superconducting proton-proton collider housed in the 27 km circumference tunnel originally constructed for the Large Electron-Positron collider (LEP), now decommissioned. It is designed to provide proton-proton collisions with unprecedented luminosity (10^{34} cm^{-2} s^{-1}) and a centre-of-mass energy of 14 TeV for the study of rare events such as the production of the Higgs boson if it exists. In order to reach the required energy in the existing tunnel, the dipoles must operate at high field (8.3 T) and therefore have to be cooled in superfluid helium at 1.9 K to increase the critical current of the NbTi conductor to the required value. In addition to p-p operation, the LHC will be able to collide heavy nuclei (Pb-Pb) with a centre-of-mass energy of 1150 TeV (2.76 TeV/U and 7 TeV per charge). By modifying the obsolete antiproton ring (LEAR) into an ion accumulator (LIER) in which electron cooling is applied, the luminosity can reach 10^{27} cm^{-2} s^{-1}.

The basic layout of the LHC is shown in Figure 1. The machine has eight arcs and straight sections approximately 528 m long. Four of the straight sections house the LHC detectors. The two high luminosity detectors, ATLAS and CMS, are located at diametrically opposite straight sections at Points 1 and 5 respectively. The two other detectors (ALICE and LHCb are located at Points 2 and 8, which also contain the injection systems for the two rings.

The other four straight sections contain machine utilities. Points 3 and 7 contain two collimation systems for capturing stray particles. Point 3 is designed to capture off-momentum particles whilst the collimation layout at Point 7 is designed to control the beam halo. Point 4 contains the Radio Frequency superconducting acceleration cavities operating at 400 MHz, twice the frequency of the LHC injector. Finally, Point 6 contains

the beam abort systems for the two beams which will allow the beams to be extracted safely and deposited onto external dumps capable of absorbing the considerable stored energy (up to 350 MJ at top energy and intensity).
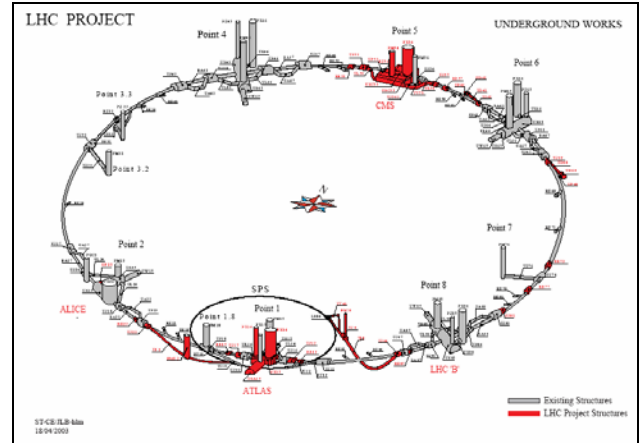
Figure 1: Machine layout.

INSTALLATION AND COMMISSIONING OF MAJOR SYSTEMS

Magnets

The full list of superconducting magnets and their function is shown in Table 1. All magnets have now been delivered. They range from the large 15 m long, 35 ton dipoles to the 11 cm long, 5 kg decapole-octupole correctors inside the dipole cold mass which correct for unwanted multipoles of the dipole field. Half of these correctors (616 units) and half of the sextupole correctors (MCS, 1232 units) were built in India under the supervision of RRCAT. All magnets were tested at 4.2 K at RRCAT before being shipped to the European manufacturers of the dipoles to be integrated into the cold masses.

Figure 2 shows the history of the main dipoles from production to installation. Delivery of all 1232 dipoles (excluding spares) is now complete (top curve). On arrival, the dipoles are inserted into their cryostats and connected to one of the cryogenic test stands (Figure 3), where they are cooled to their operating temperature of 1.8 K. Cold tests include electrical quality assurance and a training campaign where the dipoles are taken above their operational field of 8.3 T. A random sample of about 20 % is used for magnetic measurements in order to check that the correlation between warm measurements at the factories (all dipoles are measured warm) and cold measurements remains good. The cold testing of all magnets has been an enormous effort with the test stations running 24 hours per day, 7 days per week for over 3 years with only one short shutdown per year for maintenance. This would not have been possible without

01 Circular Colliders
A01 - Hadron Colliders

RECORD LUMINOSITIES AT THE TEVATRON & FUTURE POTENTIALITY[*]

S. Werkema[#], Fermilab, Batavia, IL 60510, U.S.A.

Abstract

Fermilab Collider Run II has been in progress for nearly six years. During this tine the D0 and CDF experiments have each acquired total integrated luminosities of nearly 2.2 fb^{-1}. Also during this time the peak instantaneous luminosities increased by more than a factor of 25 – from 10 to as high as 270×10^{30} cm^{-2} s^{-1}. An aggressive collider upgrade program continues to make significant progress along side luminosity production operations. This paper will give the status of Tevatron operations and expectations for the remainder of Run II.

PRESENT OPERATIONS

At the present time the Fermilab accelerator complex is providing beam for several high energy physics experiments. In addition to two collider experiments (CDF and D0), proton beam is made available for 120 GeV fixed target experiments and two neutrino experiments (NuMI and MiniBooNE).
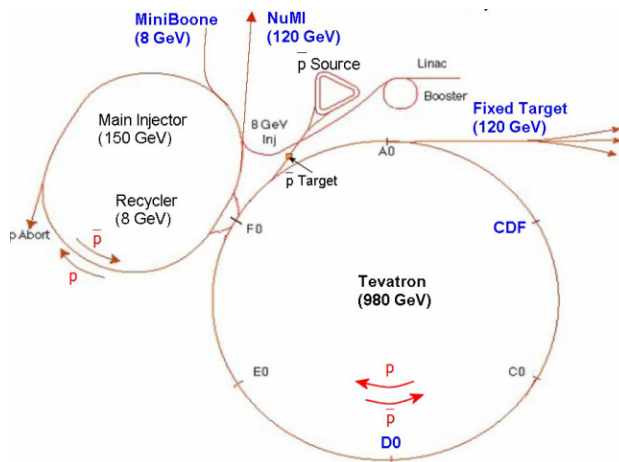
Figure 1: The Fermilab accelerator complex. Four high energy physics programs are supported: collider experiments CDF and D0, NuMI, MiniBooNE, and 120 GeV fixed target experiments.

The layout of the Fermilab accelerator complex and experiments is shown in Figure 1. Protons are accelerated and directed toward their final destination as follows:

- Protons from the Linac are accelerated to 8 GeV in the Booster synchrotron at 15 Hz.
- 4.2×10^{12} protons at 8 GeV are directed to MiniBooNE at a rate of approximately 2.5 Hz [1].
- 8.2×10^{12} protons at 8 GeV are accelerated to 120 GeV in the Main Injector every 2.4 sec for antiproton production.

- 11.5×10^{12} protons at 8 GeV are accelerated to 120 GeV in the Main Injector every 2.4 sec for neutrino production for the NuMI experiment.
- Varying amounts of 8 GeV protons are accelerated to 120 GeV and slow extracted every 61 sec for switchyard fixed target experiments

The contention for protons amongst the various experimental programs places some constraints on the operation of the Tevatron for the collider experiments.

During routine operation the injector chain operates to accumulate antiprotons while a collider store spins in the Tevatron. The average length of a collider store is about 20 hours. After a collider store is terminated a new store is inserted using the newly accumulated antiprotons.

Present and anticipated parameters of the Tevatron collider are given in Table I.

Table 1: Collider Parameters

Parameter	Present[†]	Upgrade	Units
Peak Luminosity	185	300	10^{30} cm^{-2} s^{-1}
Luminosity Lifetime	8.5	[‡]	hr
Store hours per week	97	105	hr/wk
Integrated Luminosity	5.1	[‡]	pb^{-1}/store
Total Run II $\int L dt$	2.2	7	fb^{-1}
Protons per bunch	250	270	10^9
$\bar{p}$ per bunch	58	127	10^9
Number of bunches	36×36	36×36	
β* at IPs	28	28	cm
$\bar{p}$ stacking rate to Accumulator	17.5	30	10^{10}/hr
$\bar{p}$ stacking rate to Recycler	12.0	[‡]	10^{10}/hr

[†] Average values for FY2007
[‡] No upgrade goal specified

Antiproton Stacking

Antiproton stacking consists of accelerating 120 GeV protons onto a nickel target disk through a process called slip stacking [2][3]. 8 GeV secondaries are collected off of the target using a high gradient lithium lens. This beam is injected into the Debuncher ring where the 19 nsec bunch structure from the targeted protons is rotated in longitudinal phase space to produce a narrow energy spread. The beam is stochastically cooled for 2.4 sec and transferred to an orbit on the high energy side of the Accumulator ring. The newly injected pulse of antiprotons is moved with RF to an orbit near the central

NEXT GENERATION ELECTRON-ION COLLIDERS*

Ilan Ben-Zvi**, Collider-Accelerator Department, Brookhaven National Laboratory, U.S.A.

Abstract

The next generation of electron-ion colliders promises very high luminosity, very high degree of polarization in both beams, multiple interaction points (IPs) and large range of energies. It will extend the reach and variety of attainable procresses in High Energy Physics and Nuclear Physics well beyond that provided by the first and only lepton-hadron collider, HERA. Some of these promises are based on new capabilities such as Energy Recovery Linacs (ERLs). We describe plans for these colliders which are under development by various laboratories, and the technology issues that are associated with these applications.

INTRODUCTION

Electron-ion (and positron-ion) collisions have unique properties that make them very valuable for high-energy and nuclear sciences. This was proven over 50 years ago by the seminal work on the form factor of nucleons by Robert Hofstadter which led to a Nobel Prize, and continued with ever increasing energy and luminosity to culminate in the lepton-proton HERA collider [1], providing an unprecedented energy reach, luminosity and lepton polarization. Not surprisingly new questions keep coming up and the need for accelerators with greater reach and greater variety of colliding species is ever present. In particular, the need to study QCD, improve the understanding of the structure and spin structure of hadronic matter, understanding the transition from the deconfined state of free quarks and gluons in the Big Bang to stable hadron matter can be addressed with higher precision in lepton-ion collisions. Hence, the new generation of electron-ion colliders is one of the key instruments to unravel the crucial fundamental physics questions.

Where does one go depends on the science one would like to pursue, and there is no single answer. The interest of nuclear and elementary particle physics span through a very large range of center-of-mass energies and energy ratios, variety of nuclear projectiles (from protons to uranium), use of electrons and positrons, very high luminosity and sometime very high degree of polarization.

In this work I will first outline what the accelerator physics issues are, and then describe three possible future machines which are quite different in approach and maturity of design: eRHIC, ELIC and LHeC.

ISSUES AND TECHNOLOGIES

The luminosity of an electron-ion collider can be written in terms of the fundamental machine limits, the beam-beam parameters and angular acceptance of the IP quads as

$$L = \left(\frac{4\pi\gamma_i\gamma_e}{r_i r_e}\right)(\xi_i\xi_e)(\sigma_i'\sigma_e')f$$

where round beams of the same size are assumed at the IP and subscripts *i* or *e* denote ions or electrons. The ξ are the respective beam-beam parameters, *r* are the classical radii and γ are the relativistic factors, and *f* the collision frequency. The angular rms spreads σ' at the IP are limited by the aperture of the final focus quadrupoles. Clearly the achievable luminosity scales with the assumed beam-beam parameter and a good understanding of this limit is necessary in any machine.

An ion beam-beam parameter limit of $\xi_i=0.015$ is supported by the performance of the RHIC, Tevatron and SPS proton colliders. HERA had limited operation to ξ_i ~0.003 to avoid increase of detector background due to beam loss caused by larger beam-beam parameter. The subject of the detector background requires further study. A very slow beam loss with lifetime of about 20 hours can be strongly affected by both the detector and collimation design as well as by electron cooling.

In approaching the design of a new accelerator one has to consider and resolve some of the issues outlined below.

Performance is mostly driven by the potential users of the proposed facility, and include: Richness of the selection of beam species, CM energy, variability of energy and energy-ratio (between the two colliding species), luminosity, polarization, bunch spacing, background, length of IP free of accelerator elements, number of IP's available, prospects of upgradeability and more. All of these affect the utility of the proposed facility to its users, and the users are usually the ones who have to make difficult choices.

Cost is in potential conflict with **performance**; New electron-ion colliders must use to a larger or lesser degree existing facilities in order to reduce the cost and/or improve performance. Of these, the ion machines and their injector-chains are the more expensive elements. Another variable of the cost vs. performance equation is **innovation**. One can use new technical solutions which, if used, can increase performance and/or reduce cost. However, using a new and untried approach may lead to **risk**. This has consequences - reviewers tend to be skeptical of new approaches and the contingency one has to carry influences the cost. Yet, progress requires some risks to be taken. Jawaharlal Nehru said wisely: "The policy of being too cautious is the greatest risk of all". In this paper I will try to portray the different path taken by

OVERVIEW OF SYNCHROTRON RADIATION LIGHT SOURCES

A.F. Wrulich, PSI, Villigen

Abstract

Third generation light sources are, at present, the most intense and stable sources of short X-ray pulses. Their successful operation has triggered several new projects, resulting in a constant growth of the user community and an expansion in experimental techniques. With the recent conceptual and technological advancements, the performance of third generation light sources has however reached its limits. Novel techniques have been developed to further the scientific endeavors. Energy Recovery Linacs (ERL) are able to overcome some of the intrinsic performance limitations of storage ring based light sources. An even higher performance can be achieved with Free Electron Lasers (FELs) based either on storage rings, ERLs or linear accelerators. X-ray FELs based on Linacs represent the next generation of sources of intense X-ray pulses. The dramatic increase in flux and time resolution brought about by X-FELs will not only represent another breakthrough in technical achievement, but will provide a new frontier in which great scientific discoveries can be envisaged. The evolution of light sources will be presented with emphasis on the conceptual and technical innovations.

PAPER NOT YET RECEIVED

COMMISIONING OF THE INDUS-2 STORAGE RING

V.C. Sahni

Raja Ramanna Centre for Advanced Technology (RRCAT), Indore-452 013 &
Bhabha Atomic Research Centre (BARC), Mumbai-400 085

Abstract

An overview of the 2.5 GeV synchrotron radiation source, Indus-2, which has been set up at RRCAT, Indore will be presented with emphasis on commissioning details. The accelerator is used both as a booster and as a storage ring. Using an injection energy of 550MeV, the beam energy has been ramped up to 2.4 GeV. Two beam lines have also been installed, one for x-ray diffraction (XRD) and another for extended x-ray absorption fine structure (EXAFS) studies. To condition the vacuum chamber of the ring, regular operation has been restricted to 2 GeV. To test the XRD beam line, first diffraction pattern from a pyrolitic graphite sample was recorded with bending magnet synchrotron light with ring operating at 2 GeV. Indigenous technological base created in setting up Indus-2 would be used while participating in up coming international accelerator projects.

INTRODUCTION

A programme to build synchrotron radiation sources (SRSs) in the country was started in the eighties by the Department of Atomic Energy. A separate laboratory named Centre for Advanced Technology at Indore was created. The injector accelerators, namely, 20 MeV microtron and a 450-700 MeV booster synchrotron and the first 450 MeV storage ring Indus-1 were commissioned during the 90's. Originally, SRS Indus-2 was planned to be a 2 GeV ring. However, in November 1997, based on the advice of an International Panel, this energy was raised to 2.5 GeV. The design work on the new components, needed for the enhanced energy ring, was started in 1998 along with the civil construction of the building. Development of the prototype components and their large scale manufacture, partly in industry and partly in house, was spread over the next five years. The installation of the different subsystems was taken up from 2003-04 onwards. The complete assembly of Indus-2 & transport line (TL-3) connecting it to booster synchrotron, was finished by early 2005. Thereafter the evacuation of the ring and subsystem commissioning was taken up. By the end of 2005 we had started accumulating electrons in Indus-2 of ~450 MeV energy and the first signatures of the SR from Indus-2 were recorded using a CCD camera mounted over the sighting beam line. Over the past year beam energy ramping experiments were successfully completed, reaching up to 2.4 GeV in stages. In parallel work on building the beam lines for using the SR have also gone on. This paper will concentrate on the progress during the past year and a half. Main developments during the earlier periods have been described before [1].

INDUS ACCELERATOR PROGRAM AT RRCAT

Figure 1 gives a schematic view of the Indus Accelerator Complex and the present status of the machines and the transport lines. A sketch of Indus-2 lattice is given in figure 2 and Table 1 contains the parameters of the ring [1].
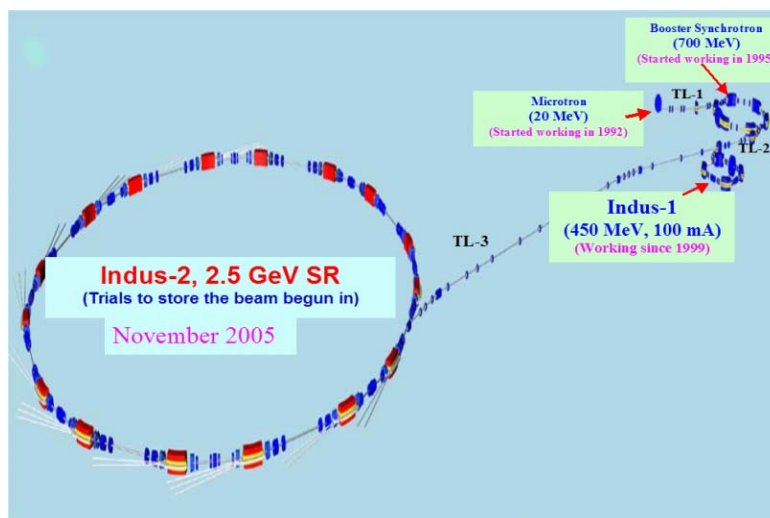
Figure 1: Schematic view of the Indus Accelerator Complex.

COMMISSIONING AND STATUS OF THE DIAMOND STORAGE RING

R.P. Walker, Diamond Light Source (DLS), Oxfordshire, U.K.,
on behalf of the Diamond Machine Commissioning Team

Abstract

The commissioning of the Diamond storage ring at 3 GeV, as well as the current status and future plans, are described.

INTRODUCTION

The construction phase of Diamond, the UK's new medium-energy 3rd generation synchrotron light source [1,2] concluded at the end of December 2006. Diamond has now entered the operational phase, with first external users starting at the end of January 2007, in line with the original programme. The main parameters of Diamond are given in Table 1.

Table 1: Main parameters of the Diamond storage ring.

Energy	3 GeV
Circumference	561.6 m
Lattice	24-cell DBA
Straight sections	6 x 8 m, 18 x 5 m
RF frequency	500 MHz
Nominal current	300 mA
Nominal rms emittances (H,V)	2.7, 0.03 nm rad
Nominal rms energy spread	0.096 %

This report will concentrate on the recent commissioning of the storage ring at the full energy of 3 GeV which began in September 2006. The earlier commissioning of the 100 MeV linac (August-October 2005) and 3 GeV booster (December 2005 – June 2006), as well as the initial phase of storage ring commissioning (May 2006), were described at EPAC 2006 [2-5].

The first phase of storage ring commissioning took place at 700 MeV, because of the lack of water cooling at that time for both magnets and radiation absorbers. The low energy made commissioning very difficult, however it did prove possible to accumulate a current of 2 mA. Following this period the ring was shut-down for 3 months both to complete the water cooling systems, as well as to install the insertion devices, and further front-ends. By the beginning of September all seven Phase I insertion devices had been installed.

Commissioning at 3 GeV began on the evening of the 4th September 2006. Operation was restricted to outside normal working hours until the radiation shielding had been verified. On the first evening the beam was circulated for 5 turns, with correctors, sextupoles and RF off. The next evening 120 turns were obtained, with sextupoles on. The following evening the RF was turned on and a beam of 2 mA was accumulated. In 3 evenings therefore we had accomplished what had taken a month at 700 MeV, because of calibration, stability and other beam dynamics issues [2].

At that stage the current was deliberately limited at 2 mA until cooling water and interlocks on the radiation absorbers had been fully tested. Two days later this work had been carried out and beam was accumulated up to 10 mA. Another limit was placed at this level since the orbit interlock for protecting the vacuum vessel in case of mis-steered photon beams was not yet in operation. Nevertheless the current was sufficient to allow progress to be made with closed orbit correction and optics optimisation. Once the orbit interlock was operational the current was gradually increased, carefully checking for beam instabilities and monitoring vessel temperatures and vacuum pressures. By the beginning of October, 60 mA had been reached and the target for initial operation of 100 mA was achieved on Nov. 11th. Further progress was limited by the time available for high current operation and RF conditioning, since an increasing amount of time was devoted to beamline commissioning. First light was let into a beamline optics hutch on Oct. 12th, and regular daytime beamline commissioning started on Oct. 23rd.

ACCELERATOR PHYSICS

Closed-orbit

Initial correction of the closed orbit quickly reduced the error to the level of 0.7 mm rms in both planes, but no less. A "beam based alignment" (BBA) was then carried out to determine the offset between the centre of each beam position monitor (BPM) and the magnetic centre of the nearest quadrupole magnet.
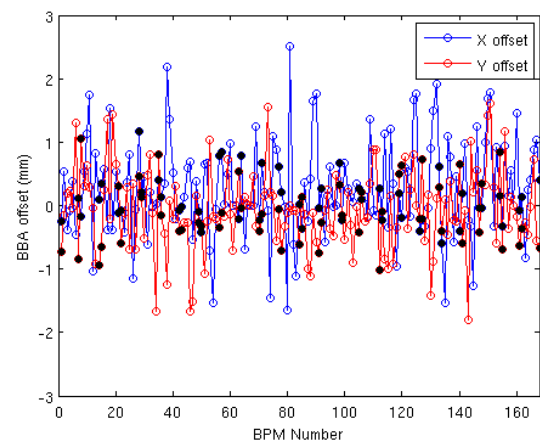
Figure 1: BPM-quadrupole offsets; black dots denote "primary" BPMs.

The Accelerator Toolbox Middlelayer routine "quadcenter" [6] was used for this task. A complete scan of all 168 BPMs required 8 hours. The first measurement did not result in a very accurate determination of the offsets, but nevertheless when the offsets were taken into account the closed orbit could be improved. A further series of iterations was then carried out, each time

DESIGN OF THE TRANSFER LINE-2 FOR THE CTF-3 AT CERN

Amalendu Sharma, Abdurrahim, A.D. Ghodke, Gurnam Singh
IOAPDD, Raja Ramanna Centre for Advanced Technology, Indore (M.P.)

Abstract

The design of the Transfer Line-2 (TL-2), which will transfer an electron beam from the Combiner Ring (CR) to CLEX area (CLIC experimental area) of CTF-3 (CLIC Test Facility-3) at CERN, is presented in this paper. This line will be used to control the bunch length and Twiss parameters at the entrance to the CLEX area. The line will have a wide tunability of R_{56} parameter, ranging from – 0.35m to +0.35m. This has been designed considering the constraints imposed by the building geometry and the magnetic elements to be used. The design optimization of the line has been done up to second order for the entire R_{56} range, keeping T_{566} practically zero and emittance dilution below 10%.

INTRODUCTION

CLIC (Compact Linear Collider) at CERN is based on the new scheme of RF generation at 30 GHz. The RF generation scheme is based on the frequency multiplication and bunch compression of the drive beam. The CTF-3 is to demonstrate the feasibility of such a scheme to provide the 30 GHz RF power source with CLIC nominal peak power and pulse length. The electron beam at nominal energy of 150 MeV after frequency multiplication will be extracted from the Combiner Ring (CR) and it will be transported to CLEX area with required bunch length compression by the TL-2. The general description and layout of the CLIC and CTF-3 can be found in references [1, 2, and 3]. Here in RRCAT, we have carried out the optics design of the TL-2, with required tuning range to handle the bunch length control before delivering the beam in CLEX area. In this paper we have provided the basic theory of bunch length control in the magnetic optics and design of TL-2.

BUNCH LENGTH COMPRESSION

Bunch length compression is possible by establishing the energy time correlation in the bunch by a RF field and then passing it through the magnetic channel to establish the required length energy correlation [4]. When bunch passes through the RF field, the energy time correlation is given by

$$z_1 = z_0 \tag{1}$$

$$\delta_1 = \left(1 - \frac{qV_{RF}}{E_0}\sin\phi_s\right)\delta_0 + \left(\frac{qV_{RF}}{E_0}\cos\phi_s\right)kz_0 \tag{2}$$

Here z gives the longitudinal position of the particle with respect to reference (synchronous) particle. V_{RF}, q, δ and ϕ_s carry their usual meanings. Subscripts 0 and 1 are used for entrance and exit of the cavity. In the approximation

used here, it is assumed that cavity has zero length and thus z does not change. The equation 2 can be written as

$$\delta_1 = R_{65}z_0 + R_{66}\delta_0 \tag{3}$$

Here R_{ij} is the element of 6x6 first order transfer matrix. After that the particle passes through the magnetic channel, which has opposite effect of the cavity, i.e. the δ remains unchanged and z is modified. For a magnetic channel, the first order relations can be written down as

$$z_2 = z_1 + R_{56}\delta_1 \tag{4}$$

$$\delta_2 = \delta_1 \tag{5}$$

Z_2 and δ_2 are the longitudinal position and momentum deviation after the magnetic channel. Here R_{56} depends on the dispersion distribution inside the dipole magnets of the magnetic channel. It is given by (in sign convention of MAD-8 [5])

$$R_{56} = -\int \frac{\eta ds}{\rho} \tag{6}$$

Therefore by controlling the dispersion distribution inside the dipole magnets, R_{56} parameter can be controlled and by selecting the proper values of R_{65}, R_{66} and R_{56}, the required bunch length compression can be obtained. Introducing second order terms in the analysis, the equation 4 will be modified as

$$z_2 = z_1 + R_{56}\delta + T_{566}\delta^2 \tag{7}$$

Here T_{ijk}- is the element of the second order transfer matrix. In the present paper we outline the design of the TL-2, which has a wide tuning range of the R_{56} parameter to control the bunch length and in whole tuning range second order term T_{566} is compensated.

OPTICS DESIGN OF THE TL-2

General Layout

The beam parameters of TL-2 are provided in the table-1. The line is to be accommodated in the existing LPI-complex (LEP Pre Injector complex), which has several geometrical constraints and the magnets to be used here to be selected from a stock of already magnets available at CERN. These constraints poses a challenge in the design of the line with such wide tuning range of R_{56} parameter (from -0.35m to +0.35m) with T_{566} corrected to zero and emittance dilution below 10%. The layout of the complete line inside the building is shown in the figure-1. Parameters and numbers of the available magnets are shown in the table-2.

The design of the line can be broken in three modules. Following sections describe the details of each module of this line.

RHIC STATUS*

Thomas Roser

Brookhaven National Laboratory, Upton, New York 11793-5000, USA

Abstract

As the first hadron accelerator and collider consisting of two independent superconducting rings RHIC has operated with a wide range of beam energies and particle species. Machine operation and performance will be reviewed that includes high luminosity gold-on-gold and copper-on-copper collisions at design beam energy (100 GeV/u), asymmetric deuteron-on-gold collisions as well as high energy polarized proton-proton collisions (100 GeV on 100 GeV) with beam polarization of up to 65%. Plans for future upgrades of RHIC will also be discussed.

THE RHIC FACILITY

With its two independent rings RHIC is a highly flexible collider of hadron beams ranging from colliding intense beams of polarized protons to colliding fully stripped gold ions. The collision of 100 GeV/nucleon gold ions probes the conditions of the early universe by producing extreme conditions where quarks and gluons are predicted to form a new state of matter. Several runs of high luminosity gold-gold collisions as well as comparison runs using proton, deuteron and copper beams have demonstrated that indeed a new state of matter with extreme density is formed in the RHIC gold-gold collisions.
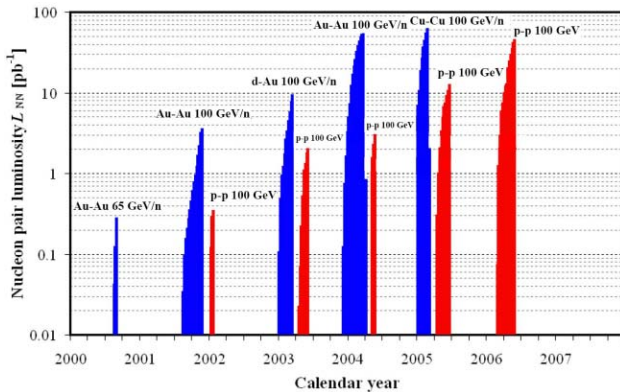
Figure 1: Integrated nucleon-pair luminosity for all the RHIC running modes since start of operation.

The RHIC polarized proton collider has opened up the completely unique physics opportunities of studying spin effects in hadronic reactions at high-luminosity high-energy proton-proton collisions. It allows the study of the spin structure of the proton, in particular the degree of polarization of the gluons and anti-quarks, and also verifica-
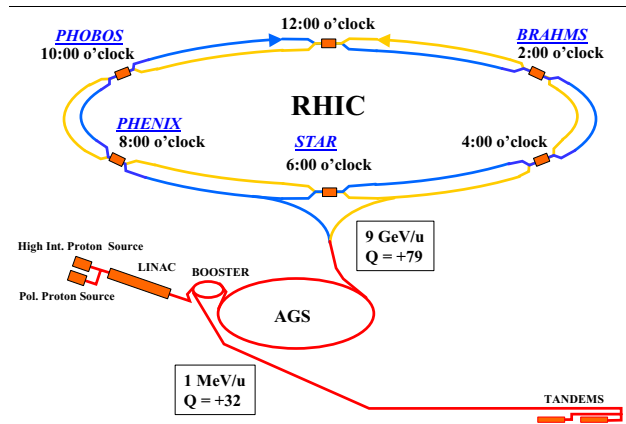
Figure 2: Layout of RHIC and the injector accelerators. The gold ions are stepwise ionized as they are accelerated to RHIC injection energy.

tion of the many well-documented expectations of spin effects in perturbative QCD and parity violation in W and Z production. The RHIC center-of-mass energy range of 200 to 500 GeV is ideal in the sense that it is high enough for perturbative QCD to be applicable and low enough so that the typical momentum fraction of the valence quarks is about 0.1 or larger. This guarantees significant levels of parton polarization.

During its first six years of operation RHIC has already exceeded the design parameters for gold-gold collisions, has successfully operated in an asymmetric mode of colliding deuteron on gold with both beams at the same energy per nucleon but, of course, different rigidities, and very successfully completed an additional comparison run of colliding copper beams with record luminosities. In addition, four very successful commissioning and running periods with polarized protons demonstrated the performance of RHIC as a high luminosity polarized collider. For the main part of all these runs RHIC was operating with beam energies of 100 GeV/nucleon - the gold beam design energy. Additional running at lower beam energy was also accomplished during these same running periods again demonstrating the high flexibility of RHIC. Fig. 1 shows, in semi-logarithmic scale the achieved integrated nucleon-pair luminosities for the many modes of operation of RHIC since its start of operation in 2000. Using nucleon-pair luminosity allows the comparison of the different modes properly reflecting the relative statistical relevance of the data samples and also the degree of difficulty in achieving high luminosity.

OPERATION FOR LHC CRYOMAGNET TESTS: CONCERNS, CHALLENGES & SUCCESSFUL COLLABORATION

V. Chohan , CERN, Geneva, Switzerland

Abstract

The LHC construction phase is coming to a close, with installation work progressing rapidly and beam start-up foreseen by end 2007. For the testing of the 1706 LHC cryomagnets in cryogenic conditions and its successful completion by early 2007, considerable challenges had to be overcome since 2002 to assure certain semi-routine tests operation at CERN. In particular, the majority of staff for tests and measurement purposes was provided by India on a rotating, one-year-stay basis, as part of the CERN-India Collaboration for LHC. This was complemented by some CERN accelerator Operation staff. While only 95 dipoles were tested till 2003, the efforts and innovative ideas coming from the Operation team contributed significantly to the completion of tests of nearly all 1706 magnets by end-2006. These included the improvements and management of the tests work flow as well as the test rates. Amongst these, certain pivotal ideas to stream-line the tests methodology as proposed and implemented successfully by the Indian Associates deserve a special mention. An insight into this as well an overall view of the tests operation will be given, together with an indication of some of the operation-related results from the tests programme.

INTRODUCTION

The Large Hadron Collider (LHC) consists of two interleaved synchrotron rings of 26.7 km circumference, to be installed in the tunnel used previously for the LEP machine [1]. Main elements of these rings are the two-in-one superconducting dipoles and quadrupoles operating in superfluid helium at a temperature of 1.9 K. Cryomagnets include 1232 dipoles (with correctors), 360 Short Straight Sections (SSS) integrated with quadrupoles and higher order poles which are needed for the different accelerator lattice functions and 114 Matching & Dispersion Suppressor region magnets integrated in Special SSS (IR-SSS).

Testing and qualification of the above magnets at cryogenic temperature is a prerequisite to their installation in the LHC tunnel. A superconducting magnet test facility equipped with 12 test benches and the necessary cryogenic infrastructure is operational at SM18 in CERN to perform the power tests and magnetic measurements for qualifying these magnets. Testing of the first series production magnets commenced in ~2001. Since early 2003, the test facility is being operated round the clock to meet the target to complete the testing of all the magnets required for the LHC by December 2006. The construction of all the 12 test benches was completed and the full usage started around June 2004.

The testing and qualification activities of a magnet is intended to verify its cryogenic, mechanical and electrical insulation integrity, qualify the performance of magnet protection systems, train the magnet up to the nominal field or higher so as to minimize training of magnets in the tunnel, characterize the intended magnetic field, accept the magnet based on its quench and training performance and generally, ensure that the magnet meets its design criteria. These may be categorized broadly within the five phases namely, to connect, cool down, cold tests, warm up and to disconnect respectively.

The workforce in the SM18 test facility consists of three teams, with the tests and measurement Operation Team as the major entity supported by the Cryogenics Team and the Magnet Connect/Disconnect Team (called ICS). The Operation Team consists mainly of associates from the Department of Atomic Energy (DAE), India, along with a number of regular CERN employees. The other two teams consist of contract employees from industrial consortia. A CERN team called Equipment Support looks after the improvements, exploitation and the troubleshooting of tests hardware and software on an on-call basis. A sub-team of ICS handles the movement of magnets within the test facility by means of a remotely controlled vehicle named ROCLA. All these teams work in mutual collaboration to complete the magnet tests within the specified time period.

In the massive effort of testing of all 1706 Cryomagnets in cryogenic conditions within a stringent time frame, considerable challenges had to be overcome since the beginning to arrive at successful completion. This paper presents a brief account of some of the major hurdles encountered in the process and the innovative strategies and techniques that were developed to overcome them. Relevant statistics are presented to highlight the effectiveness of some of these strategies.

CONCERNS & HURDLES

Like any facility of unique requirements, SM18 had also its own characteristic issues, ranging from personnel logistics to infrastructure limitations. Following is a brief account of some of the major issues and challenges that had to be addressed in the routine operation of the facility.

Personnel Logistics Issues: In early 2002, for technical and organizational reasons, the outsourcing of the tests operation was no more an option. Moreover, due to various factors, only 7 non-experienced CERN staff members from accelerator operation could be assigned to run the SM18 test facility. However, for an anticipated round the clock operation of the facility with 12 test benches, a minimum of 4 persons per shift was necessary, thereby demanding minimum staff strength of 24. It was

07 Accelerator Technology
T10 - Superconducting Magnets

MATERIAL SCIENCE CHALLENGES FOR ILC CAVITIES

G. Myneni, Jefferson Lab, Newport News, Virginia

Abstract

Fine grain high purity niobium has been the material of choice for SRF cavities during the past several decades. The current high RRR niobium material specifications will be reviewed from the historical context. The specification discussions include grain size, ductility, yield strength, thermal conductivity and residual resistance ratio. The effect of each of these material characteristic on the process and performance of the cavities will be explored. The recent progress on the single crystal - large grain niobium technology and its potential impact on the cost and performance of ILC cavities will be discussed. The possible relaxation of specifications, such as residual resistance ratio and Tantalum content will be presented from the perspective of reducing the ILC cavity fabrication costs with same performance levels. Further, a new QA step based on the measurement of critical magnetic field of niobium will be proposed.

PAPER NOT YET RECEIVED

COHERENT SYNCHROTRON RADIATION INSTABILITIES AND ITS EFFECTS ON ELECTRON BEAM QUALITIES

K.-J. Kim, ANL, Argonne, Illinois

Abstract

Coherent synchrotron radiation (CSR) can seriously affect performance of high-brightness, short pulse electron accelerators for high-performance light sources based on storage rings, energy recovery linacs, and x-ray free electron lasers. This paper is a review of the physical mechanism, its effects on electron beam qualities, and possible cures of CSR.

PAPER NOT YET RECEIVED

ION INSTABILITY ISSUE IN ELECTRON RINGS [*]

T.-Y. Lee[#], H. S. Kang, J. Choi

Pohang Accelerator Laboratory, San 31, Hyoja-dong, Pohang, Kyungbuk, 790-784 KOREA

Abstract

The fast beam-ion instability attracts interests recently for the International Linear Collider Project. In this paper, we will briefly review and discuss the instability in relation to the ILC project, and we will present a new observation of the instability in the PLS in-vacuum undulator, which shows that the vacuum pressure increase only in a small part of a ring can stimulate the instability.

INTRODUCTION

The so called fast beam-ion instability (FBII) was predicted by simulation and verified later by experiments. FBII is excited by attractive forces between electrons and ions created by passing electrons like other ion-induced instabilities. However, its unique point is that it is excited not by trapped ions but by transient ions; ions that are created by passing electron bunches and cleared by a large gap. Hence there is no periodicity but (approximate) linearity in the interacting ion density. Without trapped electrons, the number of ions that an electron bunch faces is proportional to the number of electrons that are ahead of the electron bunch. Therefore, the number of ions (and the strength of electron-ion interaction) is approximately linear with the position along the electron bunch train. Hence the amplitude of the coherent FBII oscillation grows along the electron bunch train. The difference from the ion trapping is clear. The electron-ion interaction depends also on the electron emittance, especially the vertical one.

The theoretical (and simulational) prediction and description of this picture was firstly given in Ref. [1, 2]. The first experimental observation of FBII was given in Advanced Light Source [3]. With artificially increased pressure and gaps in the bunch train large enough to avoid ion trapping, they observed a factor of 2-3 increase in the vertical beamsize along coherent beam oscillations which increased along the bunch train. Similar experiment was carried out later in Pohang Light Source (PLS) with more visual clarity [4, 5]. Especially, Ref. [5] captured the visual images of FBII with streak camera, which shows clearly the coherent oscillation increasing along the electron bunch train. Also, in the commissioning phase of Canadian Light Source when the vacumm pressure was very high, vertical beamsize blowup was observed, which could be attributed to FBII [6].

Interestingly and accidentally, the strength of FBII is such that it is hardly observed in a currently active electron storage ring of normal operation condition. A few years ago, the B-factory electron ring was considered a candidate for the FBII observation even in the normal operation condition, because of the high electron bunch current. However, FBII turned out to be invisible even in the B-factory. Recently, interests in FBII have been revived because of the future International Linear Collider (ILC) of electron and positron [7]. In ILC, electron beam (and positron beam) will have an extremely low vertical emittance. For that purpose, a damping ring will be constructed. The ILC electron damping ring is considered a strong candidate for the FBII observation, because of its tiny vertical emittance and high bunch current. In this paper, we will review and discuss FBII in relation to the ILC project, and we will present a new observation of FBII in the PLS in-vacuum undulator, which shows that the vacuum pressure increase only in a small part of a ring can stimulate FBII.

FAST BEAM-ION INSTABILITY

A schematic figure of FBII is shown in Fig. 1. The force that stimulates FBII is the attracting linear force between the electron bunch and the ion cloud [8]. The linear force on the n-th electron bunch has the following dependence

$$f_e(n) \propto \frac{\lambda_i(n)}{\sigma_y(\sigma_x + \sigma_y)}, \quad (1)$$

where $\lambda_i(n)$ is the ion density at the position of the n-th electron bunch and σ_x, σ_y are the horizontal and vertical sizes of the electron beam. On the other hand, the linear force on the ions f_i depends on the electron density λ_e instead of λ_i. Because of these linear forces, both electrons and ions oscillate coherently with separate oscillating frequencies. For example, the ion frequency has the dependence of

$$w_i \propto \left[\frac{N}{\sigma_y(\sigma_x + \sigma_y)A} \right]^{1/2}, \quad (2)$$

where N is the number of electrons in a bunch and A is the mass number of the ion. Normally A is that of CO ion.

Obviously λ_i depends on λ_e because ions are created by electrons. Note that $\lambda_i(n)$ is proportional to the vacuum pressure P and the number of electrons from the electron head to the n-th bunch, as described by

$$\lambda_i(n) \propto PNn, \quad (3)$$

where P is the vacuum pressure and N is the number of electrons per bunch. Hence we can rewrite $f_e(n)$ as

$$f_e(n) = K \frac{PNn}{\sigma_y(\sigma_x + \sigma_y)}, \quad (4)$$

ELECTRON CLOUD EXPERIMENTS, SIMULATION AND CURE*

H. Fukuma[#], KEK, Tsukuba, Japan

Abstract

This paper reviews experiments, simulations and mitigation methods of electron cloud effects. A concise review of electron cloud effects was recently given by K. C. Harkay at EPAC06 [1]. Inevitably, several topics in this report overlap with Ref. 1.

INTRODUCTION

Many electrons stay in accelerators. Primary electrons can be produced by synchrotron radiation, lost particles hitting a chamber wall, or by ionization of the residual gas. If the charge of a beam is positive, the primary electrons receive kicks from the beam toward the center of beam chamber and hit the opposite wall, then secondary electrons are produced. Under some operational conditions of machines rapid growth of the electrons known as beam induced multipacting (BIM) [2] can occur. The primary and secondary electrons form a group of the electrons called the electron cloud (EC) which is built up along a bunch train.

In proton rings with long bunches, a large number of electrons are observed at the tail of the bunch due to a mechanism called "trailing edge multipacting" [3, 4]. Before the center of the bunch passes through the EC, all the electrons, i.e. electrons surviving electrons from the last bunch, electrons emitted at the chamber surface by the beam loss and electrons produced by ionization, are trapped in the bunch, and then released at its tail of the bunch. Electrons emitted at the chamber surface between the bunch centre and the tail are not trapped but hit the opposite surface due to the negative slope of the longitudinal beam density. Then amplification of the electrons can occur towards the tail. Trapped electrons and multipacting electrons together result in the large number electrons at the tail.

The EC causes harmful effects on the accelerator performance as discussed below.

OBSERVATIONS AND EXPERIMENTS

Measurements of Electron Yield

A planar retarded field analyzer (RFA) pioneered at APS is widely used to measure the flux and energy distribution of electrons on the chamber wall [5]. Measurements showed that the energy of electrons hitting the wall is very low, typically less than 10 eV. BIM was observed at APS, where the electron yield abnormally increased at the bunch spacing of seven. The result is consistent with a simulation by POSINST [6].

Time resolved measurement by an RFA at PSR showed

numerous electrons generated at the tail of the bunch. The measurement led to the discovery of the trailing edge multipacting [3]. The full number of electrons in the beam chamber was measured by an electron sweeper originally designed at PSR. It consists of an RFA and a pulsed electrode which sweeps electrons into the RFA. A large number of electrons, which is approximately equal to that needed to cause the e-p instability, were found in the bunch gap. The long exponential tail of the decay of the electron yield in the gap implies a relatively high secondary emission yield from low energy electrons of 2-5 eV.

Pressure Rise

Electrons hitting the chamber wall desorb molecules on the wall, thereby causing a pressure rise. The pressure increases non-linearly with the beam current if the BIM occurs. In RHIC the number of bunches of the ion beam is limited to about half of the possible number by dynamic pressure rises caused by the EC [7]. The molecular desorption coefficients (MDC) were studied at RHIC [8]. For unbaked stainless steel and assuming CO, the MDC was 0.05. A conditioning effect on the MDC by the beam was observed.

Emission of Secondary Electrons

One of the most important parameters in EC formation is the secondary emission yield (SEY). The secondary electrons are classified into three categories according to their energy spectrum: true secondary electrons, elastically backscattered electrons and rediffused electrons [9]. The SEY as a function of the primary electron energy has a peak δ_{max}, typically 1.5 - 2, around 200-300 eV. As the secondary emission is a surface dependent phenomenon, the SEY depends on the material and is influenced by the surface preparation [10, 11].

A decrease in δ_{max} by electron bombardment is called scrubbing. Scrubbing has been observed in several laboratory measurements [11, 12] and also in-situ at the CERN SPS [13]. After an electron bombardment of $1mC/mm^2$, δ_{max} decreased from 1.5 to 1.1 for TiN and from 1.4 to 1.2 for TiZrV [12]. An electron dose of $1mC/mm^2$ seems necessary for δ_{max} to decrease below 1.2. A possible mechanism of the scrubbing called graphitization was found by a laboratory measurement at KEK [14]. As-received copper was irradiated by an electron beam of 5 keV. After the irradiation of electrons (total dose of 1×10^{20} e-/cm^2), δ_{max} was reduced from 1.85 to 1.02. It was found that a contaminated layer of carbon was changed to graphite which has a low δ_{max}. A further in-situ measurement of the SEY is underway in the KEKB.

ILC DR ALTERNATIVE LATTICE DESIGN[**]

Y. P. Sun[*], Key Laboratory of Heavy Ion Physics, Peking University& IHEP, Beijing
J. Gao, IHEP, Beijing; Z. Y. Guo, Key Laboratory of Heavy Ion Physics, Peking University, Beijing

Abstract

The International Linear Collider (ILC) which is based on super-conducting RF acceleration technology requires the damping rings to provide beams with extremely small equilibrium emittances, and large acceptance to ensure good injection efficiency for high emittance, high energy spread beam from the positron source. In order to reduce the cost for ILC damping rings, an alternative lattice which is different from the baseline configuration design has been designed with modified FODO arc cells , and the total quadrupole number has been reduced by half. At the same time, to decrease the total cost involved in constructing access shafts needed to supply power, cryogenics etc. for the wigglers and other systems, the number of wiggler sections is decreased from 8 to 4, and further to 2. This new lattice has been optimised to have a good dynamic aperture. This alternative ILC damping ring lattice design will reduce the cost largely compared with the baseline design.

INTRODUCTION

The International Linear Collider (ILC) damping rings should provide beams with very low natural emittances for the linear collider to reach the required luminosity, and at the same time, the damping rings also need to have a large acceptance to ensure good injection efficiency for high emittance, high energy spread beam from the positron source [1]. Another main design criteria for the damping ring comes from the requirement of providing a long beam pulse of 1 ms containing 2820 bunches (normal parameter set [2]), corresponding to an approximately 300 km long bunch train. To keep the damping ring's circumference reasonable, the bunch train has to be stored in a compressed mode with much smaller bunch spacing than in the linacs. Consequently, each bunch has to be individually injected and ejected. The ring circumference is then determined both by pulse width of the injection and extraction kicker system and electron-cloud (ion) effects. Based on the studies of the various configuration options, the ILC damping ring Baseline Configuration Design (BCD) decides that the positron damping ring should consist of two (roughly circular) rings of approximately 6 km circumference in a single tunnel and the electron damping ring should consist of a single 6 km ring, assuming that the fill pattern allows a sufficient gap for clearing ions [2, 3].

In the ILC damping ring baseline design, a lattice which has a circumference of approximately 6 km using TME arc cells has been used [4]. In this paper, with the aim to reduce the cost of the damping rings, a new lattice with modified FODO arc cells is designed

to be an alternative of the baseline design [5]. To decrease the total cost involved in constructing access shafts needed to supply power, cryogenics etc. for the wigglers and other systems, the number of wiggler sections is decreased from 8 to 4, and further to 2.

LINEAR LATTICE DESIGN

There are 120 arc cells in all for a 6 km damping ring, therefore each arc cell provides a bending angle of $\pi/60$ for the beam. The FODO arc cell length is selected as 38.9 m and the phase advance per arc cell is 90º/90º for the horizontal and vertical betatron motion, respectively. According to Equation 1, the maximum and the minimum value of the beta functions of the FODO arc cell is 66.2 m and 11.4 m, respectively. From Equation 2, the maximum and the minimum horizontal dispersion function is 1.37 m and 1.02 m respectively, which are too large to get a reasonable bunch length of 6 mm.

$$\beta^{\pm} = \frac{L_P(1 \pm \sin\frac{\mu}{2})}{\sin\mu} \tag{1}$$

$$D^{\pm} = \frac{L_P\phi(1 \pm \frac{1}{2}\sin\frac{\mu}{2})}{4\sin^2\frac{\mu}{2}} \tag{2}$$

where β^+ and β are the maximum and minimum value of the beta functions, D^+ and D^- are the maximum and minimum value of the horizontal dispersion function, L_P is the length of the cell, μ is the phase advance of the cell, and φ is the bending angle in one arc cell, T_o have smaller RMS dispersion value, the length of the drifts that are between the quadrupoles is adjusted and the ultimate value of the two long drifts are 13.7 m and 1.55 m with the maximum and the RMS horizontal dispersion function being 1.15 m and 0.77 m, respectively. The lattice functions in an arc cell are shown in Figure. 1.
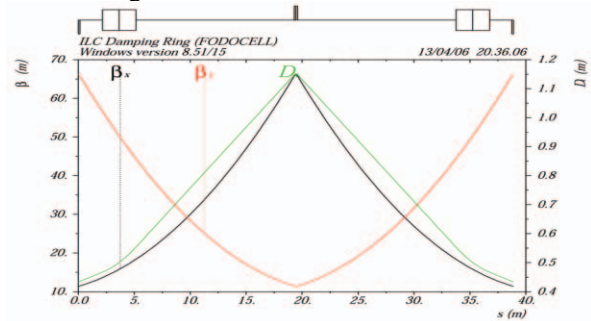
Figure 1: Lattice functions in an arc cell.

ULTIMATE ABILITIES OF CONVENTIONAL POSITRON SOURCES

P. Logachev, M. Avilov, M. Blinov, P. Martyshkin, T. Vsevolozhskaya, Budker INP, Novosibirsk, Russian Federation.

Abstract

Significant increasing of desired luminosity for future e+e- colliders leads to corresponding enlargement of positron production rate. Conventional technology of positron production has not reached yet its technical limits. Experimental study in order to find out these limits for basic subsystems of positron source is presented.

INTRODUCTION

With the advent of first linear accelerators in the middle of last century these machines were used for production and acceleration of positron beams. The first successful acceleration of positron beam was reported from Mark III accelerating system at Stanford [1]. Many linac based e$^+$ sources were built in subsequent years with significant improvements of beam intensity and quality. But the basic concept of these sources remained practically unchanged [2]. In this concept a high-energy electron beam from driving linear accelerator is focused on a thick target of high Z material, generating an electromagnetic shower in it. A part of shower positrons escapes from the target with a large spread in energy and angles. So only a small fraction of these positrons is guided by magnetic matching device into a following linear accelerator. The first part of this linac is immersed into longitudinal magnetic field of a long solenoid. This field provides transverse focusing for positrons with a large transverse momentum. Quadrupoles mounted on accelerating structure are used downstream of the long solenoid. These quadrupoles have alternating polarity for magnetic field gradient and form so-called FODO structure. A sketch of linac based positron source is shown in Fig. 1.

POSITRON PRODUCTION TARGET

For particular value of driving electron beam energy, an optimum length of positron production target exists [2]. This optimum length corresponds to the maximum of positrons density in the electromagnetic shower as it leaves the target. Space, energy and angle distributions of positrons after the target with an optimum length have a weak dependence upon the energy of primary electron beam within the range from 0.3 GeV up to 30 GeV [3]. This fact makes easier the analysis and comparison of positron sources with different energy of driving electron beam.

Thermal stability of positron production target under the heating energy deposition from the electromagnetic shower is the most important problem. Thermal damage of the target limits the intensity of driving electron beam and, hence, the intensity of secondary positron beam. This damage comes from the excess of mechanical stress limit for solid elements of target assembly.

Driving electron beam may consist of one or few intense and very short bunches usually called as a bunch train, or macro pulse. Driving electron linac produces these macro pulses with some repetition rate. In such a way, the particular time structure of the beam can be varied and depends on the particular application. But for most target designs and driving beam structures the working area for target subsystem can be defined in terms of two parameters. The first parameter is related to negative stress limit reached while the shock wave travels through the solid part of the target assembly (dynamic limit). Intense driving electron bunch or bunch train generates this wave. The second parameter corresponds to the maximum DC power density allowed for particular target design (static limit). Both parameters depends upon the power density in driving electron beam and, hence, upon the electron beam size on the target. However, the positron beam size at the exit of the target with optimum length is practically the same for any diameter of driving beam less than 1 mm. So the optimum driving electron beam transverse size on the target can be fixed at the level of 1 mm (FWHM).

The following time scales can be applied for different processes took place in a short electron bunch interaction with the target: energy deposit (up to 100 ps), time response for temperature (up to few ns) and stress (up to 300 ns). So 100 ns can be chosen as the maximum time duration for the bunch train, which generates shock waves with maximum efficiency. Finally, it is possible to define the first parameter as J=E*N/S, where E is driving electron beam energy in GeV, N is the maximum number of incident electrons in 100 ns time interval, S is the transverse cross section of driving electron beam (mm^2). The second parameter can be defined as DC power (kW) in driving electron beam with 1 mm transverse size on the target. These two parameters form 2-D plot (see Fig.2)
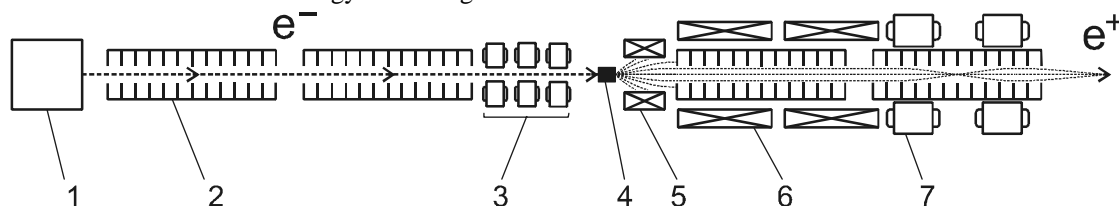
Figure 1: 1 — electron source, 2 — accelerating structure, 3 — focusing triplet, 4 — positron production target, 5 — magnetic matching device, 6 — solenoid, 7 — quadrupole lens.

OPTIMIZATION OF THE BEPCII LATTICE WITH FREQUENCY MAP ANALYSIS*

Y. Jiao[#], J.Q. Wang, D.M. Zhou, Q. Qin, G. Xu, S.X. Fang
Institute of High Energy Physics, Beijing 100049, China.

Abstract

The method of frequency map analysis (FMA) is used to analyze and optimize the lattice of the BEPCII storage ring. With the longitudinal oscillation and radiation being considered, both on- and off-momentum frequency maps are studied to have a complete picture of beam dynamics. The synchro-betatron resonances are found to be responsible for one limit of the dynamic aperture, and some efforts are made to reduce the effect of these resonances.

INTRODUCTION

BEPCII is the upgrade project of the Beijing Electron Positron Collider (BEPC) being built at IHEP. To enhance its luminosity, a double-ring design is adopted to house the micro-β scheme and multi-bunch collision. For the colliding beams the design luminosity is 1×10^{33}cm^{-2}s^{-1} optimized at beam energy of 1.89 GeV, which is about two orders higher than that of the BEPC [1]. According to the beam-beam simulations with Cai's code [2] and Zhang's code [3], the working point is chose to be close to the half integer resonance, which thus calls for elaborate analysis and optimization of the beam dynamics.

Frequency map analysis (FMA) is a very useful tool to study the single particle dynamics by constructing a one-to-one relationship between the space of initial conditions (x, y, $x' = y' =0$) and the tune space (Q_x, Q_y) [4]. With this method, we can obtain the dynamic aperture (DA) and the corresponding frequency map (FM) at the same time, and study the effects and features of only one resonance out of others. This method has been used among many light sources (ALS, NSLS, SPEAR3, SOLEIL, ESRF, SSRF, etc) [5-10] and other machines (LHC, SNS) [11, 12]. It is the first time that we systematically apply the FMA to the lattice of the BEPCII storage ring.

The paper is organized as follows. In Sec. 2, we present the FMA results of BEPCII lattices and study the effect of synchro-betatron resonances on the single beam dynamics in detail. Several ways to the optimize the lattices are discussed in Sec. 3. We summarize and conclude our work in Sec. 4.

FMA ON THE BEPCII LATTICES

BEPCII collision mode

The BEPCII lattice loses the 4-fold symmetry of the BEPC, due to the double-ring geometric structure [1]. The vertical beta function at the IP is squeezed by a pair of

defocusing superconducting quadrupoles. The dispersion functions are free at the IP, the RF region (outer ring) and the injection point. The beta functions are required to be less than 15 m at the RF cavities in both vertical and horizontal planes and largger than 20 m at the injection point in horizontal plane to save the kicker strength.

A recently designed collision mode lattice [13] with the working point of (6.51, 5.58) is put into analysis using FMA. Table 1 gives the main parameters of the collision mode and the injection mode which will be referred in the following text.

Table 1: Main parameters of the BEPCII lattices

Parameter	Unit	Collision mode	Injection mode
Beam energy	GeV	1.89	1.89
Circumference	m	237.53	237.53
RF voltage	MV	1.5	1.5
$Q_x/Q_y/Q_s$		6.51/5.58/ 0.034	6.58/5.62/ 0.034
Natural chromatity		−10.7/−21.0	−10.5/−12.1
Horizontal natural emittance	nm· rad	141	135
β_x^* / β_y^* (IP)	m	1/0.015	2.8/0.04

For the horizontal working point is much close to the half integer resonance, the nonlinear optimization of the lattice with 4 families of sextupoles by MAD [14], is not perfect. As shown in Fig 1, the average off-momentum DAs with errors (20 random seeds) from SAD [15] are only slightly largger than the required aperture for collision which is $10\sigma_x \times 10\sigma_y$ and labeled as the solid square, but smaller than the requirements for injection, i.e., $13.5\sigma_x \times 10\sigma_y$, the dashed square. The minimum DAs with errors (among 20 random seeds) for different momentum deviations are even smaller (for more details, refer to [13]).
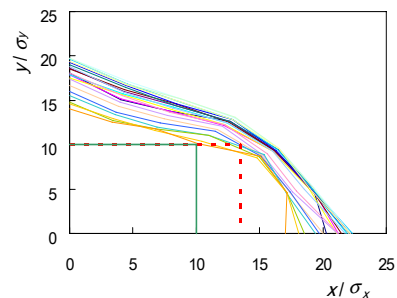
Figure 1: The average DAs with $\Delta p/p \in$ (−10σ_e, 10σ_e) from SAD, with multipolar magnetic errors[13].

For FMA analysis, tracking is done with AT [16]. Starting from the RF cavity, the particles with different

05 Beam Dynamics and Electromagnetic Fields
D02 - Non-linear Dynamics – Resonances, Tracking, Higher Order

NEW CONNECTION CRYOSTAT TO INSERT FP420 PROTON TAGGING DETECTOR IN THE LHC RING

S. Pattalwar CCLRC, Daresbury, UK

T. Colombet, S. Marque, T. Renaglia, D. Swoboda CERN, Geneva, Switzerland

B. Cox, K. Potter, F. Roncarolo Cockcroft Institute and University of Manchester, UK

D. Dattola, INFN, Torino, Italy

Abstract

FP420 is a R&D project to assess the feasibility of installing proton tagging detectors in the region 420m from the interaction points at the LHC. They would function as new sub-detectors at ATLAS/CMS, allowing the measurement of the spatial position and arrival time of outgoing protons emerging intact from the collision. Forward proton tagging in this region is expected to open a new programme of electroweak, QCD and BSM physics.

At present the 420m region is enclosed in a 'connection cryostat' (maintained at 1.9K) that provides continuity for the LHC beam, cryogenic & vacuum services and electrical power circuits through superconducting bus bars. The requirement of near room temperature operation and critical position control close to the beam pipes has made inserting FP420 detectors in this region a very complex task. The currently favoured design calls for the replacement of the connection cryostats with a new ~14m long assembly that will have all the necessary features of the existing connections cryostat as well as the appropriate environment for the operation of the detectors. This paper mainly describes the cryogenic aspects of the new connection cryostat.

INTRODUCTION

The FP420 R&D project [1] is an international collaboration with members from 29 institutes from 10 countries. The aim is to assess the feasibility of installing **F**orward **P**roton Tagging Detectors at **420m** from the interaction points (IP) of the ATLAS and / or CMS experiments at the LHC. The physics potential of forward proton tagging in the 420m region at the LHC has only been fully appreciated within the last few years. By detecting protons that have lost less than 1% of their longitudinal momentum, a rich QCD, electroweak, Higgs and BSM program becomes accessible, with the potential to make measurements which are unique at LHC, and difficult even at a future linear collider.

The drift spaces around 420m from the ATLAS and CMS interaction points are at present enclosed in a 14 m long interconnection cryostat [2] that connects the superconducting arcs and dispersion suppressor regions of the LHC. The cryostat provides continuity not only of the beam pipes held cold at 2K, but also of the isolation vacuum, electrical power, cryogenic circuits and thermal shielding. One of the key challenges for the FP420 experiment is to design a new 14 m section to replace the interconnection cryostat which will allow access to warm

beam pipes. In this paper we describe the design concepts of the proposed new connection cryostat.

EXPERIMENTAL REQUIREMENTS

The main requirements of the FP420 experiment are:

- The FP420 detector must be able to reconstruct the tracks of the outgoing protons a few mm away from the beam.
- Silicon pixel detectors [3] must be moved into a position as close to the beam as possible when stable beam conditions are reached.
- Geometry and the materials used for the modified beam pipe must not affect the normal running of the LHC.
- The new design of the cryostat with the detector assembly must ensure the continuity of the existing LHC services as well meet all the necessary criteria for cryogenic performance [4], alignment, transport and commissioning.
- The Si-detectors operate near room temperature whereas the beam pipes are maintained at 1.8K in the current design of the connection cryostat. **Providing a warm access to the beam pipe is a key challenge in designing a new cryostat.**
- The commissioning of the FP420 detectors is being planned during the LHC shutdown in January 2009. Transport, installation, decommissioning & commissioning of the cryostat including the integration of the complete FP420 detector with LHC during the beam shutdown period will be extremely critical.

THE NEW CONNECTION CRYOSTAT

Figure 1 shows the cold mass in the present design of the connection cryostat. Figure 2 shows its cross section. The three bus bars M1, M2 and M3, the two beam pipes V1 and V2 and the heat exchanger line X are all enclosed in a cold mass maintained at 1.9K. Table 1 shows the configurations of the lines in the cryostat

Figure 1: Cold Mass inside the Connection Cryostat.

SIMULATION STUDY ON BUNCH LENGTHENING

Y. P. Sun[#], Key Laboratory of Heavy Ion Physics, Peking University& IHEP, Beijing
J. Gao, IHEP, Beijing; Z. Y. Guo, Key Laboratory of Heavy Ion Physics, Peking University, Beijing

Abstract

The bunch lengthening phenomenon is resulted from one of the most severe single bunch instabilities in electron storage rings. As for BEPCII, controlling the bunch length is the most critical task to fulfil the designed luminosity goal. A new code is developed to calculate the single bunch length and energy spread in storage rings using FORTRAN. In this code, the wake field is calculated using an analytical formula. The bunch length and energy spread under different bunch current are calculated for BEPCII. The tracking results clearly show that the microwave instability threshold is around 65 mA for BEPCII storage ring. The tracking results of this code are in good accordance with those from other codes.

INTRODUCTION

The bunch lengthening phenomenon is resulted from one of the most severe single bunch instabilities in electron storage rings. It is well known that in an electron storage ring an electron will lose energy due to synchrotron radiations. Since this radiation is compensated by the RF cavities in the ring there exists a damping effect on the synchrotron oscillation with the corresponding damping time. The synchrotron radiation energy loss is in the form of randomly emitted photons, and this random quantum excitations together with the previously mentioned synchrotron radiation damping effects result in the single particle equilibrium energy spread and bunch length. The distribution in the normalized time displacement is as a Gaussian with a standard deviation that is equal to the standard deviation of the energy oscillations [1]. It follows that the fluctuating energy oscillations are accompanied by associated fluctuations in the time displacement. And the standard deviation of these fluctuations can be deduced to be (zero current case):

$$\sigma_{l0} = \frac{\alpha_P \overline{R} \sigma_{\varepsilon 0}}{\nu_s} \qquad (1)$$

where σ_{l0} is the natural bunch length, α_P is the momentum compaction factor, $\sigma_{\varepsilon 0}$ is the natural energy spread and ν_s is the synchrotron tune.

The bunch length is equal to its natural values when the bunch current is low. However, when the bunch current is higher, the bunch length and energy spread increase due to collective effects.

Numerically there are normally three kind of approach to calculate the longitudinal stability of the beam: solving of linearized Vlasov integral equation in frequency domain which has a lot of neutrally stable spurious modes [2]; solving full Vlasov-Fokker-Planck equation in time

domain which is slow but accurate [3]; particle tracking with wake fields which is fast but may be noisy [4]. For the macro-particle tracking approach with wake fields, longitudinal single bunch effect is simulated in electron storage rings to study the single bunch lengthening and energy spread. The turn by turn energy and phase deviations of N macro-particles are tracked. The input parameters consist of the usual RF and lattice associated parameters as well as the wake potential. Most of the other codes use the wake potential from the measured or calculated impedance values, but in this code an analytical wake potential is used.

STRUCTURE OF THE CODE

The phase space distribution of the bunch is represented by M randomly chosen test particles which are in Gaussian distribution in both longitudinal position and energy deviation. The turn by turn energy and phase deviations of M macro-particles are tracked as follows: [3]

$$t_m(n) = t_m(n-1) + \frac{\alpha_P T_0}{E_0} \varepsilon_m(n) \qquad (2)$$

$$\begin{aligned}
\varepsilon_m(n) = {} & \varepsilon_m(n-1) - \frac{2T_0}{\tau_\varepsilon} \varepsilon_m(n-1) \\
& - U_0\left(1 - \cos\left(\omega_{rf} t_m(n-1)\right)\right) - \hat{U} \sin\left(\omega_{rf} t_m(n-1)\right)\sin\phi_s \\
& + 2\sigma_{\varepsilon 0}\sqrt{\frac{T_0}{\tau_\varepsilon}} R_m(n) + eV_m(n)
\end{aligned} \qquad (3)$$

where m represents the mth test particle, n is the number of the turn, t and ε are the phase and energy deviations, T_0 is the revolutionary time, E_0 is the beam energy, τ_ε is the radiation damping time for energy oscillations, U_0 is the average synchrotron radiation energy loss per turn, $\hat{U}$ is the peak energy gain from RF cavity, ω_{rf} is the angular frequency of the RF cavity, Φ_S is the zero current synchronous phase angle, R_m is a Gaussian distributed random number with mean value equal to 0 and RMS value equal to 1, $\sigma_{\varepsilon 0}$ is the natural energy spread, and V_m is the wake field. In the above equations collective effects are contained in the term of wake field and the wake field gives the effect on particle m from all the particles which precede it in the bunch. Usually the bunch is separated into several bins every sigma. The spectrum of the bunch is gotten by Fourier transformation. Then the wake field is the reverse Fourier transformation of the product of impedance and the bunch spectrum.

The new contribution in this work is the treatment of the wake potential. An analytical expression that describes the wake potential of a storage ring is found to be effective on several storage rings in Ref. [5]. For the convenience of the theoretical treatment in Ref. [5], three

STUDY ON THE BEPCII LATTICE[*]

Y. P. Sun[#], Key Laboratory of Heavy Ion Physics, Peking University& IHEP, Beijing

J. Gao, IHEP, Beijing; Z. Y. Guo, Key Laboratory of Heavy Ion Physics, Peking University, Beijing

Abstract

BEPCII, the upgrading project of the Beijing Electron-Positron Collider (BEPC), has been designed with a luminosity of 10^{33} cm^{-2}s^{-1} at the τ-charm energy region. According to the beam-beam simulation results, the luminosity of BEPCII with a crossing collision angle of 11 mrad is about 0.50×10^{33} cm^{-2}s^{-1} with the original operation mode at the working point of 6.53/5.58. To increase the operating luminosity of the BEPCII, a low momentum compaction factor (α_P) collision mode has been studied which can increase the luminosity to 0.54×10^{33} cm^{-2}s^{-1}. If the bunch length of the low α_P mode is reduced from 1.5 cm to 1.2 cm, a mode with vertical beta function at IP equal to 1.2 cm could push the luminosity to 0.828×10^{33} cm^{-2}s^{-1} at the working points 6.53/5.56. Also, the BEPCII synchrotron radiation mode is optimized to get a larger dynamic aperture and much more stable tunes.

ON COLLISION LATTICE

BEPCII is an upgrading project of the Beijing Electron-Positron Collider (BEPC), where a new inner ring will be installed inside the old one. The double-ring geometric structure of the BEPCII makes each ring not to be a 4-fold symmetrical structure, though symmetry still exists between the electron and positron rings. Based on several design criteria, a geometric design which satisfies both collision and synchrotron radiation modes requirements is done [1].

From Eq. 1, one can calculate the head-on collison luminosity.

$$L(\text{cm}^{-2}\text{s}^{-1}) = 2.17 \times 10^{34}(1+R)\xi_y \frac{E(GeV)k_b I_b(\text{A})}{\beta_y^*(\text{cm})} \quad (1)$$

where $R = \sigma_y^*/\sigma_x^*$ is the beam aspect ratio at the interaction point (IP), ξ_y the vertical beam-beam parameter, E the beam energy, β_y^* the vertical envelope function at IP, k_b the bunch number in each beam and I_b the bunch current.

The beam-beam interaction simulation was carried out with several computer codes, which shows a luminosity reduction in different degrees compared with the designed luminosity. The results from one of the codes show that the luminosity of BEPCII with a crossing collision angle of 11 mrad is about 0.50×10^{33} cm^{-2}s^{-1} with the original operation mode at the working point of 6.53/5.58 [2]. To increase the luminosity of BEPCII, in this paper we will discuss how to adjust the lattice to reach high luminosity. First, the BEPCII lattice is adjusted to reduce the momentum compaction factor α_P while keeping the vertical beta function at 1.5 cm [3]. The corresponding luminosity can be increased to 0.54×10^{33} cm^{-2}s^{-1}.

The threshold of microwave instability can be estimated according to the Boussard or the Keil-schnell criteria [4]:

$$I_{th} = \frac{\sqrt{2\pi}\alpha_p \frac{E}{e}\sigma_{e0}^2 \sigma_{l0}}{R \mid \frac{Z}{n} \mid_{eff}} \quad (2)$$

For low alpha mode, α_P=0.0188, σ_{l0}=1.08 cm, other parameters are the same as in the original mode [1], it can be calculated from Eq. 2 that the threshold of microwave instability will be 34 mA which is much larger than the BEPCII designed single bunch current 9.8 mA.

Secondly, the quadrupoles in the ring are adjusted to give the vertical beta function equaling to 1.2 cm at IP, with the working point kept at 6.53/5.58 [5]. Finally, with the vertical beta function being 1.2 cm at IP, the working point is moved to 6.53/5.56. At the same time, maintaining a low horizontal emittance is very important for gaining a high luminosity.

In the following sections, the matching procedure for the lattice with α_P=0.0188 and β_y^*=1.2cm, the chromaticity correction, and the dynamic aperture tracking results are presented.

As the vertical beta function at IP should be decreased to 1.2 cm, the strength of the quadrupole in the mini-beta insertion should be increased. Here the K1 value of R3OQ1A is kept the same as the original value 1 and the K1 value of R3OQ1B is adjusted from 0.7232 to 0.73. The quadrupoles in region 3 and 4 are adjusted to satisfy other criteria. The quadrupoles in Region 1 and 2 is not changed. In that way the phase advance between kickers and the beta function at the RF cavity are not changed.

The TWISS parameters of the ring are shown in Figure. 1.
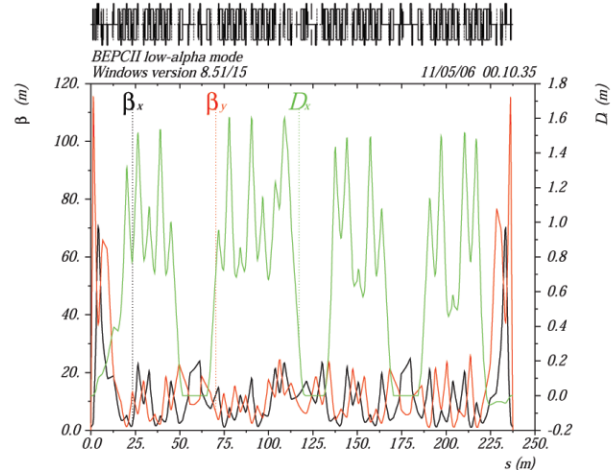
Figure 1: TWISS parameters of the BEPCII high luminosity collision mode

STATUS OF THE VEPP-4M ELECTRON-POSITRON COLLIDER

V. Petrov for the VEPP-4 team

Budker Institute of Nuclear Physics, Novosibirsk, Russia

Abstract

The VEPP-4M electron-positron collider is now operating for high-energy physics experiments in the 1.5-2.0 GeV energy range. The most important of them is precise measurement of the tau-lepton mass at the producing threshold. During all the high-energy physics experiments, absolute calibrations of beam energy by the resonant depolarization method and routine energy monitoring using the Compton back-scattering technique were realized. Monitoring of beam energy spread, which is also important, was implemented using several techniques. To provide the VEPP-4M high performance, some investigation and further development of the machine have been done, the most important results are described.

HIGH-ENERGY PHYSICS EXPERIMENTS

Since 2004, the VEPP-4M electron-positron collider [1] is operating for high-energy physics experiments in the 1.5-2.0 GeV energy range. The most important of them is precise measurement of the τ-lepton mass at the producing threshold. The τ-lepton mass together with the lifetime and the decay probability to $e\bar{\nu}_e\nu_\tau$ can be used to test the $\mu - \tau-$universality principle which is one of the postulates of the Standard Model, the most complete theory describing fundamental properties of matter and elementary particles.

Current situation in the world is as follows: the CLEO-c detector is now operating at the CESR collider with the luminosity of $6 \cdot 10^{31}$ cm^{-2}s^{-1}; the BES experiment is completed not long ago at the BEPC collider with the luminosity of $5 \cdot 10^{30}$ cm^{-2}s^{-1}, new BES-III detector and c-τ factory with the luminosity of 10^{33} cm^{-2}s^{-1} are now under construction.

In the 1.5-2.0 GeV energy range, peak luminosity of the VEPP-4M collider is $2 \cdot 10^{30}$ cm^{-2}s^{-1}. In spite of considerably lower luminosity, the VEPP-4M - KEDR facility have some advantages, the most principal of them are:

- wide energy range of 1.0 - 5.5 GeV in a beam;

- beam energy measurement with record high accuracy of 10^{-6} (2 keV) provided by the resonant depolarization method [2];

- routine monitoring of beam mean energy with the $5 \cdot 10^{-5}$ (100 keV) accuracy and beam energy spread with the 10% accuracy, using the Compton back-scattering method [3];

Fine adjustment of all the facilities included in the VEPP-4 accelerating-storage complex, in parallel with im-

Table 1: τ-lepton mass measurements

PDG 2006	$1776.90^{+0.29}_{-0.26}$ MeV
BES 1996	$1776.96^{+0.18}_{-0.21}\,{}^{+0.25}_{-0.17}\left({}^{+0.31}_{-0.27}\right)$ MeV
BELLE 2006	$1776.77 \pm 0.13 \pm 0.32(\pm 0.35)$ MeV
KEDR 2006	$1776.80^{+0.25}_{-0.23} \pm 0.15 \left({}^{+0.29}_{-0.27}\right)$ MeV

proving of the machine reliability, result in gradual increase of average luminosity, as it is shown in Figure 1. Total luminosity integral collected during the 2004-2006 τ-
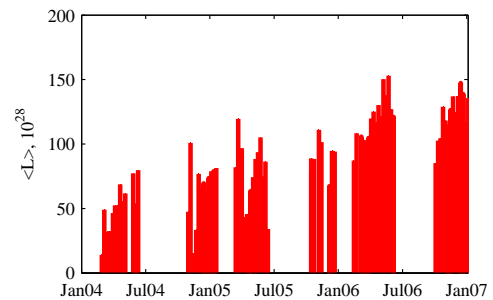
Figure 1: Average luminosity in 2004-2006.

lepton experiment is about 10 pb^{-1}. Preliminary results of the τ-lepton mass measurement at the VEPP-4 have been reported at the International Conference of High Energy Physics (ICHEP-2006) and international Tau-lepton Workshop (TAU-2006). Accuracy of this τ-lepton mass measurement is the best is the world and exceeds the accuracy reached at the BES and BELLE detectors, as it is shown in Table 1.

Along with the τ-lepton mass measurement, a series of experiments to improve measurement accuracy of the J/ψ, $\psi(2s)$ and $\psi(3770)$ mesons has been also performed. Measurement accuracy reached in these experiments is 2 times better than the world average value for $\psi(2s)$, and 3 times better for $\psi(3770)$. There are only 5 particle masses (e, p, n, μ, π) measured with better accuracy. Precise measurements of the J/ψ and $\psi(2s)$ meson masses provide the energy scale in the range around 3 GeV which is a basis for accurate determination of masses for all charmed particles. These measurements are also important for the accurate determination of the τ-lepton mass.

For the τ-lepton mass measurement, a procedure of regular particle energy calibration is essential. Absolute energy calibration is realized by the resonant depolarization method, between data collection runs of the KEDR detector. During the runs, routine energy monitoring is carried

01 Circular Colliders

A18 - Accelerators and Storage Rings, Other

MEASUREMENT OF BREMSSTRAHLUNG DEPENDENT ON STORED BEAM CURRENT

Y. Yamamoto

Ritsumeikan University SR Center, Kusatsu, Shiga, Japan

Abstract

Bremsstrahlung was measured as a function of stored beam current using the BGO scintillation spectrometer at the compact superconducting storage ring of Ritsumeikan University. Bremsstrahlung is emitted for collision of stored electrons and residual gas on the beam orbit. Yield of bremsstrahlung depend on stored beam current and residual gas density. We tried to determine gas density on the beam orbit by present measurement.

INTRODUCTION

The compact electron storage ring AURORA, manufactured by Sumitomo Heavy Industries [1], was installed at Ritsumeikan University in 1996 and has been operated successfully since then [2]. It is of the weak focusing type with the simplest lattice composed of a single body superconducting magnet, which produces an axially symmetric strong magnetic field to achieve compactness. The normal operating magnetic field is 3.8 T and the field index is 0.36 at ring energy of 575 MeV. The initial stored beam current is 300 mA in the orbit of 0.5 m in the radius. Table 1 lists the parameters of the injector and the ring. Figure 1 shows the storage ring and beamlines in the experimental hall.

The residual gas density on the beam orbit is very important parameter for storage rings. The pressure in the vacuum chambers is measured by using the vacuum gauge; the base pressure in the vacuum chamber of our storage ring is 1×10^{-8} Pa. On the other hand, the measurement of the pressure on the beam orbit in operation is difficult, because electron beam collide with the vacuum gauge.

We tried to measure bremsstrahlung which was emitted for collision of stored electrons and residual gas on the beam orbit. Yield of bremsstrahlung suggest the density of residual gas.

EXPERIMENTAL SETUP

The maximum energy of bremsstrahlung is 575 MeV to agree with the energy of the stored electron beam. Normal γ-ray survey meters can't measure such high energy bremsstrahlung. We employed BGO (bismuth germanate) scintillation spectrometer (CANBERRA) that could measure ~50 MeV X-ray. Measurement system which was composed by the detector, multichannel analyzer (ASA-100 CANBERRA) and PC was constructed behind

the beam extraction port BL-16 at the atmosphere.

Partial pressure in the vacuum chamber was measured by the partial pressure vacuum gauge (M-066QG, ANELVA) and electron beam size was measured by the SR interferometer [3] and the conventional profile monitor. Figure 2 shows schematically the structure of measurement system.

Table 1: Parameters of the injector and storage ring

Injector parameters	
Energy	150 MeV
Repetition	10 Hz
Peak current	1 mA
Pulse width	2 μs

Storage ring parameters	
Energy	575 MeV
Stored current	300 mA
Circumference	3.14 m
Radius of curvature	0.5 m
Field strength	3.8 T
RF frequency	190.86 MHz
Number of cavities	1
Harmonic number	2
Critical energy of radiation	844 eV
Vertical beam size(σ)	0.14 mm
Horizontal beam size(σ)	1.2 mm
Beam lifetime	300 min
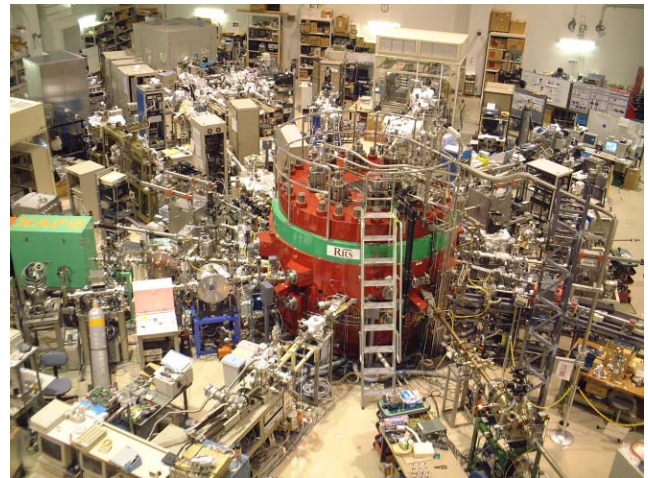
Figure 1: Photograph showing the storage ring and beamlines in the experimental hall.

STATE OF THE SLS MULTI BUNCH FEEDBACKS

M. Dehler[#], G. Marinkovic, R. Kramert, P. Pollet, T. Schilcher,
Paul Scherrer Institut, CH-5232 Villigen PSI, Switzerland

Abstract

In order to control coupled bunch oscillations in the SLS storage ring, feedback systems for all three planes were foreseen, which are realized as fully digital bunch by bunch systems. With the development of dedicated ADC and DAC boards, the feedbacks could be commissioned. Important parts of the computations for the transverse planes were implemented into the FPGA, making the DSPs originally planned to be used obsolete and allowing for an extremely low latency time of 300 ns. The systems give a larger freedom of choice for the beam optics and also lead to a better closure of the injection bump during top up mode. At present, systems for all planes have been commissioned and are in routine service.

INTRODUCTION

The Swiss Light Source (SLS) is a 2.4 GeV synchrotron light source at the Paul Scherrer Institut. As in other high current electron rings, coupled bunch instabilities can show up due to either resistive wakes and residual ions in the transverse case or due to higher order modes in the longitudinal plane.

Until now, transverse stability was obtained by a high chromaticity beam optics and by an inhomogeneous fill pattern in the ring. An additional contribution toward stable operation was obtained via Landau damping of a superconducting third harmonic cavity[1]. In order to have a higher flexibility in beam optics and a better performance in the longitudinal case, bunch by bunch feedback systems have been developed over the past years and commissioned in 2006. First, a technical overview of the systems is given, before preliminary results in operation are shown.

FEEDBACK SYSTEMS
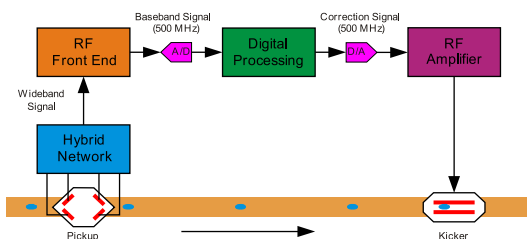
Figure 1: Functional blocks of a transverse bunch by bunch feedback system

[#]e-mail: Micha.Dehler@psi.ch

Energy	2.4 GeV
RF frequency	499.65 MHz
Harmonic number	480
Transverse	
Tunes β_x, β_y	0.43/0.73
Damping time	9.0 msec
Kicker shunt impedance	14.5/20.0 kΩ
Installed amplifier power	500 W
Filter	IIR/8 tap FIR
Longitudinal	
Synchrotron tune ν_s	$1.9 \cdot 10^{-3} - 4.8 \cdot 10^{-3}$
Damping time	15.0 msec
Kicker shunt impedance	1.5 kΩ
Installed amplifier power	250 W
Filter	IIR/16 tap FIR

Table 1: System parameters

The functional blocks of the system are shown in Figure 1. The feedback is a wide band system able to correct the positions of individual bunches, spaced 2 ns apart. Signals coming from button type pickups pass a passive hybrid network, where sum signals used for the longitudinal plane respectively difference signals for the transverse system are generated. The signals are fed into an RF front end [2] from Instrumentation Technologies mixing down the transverse signals and running a phase detection on the sum to obtain the longitudinal position. A digital system running at around 500 MS/s, consisting of an ADC, the digital filter and DAC creates the analog correction signal. Transversally, the signals are fed to the beam directly via broad band power amplifiers and strip line kickers. For the longitudinal plane, a single side band modulator mixes the signals up into the 1.25-1.5 GHz range, where they are amplified and fed to a longitudinal kicker. The analog parts have already been described in [3] and [4], hence we will concentrate on the description of the digital part.
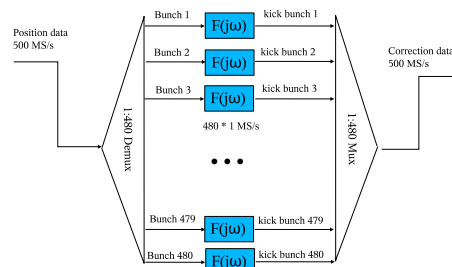
Figure 2: Data flux in the digital filter

02 Synchrotron Light Sources and FELs

A05 - Synchrotron Radiation Facilities

RADIATION SAFETY CONSIDEREATIONS OF THE OPERATION OF INDUS-1 SYNCHROTRON RADIATION SOURCE

G. Haridas, M.K. Nayak, Vipin Dev, Dimple Verma, K.K. Thakkar,
Health Physics Unit, Raja Ramanna Centre for Advanced Technology, Indore, India 452 013
P.K. Sarkar, D.N. Sharma
Radiation Safety Systems Division, Bhabha Atomic Research Centre, Mumbai 400085

Abstract

Radiological safety aspects of the operation of the electron storage ring, Indus-1 (450 MeV, 100 mA) is described in the paper. The ring is provided with a modular hybrid shielding comprising of mild steel and lead through which synchrotron radiation (SR) beam lines pass out. During the commissioning phase several radiation protection problems like streaming of high-energy bremsstrahlung x-rays through front ends of SR beam lines, shield joints, its detection and containment were encountered. Experimental measurements on the response of conventional radiation monitors with respect to water phantom were carried out to evaluate the dose build up factors in the streaming high-energy radiation field. The studies lead to the deduction of correction factors for the monitors for use in Indus-1. Improvement in monitor response on account of spectral degradation through shield and radiation levels during accidental beam loss are other problems, which are evaluated. Details of the radiation protection programme, radiation physics studies, the current status of radiation levels and access control are presented.

INTRODUCTION

Indus-1 is a 450 MeV electron storage ring [1] operated at Centre For Advanced Technology, India, giving rise to synchrotron radiation with a critical wavelength of $61A^0$ (202 eV). It has a circumference of 18.96 m with four bending dipole magnets from which synchrotron radiation is tapped through front ends and has five beam lines for different types of experiments like reflectivity, photoelectron spectroscopy etc. [2]. Bremsstrahlung x-ray photons form the major radiation hazard at intermediate energy electron storage rings like Indus-1. These photons have a continuous energy spectrum, whose maximum energy extends up to the energy of electrons in the ring. During commissioning of the storage ring, several radiation safety problems in regard to high-energy photons were encountered. For installation and commissioning of synchrotron radiation beam lines, modular hybrid shielding [3], comprising of lead and iron was installed, with a total thickness of 160 mm (80 mm lead + 80 mm iron). This modification has left shield joints and penetrations at some locations through which bremsstrahlung x-rays, produced as a result of interaction of electrons, with accelerator structures, mainly vacuum envelopes and residual gas molecules [4], streamed out to accessible areas. For proper monitoring of these high-energy photons no radiation monitors are commercially available. However, Victoreen survey meter, model 450 P (which is a pressurized ion chamber based survey meter) was used with water phantom to study its adequacy for radiation monitoring in such high-energy photon fields, experimentally. It was found that the dose rate builds up to certain thickness of water and reduces. From the measurements dose equivalent build up factor was found out. Build up factors were also calculated from Monte-Carlo calculations carried out using the code EGSnrc [5] and was found to be in good agreement with measurements. To see the spectral degradation of bremsstrahlung photons on account of radiation shield and adequacy of radiation monitors behind thick shields, photon spectrum measurements were carried out with a 50.8 mm X 50.8 mm BGO detector in the direct and transmitted photon field (through shield) from the storage ring. The transmitted spectrum showed spectral degradation and indicated good response by radiation monitors. Radiation levels around the storage ring during accidental beam loss due to different reasons like tripping of dipole, RF etc also were evaluated.

RADIATION MEASUREMENTS

Measurements of radiation dose with conventional instruments gave underestimation in streaming high energy photon field as dose was found to build up when measured with respect to different thickness of water phantom. The depth dose measured at two different locations (one at a front end in the accessible area and another near a bending magnet within the shielded enclosure) around Indus-1 is reproduced [6] in Fig 1. Monte Carlo calculations on the dose build up factors in water due to different incident bremsstrahlung photon spectra (obtained from semi-infinite copper slabs of different thickness on 450 MeV electron bombardment using EGS-4) gave comparable results with experimental values.

Fig 2 shows the average energy of the incident spectra and the respective the build up factors obtained in water when plotted as a function of the thickness of water where the maximum dose occurred (designated as shower maximum, X_{max}).

COMPUTATION OF WAKEFIELDS AND IMPEDANCES FOR THE PETRA III LONGITUDINAL FEEDBACK CAVITY

A.K. Bandyopadhyay [*], A. Joestingmeier, A.S. Omar ,
Otto-Von-Guericke University, Magdeburg, Germany.
K. Balewski, R. Wanzenberg, DESY, Hamburg, Germany.

Abstract

At DESY the existing PETRA II storage ring will be converted into a 3rd generation synchrotron radiation source, called PETRA III. The total beam current is limited by coupled bunch instabilities which are mainly driven by the parasitic modes of the RF cavities. It is planned to use longitudinal and transverse feedback systems to achieve the design current of 100 mA. Eight single cell feedback cavities will be installed into the PETRA III ring to damp the coupled bunch longitudinal phase oscillations. It is important to know the contribution of the feedback cavity to the impedance budget of PETRA III. In this article, the wake and impedance computation results, using the loss and kick parameters, will be reported. The computer codes MAFIA and Microwave Studio have been used to compute the electromagnetic fields.

INTRODUCTION

PETRA III

Beginning in mid 2007, the PETRA storage ring will be converted into a 3rd generation light source, PETRA III [1]. The planned facility aims for a very high brilliance of about 10^{21} photons /sec /0.1% BW /mm^2 /mrad^2 using a low emittance (1 nm rad) beam with an energy of 6 GeV and a total electron or positron design current of 100 mA. It is essential to use powerful feedback systems to prevent coupled bunch instabilities which are mainly driven by parasitic modes of the 500 MHz RF cavities. Eight single cell cavities will be installed to provide the required damping of $1/\tau = 800$ Hz. The cavity design has been adopted from the SLS [2] and DAFNE [3] overdamped feedback cavity designs. The cavities will be operated at a frequency of about 1375 MHz. The cavities are necessary to prevent longitudinal coupled bunch instabilities but are a potential source of higher order modes and wakefields which may cause beam instabilities. The impedance of the feedback cavities, investigated by numerical methods, are presented here.

Wakefields and potentials

The electromagnetic fields excited by a charged particle traversing any discontinuity in the beam pipe are called wakefields. The integrated effects of these fields over a given path length of a trailing charge gives rise to longitudinal and transverse wake potentials [4, 5]. The wake potential of a point charge q_1 is defined as:

$$\mathbf{W}^{\delta}(\mathbf{r}, s) = \frac{1}{q_1} \int [\mathbf{E}(r, z, t) + c_0 \mathbf{e}_z \times \mathbf{B}(r, z, t)]_{t=\frac{z+s}{c_0}} dz \tag{1}$$

where $\mathbf{E}$ and $\mathbf{B}$ are the electric and magnetic field excited by the charge q_1 at the longitudinal position $z = c_0 t$, $\mathbf{r}$ is the radial offset of the charge q_1 and the test charge, c_0 is the velocity of light in vacuum, s denotes the distance between the exciting charge and the test charge in the bunch coordinate system and $\mathbf{e}_z$ is the unit vector along the z-direction (Fig. 1). The wake potential $W(s)$ due to a charge distribution can be obtained as the convolution of the point charge wake potential with the line charge density. The loss parameter ($k_\parallel$), kick parameter ($k_\perp$) and the $k(1)$ parameters are defined according to the equations:

$$k_\parallel = \int_{-\infty}^{\infty} \lambda(s) W_\parallel(s) ds \tag{2}$$

$$k_\perp = \int_{-\infty}^{\infty} \lambda(s) W_\perp(s) ds \tag{3}$$

$$k(1) = \int_{-\infty}^{\infty} \frac{d\lambda(s)}{ds} W_\parallel(s) ds \tag{4}$$

where $\lambda(s)$ is the charge density and $W_\parallel(s)$ and $W_\perp(s)$ are the longitudinal and transverse wake potentials as functions of the bunch coordinate s. The loss parameter ($k_\parallel$) can be used to estimate the total energy loss of the beam, while the kick parameter ($k_\perp$) and $k(1)$ parameters are used to estimate the coherent tune shifts of the lowest order coupled bunch modes in the transverse and longitudinal planes.

The frequency domain description of the wakes are represented by the impedances, which are defined as the Fourier transforms of the wake potentials. The longitudinal
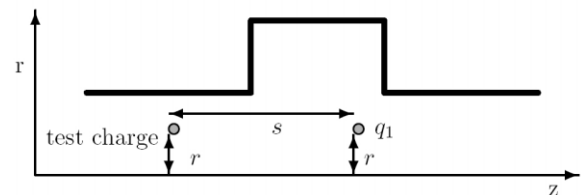
Figure 1: A charge q_1 and the test charge traversing a discontinuity in the beam pipe.

02 Synchrotron Light Sources and FELs
A05 - Synchrotron Radiation Facilities

COMPACT HARD X-RAY SYNCHROTRON RADIATION SOURCE WITH SUPERCONDUCTING BENDING MAGNETS

E.I. Antokhin, A.A. Gvozdev, G.N.Kulipanov, P.V. Logachev, N.A. Mezentsev, V.E.Panchenko, A.V. Philipchenko, Y.V. Rakshun, A.V. Utkin, N.A. Vinokurov, K.V. Zolotarev*,
Budker Institute of Nuclear Physics, 630090, Novosibirsk, Russia

Abstract

Synchrotron radiation (SR) with relatively hard spectrum (up to 50 keV) is necessary for realization many modern X-ray analytical methods. These methods can be effectively used in industrial and medical applications, in universities and scientific centers. So, the task of developing of compact source of hard synchrotron radiation is very perspective. Budker INP has a big experience for developing and fabrication of high field superconducting insertion devices for different SR centers. In frame of this activity a superconducting bending magnet with field up to 9.6 T was fabricated for BESSY-II and commissioned in 2004. This magnet also became a prototype for compact hard SR source. A project of such storage ring is under developing in Budker INP now. This design fixed beam energy to 1.2 GeV, ring circumference about 56 m. Estimated horizontal equilibrium emittance will better near 10 nm. This report includes a detailed description of main parameters and magnetic structure of designed storage ring as well as preliminary design of injector system and beamline layout.

INTRODUCTION

Development of compact and low-cost SR sources of hard (up to 50 keV) X-rays is an actual task for further application of the advanced X-ray methods in industry, medical centers, hospitals, small scientific centers and universities. Application of superconductive bending magnets allows solving this task with relatively small electron beam energies in a storage ring. Economically, a high cost of the magnetic system of such a storage ring can be compensated by cheaper injector, RF and protection systems and abrupt decrease of expenses for construction of the infrastructure of the complex. Low beam energy simplifies reduction of the emittance value and permits increasing spectral brightness of the source as compared with a high-energy storage ring with a magnetic system of a similar type.

The concept of compact SR source using superconducting magnets has been realized in different projects (AURORA, NIJI-3, SXLS, Helios, Super-ALIS etc.) (see [1, 2]) in the 1990s. However, these projects were aimed at generation of VUV and soft X-rays, which did not allow using such installations for research in the hard X-ray region.

In 1992 a prototype of superconducting bending magnet with a working field of 6 Tesla was fabricated and successfully tested at Budker INP. It was decided to organize manufacture of such bending magnets for future creation of compact SR sources consisting of superconducting and conventional bending magnets [3, 4]. Unfortunately, these projects were not realized because of serious problems in Russian economics at that time.

In 2001 a project for design and fabrication of a 9 Tesla superconductive bending magnet (Superbend) was started in the framework of collaboration between Budker INP and BESSY. In 2003 the Superbend was successfully tested and a field of 9.37 Tesla was obtained. After some work to minimize heat inleak in the cryostat and to reduce liquid helium consumption, the magnet was successfully commissioned at the BESSY site. The maximal field value of 9.6 T was achieved in 2004 during site acceptance testes at BESSY [5].

The successful commissioning of the superconducting bending magnet confirmed reliability of the BINP technology and allowed creation of a compact SR source of hard X-rays on the basis of such magnets. This project was started at Budker INP in 2006.

Besides, Siberian Synchrotron Radiation Center (SSRC) at Budker INP unites a lot of SR users from Siberian Branch of Russian Academy of Science and from other organizations. SSRC has good experience in organization of large user communities, and has the infrastructure required for research [6]. But the main problem of SSRC is the absence of a specialized SR source. This project can be considered as a way of noticeable up-grade of this center. Thus, development of such compact and bright SR source is really a very actual task.

POSSIBLE SCHEME OF COMPACT STORAGE RING

To show realizability of all the above-mentioned ideas, a scheme of such a system was suggested. Main parameters of the complex are sumarized in Table 1 and general view is presented in Figure 1. The ring perimeter is 56 m, and a 17×22 m hall can accommodate such storage ring. This variant allows organization of as many as 18 channels for hard spectrum SR extraction and of a rather large amount of channels for the soft X-radiation.

---

*Zolotarev@inp.nsk.su

BEAM BASED ALIGNMENT AND COD CORRECTION FOR THE SIAM PHOTON SOURCE

S. Rugmai[#], NSRC and Suranaree University of Technology, Nakhon Ratchasima, Thailand.
C. Kwankasem, P. Sudmuang, and P. Klysubun, NSRC, Nakhon Ratchasima, Thailand.

Abstract

The first systematic Beam based Alignment (BBA) and COD correction attempt for the Siam Photon Source (SPS) has been performed. Automated measurements were carried out using Matlab OPC Toolbox, interfacing to the accelerator control system. Calculations of theoretical parameters were performed with Accelerator Toolbox via Matlab interface. Since the Beam Position Monitors (BPMs) were not properly calibrated beam based calibrations were carried out. Preliminary calibration factors for each BPM were obtained by normalizing BPM signals to modelled corrector magnet responses. Measurements of offsets between BPM and quadrupole centers were performed by quadratic fitting for minima of orbit response to changes of quadrupole strengths. The resulting offsets were superimposed to the BPM readings. COD correction was then performed.

INTRODUCTION

The Siam Photon Source (SPS) has been in operation with currently three beamlines completed and opened for users. The machine performance has constantly been improved, including the recent energy upgrade from 1 to 1.2 GeV [1]. However, proper correction of the closed orbit has not been carried out. Many obstacles contribute to the difficulties for carrying out the COD correction. In the past, the machine control system lacked a good user interface system to enable fast and reliable beam measurements. This major obstacle has been solved by installation of Matlab OPC Toolbox to enable real time interface and programming via Matlab [2]. A project for proper COD correction and orbit stabilization has then been under way. Results of beam based BPM calibration, beam based alignment (BBA) measurements and COD correction are presented in this report.

BEAM BASED BPM CALIBRATION

The SPS contains 16 horizontal and 12 vertical corrector magnets, 28 quadrupole magnets and 20 BPMs. It is unfortunate that the BPMs of the SPS were not properly calibrated prior to installation. Dismantling the BPMs for recalibration at this stage is not a preferable option. It was therefore decided that a beam based calibration should be attempted. The calibration was carried out by calibrating the measured orbit responses to the theoretical values, i.e.

_____
[#]supagorn@nsrc.or.th

$$\Delta = \frac{\theta\sqrt{\beta_i\beta_j}}{2\sin\pi\nu}\cos\left(\left|\mu_i - \mu_j\right| - \nu\pi\right), \qquad (1)$$

where θ is the corrector kick angle, β the beta function, μ the phase advance, ν the betatron tune, and where the subscript i and j indicate the values at the BPM and the corrector positions, respectively. This calibration method therefore relies on the knowledge for corrector magnet characteristics and the theoretical model of the storage ring. The corrector magnets were accurately measured for the B-I slope and effective magnetic lengths [3]. The storage ring theoretical model was obtained by fitting the measured beta function and betatron tunes [4]. From the measured beta functions the four-fold symmetry of the ring is reasonably reproduced. For simplicity, the symmetry was therefore kept in the fitted model. The measured and fitted beta functions are shown in Figure 1. The model is used in Accelerator Toolbox [5] for calculations.
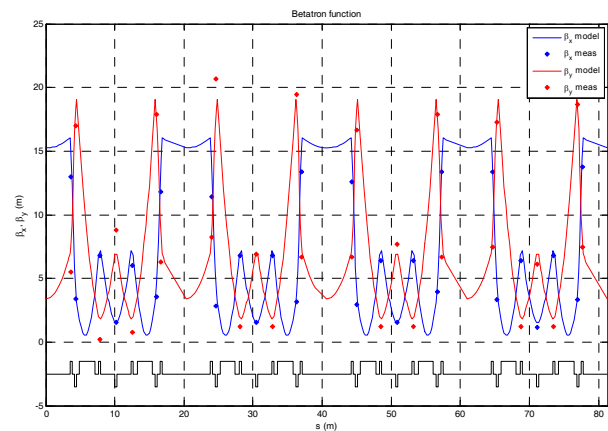
Figure 1: Measured and modelled beta functions

Even though this will contribute some errors to the calibration it is expected that the results should be good enough for preliminary COD correction. Moreover, it is hoped that this should at least give a reasonable working system to perform a more systematic refinement such as that using LOCO [6].

Automated measurements of the response matrix were carried out by varying corrector currents and measuring orbit responses. The calibration factors in the horizontal and vertical planes for each BPM were then calculated by averaging the ratios between the model and measured responses for all corrector magnets. The final calibration factors for horizontal and vertical planes were then obtained by averaging the factors obtained for all BPMs

CONSTRUCTION PROGRESS OF THE SSRF INJECTOR

D.M. Li, M.H. Zhao, H.H. Li, Z.Q. Shen, Z.T. Zhao
Shanghai Institute of Applied Physics, Shanghai 201800, P.R. China

Abstract

Shanghai Synchrotron Radiation Facility (SSRF) is a third generation synchrotron radiation source facility under construction. To meet full energy top-up injection requirements of 3.5GeV storage ring, the injector of SSRF was designed which consists of an 150 MeV linac, a two super-period 28 cells FODO type booster and two transport lines (LT and HT). The cycle rate of the booster is 1 or 2 Hz.

In this paper, the brief description of SSRF injector design, and the progress of construction of the linac, booster and transport lines are described.

INTRODUCTION

As a third generation synchrotron radiation source facility, the SSRF storage ring calls for a 3.5GeV full energy injector, a top-up injection is also demanded [1]. After the SSRF project was approved in 2004 [2], the SSRF injector was redesigned to satisfy these new demands, a new detailed scheme of SSRF injector was carried out [3]. In the finally scheme, the SSRF injector is comprised of a dedicated 150MeV linac, a two-fold 28 cells booster and two beam transport lines. The high reliable linac is used as the pre-injector to meet the requirements of the booster injection. Figure 1 shows the schematic layout of SSRF injector.

The injection cycle rate has been fixed to 2 Hz. With this cycle rate and single bunch of 1nC charge, the booster can smoothly perform normal injections and continuous top-up injections. To speed up the commissioning of storage ring, the multi-bunch mode of the injector is also included in the renewed design, which produces maximal 150 bunches occupying a total time of 300ns.
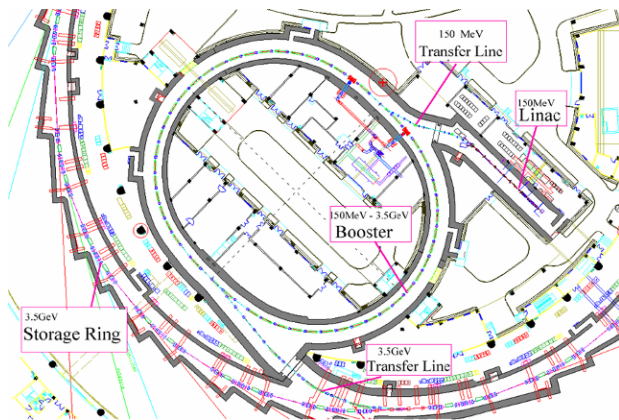
Figure 1: Schematic layout of SSRF injector

SSRF was started construction in the end of 2004. The beam commissioning will be completed in April, 2008 according to the schedule. The building construction has been basically finished. The linac installation was started in November, 2006, and the beam commissioning will be started in April, 2007. The Booster will start commissioning before October, 2007. Up to now, most of on-line installing components, power supplies, and instruments are under manufacture or purchasing for the SSRF booster and transport lines.

LINAC

The 150MeV linac is used as the pre-injector of 3.5GeV booster, which consists of four 3m long constant gradient accelerating sections and an injection section. A thermionic cathode electron gun, a 499.65MHz sub-harmonic buncher and a 2998MHz buncher, compose the linac injector section. The main beam parameters of the linac are listed in Table 1.

Table 1: The main parameters of linac

Nominal energy (MeV)	150
Repetition Rate (Hz)	1~5
Beam charge (nC)	
Single-bunch	1
Multi-bunch,	3~5
Pulse to pulse energy stability	0.25%
Relative energy spread	0.5% (rms)
Normalized Emittance (mm.mrad)	<100
Rf Frequency (MHz)	2998

The buncher and four accelerating structures are powered by two 45MW klystrons, each is driven by a 1kW solid-state amplifier. The pre-buncher is driven by a 500MHz r.f. amplifier.

Manufacture and test of all linac components have almost been finished. Mechanical and electrical installation are close to be completed. The beam commissioning will begin from April 2007. Figure 2 shows the progress of linac installation

BOOSTER AND TRANSPORT LINE

The SSRF booster performs as a synchrotron to accelerate the electrons from the linac energy of 150MeV to the storage ring energy of 3.5GeV. To achieve the emittance demands of top-up injection, the design of booster has been carefully optimized: 1) A reasonable low nature emittance and a relative large dynamic aperture. 2) Keeping bending magnet field strength at about 0.8T to limit the energy loss per turn and therefore cut down the scale and cost of RF system. 3) The booster is seated in an independent tunnel for the convenience in commissioning and maintenance.

PROJECT OF 2 GeV SYNCHROTRON LIGHT SOURCE FOR THE REPUBLIC OF KAZAKHSTAN

K. Kadyrzhanov, S. Lysukhin, INP, Almaty, Kazakhstan

E. Antokhin, K. Zolotarev, N. Mezentsev, G. Kulipanov, A. Philipchenko, V.Panchenko, A. Utkin

BINP, Novosibirsk, 630090, Russia.

Abstract

Applications of synchrotron radiation (SR) are very popular for last time in many research fields. Thus a developing of compact source for generation of hard X-ray synchrotron radiation is very actual task. The goal of this work is a developing project of SR source for Republic of Kazakhstan. This storage ring mainly dedicated for performing the high sensitive X-ray fluorescence analysis of different natural samples to be used for ore exploration, ore processing and metallurgy . But implementations of other popular techniques applied for research and education with using synchrotron radiation (XAFS, XRD, etc) are also possible. This report includes a detailed description of main parameters and magnetic structure of designed storage ring as well as preliminary design of injector system.

INTRODUCTION

The growth of Kazakhstan industry demands the developing modern methods of element analyses for ore exploration and processing. In order with traditional for XRF "light" elements Z<30 (Ti, Cr, Mn, Co, Ni, Cu, Zn) there is necessity to have express and precision methods of determination Nb, Mo, Pd, Ag, Cd, In, Sn (41<Z<50) and Hf, Ta, W, Re, Pt, Au, Th, U (Z>70), that requires hard X-ray radiation with the photon energy up to100 KeV.

To provide this requirement the electron beam working energy is planed to be 2 GeV and hard X-ray flux is possible due to using superconducting bending magnet with maximal field value up to 8.5 Tesla. Thus critical photon energy for chosen energy and magnetic field values is 20 keV, that enough for fluorescence analysis of U by studying L and K-series [1].

Horizontal equilibrium emittance should correspond to the modern synchrotron light sources of 3rd generation, but with circumference of moderate size, providing moderate capital and operation cost. Moreover the number of SR channels for XRF analysis and other synchrotron radiation techniques should be as large as possible.

LATTICE CHOICE

Based on above demands and considerations we chose the emmitance as about 10 nmrad as desired target and tried to find the appropriate lattice.

Background

The well-known formula for theoretical minimum emittance is as follows:

$$\varepsilon_x = \frac{C_q \gamma^2}{J_x} \frac{\oint \frac{\mathscr{H}(s)}{\rho^3(s)} ds}{\oint \frac{ds}{\rho^2(s)}} = \frac{C_q \gamma^2}{J_x} \frac{I_5}{I_2} = \frac{C_q \gamma^2}{J_x} A \quad (1)$$

where A is part concerning integration, C_q=3.84·10^{-13} m·rads, γ is relativistic factor, ρ is bending radius, θ is bending angle, J_x is damping coefficient.

Integrating over all dipole magnets within the cell and assuming that dipole field is isomagnetic (i.e. magnets have constant radius) one can rewrite A from (1) as [2]:

$$A = \frac{\sum_i \frac{\int_{L_i} \mathscr{H} ds}{\rho_i^3}}{\sum_j \frac{L_j}{\rho_j^2}} = \frac{\sum_i \frac{\int_{L_i} \mathscr{H} ds}{\rho_i^3}}{\sum_j \frac{\theta_j}{\rho_j}} \quad (2)$$

If for dipole magnets the values of optical functions satisfy the conditions for theoretical minimum emittance, then [3]:

$$\frac{\langle \mathscr{H} \rangle_{\min}}{\rho} = K\theta^3 \quad (3)$$

where $K = \frac{1}{12\sqrt{15}}$ for central magnet and $K = \frac{1}{4\sqrt{15}}$ for side magnet (dispersion matching cells).

Then equation (2) can be written as:

$$A = \frac{\sum_i \frac{\langle \mathscr{H} \rangle L_i}{\rho_i^3}}{\sum_j \theta_j / \rho_j} = \frac{\sum_i \frac{K_i \theta_i^4}{\rho_i}}{\sum_j \theta_j / \rho_j} = \frac{\sum_i K_i \theta_i^4 \langle B_i \rangle}{\sum_j \theta_j \langle B_j \rangle} \quad (4)$$

where $\langle B_i \rangle$ is mean magnetic field value over magnet of i-th type.

Equation (4) allows performing the estimation of theoretical minimum emittance for different lattice types, consisting of different dipole bend magnets.

Taking into account the necessary of using superconducting magnet for hard X-ray generation the appropriate lattice type seems TBA cell with superconducting bend magnet (superbend) as central magnet and 2 conventional "warm" dipole magnets as side magnets.

For TBA case with different central and side magnets formula (4) can be rewritten as:

A PROTOTYPE OF THE SSRF POWER SUPPLY CONTROL SYSTEM

J.G. Ding, H.J. Zhu, H. Zhao, L.R. Shen,
Shanghai Institute of Applied Physics, Shanghai 201800, P.R. China

Abstract

The Shanghai Synchrotron Radiation Facility (SSRF) is a third generation, 3.5GeV synchrotron light source currently being constructed at the Shanghai Institute of Applied Physics (SINAP) in Shanghai, China. There will be over 700 magnet power supplies (PS) in the Storage Ring, Booster, Linac and Transport Lines. According to the requirement of control precision, reliability and stability of the magnet power supplies, we decided to use PSI-designed digital PS control system [1][2][3] for PS control, that typical resolution reaches 1ppm and long term stability and reproducibility is better than 30ppm. Each PS has a local digital controller for a digital regulation loop and a optical point-to-point link to the VME level. The low-level EPICS [4] interface is identical for all power supplies. The VME-based front-end consists of a Single Board Computer (SBC), IP carriers and Industry Pack (IP) I/O modules. A prototype of the PS control system has been setup and tested at SINAP. Control and monitoring of the prototype has been implemented with EPICS. This paper describes the development of the prototype and the progress of the power supply control system and discusses our future plan.

OVERVIEW

The SSRF design requires a large number of magnet power supplies with a wide power range and a variety of different features. Power supplies should work with high performance of precision, stability and flexibility. The PSI (Paul Scherrer Institut, Switzerland) developed digital power supply control system was chosen as the front-end of the power supplies after investigating the control solution of the domestic and foreign labs.

The digital PS is a fully digital controlled, uniform solution for all magnet PS. It consists of two parts: a digital Power Supply Controller (PSC) and a VME 64x based system. The overall control system architecture is shown in figure 1.

One PS controller contains a pair of DSP controller card and an ADC card connected through a backplane. They executes digital regulation loop for PS. Each PS controller has two communication links to the outside. A RS232 link connects the PS controller with a Personal Computer for the local operations and system configuration. A point-to-point optical fiber link connects the PS controller with an IP module hosted on a VME carrier board for the remote control. Plastic Optic Fiber is used for the optical link. The optical communication is controlled by a FPGA on the both ends: on the DSP card and on the IP module. Each controller also has an

additional optical trigger input. The trigger input is used to start a programmable current waveform.
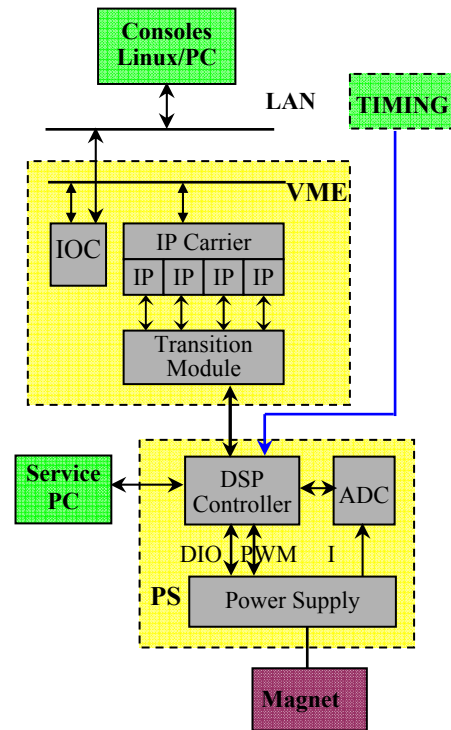
Figure 1: The PS control system architecture

The IP board is designed by PSI particularly for the solution. One IP module can serve two power supplies, each with one bidirectional 5MHz link. Four IP modules fit on an IP carrier VME card. Thus control density of eight PS per VME card can be reached. The throughput of each link reaches 10K float value frames per second.

The VME system is used as an EPICS Input/Output controller (IOC) to access the readable/writable registers of the PS controllers. IOC executes process control for power supplies by the EPICS runtime databases. The Linux/PC consoles run EPICS Channel Access (CA) clients to control/monitor the IOC execution.

SYSTEM SETUP

For SSRF project, our control platform is EPICS. The IOC for PS control is a VME 64x based system. Two kinds of SBC boards of PowerPC 74xx family have been evaluated to be used: Motorola 5500 and GE 7050. The IP carrier we use is SBS VIPC 664-ET. A Transition Module (TM) is used for the rear I/O of the carrier to connect the control system and the power supply and also executes optical/electrical signal conversion between them.

STATUS OF THE PHOTON FACTORY

S. Sakanaka, S. Asaoka, W. X. Cheng, K. Haga, K. Harada, T. Honda, M. Izawa, T. Kasuga,
Y. Kobayashi, H. Maezawa, A. Mishina, T. Mitsuhashi, T. Miyajima, H. Miyauchi, S. Nagahashi,
T. Nogami, T. Obina, C.O. Pak, H. Sasaki, Y. Sato, T. Shioya, M. Tadano, T. Takahashi, Y. Tanimoto,
K. Tsuchiya, T. Uchiyama, A. Ueda, K. Umemori, and S. Yamamoto
Institute of Materials Structure Science (IMSS), KEK, 1-1 Oho, Tsukuba, Ibaraki 305-0801, Japan
T. Ieiri, S. Isagawa, T. Kageyama, M. Kikuchi, K. Kudo, T. T. Nakamura, H. Nakanishi, K. Oide,
M. Ono, T. Ozaki, H. Sakai, Y. Sakamoto, S. Takasaki, M. Tejima, and S. Yoshimoto
Accelerator Laboratory, KEK, 1-1 Oho, Tsukuba, Ibaraki 305-0801, Japan

Abstract

The present status of two synchrotron light sources, the PF and the PF-AR storage rings at KEK, is presented. An upgrade project of the PF storage ring was successfully completed in 2005. Through this upgrade, four short-straight sections were newly created, and ten existing straight sections were extended. Two short-gap undulators were then installed in the new sections, and were commissioned. Further improvements, including a top-up operation, are in progress. The other PF-AR is a unique single-bunch hard X-ray source. During 2005-2006, two in-vacuum undulators were successfully commissioned.

INTRODUCTION

The High Energy Accelerator Research Organization (KEK) manages two synchrotron light sources [1], the Photon Factory (PF) storage ring and the Photon Factory Advanced Ring (PF-AR). The principal parameters of both rings are shown in Table 1. The 2.5-GeV PF storage ring was commissioned in 1982 as one of the major synchrotron radiation (SR) sources in the world, and it has been operated very well. The PF ring has been upgraded three times (see Table 2). Through the series of upgrades, the PF ring has become competitive [2] with other intermediate-energy third-generation light sources. We report in the next section the latest upgrade, the recommissioning, and the prospect for further improvements. The other 6.5-GeV PF-AR (see Table 3), initially named the TRISTAN Accumulator Ring, was commissioned in 1984 as a booster for the TRISTAN 30-GeV e^+e^- collider. It was converted to a dedicated SR source in 1998, and was largely upgraded in 2001. The third section describes recent improvements and operational status of the PF-AR

PF STORAGE RING

Upgrade

We carried out an upgrade project [3, 4] of the PF storage ring from March to September, 2005. This project aims at creating more space for advanced insertion devices. We refurbished the magnet lattice of about two-thirds of the ring as shown in Fig. 1. This upgrade resulted in creation of four short-straight sections of 1.4 m each, as well as extension of existing 10 straight sections.

Table 1: Principal parameters of the PF and the PF-AR storage rings.

	PF	PF-AR
Beam energy	2.5 GeV	6.5 GeV
Circumference	187 m	377 m
Natural emittance	35 nm·rad	293 nm·rad
RF frequency	500.1 MHz	508.6 MHz
Energy loss per turn	0.4 MeV	6.66 MeV
Injection energy	2.5 GeV	3 GeV
Typical number of bunches	280	1
Initial stored current	450 mA	60 mA
Beam lifetime (at initial cur.)	30-40 hrs	15-20 hrs
Number of insertion devices	9	6

Table 2: Brief history of the PF storage ring.

Year	Event
1982	Commissioned.
1986	Upgraded to lower emittance (460 → 130 nm·rad).
1997	Upgraded to lower emittance (130 → 36 nm·rad).
2005	Upgraded (extensions in straight sections) [3, 4].

Table 3: Brief history of the PF-AR.

Year	Event
1984	Commissioned as the TRISTAN injector.
1986	Parasitic SR usage started.
1998	Converted to a dedicated light source.
2001	Upgraded (beam current and lifetime) [5].

In these sections, we replaced quadrupole magnets to thinner ones, and moved them closer to bending magnets. We also renewed the beam ducts in these sections [6], and reconstructed thirteen beamline front-ends [7] so that we accommodated them both to the new lattice and to coming new IDs. We also reinforced septum magnets for injection, renewed our control system to an EPICS

DEVELOPMENT OF TRIGGER AND CLOCK DELAY MODULE WITH ULTRA-WIDE RANGE AND HIGH PRECISION *

T. Ohshima[#], Y. Fukuyama, J. Kim, JASRI/SPring-8, Hyogo, Japan,

Y. Tanaka, RIKEN SPring-8 Center, Hyogo, Japan,

E. Nonoshita, H. Sengoku, Candox Systems Inc., Saitama, Japan

Abstract

Pump and probe experiments using short pulse lasers and synchrotron radiations require precise timing relation between the laser pulse and the RF reference signal of the accelerator. The pulse laser needs clock signal for a mode-locked laser and trigger signal for a regenerative amplifier. The delay time of these two signals were usually adjusted by using a mechanical phase shifter or a cable delay. They have disadvantages of short tuning range or discontinuity in the clock signal. We developed a new delay system, which can continuously change the delay time with the range over 200 ns and the precision better than 3 ps. The key point of the system is combination of an IQ modulator and a synchronous counter. The IQ modulator can change the phase of the RF signal with infinite amount with high precision in ether positive or negative direction. The phase-modulated RF signal is fed to a frequency divider and its output is used for the clock signal of the mode-locked laser. The signal is also fed to the synchronous counter and its output is used for the trigger of the regenerative amplifier. The effectiveness of this system was confirmed by an experiment carried out at the SPring-8. Composition of the delay system, performance and its applications are described in the paper.

INTRODUCTION

The SPring-8 is one of the 3rd generation X-ray source facilities. One of outstanding features of the SPring-8 is its flexible time structure. The FWHM of the X-ray pulse width is about 40 ps. The interval of the pulses can be changed from 2 ns to 600 ns by using a various filling patterns. The interval can be increased of the order of millisecond by using a high-speed mechanical shutter (X-ray Pulse Selector: XPS). Using this feature, time resolved experiments, such as nuclear magnetic resonance, pump and probe experiments are carried out at the SPring-8. In the pump and probe experiments a time evolution of the excited state of material pumped by a laser light (or X-ray) is measured by probing X-ray (or laser light) by changing the irradiation timing of pumping light. In the experiments we need following signals:

a) Clock signal for a mode-locked laser whose frequency is 84.76 MHz, which is one-sixth of the RF reference frequency of 508.58MHz.

b) Trigger signal for a regenerative amplifier with, for

example, 949Hz repetition rate.

c) Trigger signal for a XPS with same repetition rate as b).

All these signals should be precisely synchronized to the timing of the X-ray. And the clock signal of a) should be continuous to avoid frequency jump of the mode-locked laser. Because the X-rays are generated from the electron bunches stored in the ring, and the timing of the electron bunches are determined by the acceleration RF system, the signals for the laser can be generated from the RF reference signal. Usually mechanical delay modules such as trombones or cable delays are used to change the clock timing. But they have disadvantages: the trombone has a short tuning range, and the cable delay has a discontinuity when the delay length is changed using RF switches.

To achieve the large delay range with high precision without discontinuity, we developed a new timing system. It consists from a phase delay with infinite tuning range and a synchronous counter. Detail of the composition of the system and its performance are shown below.
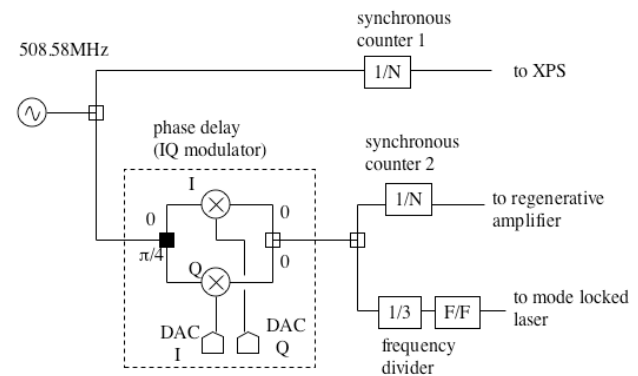
Fig. 1. Schematic diagram of the trigger and clock delay system.

COMPOSITION OF TRIGGER AND CLOCK DELAY SYSTEM

The trigger and clock delay system is composed by a phase delay and a synchronous counter. Fig. 1 shows the schematic view of the trigger and clock delay system. The 508.58MHz-RF reference signal is divided into two. One is fed to a synchronous counter No. 1 to generate a trigger signal for the XPS. The timing of the signal is adjusted to synchronize that of X-ray pulse. The other reference signal is fed to a phase shifter to make a delayed reference signal. The delayed signal is divided into two. One is fed

RADIATION SAFETY SYSTEM FOR INDUS ACCELERATOR COMPLEX

R.G.Marathe, D.S.Thakur, Vimal Bhatnagar, R.K.Gupta, K.K.Thakkar, P.Fatnani and Gurnam Singh,
Raja Ramanna Centre for Advanced Technology, Indore, INDIA

Abstract

Ionizing radiation emitted from the accelerators of Indus facility and similar facilities is a major occupational hazard. Therefore, a Radiation Safety System (RSS) is installed at Indus facility as a mandatory feature. The essential constituents of the RSS are: Shielding structure, erected as a part of the building, for protecting the personnel from ionizing radiation; Protection system for ensuring that nobody is inside the shielded area when the facility is in operation and detection and monitoring of the radiation levels inside & outside the shielded area. This paper deals mainly with the later two parts. The Protection and Monitoring systems were set-up in stages, first, for microtron and booster synchrotron, followed by that for Indus-1 ring. For Indus-2, it was commissioned in July 2005. These systems were then integrated and have been performing as intended. This paper presents the integrated radiation safety system of Indus Accelerator Complex with emphasis to the features of Indus-2 RSS.

INTRODUCTION

Indus Accelerator Complex is the first synchrotron radiation facility in India, located at Raja Ramanna Centre for Advanced Technology, Indore. It consists of a 450 MeV electron storage ring Indus–1 and 550-2500 MeV booster-cum-storage ring Indus-2. A common injector system that feeds these rings consists of a 20 MeV microtron & a 450-600 MeV booster synchrotron. All these accelerators produce intense ionizing radiation due to gradual or accidental loss of high-energy electrons in these machines. A Radiation Safety System (RSS) has been installed at this Complex to protect the personnel from this harmful radiation as a mandatory pre-requisite. Shielding structures made of thick concrete walls and roofs, form part of the Complex-building and enclose these four machines to contain the harmful radiation. The objectives of RSS are to:

- Prohibit any radiation producing activity in a shielded area till it is accessible;
- Prompt and ensure evacuation of shielded areas;
- Permit operation of accelerator / systems only after the respective area is searched and locked;
- Terminate the operation if trapping of a person is annunciated from a locked shielded area or access to such an area is attempted;
- Display the status of operation and access restrictions;
- Monitor, regulate and record the access of personnel to machine areas;
- Monitor, record and display radiation fields in the Complex and annunciate high radiation levels.

The RSS mainly consists of a hard-wired, relay-logic based Protection System and Ion-chamber-based Radiation Monitoring System to achieve these objectives.

DESCRIPTION OF RSS

The shielding structures around the machines mark the boundaries in reference to which we have set-up our RSS. The entire Complex has been divided into three zones as follows:

ZONE#1: Normal occupancy area, e.g. Foyer, offices, sitting rooms, labs – Without any monitoring of radiation field/ dose to personnel,

ZONE#2: Controlled / Restricted entry area, e.g. Experimental Areas, RF system areas, Magnet P/S areas. – With continuous monitoring of radiation field and dose to the personnel,

ZONE#3: Shielded Areas, inaccessible during operation / entry-restricted during shutdown, e.g. Microtron and Booster hall, Indus-1 hall, Indus-2 tunnel, Transport line tunnel – with continuous monitoring of radiation field & dose to personnel.

The main constituents of RSS are

- Protection System
- Radiation Monitoring System
- Access Control System
- Closed Circuit TV Surveillance System
- Moving Message Display System
- Public Address System

Protection System

This is a relay-based system and operates with 24 V dc supply. It has three parts, one for each of the three machine areas namely, Microtron & Booster, Indus-1 ring and Indus-2 ring. Each part is comprised of Search & Scram switches, door interlocks, flashing lamps, siren, key-interlocks and a central Safety Interlock Unit. Search switches are located around the machine in each of these areas. Search of each area is carried out while actuating these switches sequentially. Along with the search switches, scram switches are also provided which can be actuated to stop machine operation if needed. All access doors of these areas are fitted with limit switches interlocked with the search logic. Flashing lamps and siren are provided for audio-visual annunciation of access prohibition for machine areas. These field devices are connected to the Safety Interlock Unit of the respective machine area, which ensures that machine operation is allowed only when all the device interlocks are cleared. For Microtron and Booster ring area this system was commissioned in 1994 and for Indus-1, in 1999. These have been modified and improved since then. The system for Indus-2 is more spread-out and therefore more

OPERATION EXPERIENCE OF TOP-UP INJECTION AT TAIWAN LIGHT SOURCE

G.H. Luo, H.P. Chang, C.T. Chen, Jenny Chen, J.R. Chen, C.C. Kuo

Keng S. Liang, Y.C. Liu, R.J. Sheu and D.J. Wang

National Synchrotron Radiation Research Center, No. 101, Hsin-Ann Road, Hsinchu, Taiwan

Abstract

The storage ring of Taiwan Light Source (TLS) has one Superconducting (SC) cavity, one SC wavelength shifter, and two SC wigglers installed during last two years. The operation mode was also upgraded to have the capability of top-up injection. Top-up is an operation mode in which the beam current is maintained above certain level by frequent injections in the storage ring. The current stability maintains in the range of 10^{-3} for long period of operation. It provides constant thermal loading on all components in the storage ring and the optics components of beamlines, as well as constant signal to the beam position monitor. The top-up injection is a routine operation mode during user shifts at TLS. Statistics and operation experience with superconducting devices will be discussed in this paper.

INTRODUCTION

The Taiwan Light Source (TLS) was designed to provide 200 mA, 1.3 GeV electron beam to generate photon source for academic and industrial research scientists. The storage ring is a six-fold symmetry Triple-Bend-Archomat (TBA) lattice with six straight sections. Four of the straight sections are occupied by conventional normal-conducting insertion-devices, U9, U5, W20 and Elliptical Polarized Undulator EPU5.6.

The strong demanding of synchrotron light in x-ray regime made the beam physicists to reduce the engineering margin and pushing the beam energy to 1.5 GeV and squeeze the space at injection and RF sections to accommodate super-conducting high-field insertion devices. A 3-poles and 5.3 Tesla superconducting wavelength shifter was installed at downstream of the injection kicker #3 to provide high photon flux in x-ray regime. One 29-poles and 3.5 Tesla superconducting multipoles wiggler was installed at the RF straight section next to the Super-conducting RF (SRF) cavity to generate high flux x-ray.

It was also a strong demand to increase the photon flux and reduce the photon fluctuation due to the Higher-Order-Modes (HOM) excitation from Dories cavity. An SRF cavity was installed to replace two Doris cavities at the end of 2004. The SRF cavity was designed to be a HOM free cavity and had the capability to provide 8 MV/m accelerating gradient with power handling capability up to 200 kW. The SRF cavity extends large flexibility for tuning the cavity to optimise the operation parameters. Figure 1. shows the schematic layout and timeline of the TLS facility.
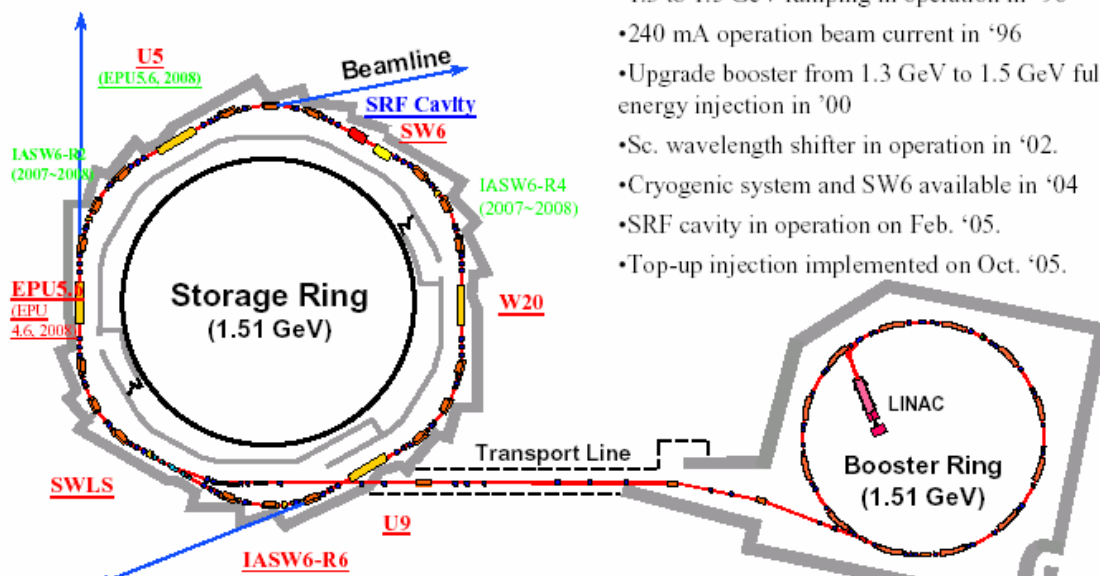
Figure 1. Schematic layout and timeline of the accelerator facility of Taiwan Light Source

SCSS PROTOTYPE ACCELERATOR TIMING SYSTEM

N. Hosoda, T. Ohata, T. Ohshima, JASRI/SPring-8, 1-1-1, Kouto, Sayo, Hyogo, 679-5198, Japan
H. Maesaka, Y. Otake, RIKEN/SPring-8, 1-1-1, Kouto, Sayo, Hyogo, 679-5148, Japan

Abstract

The 250 MeV SPring-8 Compact SASE-FEL Source (SCSS) prototype accelerator (SPA) was constructed. We observed the first amplification of light from the undulator at a 49 nm wavelength in June, 2006. We set our target time jitter of the system to be less than 1 ps. To achieve this, new timing devices, such as a master trigger unit (MTU), a master trigger distribution unit, a trigger delay unit (TDU), and a level converter unit, were developed. Reference clocks of 238 MHz and 5712 MHz RF are delivered to timing modules distributed along the accelerator. The MTU generates a master trigger synchronized both to the 60 Hz AC line and to the 238 MHz reference clock with a repetition rate of 1 Hz to 60 Hz. The TDU is an 8-ch 24-bit delay counter used to generate delayed signals from the master trigger for each component. The TDU uses 238 MHz RF as a counter clock and 5712 MHz RF to recover the time jitter. A measured jitter of 0.71 ps in standard deviation was achieved in the TDU. We measured the jitter between the arriving time of an electron beam to a monitor and a 5712 MHz RF; it was 0.34 ps. This demonstrates good stability of the timing system and the RF system of the SPA.

INTRODUCTION

The SPring-8 Compact SASE-FEL Source (SCSS) project is in progress. The 250 MeV SCSS prototype accelerator (SPA) was constructed to verify the feasibility of the source. The total length of the SPA is 60 m. We observed the first amplification of 49 nm light in June, 2006 [1].

The main acceleration radio frequency of the SPA is 5712 MHz (C-band). Three sub-harmonic frequencies of 238 MHz, 476 MHz, and 2856 MHz (S-band) are also used to compress the electron bunch length from 1ns to 1 ps before injecting to the main accelerator. All components around the facility of an electron gun, accelerator, insertion devices, and experimental apparatuses should be driven synchronously with the repetition rate from 1 Hz to 60 Hz using a 5712 MHz RF clock generated at a single source to obtain stable coherent light as the result of a stable electron beam. The distribution of stable 5712 MHz RF is one of the key technologies of the system [2]. We developed the timing system of the SPA, since the time jitter of the system was less than 1ps. This comes from a phase jitter of about 1 degree of 5712 MHz RF, which corresponds to a beam energy jitter requirement of 10^{-4} to generate and amplify 60 nm light at the SPA [3].

In this paper, we describe the timing system of the SPA.

TIMING SYSTEM

Overview

Figure 1 shows a schematic of the system. A newly developed master oscillator having a low noise characteristic generates a 5712 MHz RF. In addition, it generates a 238 MHz RF dividing the 5712 MHz RF. Ten W CW amplifiers amplify these RF signals to compensate for any cable loss in the distribution. Coaxial cables of HF-15D are used to distribute the RF signals in the SPA, because the maximum cable length is only 30 m. Its temperature coefficient is 5 ppm/K. We do not yet apply a dedicated feedback circuit to stabilize the electrical length of the cables, but no problem has occurred.

Trigger signals are needed for most equipment around the machine, for example, electron beam generation, single bunch formation, acceleration, and monitoring. To prepare the required timing triggers, we developed a trigger distribution system. A master trigger unit (MTU) generates a pulse signal, which is the master trigger of the whole operation sequence of the accelerator. Four trigger distribution units are used to distribute the master trigger. We adopted LVDS (low voltage differential signaling) for the signal transmission. Each trigger distribution unit is connected in series with 100 Ω twisted-pair cables to reduce the noise influence. Trigger delay units (TDU) receive the master trigger from the trigger distribution
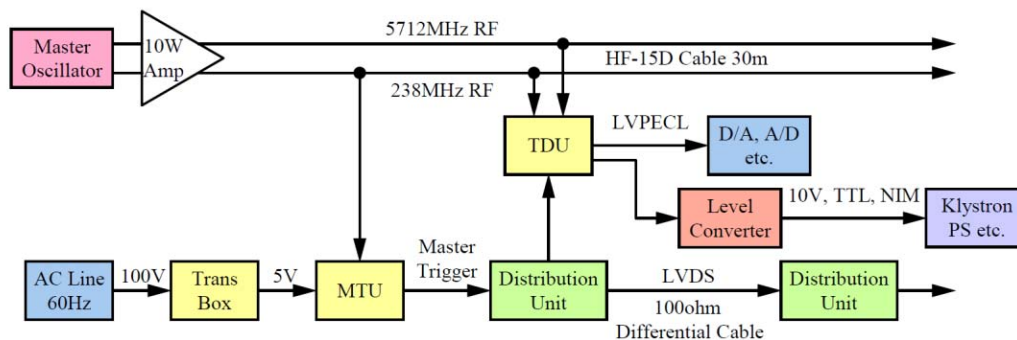
Figure 1: Schematic of the SPA timing system.

COMPARATIVE STUDIES OF ELECTRON SOURCES FOR A FREE ELECTRON LASER AT PSI

M.Dehler*, A. Anghel

Paul Scherrer Institut, CH-5232 Villigen PSI, Switzerland

Abstract

Within the scope of the low emittance gun project (LEG) at PSI, research is conducted into the development of a high brightness electron source suitable for compact, short wavelength free electron lasers. The gun, supposed to generate up to 5.5 Amperes of beam current, consists of a pulsed DC diode followed by a 1 1/2 cell RF gun. Using specialized codes, the performance of field emitter arrays is evaluated assuming realistic geometries. As an alternative, we examine the performance of conventional photo emission using copper cathodes, which we compare to that of field emitter arrays.

INTRODUCTION

High brilliance electron sources are an essential ingredient for a compact free electron laser in the Angstrom wavelength region. Their low emittance simultaneously reduces the required beam energy and saturation length for the lasing process, decreasing the cost and size of such a facility.

A study at the Paul Scherrer Institut (PSI)[1] focuses on developing suitable technologies toward a low emittance gun (LEG). We see double gated field emitter arrays as an option for a electron source with a strongly reduced initial thermal emittance, the objective being a current of 5.5 A with a slice emittance of 50 nm rad. Development of a suitable emitter is under way at PSI's laboratory for micro- and nanostructures (LMN)[2]. To avoid space charge forces destroying the emittance, fast acceleration in a pulsed DC diode gun running at high gradients up to 250 MV/m is a second focal point of research.

To simulate these devices with the required accuracy, special codes and techniques have been developed[3]. Special care has been exercised in modeling all real world effects using a realistic initial phase space distribution including also inhomogeneities in the emission density. In the following, we give an overview of current results. For comparison, similar simulations have been performed assuming emission from a copper cathode.

FIELD EMISSION CATHODES

Also known as Fowler-Nordheim tunneling, field emission is a form of quantum tunneling in which electrons pass through a barrier in the presence of a high electric field [4]. Being a cold emission process, it is seen as a possible alternative to photo emission, the advantages being a more

simple, robust setup and the potential for a higher brightness.
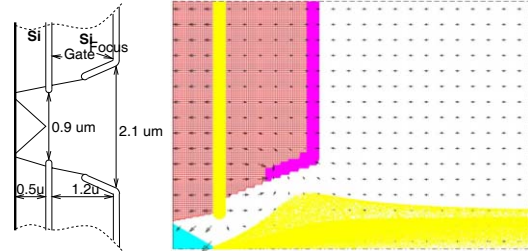
Figure 1: Geometry of double gated field emitter with beam trajectories ($I_b = 0.5mA$).

To create the required current, micron sized field emission tips are grouped into arrays, typically with a gate creating the necessary field to extract the electrons. The beamlet out of a tip will diverge strongly due to field forces and space charge effects resulting in a large emittance. A double gated geometry as in fig. 1, where the second gate acts as an electrostatic lens, avoids that in minimizing the transverse momentum spread.
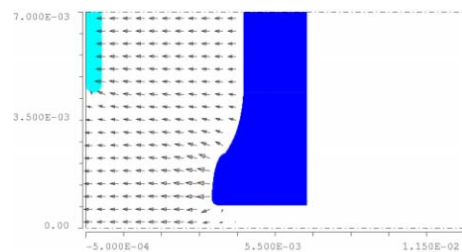
Figure 2: Gun geometry in cylindric coordinates together with accelerating field.

Parameterizing the phase space of the individual tip, we compute the beam dynamics in the pulsed DC gun[6]. The geometry is shown in Figure 2. The nominal accelerating gradient is 250 MV/m. Optimizing the cathode layout resulted in a cylindrical array of emission tips with a diameter of 500 μm. Figure 3 shows, how the slice emittance evolves from emission at the cathode ($z = -0.5mm$) to the drift following the anode. The emittance is dominated by the initial momentum spread of the individual beamlets. If, as in the second trace in Figure 3, we assume an ideal emitter geometry producing a zero emittance and divergence beamlet, a much better total performance with an emittance value of 23 nm rad could be obtained. So, optimizing the initial momentum spread of the emitted electrons further is of high interest.

* e-mail: Micha.Dehler@psi.ch

PROJECT OF INFRARED STORAGE RING
FREE ELECTRON LASERS AT AIST

N Sei[#], K. Yamada, H. Ogawa, M. Yasumoto

National Institute of Advanced Industrial Science and Technology, 1-1-1 Umezono, Tsukuba, Ibaraki 305-8568, Japan

Abstract

Development of free electron lasers (FELs) with a compact storage ring NIJI-IV in the near and middle infrared regions is planned in National Institute of Advanced Industrial Science and Technology (AIST). Infrared FELs with a linear accelerator have been already developed and used for various applications in many FEL facilities. However, there is no storage ring FEL (SRFEL) which can oscillate in those regions widely. Although an SRFEL is inferior to a linear accelerator FEL in an average power, it has an extremely stable wavelength and its spectrum line width is as narrow as that of a monochromatic light in a synchrotron radiation facility. The optical klystron ETLOK-III for the infrared FEL has been already installed in the NIJI-IV, and the spontaneous emission from the ETLOK-III has been measured. New optical cavity chambers which could suppress low-frequency vibrations are designed. They will be installed in the NIJI-IV in February. An infrared SRFEL will be achieved by the end of this year.

INTRODUCTION

Oscillations of free electron lasers (FELs) have been developed with a compact storage ring NIJI-IV in National Institute of Advanced Industrial Science and Technology (AIST). The first lasing was achieved at wavelengths of 595 and 488 nm in 1992 [1]. Improvements of the electron-beam qualities in the NIJI-IV have been advanced for shortening FEL wavelength. The wavelength of 212 nm, at which an FEL oscillation was achieved with the NIJI-IV, was the record for the shortest wavelength of FELs in 1998 [2]. The wavelength of the NIJI-IV FEL was down to 198 nm in 2003 [3], and the NIJI-IV FEL reached to the VUV region. FELs in the deep UV and VUV regions are suitable as an intense light source to observe chemical reactions which are occurred on the surface of transition-metals because the work function of the transition-metals lays around 5 eV. Then, experiments of photoelectron emission microscopy with the NIJI-IV FELs have been developed, and catalytic CO oxidation on Palladium surface was observed with video-rate time resolution [4]. FEL experiments for further shortening the wavelength below 195 nm are being carried out.

A new challenge to enhance the region of the NIJI-IV FEL wavelength has been advanced. A new optical klystron ETLOK-III, which was designed for the infrared

FEL oscillations in a wavelength region of 1-10 μm, was installed in a long straight section of the NIJI-IV in 2004 [5]. Although many infrared FEL facilities based on linear accelerators are operating, no SRFEL has been achieved in the wide infrared region. Generally, an SRFEL has the advantage of a narrow spectrum line width and stability of the lasing wavelength compare with a linear accelerator FEL. It can be used as well as synchrotron radiation passed a monochromator. The average power of the synchrotron radiation in an infrared beam line is about 10 μW at most. Then the SRFEL can be expected as a light source which is more intense than the synchrotron radiation. The output power which is our target is 1 mW. Spectra of spontaneous emission from the ETLOK-III have been already observed in the visible and near-infrared regions. New optical cavity chambers for adjusting positions and rotations of the cavity mirrors will be installed in the both ends of the long straight section in February. In this article, we explain the recent status of the development of the infrared SRFEL with the NIJI-IV.

INSERTION DEVICE

The insertion device for the infrared FEL oscillations, optical klystron ETLOK-III, has two 1.4 m undulator sections and a 72 cm dispersive section [6]. Figure 1 illustrates outline of the magnet arrangement of the ETLOK-III. Gap of the undulator section can be changed between 36 and 150 mm, and number of the periods in one undulator section is 7. The maximum K value is estimated to be 10.4 from the observed spontaneous emission spectra. Gap of the dispersive section can be changed between 42 and 188 mm. Because the magnets in the dispersive section are inserted between two tables which fix the magnets of the undulator sections, the gap of the dispersive section cannot be opened from the gap of the undulator sections over 38 mm. The dispersive section is so long that the electron beam with comparatively low energy meanders greatly in it. The electron beam passes in magnetic field of the dispersive section which is not uniform in the horizontal direction. Then the electron beam is kicked in the dispersive section and comes off the central axis of the ETLOK-III. The kick force becomes stronger as the gap of the dispersive section becomes smaller. The minimum dispersive gap at which the electron beam could be stored in the NIJI-IV was 80 mm. To cancel the kick force, we attached 5 mm iron plates to shunt magnetic field of the both end magnets in the dispersive section with a couple of 3 mm

START-UP OF FEL OSCILLATOR FROM SHOT NOISE

V. Kumar*, S. Krishnagopal, RRCAT, Indore, M.P. 452013, India
W.M. Fawley, LBNL, Berkeley, CA 94720, USA

Abstract

In free-electron laser (FEL) oscillators, as in self-amplified spontaneous emission (SASE) FELs, the build-up of cavity power starts from shot noise resulting from the discreteness of electronic charge. It is important to do the start-up analysis for the build-up of cavity power in order to fix the macropulse width from the electron accelerator such that the system reaches saturation. In this paper, we use the time-dependent simulation code GINGER[1] to perform this analysis. We present results of this analysis for the parameters of the Compact Ultrafast TErahertz FEL (CUTE-FEL) [2] being built at RRCAT.

INTRODUCTION

In an FEL oscillator driven by a pulsed radio-frequency linear accelerator, the growth of radiation starts from the noise present in the electron microbunches and gets further amplified in multiple passes, over the duration of the electron macropulse. The radiation power in the FEL cavity must saturate early enough such that one gets a temporally clean, usable radiation pulse for a significant portion of the electron macropulse. In this context, it is important to perform the start-up analysis while designing an FEL oscillator, as has been emphasized by many authors [3-9].

For typical oscillator parameters, quantum effects can be neglected [5,8] and the build-up of radiation starts from classical shot noise. Including the shot noise in the analysis of the interaction of an electron bunch with the radiation field in an FEL oscillator poses several challenges. First, the discreteness of charge has to be taken into account correctly, since the shot noise essentially results from this. Second, one has to include the broad bandwidth of radiation while studying the evolution of shot noise. This typically necessitates the use of time-dependent codes.

There have been earlier attempts to address these issues for FEL oscillators. Sprangle *et al.* [3,4] have studied the start-up process in FEL oscillators analytically, including the discrete nature of electrons, multiple radiation frequencies and finite pulse structure. The analysis, however, ignores the important non-linear effects and warm beam effects, and the three-dimensional effects are included only heuristically in terms of filling factors. Kuruma et al. [6] have studied the problem numerically using a one-dimensional, multi-frequency code where they have simulated the evolution of shot noise. Here also, three-dimensional effects have been ignored. In this paper, we simulate the start-up from shot noise of an FEL oscillator using the polychromatic FEL code GINGER [1] which

takes three-dimensional effects into account. In the next section, we discuss the details of simulations that we have performed for CUTE-FEL being developed at RRCAT. The results are discussed in the following section and finally we present some conclusions.

NUMERICAL SIMULATION

For simulating the start-up from shot noise, we have used the FEL code GINGER [1], a multidimensional [full 3D for macroparticle and 2D $(r-z)$ for radiation], time-dependent code to simulate FEL interaction in single-pass amplifier as well as oscillator configurations. GINGER utilizes the KMR [10] wiggle-period-averaged electron-radiation interaction equations and the slowly-varying envelope approximation (SVEA) in both time and space for radiation propagation. For propagation outside the undulator for oscillator problems, the code uses a Huygens integral method. Shot noise is modeled by giving a controlled amount of randomness to the initial longitudinal phases of macroparticles; the algorithm [11] generates the statistically-correct shot noise at the fundamental as well as at harmonics.

The design parameters of CUTE-FEL are given in Table 1. For the simulations reported here, we have used $\gamma = 20.53$, where γ is the electron energy in unit of its rest mass energy. We had earlier done the time-independent simulation of CUTE-FEL using the code TDAOSC [12] which is an oscillator version of the code TDA [13]. For the parameters mentioned in Table 1, we had obtained a single pass, small signal gain ($\equiv$ssg) of 88%, saturated cavity power of 9 MW and hole out-coupled power of 0.65 MW. TDAOSC models the hole outcoupling in the mirror and the optimum hole radius was found to be 2 mm. The resonator parameters were also optimized using TDAOSC. The round trip radiation loss was calculated to be 15%, of which 7.5% was due to hole outcoupling, 2.5% due to mirror reflectivity, and 5% due to diffraction loss. Because GINGER does not model hole out-coupling, we instead put a total of 10% loss mirror reflectivity. This value includes a 7.5% loss from hole out-coupling and 2.5% from the actual mirror reflectivity. Note that GINGER does include diffraction and refraction effects.

We first performed time-independent simulation using GINGER in order to verify our old results and obtain a single pass ssg of 90% and saturated cavity power of 8.3 MW. Assuming 7.5% out-coupling, the out-coupled power becomes 0.62 MW. These numbers agree quite well with earlier results of Ref. 12. We then proceeded with time-dependent oscillator simulations adopting a Gaussian longitudinal electron beam profile with a rms width of 4 ps and peak current of 20 A ($Q = 0.2$ nC). The longitudinal slice

COMPARISON OF CODES FOR SMITH-PURCELL FEL [*]

Vinit Kumar[#], RRCAT, Indore, M.P. 452013, India
Kwang-Je Kim, ANL, Argonne, IL 60439, USA
Dazhi Li, ILT, Suita, Osaka 565-0871, Japan

Abstract

Smith-Purcell (SP) free-electron lasers (FELs) using low energy electron beam are being seen as attractive option for a compact source of coherent terahertz radiation. Recently, Kumar and Kim [1] have performed numerical simulation of SP-FELs based on a computer code using Maxwell-Lorentz equations. Li et al. [2,3], and Donohue et al. [4] have performed calculations using particle in cell (PIC) codes. In this paper, we present a comparison of these methods and compare results obtained using different codes.

INTRODUCTION

Recently, there has been a lot of interest in the analysis and simulation of Smith-Purcell (SP) free-electron laser (FEL) [1-6]. The possibility of a SP-FEL based on low energy electron beam is seen as an attractive option for compact terahertz (THz) source of coherent radiation. The SP-FEL is a backward wave oscillator (BWO) for low energy electron beam [1,5]. In a BWO, like any oscillator system, the electron beam current needs to be higher than a threshold value, known as the start current, in order to produce coherent electromagnetic oscillation. If the electron beam current is higher than the start current, the coherent electromagnetic oscillations start growing and then saturate due to nonlinearity. In order to build such a device, it is important to study the start current and the saturation behaviour of SP-FEL. Kumar and Kim [1] have performed an analysis and numerical simulation of a SP-FEL system using Maxwell-Lorentz equations, where they have studied the growth of power, the efficiency at saturation and the start current in a SP-FEL. Li et al. [2] and Donohue et al. [4] have performed a more detailed 2D simulation of a SP-FEL system using a computer code MAGIC [7] which is a particle in cell (PIC) code. In Ref. 3, Li et al. have performed three-dimensional simulation of SP-FEL system using MAGIC. A natural question then arises that how do these different codes compare with each other. In this paper, we present a comparison of the results obtained using different computer codes for simulating a SP-FEL. We find that the results of the fast, 2-D simulation using Maxwell-Lorentz equation developed in Ref. 1 agree well with other more elaborate simulations.

In the next section, we discuss the numerical simulation and calculations that we have performed based on Maxwell-Lorentz equations. We then discuss the compari-
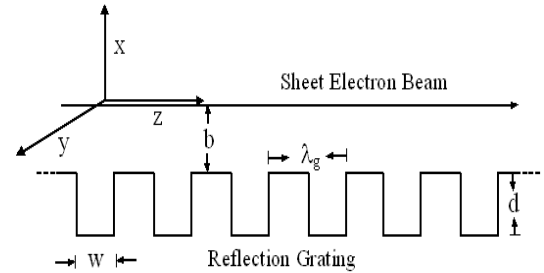
Figure 1: Schematic of an SP-FEL using a sheet electron beam. The sheet electron beam is in the plane $x = 0$.

son of results obtained using this approach with the already published results [2-4] obtained using PIC code in the following section and conclude.

DETAILS OF MAXWELL-LORENTZ SIMULATION

We start with a brief description of the SP-FEL system. Figure 1 shows the schematic of the SP-FEL setup. We assume the system to have translational invariance in the y-direction and hence ours is a 2D analysis. We assume a sheet electron beam which travels with a speed βc along the z-axis, at a height b above the grating of length L, having grooves of depth d, width w and period λ_g. Here, c is the speed of light in vacuum.

In a SP-FEL, the electron beam interacts with the co-propagating surface electromagnetic mode supported by the grating. As shown in Refs. 1 and 5, the co-propagating surface mode has a group velocity in the direction opposite to the electron beam for low electron beam energy. The backward surface mode supported by the grating is a linear combination of infinite number of Floquet-Bloch harmonics having the z-component of propagation vectors differing from each other by an integral multiple of k_g, where $k_g = 2\pi/\lambda_g$. The y-component H_y of the magnetic field of the backward surface mode can be written as $\sum A_n \exp(ik_0 z + ink_g z - \Gamma_n x - i\omega t)$, where the summation is implied over all n from $-\infty$ to $+\infty$ [1]. Here, ω is the frequency, $k_0 = \omega/c\beta$ is the propagation vector of the backward surface mode and $\Gamma_n = \sqrt{(k_0 + nk_g)^2 - \omega^2/c^2}$. The zeroth-order component of this mode has the longitudinal electric field given by $E_0(z,t) \exp(ik_0 z - i\omega t)$ at $x = 0$. The amplitude of all other components of the backward surface mode have to maintain a fixed ratio with the amplitude of the zeroth-order component such that the elec-

BEAM PARAMETERS OF THE SCSS PROTOTYPE ACCELERATOR DESIGNED BY PARMELA AND COMPARISON WITH THE MEASURED VALUES

Toru Hara*, Hideo Kitamura, Tsumoru Shintake, Hitoshi Tanaka, Kazuaki Togawa

RIKEN/XFEL, 1-1-1 Kouto, Sayo-cho, Sayo-gun, Hyogo 679-5148, Japan

Takanori Tanikawa

University of Hyogo, 3-2-1 Kouto, Kamigori-cho, Ako-gun, Hyogo 678-1297, JAPAN

Abstract

The 250 MeV prototype facility of the X-FEL project at SPring-8 was constructed in Octorber 2005 and the machine commissioning was started in May 2006. One month later, we have succeeded in confirming the amplification of synchrotron radiation. The electron beam parameters, such as peak currents and emittances, have been designed and estimated using PARMELA. In contrast to other X-FEL projects, the SCSS injector uses a thermionic pulsed electron gun. Compared with RF photocathode guns, a thermionic gun is stable and easy to handle. Its peak current, however, is smaller and compression of an electron bunch is necessary at the early stage of a low beam energy injector. In this report, we compare the simulation and the measured beam parameters, such as the bunch length and the projected emittance, on the SCSS prototype accelerator. The measured values, after the bunch compression process and the emittance degradation due to space charge, show fairly good agreement with the simulation.

INTRODUCTION

The SPring-8 Compact SASE Source (SCSS) prototype facility was constructed in 2005 as a test bench of the X-FEL project aiming at the lasing wavelength less than 0.1 nm [1]. One of the unique features of the project is the use of a thermionic pulsed electron gun instead of a laser photo-cathod RF gun. In order to reduce the initial beam emittance, a single crystal CeB_6 (ϕ 3 mm) is used as a cathode and a high pulsed voltage of 500 kV is applied to the anode to extract the electron beam [2]. The thermionic gun has clear advantages such as stable operation and easy maintenance, however, its peak current is smaller compared with that of photo-cathode guns. As a result, electron bunch compression is necessary at the low beam energy section ($\leq$ 1 MeV) of the accelerator.

Fig. 1 shows a schematic layout of the SCSS prototype accelerator. A fast deflector is installed just after the electron gun, and an 1 ns electron bunch is sliced out from a μsec electron beam of 1 A from the gun cathode. At the same time, the periphery of the electron beam, which is emitted from the cathode edge, is removed by a pinhole (ϕ 5 mm). Then the 1 ns electron bunch is compressed by a

velocity bunching scheme using a 238 MHz, 476 MHz and S-band APS cavities. The peak current is reached about 80 A after the S-band traveling wave tube with the beam energy of 40 MeV. At this point, the beam parameters are similar to those of the RF photocathode guns. Then the electron bunch is further compressed in a magnetic bunch compressor (BC), and accelerated up to the 250 MeV nominal energy using C-band accelerators.

Since the slice emittance and the peak current, which are the most important parameters for the FEL operation, does not change significantly in the C-band main accelerator, the key of the parameter design is how to obtain a large peak current without degrading the gun emittance at the BC end.

BEAM PARAMETER DESIGN WITH PARMELA

Initial Conditions

Since PARMELA can not treat a DC electron gun, 500 keV energy is immediately given to the electrons at the start, and no DC acceleration process between the cathode and anode is considered in the simulation. The bunch length and normalized emittance at the gun cathode are assumed to be 1 ns and 0.5 π mm-mrad respectively. In order to focus the electron beam, magnetic lens are used in the prototype accelerator for the beam energy below 1 MeV. The initial beam size and divergence at the cathode are determined so that the simulation reproduces the measured sizes at three locations of the injector section ((a), (b) and (c) in Fig. 1) as a function of the focusing strength. Fig. 2 shows the simulated and measured beam sizes at these locations as a function of the magnetic lens current.

Bunch Compression

The emittance degradation of the SCSS prototype accelerator is mainly due to the space charge effect at the low energy injector section. The focusing strength and the RF parameters should be chosen so as to keep the uniform transverse electron beam profile from the gun cathode during the velocity bunching process. In other words, the nonlinear divergence coming from the space charge effect should be minimized to avoid the slice emittance degradation. The optimized beam energies and peak currents along the accelerator are shown in Fig. 1.

---

* toru@spring8.or.jp

FUTURE LIGHT SOURCE BASED ON ENERGY RECOVERY LINAC IN JAPAN

Toshio Kasuga, Takaaki Furuya, Hiroshi Kawata, Yukinori Kobayashi, Shogo Sakanaka, and Kotaro Satoh

High Energy Accelerator Research Organization (KEK), Tsukuba, Ibaraki 305-0801, Japan

Norio Nakamura

Institute for Solid State Physics (ISSP), University of Tokyo, Kashiwa, Chiba 277-8581, Japan

Ryoichi Hajima

Japan Atomic Energy Agency (JAEA), Tokai, Naka, Ibaraki 319-1195, Japan

Abstract

After extensive discussions on the future light source of the Photon Factory at the High Energy Accelerator Research Organization (KEK), it has been concluded that a 5 GeV energy recovery linac (ERL) should be the most suitable candidate to foster cutting-edge experiments, as well as to support a large variety of user needs from VUV to X-rays. On the other hand, the Japan Atomic Energy Agency (JAEA), which has built a low energy (17 MeV) ERL, also proposed another 5-6 GeV ERL as a light source. These two institutes, with a participation of some members of the Institute for Solid State Physics (ISSP) of the University of Tokyo, agreed to promote an ERL-based next-generation synchrotron light source in Japan. Before constructing a 5 GeV ERL, it is necessary to develop several critical components, such as an electron gun and superconducting accelerating structures, and to prove their performance. To this end, we plan to construct a test ERL of 200-MeV class at the KEK site. An R&D team for the test ERL is going to be organized in collaboration with accelerator scientists from the other facilities, the UVSOR and the SPring-8.

INTRODUCTION

We have been investigating the feasibility of an energy recovery linac (ERL) as a light source for several years [1-3]. After the discussions on the future light source of the Photon Factory, it has been concluded that a 5 GeV class ERL should be the most suitable candidate to foster cutting-edge experiments, as well as to support a large variety of user needs from VUV to X-rays [4]. A conceptual layout of a 5 GeV ERL, proposed in the feasibility study, is shown in Fig. 1. The principal parameters are also shown in Table 1 [1]. In order to realize this kind of light source, the development of many components that compose the light source is necessary. Investigations into the beam dynamics issues, for example, the energy recovery in rf cavities, the stability of the beams, the conservation of normalized emittance, etc., are also essential. Therefore, construction of a test ERL seems to be inevitable. Both the design concept and the key technologies will be demonstrated by the test ERL. An R&D team for the test ERL is going to be organized in collaboration with accelerator scientists from KEK, JAEA, ISSP, UVSOR and SPring-8. We are planning to construct a 200-MeV class ERL, and to substantiate the principle of the ERL within several years. The principal parameters of the test ERL are also shown in Table 1.
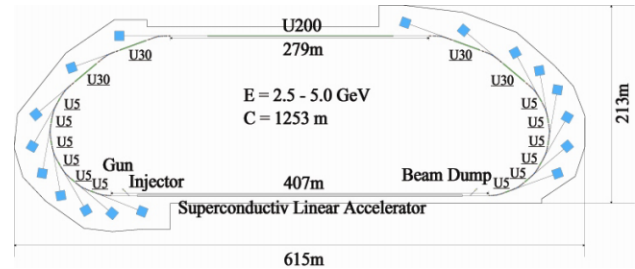
Figure 1: Conceptual layout of 5GeV ERL.

Table 1: Principal parameters of the future light source and the prototype.

	Future LS	Test ERL	
Beam energy	2.5-5.0	0.06-0.2	GeV
Injection energy	5-10	5-10	MeV
Circumference	1253	68.8	m
Beam current (Max.)	100	100	mA
Normalized emittance	0.1-1	0.1-1	mm·mrad
Energy spread (rms)	5	-	E-5
Bunch length	1-0.1	1-0.1	ps
RF frequency	1.3	1.3	GHz
Accelerating gradient	10-20	10-20	MV/m

DEVELOPMENT OF A PHOTOCATHODE DC GUN

The combination of a DC gun and a photocathode should be an optimum electron source, which fulfils the requirement of ERL light sources: electron beams of high-average current and ultra-small emittance. To demonstrate the ERL-quality electron beams, we are developing a photocathode DC gun at JAEA. The gun consists of a main chamber for DC electrodes, an NEA surface preparation chamber, and a load-lock system for transporting a photocathode between these chambers. A ceramic insulator of the gun and a high voltage stack of 250 kV-50mA power supply are located side-by-side in a pressure vessel, holding 2-atm SF6. A high-voltage test without a beam load has been completed successfully, and assembling of the load-lock system is in progress. We are proposing a superlattice semiconductor for the

DEVELOPMENT OF A PHOTOCATHODE DC GUN AT JAEA-ERL

R. Hajima[#], T. Nishitani, H. Iijima, R. Nagai, N. Nishimori

JAEA-ERL, Tokai, Ibaraki 319-1195, Japan

Abstract

An electron gun producing an e-beam with high-brightness and high-average current is a key component to realize a next-generation X-ray light source based on an energy-recovery linac (ERL). In JAEA, we are developing a photocathode DC gun for a future ERL light source. The DC gun is operated at 250 kV and 50 mA at maximum, and equipped with a load-lock chamber for cathode preparation. In order to keep small emittance at high current operation, we adopt new type of semiconductor photocathode such as AlGaAs and superlattice. In this paper, we present the status of the gun development and future plans towards the ERL test facility to construct in collaboration with KEK and other institutes.

INTRODUCTION

In JAEA (Japan Atomic Energy Agency), we have conducted a research program for a high-power free-electron laser since 1987. As a part of the research program, an energy-recovery linac (ERL) has been commissioned. The design study of the ERL was started in 1999[1]. After one-year construction period we made first demonstration of energy-recovery operation in 2002[2]. The ERL consists of a 250 kV DC gun with thermionic cathode, 2.5 MeV injector, an ERL loop for 17 MeV electrons, and an FEL undulator. The FEL wavelength is around 20 μm [3]. The ERL also generate strong radiation in millimeter wavelength region by coherent synchrotron radiation from a bending magnet[4].

Following the successful demonstration of ERLs at JAEA and Jefferson laboratory[5], several new proposal of ERLs have been suggested. Since the energy-recovery linac provides a versatile technology to generate a high-brightness electron beam of high-average current, it can be applied to various kinds of accelerators. Next-generation X-ray light source is one of the most promising direction for the future ERL development. We can produce X-rays with excellent coherence and/or ultrashort pulse duration, if we employ an energy-recovery linac equipped with a high-brightness injector such as a photocathode gun. In Cornell university, a 5 GeV ERL light source is proposed as a successor of CESR, and an injector for the ERL is under development[6]. Research and development towards next-generation light source based on an 800 MeV ERL is carried out at Daresbury[7].

In Japan, KEK and JAEA had proposed each own 5-6 GeV ERL project for a future light source independently. These two institute, however, agreed to unite their projects

into a single form in March 2006. We are now working together to construct an ERL test facility at KEK site to resolve technical and physical challenges[8]. In the joint project, JAEA is mainly responsible for the gun development and KEK has charge of superconducting cavities[9].

In this paper, we present the status of electron gun development for the future ERL light source in Japan.

ELECTRON GUN FOR ERL LIGHT SOURCES

Next-generation light source based on the ERL technology provides an evolutionary path of X-ray science, because the ERL generates coherent X-rays and femtosecond X-rays which are difficult to obtain in existing storage rings. When the divergence of an electron beam is smaller than the intrinsic divergence of an X-ray, a large part of undulator radiation becomes coherent, and this criteria is called "diffraction limit" and given by $\varepsilon < \lambda/4\pi$, where ε is geometrical rms emittance and λ is X-ray wavelength. In order to satisfy the diffraction limit for 1 Å X-rays, emittance should be less than 8 pm-rad, which corresponds to normalized rms emittance of $\sim$0.1 mm-mrad at 5 GeV. Average current of an ERL light source should be as large as 100 mA to obtain X-rays of flux comparable to 3rd-generation light sources. Thus, the requirements of an electron gun for a future ERL light source are average current of 100 mA and normalized rms emittance of 0.1 mm-mrad.

Developing an electron gun to satisfy the above requirement is a serious matter. Photocathode RF guns have been studied for high-brightness electron beams and normalized rms emittance is approaching to a value of 1 mm-mrad [10]. Recently, a DC gun with a thermionic cathode generating an electron beam of 1.1 mm-mrad was built for an XFEL[11]. These guns, however, are designed for pulsed operation with small duty cycle. The gun of JAEA-ERL is compatible with 10-mA CW operation but has rather large emittance, 13 mm-mrad, due to its gridded thermionic cathode[13].

The only candidate for the future ERL light source is the combination of a DC gun and semiconductor cathode with negative electron affinity (NEA) surface. Since GaAs with NEA surface is able to emit photo-electrons by visible lasers, it is an optimum electron source for generating high-average current. An NEA cathode can be installed only at DC guns, because stable operation of an NEA surface requires ultra-high vacuum, typically 10^{-9} Pa. A DC gun with NEA cathode has been employed at the JLAB ERL, where average current of 9 mA and normalized emittance

DEVELOPMENT OF AN INJECTOR TO GENERATE A VERY SHORT BUNCH FOR A SUPER COHERENT TERAHERZ LIGHT SOURCE PROJECT*

T. Tanaka[#], T. Muto, F. Hinode, M. Kawai, K. Nanbu, K. Kasamsook, K. Akiyama, M. Yasuda and
H. Hama, Laboratory of Nuclear Science, Tohoku University, 1-2-1 Mikamine,
Taihaku-ku, Sendai, 982-0826, Japan
H. Tanaka, N. Kumagai, RIKEN/Spring-8, 1-1-1 Koto, Sayo-cho Sayo-gun,
Hyogo- pref. 679-5198, Japan

Abstract

A project to develop a coherent Teraherz (THz) light source is in progress at Laboratory of Nuclear Science, Tohoku University. The coherent synchrotron light in the THz region is emitted from electron bunches with a very short bunch less than 100 fs (rms) generated by a thermionic RF gun and a sophisticated bunch compressor. As an injector for the linac, we have developed an independently tunable cells (ITC) RF gun and a magnetic bunch compressor which consists of a triple-bend achromat (TBA) lattice. As a result of simulation of the injector, we have obtained a very short bunch length of ~ 40 fs (rms). Results of low power tests of the ITC-RF gun and the tracking simulation of the bunch compressor will be presented in this proceeding.

INTRODUCTION

For a coherent Teraherz (THz) light source project employing an isochronous ring [1], a very short bunch less than 100 fs (rms) is required as an injected beam. A thermionic ITC-RF gun and a bunch compressor with a TBA lattice have been studied as the injector for the linac [2]. The thermionic RF gun can generate a macropulse with μs order which is an advantage for generating high average power of the radiation. Longitudinal phase space distribution can be manipulated in the ITC-RF gun so that the bunch length can be compressed effectively at the downstream of the gun. This gun can also generate a low emittance beam compared with a conventional dispenser cathode DC gun. Since the designed bunch compressor can vary R_{56} and the higher order term of the dispersion function, the bunch compression is able to be optimized even the initial longitudinal phase space distributions is changed.

GENERATION OF VERY SHORT BUNCH

Design of a thermionic RF gun

Taking the circumference of the isochronous ring (~ 150 ns) and the filling time of the gun assumed 0.3 μs into account, the macropulse duration of the injector has been chosen to be around 1.5 μs, which is possibly an

advantage for avoiding back-bombardment effect [3]. The bunch charge should be as large as possible. The momentum deviation of the injected beam for the ring should be the order of 10^{-4} to have the beam turns the ring many times without bunch lengthening. Consequently the momentum acceptance of the injector part is required to be at least 10^{-2} because the beam is accelerated from 2 MeV to 200 MeV in the linac. Normalized rms emittance of the beam has to be very small less than 2 π mm mrad because the path length difference due to the betatron oscillation should be reduced. As a cathode material, a small single crystal of LaB_6 with a diameter 1.75 mm has been chosen. This cathode has a higher current density than that of conventional dispenser cathodes. The normalized emittance can achieve a small value because of the small area of the surface. According to a simulation study, the small cathode is also effective to reduce back-bombardment effect because the beam size of backstreaming electrons is larger than the area of the cathode [4]. To control an electron distribution in the longitudinal phase space, we employed independent two cells, which don't couple with each other. Parameters of the gun are listed in Table 1.

Table 1: Design parameters of ITC-RF gun

RF frequency	2,856 MHz (S-band)
Cathode material	LaB_6
Current density @ cathode	100 A/cm^2
Cathode diameter	1.75 mm
Number of cells	2
Feeding total power	~ 5 MW
E_{total} @ exit of gun	~ 2 MeV
Bunch length (rms)	~ 100 fs
Bunch charge	~ several tens pC
$\varepsilon_{norm. rms}$	< 2 π mm mrad
$\Delta p/p$	< 2 %
Macropulse duration	1.5 μs
Filling time	0.3 μs

Study of the beam dynamics in the ITC-RF gun has been done by using a 3D FDTD PIC code [4]. We had to find out an appropriate distance between the cells and the strength of the accelerating field in each cell, because the longitudinal phase space strongly depends on these parameters. A 2D code: SUPERFISH [5] has been used to determine the radius of cells so as to resonant frequencies become 2856 MHz. The iris radius between cells has been

STUDY ON COMPACT DC ELECTRON GUN USING SINGLE CRYSTAL CATHODE OF LaB6*

K. Kasamsook[#], K. Nanbu, M. Kawai ,K. Akiyama, F. Hinode, T. Muto , T. Tanaka, M. Yasuda, H. Hama

Laboratory of Nuclear Science, Tohoku University,
1-2-1 Mikamine, Taihaku-ku, Sendai 982-0826, Japan

Abstract

A novel, compact DC gun has been developed and is currently on a test bed at LNS. Applying 50 kV high voltage for the gun, it is expected to supply a high brightness beam which the beam current of 300 mA and the variable pulse duration from 1 to 5 μsec. In addition, a floating bias voltage can be applied between the cathode and the wehnelt to manipulate electric field near cathode surface. In order to produce lower emittance beam, the size of thermionic cathode should be very small, but the cathode should be higher current density. Consequently we have chosen single crystal LaB6 as the thermionic cathode, which can provide higher current density with good homogeneity electron emission. The design parameters and initial operating experience of the DC gun are discussed. This DC gun will be used for Smith-Purcell FEL [1], advanced accelerator researches and other experiments.

INTRODUCTION

Recently, electron guns with high brightness are of great interest to achieve many applications in the field of electron beam technology such as Smith-Purcell FEL , for example. The low emittance DC electron gun at LNS is one of the candidates. The prominent point of this DC electron gun has no grid which would degrade beam emittance. The cathode is made of a single crystal material with the low work function, and heated to higher for producing electrons. We have chosen a low applying voltage (50 kV) to reduce the size of the entire system. The schematic diagram of DC gun power supply is shown in Fig.1. In spite of such low voltage, the emittance can be reduced to very small because of a very short distance between the cathode and the anode, and the bias voltage apply between wehnelt and cathode can manipulate the beam property. In order to produce low emittance beam, the cathode size should be small, so that the higher current density is required. Such high current density can be realized by some cathode materials such as single crystal LaB6 or CeB6 [2,3]. The design parameters and the drawing of the low emittance DC electron gun with solenoid lens are shown in Table 1 and Fig.2, respectively.
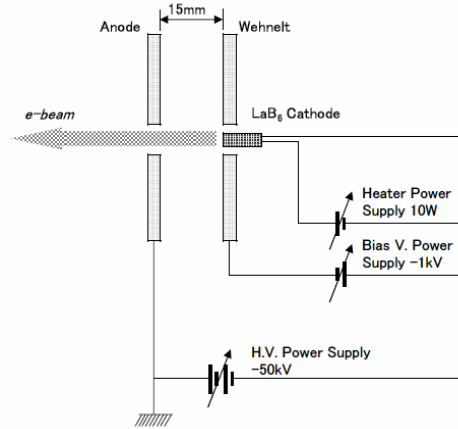
Figure 1: The schematic diagram of DC gun power supply.

Table 1: Design parameters of electron gun.

Beam energy	50 keV (Max.)
Peak current	>300 mA
Pulse width (FWHM)	1-5 μsec
Repetition rate	50 pps
Normalized emittance	<10 π mm mrad.
Normalized thermal emittance	0.25 π mm mrad* *theoretical
Cathode diameter	1.75 mm.
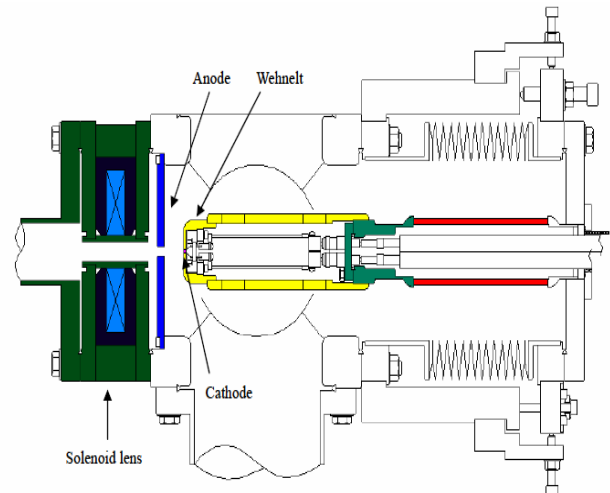
Figure 2: The low emittance DC electron gun.

INJECTION OPTIMISATION FOR INDUS-2

Ali Akbar Fakhri[*] and Gurnam Singh

Raja Ramana Centre for Advanced Technology, Post - CAT, Indore – 452 013

Abstract

In this paper commissioning experience of injection into INDUS-2, a 2.5 GeV synchrotron radiation source is discussed. In initial stage commissioning, partial beam loss was observed. In this context effect of various injection errors such as mismatch between pulse widths, jitter and magnetic field stability of kickers on injected and stored beam are studied [1]. A brief summary of the results is presented. After reducing jitter and fine adjustments of timings of kicker power supplies, partial beam loss reduced significantly.

INTRODUCTION

A multi turn injection scheme employing a compensated bump generated by four kickers has been chosen for beam injection into INDUS-2. The injector for this ring is a synchrotron with peak energy of 450-550 MeV. The synchrotron provides two bunches each one around 1ns long and separated from each other by nearly 30ns, at the required energy at a repetition rate of 1 Hz. After injecting several pulses at 450-550 MeV, the beam is accelerated to 2.5 GeV by slowly increasing the magnetic field of the bending magnets. The injection is carried out in the radial plane from the outer side of the ring by using a compensated bump generated by four kicker magnets. The Indus-2 storage ring has kicker magnets k1 to k4, placed symmetrically in a 4.5m-long straight section. The straight section part containing injection kickers is free from quadrupoles, so the deflection bump is independent of the machine optics

BEAM INJECTION

Since the synchrotron routinely delivers a beam to Indus-1 at 450 MeV, initial attempts were made to inject the beam in Indus-2 at this energy. To reduce the residual betatron oscillation of the injected beam as well as stored beam, it was decided to move septum chamber towards the beam orbit by 8 mm. By looking the beam position at BPM-1(just after up stream kicker magnet), BPM-3(located at achromat section) and just after one turn (at septum BPM) proper optimisation of position and angle was carried out by changing thick and thin septum currents. After this optimisation 2.ms Fig.1)beam rotation was observed. Further optimising RF frequency, kicker strength and time delays the beam survival time of more than 1 second was achieved. At 450 MeV beam energy the damping time in horizontal plane is 810 ms, this being comparable to the synchrotron repetition rate, the injected beam oscillations are not fully damped when the next pulse is injected into the ring. So it was decided to inject

the beam at a higher energy. The energy in the synchrotron was then ramped to 550 MeV and the beam at this energy was extracted for injection into Indus-2. At this energy the damping time is 444 ms, therefore, the beam is fully damped when the next pulse arrives after one second. Once the beam was stored for full injection cycle the kickers were adjusted to allow the beam accumulation. At this stage, it was very important to adjust the timing of the kicker pulses. Much time and efforts were spent to ensure that the stored beam traversed kickers at the proper time. Further optimisation is carried out by optimising beta functions at the end of TL-3, in which beta function is reduced from 14m to 8m, with this exercise a small beam spot on the last BPM of TL-3 and BPM 1 of Indus 2 was observed.
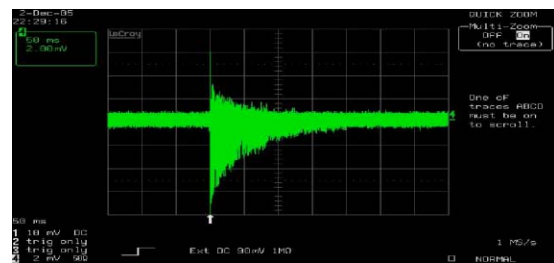
Figure 1: WCM signal indication of survival of the beam up to 200 ms.
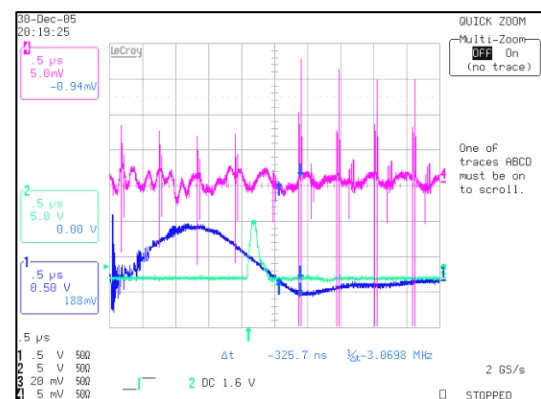
Figure 2: Beam storage to more than 1 second beam crosses injection kicker after 1 second.

In initial stage at time of injection, partial beam loss was observed. The loss was attributed to the following reasons associated with injection kickers namely 1) Magnetic field stability 2) Mismatch between pulse widths 3) Jitter. Initially effects of these errors were observed by looking at the synchrotron light monitor, which is located far away from the injection sections. Due to various injection errors, in the SLM beam spot variation was observed. A theoretical study of the effect of these errors is discussed in this paper.

INJECTION OF BEAM SHAPED LOCALLY WITH NONLINEAR OPTICS[*]

Chun-xi Wang[#], ANL, Argonne, IL 60439, USA

Abstract

We discuss nonlinear beam shaping by octupole and sextupole to fold the tails of a Gaussian beam into its core, for the purpose of improving betatron injection in storage rings by significantly reducing the beam width at the injection septum and thus reducing beam centroid offset from the stored beam. Necessary conditions as well as challenges for such nonlinear injections are explored.

INTRODUCTION

Injection is an important (yet often problematic) process in circular accelerators. Usually fast and strong kicks are used to merge the incoming beam with the stored beam (noticeable exceptions are charge-exchange H^- injection with a stripping foil and International Linear Collider damping ring injection where no stored beam exists during injection). Due to Liouville's theorem, certain phase-space separation of the incoming and stored beams are unavoidable. Here we consider the transverse injection scheme where the two beams are separated in the transverse phase space, say the horizontal plane. This injection scheme is commonly used in lepton machines where the two separated beams can be radiation damped into one. It is important to minimize the phase-space separation so that both beams can stay within the acceptance of the circular machine. This becomes more and more critical in modern storage-ring-based light sources such as the Advanced Photon Source, where acceptance is sacrificed for small emittance and narrow-gap insertion devices. On the other hand, the sizes of the stored and injected beams as well as the physical existence of a (septum) kicker requires certain clearance from the beams and thus limits the minimum separation reachable by the two beams. Therefore, the area close to the septum becomes the bottleneck of the injection process, which may result in demanding requirements for the kicker and incoming beam emittance. This note will explore possibilities to ease this bottleneck by properly folding the long tails of the Gaussian phase-space distribution of an incoming beam locally with nonlinear optics such that the incoming beam can come much closer to the septum and the stored beam.

NONLINEAR BEAM SHAPING

It is well-known that octupoles can be used to fold the tails of a Gaussian beam onto its core and make a more uniform distribution with sharper edges [1-4]. This technique is commonly used to make uniform illumination on targets. There are also proposals of using octupole beam shaping in linear colliders to make a cylindrical beam lens for final focusing or to make a nonlinear collimation system. To explore nonlinear beam shaping for injection purposes, we consider using a sextupole ($n = 2$) or octupole ($n = 3$).

To simplify the discussion we assume the nonlinear element is thin and write the beam transport from the nonlinear element to the injection point as

$$\begin{bmatrix} x \\ p \end{bmatrix} = R \begin{bmatrix} x_0 \\ p_0 \end{bmatrix} + kR \begin{bmatrix} 0 \\ x_0^n \end{bmatrix}, \qquad (1)$$

where R is the linear transfer matrix between the initial and final phase-space points $\{x_0, p_0\}$ and $\{x, p\}$, respectively; and k is the integrated strength of the nonlinear element. Using the Twiss parameters at the ends and the phase-advance Δ between them, the R-matrix can be written in the well-known form

$$R = \begin{bmatrix} \sqrt{\beta} & 0 \\ -\frac{\alpha}{\sqrt{\beta}} & \frac{1}{\sqrt{\beta}} \end{bmatrix} \begin{bmatrix} \cos\Delta & \sin\Delta \\ -\sin\Delta & \cos\Delta \end{bmatrix} \begin{bmatrix} \frac{1}{\sqrt{\beta_0}} & 0 \\ \frac{\alpha_0}{\sqrt{\beta_0}} & \sqrt{\beta_0} \end{bmatrix}. \quad (2)$$

Since our main concern is the transverse dimension of the beam at the injection point, we express the transverse position as

$$x = \sqrt{2\beta J_0}\left[\cos(\theta_0 + \Delta) + 2\,\bar{a}\sin\Delta\cos^n\theta_0\right], \quad (3)$$

where J_0 and θ_0 are the action-angle variables in the initial phase space and the parameter $\bar{a} \equiv 2^{\frac{n-3}{2}} k\,\beta_0^{\frac{n+1}{2}}\,J_0^{\frac{n-1}{2}}$. Our focus is on the beam edge given by the 3σ contour with $J_0 = 9\epsilon/2$, where ϵ is the emittance of injected beam. The first term yields the unperturbed position and the second term gives the correction due to the nonlinear kick. For a given $\bar{a}$, extreme position x_m will be reached when $\partial_{\theta_0} x = \partial_\Delta x = 0$, i.e.,

$$\begin{aligned} \sin(\theta_0 + \Delta) &= -2\bar{a}\sin\Delta\ n\cos^{n-1}\theta_0\sin\theta_0 \\ &= 2\bar{a}\cos\Delta\ \cos^n\theta_0. \end{aligned} \quad (4)$$

Let θ_m and Δ_m be a solution set, then we have the condition $\cos(\theta_m + \Delta_m) = -(n+1)\sin\theta_m\sin\Delta_m$ and the extreme value

$$x_m = \sqrt{2\beta J_0}[-(n+1)\sin\theta_m + 2\bar{a}\cos^n\theta_m]\sin\Delta_m. \quad (5)$$

Therefore, it is desirable to have the phase advance Δ_m close to a multiple of π (note that there is no solution for $\Delta_m = \text{integer} \cdot \pi$). A more geometric view of this is that, under such a condition, the peaks of the two terms in Eq. (3)

PHYSICS DESIGN OF PAL-XFEL UNDULATOR*

D.E.Kim[#], K.H.Park, J.S.Oh, C.W.Chung, and I.S.Ko, PAL, POSTECH, Korea.

Abstract

Pohang Accelerator Laboratory(PAL) is planning a 0.3 nm – 0.45 nm SASE (Self Amplification of Spontaneous Emission) XFEL based on 3.7 GeV linear accelerator. It is targeting utilization of 0.1 nm X-ray radiation using the 3rd harmonic FEL radiation. With 3.7 GeV electron beam energy, achieving 0.3 nm fundamental FEL lazing is very challenging and it requires very low emittance electron beam with minimum energy spread. It also requires small period undulator with very small gap. In this context, application of SPring8 type in vacuum undulator is seriously considered. This reflects the experiences from SPring8 SCSS project. In this report, the physics design efforts of the undulator is described. The periodic parts are optimized to achieve the highest field with other requirements. The end structures were designed to be asymmetric along the beam direction to ensure systematic zero 1st field integral. The thickness of the last magnets were adjusted to minimize the transition distance to the fully developed periodic field. The final design features 4 mm minimum pole gap, 15 mm period, peak effective field of 1.09 Tesla.

INTRODUCTION

Pohang Accelerator Laboratory (PAL) is planning to build a X-ray FEL based on SASE (self amplified spontaneous emission) process[1]. The machine is named as PAL-XFEL and will utilize the upgrade inject linac for PLS (Pohang Light Source) electron storage ring. Current electron beam energy of the linac is 2.5 GeV and it needs to be upgraded to at least 3.7 GeV for 0.3 nm FEL radiation. The SASE XFEL offers unprecedented opportunity for X-ray users. SASE XFEL radiation is supposed to be at least ten orders of magnitude brighter than the 3rd generation synchrotron light sources. The SASE XFEL is transversely coherent and the pulse length is very short, femto-second level, which also provides users with chances for new scientific research.

On the other hand, the SASE XFE is quite a scientific challenge, as is well known; the generation of an extremely low emittance electron beam through a photo-cathode RF gun, bunch compression to an extremely short length, maintaining the low emittance to the end of the linac, and keeping the beam orbit as straight as possible in the undulator. The PAL-XFEL adds a few more scientific difficulties because it is targeting relatively short radiation wavelength (0.3 nm) with lower electron beam energy (3.7 GeV). Therefore, the PAL-XFEL requires very short period undulator with minimum possible gap. This implies the use of in Vacuum undulator developed at

SPring8 is essential to the project. In this paper, the magnetic design of the periodic part, the magnetic design of the end part and other physics requirement of the PAL-XFEL undulator will be described. The major design parameters of the PAL-XFEL are summarized in Table 1.

Table 1: Major design parameters of PAL-XFEL

Beam Parameters	Value	Unit
Electron energy	3.7	GeV
Peak current	3	kA
Normalized slice emittance	1	mm mrad
RMS slice energy spread	0.02	%
Full bunch duration	270	fs
SASE FEL Parameters		
Radiation wavelength	0.3	nm
FEL parameter ρ	5.7×10^{-4}	
Peak brightness	1×10^{32}	pts/sec/m m^2/mrad^2/ 0.1%BW
Pulses repetition rate (Max.)	60	Hz
1-D gain length	1.2	m
Saturation length, L_{sat}	45	m

MAGNETIC FIELD REQUIREMENTS

A few kinds of technologies are considered for SASE XFEL undulators. For higher magnetic field at smaller magnetic period, superconducting (SC) undulator looks promising. But they believe that the technology is not mature and there is higher risk factor that hinders many laboratories to adopt SC technologies for SASE-FEL undulator. Helical undulator has advantage in getting polarized radiation with shorter saturation undulator length. But it has difficulty in manufacturing and error control. Therefore, many laboratories prefer Halbach type hybrid undulator or PPM (Pure Permanent Magnet) type undulator which can be in vacuum or out vacuum type. A lot of experiences are accumulated in this kind of planar undulator for error control and tuning procedures. It achieves comparatively higher flux density and it is believed that the tight SASE-XFEL undulator requirements can be met.

The basic magnetic structure of the undulator will be a Halbach type hybrid structure that use strong rare earth high performance magnets and ferromagnetic poles. This type can produce higher flux density and the field is mostly dominated by the mechanical manufacturing accuracy instead of less controllable material property of the magnets. Due to these advantages, the ambitious EURO-XFEL at DESY, SLAC LCLS (Linac Coherent Light Source) and SCSS at SPring8 projects are planning to use the Halbach hybrid type undulator.

INSERTION DEVICES FOR SESAME

Hamed Tarawneh, Geatano Vignola

SESAME, c/o UNESCO Amman Office, P.O. Box 2270, Amman 11181, Jordan

Abstract

The Phase-I SESAME beamlines have been defined by the scientific research programme of the SESAME users and Insertion Devices (IDs) will be the primary photon sources. It foresees two planar wigglers dedicated for WAFS/XRF and powder diffraction beamlines covering spectral range of 3-30 keV and 3-25 keV respectively, one elliptically polarizing undulator dedicated for Photo-absorption spectroscopy that covers a spectral range of 0.1-1 keV, one undulator dedicated for material science that covers 8-12 keV, one In-vacuum undulator dedicated for MAD protein crystallography covering 5-15 keV and two IR ports from a bending magnet dedicated for IR Spectromicroscopy covering 0.01-1eV. This paper describes the proposed designs for the first two devices and their effects on the SESAME lattice [1].

INTRODUCTION

SESAME is a third generation synchrotron light source, with an electron beam energy of 2.5 GeV and 400 mA beam current, located in Allan, Jordan. The SESAME storage ring is optimized for the use of Insertion Devices (IDs) and can allocate up to 12 IDs which will serve the SESAME users community. In this note, the magnetic design for two IDs, Hybrid Multipole Wiggler (HMW) and an Elliptically Polarizing Undulator (EPU), suitable for the Phase-I beamlines of SESAME will be presented.

Both devices fulfill the electron beam stay clear requirements defined by the SESAME lattice leading to an acceptable vacuum lifetime. The beam lifetime is an important issue for the 2.5 GeV SESAME storage ring since the injection energy is 800 MeV and top-up injection will be implemented in a second stage.

The magnetic design and optimization of the two IDs was done using the computer codes Radia [2] and FEMM [3] whereas the characteristics of the output photons are studied with the SPECTRA code [4]. The effects of the IDs on the electron beam were studied numerically using the particle tracking code BETA [5].

EPU UNDULATOR

The Apple-II type helical undulator[6] has been chosen to provide high flux circularly polarized radiation in the soft X-ray spectral range. This magnet will operate out of vacuum with minimum magnetic gap of 13 mm, period length of 60 mm and 28 periods. This satisfies a stay clear aperture 8.5 mm for an ID length of about 2 m [1] and fundamental photon energy of elliptically polarized light less than 100 eV at the minimum undulator gap.

In this undulator, NdFeB magnet blocks with a remanent field B_r= 1.22 T and a relative permeability of 1.05

parallel to and 1.17 perpendicular to the easy axis of the blocks are used. The blocks have a thickness of ¼ period and 40 mm × 40mm cross section with 5 mm × 5mm cuts needed to clamp the blocks in the holders.

The magnet structure has four sub-assemblies, two above and two below the beam axis. By moving the sub-assemblies longitudinally relative to each other, the relative strength of the transverse components of the magnetic field is altered leading to change in the polarization of the emitted radiation. Only the helical mode of operation has been considered where horizontal, vertical and elliptical polarized light can be obtained.

An asymmetric layout has been adopted for the SESAME EPU, i.e. the vertical magnetic field has the same polarities at the entrance and exit of the magnet, with the end sections of the Elettra type [7]. The achieved magnetic flux densities for the three modes of operation as a function of the undulator gap and phase are shown in Fig. 1. Tab. 1 summarizes the main magnetic properties of the SESAME EPU at minimum gap.
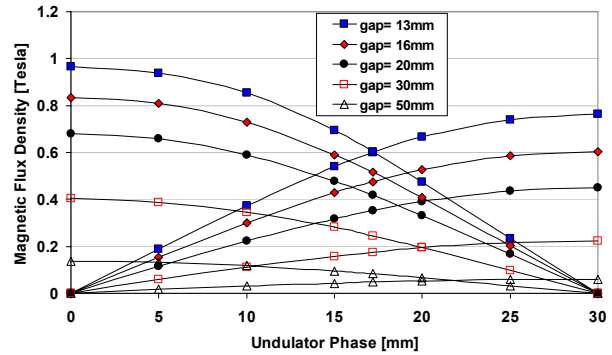
Figure 1: On-axis magnetic flux densities of the SESAME EPU undulator at different gaps and phases.

Table 1: Flux densities, K-values and minimum photon energies at minimum gap of 13 mm.

Undulator Phase	B_x [T]	B_z [T]	K-value	Ph Energy [eV]
Horizontal. 0mm	-	0.97	5.44	62
Circular 17.2mm	0.60	0.60	3.36	79
Vertical 30mm	0.76	-	4.26	98

HMW WIGGLER

The HMW will provide photon energies from 3-25 keV, which are defined by the scientific case of the SESAME. The HMW is a hybrid device with period length of 160 mm, a minimum gap of 14.5 mm, maximum flux density of 2.10 Tesla and total magnetic length of 3.092 m.

The magnet configuration consists of NdFeB magnet blocks with B_r= 1.3 T to produce the magnetic field and Vanadium Permendur material is chosen for the pole

BEAM DYNAMICS EFFECTS WITH INSERTION DEVICES FOR THE PROPOSED 3 GEV RING IN TAIWAN

H. C. Chao*, C. C. Kuo,

NSRRC, Hsinchu 30076, Taiwan, R. O. C.

S. Y. Lee

Department of Physics, Indiana Univeristy, Bloomington, Indiana, 47405, USA

Abstract

The effects of insertion devices on beam dynamics of storage rings were studied. We will focus on the changes of the emittance and the energy spread in the presence of insertion devices. Formulas for the beam emittance and the energy spread with insertion devices are also derived, in which an intrinsic parameter depending on the design of the lattice is introduced in the calculations. Simulation results and comparisons of achromatic and non-achromatic cases in the proposed 3 GeV synchrotron radiation light source in Taiwan are shown.

INTRODUCTION

A new 3 GeV third generation synchrotron radiation light source is proposed by National Synchrotron Radiation Research Center (NSRRC) in Taiwan[1]. The circumference of the storage ring is 486 m with natural emittance 1.7 nm-rad for non-achromatic case and 5.2 nm-rad for achromatic case. The twiss functions of non-achromatic case are shown in Figure 1. The lattice has a structure of 24 cells of DBA with 6-fold symmetry. It has 24 straights including 6 long straights (10.9 m) and 18 standard straights (5.8 m) for injection or insertion devices (IDs).
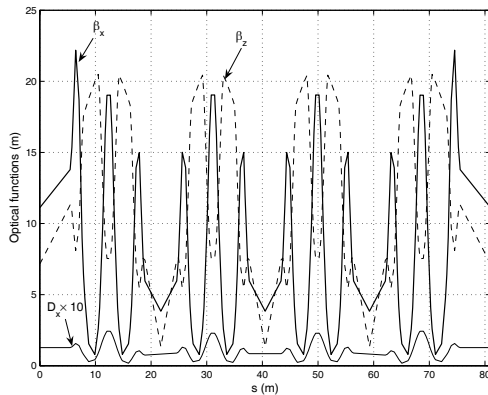
Figure 1: Optical functions of one superperiod (non-achromat lattice)

IDs are often used to produce partial coherent light or to shift energy ranges of synchrotron radiation light source.

* hjjhao@nsrrc.org.tw

In the meanwhile, they bring some effects on electron beam parameters. First consider the synchrotron radiation integrals defined by

$$I_2 = \oint \frac{1}{\rho^2} ds \qquad (1)$$

$$I_3 = \oint \frac{1}{|\rho|^3} ds \qquad (2)$$

$$I_4 = \oint \frac{D_x}{\rho} (\frac{1}{\rho^2} + 2K) ds \qquad (3)$$

$$I_5 = \oint \frac{\mathcal{H}}{|\rho|^3} ds, \text{ where } \mathcal{H} = \frac{D_x^2 + (\alpha_x D_x + \beta_x D_x')^2}{\beta_x} \qquad (4)$$

The integrals are taken over the whole ring. K is the focusing function. β_x is the horizontal betatron amplitude funcion and $\alpha = -\beta_x'/2$. D_x is the horizontal dispersion function and D_x' is its differential.

Some important parameters of beam dynamics can be characterized by synchrotron radiation integrals.

- Energy loss per turn

$$U_0 = C_\gamma \frac{\beta^3}{2\pi} E^4 I_2 \approx \frac{C_\gamma E^4 I_2}{2\pi} \qquad (5)$$

$$C_\gamma = \frac{4\pi}{3} \frac{r_0}{(mc^2)^3} = 8.85 \times 10^{-5} \text{ m/(GeV)}^3$$

- Energy spread

$$(\frac{\sigma_E}{E})^2 = C_q \gamma^2 \frac{I_3}{2I_2 + I_4} \qquad (6)$$

$$C_q = \frac{55}{32\sqrt{3}} \frac{\hbar}{mc} = 3.83 \times 10^{-13} \text{ m}$$

- Natural emittance

$$\varepsilon_{x0} = C_q \gamma^2 \frac{I_5}{I_2 - I_4} , \qquad (7)$$

where r_0 and m are the radius and the mass of the particle (here electron); γ is the Lorentz factor; c is the speed of light in vaccum; E is the particle energy; and $\hbar$ is Planck's constant.

EFFECTS OF INSERTION DEVICES

Adding IDs brings additional magnitudes of synchrotron radiation integrals. Taking this effect into account the

A HAMILTONIAN FOR WAVE LENGTH SHIFTER AND ITS STUDIES ON INDUS-1

Ali Akbar Fakhri*, and Gurnam Singh

Raja Ramanna Centre for Advanced Technology, Post - CAT, Indore – 452 013

Abstract

The INDUS-1 is a 450 MeV synchrotron radiation source for the production of VUV radiation. In order to produce the radiation of shorter wavelengths ($\lambda_c = 31$ A^o), a superconducting wavelength shifter (WLS) with peak field of 3T is being considered for Indus-1. In this paper, L. Smith's Hamiltonian for Halbach's magnetic field model has been re-derived to estimate focussing component under the compensated electron beam trajectory transformation. Various linear compensation schemes are presented to minimize the linear effects of WLS and its effects on machine operation are also theoretically studied.

INTRODUCTION

It is well known that an insertion device perturbs [2,3] the motion of an electron in storage rings. It produces the linear and non-linear beam dynamics effects. In the case of the WLS nonlinear contribution would be small but due to its linear effect, linear optics will be distorted and it will disturb the nonlinear optics of the ring. So it is necessary to predict precisely quadrupole component for WLS. For this purpose, Hamiltonian for WLS has been rederived for compensated electron bump trajectory transformation and its effects on Indus-1 machine operation are studied theoretically.

A HAMILTOINAN FOR WAVELENGTH SHIFTER

Magnetic Field

The components of the transverse magnetic field in a WLS with finite pole width may be obtained from Halbach's [1] expression.

$$B_x = \frac{k_{mx}}{k_{my}} B_m \sinh k_{mx} x \sinh k_{my} y \sin k_m (z - c_m)$$

$$B_y = B_m \cosh k_{mx} x \cosh k_{my} y \sin k_m (z - c_m)$$

$$B_z = -\frac{k_m}{k_{my}} B_m \cosh k_{mx} x \sinh k_{my} y \cos k_m (z - c_m)$$

$$k_{mx}^2 + k_{my}^2 = k_m^2 = (\pi / d_m)^2$$

If k_{mx}^2 is small then $k_{my}^2 \sim k_m^2 \sim (\frac{\pi}{d_m})^2$ and $B_1 = B_3 = -\frac{B_2 d_2}{2 d_1}$

Where subscripts m denotes pole number 1,2, 3, B_m is used to denote peak magnetic field, d_m is used to represent corresponding pole length and c_m denotes phase adjustment (c_1=0, c_2=d$_1$ c$_3$=d$_1$ +d$_2$) for different pole. In

_____

* fakhri@cat.ernet.in

present case d$_1$= d$_2$= d$_3$ & $k_{x1} = k_{x2}$. B_2 is the its' peak magnetic field and x, y and z are horizontal, vertical and beam directions respectively.

Electron beam trajectory

The equation of motion for the first pole in the horizontal plane, with coshk_xx~1and y=0. is :

$$\frac{d^2 x}{ds^2} = \frac{B_2}{2 B \rho} \sin k (s - c_1)$$

Where ρ =radius of curvature in the field B and ds = vdt
The first integral of equation is

$$\frac{dx}{ds} = -\frac{B_2}{2 k B \rho} [\cos k (s - c_1) - 1]$$

By using the relation $z_e'^2 = 1 - x_e'^2 \sim 1$
After second integration

$$x = -\frac{B_2}{2 k B \rho} \left[\frac{\sin k (s - c_1)}{k} - s \right]$$

Similarly for the second pole and third pole, we can write

$$x = \frac{B_2}{k_2 B \rho} \left[\frac{\sin k (s - c_2)}{k} + \frac{d}{2} \right]$$

$$x = -\frac{B_2}{2 k B \rho} \left[\frac{\sin k (s - c_3)}{k} + s - 3d \right]$$

In above equations on right hand side second additional term is due to compensated electron bump trajectory.

A Hamiltonian for Betatron motion

The Hamiltonian of the motion of an electron under above magnetic field [2] can be written as,

$$H = \frac{1}{2} \left[p_z^2 + (p_x - A_x \cos k_m (z - c_m))^2 + (p_y - A_y \cos k_m (z - c_m))^2 \right]$$

Where: $A_{mx} = -\frac{B_m}{k_m B \rho} \cosh k_{mx} x \cosh k_{my} y$

$$A_{my} = \frac{B_m k_{mx}}{k_{my}} \frac{\sinh k_{mx} x \sinh k_{my} y}{k_m B \rho}$$

A canonical transformation is required to change variables from (x, y, z) to (x_β, y_β, s) where s is distance along the equilibrium orbit, x_β is a displacement in the (x, z) plane perpendicular to the equilibrium orbit and $y_\beta = y$ is vertical displacement from the equilibrium orbit. Transformation between variables for first pole, second pole and third pole can be written as

$$x = x_e + z_e' x_\beta = x_e - \frac{B_2}{2 k B \rho} \left[\frac{\sin k (s - c_1)}{k} - s \right] \sim x - a_1$$

$$z = s - x_e' x_\beta = s - x_e' \frac{B_2}{2 k B \rho} \left[\frac{\sin k (s - c_1)}{k} - s \right] \sim s$$

ILC ACTIVITY AT JINR AND SITING IN DUBNA REGION

Yu.Budagov, Yu.Denisov, I.Meshkov, G.Shirkov, A.Sissakian, G.Trubnikov[#].
Joint Institute for Nuclear Research, Dubna, 141980, Russia

Abstract

JINR actively participates in ILC project. JINR physicists are taking part in several fields of activity in ILC: works on photo injector prototype, participation in design and construction of cryomodules, laser metrology, etc. Moreover Joint Institute is officially approved candidate for possible hosting of ILC in the region near Dubna. International intergovernmental status of JINR, comfortable location of site, well developed infrastructure, geological, climate and relief conditions may become powerful advantages of Dubna siting among other proposals of ILC location. All above mentioned topics are discussed in the presented report.

INTRODUCTION

Prominent achievements of the fundamental science form the material and technical basis of the modern civilization. The crucial role here belongs to the elementary particle physics. Its main discoveries and laws are the result of complicated experiments, many of which have been carried out on beams of the elementary particle accelerators.

Expressing the undivided opinion of many leading scientists of the present time, the International Committee for Future Accelerators (ICFA) and the International Union of Pure and Applied Physics (IUPAP) declared about the major decision to join efforts of world scientific centers in construction of the advanced accelerating complex – the International Linear Collider (ILC) [1].

The unprecedented task of the ILC is to provide measurements in the field of elementary particle physics at the unprecedented accuracy in the wide region of maximally high energies of colliding particles (electrons and positrons). The possibility of energy variation (in the system of the center of mass of colliding particles from 500 to 1000 GeV) is of key importance to provide the maximal accuracy of measurements.

Today the ILC project is seen as a completely international scientific project, which must be developed, financed, governed, maintained and exploited in the framework of the wide international scientific cooperation organized properly.

The following main parameters of the facility are recommended at the international meeting in Snowmass. The luminosity at the energy of electrons 500 GeV is $2 * 10^{34}$ cm^2 s^{-1}. For a 500 GeV facility based on the resonator of the TESLA type the maximal acceleration rate of all the 20000 resonators must be 35 MV/m and operating gradient – 31.5 MV/m at the length of each of two linear accelerators 10.6 km. At the subsequent increase of energy up to 1 TeV the resonators having the maximal gradient 40 MV/m and operating gradient 36 MV/m are recommended, which will lead to the increase

of length for 9.3 km of each of two linear accelerators (Fig.1). In this case, the total length of two linear accelerators will be about 40 km and the length of the whole facility (total tunnel length) – about 50 km.

Figure 1. Schematic layout of the 500 GeV machine

PROJECT ORGANIZATION

Organization and scale of the works to construct the ILC accelerator are unprecedented. Wide interstate relations at every stage of the project realization will allow the participants to use mutually the best scientific and technological achievements in their countries. Involvement of scientists and specialists from the Russian Federation (RF), JINR and its Member States in a high-tech project of the accelerator construction of such scale will contribute to accelerated development of advanced technologies in these countries and, first of all, in Russia. By now scientific, technological and organizational development in the framework of the ILC project has started. In accordance with the schedule, the basic and alternative configurations of the facility have been formulated at the end of 2005. As a result, the Baseline Configuration Document (BCD) has been prepared. On the basis of this document in the course of 2006 the designing is carried out, the cost is estimated and the physical program of investigations at ILC is formed. The accelerator project is worked up by scientists and specialists from leading research centers and engineering companies of America, Asia, Europe, including Russian Institutes and JINR in Dubna.

COST OF THE PROJECT

Currently, cost of the full-scale ILC project is estimated about 8-9 B$, by the GDE. The estimate is performed for the ILC length of 50 km and is obtained by the extrapolation of the approximate cost of the TESLA collider, 33 km long, (Germany). The cost of experimental installations is not included here. Expenses for labor resources are not taken into account either, since they are proposed to be covered by the organizations participating in the project. The given estimate will be corrected after preparation of the BCD document, which will make the ILC parameters clearer.

By the GSPI (Moscow) specialist estimate, in case of placing the accelerator in the vicinity of Dubna, the total cost of building and assembly works of underground and

ENERGY EQUALIZATION BY USING S-BAND AND X-BAND ACCELERATOR MODULES

Kazue Yokoyama[#], Takuya Kamitani

Accelerator Laboratory, High Energy Accelerator Research Organization (KEK),

1-1 Oho, Tsukuba, Ibaraki 305-0801, Japan

Abstract

To reduce the beam loss and to restrict the expanse of the bunch length of the positron beam from the KEKB injector, an energy spread of ± 0.25% or less is required for the beam-transport (BT) line of the KEKB ring [1]. Generally, a positron beam has a large energy spread because the original bunch length is large and all positrons do not see the same accelerating field. Thus, an energy compression system (ECS) that consists of a magnetic chicane and two 2-m S-band accelerating structures was implemented at the end of the linac and has been used, but it has a demerit that the beam bunch is lengthened [2]. In this paper, we propose a new method to suppress the energy spread without enlarging the bunch length. This method utilizes superimposed acceleration of the S-band modules and X-band modules.

ENERGY COMPRESSION BY USING DIFFERENT FREQUENCY

A large energy spread of a positron beam is due to a position dependence of the energy gain. Assuming that the energy gain of beam particles riding on the rf wave crest is to be E_{e^+} at the end of the linac, the total energy gain of the linac can be approximately expressed as

$$E_{total\ gain} = E_{e^+} \cos(2\pi \frac{z}{\lambda_s}) \qquad (1),$$

where z is the distance from the centre of the bunch and λ_s is the wavelength of the S-band frequency. Equation (1) signifies that a large energy spread of the positron beam is due to a position dependence of the energy gain, considering that its original bunch length is large. Therefore, the positrons away from the centre bunch require a higher electric field to compensate for the energy variation. A correction function can be obtained by the Taylor expansion up to the 2nd order; it is proportional to the square of z, as follows:

$$E_{equalizer} = E_{e^+} - E_{e^+} \cos(2\pi \frac{z}{\lambda_s}) \approx \frac{1}{2} E_{e^+} (2\pi \frac{z}{\lambda_s})^2$$

(2)

The correction function, which is proportional to the square of z, can be realized by superimposing a different frequency of the same energy gain as the S-band. It can be expressed as

---

[#] Kazue.Yokoyama@kek.jp

$$E_{equalizer} = \Delta E \cos(2\pi \frac{z}{\lambda_s}) - \Delta E \cos(2\pi \frac{z}{\lambda_a})$$

$$= \Delta E \cos(2\pi \frac{z}{\lambda_s}) - \Delta E \cos(2\pi \frac{z}{\lambda_s} \times k) \qquad (3),$$

$$\approx \Delta E \times \frac{1}{2}(2\pi \frac{z}{\lambda_s})^2 (k^2 - 1)$$

where λ_a is the wavelength of the rf frequency, which we try to use, also $\lambda_s = k\ \lambda_a$. To compensate for energy variation up to the 2nd order, an acceleration of

$$\Delta E = \frac{E_{e^+}}{k^2 - 1} \qquad (4)$$

is required from Eq. (2) and Eq. (3).
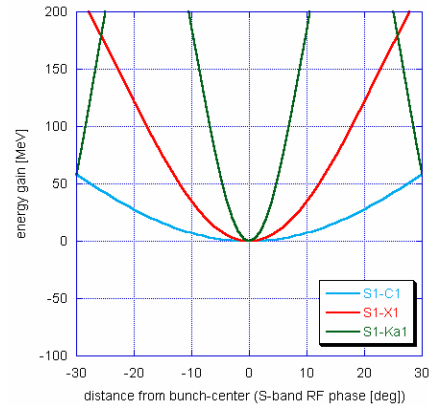
Figure 1: Comparison of the correction functions for three different frequencies with same energy, ΔE.

The legends of S1-C1, S1-X1 and S1-Ka stand for C-band ($k = 2$), X-band ($k = 4$) and Ka-band ($k = 10$), which are innovated for compensation, respectively.

Figure 1 shows that energy gain depending on the rf frequency which supplies the accelerating electric field when the correction function is obtained with the same energy, ΔE = 160 MeV corresponds to the energy of an accelerator module of the KEKB injector. This shows that a higher frequency is more effective for compensation than a lower frequency when comparing it with the same energy of the energy correction. For example, an energy of about 1166 MeV from the C-band ($k = 2$) module is required to compensate for a 3.5 GeV positron at the KEKB injector, while it is achieved by an energy of only about 233 MeV from the X-band ($k = 4$) module. Thus, in this method, innovating X-band modules is more practical than the C-band modules for savings in both cost and space. In addition, the aperture of a X-band accelerating structure is one 4th the size of the S-band accelerating

NEW TIMING SYSTEM FOR THE L-BAND LINEAR ACCELERATOR AT OSAKA UNIVERSITY

Shigeru Kashiwagi*, Goro Isoyama, Ryukou Kato, Shoji Suemine
ISIR, Osaka University, 8-1 Mihogaoka, Ibaraki, Osaka 567-0047, Japan
Takao Asaka, Yoshitaka Kawashima
SPring-8, 1-1-1, Kouto, Mikazuki, Sayo-gun, Hyogo 679-5198, Japan

Abstract

A highly precise and flexible timing system has been developed for the L-band linac at ISIR, Osaka University. It provides four RF signals and several timing signals for operation of the linac and for experiments with the linac. In order to realize long-term stability of the timing system and hence operation of the linac, a rubidium atomic clock producing a 10 MHz RF signal with the fractional stability of 10^{-15} is used as a time base for the synthesizer used as a master oscillator for generating the acceleration frequency of 1300 MHz. The 1300 MHz signal from the master oscillator is directly counted to produce the four RF signals and the clock signal of the timing system at 27 MHz. The master timing signals for linac operation is taken from the AC line frequency and it is precisely synchronized with the 27MHz clock signal. To make an arbitrary delayed timing signal, a standard digital delay generator is used to make a gate signal for a GaAs RF switch, with which one of the 27MHz clock pulses is sliced out to generate the delay timing signal. Any timing signal can be made in an interval of 37 ns and the timing jitter of the delayed signal is achieved to be as small as 2 ps (rms).

INTRODUCTION

The L-band electron linear accelerator is used for studies on nanotechnology and beam science as well as for basic studies in the related fields at the Radiation Laboratory of the Institute of Scientific and Industrial Research (ISIR), Osaka University. The L-band linac can produce electron beams of different time structures, like a single-bunch, multi-bunch with 9.1 ns spacing and so on, corresponding to various beam experiments. The high intensity single-bunch beam is the most characteristic beam of this L-band linac and it is very useful for radiation chemistry studies by means of pulse radiolysis in the time range down to sub-picoseconds [1,2] and basic study of Self-Amplified Spontaneous Emission (SASE) in the far-infrared region [3,4].

The timing system of the linac plays a very important role in generating a high quality and stable electron beam. Timing jitter between a trigger signal for the electron gun and a reference RF signal of accelerator system directly affects the stability of the electron beam in terms of intensity and energy. Experiments using the L-band linac require synchronized trigger pulse for their data acquisition, and RF signals for laser oscillator. In order to enhance the stability of the linac, we have developed a new highly precise and flexible timing system for the L-band linac at ISIR, Osaka University.

CONFIGURATION OF L-BAND LINAC AND LASER SYSTEM

The fundamental accelerating frequency of the L-band linac at ISIR is 1300 MHz. The linac has been optimized for generating the high-intensity single-bunch beam. The L-band linac is consisted of a high-current triode electron gun, three stage sub-harmonic bunchers (two operate at 108 MHz, which is a 12th subharmonic of the fundamental frequency and one at 216 MHz, a 6th of 1.3GHz), two fundamental traversing wave bunchers and 3m-long main accelerating structure. The SHB system is used mainly for single-bunch operation. The timing system is required to generate three RF signals for these RF components.

Two grid pulser circuits of the electron gun are used for generating single-bunch and multi-bunch beam. The trigger pulse for the gun grid has to be synchronized with RF signals precisely. In single-bunch operation, one trigger pulse for the gun grid with 120V height and 50ns duration is distributed from the timing system. In multi-bunch operation, two triggers for a start and a stop of pulse are necessary to decide the pulse length of multi-bunch beam in the grid pulser circuit. The trigger pulse for single-bunch and the start trigger of multi-bunch generation are common, and the input trigger pulse for the trigger circuit of the gun is switched by operation mode of the linac.

The femtosecond laser system for picosecond pulse radiolysis experiment consists of a CW green laser, a femtosecond Ti:sapphire laser operated at 81 MHz, Nd: YLF laser with a regenerative amplifier operated at 960 Hz, an optical parametric amplifier (OPA) and pulse generator. Thus, the laser system requires 81 MHz RF signal and 960 Hz and 60Hz trigger pulses to the timing system of the linac.

NEW SYNCHRONOUS TIMING SYSTEM

To achieve the stable and precise synchronization between RF signals and trigger pulses for the accelerator system, the timing system has been replaced with a new one. The new timing system of the linac comprises of a master RF part and a synchronous timing part. It provides four synchronous RF signals and a 27 MHz clock signal as well as various timing signals for operation of the linac and for the experiments. Fig. 1 shows a block diagram of new timing system for the L-band linac.

_____
*shigeruk@sanken.osaka-u.ac.jp

03 Linear Colliders, Lepton Accelerators and New Acceleration Techniques

A08 - Linear Accelerators

PERFORMANCE OF THE RENEWED L-BAND LINAC AND RECENT PROGRESS OF DEVELOPMENT OF FEL AND SASE AT OSAKA UNIVERSITY

G. Isoyama, T. Igo, S. Kashiwagi, R. Kato, Y. Kon, S. Suemine, T. Yamamoto, ISIR, Osaka

Abstract

The 40 MeV, L-band electron linac at the Institute of Scientific and Industrial Research, Osaka University is used for various studies on advanced beam sciences. The linac was constructed in 1975-1978 and largely remodeled in 2002-2004 for higher operational stability and reproducibility. We have evaluated performance of the renewed linac. The beam intensity is measured for longer than an hour at the exit of the linac operated in the transient mode for pulse radiolysis experiments in the nanosecond region. The intensity fluctuation is 0.27 %, which is one tenth of the value before remodeling. We are conducting development of an FEL and basic study of SASE in the far-infrared region with the linac. The experiment was suspended and resumed again after the remodeling. We have developed a strong focus wiggler for FEL and SASE based on the edge-focusing scheme, which can make the current density of the electron beam and hence the gain of FEL higher. The renewed linac can provide a long pulse electron beam up to 8 us for FEL and we are now commissioning the linac in this operation mode. We will report the performance of the renewed linac and recent development of FEL and SASE.

PAPER NOT YET RECEIVED

PROGRESS OF RFQ ACCELERATORS AT PEKING UNIVERSITY*

C.E.Chen Z.Y.Guo J.X.Fang Y.R.Lu X.Q.Yan K.Zhu S.X.Peng Z.Wang C.Zhang
S.L.Gao J.F.Guo W.G.Li Z.Z.Song J.X.Yu M.L.Yu
IHIP, School of Physics, Peking University, Beijing 100871, P.R.China

Abstract

The progress of two RFQ accelerators at Peking University is presented: one is Separated Function RFQ (SFRFQ), which separates the focusing and acceleration of traditional RFQ to get higher acceleration efficiency. The first prototype of the SFRFQ is designed to accelerate O^+ from 1MeV to 1.5MeV and used as a postaccelerator for ISR RFQ-1000 (Integral Split Ring) [1]. The other is high current deuteron 201.25MHz RFQ, it will accelerate 50mA D+ beam to 2MeV with a duty cycle of 10%. The design study of SFRFQ and high current Deuteron RFQ accelerator are outlined.

INTRODUCTION

The RFQ accelerators are extensively used to accelerate low energetic heavy ions and proton nowadays. Accelerator Driven Subcritical system (ADS), Spallation Neutron Source and other applications drive the RFQ developing towards high average beam power [2-4]. The RFQ team at Peking University has been engaged in developing RFQ technology since 1980s. A 300keV heavy ion Integrated Split-ring Resonator RFQ (ISR RFQ-300) with the mini-vane electrodes was constructed and put into operation in 1994[5]. Based on these experiences, A 1MeV heavy ion ISR RFQ was completed and run successfully in 2000[6]. The experiment [7] and simulation [8] for simultaneous acceleration of both positive and negative ions were realized.

To increase accelerating efficiency, a new accelerator structure, Separated Function RFQ (SFRFQ), has been proposed and investigated. It separates the transverse field for the focusing and axial component for ion acceleration by inserting a series of periodical gaps [9-12]. In order to explore the feasibilities of SFRFQ, a prototype is going to be manufactured. A match section between 1MeV RFQ and SFRFQ is designed for the transverse emittance matching. Meanwhile to upgrade the beam current to mA for ISR RFQ-1000, a new designed ECR ion source for this accelerator has been developed in the last two years [13].

A high power Deuteron RFQ accelerator has been launched for neutron radiography. The beam dynamics has been studied in detail and improved by equipartition method[14-16]. The RFQ structure, mechanical and cooling system design have been investigated.

SFRFQ

SFRFQ is an accelerating structure which is suitable for accelerating middle energy beam [10]. A SFRFQ prototype is being constructed to explore its feasibilities, which compose an accelerating system with ISR-1000. The whole system include ECR ion source, LEBT, ISR1000, match section and SFRFQ. Figure 1 gives the sketch map. Figure 2 shows SFRFQ's structure schematically, where diaphragms were mounted onto the electrodes.
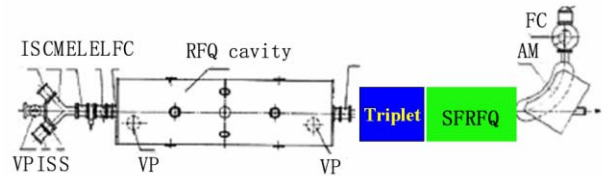
Fig. 1: Accelerating system composed by ISR-1000 and SFRFQ
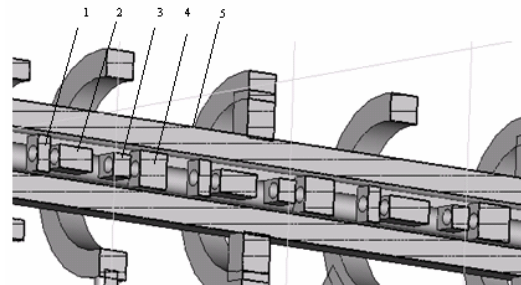
Fig. 2: Schematic view of the SFRFQ 1,2,3&4 diaphragm, 5 electrode
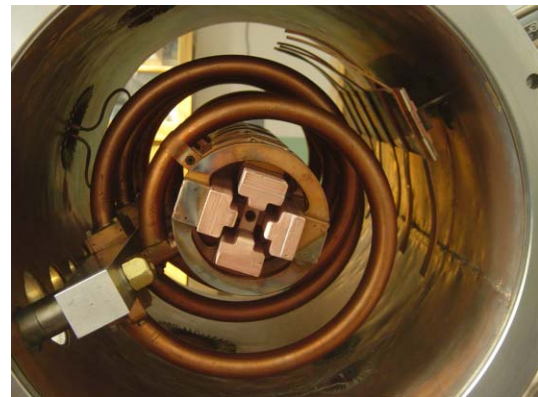
Fig. 3: Power test model of SFRFQ

STATUS OF THE CTF3 FREQUENCY MULTIPLICATION RINGS

A. Ghigo*, C. Biscari*, R. Corsini, S. Doebert, G.Geschonke, F. Marcellini*, L.Rinolfi,

M.Serio, A. Stella*, F. Tecker, P. Urschütz

CERN, Geneva, Switzerland. *INFN-LNF, Frascati, Italy

Abstract

The CLIC Test Facility (CTF3) is in construction at CERN by an international collaboration to demonstrate the feasibility of the two beam acceleration scheme at the CLIC parameters. The drive beam of CTF3 is accelerated by a fully loaded Linac that generates a long bunch train and two rings that provide the high current and bunch frequency multiplication by interleaving bunch trains. The status of the commissioning of the first ring (Delay Loop) and of the transfer lines are reported together with the installation of the second ring (Combiner Ring).

INTRODUCTION

The Compact LInear Collider (CLIC) Test Facility project [1,2] has the aim to demonstrate the feasibility of a 3 TeV electron-positron linear collider with reasonable length and cost using the dual beam accelerator scheme [3,4,5]. The layout is shown in Figure 1.

The two main characteristics of the CLIC accelerators are:

- the high accelerating gradient (>100MV/m) in high frequency RF accelerating cavities
- the production of high RF power by extracting power from a low energy high intensity electron beam, the Drive Beam, manipulated in order to create the appropriate time structure.

An international collaboration has been set to develop the CTF3 project with the following participating Institutes: Ankara Un. (Turkey); BINP, JNR, IAP (Russia); CCLRC-RAL (UK); CERN; CIEMAT, UPC, IFC (Spain); DAPNIA, LAL, LAPP, LURE (France); HIP (Finland); INFN-LNF (Italy); KEK (Japan); LLBL, LBL, NW Un., SLAC (USA); PSI (Switzerland); RRCAT (India); Uppsala

Un.(Sweden) Incoming partners are Pakistan, Iran, Cockroft Inst., J.Adams Inst., JLAB, EPFL, INFN-Mi.

CTF3 is based at CERN in the building that hosted the LEP pre-injector complex, whose hardware and infrastructure are largely reused. Drive Beam is generated by a fully loaded Linac, 70 m long, followed by two rings in which the beam manipulation is performed: the Delay Loop (DL) 42 m long and the Combiner Ring (CR) 84 m long.

The drive Linac operates at 3 GHz and produces electron beam pulse trains at the energy of 150 MeV with a 1.4 μsec pulselength and 3.5A current at 1.5 GHz bunch frequency. The Linac RF power is transferred to the electron beam and an efficiency of 94% has been measured.

A RF power production station has been also installed, halfway along the linac, to test the RF power extraction structures (PETS). The electron beam is alternatively extracted in a dog-leg line and is sent to the PETS: the 30 GHz power extracted is transferred through 30 GHz waveguide to an external laboratory where the accelerating structures are conditioned and tested.

In the frequency multiplication system successive trains of bunches coming from the Linac are interleaved in the two rings by injecting with RF deflectors.

The time structure necessary for the recombination process is produced in the injector: a high current thermoionic electron gun is followed by three sub-harmonic buncher cavities at 1.5 GHz and 3 GHz bunching system. The sub-harmonic cavities and their sources are wide-band system and allow fast phase shift along the bunch train. The 1.5 GHz electron pulse, 1.4 μsec long, is composed by up to 10 sub trains in which the phase is shifted by 180.
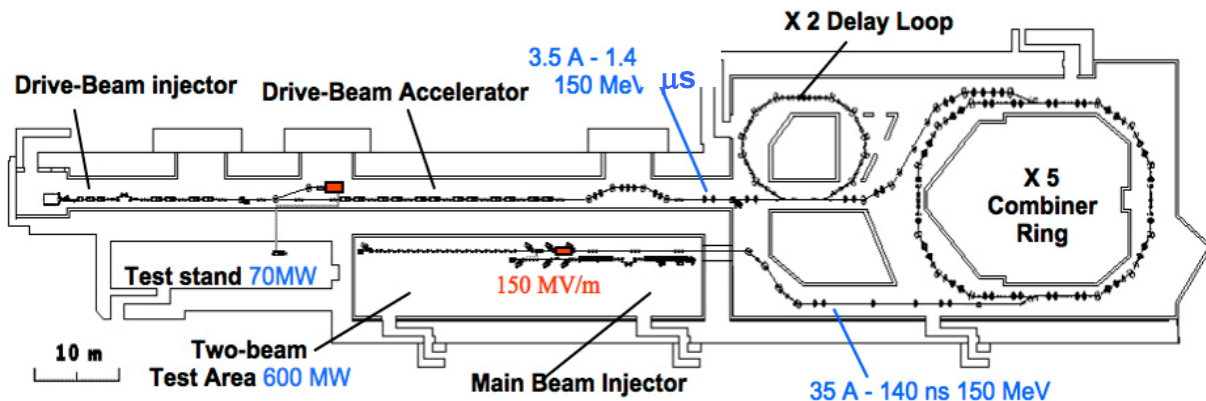
Figure1: CLIC Test Facility accelerator and building layout.

DESIGN AND DEVELOPMENT OF BEAM TRANPORT ELEMENTS FOR BARC-ECIL LINAC

P. Roychowdhury, P. Jain, D.P. Chakravarthy, K. C. Mittal, and A. K. Ray

Accelerator and Pulse Power Division

Bhabha Atomic Research Centre, Mumbai- 400 085

Abstract

A 10 MeV, 2 kW RF electron linac is under development for cargo scanning. It consists of electron gun, RF linac structure, solenoid focusing magnets, steering magnet, beam diagnostics and x-ray target. To obtain properly resolved x-ray images, a beam diameter of 2mm is required at the target. Since the beam diameter at the target is critical; the transverse beam optics of the whole RF accelerator from gun end to the target has been simulated by solving the beam envelope equation. The envelope equation has been solved using Runga Kutta method consisting of external focusing field, RF field, space charge field and emittance. Various combinations of solenoid magnet focusing have been studied. It has been found that two solenoid magnets in the gun region and one after the linac region are sufficient to transport the beam and focus to a diameter of 2mm at the target. Based on these studies three solenoid magnets have been designed and fabricated.

INTRODUCTION

The industrial linacs are now making a major contribution to cargo inspection for manifest verification. This kind of system can easily inspect the contraband goods hidden in high density materials or fully loaded containers/ vehicles and show high quality scanning images. A 10 MeV, 10 kW RF linac for industrial application [1] has been installed at electron beam centre (EBC), Kharghar, Navi Mumbai and commissioned with 10 MeV, 15 mA, 10 µs pulse at 100 Hz PRF. The system consists of LaB_6 based electron gun injected into a standing wave on-axis coupled cavity linac, which accelerate the beam to energy of 10 MeV. A 2856 MHz, 3.5 MW Klystron based RF power source has been used to established the required electric field inside the linac. A similar system with x-ray target is under development at ECIL, Hyderabad for cargo scanning. This linac as a radiation source will be situated in a shielded room with concrete walls.

The electron gun of the linac produces electron beam of 50 keV, 10 µs, 100 Hz with maximum peak current ~1A. The beam is then focused by two solenoid magnetic lenses S1 and S2 and enters in the standing wave linac section L. In the drift section D1, a beam current transformer is incorporated to measure the gun current. The beam after coming out of linac hits the tantalum target T located beyond one meter concrete wall and produces x -radiation. A second beam current transformer is located in the drift region D3 to measure the beam current from the linac. A solenoid magnetic lens S3 is employed in front of the target to focus the accelerated beam to 2mm diameter.

THE ENVELOPE EQUATION

The generalized paraxial rms beam envelope equation for a cylindrically symmetric system which explicitly includes the effects of rf acceleration and external focusing is given as [2]

$$A'' + [\{\gamma'^2 (\gamma^2 + 2)\}/ 4\beta^4 \gamma^4 + K_{r,rf} + K_{r,B}] A - \beta\gamma Q/ A - \varepsilon_n/ A^3 = 0 \qquad (1)$$

where, $K_{r,rf} = 1/8 (e E_0/ \beta\gamma m_0 c^2)^2$ is the rf focusing strength, $K_{r,B} = (eB_z(z) / \beta\gamma m_0 c)^2$ is the solenoidal focusing strength and for the standing-wave accelerating structure, $\gamma' \approx e E_0 /2mc^2$. The normalized rms beam size $A = \sigma_r(\beta\gamma)^{1/2}$, the normalized rms emittance $\varepsilon_n = \beta\gamma\varepsilon$, and the perveance of the beam $Q = I/\beta^3\gamma^3 I_0$, with $I_0 = ec/r_e \approx 17$ kA for electrons. The input beam parameters of the 50 keV beam from the electron gun are the following: r = 5 mm, r' = 25 mrad, and I = 100 mA. The average accelerating gradient E_0 = 12 MV/m.
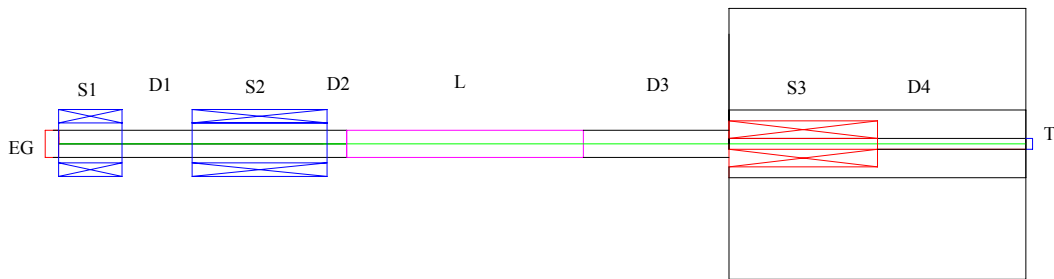
Figure 1: Schematic of beam transport elements: EG-Electron Gun, S-Solenoids, D-Drifts, L-Linac, T-Target.

HIGH QUANTUM EFFICIENCY PHOTOCATHODES FOR RF GUNS*

D. Sertore[#], P. Michelato, L. Monaco, C. Pagani, INFN Milano - LASA, Segrate (MI), Italy
F. Stephan, DESY-Zeuthen, Zeuthen, Germany
S. Schreiber, DESY, Hamburg, Germany.

Abstract

High Quantum Efficiency Photocathodes are nowadays routinely used as electron sources for laser driven RF guns. In this paper, we review the production, characterization and operation performances of the Cs_2Te photocathodes prepared at INFN Milano – LASA and operated at DESY for the FLASH and PITZ photoinjectors.

INTRODUCTION

Since the 90s, INFN Milano is involved in the study of the growth process of photocathodes based on alkali antimonide and more recently alkali telluride. The figure of merit for the photocathode characterization are the operative lifetime, the achievable current density, the extracted charge, the dark current, the sensitivity to gas exposition, the Quantum Efficiency (QE), and the uniformity of the cathode sensitive layer response.

The growth process was studied applying surface science techniques like XPS (X-ray Photoelectron Spectroscopy) and AES (Auger Electron Spectroscopy) [1]. We applied the same techniques also for investigating the response to gas exposition.

Since 1998, INFN Milano is in charge of the production of the photocathodes for TTF, now FLASH. From the year 2000, we have also responsibility for the production of the photocathodes for the PITZ facility. In the production process, we apply the knowledge gathered in previous years of R&D activities. Up to now, none of the cathodes has shown any limitation in the extracted charge, even after long periods of usage. The main reason to change cathodes during the gun operation is the growth of dark current to high values. Since the start-up of the cathode delivery, we have collected many parameters that characterize both the plug preparation and the growing process. In the following section we briefly review the preparation, characterization and operational performances of the cathodes, from their deposition at INFN Milano-LASA to their use at FLASH and PITZ.

PHOTOCATODES PRODUCTION

The Preparation System

The preparation system consists of a UHV chamber whose base pressure is few 10^{-10} mbar (low 10^{-9} mbar during cathode growing). A CF63 sapphire viewport allows the cathode illumination for photocurrent measurements. The sources for Te and Cs evaporation are

hosted on a frame that holds up to 6 sources. The Te sources are made from pure Tellurium (99.9999 %). Cs is evaporated from SAES® sources based on Cesium chromate. A circular masking system, placed in front of the cathode, shapes the round active layer (Φ= 5 mm) and assures its centering on the plug. The cathodes are loaded in the transport box and moved into the chamber by a magnetic-coupled manipulator. The box is then sent to FLASH or PITZ maintaining the UHV condition at all times.

The Coating Growth Procedure

The cathode plug is made out of pure Molybdenum with a 16 mm front surface diameter. The surface is cleaned and polished to optical quality with an automated lapping procedure. In addition to normal cleaning, some cathodes have been cleaned with a buffered chemical polishing method (BCP) or with electro-polishing (EP). Thin films of Tellurium and Cesium are then deposited in UHV condition. Tellurium and Cesium react to produce Cs_2Te. During the evaporation, the plug is heated to 120 °C. First, a thin layer of 10 nm of Tellurium is produced, and then Cesium is evaporated at a rate of 1 nm/min. The film is illuminated with UV light (λ=254 nm) of a Hg lamp to monitor the quantum efficiency. The evaporation is stopped, when the QE is at maximum. The final photoemissive layer thickness is some tens of nanometers.

For special purposes, we produce also KCsTe photocathodes that have higher QE then Cs_2Te but shorter lifetime. After the preparation, the plug is heated to 120 °C for the deposition of a 10 nm layer of Te. The temperature is then risen to 150 °C for a K layer deposition. Also in this case we use UV light from an Hg lamp to monitor the quantum efficiency. Once the maximum of the photocurrent arrives, the plug is cooled down to 120 °C for the final Cs layer deposition, until the maximum QE value is reached.

Some Statistics on Produced Cathodes

So far we have produced 51 Cs_2Te photocathodes and 2 KCsTe. 37 Cs_2Te photocathodes have been delivered to FLASH and 14 to PITZ. The overall number of uncoated Mo plugs delivered to different labs is 28 (11 to FLASH and 17 to PITZ). They are used for gun conditioning and dark current measurements.

Fig. 1 reports a summary of the QE measured at LASA for the whole photocathode production. Green dots are QE measurement before the shipment and the magenta ones after their use in the gun and return to LASA from the different labs. These data are available on-line from the Web interface to a database [2]

03 Linear Colliders, Lepton Accelerators and New Acceleration Techniques

T02 - Lepton Sources

IONS FOR LHC: STATUS OF THE INJECTOR CHAIN

D. Manglunki, A. Beuret, J. Borburgh, Ch. Carli, M. Chanel, L. Dumas, T. Fowler,
M. Gourber-Pace, S. Hancock, M. Hourican, J.M. Jowett, D. Kuchler, E. Mahner, M. Martini,
S. Maury, S. Pasinelli, U. Raich, A. Rey, J.-P. Royer, R. Scrivens,
L. Sermeus, G. Tranquille, J.-L. Vallet, B. Vandorpe

CERN, Geneva, Switzerland.

Abstract

The LHC will, in addition to proton runs, be operated with Pb ions and provide collisions at energies of 5.5 TeV per nucleon pair, i.e. more than 1.1 PeV per event, to experiments. The transformation of CERN's ion injector complex (Linac3-LEIR-PS-SPS) to allow collision of ions in LHC in 2008 is well under way. The status of these modifications and the latest results of commissioning will be presented. The remaining challenges are reviewed.

INTRODUCTION

The commissioning of the new ion injection chain for the LHC is advancing in stages, as planned [1]. After the successful first operation of the Low Energy Ion Ring (LEIR) in 2005 [2], the Proton Synchrotron (PS) has now been commissioned with the ion beam.

This paper summarizes the operation in 2006 of all the machines involved in the ion injection chain, except for LEIR which is described in a separate paper [3]. Most of the work presented here was achieved while the machines operated in parallel.

SOURCE AND LINAC 3

In 2006 the Grenoble Test Source for LHC was running most of the time for the commissioning of the LEIR and the PS with lead. During this time the source provided ~100 eµA of Pb^{27+} and Linac 3 gave more than 20 eµA of Pb^{54+}. The beam was stable and the source required very little retuning. Besides beam delivered for LEIR and PS commissioning, studies of the source biased disc were made [4] and the extraction and acceleration of Pb^{29+} was tested. With a similar ion current out of the Linac, Pb^{29+} has the advantage of lower RF fields in the tanks, which reduces the x-ray emission.

PROTON SYNCHROTRON

Beside acceleration, the role of the PS is to adapt the beam from LEIR according to a variety of constraints imposed by the downstream machines. Notably, it is the PS machine that imposes the bunch spacing required by LHC experiments, while the bunch length and repetition frequency at PS ejection must lie within the narrow ranges acceptable by the rf system of the SPS. In the nominal scheme, this requires complex rf gymnastics [5] to be performed at an intermediate energy in the PS cycle. In order to minimize the risk to beam lifetime, the intermediate plateau was chosen close to the highest

energy consistent with the frequency range of the cavities performing the gymnastics.

The aim of the commissioning period was to make sure the PS would be able to deliver the "Early beam"; the achieved performance is summarized and compared with the design values, in table 1. However, a lot of time and effort was invested to prepare the "Nominal Beam", in order to identify potential problems and devise solutions [6].

Table 1: Performance of the Early Beam. Transverse emittances are given as normalised RMS values: $\varepsilon^{*}_{H,V} = \sqrt{\gamma^2 - 1}\, \sigma^2_{H,V} / \beta_{H,V}$

	Design	Achieved
N [E8 ions/bunch]	1.20	1.1
ε^{*}_H [µm]	1.00	0.85
ε^{*}_V [µm]	1.00	0.73
$\varepsilon_{//}$ [eVs/u]	0.05	0.03
τ_B [ns]	3.9	3.0

First injection into PS ring

In order to inject ions from LEIR into the PS, the new septum in its refurbished tank and kicker previously used for antiproton transfer from PS to LEAR, are complemented by a 2-dipole bump in order to cope with the higher magnetic rigidity of the Pb^{54+} beam [5]. The first injections took place on a flat cycle to study the beam behaviour at low energy. The lower limit for the beam lifetime was measured and exceeded 700 ms, confirming the excellent quality of the vacuum in the PS.

LEIR to PS transfer line matching

The transverse matching of the beam delivered has been measured with three secondary emission profile monitors (SEM) installed in the PS. One should note that due to imperfections (one vertical monitor "blind" at the center), the vertical trajectory had to be distorted strongly for the vertical measurement. The dispersion has been determined by measuring the beam position as a function of the momentum offset and the betatron functions and emittances from the beam sizes.

During a first measurement campaign, good betatron matching, but a significant (even though acceptable in terms of induced emittance blow-up) dispersion mismatch has been observed.

Based on the first measurement, a new setting of the transfer line has been implemented and investigated

LEIR: TOWARDS THE NOMINAL LEAD ION BEAM

M. Chanel, M.E Angoletta, V. Baggiolini, P. Belochitskii, A.Beuret, A. Blas, J. Borburgh, C. Carli, K. Cornelis, T. Fowler, M. Gourber-Pace, S. Hancock, C.E. Hill, M. Hourican, D. Kuchler, E. Mahner, D. Manglunki, S. Maury, M. Paoluzzi, S. Pasinelli, J. Pasternak, U. Raich, F. Roncarolo, C. Rossi, J.P. Royer, M. Royer, R. Scrivens, L. Sermeus, G. Tranquille, M. Vretenar,

CERN, Geneva, Switzerland.

Abstract

The Low Energy Ion Ring (LEIR) is a central piece for LHC ion operation at CERN, transforming long Linac3 pulses into high density bunches needed for LHC. The first phase of LEIR commissioning successfully attained its goal of providing the so-called "early ion beam" (one bunch of 2.25×10^8 Lead ions) needed for the first LHC ion runs with reduced luminosity. Studies in view of generating the beam needed for nominal ion operation (2 bunches of 4.5×10^8 ions in LEIR) were carried out in parallel with the setting-up of the early beam in the accelerators further downstream in the LHC injector chain. The main characteristics of the machine using a new state of the art electron cooler are discussed together with the latest results.

INTRODUCTION

The LHC [1,2], presently in construction at CERN will, in addition to proton operation, provide Pb ion collisions. The ion accelerator chain existing before the LHC era was by far not sufficient to provide the ion beams needed. The most fundamental upgrade of this ion accelerator chain [3-5] was the addition of the Low Energy Ion Ring. The role of this small accumulator ring, equipped with a new state-of-the-art electron cooler (built by BINP-Novosibirsk), is to convert several (200 µs) long Linac pulses into short high brilliance bunches needed for LHC ion operation.

Since nominal LHC ion operation is very demanding for both the LHC and the injector chain, first LHC ion operation will take place with a lower luminosity and less bunches using the so-called "early scheme" [3-5]. During the LEIR commissioning [6-9], the beam for this early scheme has been produced and transported to the PS injection region. The goal of the first LEIR operation run during last fall was to send the early beam to the PS to commission it[10], and to explore the way to the nominal beam in LEIR.

THE "EARLY SCHEME"

In LEIR, the simple "early scheme" consists in accumulating 2.2×10^8 lead ions(54+), bunching this beam on h=1, accelerating it from 4.2 to 72 MeV/n and sending it to the PS (Figure 1).The main results of this run are:

- The Ion Source performance was significantly improved such that LEIR received regularly, from the Linac3, an intensity of 22 eµA or more.

- Only one shot was needed to produce the early beam. The beam was cooled, accelerated on a cycle of 2.4 s and extracted toward the PS without particular difficulties.

Figure 1: The "early ion beam" in LEIR (200ms/div). The red trace is the main bending field, the green trace is the beam current (8×10^7 ions/div), the blue trace is the electron cooling cathode voltage which is reduced just before the ramp.

- The injection efficiency was strongly influenced by shot to shot trajectory fluctuations in the injection line. This has been caused by stray fields generated by pulsed magnets (PS ring and ejection line). Magnetic shielding will be implemented to cure the problem during the present machine shut down.

- The new fully digital RF system was for the first time used in operation (see below). It performs very well and reliably apart from a fault related to commissioning the system.

- The normalised transverse emittances measured along the transfer line to the PS by the 3 profiles method (3 secondary emission grids distant by about 60 degrees phase advance) were found to be about 0.3 µm. The longitudinal emittance is $\varepsilon_l < 0.02$ eVs/n. All these measurements are well within specifications.

- The availability of the beam for the PS commissioning was about 78%. The stops were mainly due to 3 faults; delay of the start-up by a vacuum leak in the electron cooler; a general stop of the power network at CERN; an error introduced in the RF digital system while commissioning a voltage loop in parallel to sending beam to the PS.

HIGH POWER RF TESTING OF A CELL COUPLED DRIFT TUBE LINAC PROTOTYPE FOR LINAC4

M. Vretenar, Y. Cuvet, F. Gerigk, J. Marques Balula, M. Pasini, CERN, Geneva, Switzerland

Abstract

A Cell-Coupled Drift Tube Linac (CCDTL) accelerating structure at 352 MHz has been adopted for the energy range 40 to 90 MeV of Linac4, the new 160 MeV injector linac for the CERN accelerator complex. With regard to a conventional DTL in this energy range this structure presents the advantages of lower construction cost and easier access, cooling and alignment of the focusing quadrupoles placed between tanks.

A full-scale high-power prototype representing 1/3 of a complete module has been designed and built at CERN. It is fed by a waveguide input coupler of novel conception.

This paper summarizes the main mechanical features of the prototype and reports the RF tuning procedure and the results of high-power RF testing.

THE CCDTL PROTOTYPE

A CCDTL module, in the geometry adopted for Linac4 [1], consists of three DTL-type tanks containing two drift tubes each, connected by off-axis coupling cells. Between tanks are placed electromagnetic quadrupoles and diagnostic equiment whose installation, alignment and access is greatly simplified with respect to a DTL. The module resonates at 352 MHz in the $\pi/2$ mode, leaving the couping cells unexcited. Figure 1 shows an open 3D view of a module, together with its support and the short-circuited WR2300 waveguide coupled to the central tank.
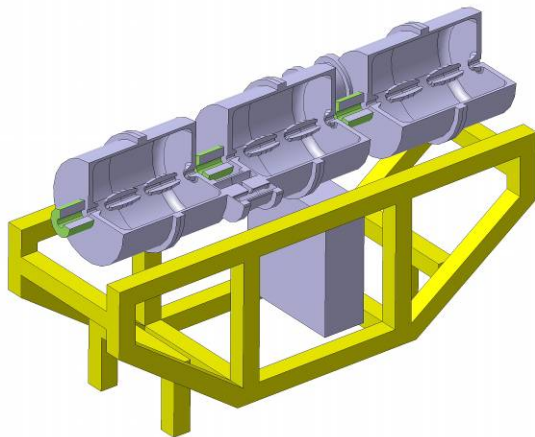
Figure 1: open view of a CCDTL module.

A CCDTL prototype consisting of two half accelerating cells connected by a coupling cell (Fig. 2) has been recently designed and built [2]. The chosen geometry is the smallest presenting the same electric field and thermal distribution as the final CCDTL structure. The half-tanks are made of copper-plated stainless steel, with cooling channels directly machined in the external part of the tank cylinder. Each half-tank contains a drift tube made in copper and cooled via the supporting stem. The half-tanks are connected via coupling slots to a coupling cell and are closed by disc covers, to provide the correct boundary conditions for the electric fields. In the final CCDTL configuration, two half-tanks are connected to form a complete tank. Vacuum and RF tightness between half tanks and covers and between the coupling cell elements are provided by "Helicoflex" type contacts. The end walls are EB welded to the tank cylinder, as well as the coupling cell end wall. Table 1 summarises the geometrical dimension of the prototype cavity.
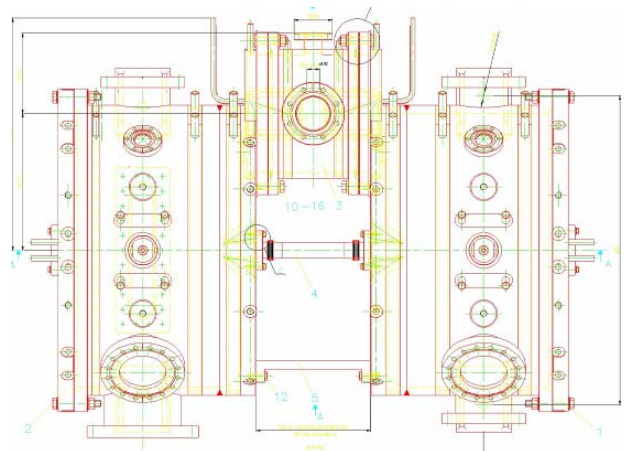
Figure 2: View from top of the CCDTL prototype. The coupling cell is off-axis; the quadrupole is replaced by a tube.

Each accelerating cell is equipped with two ports for tuners and one port for vacuum pumping. One of the accelerating cells has the port for the waveguide input coupler. The coupling cell is equipped with two tuning ports. All cells have a RF pickup port. Figures 3 and 4 show the prototype at different stages of its assembly.

Table 1: Geometrical dimension of the accelerating and coupling cell of the CCDTL prototype.

Accelerating tank diameter	495 mm
Drift tube diameter	85 mm
Full bore aperture	28 mm
Half accelerating cell length	302.5 mm
Gap length	49.05 mm
Coupling cell length	240 mm
Coupling cell nose diameter	93 mm
Coupling cell diameter	233 mm
Coupling cell gap	22.8 mm

04 Hadron Accelerators
A08 - Linear Accelerators

THERMO-STRUCTURAL ANALYSIS OF 400 KEV DEUTERON RFQ COMPONENTS

Piyush Jain[#],Vlsrao. Sista, Rajesh Kumar, P. K. Nema, P.Singh

Bhabha Atomic Research Center, Mumbai-400085, India

Abstract

In this paper we are presenting Thermo-structural analysis of 400KeV, 1mA RFQ components i.e. RF Coupler, Tuner and Vacuum port. This investigation will help us to design local cooling schemes for these components. Parametric studies are also included in this paper. Feasible cooling schemes which meet cooling requirements of components will also be shown.

INTRODUCTION

The renewed interest in Accclerator Driven Systems (ADS) has spurred tremendous interest in developing high intensity proton accelerators, and has set challenging demands in terms of delivering high current (~ tens of mA) and high energy (≥ 1 GeV) required for the spallation process. In Indian context, ADS will be used for the utilization of thorium resources for the energy production. In view of the importance of ADS, a project to design and build a 20 MeV, 30 mA CW proton accelerator (LEHIPA) as an injector to 1 GeV Linac has been initiated.

The LEHIPA mainly consists of a 50 keV ECR ion source, Low Energy Beam Transport (LEBT) line, 3 MeV Radio Frequency Quadrupole (RFQ) accelerator, Medium Energy Beam Transport (MEBT) line and a 20 MeV Drift tube Linac (DTL). 400 KeV, 1mA prototype deuteron RFQ will be build in order to understand the accelerator technologies required for LEHIPA project mainly regarding handling of very large RF power at 350 MHz. This RFQ will be utilized to replace 14 MeV neutron generator presently working at BARC.

RFQ will be made of OFHC copper. Because of the surface resistance offered by RFQ materials a portion of RF power gets dissipated in cavity itself. Average thermal load resulting from the RF power for the 400 keV RFQ is 68 KW. Main Coolant channels [1] have been designed to take care of this dissipated power. But these Main Coolant channels are not capable of eliminating potential Hot-Spot in RFQ components i.e. RF Coupler, Tuner, and Vacuum Port. Hence, Local Cooling of these components is required.

THERMO-STRUCTURAL ANALYSIS

Analysis is performed with help of FEM code 'ANSYS'. Modelling is done in ANSYS itself, this will facilitate easy remodelling. Investigation of temperature rise can be carried out with Thermal analysis, and deformation and stress pattern can be investigated with help of structural analysis. But in our case results of thermal analysis affect loading conditions in structural analysis, so coupling of thermal and structural filed is done. In Thermal analysis load is Heat flux, which is applied on mesh nodes by importing heat flux files from physics design calculations. 30% extra Heat Flux is added for safety margin. After performing thermal analysis elements are switched to structural elements while keeping model, material, mesh pattern unchanged. Now, temperature at nodes of mesh (which works as structural load) is imported from thermal analysis result file. Other boundary conditions like symmetricity, restriction of movement on flange are also applied. In following discussions h denotes Convective Heat Transfer Coefficient (in SI units) and Temperature is in Celsius. All the temperature profiles are shown on half-symmetric model.

RF Coupler

Co-axial type of coupler [2] has been chosen for this RFQ. Coaxial coupler mainly consists of Inner conductor, Outer Conductor, Ceramic window, Loop and Flange. Power dissipation in each coupler is 1.2 KW and peak Heat Flux is 35 W/cm^2.

Analysis without local cooling channel shows that temperature of loop and nearby portions may rise up to melting point of OFHC copper. Hence, local cooling scheme has been designed based on temperature profile which we got without local cooling channels. Inner conductor will be cooled by coaxial coolant channel. Outer conductor will be cooled with help of jacket from outside. Analysis shows that portion of outer conductor which penetrates inside RFQ is not required to cool locally; still temperature rise may be kept in check. Inner cooling channel and cooling jacket is shown in Figure 1. Temperature profile (with deformations) with this kind of cooling scheme is shown below in Figure 2. In this case, convection heat transfer coefficient (h) is 15000 with coolant temperature 16°C.

piyushj@barc..gov.in

ELECTRON COOLING RATES IN FNAL'S RECYCLER RING *

A. Shemyakin [#] and L.R. Prost
FNAL, Batavia, IL 60510, USA

Abstract

A 0.1-0.5 A, 4.3 MeV DC electron beam provides cooling of 8 GeV antiprotons in Fermilab's Recycler storage ring. The paper presents cooling rate formulas derived in the framework of a simple non-magnetized model and compares them with measurements.

INTRODUCTION

Since the first cooling demonstration in 2005 [1], the Recycler Electron Cooler (REC) is used for storing and preparing antiproton bunches for every Tevatron store. To understand and improve the cooling process, dedicated cooling measurements of two types are performed.

In drag rate measurements [2], a low-intensity, coasting antiproton beam is first deeply cooled. Then the electron energy is changed by a jump, and the evolution of the average antiproton momentum is analyzed.

In the measurements of the second type, an antiproton beam with a Gaussian velocity distribution is kept between barrier buckets at a constant length. After turning the electron beam on, the initial derivatives of the momentum spread and transverse emittance are recorded.

In this paper, we compare results of these measurements with a non- magnetized model.

COOLING MODEL

The REC employs a weak 105 G longitudinal magnetic field to focus the electron beam in the cooling section. The simplest model to estimate the cooling rates of the antiproton beam is as follows:

1. The influence of the magnetic field on the cooling dynamics is neglected (so-called non-magnetized cooling).
2. The electron beam properties are assumed to be the same along the cooling section and across the beam.
3. The angle and momentum distributions of both electron and antiproton beams are Gaussian.
4. Variation of the Coulomb logarithm L_c over the range of relative velocities is neglected, and it is taken out of the cooling force integral.
5. For both beams, velocity spreads in x and y directions are equal in the cooling section.
6. The antiproton beam is assumed to be coasting, i.e. effects of RF barriers are neglected.
7. Antiproton motion in all three directions is uncoupled.

Cooling force

Under these assumptions, the formula for the non-magnetized cooling force [3] can be reduced to a one-

dimensional integral [4] (similar to what is called "Binney's formula" in [5]):

$$F_{b\_xi}(\vec{V}_p) = -A \cdot \frac{\partial}{\partial V_{xi}} U(V_{px}, V_{py}, V_{pz}), \; A = 4\pi \cdot m_e r_e^2 c^4 n_{eb} \eta \cdot L_c$$

$$U(V_{px}, V_{pz}, V_{pz}) = \frac{2}{\sqrt{\pi}} \cdot \int_0^\infty dt \frac{\exp\left(-\frac{t^2 V_{px}^2}{1 + 2 \cdot \sigma_{ex}^2 t^2} - \frac{t^2 V_{py}^2}{1 + 2 \cdot \sigma_{ey}^2 t^2} - \frac{t^2 V_{pz}^2}{1 + 2 \cdot \sigma_{ez}^2 t^2}\right)}{\sqrt{(1 + 2 \cdot \sigma_{ex}^2 t^2)(1 + 2 \cdot \sigma_{eyf}^2 t^2)(1 + 2 \cdot \sigma_{ez}^2 t^2)}}$$

(1)

where F_{b_xi}, V_{pxi}, and σ_{exi} are the xi components of the cooling force, antiproton velocity, and electron r.m.s. velocity spread, correspondingly; n_{eb} is the electron density, m_e is the electron mass, r_e is the classical electron radius, c is the speed of light, η is the portion of the ring occupied by the cooling section. All values are in the beam frame.

Cooling rates

The beam-frame longitudinal cooling rate is derived by averaging the cooling force power over the antiproton velocity distribution $f_p(\vec{V}_p)$ [6]:

$$M_p \frac{d\sigma_{pz}}{dt_b} \sigma_{pz} = \int F_{b\_z} V_{pz} f_p(\vec{V}_p) d\vec{V}_p =$$

$$\sqrt{\frac{2}{\pi}} \frac{A \cdot \sigma_{pz}^2 \cdot f_{long}(\alpha)}{\sqrt{\sigma_{ez}^2 + \sigma_{pz}^2}(\sigma_{ex}^2 + \sigma_{px}^2)},$$

(2)

$$f_{long}(\alpha) = \frac{1 - \sqrt{\frac{\alpha}{1-\alpha}} \cdot \arccos(\sqrt{\alpha})}{1 - \alpha}, \; \alpha = \frac{\sigma_{ez}^2 + \sigma_{pz}^2}{\sigma_{ex}^2 + \sigma_{px}^2},$$

where M_p is the proton mass, σ_{pxi} is the xi component of the antiproton r.m.s. velocity spread, and the case where $\sigma_{ex} = \sigma_{ey}, \sigma_{px} = \sigma_{py}$ is considered. Eq. (2) is valid for $\alpha < 1$. This is typical for the REC parameters and will further be assumed in this paper. When $\alpha > 1$, the result is expressed through $\cosh^{-1}(\sqrt{\alpha})$. In the lab frame, the time derivative of the momentum r.m.s. spread δp is calculated as

$$\delta \ddot{p} \equiv \frac{\delta p}{\tau_{long}} \equiv \frac{d}{dt_l} \delta p = \frac{d\sigma_{pz}}{dt_b} M_p.$$

(3)

A similar integration for the transverse velocity gives

$$\frac{d}{dt_b}\left(\sigma_{px}^2\right) = \sqrt{\frac{2}{\pi}} \frac{A \cdot \sigma_{px}^2 \cdot f_{tr}(\alpha)}{M_p(\sigma_{ex}^2 + \sigma_{px}^2)^{3/2}},$$

$$f_{tr}(\alpha) = \frac{\arccos\sqrt{\alpha} - \sqrt{\alpha(1-\alpha)}}{2(1-\alpha)^{3/2}}.$$

(4)

Eq. (4) takes into account a decrease of the cooling rate by a factor of 2 due to averaging over the betatron phases. Transition to the lab frame gives the expression for the time derivative of the transverse emittance:

$$\tau_{tr}^{-1} \equiv \frac{1}{\varepsilon} \frac{d\varepsilon}{dt_l} = \sqrt{\frac{2}{\pi}} \frac{A \cdot f_{tr}(\alpha)}{\gamma M_p(\sigma_{ex}^2 + \sigma_{px}^2)^{3/2}}$$

(5)

CHARACTERISTICS OF THE MAGNETIC CHANNEL IN THE YOKE HOLE OF K500 SUPERCONDUCTING CYCLOTRON

J. Pradhan, U Bhunia, J Debnath, S Paul, Z A Naseer, A Dutta, S Bhattacharya, MK Dey, C Mallik and RK Bhandari,

Variable Energy Cyclotron Centre, I/AF, Bidhan Nagar, Kolkata-700 064, INDIA

Abstract

The detail magnetic field measurement of K-500 superconducting cyclotron has been carried out. The last magnetic channel of the extraction system placed in the yoke hole of the cyclotron before external beam line is active, unlike others, which are all passive. This channel comprises a coil and a special shaped iron to produce both quadrupole and dipole field for focussing and radially aligning the different ion species coming out from the cyclotron, with the external beam transport line. The magnetic field inside the channel along with the outside stray field has been measured for different channel currents as well as main magnet excitations. A 3-D model of the full magnet is constructed using magneto- static code RADIA [2] to simulate the yoke field. This paper reports the comparative study of measured and calculated field and studies the trajectories for the representative ions through the stray field calculated from the model. The later being used to locate the starting point (or matching point) for the external beam transport line.

INTRODUCTION

The main magnet of K-500 superconducting cyclotron (SCC) consist of two coils (α coil and β coil), which has been excited to different measurement grid points and detail field mapping is carried out. The last magnetic channel of the extraction system is located in the yoke hole and is active unlike others, which are all passive. This channel is used to focus the beam radially as it passes through the yoke and also help to align the beam with the central trajectory of the external beam line. The magnetic field can be changed by varying channel current in both positive and negative direction, depending on the requirement of different ion species. The channel consists of ten pancake coils made up of 6mm $\times$ 6 mm hollow copper conductor. Its tapered iron pole piece (as shown in fig. 2) produces constant gradient field. The uniformity of the field gradient is maintained to avoid the deterioration of the exit beam quality. The detail design studies have been published elsewhere [1]. This paper reports the results of field measurement inside the channel and its comparison with the results of 3-Dimensional magneto-static code RADIA [2]. Particles with different charge to mass ratio and final energy have different trajectories along the extraction path. So the particle tracking for different representative ions is performed to locate the matching point of the external beam transport line.

MEASUREMENT SCHEME

The magnet was mapped using a special zig, which is inserted inside the channel. The field is measured with the help of transverse hall probes and F W Bell make gauss meter. The measurements are performed under three main coil excitations: I_α / I_β= 300 A/300 A; I_α / I_β= 575 A/75 A; and I_α / I_β= 459 A/471 A. The channel current is varied from 0A to 300A in both positive and negative direction. Fields have been measured on a rectangular grid aligned with channel, having long dimension (+z) pointing in the direction of the beam. In the transverse direction (x), there were three points for each z, measured at –8mm, 0, +8 mm from the centre of zig. The measurement step is 0.5 inch along z direction. The stray magnetic field outside the main magnet is also measured up to about 5 m from the yoke.

FIELD SIMULATION AND RESULTS

This active magnetic channel is situated in the yoke hole and it is necessary to generate the yoke field for estimating the actual field inside the channel and compare it with the experimentally measured data. A complete 3-D model of K-500 SCC main magnet is made with the help of code RADIA. This is three sector cyclotron having mirror symmetry about its median plane. The median plane view of the magnet along with channel in the yoke hole is shown in figure 1.

Channel inside the yoke hole (magnified view in figure 2)
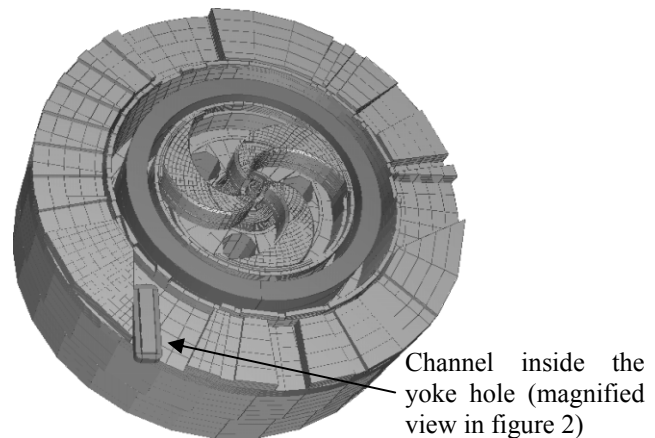
Figure 1. Median plane view of main magnet of K-500 Superconducting Cyclotron (SCC)

ADIABATIC DAMPING OF THE BUNCH-LENGTH IN THE INDUCTION SYNCHROTRON

Tanuja Dixit[#], The Graduate University for Advanced Studies, Hayama, Miura, Kanagawa 240-0193, Japan
Yoshito Shimosaki, Ken Takayama, Accelerator Laboratory, High Energy Accelerator Research Organization (KEK), 1-1 Oho, Tsukuba, Ibaraki, 305-0801, Japan

Abstract

It was observed that a bunch-length shrunk with acceleration in the Induction Synchrotron (IS) experiment, where a single proton-bunch injected from the 500 MeV Booster was accelerated to 6 GeV in the KEK-PS. A novel technique capable of quantitatively predicting the adiabatic phenomenon of bunch shortening has been developed, based on a hypothesis that the particle oscillation amplitude varies inversely proportional to the square root of its oscillation frequency. The experimental result and analytical prediction is in good agreement with each other.

INTRODUCTION

The induction acceleration experiment was carried out using the KEK 12 GeV proton synchrotron (12GeV-PS) in a series of experiments to demonstrate a proof of principle of the IS [1], the schematics of which is shown in Fig. 1. Details of the experiments have been described in the literatures [2,3,4].

A specific property of the functional separation of acceleration and confinement in the IS allows us to control the beam size through the entire period of acceleration. However, the accelerated beam bunch is subjected to adiabatic damping, as seen in the conventional RF synchrotron. It is quite important to know how the bunch size evolves through the entire acceleration in the IS and what factors dominantly determine the bunch size. A theoretical approach to predict the temporal evolution of the bunch size is developed. After the approach is carefully justified by comparing with computer simulations, the theoretical prediction is compared with the experimental results. Last we will discuss how this theoretical approach can provide a useful tool to estimate a temporal evolution of the bunch size associated with adiabatic changes in the external parameters, such as the barrier voltage amplitude and a time-interval between barrier voltages.
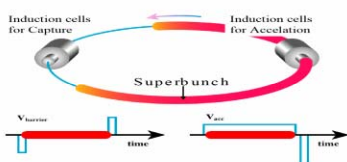
Figure 1: Schematic view of the Induction Synchrotron

EXPERIMENTAL RESULTS

The bunch profile which was monitored by the wall current monitor, was recorded every 33 msec from the injection to the end of acceleration. Experimental results through the entire acceleration period are plotted for typical four shots in Fig. 3, where the bunch size is defined as a width measured at 5% of the peak height. From Fig. 3, we can clearly identify four regions: At the injection (I), the bunch width is 100 nsec but it quickly increases to ~ 400 nsec because of mismatching to the barrier bucket [3]. Tumbling of the bunch in the phase space and the succeeding filamentation are apparent there, leading to a long bunch width. In the remaining minimal field region (II) before acceleration, the bunch size is almost constant. This implies good matching with the barrier bucket shape throughout the region. The initial acceleration region (III) is characterized by serious beam loss as shown in Fig. 2. Quick shrinking of the beam size is caused by the beam loss in addition to damping associated with acceleration. The reason of beam loss is not fully understood, although it is speculated that the control of the trigger pulse density is not enough at this transient region. There is no beam loss in the constant acceleration region (IV). A steady state damping is clear. Near the end of acceleration region, the bunch width is almost constant. We will discuss more about this region hereafter.
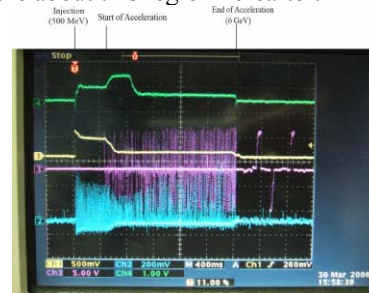
Figure 2: Experimental results. From top to bottom, ΔR signal, beam current, acceleration voltage pulses, and bunch signal

THEORY

To develop the theory, we set a hypothesis that the phase oscillation evolves such that the instantaneous oscillation amplitude is inversely proportional to the square root of the phase oscillation frequency. This hypothesis is originated from an analogy of the WKB solution for a harmonic oscillator with slowly varying

INSTALLATION AND RADIATION MAINTENANCE SCENARIO FOR J-PARC 50 GEV SYNCHROTRON

M. Yoshioka, T. Fujino, H. Kobayashi, Y. Hori, K. Ishii, T. Kubo, H. Matsumoto, T. Oogoe, Y. Saito, Y. Sato, M. Shimamoto, Y. Takeuchi, M. J. Shirakata, M. Uota, Y. Watanabe
KEK, 1-1 Oho, Tsukuba, Ibaraki, Japan
M. Hosokawa, THK CO., LTD., 2-2-7 Sasano-cho, Hitachinaka, Ibaraki, Japan
Y. Kuniyasu, Mitsubishi Electric System & Service Co., LTD.,
2-8-8 Umezono, Tsukuba, Ibaraki, Japan
H. Oki, KDC Engineering Co., LTD., 1-58-4 Yayoi-cho, Nakano-ku, Tokyo, Japan

Abstract

This paper describes the installation of the accelerator components and the installation schedule for the 50 GeV J-PARC Synchrotron and the maintenance scenario for the handling of radioactive components.

INTRODUCTION

J-PARC is a high intensity proton synchrotron, which KEK and JAEA are jointly constructing at Tokai [1,2]. The accelerator is composed of a 181 MeV linac, a 3 GeV Rapid Cycling Synchrotron (25Hz, RCS), and a 50 GeV Slow Cycling Synchrotron (0.3Hz, MR) which has a circumference of 1568 m. The RCS primarily provides a 1 MW proton beam to a material and life science experimental facility. The MR receives part of the RCS beam (~5%) through the beam transport line (BT), which is 220 m long; after the MR accelerates it to the maximum 50 GeV, the extracted beam with an intensity of 750 kW is sent to two experimental facilities. Fast extraction delivers a beam for the long base line neutrino experiment T2K, slow extraction is used for the Hadron experiment. This paper describes the installation of accelerator components for the MR and a maintenance scenario for the handling of radioactive components.

Beam loss is the major factor which limits the operation of J-PARC. Once accelerator components become highly activated by any lost beam, it becomes very difficult to maintain components in the area. Our experience with KEK's 12 GeV proton synchrotron (PS), which was decommissioned in March last year, has shown us that the radiation exposure to workers would exceed the permissible level unless the radioactivity at the location where the workers would be is less than 0.5 mSv/h. The beam intensity of the PS was 5 kW, which is less than 1% of the J-PARC design, but beam losses sometimes reached 500 W, producing radiation levels exceeded 10 mSv/h in the immediate area. For the J-PARC MR, the expectation is that the beam losses should concentrate in the five areas shown in Figure 1 and that the beam loss everywhere outside these five areas should be at less than 0.5 W/m. According we designed the aperture of MR carefully considering this scenario. In order to cut the beam halo locally, there will be two collimator systems [3], one upstream in the BT and one in the MR. Septum magnets for beam injection and extraction are the most

critical MR components in this regard. Necessarily the septum magnets aperture is ultimately a trade-off where electromagnetic and mechanical requirements are compromised, and we have to accept a certain amount of beam loss. Given that, we have worked out a safe and yet practical maintenance scenario for possible required replacement of the units comprising the two collimators, the beam injection, slow extraction, and fast extraction systems.
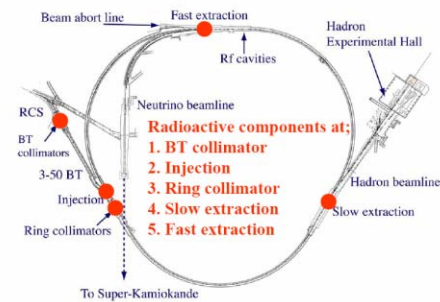
Figure 1: Location of radioactive components

INSTALLATION OF MAGNETS

Installation

The BT and MR magnet quantities and weights are shown in Table 1.

Table 1: BT and MR magnets

	Type of Magnet	Qty.	Weight (ton)
MR	Dipole	96	33
	Quadrupole	216	10~15
	Sextupole	72	2
	Resonant Sextupole	8	2
	Corrector dipole	186	0.3
BT	Pulse dipole	1	16
	Horizontal dipole	3	14~18
	Vertical dipole	2	4.5
	Quadrupole	38	3.5~5.5
	Corrector dipole	14	0.75

The floor level of the accelerator tunnel is excavated ~11 m below the ground surface. Magnets are unloaded at a carry-in vertical shaft by crane and conveyed to the accelerator tunnel by truck. The BT has a crane which is used to install the magnets in the accelerator tunnel. The two straight sections for fast and slow extraction in the

TRANSVERSE MATCHING OF THE SNS LINAC BASED ON PROFILE MEASUREMENTS*

Dong-o Jeon[#] and Paul Chu, Oak Ridge National Laboratory, Oak Ridge, TN37831, U.S.A.

Abstract

For a high intensity linac such as the SNS linac, it matters to match adequately to minimize the beam mismatch and potential beam loss. The technique of doing the matching using the wire-scanners in series was employed [1]. It was verified that matching was improved through the matching technique based on the beam profile measurements from wire-scanners in series.

INTRODUCTION

The Spallation Neutron Source (SNS) accelerator system is designed to accelerate intense proton beams to energy of 1-GeV, delivering more than 1.4 MW of beam power to the neutron production target [2]. Being a high intensity linac, a primary concern is potential damage and radio activation of accelerator components resulting from uncontrolled beam losses. A major source of loss is beam halo that intercepts the bore of the linac. It is important to accomplish adequate level of transverse matching between sections of linac.

When emittance measurement device is available, minimization of rms emittance proves to be effective in doing the matching as for the SNS DTL (Drift Tube Linac) tank 1 commissioning [3,4].

Alternatively wire-scanners installed in series can be used to do the matching [1]. For the purpose of transversely matching between two different structures of the SNS linac, four wire-scanners are installed in series. During the beam commissioning runs, the matching technique based on beam profile measurements was tested and the results are presented here.

MATCHING SCL TO HEBT

We applied the technique based on profile measurements to matching the Superconducting Linac (SCL) to the High Energy Beam Transport (HEBT). We performed a Gaussian fit to the measured beam profile and obtained its beam size σ. By fitting the beam envelope from the Trace3D code to the wire-scanner profile data, we obtained the input beam Courant-Snyder parameters β and α, and the beam emittance ε, as shown in Fig. 1. Table 1 lists the incoming beam parameters determined above. The solid circles in Figs. 1 and 2 represent the beam profile data from the wire-scanners in the HEBT and the solid lines represent simulated beam profile obtained from the Trace3D code. It should be noted that there is a mild oscillation in the beam core before the beam enters HEBT at $Z=8 \times 10^4$ [mm]. The blue color represents the x beam size and the red the y beam

size. HEBT starts from 8×10^4 mm in the figure and the upstream of that point is the SCL.

With the beam parameters of the incoming beam determined, the matching quadrupoles are optimized using the Trace3D code to do the matching. When the matching routine completes the matching, we change the matching quadrupoles as suggested and subsequent wire-scanner measurement is done as shown in Fig. 2.
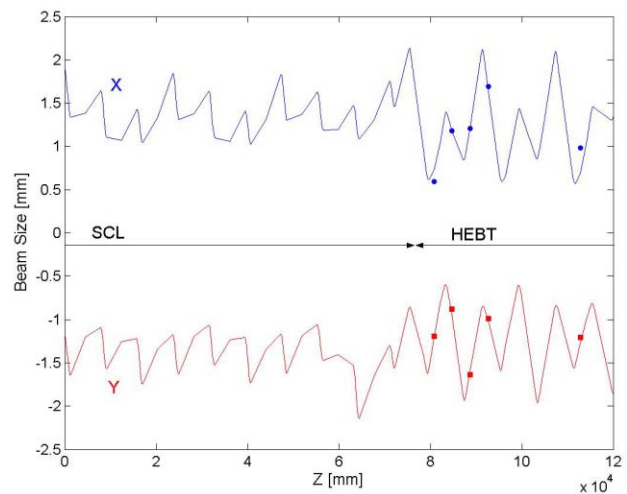
Figure 1: Plots of beam profiles before matching SCL to HEBT. Solid lines are plots of beam size σ [mm] from the Trace3D program and solid circles are wire-scanner measurement data.
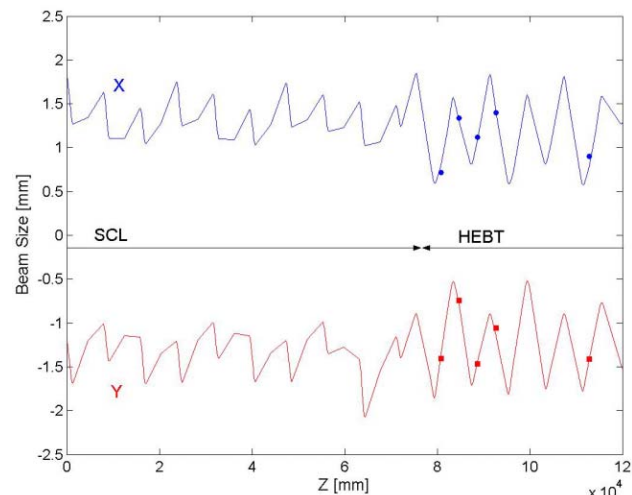
Figure 2: Plots of beam profiles after matching SCL to HEBT. Solid lines are plots of beam size σ [mm] from the Trace3D program and solid circles are wire-scanner measurement data.

BENCHMARKING OF MULTIPARTICLE PHASE SCAN AND ACCEPTANCE SCAN TECHNIQUES FOR THE SNS DTL*

Dong-o Jeon[#], Oak Ridge National Laboratory, Oak Ridge, TN 37831, U.S.A

Abstract

It is important to bring the cavity rf field amplitude and phase to the design for a high intensity linac such as the Spallation Neutron Source (SNS) linac. A few techniques are available such as the acceptance scan and multiparticle phase scan for tuning the Drift Tube Linac (DTL). During the SNS linac commissioning, tuning of cavities was conducted using the acceptance scan and phase scan technique based on multiparticle simulations. The two techniques are benchmarked.

INTRODUCTION

The Spallation Neutron Source (SNS) accelerator system is designed to accelerate intense proton beams to energy of 1-GeV, delivering more than 1.4 MW of beam power to the neutron production target [1]. The design peak current in the linac is 38mA and the macropulse average current is 26mA due to chopping.

Being a high intensity linac, it is crucial to minimize the machine activation induced by beam loss. Finding the right rf set-point can minimize longitudinal halo formation. Because bunch length is relatively long for the DTL, multiparticle tracking is important to accurately simulate the behavior of beam through each tank.

A few techniques for setting rf set-points were studied in depth in the past [2]. In this paper, we describe and compare the results of two techniques used for tuning the DTL, namely, phase scan using BPMs and acceptance scan using Energy Degrader and Faraday Cup (ED/FC). Experimental data were compared with the multi-particle simulations using the PARMILA code [3]. For general SNS linac commissioning results, please refer to [4].

MULTIPARTICLE PHASE SCAN
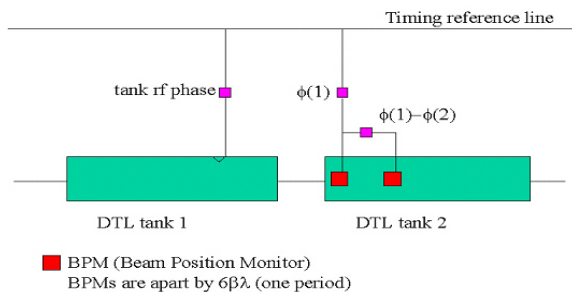
Figure 1: Schematic plot of phase scan with two down-stream BPMs.

The schematic plot of the Phase Scan is in Fig. 1. The

two down-stream BPMs of, say, DTL tank 1 are inside DTL tank 2. They are $6\beta\lambda$ apart (a complete period). Phase advance plays an important role in this technique and is a function of tank rf amplitude and the offset from the design rf phase.

Phase Scans were performed using two down-stream BPMs during the SNS linac beam commissioning. The cavity field amplitude, cavity field phase and beam energy are varied to best match the measured values. The simulation is based on multiparticle tracking because bunch is relatively long for DTL tanks 1, 2 and 3.

Phase scan was performed for the DTL tank 1 and the data are shown in Fig. 2. Lines with circles represent the measurement data showing the difference of two BPM phase data $\phi(1)-\phi(2)$. Solid lines are Parmila simulations. The agreement between the measurement and simulation is excellent. The rf set-point obtained from this phase scan is $(A, \phi)=(0.179, -125.5°)$. Here, A is the Low Level RF amplitude and ϕ the LLRF phase. The incoming beam has an energy deviation of -0.0265 MeV from 2.5MeV, that is -1.060 %.
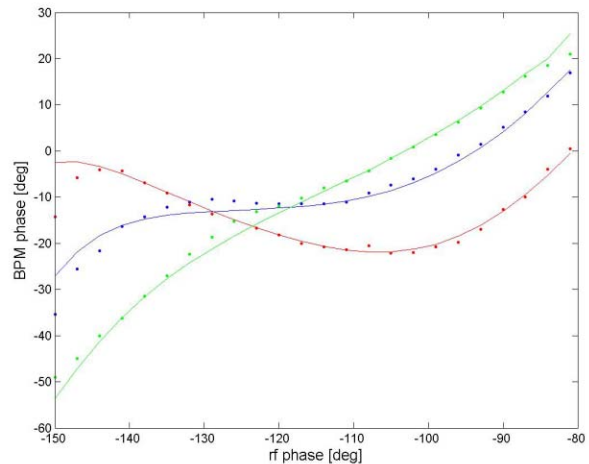
Figure 2: Plots of DTL tank 1 phase scan. Plotted are experimental data (solid lines with circles) and simulation results (solid lines) for three different rf amplitudes.

Phase scan was also performed for the DTL tank 2. The obtained rf set-point is $(A, \phi)=(0.483, 166.5°)$. The incoming beam has an energy deviation of -0.0236 MeV from 7.523MeV, that is -0.314 %. The plotted data in Fig. 3 are also the phase difference of two BPMs phase data. Now the agreement between the measurement and simulation becomes better.

THERMAL-INDUCED FREQUENCY DETUNING OF 350 MHz RFQ STRUCTURE

N. K. Sharma, S. C. Joshi, N. Kumar

Raja Ramanna Centre for Advanced Technology, Indore 452013, INDIA

Abstract

A 350 MHz, 4.5 MeV RFQ structure is being developed for high power Proton Linac for Indian SNS. RFQ structure operated at higher duty factor will be subjected to thermal deformations and hence the detuning of resonating structure due to RF induced heating. A detailed Thermal-Structural-Electromagnetic sequential analysis of RFQ has been performed using Multi-physics ANSYS (Finite Element Analysis Software). A cooling scheme has been designed for efficient heat removal from the structure to minimize the thermal induced frequency shift. During analysis the parameters such as cooling water flow rate and bulk water temperatures are varied to study their effect on temperature distribution and associated frequency variation. The frequency shift is found highly sensitive to vane tip cooling parameters.

RFQ FOR LOW ENERGY H⁻ ION LINAC

A 350 MHz integrated vane type RFQ structure has been selected for accelerating proton/H- ion from the ion source to 3- 4.5 MeV. The operating frequency 350 MHz is selected on the basis of available RF power sources. Higher output energy from RFQ like 4.5 MeV is preferred from the injection point of view into the following linac structures like DTL/ low beta SC cavities. An intervane voltage of 65 kV is selected for the high duty operation of RFQ. While lower inter-vane voltage in RFQ reduces the power dissipation per unit length in the structure, however it results in increased length of RFQ structure.
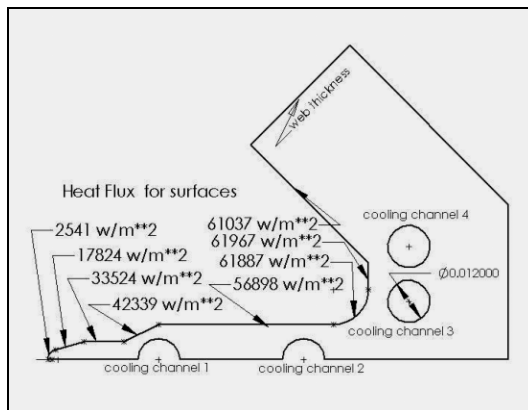
Figure 1: RFQ geometry with heat flux

COUPLED FIELD ANALYSIS OF RFQ

The RFQ cavity structure has been designed using SUPERFISH for the inter-vane voltage of 65 kV. The total power loss in the RFQ structure is 539 kW. Figure 1 shows the surface heat flux in RFQ. The power loss for the thermal analysis has been considered 50% more than the power loss calculated by SUPERFISH to compensate for the deviation in ideal surface conditions, theoretical electrical conductivity and joints etc. The material for the construction of RFQ is OFHC copper. The RFQ cavity has been analyzed using FEA software ANSYS considering six cooling channels per quadrant of RFQ cavity. Thermal analysis of RFQ has been performed to remove the RF induced heat from the structure The circular shape, 12 mm diameter of cooling channel is selected due to ease in machining. The relative locations of remaining five channels were determined by parametric thermal design optimization. Parametric studies are performed to evaluate the effect of cooling water flow rate and cooling water bulk temperature and their effect temperature distribution are shown in the figures.

Thermal-Structural-Electromagnetic sequential Analysis of RFQ

Thermal-structural-electromagnetic sequential analysis has been performed to evaluate the thermal induced frequency shift of RFQ structure. The RFQ geometry is modeled by using Plane 2D elements for OFHC Copper walls and a corresponding MESH 200 unsolved elements for cavity space. The temperature distribution obtained from the thermal analysis was taken as an input for the structural analysis. The displacement constraints were applied such that the RFQ structure is free to expand in the radial direction. The deformation due to self weight of the structure is also incorporated in the analysis. During thermal and structural analysis the MESH 200 elements act as a dummy element. The high frequency electromagnetic analysis is performed for resultant deformed cavity to evaluate the thermal induced detuning of the structure. During HF electromagnetic analysis, the unsolved MESH200 elements are converted into corresponding high frequency elements. Various multiple iterative ANSYS macros have been incorporated in the sequential analysis to evaluate the effect of cooling channel flow rate and bulk water temperature on resonating frequency. Figure 3 and Figure 4 shows the effect of flow rate and bulk water temperature in various cooling channels on temperature rise in RFQ.

04 Hadron Accelerators
A15 - High Intensity Proton Machines

PRESENT STATUS OF J-PARC MR SYNCHROTRON

T. Koseki[#,A)], H. Kobayashi[A)], M. Yoshioka[A)], H. Matsumoto[A)] and J-PARC MR Group[A),B)]

[A)]Accelerator Laboratory, KEK, Tsukuba, Japan

[B)]JAEA, Tokai, Japan

Abstract

The J-PARC (Japan Proton Accelerator Research Complex) is a joint project of High Energy Accelerator Research Organization (KEK) and Japan Atomic Energy Agency (JAEA). Presented in this paper is a recent status of a 50-GeV slow cycling main ring synchrotron (MR) of J-PARC. Installation and performance test of accelerator components are now in progress. Beam commissioning of the MR is scheduled to start in May 2008.

INTRODUCTION

The J-PARC facility consists of a 400-MeV linac, a 3.0-GeV rapid cycling synchrotron (RCS), a 50-GeV slow cycling main ring synchrotron (MR) [1, 2] and related experimental facilities for use in various fields of science and technology. The RCS will provide a 3.0-GeV, 1-MW proton beam to neutron and muon targets in the Materials and Life Science Experimental Facility (MLF). The MR will provide a 50-GeV, 0.75-MW proton beam to the Hadron Beam Facility (HD) and a neutrino production target in the Neutrino Facility.

The J-PARC project is being promoted in two phases. The facilities mentioned above are constructed in Phase I. However, the maximum beam energy of the MR is 40 GeV in Phase I because of flywheel electric power system will be ready for only Phase II. Furthermore the Linac starts with a beam energy of 181 MeV, then the beam power of the RCS will be limited to 0.6 MW in maximum.
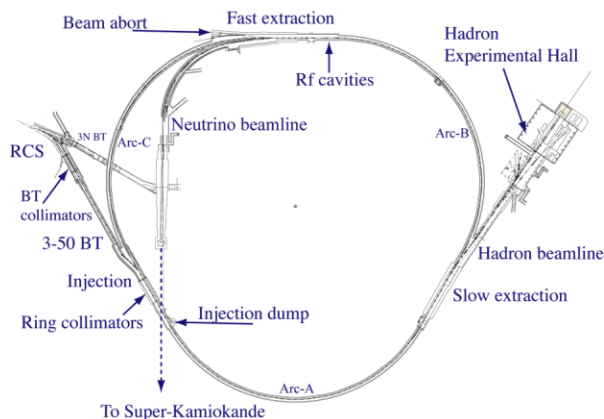
Figure 1: Plan view of MR and experimental facilities.

Figure 1 shows a plan view of the MR and the experimental facilities. The MR has an imaginary

transition lattice structure to avoid transition crossing during acceleration. It has a three-fold symmetry and a circumference of 1567.5 m. Three dispersion-free 116-m long straight sections are dedicated to "injection and beam collimators", "fast extraction and rf system", and "slow extraction". The slow extraction beam is delivered to the HD experimental Hall for particle and nuclear physics experiments. The fast extraction beam is delivered to the neutrino production target. The produced neutrino beam is sent to Super-Kamiokande, a large water Cherenkov detector, located 300 km west for long baseline neutrino oscillation experiment. The main parameters of the MR are summarized in Table 1.

Table 1: Main Parameters of MR.

Circumference [m]	1567.5
Superperiodicity	3
Repetition rate [Hz]	~ 0.3
Injection Energy [GeV]	3.0
Extraction Energy [GeV]	30/40(Phase I), 50 (Phase II)
Harmonic number	9
Number of bunches	8
Transition γ	j31.7
Typical tune	22.4, 20.8
Transverse emittance at inj. [πmm-mrad]	54
Transverse emittance at ext.[πmm-mrad]	10(at 30 GeV) 6.1(at 50GeV)
Rf frequency [MHz]	1.67 – 1.72

Beam commissioning is started from the upstream accelerators while the construction of the downstream accelerators and experimental facilities is in progress. The construction of the linac has been completed and beam commissioning started in November 2006. Recently, we have achieved beam acceleration up to the nominal beam energy of 181 MeV [3]. The construction of the RCS will be completed in April 2007. The beam commissioning of the RCS is scheduled to start in this September.

For the MR, civil construction of the accelerator tunnel has been completed at the November 2006. Installation of the accelerator components is now in progress.

CONSTRUCTION STATUS

The MR lattice requires 96 dipoles, 216 quadrupoles with eleven families, 72 sextupoles with three families. The MR also has eight sextupoles with two families to excite the third order resonance for the slow extraction. The mass production and magnetic field measurement of

DESIGN OF HIGH CURRENT RF ION SOURCE FOR MICROMACHINING APPLICATIONS

P.Y. Nabhiraj, Ranjini Menon, C. Mallik, R.K. Bhandari
Variable Energy Cyclotron Centre, 1/AF, Bidhan Nagar, Kolkata, India
G. Mohan Rao, S. Mohan
Department of Instrumentation, Indian Institute of Science, Bangalore, India

Abstract

Liquid Metal Ion Source (LMIS) and Gas Field Emission Ion Source (GFEIS) are the major ones in micromachining applications so far. They have limitations of contaminations and low throughput. Plasma based ion sources can produce heavier ions for higher throughput, lighter ions for fabrication of higher resolution structures, ions for doping, ion assisted direct writing of metallic, oxide, nitride and carbide layers and lines. Considering wide range of applications, a 13.56 MHz inductive coupled plasma (ICP) ion source for producing high brightness ion beams with very low energy spread has been developed. It is a very compact ion source with external helical antenna wound around a 30 mm quartz tube. 1 mA of Argon and 0.5 mA of proton ion beams have been extracted from 2 mm dia aperture in plasma electrode at 4.0 kV extraction potential and ~200W of RF power. Using LabView software an automated plasma diagnostic system has been designed and used to measure the plasma parameters. Retarding Field Analyser (RFA) has been designed and developed for ion energy spread measurements. This paper describes the features of the ion source, ion beams produced, some results of the plasma diagnostics.

INTRODUCTION

Ions in keV energies when incident on solid surface produce several effects such as sputtering of target atoms, secondary electron emission, inducing chemical reactions, creation of defects, implantation of ions and altering the surface properties. Some of these effects are put into use in the field of micro electro mechanical system (MEMS)/ nano electro mechanical system (NEMS) and semiconductor device manufacturing. The conventional lithographic techniques using UV, electron beam, X-rays have reached the limitations. Ion beams are most suitable to overcome these limitations as they have least proximity effect due to their low scattering and absence of diffraction effects. During 1950's Feynman [1] in his visionary speech proposed to use FIB for creation of structure of nanometer sizes. With the use of ion beams for the processes, resist can be avoided and the ion doses and energies can be varied accurately making them versatile in many applications. Development of liquid metal ion sources (LMIS) producing typical semiconductor dopants, broadened the field of applications [2], [3]. In case of resist based lithography, resists have higher sensitivity for ion beams facilitating higher throughput. Conventional LMIS has many

limitations like, production of ion beams of a fewer elements, shorter life time of the source etc. Gaseous field ion source can give stable beam for longer time. But technology is cumbersome due to the involvement of cryogenics. The other problem using LMIS is that these metallic ions get trapped in the target producing impurities in the deposited films. To overcome the limitation of LMIS, Inductive Coupled Plasma (ICP) based ion sources are being developed for focused ion beam applications. These ion sources can produce ion beams of all the typical dopants for semiconductor fabrication applications and heavy gaseous ion beams for micromachining applications. A mini ICP with external helical coil, measuring 30 mm in diameter has been developed for this application. Small volume ICP source can produce very high density plasma at low powers. ICP based gaseous ion sources are one of the excellent tools to grow thin films of practically any materials with least contamination.
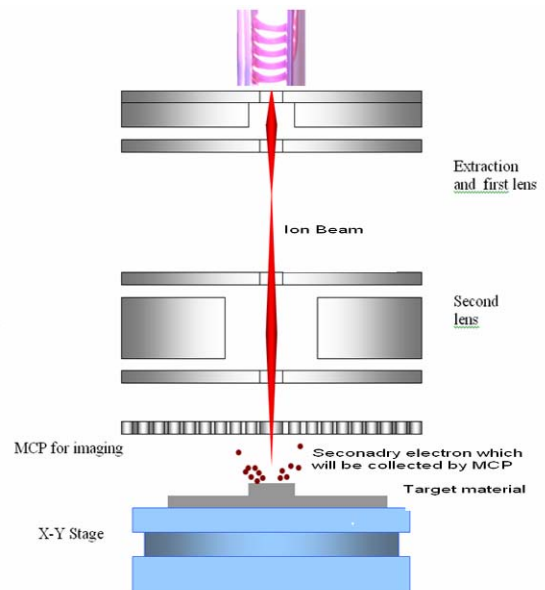
Figure 1: Schematic of focused ion beam system.

Fig 1. shows the schematic of focused ion beam (FIB) systems with the inductive coupled plasma ion source. This set up is being designed for micromachining applications in the micro and sub-micro scales. Typical FIB column consists of ion source, extraction system, focusing elements, ion beam scanning and blanking systems, micro channel plates for ion and secondary electron detection for real-time imaging of the surface by

SIMULATION OF NON-UNIFORM HIGH DENSITY ELECTRONEGATIVE PLASMA FOR OPTIMIZATION OF H⁻ ION AND THEIR EXTRACTION

Ajeet Kumar* , V. K. Senecha and S. Kotaiah, Power Supply Division, RRCAT, Indore, India-452013

Abstract

Numerical simulations of radio frequency multi-cusp volume type H^- ion source have been performed under non-uniform electronegative plasma equilibrium conditions in order to understand the physics of formation of various ion species (H^+, H^-, e^- etc.) and for optimization of H^- ion formation and extraction. Coupled momentum balance equations along with continuity equations were solved in a cylindrical geometry to obtain the density profile of various ion species. The relevant cross-section data available in the literature as a function of temperature has been used in the computation. The hydrodynamic model of plasma in equilibrium with background neutral gas has been used. Low degree of ionization ($\approx 1\%$) has been assumed. The collision less sheath formation, penetration of electric and magnetic field and power requirment to sustain the plasma has been worked out numerically. An effort has been made to give a self-consistent numerical scheme for the solution of inductively coupled plasma(ICP) in equilibrium, and the results obtained have been presented.

INTRODUCTION

In order to meet the high current requirement of H^- ion for spallation neutron source, which is being proposed to be developed at RRCAT, a detailed theoretical investigation of H^- ion source has been carried out. The fluid model has been applied by various authors, to study various aspects of ion source [1, 2, 4]. In our numerical model we have retained the inertial derivative term. The effective collision frequency of electron and RF field frequency has been computed assuming Maxwellian velocity distribution. This was crucial because the discharge is assumed to be operated at 13.56 MHz, and typical plasma parameters are such that, neither high frequency nor the dc limit will be suitable. At this frequency it is safe to assume that electron respond to RF field while ions respond to the average field.

STEADY STATE FLUID MODEL

The steady state equilibrium of different species in the RF field implies the average value of different measurable parameter over several RF cycles remain unchanged. We have numerically solved the steady state equlibrium values in cylindrical geometry for H^+, H^-, e^- species in H^- ion source. It is assumed that the background hydrogen molecular density to be uniform, depending only on the pressure of the plasma chamber. The particle balance equation in

* ajeet@cat.ernet.in

the steady state for i^{th} species is:

$$\vec{\nabla} \cdot \vec{\Gamma}_i = (G - L)_i \tag{1}$$

where $\vec{\Gamma}_i$ is the flux of the ith species and G and L are the gain and the loss term of the ith species. It has been evaluated from the cross-section data [2]. The flux of the ith species is given by $\vec{\Gamma}_i = n_i\vec{u}_i$, where n_i is the density and $\vec{u}_i$ is the diffusion velocity. The momentum balance equation in steady state for i^{th} species is written as:

$$m_i n_i (\vec{u}_i \cdot \vec{\nabla})\vec{u}_i = -\vec{\nabla}P_i - en_i\vec{\nabla}\phi + en_i\mu\vec{u}_i \times \vec{H} - f_i\vec{u}_i \tag{2}$$

Where ϕ is electric potential. For neutral species the forces due to electric and magnetic field would be absent. Here f_i is the effective coefficient of frictional force on i^{th} species assumed to be proportional to diffusion velocity. It arises due to loss of momentum in the collisions with background molecules and in the creation and distruction of the species inside the plasma. It can also be evaluated using cross-section data and collision frequencies.

Plasma eqilibrium in RF field

The discharge is assumed to be created by inductive coupling of RF power through antenna coil wound over cylidrical ceramic chamber. Cylindrical co-ordinate system has been used with $\hat{z}$ axis coinciding with the antenna axis. Due to cylindrical symmetry any variation in the $\hat{\theta}$ direction has been ignored. The z variation in the plasma has been ignored which is a good approximation if $Z >> R$ or in the mid plane of the plasma cylinder. Hence we can write:

$$\vec{H} = H(r,t)\hat{z} \tag{3}$$

$$\vec{E} = E_r(r,t)\hat{r} + E_\theta(r,t)\hat{\theta} \tag{4}$$

$$\vec{u}_i = \tilde{u}_{ir}(r,t)\hat{r} + \tilde{u}_{i\theta}(r,t)\hat{\theta} \tag{5}$$

$$n_i = n_i(r,t) \tag{6}$$

Where $\vec{u}_i$ and n_i are the velocity and density of the ith species respectively. The presence of Magnetic field in the ICP cannot be ignored altogether. Neglecting screening effect, it can be shown that the $\frac{F_{mag}}{F_{elec}} \approx \frac{R(Plasma\ Radius)\ w(rad/sec)}{V_t(Thermal\ velocity)}$ where w is RF frequency. Typically for H^- ion source the, electron temperature is $5\,eV$ and the ion temperature is $\approx 0.5\,eV$. Hence magnetic field has been ignored in the momentum balance of heavy ions while it has been considered in the momentum balance of electron. From the $\hat{\theta}$ component of the momentum balance of electron, writing $E_\theta(r,t) =$

PERIODIC ION CURRENT BURST IN 6.4 GHZ ECR SOURCE

G.S. Taki[#], P.R. Sarma, R.K. Bhandari, Variable Energy Cyclotron Centre, Kolkata, India
A.G. Drentje, Kernfysisch Versneller Instituut, Groningen, The Netherlands
T. Nakagawa, Institute of Physical and Chemical Research (RIKEN), Wakoshi, Japan
P.K. Ray, Bengal Engineering and Science University, Howrah, India

Abstract

We studied the enhancement in extracted ion current in the 6.4 GHz ECR ion source at VECC, Kolkata by inserting a negatively biased disc. In addition to the expected increase in current, we observed a sudden jump in the current at some low bias voltage. We recently measured and analyzed the time spectra of high charge state ion current for neon to understand the origin of the jump. It revealed the presence of a burst frequency in kilohertz range. This frequency shows a synchronous jump with the ion current and also a good linear correlation with it. This may signify that current per burst is a constant factor ; higher current means that there are more number of bursts.

INTRODUCTION

Various techniques are employed for enhancing the extracted beam current from Electron Cyclotron Resonance (ECR) ion sources. The most common method is to add a lighter gas to the sample gas in order to reduce the ion temperature thereby increasing the retaining time and thus the ion current [1]. Another approach is to supply low temperature electrons to the main stage plasma. In this process the plasma becomes more stable, as a result of which the ion confinement time increases. Wall coating [2], use of an electron emitter [3], and the insertion of a biased disc [4-6] are the cold electron supplying techniques.

The use of biased disc in ECR sources was first demonstrated by Melin et al. [4]. In recent years, this technique has become the most popular method of increasing the extracted ion current from an ECR ion source. Melin [4] and Gammino et al. [7] systematically studied the improvement in ion current by biased probes. The improvement was thought to be due to an increase in the electron density with the application of a negative potential. D. Meyer [8] suggested that when negative potential is applied on the disc, the plasma potential decreases making the ECR plasma more stable. As a result, high charge state production increases. Tarvainen et al. [9] and Mironov et al. [10] made measurements on the plasma potential and found that it decreased when the negative potential at the biased disk was increased.

In order to study the performance of the biased disc systematically we made measurements on the extracted ion current by varying the disc bias potential [11,12]. The modification undertaken on the vacuum system allowed

the source to sustain a base pressure of 6×10^{-8} Torr on the injection side. The measurements showed that as the negative bias potential was increased, the extracted ion current for any species showed a small decrease and then at a small negative potential it jumped to a high value. As the potential was further increased, the ion current also increased and saturated at a large bias potential.

Fig.1. shows typical results of the measurement on ions of various charge states. It is to be noted that the potential at which the current abruptly jumps is the same for all species. Another interesting feature is that for H^+ the ion current jumps to a lower value.
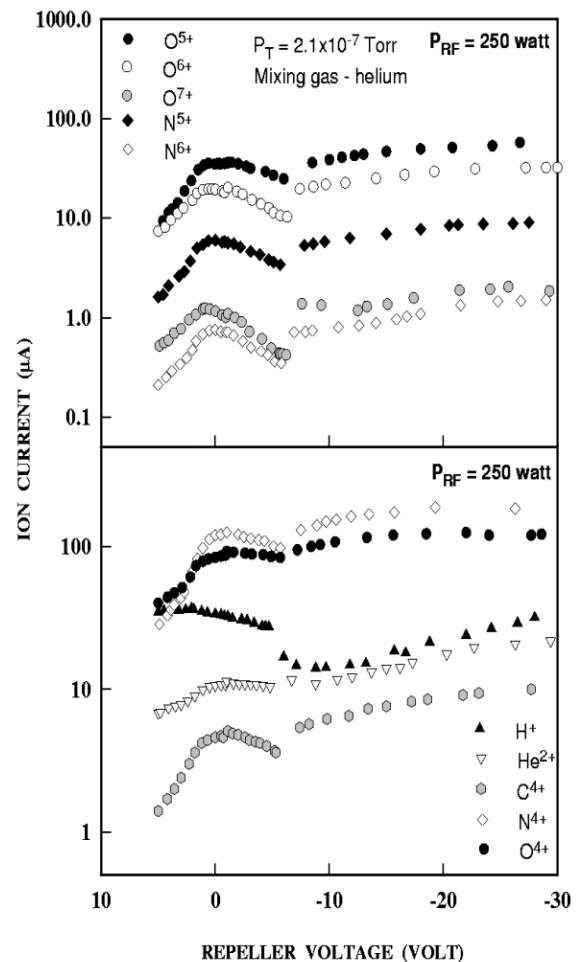
Figure 1: Variation of ion current with bias voltage.

_____
[#] gstaki@veccal.ernet.in

BEAM LINE DESIGN FOR PEFP USER FACILITY*

Y.S. Cho[#], B.C. Chung, K.Y. Kim, Y.H. Kim, K.R. Kim, Y.Y. Lee, B.H. Choi, Proton Engineering Frontier Project, Korea Atomic Energy Research Institute, Daejeon 305-353, Korea.

Abstract

In the Proton Engineering Frontier Project (PEFP), 20MeV and 100MeV proton beams from a 100MeV proton linear accelerator [1] will be supplied to users for beam applications. The basic lattice for beam transport line will be FODO from the linac to the targets. Dipole magnets exited with shaped AC currents will distribute the beam from the linac to five targets simultaneously. To provide flexibilities of irradiation conditions for users from many application fields, we design beam lines to the targets with wide or focused, external or in-vacuum, and horizontal or vertical beams. The details of the beam line design will be reported.

INTRODUCTION

The main concept of the PEFP proton beam facility is that a high power proton accelerator supplies proton beam to many users simultaneously. This concept can be compared with a facility with many low power proton accelerators for many users. Based on the user demand survey for proton beam applications, we have chosen a facility with a high power accelerator. There are many types of proton accelerator for proton beam applications, such as cyclotron, synchrotron, and linac. Because the capability of high beam power is the most important feature, we have decided to choose a linac for the main accelerator of the facility. Figure 1 shows the schematic diagram of the PEFP user beam line.

Proton beams of 100MeV and 20MeV will be extracted and distributed to maximum five users simultaneously by AC magnets with a programmable current power supply. We will control the beam energy stepwise with RF ON/OFF of each DTL tank. To control the beam energy continuously, we will put energy degraders and energy filters in the beam lines for special applications.

BEAM LINE REQUIREMENTS

The surveys for proton beam demand from many application fields, such as nano-technology (NT), bio-technology (BT), space technology (ST), and radio-isotope production, have been done through the homepage (http://www.komac.re.kr) and the user program from 2003 to 2006. From these activities, we have selected the common requirements for many applications and have summarized the beam line requirements for 10 beam lines of 100MeV and 20MeV, which are shown in Table 1 and 2. In the selection process, we have put more weighting to high beam power applications, which will be main applications in this facility.

Table 1: 100MeV beam line requirements

Beam Line No.	Energy	Avg. Current	Irradiation Condition	Max. Target Size
BL100	100MeV	~1.8mA	Horizontal Vacuum	Beam Dump
BL101	33,45,57, 69,80,92, 103MeV	30~ 300μA	Horizontal Vacuum	100mm
BL102	20~ 103MeV	~10μA (10nA)	Vertical External	300mm
BL103	20~ 103MeV	30~ 300μA	Horizontal External	300mm
BL104	20~ 103MeV	10nA ~10μA	Horizontal External	300mm
BL105	103MeV	30~ 300μA	Horizontal Vacuum	100mm
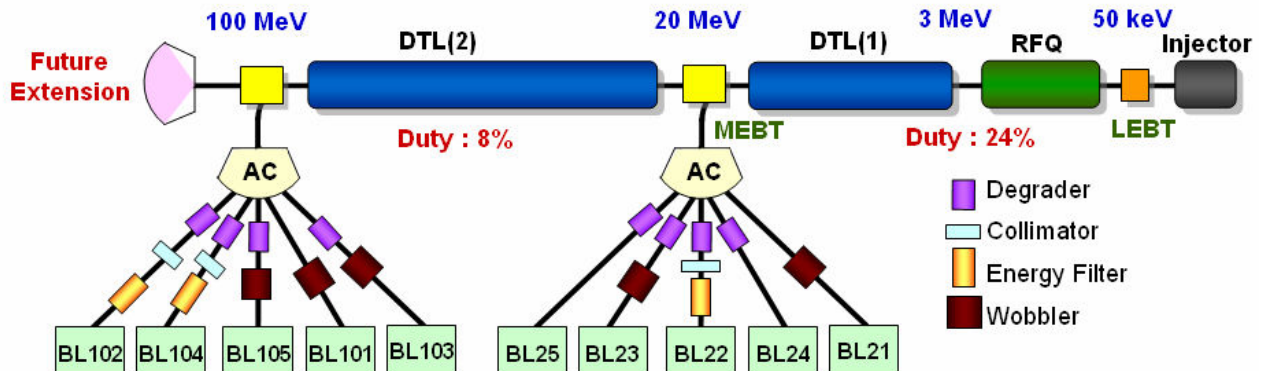
Figure 1: Schematic diagram of PEFP user beam line.

04 Hadron Accelerators

T12 - Beam Injection/Extraction and Transport

HIGH POWER NEUTRON CONVERTER FOR LOW ENERGY PROTON/DEUTERON BEAMS: PRESENT STATUS*

A.Antoshin, M.Avilov, D.Bolkhovityanov, S.Fadeev, K.Gubin, N.Lebedev, P.Logachev,
P.Martyshkin, S.Shiyankov, BINP, Novosibirsk, Russia,
L.Tecchio, INFN-LNL, Legnaro, Italy.

Abstract

In BINP, Russia, the high temperature neutron target for SPES project (INFN-LNL, Italy) is proposed. The target is designed to produce up to 10^{14} neutron per second within the energy range of several MeV under irradiation by proton/deuteron beam of power up to 200 kW. By now, the target prototype is successfully tested. The development of liquid metal driving system and target general design is started. This paper describes the design of the target and the target prototype as well as the results of prototype tests under high-power electron beam.

Special attention is paid to the carbon material with high content of ^{13}C isotope. The material is produced in accordance with the original technology and is used for manufacturing the converter irradiated with the proton beam.

INTRODUCTION

In the framework of the European program, to define a second generation Radioactive Ion Beam (RIB) facility, the Legnaro National Laboratories (LNL) are proposing the construction in the next years of a specialized national facility for RIB originated by fission fragments produced by fast neutrons (SPES) [1]. Protons/deuterons of 40 MeV and 150 kW will produce in a converter about 10^{14} neutrons per second centered at around 14 MeV that will induce fission in a suitable fissile target, with the aim of 10^{13} fission per second at least.

The neutron energy distribution, the target size and its constituents are the most important parameters to be investigated in order to maximize the efficiency for RIB production. A few different methods for producing fast neutrons and their induced fissions following the (p,xn) or (d,xn) reactions on different materials were investigated.

Designing the SPES facility, simulations of neutron spectra for several beam converter materials/configurations have been performed with the MCNPx [2] and the PRIZMA [3] codes. Furthermore, the isotopic distributions are evaluated combining the MCNPx with the code SP-FISPACT2001 [4] that allows the neutron transport below 20 MeV. The simulations performed were compared with experimental angular distributions measured at energies of 20, 40, 50 and 90 MeV for ^{12}C, ^{13}C and beryllium converters.

Results of simulations show the difference of neutron yield between different converter material are not critical, optimal target construction is more important. Calculated neutron angle-energy distributions allowed to estimate the different isotopes production and radiation shielding, to propose and optimize the full target system assemblage (see fig.1).

The design of the converter and its prototype and the results of the prototype tests are discussed in detail in the following paper.
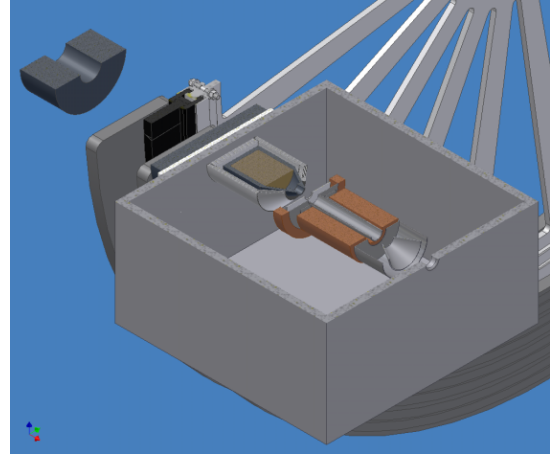
Figure 1: Layout of the SPES target system. Left to right: protecting collimator, neutron converter inside the cooling panels, fission target, ion source.

CONVERTERS AND PROTOTYPE DESIGN

The proposed target design [5] comprises the carbon converter assembled with plates, which are mounted on rotating metal disk (see fig.1). The converter material considered is ^{13}C (for proton beam) and natural carbon (for deuteron beam), both under graphite form with thickness of 10 mm, suitable to stop full beam inside it. The diameters of the wheel and of the rotating shaft are close to 100 cm and 5 cm, respectively. The thermal power deposited in the converter material is dissipated only by thermal radiation. Heat removal from vacuum chamber is carried out by water circulating inside aluminum cooling channels fixed to the chamber's walls. Before the converter a collimator acts as a beam position monitor. Beyond the converter, a graphite plate serves to survey and monitoring eventual damages of the converter and, at the same time, protects the vacuum chamber from primary beam.

The converter prototype is described in detail in paper [6]. It is scaled to 1/3 of the real power (50 kW) by reducing its dimensions and limited to 20 MeV equivalent proton beam energy to match the energy and power of the electron accelerator used to perform experimental tests. All construction is assembled inside the special cooled vacuum chamber. The rotation of prototype is carried out

ELECTRON ACCELERATION IN THE WAKE FIELD EXCITED BY 200TW FEMTO SECOND LASER IN UNDERDENSE PLASMA

R. Taki[a], W. M. An[b], Y. Q. Gu[c], Y. Guo[c], W. Hong[c], J. F. Hua[b], W. H. Huang[b], C. Y. Jiao[c],
T. Kameshima[a], S. Kurokawa[ad], Y. Z. Lin[c], H. J. Liu[c], K. Nakajima[ad], H. S. Peng[c], L. Sun[c],
C. M. Tang[c], C. X. Tang[b], X. D. Wang[c], X. D. Wang[e], T. S. Wen[c], X. L. Wen[c], Y. C. Wu[c],
B. H. Zhang[c], K. N. Zhou[c] and Q. H. Zhu[c]

[a]Department of Accelerator Science, Graduate University for Advanced Studies, 1-1 Oho, Ibaraki 305-0801, Japan

[b]Department of Engineering Physics, Tsinghua University, Beijing 100084, P.R.China

[c]Laser Fusion Research Center, China Academy of Engineering Physics, Mianyang, Sichuan 621900, P.R. China

[d]High Energy Accelerator Research Organization, 1-1 Oho, Ibaraki 305-0801, Japan

[e]University of Southern California, Los Angeles, California 90089-0484, USA

Abstract

Laser-plasma acceleration experiment has been carried out using 200TW, 30fs Ti:Sapphire laser pulses focused on helium gas-jets with F/8.75 optics. Intense mono-energetic electron beams have been produced by controlling plasma length and density precisely. Energy spectral oscillations of accelerated electrons in respect to ejection angle have been also observed. Measurement of images from Thomson scattering and fluorescence side scattering from plasma indicate highly relativistic effects such as a long self-channeling and filamentation. It seems that these nonlinear phenomena strongly disturb high energy gain acceleration and high quality beam generation.

INTRODUCTION

Wake-field acceleration including plasma beat wave, plasma wake-field and laser wake-field acceleration has been studied to take advantage of high acceleration gradient which promises a compact accelerator. Recently good quality and high energy electrons have been demonstrated based on laser wake-field acceleration [1-3]. The recent development of laser technology enables us to use ultra-high power and short pulse lasers which can excite a large amplitude plasma wave. Electron motion in large amplitude plasma is involved in nonlinear dynamics. It has been studied theoretically and in particle-in-cell simulations [4,5], however, not well demonstrated experimentally yet. Here we present the results of electron acceleration in the nonlinear plasma wave excited by 200 TW femto second pulses.

EXPERIMENTAL SETUP

The experiment was performed with Ti:Sapphire laser system "SILEX-1" at CAEP [6]. The laser pulses of 800 nm wave length and 30 fs duration with 4 - 8.3 J were focused with F/8.75 optics onto helium gas-jets. The laser spot radius, w_0, was 12 μm, which yields peak intensity

up to $1.8 – 3.8 \times 10^{19}$ W/cm^2 and the laser strength parameter, a_0, up to 2.9 – 3.8 on assumption that the energy concentration is 30%. The laser was polarized in horizontal axis. The experimental setup for electron energy measurements is shown in Fig. 1. Thomson scattering images from plasma were recorded by a charge-coupled device, CCD, camera (CCD1) which was set on top of a gas-jet applying a band-pass filter with the wave range of 800 nm ± 10 nm in front of the CCD camera. Fluorescence side scattering images were also monitored by a CCD camera (CCD2) followed by a band-pass filter with the wave range of 400 nm ± 10 nm. Accelerated electrons were momentum analyzed using a permanent magnet, a phosphor screen, DRZ, placed just after the exit of the magnet, and a CCD camera (CCD3). Backward Raman scattering was measured by an optical multi-channel analyzer (OMA) system.
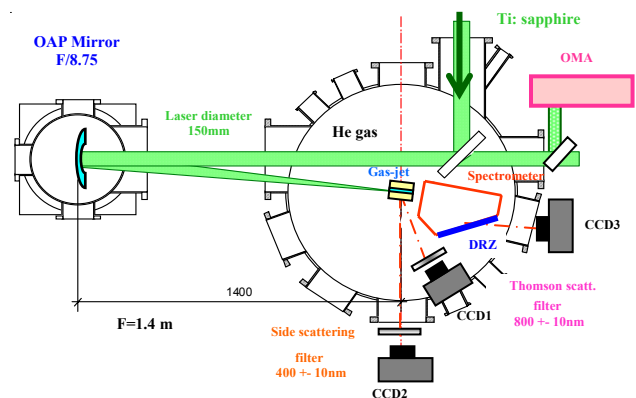
Figure 1: Schematic layout of the experimental setup for electron energy measurements.

Helium gas-get nozzles

We used two kinds of nozzles shown in Fig. 2(a) and (b) to adjust the plasma lengths. The nozzle in (a) is a supersonic Laval nozzle [7] which has a rectangular slit

MULTIPACTING IN A COAXIAL CAVITY

M.M. Rahman, University of Chittagong, Chittagong;
K. Hosoyama, S.-I. Kurokawa, KEK, Ibaraki

Abstract

Residual Gas Molecules on Multipacting

PAPER NOT YET RECEIVED

STATUS OF KEKB AND UPGRADE PLAN TO SUPERKEKB

Mi. Yoshida[#], T. Agoh, K. Akai, M. Akemoto, A. Akiyama, M. Arinaga, K. Ebihara, K. Egawa,
A. Enomoto, J. Flanagan, S. Fukuda, H. Fukuma, Y. Funakoshi, K. Furukawa, T. Furuya, J. Haba,
K. Hara, T. Higo, S. Hiramatsu, H. Hisamatsu, H. Honma, T. Honma, T. Ieiri, N. Iida, H. Ikeda,
M. Ikeda, S. Inagaki, S. Isagawa, H. Ishii, A. Kabe, E. Kadokura, T. Kageyama, K. Kakihara,
E. Kako, S. Kamada, T. Kamitani, K. Kanazawa, H. Katagiri, S. Kato, T. Kawamoto, S. Kazakov,
M. Kikuchi, E. Kikutani, H. Koiso, Y. Kojima, I. Komada, T. Kubo, K. Kudo, N. Kudo,
K. Marutsuka, M. Masuzawa, S. Matsumoto, T. Matsumoto, S. Michizono, K. Mikawa, T. Mimashi,
S. Mitsunobu, K. Mori, A. Morita, Y. Morita, H. Nakai, H. Nakajima, T. T. Nakamura,
H. Nakanishi, K. Nakanishi, K. Nakao, H. Nakayama, S. Ninomiya, Y. Ogawa, K. Ohmi,
S. Ohsawa, Y. Ohsawa, Y. Ohnishi, N. Ohuchi, K. Oide, M. Ono, T. Ozaki, K. Saito, H. Sakai,
Y. Sakamoto, M. Sato, M. Satoh, K. Shibata, T. Shidara, M. Shirai, A. Shirakawa, T. Sueno,
M. Suetake, Y. Suetsugu, R. Sugahara, T. Sugimura, T. Suwada, S. Takano, S. Takasaki,
T. Takenaka, Y. Takeuchi, M. Tawada, M. Tejima, M. Tobiyama, N. Tokuda, S. Uehara, S. Uno,
N. Yamamoto, Y. Yamamoto, Y. Yano, K. Yokoyama, Ma. Yoshida, S. Yoshimoto, K. Yoshino
KEK, Tsukuba, Ibaraki 305-0801, Japan

Abstract

KEKB is an electron-positron two-ring collider for the leading B meson factory. It consists of an 8 GeV electron ring (HER) and a 3.5 GeV positron ring (LER) and their injector linac. It has been operated since December 1998, and has recently marked the peak luminosity of 17.12 /nb/s. This peak luminosity is obtained under the crab-ready beam optics having the robust operating condition by some efforts to solve the optics problems. We are aiming more luminosity improvement after the crab cavity installation. Further the major upgrade plan for SuperKEKB is expected to achieve 400 /nb/s keeping the baseline of the original proposal. This paper describes the recent status of KEKB and upgrade plans for SuperKEKB.

OVERVIEW

The 8 GeV electron and 3.5 GeV positron rings are built in the 3 km-long TRISTAN tunnel. This collider aims to make a detailed study of the B-meson. Especially the CP violation effects are measured in its decay. The energy difference between the electron and positron beams gives a boost to the produced B-meson pairs. This boost makes it possible to measure the time dependent features of B-meson decay due to the large CP asymmetry predicted in B-meson system.

Since the construction of KEKB started in 1994 and the first event was observed by Belle detector in June 1999, the KEKB continuously accumulate its integrated luminosity for 7 years. Figure 1 shows 7-year's history of the KEKB luminosity and beam currents. The KEKB has recently marked the peak luminosity of 17.12 /nb/s (= 1.712×10^{34} /cm^2/s) which is 70 % higher luminosity than the designed peak luminosity of 10 /nb/s. Not only the peak but also the integrated luminosity of 710 /fb has been accumulated with the peak increasement of 1.232

_____
[#]mitsuhiro.yoshida@kek.jp

/fb/day which is obtained in the continuous injection mode operated after 2004.

RECENT STATUS OF KEKB

The recent status of KEKB mainly in 2006 is summarized. A status report before this was written in the previous report [1, 2]. Table 1 shows present machine parameters of KEKB compared with those of about one year ago and the design parameter. The performance progress in the past one year is not very remarkable compared with earlier years. We describe the recent status of KEKB including causes of the present performance limitations.

Table 1: Machine parameters of KEKB

	Design		Dec. 2005		Dec. 2006	
	LER	HER	LER	HER	LER	HER
Energy [GeV]	3.5	8.0				
Circumference [m]	3016.26				3016	
I_{beam} [mA]	2600	1100	1719	1347	1662	1340
# of bunches	5000		1388		1388	
I_{bunch} [mA]	0.52	0.22	1.23	0.97	1.20	0.965
Bunch Spacing [m]	0.59		1.8 - 2.4		2.1	
Emittance [nm]	18	18	18	24	18	24
β_x^* [cm]	33	33	59	56	59	56
β_y^* [cm]	1.0	1.0	0.65	0.62	0.65	0.59
Ver. Size@IP [μm]	1.9	1.9	2.1	2.1	1.9	1.9
RF Voltge [MV]					8.0	15.0
ν_x	45.52	47.52	45.506	44.512	45.505	44.509
ν_y	46.08	43.08	43.531	41.578	43.534	41.565
ξ_x	0.039	0.039	0.117	0.073	0.117	0.070
ξ_y	0.052	0.052	0.096	0.055	0.105	0.056
Lifetime [min.@mA]			135@ 1719	222@ 1347	110@ 1600	180@ 1340
Luminosity [/nb/s]	10		16.27		17.12	
Lum/day [/fb]	~ 0.6		1.183		1.232	
Lum/7 days [/fb]	-		7.358		7.809	
Lum/30 days [/fb]	-		29.018		30.21	

THE BEPCII: CONSTRUCTION AND INITIAL COMMISSIONING

C. Zhang and Q.Qin for the BEPCII Team, IHEP, CAS, P.O.Box 918, Beijing 100049, China

Abstract

The BEPCII, as a natural extension of the BEPC (Beijing Electron-Positron Collider), is a double ring e-e+ collider and a synchrotron radiation (SR) source with its outer ring, or SR ring. As an e-e+ collider, the BEPCII will operate in the beam energy region of 1-2.1 GeV with design luminosity of 1×10^{33} cm-2s-1 at 1.89 GeV. As a light source, the SR ring operates at the beam energy of 2.5 GeV with the design intensity of 250 mA. The project started construction in the beginning of 2004. The upgrade of the injector linac completed in late 2004. The BEPC ring dismount started in July 2005. Installation of the storage ring components except the superconducting (SC) insertion magnets completed in early November, 2006. The improvement of the cryogenics of SC megnets is in progress. The commissioning of the SR ring with conventional magnets in the interaction region (IR) started on Nov. 13 and the first electron beam stored on Nov. 18. The BEPCII has been operating for SR users since Dec. 25, 2006 at 2.5 GeV with the peak beam current of 100-150 mA. The beam lifetime increases steadily and reached about 7 h at beam current of 80 mA with an accumulated beam dose of 45A·h. This paper provides an overview of the construction and initial commissioning of the BEPCII.

GENERAL DESCRIPTION

The BEPCII serves the purposes of both high energy physics experiments and synchrotron radiation applications. The details of the BEPCII design can be found in its design report [1]. The goals of the BEPCII are shown in Table 1.

Table 1: The design goals of the BEPCII

Beam energy	$1-2.0$ GEV
Optimum energy	1.89 GEV
Luminosity	1×10^{33} cm^{-2}s^{-1} @189 GeV
Linac injector	Full energy inj.: $1.55-1.89$GeV Positron inj. rate $\geq$50 mA/min
Dedicated SR	250 mA @ 2.5 GeV

Serving as a collider, the BEPCII will operate in the beam energy region of 1.0-2.1 GeV so that its physical potential in τ-charm range is preserved. The design of the BEPCII aims at a high luminosity. The luminosity of an e+-e− collider is expressed as

$$L(\mathrm{cm}^{-2}\mathrm{s}^{-1}) = 2.17\times10^{34}(1+r)\xi_y\,\frac{E(GeV)k_b I_b(\mathrm{A})}{\beta_y^*(\mathrm{cm})}, \quad (1)$$

where $r=\sigma_y^*/\sigma_x^*$ is the beam aspect ratio at the interaction point (IP), ξ_y the vertical beam-beam parameter, β_y^* the vertical β-function at IP, k_b bunch number in each beam and I_b the bunch current. The strategy for the BEPCII to reach the design luminosity is to apply multi-bunch collisions (k_b=93) with double rings and micro-β at IP with short bunches whose length is compatible to the β_y^* value. The layout and installed double-ring accelerator units in the BEPCII tunnel are shown in Fig. 1.
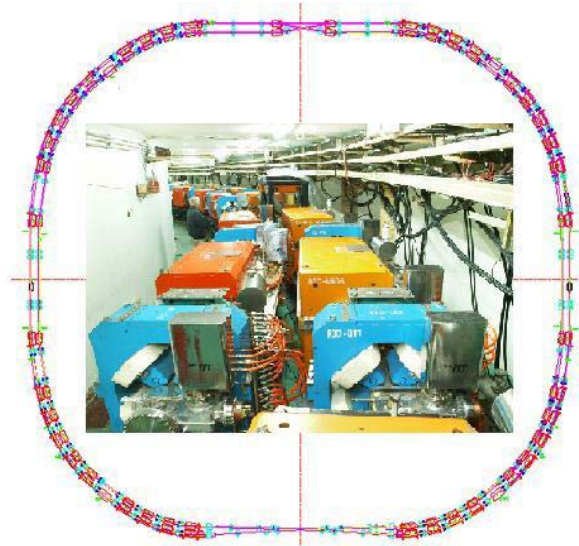
Figure 1: Layout and installed double-ring units.

The inner ring and the outer ring cross each other in the northern and southern IP's. The horizontal crossing angle between two beams at the southern IP, where the detector locates, is 11mrad×2 to meet the requirement of sufficient separation but no significant degradation to the luminosity. While in the northern crossing region, the two beams cross horizontally and a vertical bump is used to separate two beams, so that the optics of the two rings can be symmetric. For the dedicated synchrotron radiation operation of the BEPCII, electron beams circulate in the outer ring with a pair of horizontal bending coils in SC magnets serving this purpose and in the northern IP a bypass is designed to connect two halves of the outer ring. The machine physics issues are intensively studied [2].

The milestones of the BEPCII are as follows:

January 2004	Construction started
May. 4, 2004	Dismount of 8 linac sections started
Dec. 1, 2004	Linac delivered e− beams for BEPC
Mar. 19, 2005	First e+ beam of 50mA obtained
July 4, 2005	BEPC ring dismount started
Mar. 2, 2006	BEPCII ring installation started
Nov. 13, 2006	BEPCII ring commissioning started
Nov. 18, 2006	First e- beam stored in the ring
Dec. 25, 2006	Beams with 2.5 GeV, ~100 mA, ~3h lifetime provided for SR users

INTERNATIONAL COLLABORATIONS IN ILC: R AMP; D ISSUES

C.S. Mishra, Fermilab, Batavia, Illinois

Abstract

ILC Collaborations

PAPER NOT YET RECEIVED

THE INDIA BASED NEUTRINO OBSERVATORY - PRESENT STATUS

V. M. Datar* (on behalf of the INO collaboration), NPD, BARC, Mumbai - 400085, INDIA

Abstract

The current status of the India based Neutrino Observatory (INO) is summarized. The two major physics goals are (a) unambiguous demonstration of neutrino oscillation and a more precise measurement of the associated neutrino parameters and (b) to search for matter effects in neutrino oscillation, using the charge identification capability of the magnetized iron calorimeter, which would help determine the sign of one pair of neutrino mass differences. The status of the 1 m^3 prototype iron calorimetric detector, the design of the 50 kton magnet, the experience with resistive plate chambers used for tracking the charged particles produced in neutrino-iron interactions and the planned electronics and data acquisition system will be presented.

INTRODUCTION

The neutrino was invented by Pauli [1] in 1930 to resolve the energy-momentum conservation and spin-statistics crisis in beta decay. The first evidence of the existence of the electron (anti)neutrino was provided in a pioneering reactor experiment [2]. This was followed by the discovery of the muon neutrino and, much later, the tau neutrino [3]. The helicity of the neutrino was shown [4] to be -1 ± 0.3 in agreement with the two component neutrino theory. An upper limit of the anti-neutrino mass was set at about 55 eV/c^2 through a careful measurement of the beta spectrum in tritium decay near the end point [5]. After unsuccessfully searching for neutrinos at a reactor (which is a copious source of *anti*neutrinos) [6] Davis used the radiochemical detection technique, involving the separation of ^{37}Ar from 600 tons of the cleaning fluid C_2Cl_4 containing ^{37}Cl, to measure neutrinos produced in nuclear reactions, and beta decays of the unstable nuclei produced thereby, in the hot core of the sun [7]. The roughly threefold shortage came to be known as the solar neutrino problem [8]. One of the explanations proposed to explain this shortfall was that the electron neutrinos produced in the solar interior change into another type (flavour) of neutrino, which is not measurable by the ^{37}Cl based detector. This chameleon like behaviour, known as neutrino oscillation, was first proposed by Pontecorvo [9]. The solar neutrino problem was resolved in a definitive manner by the Sudbury Neutrino Observatory experiment [10] using 1 kton of heavy water. Charged current interactions measured the electron neutrinos while neutral current events measured all neutrinos, irrespective of their type or flavour (ν_e, ν_μ, ν_τ). The shortfall in the ν_e flux was recovered in the flux of $\nu_\mu + \nu_\tau$.

Table 1: Best values of neutrino parameters.

Parameter	Exp. value (1σ)
Δ_{21}^2	$(7.9\pm0.4)\times10^{-5}$ eV^2
Δ_{23}^2	$\pm2.4\pm0.2\times10^{-3}$ eV^2
θ_{12}	$34.1°\ ^{+1.6°}_{-1.2°}$
θ_{23}	$41.6°\ ^{+5.7°}_{-2.9°}$
θ_{13}	$<8°$

An equally intriguing problem resulted from the detailed measurements of atmospheric neutrinos. The IMB [11] and Kamiokande [12] collaborations found an anomalous ν_μ/ν_e ratio as a function of zenith angle. This ratio is expected to be close to 2, for high energy neutrinos, and the same for all directions in the absence of oscillations. If ν_μ oscillates into ν_τ the above ratio would be 2 for down going neutrinos but smaller than 2 for upgoing neutrinos. SuperKamiokande provided the first definitive results [13] which showed that neutrinos oscillate and therefore possess a small mass. It may be mentioned that atmospheric neutrinos were first detected at Kolar Gold Fields by an Indian team, just ahead of an experiment led by Reines in a South African mine [14].

The above mentioned, as well as a few more, key experiments have led to a dramatic change in our understanding of neutrinos and cannot be understood within the hitherto successful standard model of high energy physics. The widely accepted explanation of the experimental observations is that neutrinos switch identities, or oscillate into other flavours, as they propagate. This can occur if the flavour eigenstates (electron, muon and tau) are not simultaneously mass eigenstates (m_1, m_2, m_3). In general these two bases are connected by a unitary matrix. For 3 active flavours there are 7 independent parameters *viz.* the 3 mass parameters, 3 mixing angles θ_{12}, θ_{13}, θ_{23} and δ_{CP}. If the neutrino is its own (Majorana) antiparticle there are two additional phases which, however, would not be observable in ν-oscillation experiments. Table 1 lists the presently known experimental values [15]. Here Δm_{ij}^2 is defined as m_i^2-m_j^2.

There are several experiments planned in the near future which will improve the precision further and might even throw up unexpected results. Neutrinos are providing us the first clues to physics beyond the standard model and their study is expected to provide even more surprises. With a view of reentering this exciting area an initiative has been taken to set up an underground laboratory in India. One of the main experiments is aimed at making precision

ASIAN WIDE COLLABORATION ON ACCELERATOR SCIENCES

S.-I. Kurokawa, KEK, Ibaraki

Abstract

Indo Japan Collaboration in Accelerator Science

PAPER NOT YET RECEIVED

REAL-TIME FEEDBACK ON BEAM PARAMETERS

Ralph J. Steinhagen (CERN, Geneva, Switzerland)

Abstract

Traditionally, tight beam parameter stability requirements were most pronounced for light sources and lepton colliders but have now become increasingly important for present and future hadron accelerator operation, not only for performance but also for reasons of machine protection, as recent improvements have led to significantly increased stored beam energies.

In the latest generation machines, performance depends critically on the stability of the beam. In order to counteract disturbances due to magnetic imperfections, misalignments, ground motion, temperature changes and other dynamic effects, fully automated control of the key beam parameters – orbit, tune, coupling, chromaticity and energy – becomes an increasingly important aspect of accelerator operation.

This contribution presents an overview of beam-based feedback systems, their architecture, performance limitations and design choices involved.

INTRODUCTION

With respect to beam-based feedback systems, the wide range of accelerators can be grouped roughly into synchrotron light sources, lepton and hadron colliders that are distinct in their requirements of number and type of feedbacks deployed.

The requirements on beam stability in synchrotron light sources are determined by the quality and properties of the photon beam seen by experiments. Depending on the time scale of the experiment's data integration and perturbation frequency, movements of the beam centroid may either "smear out" the effective emittance, which has a deteriorating effect on the photon beam quality, or lead to an increase of measurement noise. Due to synchrotron radiation, the beam emittance is usually much smaller in the vertical plane. To preserve and minimise the effective emittance, nearly all light sources deploy fast orbit and energy feedbacks. These minimise transverse beam movements, spurious dispersion by centering the beam in the quadrupoles and maintain a stable vertical orbit inside the sextupoles that would otherwise give rise to emittance coupling. A summary and overview of beam stability requirements and stabilisation in synchrotron light source can be found in [1–4].

The beam stability requirements in lepton and present hadron colliders are driven by luminosity optimisation inside the experimental insertions. They favour, similar to light sources, small emittance and stable beam overlap at the interaction point ([5–7]). In addition to orbit feedbacks,

tune feedbacks are often also deployed ([8, 9]) to stabilise the beam during acceleration and to avoid resonances that may cause increased particle loss.

Recent improvements in hadron colliders lead to significantly larger stored beam energies which require an excellent control of particle losses inside a superconducting machine. In case of the LHC, the energy stored in the beam is sufficient to quench all magnets and cause serious damage [10]. Thus, most requirements on key beam parameters in superconducting hadron colliders strongly depend on the capability to control particle losses inside the accelerator. In the case of the LHC, the Cleaning System has the tightest constraints on the orbit and requires a stability better than $25\,\mu m$ during nominal operation at the location of the collimators [11, 12]. Other requirements range from 0.5-0.2 mm r.m.s. for global stabilisation down to $10\,\mu m$ for physics analysis improvements in the TOTEM experiment [13].

In contrast to lepton machines that require tune stability in the order of $\delta Q \approx 10^{-2}\ldots 10^{-3}$ to avoid up to 4th order resonances, synchrotron radiation damping is negligible in hadron colliders. In order to provide sufficient beam lifetime, resonances of up to the 12th order have to be avoided [14]. The corresponding tune stability δQ is thus required to be better than 0.001 at the LHC. The chromaticity has to be controlled within $Q' \approx 2 \pm 1$, while the uncorrected chromaticity changes are expected to exceed more than 100 units within a few hundred seconds after the start of the ramp [14].

PARAMETER STABILITY

The wide range of perturbation sources that may affect orbit, tune, coupling, chromaticity and energy can be grouped into:

1. Environmental sources, driven by temperature and pressure changes, ground motion, tides and noise induced by human activity which are mostly propagated through quadrupoles and their girders onto the beam,

2. Machine-inherent sources, such as the decay and snap-back of magnet multipoles, cooling liquid flow, vibration of pumps and ventilation, eddy currents and changes of machine optics (final focus),

3. Machine element failures, which are mainly important for large machines such as the LHC where the single circuit failure out of more than 1300 corrector circuits is non-negligible during regular operation.

Their time scale ranges usually from long-term (month to days) over medium term (days to hours) down to short term

BEAM INSTRUMENTATION EXPERIENCE AT ATF[*]

Yosuke Honda, High Energy Accelerator Research Organization (KEK), Tsukuba, Japan
ATF International Collaboration

Abstract

With its low-emittance stable electron beam, ATF in KEK has been an unique facility to develop various beam instruments. This paper reviews some of those devices that are used in the operation, were tested in the past, and being under development.

INTRODUCTION

Accelerator Test Facility (ATF) in KEK is a test accelerator to produce a high quality electron beam required in ILC. It consists of an injector linac, a damping ring (DR) and an extraction line. Beam energy is 1.3 GeV, nominal beam charge is 1×10^{10} e/bunch, and pulse repetition rate is 1.56 Hz in the usual operation. There are three types of operational modes, a single bunch mode, a multi-bunch mode of 20-bunches with 2.8 nsec bunch spacing, and a 3-bunches mode with 150 nsec spacing.

The damping ring reduces transverse emittances of the beam down to 1.5 nm·rad and 6 pm·rad in horizontal and in vertical plane, respectively ([1]). Emittance tuning procedures are routinely performed applying corrections to reduce dispersions and couplings based on beam orbit measurements around the DR. The emittance realized in the DR can be measured by three types of monitors, SR-interferometer, X-ray SR imaging monitor and Laserwire monitor. The typical dimensions of the damped beam are 100 μm in horizontal, 10 μm in vertical, and 8 mm in longitudinal.

After beam reaches to the equilibrium in the DR, it is kicked out to the extraction line. The emittance in the extraction line is measured with wire-scanners. The extracted low-emittance beam has been useful to test various devices, such as cavity BPMs, laser-wire, ODR, OTR and fast feedback system (FONT). Recently, most of the beam operation shifts are devoted for development works of these new instruments.

It is scheduled to extend the extraction line for building a test beam line for ILC final focus (ATF2 [2]). Its construction will start in the summer of 2007. Monitors to be used in ATF2 are also being tested.

This article reviews development works of various instruments in ATF. In the following, the instruments are categorized into four sections, beam position monitors, beam size monitors, bunch length monitors, and beam control.

BEAM POSITION MONITORS

Beam position is the most essential information. Single shot pick-up BPMs are used for usual operation. Recently, lots of works were done on cavity BPMs using the extracted beam. In the new beam line of ATF2, cavity BPMs will be used as main monitors for operation.

Pick-up BPM

The diameter of the beam duct is 24 mm in the most part of the beam line. Button type pick-ups are used in the DR, and strip-lines are used in the linac and in the extraction line. In order to quickly measure beam positions in shot-by-shot basis, a single-shot wide-band detection system was developed. The band width of the processor reaches up to 1 GHz, which almost covers the spectrum of the signal after transported to the outside of the tunnel. Bi-polar signals from pick-ups are clipped into uni-polar signals with a diode detector, then they are recorded by 14 bit charge sensitive ADCs. Each channel of the processors was calibrated using a dummy pulse distributed to all channels at the same time. The resolution reaches to 2 μm at 10^{10} e/bunch beam intensity.

Damping ring BPM upgrade

In order to realize further small vertical emittance, tests to improve the DR BPM by replacing it to a narrow-band system have started. Heterodyne receivers following narrow-band BPFs are installed closely to the pick-ups. On board processors with digital waveform recorders process signals of every beam revolutions. It is expected to have 100 nm resolution with 500 nm accuracy in a machine cycle.

Cavity BPM

Electro-magnetic modes in a cavity-like structure on beam ducts are excited by the beam passage. Among the various resonant modes, transverse dipole modes are useful to measure the beam positions because their field strength are proportional to the product of beam charge and the beam offset with respect to the electrical center. The beam signal is read out through a selective coupler which couples only with the dipole mode. Its strong and narrow-band signal enables us to measure the beam position with ~nano-metre resolution. Mechanical rigidness and reliability of the electric center are also advantages of cavity BPMs. This types of BPMs are expected to play important roles in ATF2 and future accelerators.

CHALLENGES IN ILC INSTRUMENTATION

M.C. Ross, SLAC, Menlo Park, California

Abstract

Challenges in ILC Instrumentation

PAPER NOT YET RECEIVED

UPGRADES TO THE ISIS SPALLATION NEUTRON SOURCE

C.R. Prior, CCLRC Rutherford Appleton Laboratory, Chilton, Didcot, Oxon, U.K.

Abstract

With studies of a European Spallation Source (ESS) suspended and high-level discussions taking place over the future of neutrons in Europe, efforts are being made to ensure the sustained success of ISIS well into the foreseeable future. Recent developments include upgrading the injector by replacing the Cockcroft Walton with an RFQ, and installation of a new dual harmonic RF system that should eventually enable up to 50% more protons to be accelerated in the ring. A programme of ion source development also aims at improved reliability, enhanced beam current and longer life-time. This promise of more beam power has led to construction of a second target station providing users with additional experimental facilities starting in October 2008. In the longer term, ideas are forming either for a new high intensity proton driver or for a phased development of ISIS to the 5 MW level. As an alternative to generating neutrons, such a machine might also be part of a neutrino factory, a complex of accelerators generating neutrinos from muon decay. This paper describes these activities and identifies their relative importance on an international development scale.

INTRODUCTION

At the heart of the ISIS facility at the Rutherford Appleton Laboratory (RAL) in the United Kingdom is a set of accelerators that together form an extremely robust, reliable and stable machine. The ISIS source celebrated its twentieth anniversary of neutron production in 2004, and with a proton beam output of 0.16 MW has held the accolade of the world's most powerful pulsed proton source for a number of years. Much high quality research has been carried out, with important developments over a range of topics relating to physical and biological sciences. Operational experience and technological progress have provided valuable guidance for studies towards future accelerator-based neutron sources. ISIS is increasingly seen as a benchmark not only for neutron production but also as a starting point for a high power proton accelerator. Many of the ideas behind its design have had a bearing on the US spallation neutron source (SNS), the Japanese high intensity accelerator facility (J-PARC), and spallation neutron facilities proposed for Europe, China and India.

However ISIS is now an elderly machine. Its purported successor - a new European Spallation source (ESS) [1] - was developed between 1990-2002, and discussions over its construction continue at a high level but no decision has yet been reached. Given the high demand for neutrons in Europe, it is important in the first instance to ensure that ISIS continues to run reliably at its present level. At the same time there is a need to look towards the future. A relatively modest upgrade seems feasible in the medium term, and regardless of whether ESS is or is not built, ways to increase the beam power to at least 1 MW and possibly as high as 5 MW are being explored.

ISIS

The ISIS accelerating system (Figure 1) is based on a 70 MeV H^- linac injecting via an Al_2O_3 stripping foil into an 800 MeV, 50 Hz proton synchrotron. Between 5 and 10% of the injected beam is lost during trapping and initial acceleration. Each pulse consists of two bunches of about 120 ns duration, directed onto a tantalum-clad tungsten target, where a variety of experiments are carried out for condensed matter research.
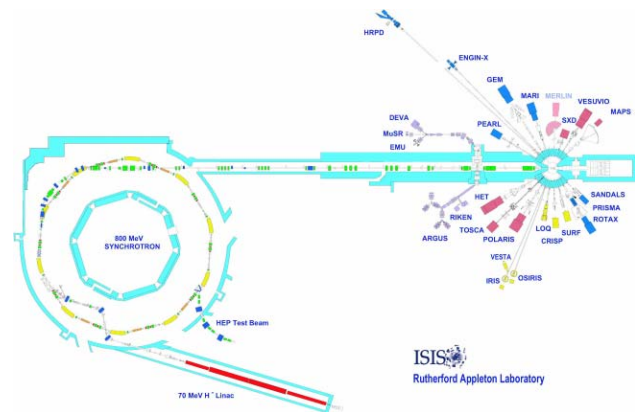
Figure 1: The ISIS Spallation Neutron Source

In its present configuration, the machine is limited by space charge to an intensity of 2.5×10^{13} protons per pulse, but a programme of development aims to increase this by perhaps as much as 50% at relatively modest cost. The key to this was identified in an earlier study [2] and involves a combination of $h = 2$ and $h = 4$ RF cavities. By carefully balancing parameters, stable areas of longitudinal phase space can be increased, allowing more beam to be injected without change in either the peak bunch current or the transverse tune shift. It is important to keep beam loss as small as possible, which is achieved by modulating the peak voltages during the accelerating cycle and controlling the relative phases between the RF harmonics in a specific way The new cavities were installed in

CHINA SPALLATION NEUTRON SOURCE DESIGN*

J. Wei[†3,1], S.-X. Fang[1], J. Feng[2], S.-N. Fu[1], H.-F. Ouyang[1], Q. Qin[1], H.-M. Qu[1],
J.-Y. Tang[1], F.-W. Wang[2], S. Wang[1], Z.-X. Xu[1], Q.-W. Yan[2], J. Zhang[2], Z. Zhang[2]
for the China Spallation Neutron Source (CSNS) teams
Institute of High Energy Physics, China[1]; Institute of Physics, China[2];
Brookhaven National Laboratory, USA[3]

Abstract

The China Spallation Neutron Source (CSNS) is an accelerator-based high-power project currently in preparation under the direction of the Chinese Academy of Sciences (CAS). The complex is based on an H^- linear accelerator, a rapid cycling proton synchrotron accelerating the beam to 1.6 GeV, a solid tungsten target station, and five initial instruments for spallation neutron applications. The facility will operate at 25 Hz repetition rate with a phase-I beam power of about 120 kW. The major challenge is to build a robust and reliable user's facility with upgrade potential at a fractional of "world standard" cost.

INTRODUCTION

There exist three classes of high-power spallation neutron facilities[1, 2]: continuous-wave (CW) facilities driven by high energy, high intensity cyclotrons or linacs (e.g. the operating SINQ isochronous-cyclotron at PSI with a beam power of 1.2 MW at 590 MeV [3]); long-pulse (ms) facilities driven by high energy, high intensity linacs (e.g. the operated LAMPF proton linac with a beam power of 1 MW at 800 MeV [4] and the PEFP under construction in Korea with a high-duty 100 MeV linac [5]); and short (μs) pulse facilities driven by a combination of high intensity linacs and rings, as shown in Fig. 1 [4, 6, 7, 2]. Among the short-pulse facilities are two types of accelerator layout: a full-energy linac followed by an accumulator (e.g. the operating LANSCE linac and PSR with a beam power of 80 kW at 800 MeV [4] and the SNS project just commissioned at ORNL with a 1 GeV superconducting (SC) RF linac and an accumulator [8]) and a partial-energy linac followed by a rapid cycling synchrotron (RCS) (e.g. the operating ISIS facility at RAL with a beam power of 160 kW from a 70 MeV linac and a 800 MeV synchrotron [9] and the J-PARC under construction in Japan with a 400 MeV linac and 3 GeV and 50 GeV synchrotrons [10]).

CSNS is an accelerator-based short-pulse facility with a partial-energy linac followed by a RCS. CSNS provides a multidisciplinary platform for scientific research and applications by national institutions, universities, and industries [12, 13, 14]. The high-flux pulsed neutrons from CSNS will compliment cw neutrons from nuclear reactors and synchrotron lights from synchrotron radiation facilities. Strongly advocated by the users groups, the CSNS
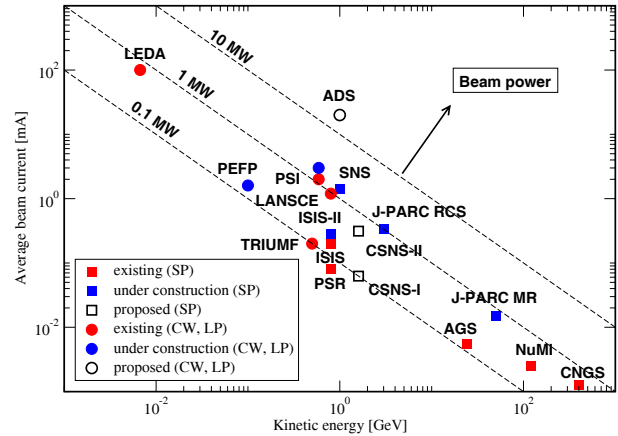
Figure 1: Accelerators at the power frontier (short pulse SP, long pulse LP, continuous wave CW).

project was approved by the Chinese central government in 2005.

As shown in Fig. 1 and Table 1, the CSNS accelerator is designed to deliver a beam power of 120 kW with the upgrade capability of up to 500 kW by raising the linac output energy and increasing the beam intensity.

Table 1: CSNS accelerator primary parameters.

Project Phase	I	II	II'
Beam power on target [kW]	120	240	500
Proton energy on target [GeV]	1.6	1.6	1.6
Average beam current [μA]	76	151	315
Pulse repetition rate [Hz]	25	25	25
Proton per pulse on target [10^{13}]	1.9	3.8	7.8
Pulse length on target [ns]	<400	<400	<400
Linac output energy [MeV]	81	134	230
Ion source/linac length [m]	50	76	86
Linac RF frequency [MHz]	324	324	324
Macropulse ave. current [mA]	15	30	40
Macropulse duty factor [%]	1.1	1.1	1.7
LRBT length [m]	142	116	106
Synchrotron circumference [m]	230.8	230.8	230.8
Ring filling time [ms]	0.42	0.42	0.68
Ring RF frequency [MHz]	1.0-2.4	1.3-2.4	1.6-2.4
Max. uncontr. beam loss [W/m]	1	1	1
Target material		tungsten	
Moderators		H_2O, CH_4, H_2	
Number of spectrometers	5	18	>18

HIGH POWER PROTON ACCELERATOR IN KOREA*

Byung-Ho Choi, Jun Yeon Kim, Kye Ryung Kim, Hyeok-Jung Kwon, Ji-Ho Jang, Kui Young Kim,
Jae Won Park, Sun An, Byungchul Chung, Yong Young Lee and Yong-Sub Cho[#]
PEFP, Korea Atomic Energy Research Institute
P.O.Box 105, Yueong, Daejeon 305-353, Republic of Korea

Abstract

A high power proton accelerator project, Proton Engineering Frontier Project (PEFP), as one of the 21C Frontier Projects promoted by Korean Government, has the goals to develop a 100 MeV high current proton linear accelerator and the user programs for its beam utilization and industrial applications. The upstream part of the 100 MeV linac, the 20 MeV linac, was successfully developed and tested. The rest part of the accelerator and beam lines and user facilities are under development, and also the site preparation and construction works are in progress. In parallel, proton beam utilizations and accelerator application technologies have been extensively studied and developed. In this paper, the status and the future plan of the project, including beam test results of the 20 MeV linac, site preparation and construction works, and development of proton beam utilization and user program are presented.

INTRODUCTION

A high-power proton accelerator (HPPA) can produce intense beams of protons and secondary particles, such as neutrons, radioisotopes, mesons, and neutrinos. Such intense beams provide us with the practical and efficient means to realize quantum engineering. High-current proton beams with low energy (< 10 MeV) are useful in industrial and defense applications, such as ion-cutting, power semiconductors, mine detection, boron neutron capture therapy, and neutron radiography. Low-current proton beams with moderate energy (10–250 MeV) are valuable in biological and medical researches and applications, for example, mutations of plants and micro-organisms, proton and neutron therapy, and radioisotope production. High-power proton beams with energies around 1 GeV are widely utilized in spallation neutron sources, radioisotope beam facilities, nuclear and high-energy physics experiments, and accelerator-driven systems.

The PEFP was launched by the Korean government in 2002 to realize potential applications of the intense proton beams. Its primary goal in the first stage is to develop a high-current proton linear accelerator to supply 100 MeV, 20 mA proton beams and to construct beam line facilities, with which the users can access the proton beams with wide ranges of energies and currents for their research

and development programs [1]. In addition, the PEFP accelerator can be exploited as a proton driver for various applications in the low- to medium-energy range, or an injector for a high-energy proton machine in the next stage of development.

ACCELERATOR DEVELOPMENT

We have successfully developed a 20 MeV proton linac in the first phase of the project, which consists of a 50 keV proton injector, a 3 MeV RFQ, and a 20 MeV drift tube linac (DTL). In the second phase, we will develop the high energy part of the PEFP 100 MeV linac and beam line facilities which supply the users with the low and medium energy proton beams. Two user facilities are to be installed to utilize the 20 MeV and 100 MeV proton beams at the end of the 20 MeV and 100 MeV accelerating structures, respectively. The schematics of the PEFP linac and beam line facilities are illustrated in Fig. 1. Some characteristic parameters of the accelerator are given in Table 1 [2].
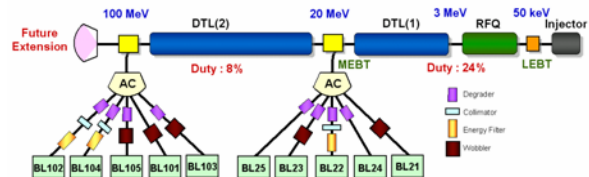
Figure 1: Schematics of the PEFP 100 MeV linac and beam line facilities.

Table 1: Characteristics of the PEFP accelerator.

Energy (MeV)	20	100
Energy spread (%)	< 1%	< 1%
Peak current (mA)	1~20	1~20
Max. beam duty (%)	24	8
Average beam current (mA)	0.1~4.8	0.1~1.6
Pulse width (ms)	0.1~2	0.1~1.33
Max. repetition rate (Hz)	120	60
Max. beam power (kW)	96	160

The injector consists of a duoplasmatron H^+ ion source and a low-energy beam transport (LEBT). The extracted beam current from the source reached up to 50 mA at a voltage of 50 kV. The extracted beam has the normalized emittance of 0.2 π mm-mrad with the proton fraction more than 80%. To achieve a pulsed operation, a high-voltage switch is installed, of which rising and falling times are less than 50 ns, respectively [3]. The LEBT consists of two solenoid magnets, which focus the protons and filter the H_2^+ ions, and two steering magnets which control the beam position at the entrance of the RFQ.

SUPERCONDUCTING CYCLOTRON PROJECT AT VECC

Rakesh Kumar Bhandari (for the VECC Staff)

Variable Energy Cyclotron Centre, I/AF Bidhan Nagar, Kolkata-700 064, India

Abstract

Construction of the K-500 superconducting cyclotron at Kolkata is now in final stages. The main magnet was operated satisfactorily for almost one year during 2005-2006. The coil was continuously kept cooled at 4.5K temperature during the entire period. Extensive magnetic field measurements were done for correction of the imperfections, centering of the main coil, calculation of operational settings, calculation of extraction trajectory etc. Subsequently, in April 2006 the coil has been warmed up to facilitate assembly of other systems of the machine. All major systems have been fabricated and the assembly is currently going on. We plan to start the commissioning tests later in the year 2007. In this paper our experience with the operation of the main superconducting magnet and magnetic field measurements will be discussed. Developmental highlights of various systems will be briefly presented.

INTRODUCTION

The main magnet of the superconducting cyclotron is designed to operate at about 800A current in each α as well as β coil producing a maximum of about 6T magnetic field [1]. The main magnet iron structure, weighing about 80 tonnes, along with superconducting coil and cryostat had been installed at the new cyclotron building in later part of 2004. The liquid He plant, cryogenic delivery system, power supplies and the control systems were successfully commissioned. The magnet was cooled down to liquid He temperature and energised first time in the early 2005.

In the subsequent months, the magnet was operated satisfactorily for almost one year. The coil was continuously kept cooled at 4.5 K temperature during the entire period. Extensive magnetic field measurements were done for correction of the manufacturing defects and assembly errors in the iron structure, centering of the main coil, calculation of operational settings, calculation of extraction trajectory etc. After completion of magnetic field measurement activity in April 2006, the coil was warmed up to facilitate assembly of the RF system and other major systems of the machine. All major components of the RF system have been fabricated and the assembly work is currently going on. The installation of ECR ion source has been started. Installation work of injection beam line has also started.

INSTALLATION AND COMMISSIONING OF DIFFERENT SYSTEMS

The superconducting magnet along with cryogenic delivery system (fig. 1) and other related subsystems was installed by early 2005 [1]. The low carbon iron frame

and the annular cryostat, housing Nb-Ti superconducting coil, were assembled and aligned concentrically. The coil is suspended inside the cryostat by nine glass epoxy support links - 6 vertical and 3 radial. The tensile forces on the support links are monitored by strain-gauged-studs. The 200W (at 4.5K) helium refrigerator/liquefier had already been installed alongside the cyclotron building. The transfer lines along with valves, manifolds and sensors have been installed connecting the cold box and nitrogen delivery system to the cryostat. The control system based on industrial PLC and HMI software was commissioned. A turbo-molecular pump, backed by scroll pump, maintains $\sim 10^{-6}$ mbar pressure in the cryostat outer vacuum chamber. Two 1000A, 20V power supplies with 10-ppm stability for the main coil along with dump resistors and control software have been installed. The magnetic field measurement setup that uses optical encoders for accurate position measurement and stepper and smart motor driver for the search coil was also installed and tested thoroughly.

Figure 1: Main magnet with cryogenic delivery system.

Cooling of the Coil and Cryostat

The moisture level in the liquid helium chamber was reduced below 10 ppm, before starting the cool down process, by repetitive evacuation and purging with pure helium gas and heating the coil with 5A current. Then the temperature was brought down by sending cold helium gas from the plant to the cryostat. Initially, the liquid nitrogen flow to the radiation shield was not available. Still the liquid helium plant was capable enough to cool

STATUS AND PLANS FOR THE TRIUMF ISAC FACILITY

P. W. Schmor, TRIUMF, Vancouver, Canada

Abstract

The TRIUMF 500 MeV cyclotron provides up to 100 μA of protons for the production of exotic beams, primarily via spallation in a thick target, at ISAC. The cyclotron is being upgraded and refurbished to meet the ISAC requirements for reliability and stability. The ISAC (Isotope Separator and Accelerator) at TRIUMF uses the ISOL (On Line Isotope Separator) technique to provide mass-separated isotopes at energies up to 60 keV for low-energy experiments. For higher energies, the ion beam is transported at 2 keV/u, injected into a room temperature RFQ Linac and then into a five-tank drift tube linac that provides variable-energy accelerated exotic-beams from 0.15 to 1.8 MeV/u for nuclear astrophysics experiments. The first stage of a Linac using super conducting rf cavities has been recently commissioned to increase the energy to 4.0 MeV/u for $A/q = 7$. In January, 2007 a $_{11}$Li beam was accelerated to an energy of 3.6 MeV/u for the first experiment in the ISAC II experimental hall. Additional super conducting rf cavities will be added to the linac chain to permit a further increase in the maximum energy of the exotic beams to 6.6 MeV/u by 2010. An ECR-based charge state booster is also being added in front of the RFQ to increase the available mass range of the accelerated isotopes from 30 to about 150. A second proton beam line and new target station for target and ion source development have been proposed for ISAC. In the future this new target station could be used as an independent simultaneous source of exotic beams for the experimental program.

INTRODUCTION

There are two main techniques for creating these exotic beams, namely, the fragmentation method and the ISOL method. At TRIUMF the ISOL approach is used. ISOL type facilities typically use a light-ion driver-accelerator to produce a variety of isotopes in a target. At TRIUMF the driver is an H-, 500 MeV, cyclotron that has been shown to have the capability of accelerating over 400 μA to 500 MeV. The TRIUMF cyclotron can simultaneously extract multiple independent proton beams into different locations. The transport beamline from the cyclotron to the target area in ISAC is shielded for a maximum current of 100 μA of 500 MeV protons on a thick target where the exotic isotopes are created & ionized.

The extracted beam is transported through a beamline with electrostatic focusing and steering elements. The electrostatic approach allows isotopes with adequate intensities to be used for tuning purposes and then, to adjust only the mass selecting system to the low flux isotopes. These fluxes cannot be, in general, observed on the normal beam diagnostic elements. However, with the electrostatic focusing elements, the beamline tune is not sensitive to the mass, only to the beam energy and that is kept constant. Therefore the low intensity isotope can be transported through the line without needing to readjust the beam optics elements and requires only a minimum of low intensity diagnostics for optimizing the transport efficiency to the experimental target. An off line ion source (OLIS) is used to provide stable beams for commissioning beamlines, accelerators, setting up tunes and experimental calibrations. The required beam quality, the beam intensity, the beam energy and the momentum spread of the accelerated exotics depend on the particular experiment. For ISAC I the user input led to a continuously variable energy from 0.15 to 1.5 MeV/u for isotopes having an A/q ≤ 30. Recently ISAC II was added with super conducting linac to increase the energy of the isotopes. The accelerator layout is shown in figure 1.

The production of exotic isotopes in an ISOL target depends on a number of variables such as driver beam-current & energy, nuclear cross-section for production, target material and target thickness. The observed yield of a particular exotic isotope also depends on the half-life of the isotope, the time that it takes the isotope to leave the target and reach the ion source, and the efficiency for ionization in the ion source. The time required to reach the ion source following production depends on material properties that are temperature dependent. The observed exotic flux from an ISOL target varies non-linearly with the proton beam current because of changes in the target temperature and factors such as radiation induced diffusion. Enhanced variations of the exotic beam flux compared to the proton beam current variations, introduce difficulties for both the experimenter and the accelerator operator. To minimize these problems it is necessary to require beam size, beam position, beam profile and beam current stability tolerances on the proton beam from the driver accelerator. In addition each accelerator event that causes an interruption in beam delivery results in an even longer interruption to the delivery of exotic ions. The target temperature at high beam powers is primarily determined by the driver beam power. The time to restore the equilibrium operating temperature in the target when the beam is restored to the operating level exceeds the time for the temperature to drop to unusable levels when a short beam interruption occurs. Consequently it has become important to monitor, analyze, and take actions to reduce the mechanisms causing the beam interruptions and beam instabilities.

MULTI-BUNCH FEEDBACK ACTIVITIES AT PHOTON FACTORY ADVANCED RING

Weixing Cheng, Takashi Obina

Photon Factory, Institute of Materials Structure Science (IMSS),

High Energy Accelerator Research Organization (KEK),

1-1 Oho, Tsukuba, Ibaraki 305-0801, Japan

Abstract

The photon factory advanced ring (PF-AR) is a dedicated single bunch light source operating at KEK, normally it's operated at 6.5 GeV with 60mA injection beam current. However, there has some users' experiment require multi-bunch operation for high intensity x-ray beams. The old transverse damping system can suppress only one (or two) bunches, new multi-bunch feedback system has been successfully tested to a maximum of 64 bunches.

Both analog and digital transverse feedback loop has been tested at AR to store multi-bunches. For analog feedback control loop, long cables are used to delay the bunch position error signal from BPM buttons. Betatron phase advance between stripline kicker and BPM are well selected to be around 90 deg. A digital feedback loop based on FPGA evaluation board has been successfully operation, which include two ADCs, one Virtex4 FPGA chip and two 14 bit DACs. Bunch position error signal sampled by ADC, filtered by 10-tap FIR filter implemented in FPGA and send to DAC output for correction. Phase shifter in the FIR filter can be adjusted depend on the kicker and BPM betatron phase advance, FIR filter will also cut the DC components and pass through the betatron oscillation signal which increase the system dynamic range a lot. Digital delay can also be implemented inside FPGA instead of long cable delays.

Maximum beam current of 97mA has been achieved for several bunches' storage, betatron oscillation of the stored beam can be suppressed well.

INTRODUCTION

The PF-AR is a dedicated single bunch ring, injection beam current of 60mA with a typical lifetime of 15 hours has been achieved. Some user's experiment need more high intensity x-ray radiation, one example is clinical application at 5.0 GeV mode[1], for this reason, multi-bunch injection and storage has been tested at PF-AR.

There has injection threshold around 20mA even for single bunch injection at PF-AR, feedback damper system is needed to suppress the injection oscillation, as well as stored beam betatron oscillation. The old transverse damping system has been operated in PF-AR for more than 20 years, key component of the damper system is such a called BOD (Bunch Oscillation Detector[2]), which can detect and damp one bunch oscillation. There has two such kind of BOD detection circuits available, that means

it's possible to store 2 bunches. For more bunches injection and storage, new feedback systems is required, benefits of highly developed digital technology makes it possible to implement the required feedback control loop relatively simple in these days. Compared to digital feedback control, analog control suppress the beam oscillation in a more direct way, there has many good review paper for feedback control.[3,4] Both analog and digital feedback loop has been successfully tested for multi-bunch injection and storage. Table 1 list the main parameters of PF-AR feedback system.

Table 1: Parameters of PF-AR Feedback System.

Beam Energy	6.5 GeV/ 5 GeV
Injection Energy	3.0 GeV
RF frequency	508.57 MHz
Harmonic Number	640
Circumference	377.26 m
Revolution frequency	795 kHz
$Q_x/Q_y/Q_s$	10.15/10.21/0.03
Emittance	294 nm.rad
BPM SW20 β_x/β_y	13.6527/2.43916 m
Kicker β_x/β_y	3.81227/12.1319 m
BPM->Kicker $\Delta\Phi_x/\Delta\Phi_y$	9.73924/9.73916
Kicker length	1300 mm
Kicker shunt impedance	>100 kOhm @20MHz

FEEDBACK IMPLEMENTATION

For analog feedback system, it's convenient to use two BPMs to detect bunch position signal. Two BPMs vector sum can produce arbitrary phase advance between BPM and kicker. Figure 1 shows the betatron phase relations of BPMs and kicker. During the machine study at PF-AR, to make the RF electronics simple, only one BPM signal is used to detect the betatron position oscillation, phase advance from the BPM to kicker is well selected to be around 90/270 deg, which means the fractional part of BPM-> kicker phase advance should be near 0.25 or 0.75, BPM SW20 can fulfill it in both vertical and horizontal plane as shown in Table 1.

FABRICATION AND PERFORMANCE TEST OF THE CAVITY BPM FOR KEK ATF2 AND PAL XFEL*

J. Y. Huang[#], S. H. Kim, Y. J. Park, W. H. Hwang, S. J. Park, *PAL, KOREA*
Y. Honda, H. Inoue, T. Tauchi, J. Urakawa, *KEK, Japan*
M. Ross, *FNAL, USA*

Abstract

A high-resolution beam position monitor (BPM) based on a pill-box type microwave cavity has been developed for the accurate beam position measurement in the KEK-ATF2. Based on the prototype cavity BPM designed in the KEK, the cavity structure and the isolation between horizontal and vertical modes are further improved by the collaboration between KEK, SLAC and PAL. The resonant frequency of the cavity and the isolation between horizontal and vertical modes can be tuned efficiently using tuning pins brazed on the cavity rim instead of the conventional tuning plunger. Offset between electrical and mechanical centers could be reduced by tuning within +/- 5 um, the isolation tuned better than 50 dB, and the 100 nm resolution of the cavity BPM has been proved through the beam tests in the ATF extraction beamline. Technical design considerations, fabrication, and test results of the cavity BPM are described in this paper.

INTRODUCTION

In the next generation linear accelerators like the International Linear Collider (ILC)[1] and the X-ray Free Electron Laser (XFEL)[2,3], precise beam trajectory control as well as the beam-based accelerator alignment are very important for achieving nanometer-sized beams at the interaction point (IP) of the ILC or keeping the orbit stability better than a few micrometers in the XFEL for the stable FEL amplification along the undulator. A Resolution as good as 100 nanometers and a long-term stability within a few micrometers are required for the beam position monitors (BPM). Although BPMs with pickup electrodes or striplines have been improved for a better resolution, it has been limited to a few micrometers. For the ultra-short, high peak current bunches, a pill-box type cavity BPM has been considered as a promising candidate providing higher electrical sensitivity and mechanical stability. In a cavity BPM, a beam with a position offset from the electrical center excites large signal of TM110 transverse dipole mode. This signal is coupled to a waveguide through a coupling slot, and then picked up with a pickup electrode positioned at the waveguide wall.

The KEK-ATF2 [4] is an advanced accelerator test facility being built by extending the extraction beamline of the existing ATF to test advanced beam diagnostic systems and beam dynamics required for the final focus area of the ILC.

Three prototype cavity BPM have been developed and fabricated for the KEK-ATF2. With the successful results from beam tests done in the ATF, 11 cavity BPMs have been produced. The remaining 28 cavity BPMs are being fabricated by the PAL and will be installed in the KEK-ATF2.

PROTOTYPE DESIGN AND FABRICATION

Design of the cavity and waveguide structure of the cavity has been done in the KEK with computer simulation codes, and a prototype cavity BPM was fabricated and tested in the KEK-ATF by Y. Honda. A C-band cavity tuned at 6.426-GHz TM110 dipole mode was selected as the pickup cavity. Mechanical and electrical design parameters of the cavity BPM are summarized in the Table 1 [5].

Table 1. Design parameters of the cavity BPM

Tuned frequency	6.426 GHz
Resolution	100 nm
Dynamic range	500 um
Isolation (x/y)	< -30 dB
Q_0	> 5000
Offset of e-center	< 10 um
Coupling	> 0.3

Offset of the beam excites TM110 transverse magnetic mode in the cavity and the signal is coupled to the electrical pickups in the waveguide through four 1.5 x 13 mm^2 rectangular coupling slots. (See Fig. 1) Waveguide structure was optimized to reduce reflections, to increase coupling, and to reject common modes.

Two variations of the prototype cavity BPMs - a perfect cylindrical cavity, and a cavity with two dents on the symmetrical positions along the inner rim of the cavity to enhance the mode separation - are fabricated and tested for comparison of isolation between horizontal and vertical modes. Fig. 1(a) shows the schematic for the two types of the prototypes. Pair of 0.1-mm dents made with 6-mm milling drill (cavity diameter = 53.822 mm) on the inner surface of cavity rim has given resonance frequency shift of 500 kHz.

The effects of machining errors and deformations of the cavity components are tested before the final design. The 1- mm thick septum for the coupling slot between the cavity and the waveguide was found to be deformed during brazing, so the thickness was increased to 1.5 mm. For the compensation of the mechanical error of the cavity, four tuning pins are brazed into the recess of cavity body on the diagonal positions of the cavity. Tuning pins can push or pull cavity wall slightly for the compensation and cancellation of the mechanical errors,

06 Beam Instrumentation and Feedback
T03 - Beam Diagnostics and Instrumentation

EXPERIMENTAL VERIFICATION OF HALO FORMATION MECHANISM OF THE SNS FRONT END*

Dong-o Jeon[#], Oak Ridge National Laboratory, Oak Ridge, TN37831, USA

Abstract

A series of emittance measurements were performed at the end of Drift Tube Linac tank 1 of the Spallation Neutron Source to verify experimentally the previously proposed halo generation mechanism and its mitigation schemes [1]. The emittance measurements clearly showed a visible reduction in the halo as well as a significant reduction in the rms emittance when the proposed round beam optics is employed. This confirms experimentally the new halo generation mechanism.

INTRODUCTION

The Spallation Neutron Source (SNS) accelerator system is designed to accelerate intense proton beams to energy of 1-GeV, delivering more than 1.4 MW (upgradeable to 2 MW) of beam power to the neutron production target [2]. The peak current in the linac is 38mA and the macropulse average current is 26mA due to chopping. The SNS linac has the following structure; ion source, LEBT (Low-Energy Beam-Transport), RFQ (Radio-Frequency Quadrupole), MEBT (Medium-Energy Beam-Transport), DTL (Drift Tube Linac), CCL (Coupled Cavity Linac), and SCL (SuperConducting Linac). A primary concern is potential damage and radio activation of accelerator components resulting from uncontrolled beam losses. A major source of loss is beam halo that intercepts the bore of the linac.

The uncertainty in the initial matching condition is Beam dynamics simulations of the SNS linac showed that the beam halo develops at low energy, but some halo particles survive acceleration to higher energies before being lost primarily on the CCL bore. This particle loss at higher energies results in radio activation of the CCL. In order to find ways to mitigate this halo related beam loss, studies were conducted to identify the sources and mechanism of halo formation. It turns out that the MEBT is the largest contributor to Front End (FE) halo generation in the SNS linac.

A new halo generation mechanism was reported in the non-periodic lattices such as the SNS linac MEBT (Medium-Energy Beam-Transport between RFQ and DTL) [1]. It was found that the nonlinear space charge force resulting from large transverse beam eccentricity ~2:1 in the ~1.6-m-long MEBT chopper section shown in the upper plot of Fig. 1 is responsible for halo formation. This MEBT optics is called as "nominal optics". As a result, the beam distribution, based on the Front End emittance measurements and multiparticle simulation studies, develops halo that leads to beam loss and radio activation of the SNS linac. Designing lattices with

transverse beam eccentricity close to 1:1 as shown in the bottom plot of Fig. 1 suppresses this kind of halo generation. This optics is called as "round beam optics". Multiparticle simulations show that the rms emittance in both planes and halo are reduced significantly when the round beam optics is employed. Modifying the MEBT optics and introducing adjustable collimators in the MEBT significantly reduced beam losses in the CCL, which is a preferred scheme for mitigating halo. For the details, please refer to the previous study [1].
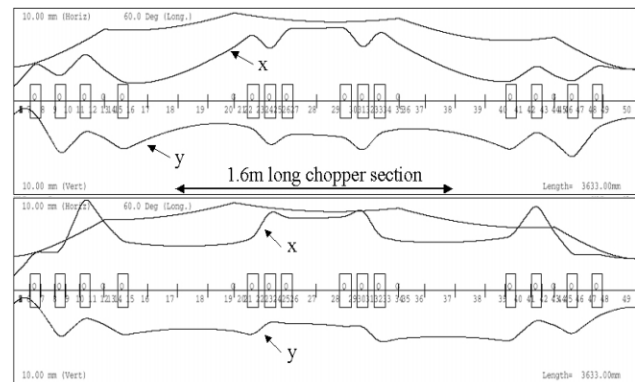
Figure 1: MEBT beam profiles obtained from Trace3D for the "nominal optics" at the top and for the "round beam optics" at the bottom employed for the emittance measurements. The beam is going from left to right.

A series of measurements were conducted to verify the effectiveness of the proposed halo mitigation scheme. One set of measurements was dedicated to see if the proposed round beam optics reduces halo and rms emittance. Round beam optics was adopted with transverse beam eccentricity close to 1:1 as shown in the bottom plot of Fig. 1. Matching was performed prior to measurements by minimizing the rms emittance in both planes. The other set was dedicated to see the effectiveness of the halo collimation in MEBT. For the DTL tank 1 commissioning, dedicated "Diagnostics-plate" [3] is attached at the end of DTL tank 1. There are horizontal and vertical emittance slits and harps installed for the emittance measurements, enabling emittance measurements in both planes. The arrows indicate the horizontal slit and harp.

A LARGE AREA SCANNING MAGNET FOR HOMOGENOUS IRRADIATION OF TARGETS

A.Mandal, G.Rodrigues, S.K.Suman and Rajesh Kumar
Inter University Accelerator Centre, New Delhi-110067

Abstract

The scanner is an important tool for accelerator based material science research. For high energy (~100 MeV) ion beam scanner has to be magnetic one. Major problem faced with magnetic scanner is its high inductance which causes large impedance to the a.c. power supply used to energise the magnet. We have designed a magnetic scanner keeping attention to minimise its inductance. The scanner is composed of two independent H-type dipole magnets which are fed by saw tooth pulses. It can scan over an area of 50 mm x 50 mm at a distance of 3 metre. The power supplies for this scanner have also been designed. These are bipolar, wideband, high speed amplifiers that can reproduce complex waveform without any distortion. The ratings are 60 V, 50 A operating at 50 Hz for x-scanner and 5V, 70A at 0.2 Hz for y-scanner.

INTRODUCTION

Beam Scanner is an important tool in Accelerator based research in Material Science in the scientific laboratory as well as in industry. It helps in scanning ion beam over a large area of the sample in a considerably less time, thus saving a lot of costly beam time which in turn helps in reducing price of the product in the industry. The scanner used in the low energy accelerator is electrostatic whereas it is magnetic in the high energy end. We have developed a magnetic scanner for homogenous irradiation of samples in material science beam line in beam hall – II of 15 UD pelletron [1]. The problem encountered in magnetic scanner is the high inductive impedance of the magnet which poses great problem in developing suitable power supply for energising the magnet. Keeping this in view we have made the design criteria of the magnet to have low inductance ~ 4mH. We have also developed suitable power supply for the magnet. The following sections describe the design of the magnet and power supply.

DESIGN OF THE MAGNET

The scanning magnet has been designed with the following beam and geometrical specifications:

ME/Z^2 for the beam = 400 a.m.u.MeV where M is mass in a.m.u and E, the energy in MeV and Z is charge state of the ion. L, the distance of the target from the magnet = 3 metre and scanning area = 50 mm x50 mm

To reduce the indutance we have considered two separate H-shaped magnets for scanning in horizontal (X) and vertical (Y) planes. The first dipole is for scanning in Y-

plane and the second one for X-plane. The ratio of operating frequency for X and Y magnets is 100: 1. Since operating frequency for X is large compared to Y magnet, the length of X magnet has been increased compared to Y-magnet to have same scanning length in both planes at reduced current. The linear deflection of the beam by a dipole magnet of magnetic field B at a distance L is given by the formula:

$$D \text{ (mm)} = 6950 \text{ L} \int B \text{ dl}/ (ME/z^2)^{0.5}$$

For a deflection of 25 mm at a distance of 3 metres, $\int$ B.dl = 0.02398 T.m. Taking the effective length of the x-magnet 0.2 m we get B =0.12 T. Ampere-turn is calculated using the formula NI = Bg/μ where g is the pole-gap and μ is the permeability of the air medium. Taking pole gap 53 mm, NI comes out to be 4774. If we take I= 50 A, N=96. Hence the number of turns per pole is 48. Taking the effective length for y magnet as 0.125 m, B turns out to be 0.19T. This is achieved by energising it at a current of 75 A for N = 96. The physical design specifications of the magnet is given below:

Pole gap	53 mm
Physical length (mm)	175(x magnet), 100 (y magnet)
Pole width	100 mm
Pole height	60 mm
Turns/coil	48
DC resistance	25 mili-ohm/coil
Inductance	~ 4 mH (2-coils)
Impedance	~ 1.2 ohm at 50Hz
Current	50 A (x), 75 A (y)
Voltage	60 V (x), 5 V (y)
Power	3 KW (x), 0.4 KW (y)

The schematic design of the magnet is shown below.
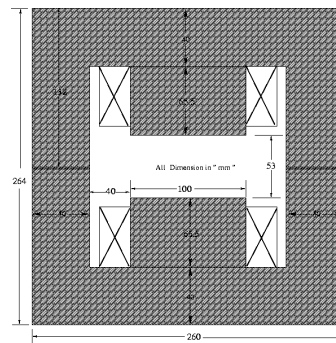
Figure 1: Schematic design of the magnet

MAGNETIC FIELD CALCULATIONS OF A 10 MEV HIGH CURRENT COMPACT CYCLOTRON

V. S. Pandit[#], P. Sing Babu, A. Goswami and P. R. Sarma
Variable Energy Cyclotron Centre, 1- AF, Bidhannagar, Kolkata, India

Abstract

In this paper we present the design study of the main magnet of the 10 MeV compact cyclotron. The preliminary dimensions of the magnet and the properties of the equilibrium orbits were first obtained using hard edge approximation. The primary size of the magnet was estimated using two-dimensional POISSON code. Finally a 3D code was utilized for the field optimization. The profile of magnet sectors was optimized based on the computed results to get the desired values of isochronous field and the betatron tunes.

INTRODUCTION

Under the ADS development programme of the DAE, a 10MeV, 5-10mA compact radial sector proton cyclotron, is being developed at VECC in Kolkata [1, 2]. A 2.45 GHz microwave ion source will produce ~30mA of proton beam at 100keV. The extracted beam will be first collimated using slits and then it will be bunched using a sinusoidal buncher. It will be injected axially in the central region of the cyclotron where a spiral inflector will place the beam on the proper orbit. Two delta type resonators, each having ~ 45 degree angle located in the opposite valleys, will be used for providing acceleration to the beam. Finally, this beam will be extracted using an electrostatic deflecting channel. The main aim of this project is to study and settle various physics and technological issues associated with the production, bunching, acceleration, injection, extraction, etc. of the high intensity beams.

In our design there are four magnet sectors. We have tried to keep a maximum magnetic field of 1.5T at the hill centre, and an average magnetic field of 0.689T, which correspond to a particle revolution frequency of 10.5MHz for proton. The hill gap is 4 cm and the valley gap is 64 cm, same as the distance between the upper and lower return yokes. For the injection system, one hole is provided at the center. We have provided four holes in the four valleys, two of them will be used for vacuum pumps and the rest two will be used for the RF cavities vertically. Apart from using a high dee voltage, we have chosen a low average magnetic field and hence a large extraction radius of ~65 cm for 10 MeV cyclotron to have a reasonable turn separation at the extraction radius. Though this method increases the cost of the cyclotron, it gives more flexibility and a clear advantage for injection and extraction. The harmonic mode *h* of operation is equal to 4. The magnet design combines the advantages of solid pole cyclotron and separated sector cyclotron. A high flutter provides strong focusing in the vertical direction. The main idea was to provide the vertical

---

[#]pandit@veccal.ernet.in

betatron tune > 0.5 at all radii. This is necessary for handling the beam space charge defocusing force at the average beam current of ~ 5mA. In order to meet the isochronism, the shaping of the azimuthally averaged magnetic field was done with the help of varying the sector angular width along the radius.

The primary size of the magnet was estimated using two-dimensional code. Finally a 3D code was utilized for the field calculation and optimization. The profile of magnet sectors was optimized based on the computed results to get the desired values of isochronous field and the betatron tunes.

CYCLOTRON PARAMETERS

The conceptual dimensions of the magnet and the properties of the equilibrium orbits (EO) were first determined by a computer code based on hard edge approximation and matrix method [3, 4]. Here we outline the procedure briefly. Details are given in reference [5]. For an N sector cyclotron with magnetic fields B_H and B_V in the hill and valley respectively, the angles of turning of orbits η and ξ can be given as

$$\eta = \frac{B_H B_V}{B_H - B_V} \cdot \frac{2\pi}{N} \cdot \left(\frac{1}{B_V} - \frac{1}{\gamma B_0} \right), \ \xi = \frac{2\pi}{N} - \eta \quad (1)$$

where γ is the usual relativistic term and B_0 is the central magnetic filed. One can easily obtain the angular widths of the hill and valley η_0 and ξ_0 on an equilibrium orbit for a given energy by solving

$$\cot(\frac{\eta_0}{2}) = \cot(\frac{\pi}{N}) + \frac{B_H}{B_V}\left(\cot(\frac{\eta}{2}) - \cot(\frac{\pi}{N}) \right),$$

$$\xi_0 = \frac{2\pi}{N} - \eta_0 \quad (2)$$

In order to calculate betatron tunes we need entry and exit angles to the hill (which becomes the exit and entry angles for the valley), which are given by

$$\phi_1 = \varepsilon_1 + \frac{\eta - \eta_0}{2} \ , \ \phi_2 = \varepsilon_2 - \frac{\eta - \eta_0}{2}$$

$$\tan \varepsilon_2 = \tan \varepsilon_1 + R \cdot \frac{d\eta_0}{d\gamma} \cdot \frac{d\gamma}{dR} \quad (3)$$

Here ε_1 is the spiral angle at the entry of the hill, which is zero in the present case. The effective spiral angle ε_2 at the exit of the hill includes spiral angle as well as flaring effect [4]. We have used the well-known matrix method to estimate the betatron tunes. Here hills and valleys are treated as bending magnets of lengths $\eta\rho_H$ and $\xi\rho_V$ having focusing strengths of $1/\rho_H$ and $1/\rho_V$, ρ_H and ρ_V being the radius of curvature in the hill and valley respectively. The

8 GEV BEAM LINE OPTICS OPTIMIZATION FOR THE RAPID ANTIPROTON TRANSFERS AT FERMILAB*.

V. Nagaslaev[#], V. Lebedev, J.Morgan, D.Vander Meulen
Fermilab, PO Box 500, Batavia IL 60510, USA

Abstract

Tevatron Run-II upgrade requires a significant increase of the efficiency and speed of the antiproton transfers from the Accumulator to the Recycler. The goal for the total transfer time is challenging a reduction from 1 hour down to a few minutes. Here we discuss the beam line optics aspects of this project. Results of lattice measurements and optimization are analyzed in terms of transport efficiency and stability.

INTRODUCTION

The transport of antiprotons between the Accumulator and Recycler involves 3 machines and 5 beam lines. The total length of the beam lines is over 1 km and each machine performs RF manipulations with the beam on its way. Because some of the beam lines are also used for transfers at 120GeV and 150GeV in addition to 8GeV, an initial tune up is made with the reverse proton beam prior to transporting antiprotons. The antiproton beam is sent from the Accumulator in multiple transfers, usually 5 or 6. A 2.5 MHz H=4 RF system (ARF4) is used to bunch a portion of the stack and accelerate it to the injection/extraction orbit about 140 MeV away. The extraction kicker (EKIK) then kicks this portion into the 8GeV transport line. This beam passes through the AP3, AP1, P2 and P1 beam lines on its way to the Main Injector. Main Injector RF synchronously captures the beam and decelerates it by about 40 MeV to match the Recycler ring energy.
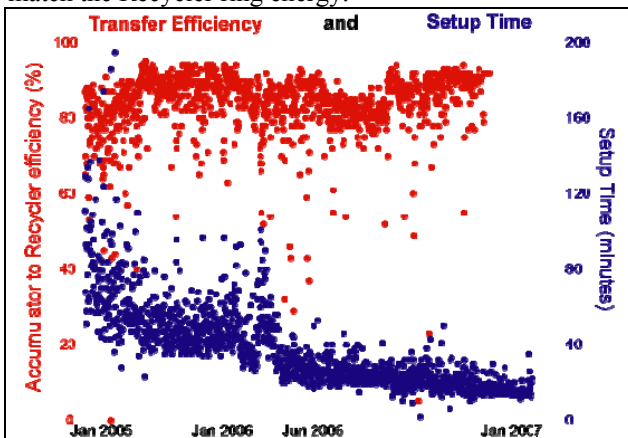
Figure 1. Accumulator to Recycler transfer efficiency and the shot set up time in 2005 through 2007. Transfer efficiency data is unavailable for the past few months but is thought to be near the historic best.

Antiprotons are then transported to the Recycler

through the R22 beam line. Recycler RF forms barrier buckets to isolate the injected beam and pre-cool it before merging with the main antiproton stack. In the transfer process (shots) each machine is changing its state and mode of operation synchronously with others. The most complex transformation takes place in the Accumulator ring. It has to change from pbar accumulation (stacking) mode, where it injects antiprotons from the Debuncher and stochastically cools them into the dense core, to the transport (unstacking) mode. This process historically involved manipulation of thousands devices. Factoring in cooling the core down before the transfers, the whole process used to take more than an hour prior to 2006.

STEPS TO EFFICIENT TRANSFERS

In order to maximize the rapid transfer efficiency good beam orbit control is required. Beam line lattice functions should be well matched to the optics of the downstream machine to avoid emittance dilution. Effective apertures should be maximized, achieved by the lattice optimization and proper beam steering. A number of hardware upgrades are needed in order to meet the goals of rapid transfers.

Magnet ramping

In 2003 the optics of the beam line was modified in order to avoid changing polarity on some magnets when switching between 120GeV and 8GeV beam line power supplies. This facilitated a faster transition between modes and improved the reproducibility of magnetic fields. The 2 sets of power supplies were originally used to improve power supply regulation. The next step is to avoid switching between power supplies. AP1 line is now being converted to single power supply operation with installation of waveform generating cards. The P1 and P2 beam lines already ramp and the AP3 beam line is dedicated to 8GeV operation.

BPM upgrade

An upgrade of the beam line Beam Position Monitor (BPM) system has been recently completed. New advanced system allows taking data at both 53 MHz (protons) and 2.5 MHz (pbars) for all transfer modes in real time. In particular it has made it possible to take good quality orbit data during antiproton transfers which have many advantages.

MI dampers

There is a transverse narrowband damper system in the Main Injector used for damping oscillations in proton beams arriving from the Booster. Switches have been installed in this system to make them bi-directional, so

DESIGN AND OPERATING EXPERIENCE OF TRIODE ELECTRON GUNS FOR INDUSTRIAL ELECTRON ACCELERATORS

Arvind Jain, A.R.Chindarkar, K.C.Mittal

Accelerator and Pulse Power Division, Bhabha Atomic Research Centre, Mumbai 400 085

arvjain@ barc.gov.in

Abstract

The Accelerator and Pulse Power Division of BARC is presently constructing three industrial electron accelerators for radiation applications. a) a 500keV, 10 KW Cockcroft-Walton accelerator b) a 10MeV , 10kW electron linac and c) a 3MeV, 30kW DC machine. While the DC machines require an almost parallel beam with less than 1.0 degree divergence, the RF linac gun requires a 50keV, 2 ampere pulsed beam of low emittance. Using relativistic electron optics, including space charge effects, very simple triode gun designs with flat cathode, grid and anode apertures which fulfil these requirements and are easy to fabricate experimentally are described. Our operating experience with these guns are also described.

INTRODUCTION

The Accelerator and Pulse Power Division of BARC is presently constructing three industrial electron accelerators for radiation applications. a) a 500 keV, 10kW Cockcroft-Walton accelerator b) a 10 MeV , 10 KW electron linac and c) a 3 MeV, 30 KW DC machine. These accelerators, for irradiation purposes, require electron guns with special requirements. The two DC machines require an almost parallel beam with less than 1.0 degree divergence from the gun to enable the beam to drift through the accelerating modules. The linac requires a 50 to 80 keV , 1 to 3 ampere pulsed beam with a duty cycle of 0.1% . In this case a normalized emittance of the electron beam less than 100π mm mR MeV/c is required. Using relativistic electron optics, including space charge effects, very simple gun designs are presented which fulfill these requirements. A triode gun, having a flat cathode and parallel discs with apertures for the grid and anode have been used in the designs. The electron trajectories have been obtained using the SLAC gun design code EGUN [1].

GUN DESIGN

The triode gun is shown schematically in Fig.1. In the figure, C is the flat cathode, G the grid and A the anode. The diameter of the grid aperture is D_g and that of the anode is A_g. 'g' is the distance between the cathode and grid and 'a' the distance between the grid and the anode. The thickness of the grid and anode are t_g and t_a respectively. These parameters completely define the gun. All three, viz. the cathode, grid and the anode are separated by insulators and can take independent potentials.

Different values were tried in the program EGUN for the grid aperture D_g and the anode aperture A_g , the cathode-grid spacing 'g' and the grid-anode spacing 'a' in the program [2]. The electron beam profile obtained if the correct parameters are not used in the design is shown in Fig.1(a). By trial and error, the correct geometry has been obtained which results in a parallel beam as shown in Fig.1(b).
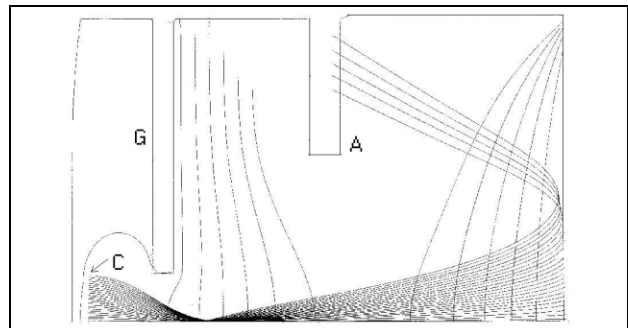
Figure 1(a): The effect on the electron trajectories if the proper apertures are not used.
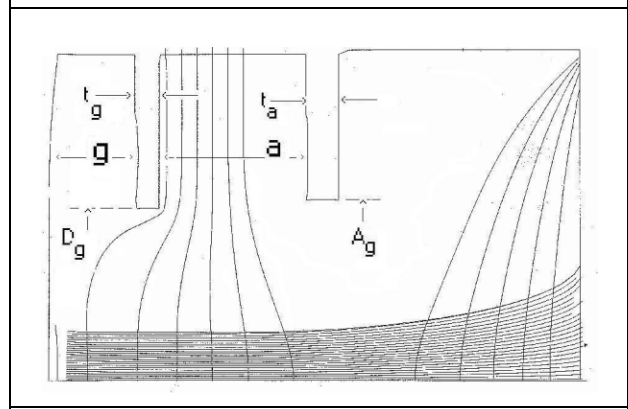
Figure 1(b): With the proper parameters, a parallel beam is obtained.

In our DC machines, the electron gun is followed by the NEC (National Electrostatic Corporation) accelerating tube section. The first three accelerating electrodes of the NEC accelerating tube were included in the EGUN program to see their effect on the electron trajectories. The first three electrodes were given potentials of +13kV, +33kV, and +53kV respectively . The results are shown in Fig.2(a).

05 Beam Dynamics and Electromagnetic Fields
D01 - Beam Optics – Lattices, Correction Schemes, Transport

ANALYSIS AND CORRECTION OF THE MEASURED COD IN INDUS-2

Riyasat Husain[#], A.D.Ghodke and Gurnam Singh

Raja Ramanna Centre for Advanced Technology, Indore-452013(MP) INDIA

Abstract

In Indus-2 there are 56 button type beam position monitors (BPMs), 48 horizontal and 40 vertical corrector magnets. The measured orbit has been fitted by effective quadrupole misalignments by using SVD of the response matrix generated between BPMs and the quadrupole misalignments in the model obtained by setting the magnet strengths as per the current set in the magnets. We present the global orbit correction algorithm developed for minimizing the orbit. The preliminary result for the orbit correction, at injection energy, in horizontal plane using best orbit correctors identified by an SVD of the response matrix is presented.

INTRODUCTION

The synchrotron light sources are characterized by low emittance of the electron beam and high brightness of the photon beams radiated from dipoles and insertion devices. Indus-2 is a 2.5GeV synchrotron radiation source with expanded Chasman Green lattice. The source consists of 8 unit cells; one unit cell contains 2 dipoles, 9 quadrupoles and four sextupoles. There are 7 beam position monitors (BPMs), 6 horizontal and 5 vertical corrector magnets in each cell for orbit measurement and its correction. One unit cell is shown in figure (1). The ring comprises of 72 quadrupoles divided into five families of quadrupole magnets. The closed orbit results from field errors and the errors arising from magnetic element positioning. The most severe effects come from misalignment of quadrupole magnets, where the resulting dipole field is proportional to both gradient and alignment errors. Indus-2 ring is being commissioned and measurement and correction of the beam dynamics parameters such as closed orbit distortion, tune, chromaticity etc. are being done. In this paper we describe the COD correction algorithms and its measurement and correction.

Figure 1: One unit cell of Indus-2 ring: Rectangles: empty-dipoles; blue-focusing quadrupoles; red-defocusing quadrupoles; yellow-focussing sextupoles; black-defocusing sextupoles; green-beam position monitors; magenta-horizontal corrector magnets and cyan-vertical corrector magnets. LS and SS stand for long straight section and short straight section.

The measured orbit has been fitted by effective quadrupole misalignments by singular value decomposition (SVD) of the response matrix generated between BPMs and the quadrupole misalignments in the model obtained by setting the magnet strengths as per the current set in the magnets. We present the global orbit correction algorithm developed for minimizing and controlling the orbit. The preliminary result for the orbit correction, at injection energy, in horizontal plane using most effective correctors identified by SVD of the response matrix is presented.

ALGORITHM

Considering M BPMs and N correctors used for closed orbit correction in the storage ring, the response matrix Rij corresponding to the beam motion at the ith BPM per unit angle of kick by the jth corrector is given by

$$R_{ij} = \frac{\sqrt{\beta_i \beta_j}}{2\sin(\pi\upsilon)} \cos\left(\left|\varphi_i - \varphi_j\right| - \pi\upsilon\right) \quad (1)$$

where (β_i, φ_i), and (β_j, φ_j) are the beta function and phase advance at BPM and corrector locations, υ is the betatron tune.

The solution of the problem of the system of simultaneous linear equations between BPMs and the correctors is to effectively find out the inverse of the response matrix, R^{-1}. By SVD, the response matrix R can be decomposed into U, S, V [2]

$$R = U \times W \times V^T \quad (2)$$

Where U is an MxM unitary matrix ($UUT = UTU = 1$) and V is an NxN unitary matrix ($VT V= VTV = 1$), W is an MxN diagonal matrix with positive or zero. We call these diagonal elements $W_n (\geq 0, 1 \leq n \leq \min(M,N))$ the eigenvalues, which represent the coupling efficiency between the BPMs and correctors. The matrix R is singular if any of the eigen values are equal to zero. The R^{-1} can be calculated as

$$R^{-1} = V \times (W_{inv}) \times U^T \quad (3)$$

Here, W_{inv} is a diagonal matrix of dimension NxM and the elements are given by

$$W_{inv} = q_{\min(i,j)}\delta_{ij} \quad (4)$$

with

[#]riyasat@cat.ernet.in

INHOMOGENOUS FIELD WIEN FILTER DESIGN

Puneet Jain [#] , P. Roychowdhury, D. P. Chakravarthy, Asish K. Ray
Accelerator and Pulse Power Division, BARC, Mumbai 400085, INDIA

Abstract

The Wien velocity filter is a useful device that transports pure proton fraction from high-power ECR proton source to the RFQ. It is a deflecting device, which has crossed electrostatic, and magnetostatic fields. Both fields are perpendicular to the beam trajectory that deflects and eliminates the undesired species of ions from the main beam. A tilted-pole Wien filter [1] surpasses the classical parallel-rectangular-poles Wien filter in performance as the former eliminates the astigmatism. The present paper describes the design of an inhomogeneous field Wien filter where the equations of motion are developed and solved up to a second-order approximation for a paraxial ion beam inside an E×B mass separator without considering the space charge effects.

INTRODUCTION

A high current low emittance ECR proton source is being developed at Accelerator and Pulse Power Division (APPD), Bhabha Atomic Research Centre (BARC) for Accelerator Driven sub critical Systems (ADS) applications [2]. This source (50 keV, 30 mA) will be an injector to 3 MeV RFQ, a subsequent accelerating structure. The beam coming out of the source [3] may contain molecular hydrogen ions (H_2^+) species besides pure proton (H^+). It is desired to have more than 80% of proton fraction before it reaches RFQ. To remove the undesired species of molecular hydrogen ions, a device viz. Wien filter is used. The protons and molecular hydrogen ions in the beam have same energy (50 keV) but owing to different masses, have different velocities. The Wien filter removes the undesired molecular hydrogen ions species and hence this device is also called mass separator or Wien velocity filter (WVF). The WVF is a mass-dispersive electromagnetic optical device, having mutually perpendicular electrostatic and magnetostatic fields both being transverse to the direction of the charged particle beam. An appropriate choice of the separator's electric (E) and magnetic (B) field strengths, deflection forces sets up inside the device, which in turn cancel out for the desired beam species having axial velocity v = E/B. A classical WVF [4] consists of rectangular-parallel surfaces of electrodes and magnetic poles respectively (Figure 1). Along with spatial dispersion, the forces inside E×B separators also cause focusing of the beam. This focusing is not axisymmetric and astigmatism is introduced into the undeflected beam. A circular beam emerges out as an elliptical one out of the classical separator. This paper discusses how the astigmatism is removed up to a certain limit by introducing field gradients both in E and B.

[#] Email : pun12j@yahoo.co.in
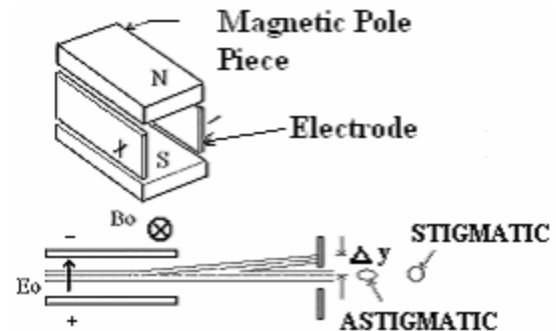
Figure 1: Schematic of classical Wien Filter

ELECTRODES GEOMETRY

We shall be using right-handed Cartesian coordinate system as shown in Figure 2.
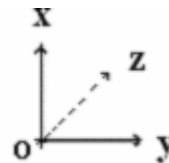
Figure 2: Coordinate system used in our analysis

For a parallel plate capacitor, one needs to choose electrodes profile as constant y lines. Obviously constant x lines shall be the electric field lines. To get an electric field gradient symmetric to y-axis we make a complex plane transformation given by w = Sin (ζ), where w (u, v) = u (x, y) + i v (x, y) and ζ (x, y) = x + i y. The equipotential curves are given by v = Cos (x) Sinh (y) and the orthogonal curves u = Sin (x) Cosh (y) shall be the corresponding field lines (Figure 3). The electrodes geometry shall therefore be according to constant v curves.
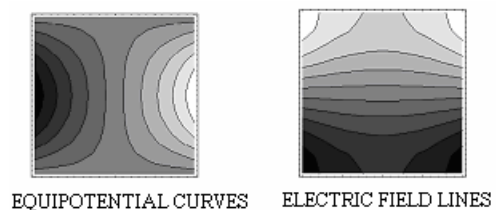
Figure 3: Electrodes profile (left figure) and the electric field lines (right figure)

MAGNETIC POLES GEOMETRY

The magnetic field used in the WVF should have a quadrupole component also besides a dipole. Such a configuration can be conceived by using tilted magnetic

CHARACTERISTICS OF BEAM EXTRACTION SYSTEM OF K500 SUPERCONDUCTING CYCLOTRON

S. Paul[#], J. Debnath, M.K. Dey, J. Pradhan, A. Dutta, C. Mallik, R. K. Bhandari
Variable Energy Cyclotron Centre, 1/AF Bidhannagar, Kolkata 700 064

Abstract

Extensive Magnetic Field measurement of the K500 Superconducting Cyclotron has been completed. In this paper we report the beam dynamical calculations along the extraction system based on the measured magnetic field data. The beam matching to the external beam transport system, for different ion species spanning the operating region is also explored.

INTRODUCTION

The K500 Superconducting Cyclotron at VECC, Kolkata uses 2 electrostatic deflectors, 8 passive magnetic channels and 1 active magnetic channel as its extraction elements [1]. Except for the active magnetic channel, all the other elements are radially movable, typically by ± 0.25 inches around a centre position. This maneuverability is due to the fact that not all the ions spanning the operating region of the cyclotron will have the same optimum beam extraction radius. Though it is possible that by adjusting the position and electric field of the electrostatic deflectors only, one can guide the extracted trajectories along a fixed common path, it is extremely difficult given the azimuthal length of the extraction path ($\sim 330^0$), the total number of extraction elements involved, and the large variations in orbit scalloping across the anticipated range of magnetic fields. During the magnetic field mapping exercise, the magnetic field and magnetic field gradient along the extraction path has been measured both in the absence and presence of the magnetic channels at its central position, at different main magnet excitations, using a specially designed flexible zig and hall sensors.

The extraction elements

The different parameter of the extraction elements that affects the beam behaviour is listed in Table 1. For the deflectors, the septum to electrode gap is set to 6mm and the maximum voltage is set at 100 kV. To compensate the field perturbation effects of the magnetic channels on the inner orbits, 2 compensating bars (C_1 and C_2) are used, whose locations are also enlisted. C_1 compensates the effect of M_1 while C_2 compensates the overall effect of the remaining magnetic channels. The entries in Table 1. are as follows:

θ_i , θ_f : Initial and final azimuth of the element listed,

R_i , R_f : Average central ray radius at the initial and final azimuth of each element,

B : Magnetic field for the element

$\delta B/\delta x$: Gradients for the element.

[#]spaul@veccal.ernet.in

Table 1: Extraction element's parameter

Element	θ_i (deg.)	θ_f (deg.)	R_i(in)	R_f(in)	B (kG)	$\delta B/\delta x$ (kG/in)
E_1	-23	32	26.6	26.93	-	-
E_2	94	137	27.1	27.68	-	-
M_1	140	153	27.7	27.76	1.14	8.3
M_2	200	206	28.28	28.39	1.14	8.3
M_3	226	232	28.89	29.08	1.04	13.3
M_4	236	242	29.21	29.44	1.04	13.3
M_5	256	262	30.09	30.46	1.04	13.3
M_6	266	272	30.75	31.24	1.04	13.3
M_7	276	282	31.62	32.31	1.14	8.3
M_8	286	292	32.88	33.95	0.96	11.6
C_1	320	334	27.75	27.75	-	-
C_2	46	58	28.95	28.95	-	-

SYSTEM CHARACTERISTICS

Figure 1. shows a plot of the magnetic field and radial gradient ($\delta B/\delta x$) across a typical magnetic channel. The field and the gradient is constant within ± 5 % across the beam width ($\sim$ ± 0.15 inch) and is therefore quite sufficient.
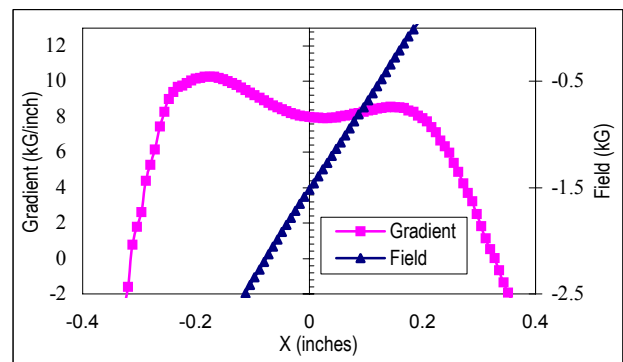
Figure 1: Field and gradient across a magnetic channel.

The properties of beams from the K-500 Superconducting Cyclotron were calculated by the ray-tracing method. In this calculation, the effect of the magnetic channels were included using the result of the magnetic field measurement. Three different species (Table 2.) spanning the operating-region of the cyclotron

ELECTRON GUNS AND BEAMLINES IN THE VIEW OF EMITTANCE COMPENSATION

S. V. Miginsky[#], Budker INP, Novosibirsk, Russia

Abstract

Space charge effect is ever of fundamental importance for low-energy parts of accelerators. Simple and robust estimations of the emittance degradation in various electron guns were obtained analytically and numerically. Nonuniform longitudinal and transverse distribution of current and the effect of gun electrodes were taken into account. The parameters of optimal beamlines for emittance compensation were estimated.

INTRODUCTION

Emittance compensation technique has been mentioned first probably in [1]. It was explained and developed further in [2] and other papers. The two basic effects, caused by the longitudinal nonuniformity of charge density and the transverse one, and their combination in uniform and nonuniform beamlines were considered in [3] and [4], also with accelerating and bunching. The main results of the two latter works is that the charge phase advance through the beamline should be $2n\pi$ (n is integer) and the focusing should be optimal. Then the normalized emittance dilution is well estimated as

$$\varepsilon_n \cong \xi r \sqrt{\frac{I}{I_0 \beta\gamma}}, \tag{1}$$

where r is the rms size of the beam at the entrance; I is the peak current; $I_0 = 4\pi \cdot mc^2 / Z_0|e|$, ≈ 17.045 kA for electrons; $\beta = v/c$; $\gamma = 1/\sqrt{1-\beta^2}$; v is the longitudinal velocity; and ξ is the dimensionless coefficient depended on the type of the beamline.

In this paper we consider electron guns in the same view. We take into account only macroscopic space charge effect and neglect thermal and grid emittance. There are at least three significant differences from the previous cases:

- Metallic electrodes always exist near the emitter. Its charge depends on the one of the beam and generates comparable fields.
- A bunch ever starts at very low energy, so its velocity and length are small enough. If the length of a bunch in the moving frame is comparable to or less than its radius, the interaction between its slices can't be neglected.
- The head and the tail of a bunch are in different conditions. If we consider them at the same position, the bunch will have lower energy in the first case and the transverse force will be smaller due to nonlocal interaction.

We use a steady-state code that takes into account the first effect, but not the two others.

[#]S.V.Miginsky@inp.nsk.su

EMITTANCE DILUTION IN GUNS

Phenomena and Basic Scaling

If the emitter is round and the beam is homogeneous and stationary, the gun geometry can be optimized so that the space charge effect doesn't affect the emittance, as in the well known Pierce gun [5]. If the beam is not uniform in the longitudinal direction, the transverse phase portraits of its slices differ and their emittances are not equal to zero. Let's consider these phenomena and estimate the total emittance.

Particle motion in the same gun is similar if its voltage and current meet Child-Langmuir law $I \propto U^{3/2}$. In this case the emittance (not normalized!) doesn't depend on the current. The quality factor of a gun

$$\frac{\varepsilon}{r\sqrt{\dfrac{I}{I_0(\beta\gamma)^3}}} \equiv \frac{\varepsilon}{r\sqrt{j}}, \tag{2}$$

where r is the emitter radius, also doesn't depend on the current. At the same time, brightness $I/\varepsilon_n^2 \propto \sqrt{U}$. If all the dimensions of a gun are changed proportionally, its quality factor preserves while its brightness is $\propto \sqrt{U}/r^2$. Thus, one should find the quality factor and the optimal compensation beamline for any gun.

Charge Amplitude and Phase

Consider round beams and small deviations δ from the principal trajectories in the transverse phase space as in [3] and [4]. Then the motion is described by a second order differential equation with variable coefficients and a transform matrix exists for each beamline

$$\begin{pmatrix} \delta \\ \delta' \end{pmatrix} = \begin{pmatrix} C & S \\ C' & S' \end{pmatrix} \cdot \begin{pmatrix} \delta_0 \\ \delta_0' \end{pmatrix}. \tag{3}$$

$\delta' = 0$ (see [3] (3)) at the emitter and we should zero it at some point after the gun to minimize the emittance. Thus, only C and C' are significant in our case and one can define the charge phase advance as

$$\varphi = \arctan\left(\frac{-C'x}{C\sqrt{j}}\right), \tag{4}$$

where x is the rms-size of a slice. The quadrant should be taken so that the signs of $\cos\varphi$ and $-\sin\varphi$ coincide to ones of C and C' respectively. This definition possesses a critical property: if a uniform beamline with the phase advance $\pi - \varphi$ and x, j, and $\beta\gamma$ equal to ones at the exit of an arbitrary beamline with the phase advance φ, the total phase advance is π.

A GENERAL MODEL OF THE RESISTIVE WALL INSTABILITY IN LINEAR ACCELERATORS *

J. R. Delayen[#], Thomas Jefferson National Accelerator Facility, Newport News, VA 23606, USA
and Old Dominion University, Norfolk, VA 23529, USA

Juhao Wu, Stanford Linear Accelerator Center, Menlo Park, CA 94025, USA

Abstract

A general model for wakefield-generated instabilities in linear accelerators, originally developed for cumulative beam breakup [1], is applied to the resistive wall instability. The general solution for various bunch charge distributions and application to various accelerator configurations are presented.

INTRODUCTION

The beam breakup instability caused by the resistive wall impedance has been studied for the cases of a uniform single bunch and of a point-like bunch train [2] in the asymptotic limit of strong coupling. However, in the final focus of a linear collider or in light sources, the beam current profile is typically non uniform and the coupling, while not negligible, is relatively modest. The formalism developed previously for cumulative beam breakup [1] is applied here to investigate the resistive wall instability for arbitrary beam current profile and arbitrary strength of the wake field

FORMULATION AND SOLUTION

In a continuum approximation, the transverse motion of a relativistic beam under the influence of focusing and transverse wakefield can be modeled by [1]

$$\left[\frac{1}{\gamma} \frac{\partial}{\partial s}\left(\gamma \frac{\partial}{\partial s} \right) + \kappa^2 \right] x(s,\zeta)$$
$$= \varepsilon \int_0^\zeta d\zeta_1 \, w(\zeta - \zeta_1) F(\zeta_1) x(s,\zeta_1) \tag{1}$$

where γ is the usual energy parameter; s is the distance from the front of the accelerator; κ is the focusing wave number; $\zeta = t - s/c$, is the time measured after the arrival of the head of the beam at location s; $F(\zeta) = I(\zeta)/\bar{I}$, the current form factor, is the instantaneous current divided by the average current; $w(\zeta)$ is the wake function; ε is the coupling strength between the beam and the deflecting field, and includes properties of the beam and the transport channel. If the wakefield source is the resistive-wall of a cylindrical pipe, then the long-range wake field is [3]

$$W(\tau) = \frac{\varepsilon}{\sqrt{\tau}}, \tag{2}$$

where

$$\varepsilon = (4c^2 \bar{I})/(c\gamma b^3 I_A)\sqrt{\varepsilon_0 / \pi \sigma_c}. \tag{3}$$

In the above expression, c is the speed of light, γ is the Lorentz factor, b is the radius of the pipe, $I_A = 17,045$ Amp is the Alfven current, ε_0 is the vacuum permittivity and σ_c is the pipe conductivity. With this definition we have

$$w(\zeta) = \zeta^{-1/2} \quad \text{for} \quad \zeta > 0. \tag{4}$$

While Eq. (1) assumes a perfectly aligned accelerator, misalignment of the cavities and focusing elements can also be included in the following analysis in a straightforward fashion [1].

Without loss of generality, we will assume a coasting beam. As shown in [1], the analytical results can be extended to an accelerated beam by suitable coordinate and variable transformations. We will also assume that the beam is injected parallel to the axis with a time-independent offset x_0. Under these assumptions, the equation of motion becomes [1]

$$\frac{\partial^2}{\partial s^2} x(s,\zeta) + \kappa^2 x(s,\zeta) =$$
$$\varepsilon \int_0^\zeta d\zeta_1 \, w(\zeta - \zeta_1) \, F(\zeta_1) x(s,\zeta_1). \tag{5}$$

and the solution is

$$x(s,\zeta) = x_0 \sum_{n=0}^\infty \varepsilon^n \, h_n(\zeta) \, j_n(\kappa, s), \tag{6}$$

with

$$h_0(\zeta) = 1; \qquad h_{n+1}(\zeta) = \int_0^\zeta d\zeta_1 \, w(\zeta - \zeta_1) \, F(\zeta_1)$$
$$j_n(\kappa, s) = \frac{1}{n!}\left(\frac{s}{2\kappa}\right)^n \sqrt{\frac{\pi \kappa s}{2}} J_{n-1/2}(\kappa s) \tag{7}$$

Once the profile of the charge distribution in the bunch is determined, the functions $h_n(\zeta)$ can be calculated and then the shape and position of the bunch at any location s determined form Eqs. (6) and (7).

UNIFORM CHARGE DISTRIBUTION

In the case of a uniform charge distribution, the functions $h_n(\zeta)$ can be calculated in closed form and are

THE BUNCH LENGTHENING DUE TO ELECTRON CLOUD IN POSITRON STORAGE RING*

Y. D. Liu[#]

Institute of High Energy Physics, CAS, P.O. Box 918, 100049, Beijing, China

Abstract

The electron cloud generates not only the transverse wake field but also the longitudinal wake field. The mechanism of the bunch lengthening due to longitudinal wake produced by the electron cloud in the positron storage ring is analyzed. The longitudinal field, which depends on the density of the electron cloud in the storage ring, arises from the accumulation of the electrons near to the centre of the bunch during the bunch passage. Based on the longitudinal wake field, tracking method is used to simulate variation of the bunch longitudinal profile in different electron cloud density. According to simulation, the longitudinal action on the bunch from electron cloud is the same as the potential-well distortion to shift the bunch distribution and give a rise to the bunch deformation.

INTRODUCTION

The electron cloud accumulated in the vacuum chamber is usually associated with the transverse coupled bunch instability and bunch blow up. Experimental studies and numerical simulation have been developed for these phenomena [1]. In fact, electron cloud interacts with a positron bunch not only in transverse direction. Longitudinal instability was first discussed by G. Rumolo and F. Zimmermann as a single bunch effect, such as bunch lengthening [2]. The accurate simulation on the longitudinal interaction between electron cloud and the bunch need a fully self-consistent three dimensional plasma particle in cell model to solve Maxwell's equation as code OSIRIS which will spend much longer time [3]. In this paper, a simplified 2D approach is use to estimate the longitudinal electron cloud wake excited by a bunch passing through the electron cloud. Based on the longitudinal wake field, tracking method is used to simulate variation of the bunch longitudinal profile due to electron cloud.

PHYSICAL MODEL FOR THE LONGITUDINAL WAKE

During the passage of a bunch through the electron cloud, the electrons are attracted by the beam electric field and accumulate around the positron beam. The positron bunches have to lose some mount of their kinetic energy to build the electron cloud during the interaction with the electrons. The energy variation inside the bunch can be seen as a longitudinal wake. The bunch particles have an additional energy spread due to the longitudinal

wake from the electron cloud. The electromagnetic field of the electron cloud can drive from the Maxwell equations as following formula [4]

$$\nabla \cdot \vec{E} = \frac{\rho}{\varepsilon_0} \qquad (1)$$

$$\nabla \times \vec{H} = \vec{j} + \varepsilon_0 \frac{\partial \vec{E}}{\partial t} \qquad (2)$$

$$\nabla \times \vec{E} = -\mu_0 \frac{\partial \vec{H}}{\partial t} \qquad (3)$$

where ρ and $\vec{j}$ are the charge density and current density of the electron cloud, respectively. Here, ρ, $\vec{j}$, $\vec{E}$, $\vec{H}$ are the function of time t during the bunch passing. For azimuthally symmetrical fields and the assumption that the electron cloud has a periodic structure, the equations can be expressed as

$$\frac{1}{r}\frac{\partial}{\partial r}(rE_r) - \frac{\partial E_z}{c\partial \tau} = \frac{\rho}{\varepsilon_0}, \qquad (4)$$

$$\frac{\partial H_\theta}{c\partial \tau} = j_r + \varepsilon_0 \frac{\partial E_r}{\partial \tau}, \qquad (5)$$

$$-\frac{\partial E_r}{c\partial \tau} - \frac{\partial E_z}{\partial r} = -\mu_0 \frac{\partial H_\theta}{\partial \tau}, \qquad (6)$$

where $\tau = z/c$, is the time difference to synchrotron particles. According to the relation $Z_0 = \frac{1}{\varepsilon_0 c} = 120\pi\Omega$, the integration in the radial direction and the boundary condition $E_z(r = a, \tau) = 0$, the longitudinal electric field of the electron cloud is expressed as,

$$E_z = Z_0 \int_r^a j_r dr, \qquad (7)$$

where Z_0 the impedance in free space and j_r is transverse current density of electron cloud.

As an example of BEPCII, assuming the bunch current is 9.8mA and central density of the electron cloud is 1.0×10^{13}m^{-3}, the bunch longitudinal distribution and its electric field caused by electron cloud is shown in Figure 1.

From Figure 1, the longitudinal electric field is much smaller than the transverse filed which is on the order of 10^4 V/m [5]. During the passage of a positron bunch the transverse distribution of the electron cloud also has some significant change as displayed in Figure 2.

05 Beam Dynamics and Electromagnetic Fields
D04 - Instabilities – Processes, Impedances, Counter-measures

DEGRADATION OF THE BEAM PASSING THROUGH IDLE COUPLED CAVITIES

Y. Shobuda, JAEA, Tokai_mura, Ibaraki, Japan
S. Machida, CCLRC/RAL/ASTeC, Chilton, Didcot, Oxon, U.K.

Abstract

Effects of wake fields on a high intensity proton beam are studied, when it passes through idle coupled cavities (The same number of modes as that of gaps that compose of the cavities build up.). Since the cavities are designed for an accelerated beam, the shunt impedance for the respective mode is different from the designed value, when the beam is not accelerated. This change of shunt impedances reduces the detuning effects in the sense of the reduction of the beam degradation.

INTRODUCTION

J-PARC (Japan Proton Accelerator Research Complex) is composed of linac, 3GeV RCS (Rapid Cycling Synchrotron) and Main ring [1]. In the first stage, 181[MeV], 30[mA] proton beam will be injected into RCS. In the upgraded J-PARC, it is planned that 400[MeV], 50[mA] proton beam will be injected into RCS through ACS (Annular Coupled Structure linac).

Before we inject the beam into RCS in case of the upgraded J-PARC, it is necessary to investigate the beam degradation due to the idle ACS, because RCS in J-PARC requests the momentum spread should be below 0.1%[1] before injection. It is not clear that we can reduce the beam degradation, especially when the chopped beam is injected into the cavity, by selecting the most appropriate frequency of the cavity, because the coupling effects between gaps (the shunt impedance for the non-accelerated beam is different from the designed value, because the ACS is designed for the accelerated beam.) is not negligible for the proton beam.

Further, as our commissioning, it is necessary to let beam pass through idle cavities, in order to adjust parameters of the accelerator. Tuning phase and amplitude of the powered cavity is one of the important processes at the commissioning of linac. The scheme of measurements of TOF (time of flight) is sometimes used for this purpose. Since many cavities exist between monitors for the measurements, it is severer the measurement of TOF as the intensity of beam becomes higher. Under this situation, it is important to investigate wake field effects on the beam quality [2].

In section 2, we consider the situation that the 181[MeV], 30[mA] chopped beam passes through the idle ACS. In section 3, we discuss the possibility of the correction scheme of TOF. Conclusions follow in section 4.

THE BEAM DEGRADATION

In the upgraded J-PARC, it is planned that 400[MeV], 50[mA] proton beam will be injected into RCS through

ACS. The ACS is composed of 42 cavities. One cavity is composed of N_g=17 gaps [3]. Parameters for the ACS were already calculated by M. Ikegami: the shunt impedance ZT^2=41.223[MΩ/m], the quality factor Q=20300 and the frequency of the cavity $f_{\pi/2}$=972[MHz] [3].

Let us consider the situation that 181[MeV], 30[mA] chopped beam described in Fig.1 passes through the idle ACS. J-PARC RCS condition requires the momentum spread should be below 0.1%[1] before injection. It is not clear that we can reduce the momentum (energy) spread by selecting the most appropriate frequency of the idle cavities, because the coupling effects between gaps are not negligible for proton beam. Further, the chopped beam has many intrinsic frequencies.
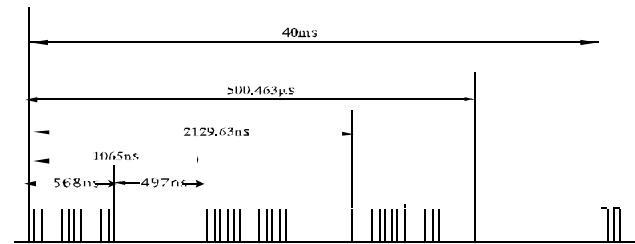
Figure 1: The chopped beam at J-PARC is described. Time period of the smallest pulse is 324[MHz]. The time period of the bunch (1065[ns]) corresponds to 0.93[MHz]. The interval of bunches is fluctuating around 1065[ns] (typically ~3[ns]). The repetition rate of the beam is 25[Hz].

Let us explain how to calculate frequencies and the shunt impedance of the coupled cavity when beam is not accelerated. When ACS has only one tuner, Brillouin curve for the detuned cavity is obtained by solving

$$D_{N_g} = \begin{vmatrix} i\left(\frac{\omega}{2\pi f_{\pi/2}} - \frac{2\pi f_{\pi/2}}{\omega}\right) & i\frac{\kappa}{2} & \cdots & 0 \\ i\frac{\kappa}{2} & i\left(\frac{\omega}{2\pi f_{\pi/2}} - \frac{2\pi f_{\pi/2}}{\omega}\right) & \cdots & \vdots \\ \vdots & \vdots & \ddots & i\frac{\kappa}{2} \\ 0 & \cdots & i\frac{\kappa}{2} & i\left(\frac{\omega}{2\pi f_{\pi/2}} - \frac{2\pi f_{\pi/2}}{\omega}\right) \end{vmatrix} = 0, \quad (1)$$

where the only $((N_g+1)/2, (N_g+1)/2)$ component of D_{N_g} is replaced by $i(\omega/2\pi(f_{\pi/2}+df) - 2\pi(f_{\pi/2}+df)/\omega)$ and df is the amount of detuned frequency (D_{N_g} is the determinant of N_g*N_g.)[4]. Here κ=0.055 [5] is the coupling constant. One of detuned cases is represented in Fig.2. The frequency f_k is changed only when the mode index (k) is odd. We approximately reproduce the well-known Brillouin curve formula:

$$f_k = f_{\frac{\pi}{2}}\left(1 - \frac{\kappa}{2}\cos\left[k\frac{\pi}{N_g+1}\right]\right), \quad (2)$$

BEAM COUPLING IMPEDANCE STUDIES OF THE CSNS RING

N. Wang*, Q. Qin

Institute of High Energy Physics, Beijing 10049, P. R. China

Abstract

The China Spallation Neutron Source (CSNS) is a high intensity proton accelerator with an injection energy of 80 MeV. The knowledge of the impedance in the vacuum chamber is necessary for optimizing the beam performance. In this paper, the longitudinal and transverse coupling impedances of the CSNS Rapid Cycling Synchrotron (RCS) are estimated.

INTRODUCTION

The CSNS is comprised of an 80 MeV Linac and a 1.6 GeV RCS ring [1]. Two bunches of 1.88×10^{13} protons are accelerated in the ring with a repetition frequency of 25 Hz. Many elements installed in the ring will cause beam instability via coupling impedance. Impedance from sources, such as space charge, vacuum wall and vacuum components, is calculated with analytical formulae. Impedance of other devices such as kicker magnets and RF cavities are difficult to calculate and should be measured. The results have been derived according to their preliminary design, rather than the impedance threshold given by the beam instability criterion. For further study, we will calculate the beam current threshold based on the impedance budget obtained, and then re-evaluate the impedance according to the stability criterion. This iteration will compromise the requirements of mechanical design for each vacuum component under an acceptable beam instability effect.

The main parameters of the CSNS/RCS are shown in Table 1.

Table 1: CSNS/RCS ring parameters

Circumference	m	230.8
Inj./Ext. energy	GeV	0.08/1.6
Repetition rate	Hz	25
Beam power	kW	120
Average Current	mA	63
RF harmonics		2
Trans. acceptance	$\pi\mu m\cdot rad$	540

COUPLING IMPEDANCE

Transverse and longitudinal coupling impedance are calculated analytically for both injection and extraction energies.

Space Charge

The transverse space charge impedance for a round beam of radius a in a round pipe of radius b is given by

$$Z_\perp = -j\frac{Z_0 R}{\beta^2\gamma^2}\left(\frac{1}{a^2}-\frac{1}{b^2}\right), \qquad (1)$$

where $Z_0 = 377\ \Omega$, $\beta = v/c$, γ is the Lorentz factor, and $2\pi R$ is the accelerator circumference. The longitudinal space charge impedance under the same condition is

$$\frac{Z_{//}}{n} = -j\frac{Z_0}{2\beta\gamma^2}\left[1+2\ln\frac{b}{a}\right], \qquad (2)$$

where $n = \omega/\omega_0$ and ω_0 is the revolution frequency.

Chambers in the dipole magnets will be designed to have racetrack cross-sections. They are taken as rectangular chambers in calculation for simplicity. The space charge impedance for a rectangular beam pipe is given as [2]

$$Z_{H,V}(\omega) = -j\frac{Z_0 R}{\beta^2\gamma^2}\left[\frac{1}{a^2}-\frac{8}{h^2}\left(\xi_1^{H,V}-\varepsilon_1^{H,V}\right)\right],$$

$$\frac{Z_{//}(\omega)}{n} = -j\frac{Z_0}{2\beta\gamma^2}\left[1+2\ln\left(\frac{2h}{\pi a}\tanh\left(\frac{\pi w}{2h}\right)\right)\right], \qquad (3)$$

where w and h stand for width and height of the chamber, and $\xi_1^{H,V}$ and $\varepsilon_1^{H,V}$ are electric image coefficients. For the CSNS/RCS ring, the space charge impedance are $Z_{//}/n = -j\ 792\ \Omega$, $Z_{\perp x} = -j\ 17.5$ MΩ/m and $Z_{\perp y} = -j\ 9.5$ MΩ/m at 80 MeV, and $Z_{//}/n = -j\ 102.8\ \Omega$, $Z_{\perp x} = -j\ 4.7$ MΩ/m and $Z_{\perp y} = -j\ 4.5$ MΩ/m at 1.6 GeV. It plays a dominant role in the whole impedance.

Resistive Wall

The RF shielded ceramic chambers will be chosen in the dipoles and quadrupoles due to the rapid field variation, and stainless steel (or titanium) chambers could be at the field free regions.

We choose ~ 0.5 mm in thickness and 5 mm in width copper stripes as the RF shield. The selection of the thickness of the copper stripes compromises the shielding efficiency and the ohmic loss due to eddy current.

A quick disconnect Ti flange will be welded to a sleeve attached to the ceramic segment by metal and brazing. Beam chambers in the straight sections, the vacuum chambers for steering magnets, DC bumpers, and extraction septum, are stainless steel pipes. They present an important portion for the resistive wall impedance due to its low conductivity [3].

For a round beam pipe, whose skin depth is small compared to the thickness of the vacuum chamber, the resistive wall impedance is [4]

$$Z_{//}(\omega) = (1+j\,\text{sgn}(\omega))\frac{l}{2\pi b\sigma\delta},$$

$$Z_\perp(\omega) \approx 2cZ_{//}(\omega)/(\omega b^2), \qquad (4)$$

where we have introduced the skin depth at ω

05 Beam Dynamics and Electromagnetic Fields
D04 - Instabilities – Processes, Impedances, Counter-measures

A STUDY ON THE APPLICABILITY OF LANDAU CAVITY TO THE 1.2GeV BOOSTER SYNCHROTRON AT TOHOKU UNIVERSITY*

F. Hinode [#], K. Akiyama, H. Hama, M. Kawai, K. Kasamsook, A. Kurihara, T. Muto, K. Nanbu, Y. Shibasaki, S. Takahashi, T. Tanaka, M. Yasuda

Laboratory of Nuclear Science, Tohoku University, Sendai 982-0826, Japan

Abstract

A 1.2 GeV Stretcher-Booster (STB) ring at Laboratory of Nuclear Science (LNS), Tohoku University, has been mainly operated for experiments of nuclear physics. One of the many issues limiting performance of the STB ring is supposed to be strong longitudinal coupled-bunch instability. In order to suppress the instability, applicability of a third-harmonic Landau cavity has been studied. The 1.5 GHz harmonic cavity was manufactured and installed in the ring. As a preliminary result of the beam test, it was turned out that the very strong signal of collective synchrotron oscillation was able to damp drastically depending on tuning angle of the harmonic cavity. Present status of the STB and the first test result of beam operation with harmonic cavity are described in the paper.

INTRODUCTION

In these years, the STB ring has been mainly operated in the booster-storage mode in which the high energy gamma-ray beam generated via bremsstrahlung from internal target wire has been utilized for experiments of nuclear physics [1]. The STB ring had been designed and constructed so as to have functions of: 1) pulse-beam stretcher [2], and 2) booster ring as an injector for a light source project [3]. The main parameters of the ring are listed in table 1. The STB is not the light source ring but also has storage ring-like function. Although the stored beam current is sufficient level (~15 mA) in the present operation for the nuclear physics user, it has still continued to increase the stored current toward the future application such as light source. The injected beam from linac is ramped up to variable top energy (1.2 GeV max.) during about 1 sec. The flat top time is also variable. The injection energy is not high enough (150 or 200 MeV), so that radiation damping time is much long (~ 1 s in the longitudinal direction). Although the injector linac provides sufficient beam current without beam stacking, circulating beam current decays rapidly due to instabilities before the beam reaches the top energy. One of the main causes of the beam current limitation might be supposed due to strong coupled-bunch instability because any care for the ring impedances had not been taken. Actually very strong synchrotron oscillation signal have been observed around 3.6 GHz. Since the main rf cavity itself does not have adequate HOM in such frequency region, any other possibility for the narrow

band impedance source has been investigated. On the other hand, Landau cavity might be effective in order to suppress the instability. It is also supposed that the Landau cavity can improve the beam lifetime by increasing the bunch length. This approach is successfully employed in many light sources such as MAX-II, ALS and BESSY-II so far [4-6]. This technique is getting well established, but there may still remain difficulty and/or less knowledge in low energy ring where the radiation damping is very weak. Especially in the booster ring with large energy deviation from injection to flat top, to study the effect of the harmonic cavity seems to be interesting for longitudinal beam dynamics.

Table 1: The main parameters of STB ring

Lattice type	Chasman-Green
Superperiodicity	4
Circumference	49.7 m
Maximum energy	1.2 GeV
Injection energy	0.2 or 0.15 GeV
Betatron tune (ν_x,ν_y)	(3.22, 1.15)
Chromaticity (ξ_x,ξ_y)	(~ -5.5, ~ -4.7)
RF frequency	500.14 MHz
RF voltage	140 kV
Harmonics	83
Natural emittance	170 nmrad (@ 1.2 GeV)
Momentum compaction	0.0378

HIGHER HARMONIC CAVITY FOR STB

Among some choices we decided to test the normal-conducting passive third harmonic cavity because of that simplicity and easier understanding of beam dynamics. The tentative target was set to 100 mA for the design of higher harmonic cavity. The parameters of the cavity are listed in table 2.

Table 2: Parameters of the harmonic cavity (measured)

Frequency (@0mm,30°C)	1499.1		MHz
Frequency range (tuner position)	+11.4 -1.2	(+25 mm) (-15 mm)	MHz
Pickup probe coupling	-30		dB
Loaded Q	22,270		
Shunt impedance*	3.8		MΩ

* Rsh =V^2/P : calculated value assuming R/Q by SUPERFISH

For the full energy operation, analytic modeling and simulations were first performed without consideration of HOMs in the rf cavities [7]. This allows the study of Robinson instabilities and coupled-bunch instabilities

EFFECT OF MAGNETIC FIELD COUPLING ON INDUS-2 QUADRUPOLE MAGNETS

G Sinha, A. Kumar, A. K. Mishra and Gurnam Singh

IOAPDD, Raja Ramanna Centre for Advanced Technology, Indore-452013

Abstract

The distances between the magnets in the Indus-2, are small and as a result, the magnetic field of one magnet may affect the fields of the adjacent magnets. Therefore, it is important to find out the effect of mutual coupling between magnets in the actual condition in the ring and the ways to overcome this problem. In this paper, we will discuss how the field quality of quadrupole magnets (QP) in the ring is affected when accompanied by various corrector dipole magnets (CDP)(vertical and horizontal) and sextupole magnets (SP). Variations of integrated quadrupole field strength in presence of CDPs are measured at various field excitations and also by varying the distance between the magnets using a rotating coil. Experimental results are compared with the results obtained from 3D simulations. Possibilities of studying the interference effect by scanning the field by a Hall probe, is explored. Dependence of field interference on the distance between magnets, pole gap and the steel length are studied. Effects of the adjacent magnets on the higher order multipole of QP are also examined.

INTRODUCTION

Double Bend Achromat Indus-2 lattice consists of eight super periods each having two dipole bending magnets, four focusing and five defocusing QPs and four SPs and seven CDPs (used for closed orbit correction). There are total 72 QPs in the ring. These are divided in five different categories named as Q1, Q2, Q3, Q4 and Q5. All of these magnets have the same maximum gradient of 16 T/m. and same bore diameter of 85 mm and same cross section. Steel lengths of the Q1, Q2, Q3, Q4 and Q5 magnets are 262.5, 512.5, 362.5, 362.5 and 362.5 mm, respectively. There are two quadrupole triplets (Q1, Q2 and Q3) for the adjustment of beam sizes in the long straight section (LSS) and four CDPs are placed in between them (Figure 1). The achromat section consists of a triplet QP having two Q4s and one Q5 and four SPs and three CDPs. The distance (steel edge to steel edge) between a QP and a CDP vary from 176.25 mm to 383.75 mm in the LSS. In the achromat section, SP is placed as close as 195.75 mm from QP. It is clear that the fringe field of a QP is extended beyond the location of the adjacent magnets.
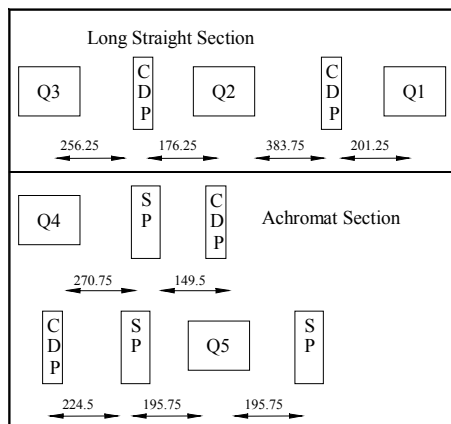
EXPERIMENTAL RESULTS

Integrated QP field strength is measured at a reference radius of 32mm using a rotating coil system [1]. Around 150 A current in QP produces required maximum field gradient of 16 T/m. To find the effect of the adjacent CDP
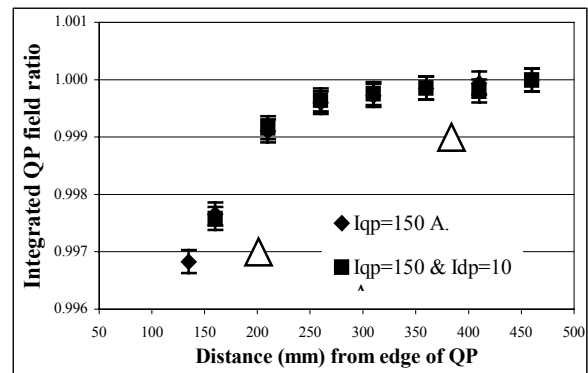
Figure 2: Variation of the ratio of the measured integrated quadrupole gradient, to the nominal gradient, with distance between the quadrupole (Q1) and the CDP. In one case current in QP is 150 A. and no current in CDP. Other case QP and CDP are having 150 A and 10 A currents, respectively. Open triangles indicate the minimum and the maximum distances in the ring.

on a QP, the current in Q1 is fixed at 150A and the distances between them are varied from 135 mm to 460 mm. In the first case there is no current in the CDP. Then the same experiment is repeated while the current in the CDP is set to 10 A to check whether the field interference depends on the field excitation of the CDP. The integrated quadrupole field strength ($B_2.L$) of Q1 (steel length is

Figure 1: Block diagram of the portion of the unit cell where field interference between various magnets can occur. Distances are in mm.

PROGRAM FOR THE GENERATION OF HIGH CURRENT RFQ

Vlsrao.Sista[#], S.C.L. Srivastava, T.Basak, Rajni Pande, Shweta Roy and P.Singh
Bhabha Atomic Research Centre, Mumbai-400085, India

Abstract

In general design of the linear accelerators, the beam dynamics parameters are calculated from data describing the accelerator structure. In this approach, the desired phase advances (beam dynamics parameters) are obtained after several iterations of structure parameters. A program has been written for the generation of RFQ Linac, which is based on choosing the zero current transverse and longitudinal phase advances. Given the zero current transverse and longitudinal phase advances, the structure parameters are calculated using the analytical formulae. In this paper, we discuss the design of the high current RFQ using this procedure and compare it with the ones obtained from the standard codes.

INTRODUCTION

The renewed interest in Accclerator Driven Systems (ADS) has spurred tremendous interest in developing high intensity proton accelerators, and set challenging demands in terms of delivering high current (~ tens of mA) and high energy (≥ 1 GeV) required for the spallation process. In Indian context, ADS will be used for the utilization of thorium resources for the energy production. In view of the importance of ADS, a project to design and build a 20 MeV, 30 mA CW proton accelerator (LEHIPA) as an injector to 1 GeV Linac has been initiated.

The LEHIPA [1] mainly consists of a 50 keV ECR ion source, Low Energy Beam Transport (LEBT) line, 3 MeV Radio Frequency Quadrupole (RFQ) accelerator, Medium Energy Beam Transport (MEBT) line and a 20 MeV Drift tube Linac (DTL).

The Linac for the ADS system requires extremely low beam loss in order to allow hands-on maintenance. It has also been studied that if the beam is not in thermal equilibrium, the equipartitioning process caused by the strong coupling between the transverse and longitudinal motions can lead to emittance growth [2] and halo formation [3,4]. Hence we have studied ability of the RFQ to prepare an equipartitioned beam. The choice of the phase advances per focusing period (with, without space charge) of the transverse (σ_t, σ_{0t}) and longitudinal (σ_l, σ_{0l}) oscillations are crucial for the design of high current accelerators. These parameters not only determine the motion stability but also the emittance growths and the halo formation which can produce undesirable beam losses in high current accelerators. The zero current

_____
[#]vlsrao.sista@gmail.com

phase advance parameters (σ_{0t} and σ_{0l}) determine the structure parameters. A program has been written for the generation of RFQ by choosing the phase advances at the end of the gentle buncher.

DESIGN STRATEGY

An equipartitioned beam has equal transverse and longitudinal temperatures, $T_l = T_t$. Theoretically, for a matched bunch in a smooth-focusing system, the temperatures can be related to the rms beam widths and normalized rms emittances [5].

$$\frac{T_l}{T_t} = \frac{\varepsilon_{\ln}^2}{\varepsilon_{tn}^2} \cdot \frac{a^2}{(\gamma b)^2} \tag{1}$$

Where ε_{tn}, $\varepsilon_{\ln}$ denotes the full (100%) normalized emittance of a uniform beam distribution, a and b corresponds to full beam radii in the transverse and longitudinal directions respectively, γ is the relativistic factor. From the envelope equations the full current phase advances (σ_t, σ_l) are given by

$$\sigma_t = \frac{\varepsilon_{tn} \lambda}{a^2 \gamma} \tag{2}$$

$$\sigma_l = \frac{\varepsilon_{\ln} \lambda}{b^2 \gamma^3} \tag{3}$$

where λ is the wavelength.

From the smooth approximation theory the phase advances with space charge for the uniformly ellipsoidal beam bunch are related to the external focusing forces in the form of:

$$\sigma_t^2 = \sigma_{0t}^2 - \frac{Q(1-ff)}{2a^2 b} \tag{4}$$

$$\sigma_l^2 = \sigma_{0l}^2 - \frac{Qff}{a^2 b} \tag{5}$$

where the bunch form factor *ff* is a function of $\gamma b/a$ [6]

when $0.85 \leq \gamma b/a \leq 5$ then $ff = a/3\gamma b$, and $Q = \dfrac{3Z_0 q I \lambda^3}{4\pi m_0 c^2 \gamma^3}$

with $Z_0 = 377\Omega$

The Q parameter is then fixed by the choice of the beam current, I, the particle rest mass ($m_0 c^2$), charge, and energy (W) and the operating frequency of the system.

For the equipartitioned beam the ratio of the transverse and longitudinal temperatures should be equal to one.

STUDY OF SPACE CHARGE COMPENSATION IN LEBT

S.C.L.Srivastava[#], Vlsrao.Sista, Rajni Pande, Shweta Roy, T. Basak and P.Singh
Bhabha Atomic Research Centre, Mumbai-400085, India.

Abstract

A 20 MeV, 30 mA CW proton accelerator is being built in BARC which consists of 50 keV ECR ion-source, LEBT, 3 MeV RFQ, MEBT and 20 MeV DTL. In designing low energy beam transport (LEBT) line, which matches the beam from ion-source to RFQ, the expansion of the proton beam is a severe problem. As the energy of the beam is 50 keV, Coulomb repulsion is enormous and for minimization of this repulsion, space charge compensation is done. To simulate the beam dynamics part, a PIC code is written, which allows beam of different distributions like KV, Parabolic and Waterbag. This is an electrostatic code, which can also take care of external magnetic fields. A Monte Carlo collision scheme is being implemented for the ionization of the background gas. In this paper, we are presenting the simulation of space charge compensation of the 30 mA proton beam at 50 keV.

INTRODUCTION

Newly proposed accelerators with application to nuclear waste transmutation, subcritical nuclear reactors, neutron spallation sources require high intensity linacs. A 20 MeV, 30 mA CW proton accelerator is being built in BARC which consists of 50 keV ECR ion-source, LEBT, 3 MeV RFQ, MEBT and 20 MeV DTL [1]. In the low energy section of such accelerators beams of tens of mA are strongly subjected to the Coulombian repulsion. The transport of such space-charge dominated beams are challenging task because of the same reason. Apart from applying the usual magnetic fields based structure for focussing; the method of space-charge neutralization has also been tried for the same. In this process, a gas is introduced in the beam pipe, which gets ionized by the beam. The produced electrons are trapped in the beam potential and reduce the repulsive space charge forces. A better understanding of the kinetics of the process will make it more efficient and may find different application in other fields. To study this kind of situation, we need to solve the full Poisson-Vlasov model including the different kind of collisions. This makes PIC-MCC simulation technique as a competitive candidate.

BASICS OF A PARTICLE-IN-CELL/ MONTE CARLO MODEL

In the PIC method, so-called ''superparticles'' move in the simulation region through an artificial grid on a timestep basis. Each of these superparticles represents typically about 10^8 real particles. Only charged particles are simulated with these superparticles; neutrals are assumed to form a continuum. In the beginning of the simulation, every charged particle is assigned to a specific position on the grid, leading to a self-generated electric field. The particles move in response to both the applied and self-generated fields, according to Newton's laws. This gives rise to new positions for the particles, changing the self-generated field, and hence changing the force acting on the particles. Mathematically, this is done every timestep by first *weighting* the positions of the particles to the grid, yielding the charge densities on the grid points. The potential and electric field on the grid points are then determined from the calculated charges, by Poisson's equation. A weighting procedure is applied again, to obtain the forces on the positions of the particles from the previously obtained field on the grid points. From the force on the positions of the particles, first, the velocity of every particle is calculated and, from the velocity, the position is determined, using a leap-frog algorithm [2]. After the particles are placed in their positions, a Monte Carlo algorithm is used to simulate collisions between particles. This procedure is repeated for many timesteps, until convergence is reached.

In the MC module, a random number between 0 and 1 is chosen to determine for every particle whether a collision occurs or not. If a collision takes place, a second random number is generated to determine the collision type. The energy and direction of the particles after the collision are determined, depending on the collision type, again using random numbers. We make use of the ''null-collision'' method [3]. In this approach, a fictitious collision process (null-collision) is introduced, with a collision frequency such that when it is added to the sum of the collision frequencies of the real collision processes, a constant total collision frequency over position and energy is obtained. In this way, the maximum fraction of the total number of particles in the simulation that undergo a collision (either a real or a null collision) during a timestep Δt, is given by

$$P_{null} = 1 - \exp(-v'\Delta t) \qquad (1)$$

where

$$v' = \max_{x,E}(n_t \sigma_T v) \qquad (2)$$

In Eq.(2), x denotes the position, E is the energy of the incident particle, n_t is the density of target particles at particle position, σ_T is the total cross section for every species and v is the velocity of the incident particle. Typically the target particles are assumed to be uniformly

05 Beam Dynamics and Electromagnetic Fields
D05 - Code Developments and Simulation Techniques

BEAM POSITION MONITOR AT THE SCSS PROTOTYPE ACCELERATOR

H. Maesaka[#], Y. Otake, K. Togawa, T. Shintake, RIKEN/SPring-8, Kouto, Sayo, Hyogo, Japan,
H. Ego, T. Fukui, N. Hosoda, T. Ohshima, JASRI/SPring-8, Kouto, Sayo, Hyogo, Japan

Abstract

This paper presents the design and the performance of the beam position monitor (BPM) in the prototype accelerator of the X-ray free electron laser (XFEL) project at SPring-8. An RF cavity-type BPM has been developed, since it has the capability to achieve the required position resolution, which is less than 1 μm. The TM110 mode of a beam-induced field is extracted and its amplitude and phase yield the beam position. Conversion coefficients were determined by beam-based calibration. The position resolution was also evaluated by a beam-based method. The preliminary result was obtained to be approximately 5 μm, or better. This result is sufficient for tuning the beam of the prototype accelerator to generate the vacuum ultraviolet (VUV) FEL, and a FEL amplification has been observed. However, XFEL requires better resolution. Therefore, we are planning to perform more precise measurements and to develop a new detection circuit.

INTRODUCTION

The XFEL project, SCSS (SPring-8 compact SASE[!] source) [1], is in progress, and the prototype accelerator [2] is in operation. One of the most important subjects to produce XFEL is that the electron beam must overlap with the radiated X-ray throughout the undulator section. The position difference between the beam and the X-rays is required to be less than 4 μm [3]. Therefore, the resolution of the BPM is necessary to be less than 1 μm. The cavity type RF-BPM has a capability to achieve the required performance, since past experiments, such as Ref. [4], showed resolutions of a few tens of nanometers. Another advantage is that the agreement between the electrical center and the mechanical center is fine, since the cylindrical shape of the RF-BPM enables a precise lathe process. We describe the design and the performance of the RF-BPM used at the prototype accelerator.

MEASUREMENT PRINCIPLE

Suppose that there is a cylindrical RF cavity in a beam line. When a short bunch of charged particles passes through the cavity, it excites electromagnetic oscillations resonating with the cavity. Since the electric field of a dipole mode, such as TM110, linearly varies with the transverse offset near the cavity axis, the amplitude of the beam-induced field strongly depends on the beam position. On the other hand, the electric field of a monopole mode, such as TM010, has axis symmetry at the cavity center. Accordingly, the amplitude is almost

independent of the beam position, and is sensitive to only the beam charge. Thus, dipole modes are available for beam-position measurements. Since the TM110 dipole mode is the lowest order, we consider this mode hereafter.

The complex amplitude of the TM110 frequency is expressed as [5]

$$V_{RF} = A_1 qy + iA_2 qy' + iA_3 q + V_N . \qquad (1)$$

Descriptions of each term are:

- $A_1 qy$: Beam position signal. The amplitude is proportional to the beam displacement, y , and the beam charge, q .

- $iA_2 qy'$: Beam angle signal, which is induced by the beam angle, y' . The phase is 90 degrees different from the first term, which is the reason why the imaginary unit i is multiplied.

- $iA_3 q$: Contamination from the tail components of the frequency distribution of monopole modes. Even if the eigenfrequency is different, the finite Q value causes a measurable effect on the TM110 frequency. The phase of this term is also 90 degrees apart from the first term.

- V_N : The other components, such as thermal noise.

Here, A_1 , A_2 and A_3 are proportionality coefficients. Thus, we can obtain the beam position when we know the amplitude and the phase of the TM110 signal together with the beam charge. To measure the charge, it is effective to prepare another TM010 cavity whose resonant frequency is the same as that of the TM110 cavity. In this case, the TM010 cavity provides a phase reference of the TM110 signal in addition to charge information.

HARDWARE SETUP

The drawing of the RF-BPM installed in the prototype accelerator is shown in Figure 1. The RF-BPM consists of two cavities, a position-detection cavity (TM110) and a reference cavity (TM010). The resonant frequency is
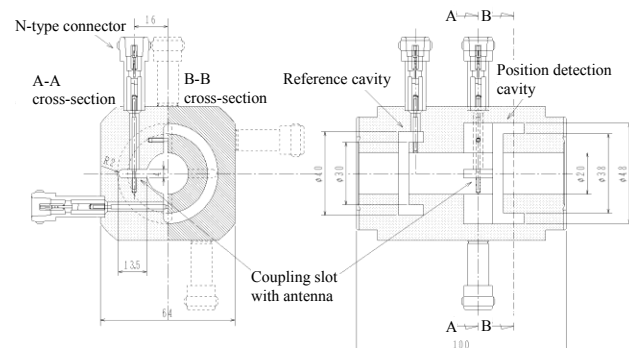
Figure 1: Drawing of the RF-BPM.

DESIGN OF A STRIPLINE KICKER FOR TUNE MEASUREMENT IN SESAME STORAGE RING

Seadat Varnasseri[#]

SESAME, c/o UNESCO Amman Office, P.O. Box 2270

Abstract

In this paper the SESAME[*] storage ring tune measurement system is described. Travelling wave electrodes are commonly used in synchrotron light sources as a tool for both excitation and beam sensing for tune measurement. Normal longitudinally symmetric stripline has a positive sine wave response in the frequency domain. An exponentially tapered stripline has a constant coupling impedance versus frequency and better frequency response, but complicated in manufacturing. In this paper the design of stripline kicker for the purpose of tune measurement in the SESAME storage ring is reported.

INTRODUCTION

In SESAME the electrons are injected from a 20 MeV microtron into a 800 MeV booster synchrotron, with a repetition rate of 1 Hz. The 800 MeV beam is transported through the transfer line to the main storage ring and after accumulation, accelerated to 2.5 GeV[1,2].   During the normal operation , injection and ramping period in the storage ring, the betatron and synchrotron tunes in the storage ring will be measured frequently. The tune as well as time structure measurements could be done with the kicker-pickup striplines combination.

HARDWARE DESCRIPTION

Betatron and synchrotron motion in circular machines is usually incoherent, except in presence of an instability, therefore their values can not be easily measured. In order to make the measurement of the tunes, it is necessary to make the motion coherent by exciting the beam at the proper frequency. At SESAME storage ring the betatron tune measurement is performed by exciting the beam externally in the horizontal and vertical planes simultaneously through a stripline as a shaker and detect the excitation by another stripline as a detector. The main components for tune measurement in the storage ring consist of stripline shaker, stripline detector, low frequency voltage amplifier, network analyzer and the associated electronics for the detector. Figure.1 shows a simplified block diagram of the storage ring tune measurement. The overall tune monitoring system

s.varnasseri@unesco.org.jo

* Synchrotron-light for Experimental Science and Applications in the Middle East is an independent intergovernmental organization developed under the auspices of UNESCO It involves at present the following member states: Bahrain, Cyprus, Egypt, Israel, Jordan, Pakistan, Palestinian Authority and Turkey. Iran is in the process of finalizing its formal membership.

provides the capability of monitoring the storage ring tunes, v_x and v_y during ramping and stored beam operation.
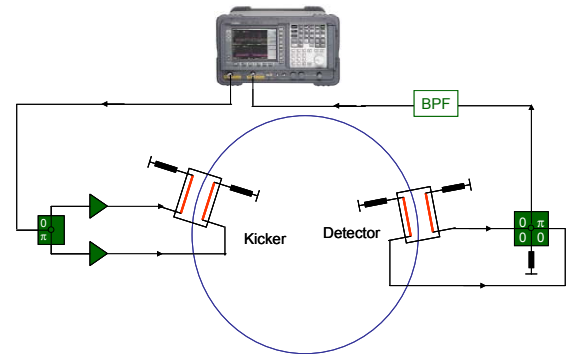
Figure 1: Simplified block diagram for tune measurement.

The horizontal/vertical tunes and other related parameters are given in Table1.

Table 1. Various tune related parameters

Injection Energy (GeV)	0.8
Stored Beam Energy (GeV)	2.5
RF frequency (MHz)	499.654
Revolution Frequency (MHz)	2.25
v_x	7.23
v_y	6.19
Fractional Tunes (kHz)	
Δv_x	517
Δv_y	427

STRIPLINE DESIGN

To simplify the design and minimize the manufacturing and development costs, two striplines with the same mechanical structure and dimensions will be used. One stripline for the excitation of the beam as the shaker and the other as the pickup to detect the excitation resonances. The stripline has four strips, one pair in each plane. For horizontal betatron tune (in order to measure directly the displacement relatively to the centre), the left pair of strips will be 180^0 out of phase with the right pair, and for y-tune the top and bottom pair will be out of phase. The strip has N-type vacuum feed through at the end and has a length of 150 mm. By a suitable choice of the ratio between the strip width and distance from the wall, the characteristic impedance is made 50 Ω [3]. The possibility of a design by means of using exponentially tapered strips in order to have smooth frequency domain response also has been investigated, but the difficulties come into the mechanical dimensions which makes extra cost. However the initial design was based on a pipe radius of 35mm, but due to the problems of radiation

06 Beam Instrumentation and Feedback
T03 - Beam Diagnostics and Instrumentation

BPM (BEAM POSITION MONITOR) OF PAL LINAC AND BTL *

S. C. Kim[#], D. T. Kim, W. W. Lee, H. J. Park, Y. J. Han, J. Y. Huang, J. H. Choi,

Pohang Accelerator Laboratory(PAL), San 31, Hyoja-dong, Pohang 790-784, KOREA

Abstract

In Aug. 2004, thirteen BPMs are installed at BTL(Beam Transport Line), and in Aug. 2005, three BPM installed at main linac for beam trajectory measurement and feedback. BPM of the Linac consist of 57mm strip-line electrodes in 100mm short chamber and SMA-R type feed-through. BPM of the BTL consist of 100mm strip-line electrodes in 150mm long chamber and used SMA-R type feed-through. These BPM electronics of Linac and BTL is adpoted 500MHz log-ratio signal processing circuits. BPM data acquisition system is developed as EPICS IOC by using NI S-series DAQ board and NI Lab-view 7.1. Maximum read-out accuracy of BPM system is measured as 20μm included BPM electronics. In this paper, we are describes on BPM characteristics of PAL Linac and BTL.

INTRODUCTION

The linac of the PAL is consists of 12 klystron-modulator systems, 11 pulse compressors, 44 accelerating columns. Pre-injector section of the linac has a 1-ns, 80 kV, 2 A thermionic electron gun, a pre-buncher, and a buncher. After passing through the pre-injector section, the beam is compressed as three μ-bunch. Operation frequency of the linac is 2,856 MHz. There are thirteen Beam Current Monitor (BCM), twelve Beam Profile Monitor (BPRM) and fifty-six Beam Loss Monitor (BLM) for diagnostics in the PLS linac and BTL. There are also two beam analysing stations in the linac. The delivery ratio of the beam current from Linac to SR is depends mainly on the beam optics. Thirteen BPMs were installed from Linac end to BTL end at Aug. 2004 and three BPM were installed main linac at Aug. 2005 for beam trajectory measurement and feedback. BPM of the linac consist of 57 mm strip-line electrodes in 100 mm long chamber, and BPM of the BTL consist of 100 mm strip-line electrodes in 150 mm short chamber beam signal pick-up is used SMA-R type feed-through. In this paper, we are describes on BPM characteristics of PAL Linac and BTL.

BEAM POSITION MONITOR(BPM) OF THE PAL

For stabilized beam injection from linac to storage ring (SR) beam trajectory measurement and energy feedback are very important and BPMs are necessary beam instrument.

BPM Chambers

A conventional strip-line type BPM was designed with a π/2 rotational symmetry. Length of strip-line was decided by BPM electronics frequency. The angular width of the electrode is 52 degree in order to avoid a strong electromagnetic coupling between electrodes and electrodes. Linac BPM consist of 57 mm strip-line electrodes in 100 mm chamber and diameter of strip-line to line is 20 mm. BTL BPM consist of 100 mm strip-line electrodes in 150 mm chamber and diameter of strip-line to line is 40 mm. A 50 Ω SMA-type feed-through is connected to the upstream side of each electrode, while downstream ends are short-circuited to the chamber. Fig 1 and 2 are show the strip-line type BPM for PAL Linac and BTL.
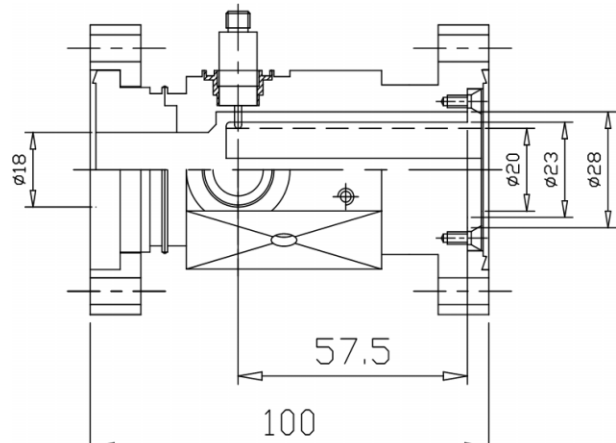
Figure 1: Strip-line type BPM for the PAL Linac
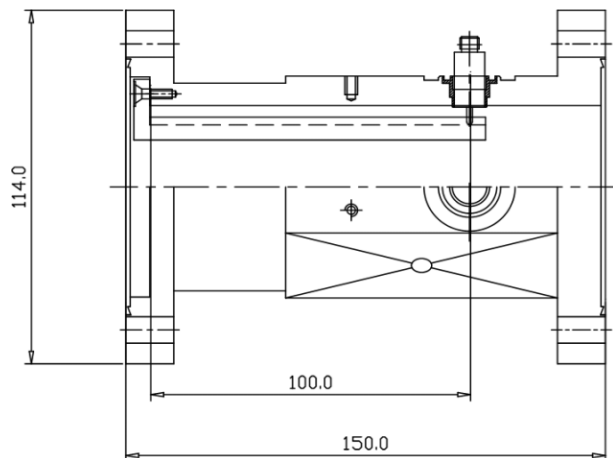
Figure 2: Strip-line type BPM for the PAL BTL

DEVELOPMENT OF WIDE BAND FCT SYSTEM FOR BOOSTER SYNCHROTRON OF INDUS-1 & 2

Prashant Pareek*, Karan singh & R.S. Shinde
Raja Ramanna Centre For Advanced Technology, Indore, India.

Abstract

A precision, non-destructive type wide band FCT for measurement of electron current of Booster synchrotron for Indus-1 & 2 has been developed. This monitoring system is composed of fast and slow FCTs using NiZnCo ferrite toroids, pulse amplifiers and electromagnetic shields. The FCT shows fast rise time (60 ns) large time constant (38 ms), high sensitivity 25 mV/mA at 50 Ω and linearity within 1%. This paper focuses on FCT design, construction and pulse response.

INTRODUCTION

For the fine operation of accelerator it is important to measure beam current and pulse shape so a wide band FCT is required to measure electron beam turn to turn current and stored current accumulation during 1μs pulse injection into booster synchrotron. The parameters required for FCT are 1) fast rise time 2) large L/R ratio 3) high signal to noise ratio 4) good linearity. It is difficult to achieve above characteristics using single large ferrite toroid. So we have developed two FCTs using large Ni-Zn-Co ferrite toroids, housed in a single box with two outputs. One FCT measures the current from 60 ns to 15 μs and another measures from 12 μs to 1 ms. The spacing between two FCT is optimized to reduce mutual coupling .The two outputs are amplified, buffered and then transmitted through 50 Ω characteristic impedance coaxial cable to control room.

CIRCUIT DESCRIPTION

Principle

The FCT picks up the magnetic field generated by electron beam [1]. A simplified equivalent electrical circuit diagram is shown in fig 1.
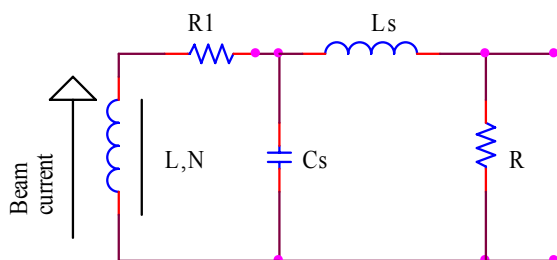
Figure 1: Equivalent electrical circuit diagram of FCT where

- L, the pickup coil or secondary inductance
- N, the number secondary turns
- R, the load resistance
- R1, the resistance of cable of secondary circuit

*ppareek@cat.ernet.in

- C_s, Stray capacitance between components
- L_s, stray inductance between the components

Due the combination of L_s & C_s results in overshoot and damped oscillation of the output signal. The stray inductance and capacitance influences the rise time. To get fast rise time 60 ns, numbers of turns are reduced in fast FCT and to get large time constant 38 ms, number of turns are increased. Secondary side reflected equivalent circuit diagram is shown in fig 2.
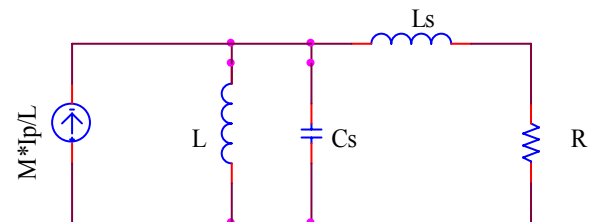
Figure 2: Equivalent secondary side reflected electrical circuit diagram of FCT

Fast FCT

Fast FCT has given 20 turns and terminated with 4.75 Ω resistance, which gives time constant 87 μs. The pickup coil wound on small region of the core, so the leakage inductance cannot be neglected. Therefore, the current transferred to secondary will be equal $M*I_{beam}$ / L_{pickup} instead of I_{beam} / N. M is the mutual inductance between pickup coil and I_{beam} acting as primary. The measured M and coupling coefficient K are 15 μH & 0.6 respectively . The signal across load resistance is amplified by differential video amplifier MC1733. A cable driver LH0033 is used to transmit the signal through 50 Ω characteristic impedance coaxial cable to control room. The electronic block diagram is shown in fig 3.
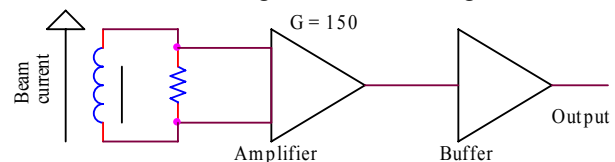
Figure 3: Electronic circuit block diagram for fast type FCT

Slow FCT

Slow FCT has given 350 turns and terminated with 3.2 Ω resistances, which gives time constant 38ms. Here the pickup coil wound on entire region of the core. The measured M and coupling coefficient K are 307 μH & 0.72 respectively. Due to large number of turns, high gain is required which is achieved in three stages using video amplifier and operational amplifier and cable driver LH0033 is used to transmit the signal through 50Ω characteristic impedance coaxial cable [2]. The electronic

06 Beam Instrumentation and Feedback
T03 - Beam Diagnostics and Instrumentation

PHOTON BEAM POSITION MONITOR WITH HYDRAULIC LEVEL SYSTEM

Y. J. Han, J. Y. Huang, S. N. Kim, Y. C. Kim, J. H. Choi, and I. S. Ko
Pohang Accelerator Laboratory, POSTECH, Pohang, 790-784, Korea

Abstract

In a synchrotron radiation source like the Pohang Light Source (PLS), a great effort has been made on beam stability improvements. For the beam line user-side orbit feedback, Photon Beam Position Monitor(PBPM) provides more practical information on the position and angle of the elector beam at the center of the bending magnet, compared the closed orbit data. For improvement of the orbit stability, PBPMs are used in PLS. However, the ground of PLS moves about 2mm every year. Therefore, we plan to measure the vertical orbit drift and angle variation considering the floor uneven settlement and the support thermal deformation by use of PBPM with Hydraulic Level System(HLS).

INTRODUCTION

Pohang Light Source (PLS) with beam energy of 2.5 GeV has provided the stable beam to the users during last 10 years. As the number of beamline requiring the micro-spot high resolution photon beam such as ID (Insertion Devices)has been increased, the stabilization of the electron beam orbit drift is strongly required. Therefore, in a synchrotron radiation source like PLS, a great effort has been made on beam stability improvement in various related field such as RF, magnet power supply, diagnostics, etc. For the beamline user-sided orbit feedback, PBPM provides more practical information on the position and the angle of the electron beam at the center of the bending magnet, compared the closed orbit data. For improvement of the orbit stability, PBPMs are used in PLS. However, the mechanical motions of main storage ring machine components such as girder, magnet, vacuum chamber, etc., have been known very important factors having potent influence on the beam trajectory. Therefore, it is necessary to measure and understand the real time movement behaviour of the storage ring components, the beamline components and their bases, i.e., the tunnel floor and the experimental hall floor. There has been a big amount of uneven settlement at the storage ring floor slab along its circumference at PLS. The amounts were almost 3mm per year at the beginning stage of measurement and it tends to converge to 2mm per year. These measurements were performed by the conventional optical surveying method at every machine shutdown period (2 times a year). To understand the real orbit drift, we have to consider the real impact of this floor uneven settlement on the beam operation. Therefore, we plan to measure the vertical orbit drift and angle variation considering the floor uneven settlement and the

support thermal deformation by use of PBPM with HLS (Fogale, Nanotech, France).

SYSTEM

PBPM

Fig. 1 shows the wire type photon beam position monitor with hydraulic level system. Here, the material of the wire is tungsten with 0.5mm diameter and 90mm length. In order to improve the electric conductivity, the

Figure 1 : Installation of Photon Beam Position with Hydraulic Level System. HLS are installed on the floor and support.

wire for PBPM is coated with gold. There is a diaphragm with 60mm horizontal aperture which can block off the miscellaneous light. Additionally, the monitor can vertically move and the moving range is ±20mm. There is generally the cooling system in the blade type PBPM, but it is structurally impossible that the cooling system is installed in the wire type PBPM. Therefore, the heat transfer analysis is very important. We have studied the effects using heat-power theoretical method and ANSYS analysis code. These methods involved radiation for cooling method. PBPM are installed to diagnostic beamline about 14m away from source point. The source of diagnostic beamline is bending magnet and PBPM's wire size is 90mm x 0.5mm at 14m away from source. Then, total power become to about 9.57W. When the ration is involved by power-heat theoretical method, the temperature of the tungsten wire is saturated at $819^{o}K$.

We also performed the heat-power analysis by ANSYS code. As the results, the maximum temperature of the tungsten wire is acquired about $1066^{o}K$. This is a bit greater than the results of theoretical method. We can estimate the tungsten wire is under safe at this temperature. Another analysis with ANSYS code is performed in order to know the structure deformation by

06 Beam Instrumentation and Feedback
T03 - Beam Diagnostics and Instrumentation

TUNE AND LIFETIME STUDIES AT THE AUSTRALIAN SYNCHROTRON

M.J. Spencer, M.J. Boland, R.T. Dowd, G. LeBlanc, Y.E. Tan, ASP, Melbourne, Australia

Abstract

The 3GeV Australian Synchrotron [1,2] will begin operation in March 2007. This paper outlines the tune and lifetime measurement systems. It also provides a summary of a number of studies completed using these systems. Three different tune measurement systems have been tested. Lifetime measurements made using the DCCT were used to optimise the strengths of the harmonic sextupoles and the location of the tunes. The vertical aperture was determined using scrapers. Beta-function measurements have been completed by shunting individual quadrupoles and noting the resultant tune changes. Chromaticity measurements have been made by observing the change in tune as the RF frequency is varied.

TUNE MEASUREMENT

Spectrum Analyser with Tracking Generator

A Rohde and Schwarz FSL spectrum analyser with tracking generator is the current default tune measurement method. The input to the spectrum analyser is a signal from a stripline. The tracking generator output is amplified to around 10 Watts before being fed, in series, to the horizontal then the vertical excitation kickers.

A C-program was written to allow MATLAB to quickly obtain the positions of the peaks.
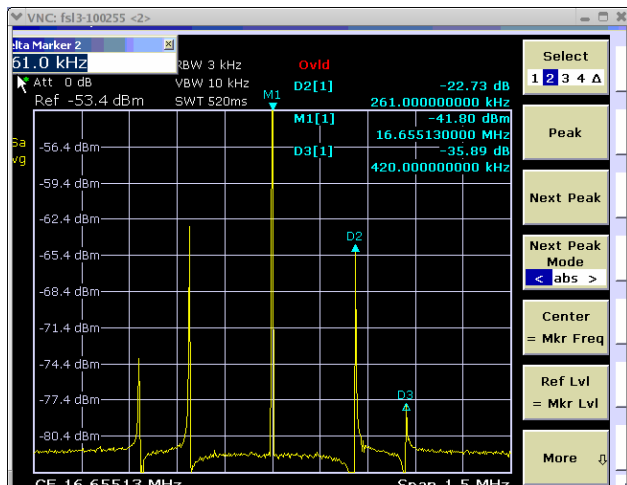
Figure 1: Tune measurement using a spectrum analyser with tracking generator.

Real-Time Spectrum Analyser in Conjunction with Arbitrary Waveform Generator

A Tektronix RSA3303A real time spectrum analyser was trialled as a tune measurement device. The stripline was used as a pickup. An Agilent 33220A arbitrary waveform generator was used to provide white noise up to 6 MHz. The signal from the noise generator was amplified and fed to the horizontal and vertical excitation kickers.
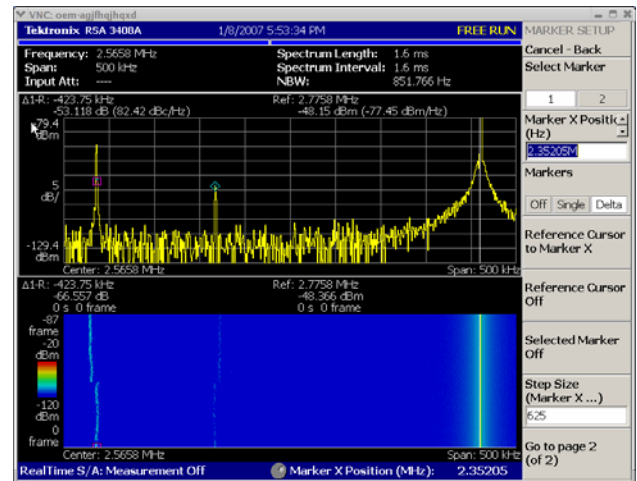
Figure 2: Tune measurement using a real time spectrum analyser and white noise generator. The waterfall plot shows a small jump in tune as a single quadrupole is shunted.

Injection Kicker with BPM Button Spectral Analysis

We have observed that our injection kickers provide a transient beam excitation in both the horizontal and vertical planes. To measure the tunes a single injection kicker is used, set to a low strength. Fourier analysis of the data from a triggered BPM button [3] reveals the tunes.
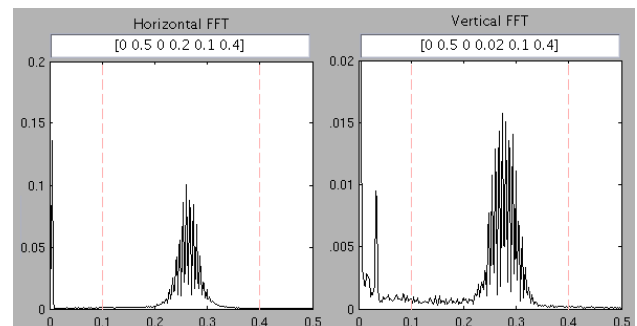
Figure 3: The tune peaks obtained by a fourier analysis of the BPM button data. Note that the large tune spread in this figure is due to the fact that the sextupoles were off.

COMMISSIONING OF THE AUSTRALIAN SYNCHROTRON WITH LIBERA EBPPS AND MATLAB

Y.-R. E. Tan, G. S. LeBlanc, M. J. Boland, R. Dowd and M. Spencer
Australian Synchrotron, Melbourne, Australia

Abstract

The Australian Synchrotron (AS) is equipped with a full compliment of 98 BPMs attached to Libera Electron Beam Position Processors (EBPPs) [1] that are capable of measuring turn-by-turn/first turn and averaged beam positions simultaneously. The BPM system coupled with Matlab applications has simplified the process of commissioning. This report will highlight how the various tools have been utilised and show the results of some studies.

INTRODUCTION

The Australian Synchrotron (AS) storage ring is a 14 cell, Chasman-Green type lattice with 3 families of quadrupoles, 4 families of sextupoles and a total of 42 horizontal correctors and 56 vertical correctors [2]. Each cell has been fitted with 7 BPMs, totalling 98 BPMs, all of which are connected to EBPPs.

EBPPs are being used at facilities such as Soleil and Diamond (just to name a few) and are versatile diagnostic tools. The specifications for the BPM system at the AS are RMS values of < 0.2 μm (slow, 1kHz BW) and < 6 μm (turn by turn, 1 MHz BW) between 10 and 200 mA. Additionally the beam current (10 – 200 mA) and thermal (± 1°C) dependence needs to be < 2 μm. Many of these parameters have yet to be characterised.

On the control side over the last few years the use of a suite of applications written in Matlab at synchrotron facilities for accelerator physics studies and commissioning has grown. The core of this suite of applications now includes AT [3], MCA, LOCO [5] and Middle Layer [4]. The integrated system of programs and scripts has made it an ideal tool for us at the AS.

The sections below will outline the BPM system and its capabilities followed by some of the applications that have been used during commissioning and the results.

BPM GEOMETRY

The four BPM buttons (from Kyocera) are separated in the vacuum chambers by 20 mm (H) and 32 mm (V). Using POISSON it is possible to simulate the fields with the geometry of the BPM blocks. The results gave BPM coefficients of $k_x = 14.60$ mm and $k_y = 14.66$ mm (LOCO results later put these values closer to ~15.3 mm ± 1%).

$$x = k_x \left(\frac{V_A - V_B - V_C + V_D}{\sum V_i} \right) \qquad y = k_y \left(\frac{V_A + V_B - V_C - V_D}{\sum V_i} \right)$$

The error estimates in the position due to the pincushion effect was also investigated (see Figure 1). Within a region of x = ± 3 mm and y = ± 2 mm the apparent position is accurate to < 5%. Given that most studies will not involve orbits > 1 mm, inverting the pincushion effect is not seen as necessary.
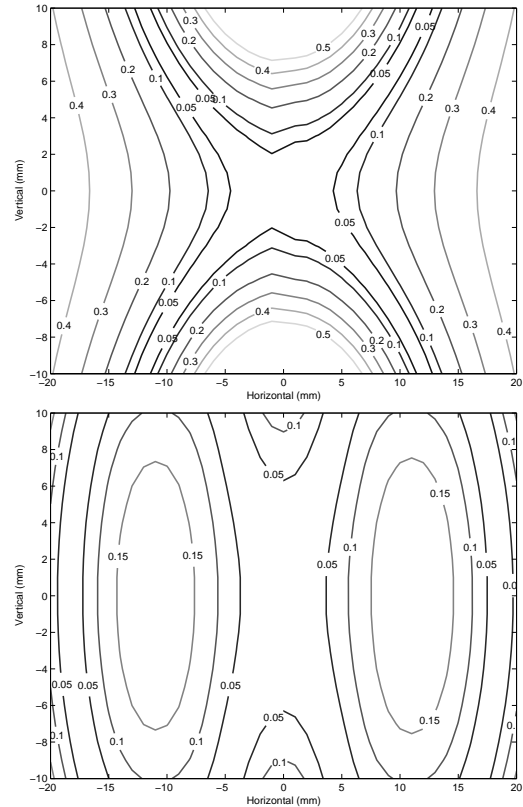
Figure 1 Relative error in the horizontal (TOP) and vertical (BOTTOM) position as a function of the actual beam position in x and y due to the pincushion effect.
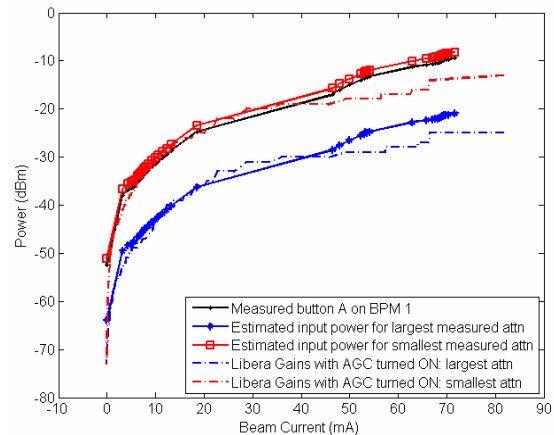
Figure 2 This plot shows a range of input power levels of the BPM signals going into the Libera based on measured signals (solid) and on gain settings of the EBPPs when Automatic Gain Control is turned on (dotted).

MEASUREMENTS USING THE X-RAY AND OPTICAL DIAGNOSTIC BEAMLINES AT THE AUSTRALIAN SYNCHROTRON

M. J. Boland, J. Bergstrom, G. S. LeBlanc, Y.-R. E. Tan, R. Dowd and M. J. Spencer, Australian Synchrotron, Clayton, Victoria 3168, Australia.

D. J. Peake and R. P. Rassool, The University of Melbourne, Victoria 3010, Australia

Abstract

First Light has been achieved on the diagnostic beamlines at the Australian Synchrotron 3 GeV storage ring. The X-ray Diagnostic Beamline (XDB) has been used to measure the beam size, divergence and emittance, while the Optical Diagnostic Beamline (ODB) has been used the measure the bunch length and turn-by-turn stability. Both beamlines receive dipole radiation from a bend magnet and provide continuous diagnostic data to the control room. The beamlines compliment each other with the ODB providing mainly longitudinal (temporal) information, while the XDB measures predominantly transverse (spatial) information. A brief description is given of the equipment on each beamline and the commissioning results are presented.

X-RAY DIAGNOSTIC BEAMLINE

The x-ray diagnostic beamline provides mostly transverse beam information and is described in more detail in Ref [1]. Measurements made during the commissioning of the storage ring are presented here.

Image Array

A pinhole array generates 9 images of the bend magnet source point which is displayed in the control room via EPICS (see Fig. 1). The spots provide a qualitative as well as quantitative diagnostic of the status of the stored beam.
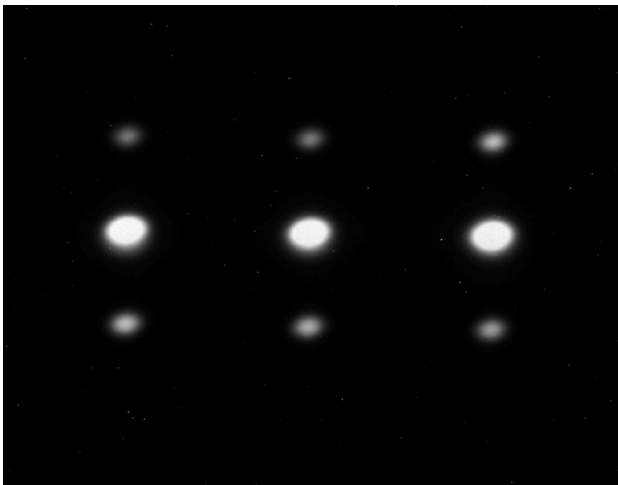
Figure 1: Array of beam spot images created by the x-ray pinhole array. The data is captured with a CCD camera viewing a YAG screen on the x-ray diagnostic beamline.

Beam Size and Emittance

The beam spot is measured from the YAG screen image and fitted with a Gaussian curve to obtain the horizontal and vertical beam sizes. The emittance was determined using the measured beam size and the beta-functions from the calibrated model that was fit using LOCO [2]. Fig. 2 shows the results of a measurement after the first correction to optics to remove beta-beating. The emittance of 17.5 nm is close to the design value of 15.8 nm for a lattice with zero dispersion in the straight sections.
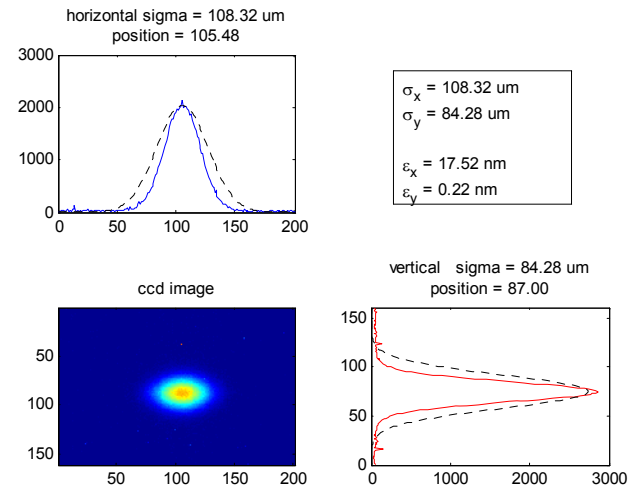
Figure 2: Emittance measurement from a single spot on the x-ray diagnostic beamline and beta-functions from a calibrated model.

Beam Stability

Using an EPICS driver to process the camera data from the Firewire CCD camera the x-ray beam centroid is monitored to track the beam stability. In order to get a good quality image the CCD integration time needs to be 50 ms or greater. With the CCD triggered at 1 Hz and a 50 ms integration time the beam stability is measured to be 2 μm rms.

Divergence

The multiple images from the pinhole array allows for divergence of the beam to be measured by fitting a Gaussian to the intensity distribution of the vertical beam spots. Fig. 3 shows the vertical profile and the Gaussian fit to the intensity distribution of the beam spot peaks.

DIAGNOSTIC SUPPORTS FOR TOP-UP OPERATION AT TLS

K.H. Hu[#], Jenny Chen, C.J. Wang, C.H. Kuo, K.T. Hsu
National Synchrotron Radiation Research Center, Hsinchu 30076, Taiwan

Abstract

The routine top-up operation of Taiwan Light Source (TLS) began in October 2005. The beam stability and integrated flux were drastically improved. Various diagnostics are needed to support the top-up operation. These tools include diagnostics for measuring beam charge and current and injection efficiency, as well as a filling pattern monitor, a tune monitor, and an instability and loss pattern monitor. This study summarizes design considerations, details and future plans.

INTRODUCTION

The accelerator system at the Taiwan Light Source (TLS) consists of a 140 keV thermionic gun, a 50 MeV linear accelerator (LINAC), a linac-to-booster (LTB) transport line, a 1.5 GeV booster synchrotron, a 70 m long booster-to-storage ring (BTS) transport line and a 1.5 GeV storage ring. The goals of the top-up mode operation are to provide high stability and a highly integrated flux photon beam and to keep the heat load of the optical components constant. A complete diagnostic of the accelerator system is required for routine monitoring and machine debugging, to support the requirements of top-up mode operation. Major diagnostics that support top-up operation include charge, transmission of transport line, current, injection efficiency, orbit stability, electron loss, profiles, tune and instability and others. Table 1 summarizes these diagnostics.

MAJOR DIAGNOSTICS SUPPORT FOR TOPUP OPERATION

Templates are provided for Microsoft Word (Mac and PC) and LaTeX. Authors are advised to use the templates provided. The JACoW Styles and Macros menu, available in the Microsoft Word .dot templates, is designed to help authors format their papers correctly. Please consult the individual conference help pages if questions arise.

LINAC and LTB Diagnostics

Diagnostic devices of the LINAC include several toroids, two fast gap monitors, and a screen monitor near the exit of LTB. These diagnostic devices can measure beam current, beam profile, energy and energy spread. A 60° bending magnet is adopted to bend the output of LINAC. An energy defining slit is located just before the last toroid to define the energy. Integrating the current waveform of this toroid monitor obtain the beam charge of the LINAC output. The energy and energy spectrum can be measured by scanning the bending angle of the bending magnet. A screen monitor is added behind the

bending magnet, to measure the emittance of the LINAC by the quad-scan method when this bending magnet is turned off.

Table 1: Main diagnostics to support top-up operation

Accelerator system	Parameters should be monitor	Descriptions
Linac	Transmission	Toroid, gap monitor, oscilloscope
	Charge	Toroid and charge integrator
Booster synchrotron	Averaged beam current	MPCT
	Filling pattern	FCT, stripline with oscilloscope
BTS	Transmission	ICT and charge integrator
	Beam position	BPM
	Position, transverse profile	Screen monitor
Storage Ring	Averaged beam current	MPCT with 1 µA resolution
	Injection efficiency	$\Delta I_{avr,SR}*t_{rev,SR}/C_{ICT,BTS}$ per injection shot
	Filling pattern	Button pickups with oscilloscope
	Isolated bunch purity	Photon counting system – in planning

Note: $\Delta I_{avr,sr}$ is increment of beam current per injection shot, $t_{rev,SR}$ is the revolution period of the storage ring, $C_{ICT,BTS}$ is the beam charge pass the BTS per injection shot.

Booster Synchrotron Diagnostics

The booster synchrotron diagnostic consists of seven sets of screen monitors, MPCT, FCT, BPMs, and a synchrotron radiation monitor. The measured parameters include beam current, closed orbit, tune and beam profile. The averaged beam current is measured by the MPCT. The filling pattern is measured by the FCT. The synchrotron radiation monitor is upgraded using an IEEE-1394 camera with an external trigger and exposure time control functions. Several approaches have been applied during the last decade was to tune measurement. Figure 1
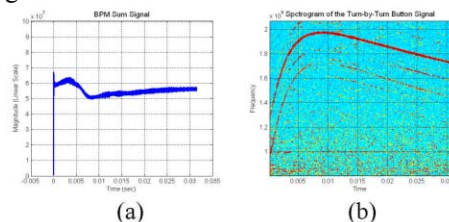
Figure 1: (a) Beam intensity of the booster synchrotron; (b) tune variation during energy ramping.

06 Beam Instrumentation and Feedback
T03 - Beam Diagnostics and Instrumentation

EXPERIENCE OF BEAM DIAGNOSTIC SYSTEMS IN COMMISSIONING STAGE OF INDUS-2

T. A. Puntambekar[#], Anil Banerji, L.K. Babbar, Akash Deep, Anil Holikatti, D.K. Joshi, A. Karnewar, S. Kotaiah, Mukesh Kumar, R.K. Nathwani, S.K. Suhane, Y. Tyagi, S.Yadav
Raja Ramanna Centre for Advanced Technology, Indore, India

Abstract

Indus-2 is a 2.5 GeV synchrotron radiation source under commissioning at this centre. Beam injection trials in the storage ring began in August 2005. Beam diagnostics systems played an important role during commissioning of the storage ring. Beam diagnostic systems installed in the machine include beam profile monitor, orbit measurement system, wall current monitor, DCCT, strip lines, tune measurement system and sighting beam line. This paper describes the diagnostic systems, experience of operation of these systems during commissioning, results obtained and the present status. During the initial stages of beam injection and circulation in Indus-2, wall current monitors, beam profile monitors and sighting beam line proved to be of utmost help. In the current stage of near routine beam operation, the main focus has shifted to the measurement of beam parameters with the objective of improving beam current and lifetime.

INTRODUCTION

Indus-2 is a 2.5 GeV energy dedicated electron synchrotron radiation source. The accelerator complex is composed of injector microtron, booster synchrotron and Indus-2 ring. Two bunches of 550 MeV are extracted from the booster synchrotron and injected in to Indus-2 through 88 m long transport line–3 (TL-3). The length of each bunch is about 1 ns and separation between them is 31.6 ns. The process of commissioning of Indus-2 started in August'05. Initially beam injection was carried out at 450 MeV energy, which was later on increased to 550 MeV to achieve higher accumulation rates. After successful beam accumulation in the storage ring, energy ramping to 2 GeV was done. Table 1 summarizes the diagnostic devices installed in Indus-2. Fluorescent screen type beam profile monitors, wall current monitors, septum hole monitors and sighting beam line were used to transport the beam effectively through the beam transfer line and achieve beam circulation and accumulation in the storage ring during the initial beam injection and commissioning stage.   The main focus has shifted to the measurement of beam parameters with the objective of improving machine performance in the current stage of near routine beam operation. Measurement of betatron tunes (Horizontal and vertical) and closed orbit distortion (COD) has been carried out [1,7].

Table 1: Beam diagnostic devices in TL-3 and Indus-2

S. No.	Name of diagnostic device	Total number
1	Beam Profile Monitor	19
2	Wall Current Monitor	5
3	DC Current transformer	1
4	Beam Position Indicator	56
5	Strip line Monitor	6
6	Sighting Beam Line	1
7	Horizontal and vertical Scraper	3
8	Thick and thin Septum Hole Monitors	2

BEAM DIAGNOSTIC SYSTEMS

An overview of the beam diagnostic systems installed in TL-3 and Indus-2, experience gained during beam commissioning and the results obtained so far are presented in the following sections.

Beam profile monitor

Fluorescent screen beam profile monitors (BPM) are installed in TL-3 and the storage ring for visual observation of beam profile and position in transport line and the storage ring [2]. The BPM uses a fluorescent screen made of chromium-doped alumina, which can be inserted into the beam path by a pneumatic cylinder based linear motion mechanism. The spot of fluorescent light generated by the beam can be viewed by a CCD camera placed vertically above the beam plane. Remote operation of BPM is achieved by BPM interface units kept near the device and video signal multiplexers. A PCI based frame grabber card is used to capture and digitise the image for further processing. Figure 1 shows photograph of a BPM and the inset shows a typical electron beam profile. One-turn beam circulation was confirmed by observing the beam spot at all eleven BPM placed in the storage ring. The septum hole monitor is used to view the position of the beam at the entrance apertures of the thick and thin injection septum. The beam passes through an opening in a fluorescent screen mounted just a few millimetres upstream of the septum aperture. It has been found to be very useful in steering the beam though the injection septum during initial beam injection into the storage ring.

[#] tushar@cat.ernet.in

COMPARISON OF THE METHODS FOR BEAM ENERGY SPREAD MEASUREMENT AT THE VEPP-4M

V.A. Kiselev, N.Yu. Muchnoi, O.I. Meshkov, V.V. Smaluk, V.N. Zhilich, A.N. Zhuravlev
Budker Institute of Nuclear Physics, Novosibirsk 630090, Russia

Abstract

The VEPP-4M electron-positron collider is now operating with the KEDR detector for the experiment of precise measurement of tau-lepton mass. In this experiment, monitoring of beam energy spread is important to know the energy spread contribution into the total systematic error. Information about the energy spread gives an opportunity to reduce the error of the tau-lepton mass measuring. Several techniques for measuring the energy spread are described in the paper. Width of the ψ' resonance measured with the KEDR detector is used as a reference.

INTRODUCTION

The basic physical program of the VEPP-4M collider consists in precise measurements of mass of J/ψ, ψ', ψ'' narrow resonances and c-τ lepton mass on the threshold production. Value of beam energy spread σ_E is directly included into accuracy of the mass measurement. Knowledge of exact value of the beam energy spread enables us to reduce significantly a systematical error in the experiment of c-τ lepton mass measurement. It is also an essential supplement to the precise measurement of average beam energy.

Clear understanding of the reasons influencing the beam spread and the ability to control this value are important tasks for our experiments.

Energy spread of the beam can be increased with the 3-pole snakes and depends on strength of Robinson wigglers. Snakes have a length about 1 m and 1.8 T maximal strength of magnetic field. They were applied only during the beam energy spread measurements described below.

MODES OF THE VEPP-4M OPERATION

Table 1: Operation modes of the VEPP-4M used for energy spread measurements

Name	E, MeV	I_{WG}, A	I_{SN}, A	Comments
PNT4	1843	1055	0	$c-\tau$ lepton production. KEDR magnetic field is on.
PSIS	1843	1055	0	KEDR magnetic field is off.
ZMEJ	1843	1055	2000	KEDR magnetic field is off.
JPSI	1548	620	0	J/ψ meson peak. KEDR magnetic field is off

The target of our experiments was not only the definition of the beam energy spread for basic modes of the collider operation, but also the comparison of several procedures for measurement of relative energy spread $\delta_E = \sigma_E / E$. The experiments were carried out at the four modes of the collider operation (Tab. 1). The modes differ both in the energy E and in the energy spread σ_E value. Application of several methods to determine the energy spread for different modes of the VEPP-4M operation enables us to realize a cross-validation of the measurements and to compare the diagnostics considering convenience and efficiency.

METHODS

Spectrum of chromatic sideband peak of beam betatron oscillation (I)

Optical system [3] was applied to measure the beam dimensions $\sigma_{x,y,z}$ and spectrum of vertical betatron oscillations.

Chromaticity of a storage ring causes appearing of synchrotron sideband peaks in a spectrum of beam oscillation. The amplitude of the central betatron frequency and the synchrotron satellites is [4]:

$$R_m(y) = \frac{1}{y^2} \int_0^\infty J_m^2(x) e^{-\frac{x^2}{2y^2}} x \, dx,$$

$$y = \left(\frac{\omega_\beta \alpha}{\omega_s} + \frac{\omega_0 C_y}{\omega_s} \right) \delta_E ,$$

m is the number of harmonic, δ_E is the relative energy spread.

Determination of energy spread is based on the measurement of the ratio of synchrotron satellites to the main peak height.

Current dependence of energy spread (II)

The experiments with method (I) were carried out at the small beam current I_0 = 10–50 mkA, when collective effects are negligible. In the course of experiments with mesons mass measurements the beam currents were close to beam-beam effect threshold restriction. This value was from 1.5 to 3.5 мА depending on the beam energy spread. Radial and longitudinal beam dimensions σ_{xz} were taken to determine current dependence of the beam energy spread.

Energy spread of the beam was derived from the measured radial size σ_x and known amplitude functions

06 Beam Instrumentation and Feedback
T03 - Beam Diagnostics and Instrumentation

CONTROL OF THE MULTI-BUNCH INSTABILITIES AT TLS

C.H. Kuo, K.H. Hu, Demi Lee, Jenny Chen, S.Y. Hsu, K.T. Hsu

National Synchrotron Radiation Research Center, Hsinchu, Taiwan

Abstract

The goals of the recent superconducting RF upgrade and top-up operation at the Taiwan Light Source (TLS) are to increase stored beam current and provide stable beams. Suppressing multi-bunch instabilities caused by the resistive wall of the vacuum chamber and cavity-like structures and suppressing ion-related instability are essential to exploiting these upgrades. FPGA-based transverse bunch-by-bunch and longitudinal feedback systems were adopted. Multi-bunch instabilities were successfully suppressed at stored beam currents of over 400 mA. Chromaticity can be reduced using a transverse feedback system, which is essential to increasing the injection efficiency in the top-up operation mode. The status of the feedback systems and an analysis of the behavior of multi-bunch instability are presented.

INTRODUCTION

The Taiwan Light Source (TLS) at NSRRC is a 1.5 GeV storage ring. Two major upgrades of TLS have been completed - the superconducting RF cavity (SRF) upgrade in the late 2004 and the top-up operation in the late 2005. Both upgrades were intended to increase the stored beam current from 200 mA to over 400 mA, to eliminate strong instability that is caused by the high-order modes (HOM) with conventional RF cavities, and thereby continue to provide a constant heat load for high-quality photon beams. The threshold current of transverse multi-bunch instability is slightly less than 40 mA. The longitudinal instability is also a problem when the stored beam current exceeds 150 mA. The major source of the transverse instability is the resistive wall and the ion effects. The cavity-like structure of the vacuum duct is assumed to contribute in the source of longitudinal instability. These instabilities can be effectively controlled by the transverse feedback system and the longitudinal feedback system. This report will present the status of instability suppression at TLS.

MULTI-BUNCH FEEDBACK SYSTEM

FPGA-based bunch-by-bunch feedback applications are extensively adopted in numerous) laboratories. The SLAC/LNF-INFN/KEK collaboration G-board project [1] and Libera Bunch-by-Bunch projects for ESRF broadband feedback system are typical examples. The feedback processor in TLS was originally developed for the SPring-8 [2, 3]. A highly flexible feedback processor design led to easy adoption for TLS applications. Figure 1 presents the block diagram of a bunch-by-bunch feedback system. The system consists of a beam position monitor (BPM), an analog front-end (analog de-multiplexer for

transverse feedback and phase detector for longitudinal feedback), a feedback processor, an SSB or QPSK modulator for a longitudinal feedback system, power amplifiers and kickers. The feedback processor is the key component of the feedback system, and is adapted from the SPring-8 design with minor modifications. The beam signals measured by the BPM are processed by an analog de-multiplexer or a phase detector into baseband signals and fed to the digital feedback processor, and converts the position or phase oscillation signal of each bunch into digital form which is filtered using the FIR filters. The filtered error signal drives the kicker to dampen the bunch motion. The latency of the system should be one or two periods of revolution of the storage ring plus the bunch propagation delay between the BPM and the kicker in the transverse feedback loop.
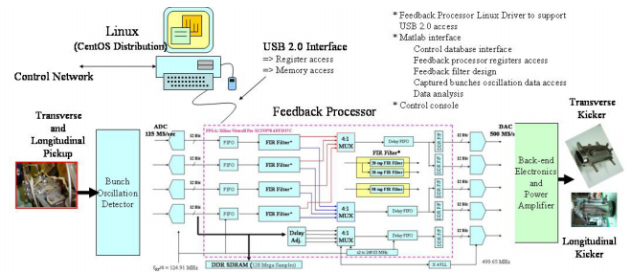
Figure 1: Block diagram of bunch-by-bunch feedback system. The feedback processor is shown in the center of the figure. The FIR filter inside the feedback FPGA consists of two 20-tap FIR filters in the transverse feedback and a 50-tap FIR filter in the longitudinal feedback.

Up to 32 sets of FIR filter coefficients can be stored in the internal register of FPGA and are selectable via a USB 2.0 interface or an external logic input control. The switching speed is about 10 ns in the latter case. This function makes the system very flexible for use in the grow-damp experiments. Up to 256 historic mega-samples of ADC are stored in the DDR memory of the feedback processor. Therefore, up to 256 ms of data can be stored in the memory. (One sample is two bytes.) The latency time of the feedback processor is about 300 ns. A favorable frequency response of the FIR filter can be easily achieved using a two-turn delay (800 ns) in the transverse feedback loop. The frequency multiplier supplies a DAC clock at the RF frequency with a cycle-to-cycle jitter of 50ps from the ADC clock. The processor with five DACs - four for the multiplexed FIR filter output and one for multiplexed raw ADC data - is used in diagnostics and tuning. The latency of the multiplexed FIR filter output can be controlled by adjusting the internal delay. Each DAC has

THE DESIGN, FABRICATION AND PERFORMANCE TESTING OF THE ANALOG I/Q RF CONTROL SYSTEM AT NSRRC

M.S. Yeh[#], L.H. Chang, F.T. Chung, Y.H. Lin, C.H. Wang, NSRRC, Hsinchu, 30076, Taiwan

Abstract

   An analog low-level RF system, based on an I/Q modulator and demodulator, has been tested at NSRRC. The I/Q RF control system has the same function blocks as the digital low-level RF system, which we plan to develop for our proposed 3-GeV light source machine. This analog I/Q RF system provides a real function structure to verify the working principle, block functions and performance evaluation of the developing digital low-level RF system. This work presents the designed function diagrams, the measured results for the characteristics of the main RF components, and the performance testing of the analog I/Q RF control system with a dummy cavity.

INTRODUCTION

   The existing low-level RF control system for the superconducting cavity of CESR-B type in NSRRC is based on analog feedback loops. It comprises four independent feedback loops, to control the gap voltage, the cavity phase, the klystron phase and the cavity frequency (tuner). These control loops ensure the required conditions of stability for operation of the superconducting cavity. Figure 1 shows a simplified block diagram of the analog low-level RF control system.
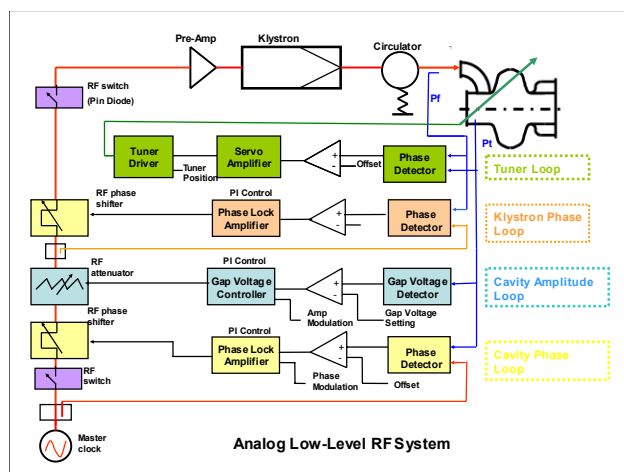
Figure 1: Functional block diagram of the analog low-level RF control system.

   The fluctuations of amplitude and phase are controllable within ± 1 % and $\pm 2°$ respectively in routine operation with the current analog low-level RF system.

   The present RF feedback control system is based on analog feedback loops for amplitude and phase. The I/Q (in-phase, quadrature) demodulation and modulator

_____
[#]msyeh@nsrrc.org.tw

techniques are currently favoured in modern accelerating structures. A translation of the amplitude and phase information into IQ is advantageous because of the symmetry of the IQ signal paths. This analog I/Q RF system also provides a real function structure to verify the working principle, block functions and the performance evaluation for the developing digital low-level RF system. A new, FPGA-based, digital, low-level RF system is proposed for development of the new Taiwan Photon Source [1]. The analog I/Q and digital FPGA LLRF systems are conceptually similar, both being based on the IQ method and PID regulation.

   This paper presents the designed function diagrams, measured results for the characteristics of the main RF vector components and the integration test of the analog I/Q RF control system

ANALOG I/Q CONTROL SYSTEM

   The analog I/Q feedback control circuits are based on NIM modules and use in-phase (I) and quadrature (Q) signal components, commonly called an I/Q detection system [2-4]. Figure 2 shows a schematic of the analog I/Q RF control system.
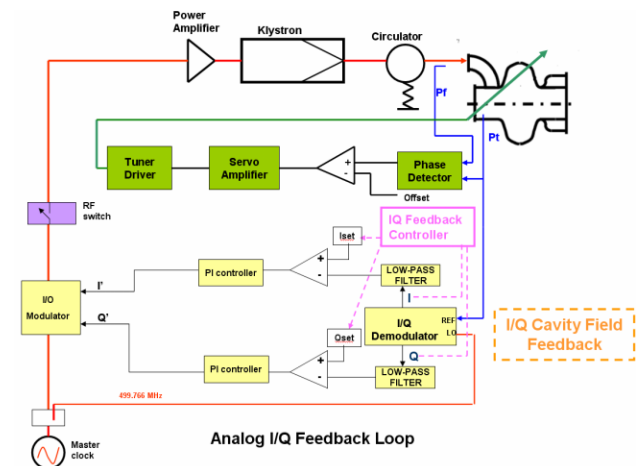
Figure 2: Function blocks of an analog I/Q control system.

   The cavity field is directly down-converted to base-band signals, for which a vector demodulator performs I/Q detection. The resulting I/Q base-band signals that describe the cavity field are fed to a pair of Proportional & Integral (PI) controllers, one for the I signal and another for the Q signal. The set points for the I/Q channels are also fed to the PI controllers in which the cavity-field error signals are generated and processed. The outputs from the I/Q PI controllers are fed to an RF vector modulator, which modifies the I and Q components of the carrier frequency from the master reference clock

CONTROL SYSTEM BASED ON PCS AND PLCS FOR THE L-BAND LINAC AT OSAKA UNIVERSITY

Ryukou Kato, Shigeru Kashiwagi, Tamotsu Yamamoto, Shoji Suemine, Goro Isoyama
ISIR, Osaka University, 8-1 Mihogaoka, Ibaraki, Osaka 567-0047, Japan

Abstract

A control system comprising of only personal computers and programmable logic controllers has been developed for the L-band electron linac at the Institute of Scientific and Industrial Research, Osaka University. The system has a simple structure consisting of a few PCs connected with Ethernet and PLCs with FL-net.

INTRODUCTION

The L-band electron linac at the Radiation Laboratory of the Nanoscience and Nanotechnology Center attached to the Institute of Scientific and Industrial Research (ISIR), Osaka University, was constructed in 1975-1978 [1] and has been used for radiation chemistry studies by pulse radiolysis technique. Recently, the linac has been extensively used for studies pertaining to nanotechnology, beam science as well as for basic studies in their related fields. In the advanced studies with the linac [2,3], stability of the electron beam and reproducibility of the linac operation are extremely important. The linac has been upgraded for higher stability and reproducibility of operation for advanced studies in beam science. A computer control system has been newly introduced for the linac not only to realize precise reproducibility of operation but also to make routine operation possible by even an unskilled operator.

In this paper, we present details of the control system and operational experiences.

HARDWARE IMPLEMENTATION

Configuration

The new control system is based on personal computers (PCs) and programmable logic controllers (PLCs). The PCs are used for operator consoles as human machine interfaces (HMIs), while the PLCs control various devices directly. The PLCs and their wiring terminals are installed in device control stations (DCSs). The DCS is the basic unit of the control hardware and all the devices of the linac except for those connected with GPIB are wired to the DCSs. The DCSs are placed at various places to form a distributed control system; three DCSs are in the control room and four in the linac room. In addition to these DCSs, the klystron modulator and the three SHB amplifiers, have their own PLCs for internal control. Network boards are added to each PLC, so that they can directly link to the control network. The schematic layout of the L-band linac and the present configuration of the control system are shown in Figures 1 and 2 respectively.

Networks

The PCs and the PLCs are connected to the networks using two different communication protocols. For the network connecting the PLCs, we have chosen FL-net, which is an open PLC network for factory automation. Protocol of FL-net is a vendor-independent open standard, and it works on compatible devices with Ethernet standard. Each PLC can share data through a common
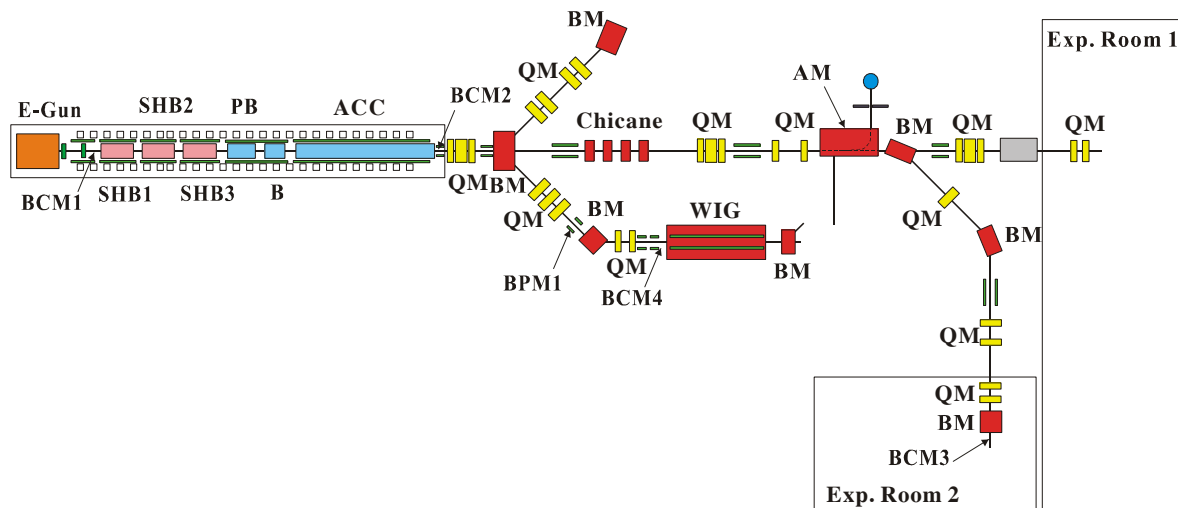
Figure 1: Schematic layout of the L-band linac. E-GUN: Electron gun, SHB1: 108MHz SHB cavity #1, SHB2: 108MHz SHB cavity #2, SHB3: 216MHz SHB cavity, PB: Prebuncher, B: Buncher, ACC: 1.3 GHz accelerating tube, BM: Bending magnet, QM: Q-magnet, AM: Analyser magnet, WIG: Wiggler, BCM1-4: beam current monitors, BPM1: beam position monitor.

IMPROVEMENT OF WEB-BASED MONITORING OF EPICS-IOC FOR PAL CONTROL SYSTEM*

J. M. Kim[#], K. M. Ha, E. H. Lee, J. H. Kim and H. S. Kang,
PAL, POSTECH, Pohang, Kyeongbuk, 790-784, Korea

Abstract

We are now operating a web-based monitoring system of PAL control system with MAC Power PC. In order to expand the IOC's web-based monitoring system, we are trying to use the X86/Linux platform. With the experience which we got in developing the web-based monitoring of EPICS-IOC based on MAC Power PC, a web-based monitoring system with an X86 Intel PC based on a new concept has been developed for lower costs, easier access and use. Its operating system employs Linux Fedora Core4. In order to drive the web-based monitoring system, EPICS Base 3.14.8 and MySQL 4.0 have been installed in the Linux Fedora Core 4. Archive engine with C language and EPICS channel access library are programmed to store the data. As a result of using the web-based monitoring system based on the X86 Intel PC, we have achieved its easier access and use, more convenient maintenance. Performance of the web-based monitoring system with an X86 Intel PC will be discussed.

INTRODUCTION

These days, web-based monitoring systems are on gradual increase. Required for the application of such systems are rapid application of newly added sub-systems and feasibility of maintenance. Currently, PAL EPICS IOC web-based monitoring system use MAC power PC G4 CPU based Linux Fedora Core 4 installed in it. By the time it was first developed in 2002, porting Linux OS in Mac system was not easy, because installation of Linux OS in Mac PC requires modification and complementation of the kernel to suit G4 CPU. Usually, Linux OS is distributed for free, and the OS kernel is seldom modified to fit any particular platform for installation. The OS kernel modification requires so specialized expertise that establishment of one system costs a great deal of time, efforts, and money. For such reason, the EPICS IOC Web Server to be newly developed adopted Intel/X86 CPU, which is easily accessible and facilitates comparatively easy system build-up.

The development experienced in MAC power PC was of great help in designing and developing new systems. The strong point of Intel/X86 PC compared to the current system is the simplicity of configuring and its low cost for the system establishment. For the operating system, Linux Fedora Core 4 was installed to maintain the compatibility with the current system. Archive Engine functioned to read data from EPICS IOC and store them

in database. IOC web sub-systems developed in the new hardware platform are Beam Current, LINAC BCM, Temperature, and Modulator.

SYSTEM ARCHITECTURE

Figure 1 shows the architecture of PAL EPICS IOC web monitoring system. EPICS IOC(Input Output Controller) consists of 19 components, and IOC Web Server is composed of three units of MAC and one unit of Intel/X86 System. The network interface is separated into two layers, Office-net and Control-net. Since SR BPM and MPS system are located in Control network, the data communication needs to be done via separate gateway. Each of the IOC Web Server system basically stores beam current data, and they are displayed as reference when the user requests a data plot from monitor screen. Each of IOC data are classified and stored through four units of IOC Web Servers. The systems which provide web service directly to users are accessed only by way of beam current web server.
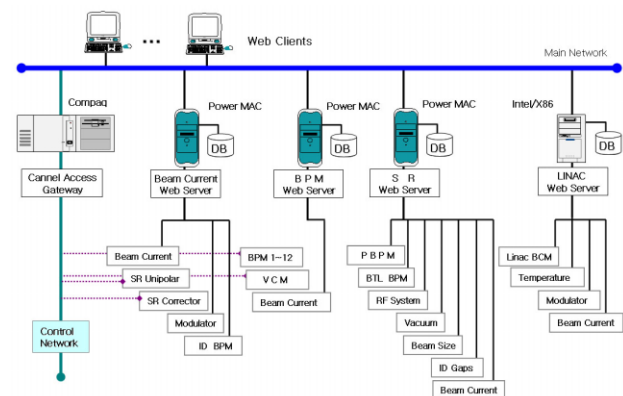
Figure 1: Architecture of IOC web monitoring system.

NEW HARDWARE SPECIFICATION

- CPU : Intel Pentium4 3.4GHz, Single.
- Memory : 2GB DDR PC400.
- Hard Disk : SATA 250GB x 2 Ea, 16MB Buffer.
- Chipset : Intel 865 + ICH5.
- Network Interface : 100Mbps.

INSTALL OF DEVELOPMENT TOOLS

In order to establish web based monitoring server, several software development tools have to be installed in advance. The tools installed are apache server for web service, EPICS 3.14.8 for channel accessing, MySQL Database for data storing, PHP Interpreter for web CGI programming, and gnuplot for tcl/tk and data plot. In

07 Accelerator Technology
T04 - Accelerator/Storage Ring Control Systems

MONITOR AND ARCHIVE SYSTEM OF INSTRUMENTATION*

Z. D. Tsai#, J. C. Chang, T. S. Ueng, Y. H. Liu and J. R. Chen

Abstract

In the accelerator field, the instrumentation includes the vacuum, magnet, RF, utility, cryogenic, power, safety, optic device and so on. The highly complicate systems have many hybrid SCADA systems to ensure precise and optimum control. For the historical data integration and analysis of those signals, the monitor and archive system is introduced to provide a distributed multi-channel acquisition platform. The system possesses various connectivity of open database, communication protocols and commercial hardware. The signal data can be collected and delivered to the central storage area network (SAN) via fiber network without latency. Finally, the unique, friendly and fast trend logger and data analysis software is also developed to view, compare, and analyze relation between facility anytime and anywhere.

INTRODUCTION

Because most of accelerator control systems are highly hybrid systems with many VME based controllers and off-the-shelf industrial controllers, the integration of SCADA (supervisory control and data acquisition) system [1] is rather complicated. For fully handling the accelerator status, the data storage must be well processed [2-3]. In TLS, we has also investigated the related mechanism and developed a set of history program to access status of signals [4-5]. Furthermore, the users always want a unique, friendly and flexible interface to monitor, compare and analysis all available signals. This article presents a full architecture of our archive system from hardware to software. On the client side, an intuitive archive viewer program has provided related functions. On the server side, more and more channel accesses and industrial protocols are adapted to the archive system.

NETWORK ARCHITECTURE AND DATA STORAGE MECHANISM

For data transparency, the system has a hybrid network infrastructure as shown in Fig. 1. The network is divided into 5 layers, including a remote viewer level, data service level, data processing level, controller level and device level.

Both controller and device levels are hardware layers. The controller with algorithms takes over machine control. Besides, the distributed controllers often have a dedicated network protocol to communicate each other or delivery related data to the upper layer's central computer.

The central computer located on data processing level is responsible for data collecting, monitoring, alert and control. Generally, the user requires user friendly graphic interface to process the related parameters and control algorithms. In the industrial SCADA systems, they always provide a set of corresponding software for their controllers and devices. A program to access the system signals via DDE (Dynamic Data Exchange), OPC(OLE Process Control) etc. must be developed. In the VME controller system or a simple data acquisition station, the process layer also needs a program to collect data via firmware. Each subsystem's central computer embedded with this channel access and time synchronous program is called an archive server. When the recorded data of the archive server excesses five minutes, the archive server will duplicate the same files into the data center sever located on the data service layer. This mechanism gives chances for data center server maintenance or avoids data loss in case of network failure. Moreover, the archive server also provides an alert with alarm and SMS (short message service) function.

The data center server located on the data service layer provides a common network service, FTP. Any client software can access the collected data from data center servers anytime and anywhere. The data center server always uses the server class computer to provide reliable service. Each component has the redundant part, such as cups, fans, powers, networks, array disks etc. These can guarantee the data center server with high reliability and robustness. Especially, the storage adopted fiber channel's array disks provides fast, reliable, extensible storage without latency. For avoiding the archive server shutdown, the data center server also takes charge of the alive monitoring of archive servers. While the archive server failure occurs, the data center server will give an alert via Email and GSM modem. This mechanism ensures the continue functioning of all archive servers. For internet security, all data center servers and archive servers are protected under firewall. A mirror server responsible for bridging and duplicating the data is also developed for outside user access.

On the top of remote viewer level, a set of archive viewer software has been used to grab data from data center server via FTP. The viewer program provides rich functions for monitoring, compare, analysis with a unique, friendly, flexible and intuitive interface. The signal data flow from IO devices to users is shown as Fig. 2.

HTS-ECRIS AND LOW ENERGY BEAM TRANSPORT SYSTEM OF THE HIGH CURRENT INJECTOR

G.Rodrigues, P.Kumar, P.S.Lakshmy, R.Ahuja, U.K.Rao, Y.Mathur, D.Naik, A.Mandal, D.Kanjilal and A.Roy

Inter University Accelerator Centre, Aruna Asaf Ali marg, New Delhi – 110067, India

Abstract

A new type of high performance electron cyclotron resonance ion source (ECRIS) called PKDELIS capable of operation at 14.5 and 18 GHz using high temperature superconducting (HTS) coils designed and developed jointly by IUAC, Delhi (earlier called NSC), Pantechnik, Caen and ISN, Grenoble is presently in operation. The source is very suitable for operation on a 400 kV high voltage platform for injecting beams from the High Current Injector (HCI) into the superconducting linear accelerator booster. Since the emittance of the source is large, the complete transport system is being made as short as possible, at the cost of some of the important beam diagnostics elements. A new type of extraction system is being developed in-house to improve the extraction conditions and better vacuum close to the beam formation region. A large aperture, 'third order' corrected analysing magnet has been fabricated for analysing the beams from the source. Typical axial and radial bremstraahlung spectra have been measured. The axial direction shows a single electron temperature component while the radial direction shows 'two electron' temperature components.

INTRODUCTION

The beam energy delivered by the 15 UD Pelletron accelerator at IUAC is above the Coulomb barrier for masses below 40. To augment the beam energy, a superconducting LINAC [2] is being installed to provide beams of ~ 5 MeV/A for the medium heavy ions. The input of LINAC demands high current, high charge state pulsed beam (150 ps). Since the pulsed beam available from the existing Pelletron is of low intensity (~ a few nA average current) and low charge state, an Electron Cyclotron Resonance (ECR) ion source based High Current Injector (HCI) is being installed to provide relatively high current (a few pµA) heavy ion beams for the LINAC.

A cryogen-free high temperature superconducting (HTS) coil based electron cyclotron resonance ion source has been developed and is being used as a part of high current injector for the superconducting linear accelerator at the Inter University Accelerator Centre. This kind of ion source is an off-shoot from the HYPERNANOGAN ECR ion sources developed by Pantechnik, France, where the resistive coils have been replaced using HTS coils [3]. By using HTS coils, the original injection field of 1.3 T has been increased to 1.8 T. The source is configured to be operated on a 400 kV high voltage platform. Power and cooling requirements for the sub-systems are designed to be minimal. Due to the use of HTS coils for the magnets, a reduction factor of 10 results in the power saving costs. In addition, the cooling requirements are also reduced tremendously. This type of ion source is first of it's kind designed to deliver highly charged ions ranging from a few keV to a few MeV depending on the extraction voltage and charge states extracted from the ion source. The source is designed to deliver A/q beams having a maximum value of 10 to be accelerated through the superconducting linear accelerator system of IUAC. A view of the high temperature superconducting ECR ion source is shown in figure 1.

DESIGN ASPECTS OF THE SOURCE

Unlike low temperature superconducting (LTS) materials, HTS coils do not require actively-cooled shields and the temperature can be controlled by standard industrial refrigeration systems. The systems are simpler to design, contruct and compact in form. LTS coils operate closer to their critical temperature as compared to HTS coils. Therefore, HTS coils can withstand wider temperature change without losing their superconducting properties. Also, the critical current density of HTS materials falls slowly as a function of temperature. In addition, the cooling costs are drastically reduced when compared to operation at lower temperatures of about 4 K. The requirements of cooling water on a high voltage platform is also negligible.

Figure 1. View of the High Temperature Superconducting ECR Ion Source, PKDELIS

The heart of the source is built using high strength Bi-2223 HTS tapes for the coils. High strength conductors were chosen instead of high current conductors to withstand the huge forces acting on the coils. Each coil consists of 10 pancakes connected in series wound on a

CONTROL SYSTEM FOR THE BENGING MPS AT PLS LINAC*

J. H. Kim[#], J. M. Kim, S. C. Kim, K. M. Ha, J. Y. Huang, H. S. Kang ,J. Choi and I. S. Ko,
Pohang Accelerator Laboratory, POSTECH, Pohang 790-784, Korea

Abstract

The former control system of the bending MPS (**M**agnet **P**ower **S**upply) was based on Supervisory Control and Data Acquisition (SCADA), RTworks[1]. It is changed based on EPICS as a framework for the full upgrade of the PLS control system. Also we have replaced the former VME 68K CPU boards with OS-9 to new Power CPU boards operated by VxWorks as IOC in the linac klystron gallery. The replaced bending MPS control system consists of a MVME5100 EPICS IOC core in the lower level control. It is implemented with the MEDM tool of EPICS to provide friendly Graphical User Interfaces. This paper describes the VME IOC and OPI and embedded local controller in MPS cabinet used for the bending MPS control in the PLS linac

INTRODUCTION

As of now, the bending MPS(Magnet Power Supply)control system have been well performed the mission to operate 2.5 GeV linac as the beam injector for the PLS storage ring. However, in early 2001, we have decided to convert the current control system into the EPICS based one because of its lack of flexibility and control speed [2]. We have been studied the key technology for EPICS control system during the development of EPICS based test-bed control system completed at the early of 2000.

Figure 1: software structure of the former and present bending MPS control system.

Originally, the former bending MPS control system has three layers of hierarchy; the operator interface computer, the supervisory control computer (SCC) for data processing and the device interface computer (DIC) for distributed data acquisition as shown fig. 1. The operator interface is designed configured on the commercial product, RTworks[1]. The VME systems under OS-9 are used for data processing and data acquisition. In order to provide EPICS structure, our bending MPS control system with three-layered architecture is changed.

Table 1 shows the difference between the former and present systems.

Table1: Comparison Table

	The former control system	The present control system
VME CPU	Eltec 16	MVME5110
I/O Board	TSVME500	TPMC866
Network	10base2	100base TX/FX
VME RTOS	OS-9	vxWorks
Core S/W	Homemade S/W	EPICSBase3.13.6
Device Interface	Serial	Serial

BENDING MPS CONTROL SYSTEM

There are 6 power supplies for bending magnet in BTL. These power supplies are placed in the BTL power supply room. A VME system for controlling them is installed in the nearest power supply [3].

As shown in fig. 2, this control system is based on the EPICS standard model. VME Systems as IOCs is used and connected via Ethernet for host and communicate with embedded controller of MPS using RS422 protocol.

This bending MPS control system has currently following features.
- All Current Set, Power/On, Off
- Individual Current Set, Power/On, Off
- Status Monitoring (Remote/Local, Polarity, Over-temperature, Over-current, etc)
- Degaussing for Bending Magnet
- Saving of individual set current value

DESIGN OF C-BAND STANDING-WAVE ACCELERATING STRUCTURE*

S. H. Kim[#], B. Park, H. R. Yang, S. D. Jang, Y. G. Son,
S. J. Park, J. S. Oh, M.H. Cho and W. Namkung
POSTECH, Pohang 790-784, Korea

Abstract

We design a C-band standing-wave accelerating structure for a compact electron linac. It is capable to produce electron beams with the beam energy of 4 MeV and the pulsed beam current of 50 mA. It is to be operated in the $\pi/2$ mode with the on-axis coupled structure. The beamline is composed of the E-gun and the accelerating column with 3 and half bunching cells and 9 and half normal cells. We design standing-wave RF cavities using the OMEGA3P code to implement the asymmetric magnetic coupling slots. For the beam dynamics study, we use the PARMELA code with the SUPERFISH fields configuration. Without the pre-buncher cavity and the focusing magnets, the lost beam power to the wall is 10 kW for the output beam power of 200 kW, while the transmission is 58%.

INTRODUCTION

The electron accelerator is widely used for industrial applications, for example, contraband detection, material processing, medical diagnosis and therapy, food sterilization, and environmental processing [1]. The environmental processing such as DeSOx or DeNOx and the sterilization processing requires the average beam power of several tens of kilowatts which depends on the processing speed. The contraband detection requires 5-10 MeV with the pulsed beam current of about 150 mA [2, 3].

We are developing an electron accelerator for an X-ray source. It uses a C-band 5-GHz RF source developed for the low-power tests on the LHCD system of KSTAR. With 1.5-MW input RF power, we designed an accelerating structure capable of producing 4 MeV at the 50-mA pulsed beam current. For compactness, a standing-wave bi-periodic structure is adopted with the $\pi/2$ mode. In this paper, we present design details of the RF cavity and the beamline with the beam dynamics.

ACCELERATOR SYSTEM

The accelerator uses a 5-GHz CPI magnetron as an RF source. It is capable of producing 1.5-MW RF with the 4-μs pulse length and the 200-Hz repetition rate. The WR187 waveguide network transports the RF power to the accelerating column. This waveguide is worked under atmospheric pressure SF6 gas except the pump-out-port waveguide which is connected to the input coupler of the accelerating column. The pulse modulator supplies the 40-kV and 90-A pulsed power to the magnetron with the 4-μs pulse length [4]. It also supplies the 40-kV pulsed

voltage to the E-gun. The E-gun is a diode-type thermionic DC gun.

The accelerating column is attached to the E-gun directly as shown in Figure 1. For the compact structure, a pre-buncher cavity with a drift tube is omitted. Furthermore, any solenoids magnet is not used since the beam current is low enough to be focused by the intrinsic focusing effect of the standing-wave electric field [5].

Table 1: Accelerator Parameters.

Accelerator Parameters	
Operating Frequency	5 GHz
Input RF Power (pulsed)	1.5 MW
Pulse Length	4 μs
Repetition Rate	200 Hz
E-gun Voltage	40 kV
Output Beam Energy	4 MeV
Output Beam Current (pulsed)	50 mA
Beam Transmission Rate	58%
Output Beam Power (pulsed)	200 kW
Loss Beam Power (pulsed)	10 kW
Type of Structure	Bi-periodic, On-axis coupled
Operating Mode	SW $\pi/2$ mode
Aperture Diameter	10 mm
Average Accelerating Gradients	10.7 MV/m
Number of Cells	13
Inter-cell Coupling	6.2%
Quality Factor[*]	7500
Effective Shunt Impedance[*]	90 MΩ/m
Transit-time Factor[*]	0.81

[*]Values for normal cells.
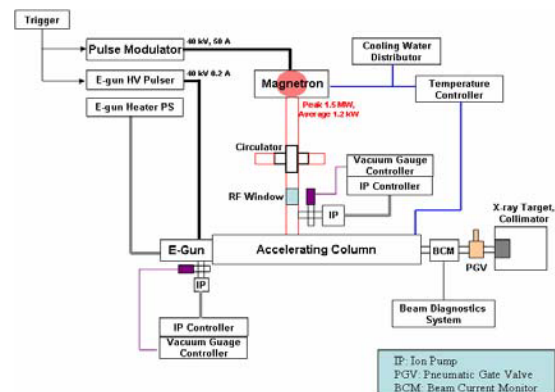
Figure 1: Block diagram of accelerator system.

07 Accelerator Technology
T04 - Accelerator/Storage Ring Control Systems

IMPLEMENTATION AND EXPERIENCE OF ENERGY RAMPING FOR INDUS-2

R. K. Agrawal[#], A. Chauhan, G. Singh, K. Saifee, M. Seema, P. Fatnani, R. Husain, Y. Sheth
Raja Ramanna Centre For Advanced Technology (RRCAT), Indore, India.

Abstract

Beam energy ramping in Synchrotron Radiation Sources (SRS) requires synchronous increase in power supply currents attached to various magnets and voltage of RF cavities. This paper describes the implementation at various layers of control system architecture, our experience of ramping beam energy from injection energy to 2.5 GeV. The total ramping system hardware and software for both magnet power supplies and voltage of RF cavities are described. The implemented ramping system provides a tracking uncertainty of better than 10 micro seconds in time.

INTRODUCTION

Indus-2 is a 2.5 GeV SRS under commissioning at Raja Ramanna Centre For Advanced Technology (RRCAT). The accelerator system at this centre has a 20 MeV Microtron as electron injector, a 450/700 MeV Booster synchrotron and a 2.5 GeV storage ring, Indus-2. The electron beam of 550 MeV from booster synchrotron is injected in the Indus-2 SRS ring from where it is ramped to energy of 2.5 GeV.

In Indus-2, the beam energy is increased from 550 MeV to higher levels by synchronously increasing the current in magnet power supplies and voltage in RF cavities (Devices). The ramp profile (sample) data is generated keeping tune and chromaticity fixed during beam energy ramp.

The ramping system is implemented in modular and distributed manner. A user interface built on PVSS SCADA layer allows the operator to send the ramp profile data to the lower layers of control system, which compute the final data. The computed data are sent sequentially to DAC on a common synchronising clock to provide a reference setting signal to interfaced ramping devices.

RAMP PROFILE DATA GENERATION

The integrated magnetic fields are calculated as per following equations:

$\int B.dl(T-m) = 3.3356.E(GeV).\theta(rad)$; for dipoles

$\int G.dl(T) = 3.3356.E(GeV).KL(m^{-1})$; for quadrupoles

$\int G'.dl(T/m) = (1/2)3.3356.E(GeV).SL(m^{-2})$; for sextupoles

where, θ is the bending angle which is 22.5 degree; KL and SL are the normalised integrated magnetic field strengths of the quadrupole and sextupole magnets.

[#]ragrawal@cat.ernet.in

The measured data of the dipole magnets for the excitation current and its first derivative versus energy and integrated magnetic field is shown in Fig. 1. The integrated magnetic field starts deviating from linearity well above 1.3GeV. The quadrupoles and sextupoles behave linearly with excitation current. The ramp profile data is generated using cubic-spline interpolation technique by fitting piece-wise cubic polynomial between two magnetic field data points. Fitting takes care of non-linear behaviour between excitation currents of dipoles, quadrupoles and sextupoles.
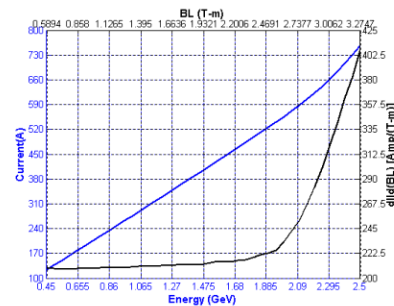
Figure 1: Measured magnetic filed data of dipole magnet.

THE SCHEME

The energy ramping process can be considered as a process in which the beam energy is changed from initial energy 'E$_1$' to final energy 'E$_N$' in '*N*' steps. Each energy level requires a set of current in magnet power supplies and voltage in RF cavities. Thus, for each device a setting is required corresponding to each energy level. This is named as **sample**. The samples are further linearly interpolated into **steps.** The number of steps between two samples is same for all the devices [3]. The samples are decided by the non-linearity of various ramping devices and steps are governed by the resolution requirements.

So, the ramping process can be seen as setting simultaneously the kth samples (1<k≤ N) on the respective ramping devices, thus arriving to a higher beam energy.

IMPLEMENTATION

The above ramping scheme is implemented modularly in software and distributed hardware on Indus-2 control system.

The INDUS–2 control system is based on three-layer architecture namely the 'User Interface Layer' (UI), the 'Supervisory Control Layer' (SC) and the 'Equipment Interface Unit (EIU) Layer' [1].

The overall ramping system is composed of:

- User Interface module.

FIRST EXPERIENCES WITH CENTRAL WEB BASED FAULT INFORMATION SYSTEM

B. S. K. Srivastava[#], P. Fatnani, RRCAT, Indore, India

Abstract

Indus Control System, which controls the Indus-1 and Indus-2 Synchrotron Radiation Sources at RRCAT, Indore, is a distributed computer system. It employs 8 VME Controllers, 300 interface modules, 7 Operator Computers for Indus-1 and approximately 100 Equipment Control VME stations, 10 Supervisory Controllers, 11 Operator Computers and 6 Server Machines for Indus-2. The machine is operated in shifts to provide synchrotron radiation from Indus-1 to users as well as carrying out commissioning experiments of Indus-2. To keep it up and running, the faults encountered during its operation are rectified at site and complete observations and rectifications of the faults are recorded electronically by the shift crewmembers in a central web based fault information system. This System is based on three tiers software architecture and has been developed using Java Servlets, HTML, JavaScript and SQL Database. Using relational database, facilities have been provided in the system for logging, e-mailing, acknowledging, exploring and analysing the fault information of various sub systems. This paper briefly describes experience, implementation aspects and functionalities provided by the system.

MOTIVATION

The main motivation of this project is to constantly monitor and improve the performance of Indus Control System. Indus-1 Control System Computers for different sub-systems are directly connected with their respective Equipment Controllers (ECs) through RS-232 serial link and these Equipment Controllers in turn are connected with different field devices e.g. Power Supplies, Vacuum Components, Radiation Monitors etc. Indus-2 Control System is based on three layer architecture for Controlling/Monitoring of various field devices. Operator Console Computers, which provide Graphical User Interface to operators, are connected with Supervisory Computers through 100 MBPS Ethernet link and Supervisory Computers are individually connected to EC Computers over RS-485 link. The EC Computers are finally interfaced to different field devices.

Seeing the complexities of different types of hardware and software involved in the control system, it was felt to have a system that would systematically track the information logged by machine crewmembers during operations of the machines.

REQUIREMENTS

Following basic requirements were considered before developing the system:

- It should be possible to use the system by multiple users simultaneously connected with CATNet (CAT Network).
- The system should be easy to use for especially non-computer experts.
- The information entered by the users should be precise and free of errors.
- It should be possible to send the entered information to concerned sub-system experts electronically.
- It should be possible to view the stored information in a structured way as per different search arguments e.g. system name, faulty device, time stamps, etc.
- It should be possible to acknowledge the stored faults by concerned sub-system persons.
- It should be possible to generate the system wise statistics of faults between a given periods of time.

It was realized that if web based system is designed then it would not only serve the above basic requirements but also offer many new features, which would not be possible with other non-web based systems. Thus this system was developed using Java, HTML, JavaScript and SQL Database. The first version of the system became operational in May 2004 and since then with various modifications and additions of new functionalities this system is being used continually by the crewmembers during operations of Indus-1 and Indus-2.
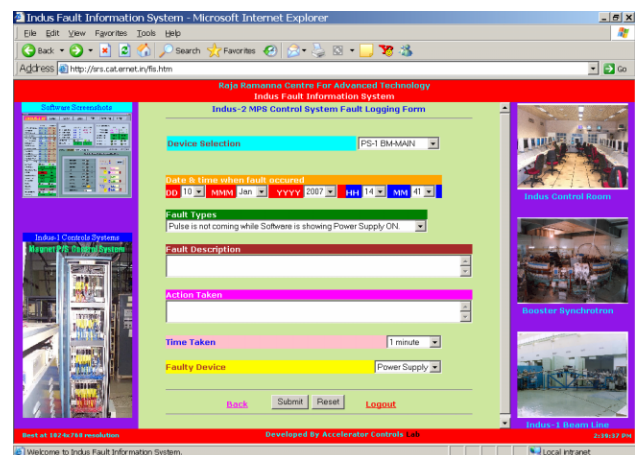
Figure 1: Fault Logger.

_____
[#]bsks@cat.ernet.in

07 Accelerator Technology
T04 - Accelerator/Storage Ring Control Systems

CONTROL SYSTEM FOR BEAM DIAGNOSTIC SYSTEM OF INDUS-2

Amit Chauhan[#], Bhavna Merh, Pravin Fatnani, Sampa Gangopadhaya

Raja Ramanna Centre for Advanced Technology, Indore-452013, India.

Abstract

This paper presents the Beam Diagnostics Control System for Indus-2 that monitors and controls the parameters related to Beam Profile Monitors (BPM), Beam Position Indicators (BPI), Direct Current Transformer (DCCT) and XZ-selection for strip-lines. The system has three-layered architecture. The middle and lower layer have VME stations with CPU cards having RTOS OS-9. The lowest layer has nine stations that house various Analog and Digital I/O boards connected to the actual devices in the field. The boards include 4-channel 16-bit ADC cards developed for BPI interfacing. The middle layer collects the data from lower layer and passes to top layer and passes the commands from top layer to the lower layer. The top layer has the GUI for operator control built using a SCADA software PVSS. It provides various features to the user for graphical display, trending, configuring, controlling, data-logging and selective data monitoring of the parameters. This system finds use right from the beam injection stage to the Orbit correction stage in addition to the normal operation stage of the machine.

CONTROL SYSTEM OVERVIEW

The control system of Indus-2 has a three-layered architecture as shown in figure-1.
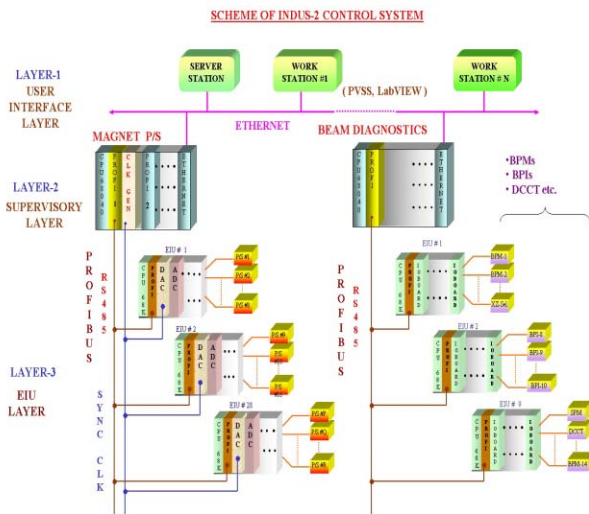
Figure 1: Scheme of Indus-2 Control system

At the lowest layer, Layer-3, known as Equipment Interface Unit (EIU) Layer there are VME stations that have various analog and digital I/O cards. These cards are interfaced with the devices in the field. The middle layer, Layer-2, is the Supervisory Layer where there are separate VME station controlling each sub-system of Indus-2 like Magnet Power supply system, beam diagnostic system, RF system, vacuum system etc. The top layer, Layer-1, is the User Interface Layer that provides the Graphical interface to the users for operating the machine.

The communication between Layer-1 and Layer-2 is on TCP/IP network using socket-based communication. Layer-2 and Layer-3 communicate using ProfiBus field-bus protocol where Layer-2 acts as the Profi Master and Layer-3 acts as Profi slave. Second and third layers make use of in-house developed Profi controller cards configured as master and slave respectively.

BEAM DIAGNOSTICS CONTROL SYSTEM

As the name suggests the Beam Diagnostics system is used for measuring the various parameters of the electron beam like its profile, position and the average current. For this various devices like BPIs, BPMs, DCCT etc. have been developed and installed in the machine by the Beam Diagnostic group at RRCAT. All the signals for controlling and monitoring of these devices are interfaced to the control system of Indus-2.

Like the control system for all other sub-system, the one for Beam Diagnostic system also has three-layer architecture as shown in Figure1.

Layer-3 has nine VME stations. Each station house a CPU card, a Profi salve card and the various digital and analog Input/output cards that are interfaced with the actual devices in the field. The OS-9 software at this layer implements Profi slave protocol, collects data from input cards and sets data on output cards.

Layer-2 has a single VME station that has one CPU card and one Profi master card. Layer-2 OS-9 software implements Profi master protocol and has socket programs for communication with Layer-1.It also holds the mapping of the various parameters of all the devices to the specific Layer-3 station, the I/O card and the channel number. So whenever a command from Layer-1 software is received, Layer-2 maps the command for the device at Layer-3 and sends it down.

Layer-1 software has been developed using PVSS, SCADA software. This software has two components. First is the API-manager written for PVSS that connects to Layer-2 on TCP/IP network and exchanges data and commands. It resides on a specific server machine. The second component is the Graphical User Interface (GUI) in the form of PVSS panels. These panels can be run on any PC on the Control Room network. Various panels have been developed for the various sections of the Beam-diagnostic sub-system like BPM, BPI, DCCT, etc

[#]amit@cat.ernet.in

CONTROL AND INSTRUMENTATION FOR THE VEC SUPERCONDUCTING CYCLOTRON CRYOGEN DELIVERY SYSTEM

T. K. Bhattacharyya[#], T. Das, C. Nandi, G. Pal and R. K. Bhandari
Variable Energy Cyclotron Centre, 1/AF Bidhan Nagar, Kolkata 700064

Abstract

The cryogen delivery system for the superconducting cyclotron supplies liquid helium to the superconducting main magnet coil and three cryopanels. It also supplies liquid nitrogen to the thermal shield of the liquid helium chamber housing superconducting coil and the thermal shield and baffles surrounding the cryopanels. A suitable efficient piping network comprising vacuum jacketed cryogenic transfer lines, liquid nitrogen shielded transfer line and distribution manifold is used in the superconducting cyclotron for distribution of cryogens. A liquid helium pump ensures the required flow of liquid helium through the cryopanels. The cryogen delivery system is fitted with necessary field instrumentation and controllers to monitor and automatically control certain important process parameters. This paper presents the overall control and instrumentation for the cryogen delivery system.

INTRODUCTION

The importance of cryogen delivery system [1] in the context of a superconducting cyclotron is immense and critical. The superconducting coils of the cyclotron are immersed in a pool of liquid helium. Liquid helium is supplied to the magnet from the liquid helium plant/refrigerator. The accelerating chamber of the superconducting cyclotron has to be maintained at high vacuum for proper acceleration of particles. Vacuum in the accelerating chamber is obtained by three cryopanels placed inside the cyclotron. These cryopanels are cooled by liquid helium. Liquid nitrogen is used to cool the thermal shields of the liquid helium chamber for the superconducting coil and the liquid helium cooled cryopanels. The delivery of liquid helium (4.2K) and liquid nitrogen (77K) from liquid helium plant and nitrogen dewars to the cryostat and cryopanels requires extreme caution, continuous monitoring and finest control. Considering its safety and control aspects an intensive data acquisition and control instrumentation has been designed, installed and successfully operated.

INSTRUMENTATION SCHEME

The system takes care of as many as hundred parameters which are extremely critical for operation of the superconducting cyclotron main magnet. The system is designed to operate in a harsh condition, without loosing its performance or speed. Each hardware component is selected considering fast action, appropriate range, continuous run and fail-safe operation. From the control point of view, the system is centralised. It employs a centralized approach to the tasks of control, monitoring, data acquisition and machine protection. The heart of the instrumentation hardware is a Schneider make level 3 premium processor based PLC. It has a three layer hierarchy with PLC at its centre. All duties related to process control, interlock generation are performed in this layer. The first layer consists of mostly field instruments of different make which acts as the gateway between process signals and the PLC. The top most layer is a supervisory control and data acquisition software, operating in two different computers in two distant locations for controlling, monitoring and data acquisition. The PC-based consoles employ Wonderware SCADA software for cryogen delivery system monitoring and control.

Hardware Layout

The first layer (Fig. 1) consists of mostly field instruments, viz. pressure transmitters, level monitors, temperature transmitters, multi-channel strain gauge scanner, vacuum gauge controllers, dewar pressurisers, valve controllers and positioners of different make. Processed analog signals from each of these transmitters/instruments are taken to/ from the second layer (PLC) for data acquisition and control. The web server facility of the PLC has enabled all the other workstations connected in the dedicated LAN to monitor some of the important parameters. Dedicated control logic was developed to process digital and analog input channels, operate various controls, generate interlocks and communicate with the supervisory control. The control parameters [2] are operated through control loops operating independently on the PLC. The PLC continuously monitors values of all the cryostat and cryopanels parameters and primarily uses these signals to control the cryogen delivery system. This also generates a "PLC_OK" signal if all the parameters are healthy. If anything goes wrong in the system, it takes necessary actions for the cryogen delivery system and also "PLC_OK" signal is withdrawn. The PLC is powered from the on-line UPS for reliable operation.

_____
[#] tamal@veccal.ernet.in

STATUS OF THE SUPERCONDUCTING INSERTION DEVICES CONTROL SYSTEM AT TLS

K.H. Hu[#], Jenny Chen, Demi Lee, S. Y. Hsu, C.H. Kuo, K.T. Hsu
National Synchrotron Radiation Research Center, Hsinchu 30076, Taiwan

Abstract

Superconducting insertion devices installed at the Taiwan Light Source serve the rapidly growing community of X-ray users. The control system supports the operation of all these superconducting insertion devices. Control system coordinates the operation of the main power supply and the trimming power supply to charge/discharge the magnet and provide essential interlock protection for the coils and vacuum ducts. Quench detection and various cryogenic interlocks are designed to protect the system. A friendly user interface and control applications are developed to support routine operation. The diagnosis of the tripping of superconducting insertion devices related to machine operation is also addressed. Design considerations and details of the implementation will be summary in this report.

INTRODUCTION

Three superconducting insertion devices a superconducting wavelength shifter (SWLS), a superconducting wiggler (SW6) and an in-achromat superconducting wiggler (IASW-R6) have been installed. Two other such devices, IASW-R2 and -R4, will be installed in the future. These superconducting IDs are applied to enhance hard X-ray production to support diffraction, scattering, spectroscopy, EXAFS, imaging, and protein crystallography. The control system of superconducting insertion devices was designed implemented and commissioned to support the operation of these devices. This control system based on the VME crate system as a standard configuration; interlock protection and a graphical user interface (GUI). The interlock logic is implemented using a programmable logic controller (PLC) to protect the coils of the magnet. The user interface and various application programs enable routine operation.

Table 1:Parameters of Superconducting Insertion Devices

Device	No.	Parameters	Applications
SWLS	1	6 Tesla, 66 poles, 30 mm periods	X-ray Imaging, Diffraction, Scattering, EXAFS, Powder Diffraction
SW6	1	3.2 Tesla, 66 poles, 30 mm periods	Protein crystallography
IASW6 -R6, -R2, -R4	3	3.2 Tesla, 66 poles, 30 mm periods	X-ray Imaging, Diffraction, Scattering, Powder Diffraction

[#]uka@nsrrc.org.tw

INFRASTRASTRUCTURE OF THE CONTROL SYSTEM

The system can be controlled using a standard VME crate to accommodate various control modules. The crate includes a PowerPC-based CPU module, which runs a LynxOS 4.0 real-time operating system as a local controller of the superconducting IDs control system. The crate includes analog input/output modules, digital input/output modules and the RS-232 interface module. The control system of superconducting IDs depends on coordinating the operation of power supplies, cryogenic instruments and interlock protection logic. Figure 1 illustrates the infrastructure of the superconducting IDs control system. Control consoles communicate with the VME host module through the control Ethernet.
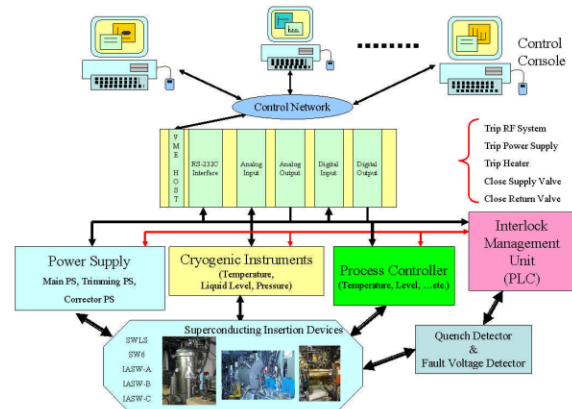
Figure 1: The control system infrastructure of the superconducting insertion devices.

Power Supplies

A precision bipolar main power supply is used to charge/discharge the magnet. The trimming power supplies are used to correct the field error. A low slew rate is used at the beginning because the inductance at low field is high when charging began. The slew rate is high after the field saturates the internal iron core, and the inductance is then considerably reduced. The control applications automatically control the slew rate. The trimming power supply can be set independently or follow the output of the main power supply, according to a predefined table. Two correctors are added upstream and downstream of all of the installed superconducting IDs. The control system coordinates the outputs of the corrector power supplies, to compensate for distortion of the beam orbit.

REJUVENATION OF LINAC CONTROL SYSTEM FOR TLS

C. Y. Wu[#], S. Y. Hsu, Demi Lee, C. J. Wang, Jenny Chen,

K. H. Hu, C. H. Kuo, K. T. Hsu, K. K. Lin

National Synchrotron Radiation Research Center, Hsinchu 30076, Taiwan,

J. Y. Hwang, National Tsing-Hua University, Hsinchu, Taiwan

Abstract

The pre-injector control system is a turn-key system, which was deployed 15 years ago. It is complicated and out-of-date nowadays in terms of system integration and hardware upgrading. It must be modernized to ensure its performance and reliability, and most importantly, to facilitate system maintenance. Modernization involves upgrading to enhance functionality, to prevent obsolesce of out-of-date control modules, and to replace old parts. The purpose of the upgrade plan is to replace the pre-injector control system by a new unit which has the same control environment as that of the main control system of the NSRRC accelerator facilities. Thus, the control system maintenance, as a whole, will be made substantially easier than the original system.

INTRODUCTION

The pre-injector of the Taiwan Light Source (TLS) comprises a 140 kV thermionic electron gun and a 50 MeV traveling wave type linear accelerator (linac). The functional block diagram and layout of the pre-injector is depicted in figure-1. The electron beam emitted from the gun is accelerated through the linac with exiting energy of 50 MeV. Then, the electron beam is guided along the linac to booster (LTB) transfer line and is injected into the booster. Brief descriptions on elements in the LTB are also given in figure-1.

The control of the linac uses a dedicated programmable logic controller (PLC) equipped with 10 MB/sec Ethernet interface. It has been operated since 1990. Besides, the vacuum interlock logic of the booster is implemented using the PLC unit and is tightly coupled with the pre-injector control system. This integral arrangement causes difficulty in carrying out maintenance and replacement of some out-of-date devices in the pre-injector system. Consequently, the control system is being rejuvenated to improve its performance in the following aspects: decouple the vacuum interlock logic from the linac control system, provide better control functionality for top-up operation, and avoid lacking of out-of-date spare units. In order to achieve this goal, one VME crate system is dedicated to linac control. A new hardware unit with a high-resolution analog interface is installed to provide dedicated service of control tasks. Two separated PLCs are newly implemented to replace the "old" PLC. A compact PLC is used to deal with the interlock logic. The

_____
[#]chunyiwu@nsrrc.org.tw

other PLC is used to be responsible for the remaining linac devices which require sequential control in routine operation. It includes: access interlock of high voltage (HV) and safety doors, delay process of klystron and electron gun warm-up etc. Both interlock and sequence control PLCs are controlled by using the VME crate. All other functions, without interlock or sequential requirement, are directly controlled by the VME crate. The upgrading linac control system is expected to provide better performance on control functionality and maintenance simplification.
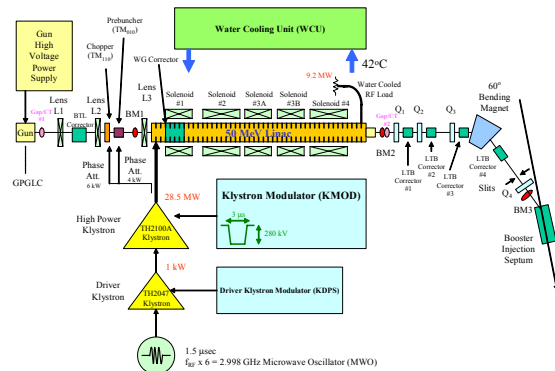
Figure 1. Synopsis of preinjector.

EVOLUTION OF THE LINAC CONTROL SYSTEM

The linac control system was embedded in the originally delivered turnkey control system of the injector, i.e. including pre-injector and booster. This system has been partly integrated with the NSRRC main control system in 1998 to enhance the operation efficiency. It reduced the resources of requirement in operating the injector and was directly benefited to performing the top-up operation. The remaining out-of-date PLC module has to be taken care of such that lacking of spare units would not jeopardize linac operation. Since top-up operation has been implemented in NSRRC in 2005, the accessible time for linac control upgrading is limited. Therefore, a long-lead transformation process toward a new control system is not avoidable. In dealing with this situation, a sideline in preparing the migration of the control environment has been exercised since July 2006 and its status is described in this report. It will become a new control system and is expected to be completed in June 2007.

A NEW, PXI BUS BASED, PATTERN MEMORY SYSTEM FOR THE SIAM PHOTON SOURCE

George Garnet Hoyes

National Synchrotron Research Center (NSRC), PO Box 93, Nakorn Ratchasema, Thailand

Abstract

A new pattern memory system has been built from PXI bus modules to ramp the booster synchrotron magnet and RF power supplies, replacing an old and proprietary Toshiba system. The new system is compact, rugged, easy to program using LabVIEW, easy to repair and low cost.

INTRODUCTION

The SPS is a modified ring which was previously SORTEC [1]. The pattern memory system for the booster was the original and proprietary system custom made by Toshiba. This old system can be considered obsolete as finding any replacement parts if difficult if not impossible. As there are no spare parts available or detailed system description we were faced with a maintenance problem for this critical sub-system and we decided to look for a replacement system well before we had a failure. One of the main requirements was that it be easily repairable from commercially available replacement modules or components.

Most existing synchrotron facilities use many VME crates and modules and therefore historically VME based pattern memory systems have been used typically. We have no such history of using VME here and a lower cost modular PXI National Instruments based Pattern Memory System has been applied to replace the (much larger) Toshiba one. We believe that this is the first time that a synchrotron facility has utilized a PXI based pattern memory system.

DEVELOPMENT OF THE NEW PXI BASED SYSTEM

The old Toshiba system provides eight, 16 bit plus strobes, RS 422 differential outputs to the Bending Magnet power supply (3), Quadrupole power supplies (4) and RF power supply (1) of the booster synchrotron. To provide differential output at the RS422 levels to the power supplies we chose the National Instruments model PXI-6534 digital I/O waveform generator with 32 Mb onboard memory for pattern storage. This module has 32 single ended outputs which we configured as 16 differential outputs by programming. As each set of 16 bit outputs also needs a strobe signal one more 6534 module was used to provide the eight differential strobe outputs.

Initially the system concept was tested with just two 6534 modules, one outputting signals to the RF power supply, which only needed one set of 16 bit input signals, and another 6534 module for outputting the strobe signals and inputting the main trigger signal from our timing system. This test worked perfectly the first

time. Figure 3 shows the input data stream and the output signals of the RF amplifier over one synchrotron injection and ramping cycle.

After the successful system concept test a complete new pattern memory system was purchased comprising of nine PXI-6534 modules, one 18 slot PXI-1045 19" chassis and one CPU controller module, a PXI-8186 P4 2.2 GHz running Windows XP. This controller has an Ethernet interface which was used to connect to our control system server for remote operation as well as for downloading the magnet and RF pattern data to the 6534 waveform generators.
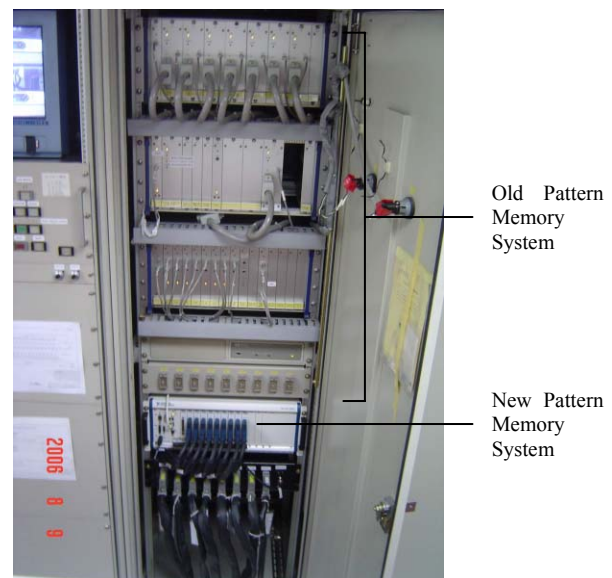
Figure 1 : Both old and new Pattern Memory Systems.

The whole system was configured, programmed and installed in the same Toshiba rack, see Fig. 1. Switching from the old system to the new system is done by simply unplugging the eight outputs from the Toshiba system and inserting them into the National Instruments system shown in Fig. 2. The Toshiba system is, for the time being, kept as a spare and eventually we shall remove it completely.

The ramping pattern is created and stored in the control server as 7001, 16 bit words for each power supply. The ramping time of the booster is 700.1mS so the data, after transfer to the digital I/O module memories, is sent during ramping to the power supplies at the rate of one word per 100 microseconds or 10kHz. This exactly emulates the old Toshiba timing although the new pattern memory can transfer data at much higher rates (up to 20MHz) allowing for the possibility of upgrading the system in the future.

THE DESIGN AND PERFORMANCE OF THE PROTOTYPE DIGITAL FEEDBACK RF CONTROL SYSTEM FOR THE PLS STORAGE RING

I.H. Yu, D. T. Kim, S.C. Kim, H.S. Kang, I.S. Park, H.Y. Kim, J.Y. Huang,
PAL, Pohang, Kyungbuk 790-784, Korea.

Abstract

At the Pohang Light Source (PLS) Storage Ring, the low level RF system based on analog technique provides RF field control for the 4 RF stations, and each station drives each RF cavity at 500.082MHz. To achieve better control system stability and accuracy, the prototype digital feedback RF control has been developed in Pohang Accelerator Laboratory (PAL). In addition to RF field control, it provides cavity resonance control, and incorporates the personnel and machine protection functions. An accelerator electric field stability of ± 0.5% in amplitude and ± 0.5º in phase is required for the RF system. In order to accomplish these requirements, a digital feedback control technique is adopted for flexibility of the feedback and feed forward algorithm implementation.

INTRODUCTION

We are developing the digital RF feedback control (DRFC) system based on recent digital technology available for the better performance. One of the advantages of the on-going digital feedback control system is to take mainstream solution using a FPGA & an embedded processor. In DRFC system, an accelerator electric field stability of ± 0.5% in amplitude and ± 0.5º in phase is required for the RF system. The digital RF feedback control system using the FPGAs and DSP Embedded Processor is adapted in order to accomplish these requirements and flexibility of the feedback and feed- forward algorithm implementation. In addition to field control, it provides cavity resonance control, and incorporates the personnel and machine protection functions

FEEDBACK ALGORITHM & SIMULATION

Figure 1 shows the block diagram of DRFC system. Cavity pick-up RF signal is down-converted to about 10 MHz IF from 500.082MHz RF and the base-band is narrowed by analog low-pass filter, and then digitally sampled at about 40 MHz by a high speed ADC.

The sampled data is sequentially arrayed as I, Q, -I, -Q, I, Q, -I, -Q. Calibration factor a and θ is used to compensate the cable loss and delay of cavity pick-up RF signal with respect to RF cavity voltage using the vector rotator(XILINX CORDIC3.0). The arithmetic FIR Digital filter is applied to reduce the noise and make the appropriate bandwidth of the feedback. The digitally filtered output is compared with I set point table and Q set

point table which are 10 MHz array data.

Figure 1: The block diagram of DRFC system.

The error output is passed to PI controller where the proportional gain and the integral gain are appropriately set based on cavity field simulation. Feedback variables such as calibration factor 'a' and 'θ', the proportional gain and the integral gain, digital filter coefficient are set by remote control system.

A base band analysis, where only the bandwidth near the operation frequency is considered, enables a simplified state-space equation:

$$\frac{d}{dt}\begin{bmatrix} V_I \\ V_Q \end{bmatrix} = \begin{bmatrix} -\omega_{1/2} & -\Delta\omega \\ \Delta\omega & -\omega_{1/2} \end{bmatrix}\begin{bmatrix} V_I \\ V_Q \end{bmatrix} + \frac{\omega_{rf}}{2}\frac{R}{Q}\begin{bmatrix} I_I \\ I_Q \end{bmatrix},$$

Where $\omega_{1/2} = \omega_{rf}\big/2Q$ is the half width of the resonance, $\Delta\omega = \omega_0 - \omega_{rf}$ the cavity detuning, and ω_0 the resonance frequency of the cavity.

Since the RF amplifier has a wider bandwidth of about 1MHz, the dominant RF device to determine the FB characteristics is the cavity.

Figure 2: The detailed block diagram of the feedback algorithm.

DRIVE SYSTEM INSTRUMENTATION FOR VEC SCC AXIAL-HOLE MAGNETIC FIELD MEASUREMENT

T K Bhattacharyya*, T Das, C Nandi, G Pal, C Mallik and R K Bhandari
Variable Energy Cyclotron Centre, 1/AF Bidhan Nagar, Kolkata 700064

Abstract

Characteristics of beam in the central region of the superconducting cyclotron are to a large extent influenced by the magnetic field it experiences during its passage through the axial-hole. Accurate knowledge of magnetic field in axial-hole is required in order to design the central region components and position the extraction elements. A probe drive with high resolution and repeatability was developed along with the required HMI to map the magnetic field through out this hole from median plane upto 3 meter above it. This paper describes the drive system, its control, data acquisition and instrumentation scheme.

DRIVE SYSTEM

The mechanical arrangement [1] for the measurement set -up can be divided into two parts: drive mechanism and probe holding mechanism. The drive mechanism has three lead screws and nuts. Lead screws of 1.5 m length are used to avoid complexity and to reduce fabrication problem and inaccuracy of the system. A stepper motor drives the lead screws. Rotational movement of the lead screws is restricted by two plates carrying hall probes, fixed at the top and the bottom ends of the lead screws. The stepper motor is fixed and the lead screws move up and down. Since the total required span of measurement is 3 m and the movement of the lead screws is restricted to 1.5 m, an extension of 1.5 m with bottom plate for mounting hall probes has been added. The plate at the end of the lead screw and extension form the probe holding mechanism. Two probes, one axial probe at the centre and one transverse probe at the outer radius, are fixed to each of the end plates. The end plates have provision to manually re-position the transverse probes at an angle of 90º. During one complete scan, the system can collect data over the complete required length of 3 m from the cyclotron median plane.

CONTROL AND DATA ACQUISITION

The axial-hole drive system can be broadly divided into two parts, the open-loop control of the drive system, and the magnetic field data acquisition system.

Control Scheme

The control scheme can be subdivided into following steps:

i. Optical limit switches are placed at both ends. At the start of each run, the drive is initialised by automatically moving it back till it touches the starting limit switch. As this operation is carried out

---

* tamal@veccal.ernet.in

in steps, an accuracy of 15 micron can be achieved.

ii. The system is then driven in steps upto 1500 mm. The heart of the control system is a stepper motor. It drives the three gear mounted lead screws which eventually move the hall probe assembly and position them correctly at 1.005 mm intervals. At this stage, the control software calculates the present absolute distance from the starting point and stores it in a file for ready reference. The control software confirms that the motor is powered (24VDC) before sending the drive pulses. In case of sudden power failure, the next drive signal is not sent and the last absolute position value is stored. When the mapping starts again after resumption of motor power, the software can easily recollect the last position value and starts scanning from that point.

iii. The motor stops after reaching the end point optical limit switch. The software scans the limit switch before each step. This results in end point detection at the theoretical accuracy of 15 micron. After reaching the end point, it shows mapping completion message on the human-machine interface (HMI) screen.

iv. After completion of a full length scan, the system automatically resets back to its initial position showing probe resetting message. It stops only if it reaches the starting point. Then it gives an option of another scan/ stop to the user.

Data Acquisition Scheme

The data acquisition scheme can be subdivided into following steps:

i. The data acquisition starts after the probe assembly stops at 1.005 mm interval. A delay of 5 seconds is given before each set of magnetic measurement to eliminate the chance of any kind of mechanical vibration.

ii. The control software communicates with the three channel FW Bell hall probe monitor through RS 232 serial port. Although four hall probes are installed in the assembly, the monitor can only read three of them at a time. Two successive scans give complete data for a fixed magnet current. The software initialises the serial port and sends command to measure the magnetic field for each channel. The hall sensors' data are collected from the read buffer of the monitor and channel-wise separated by the software. Ten sets of data are collected during the total measurement time of 5 seconds.

HIGH POWER TEST OF C-BAND ACCELERATING SYSTEM FOR JAPANESE XFEL PROJECT

K. Shirasawa[#], T. Inagaki, H. Kitamura, T. Shintake, RIKEN,SPring-8 Harima, Hyogo, Japan

S. Miura, MHI, Hiroshima, Japan

H. Matsumoto, H. Baba, KEK, Ibaraki, Japan

Abstract

The C-band (5712 MHz) accelerating system will be used as the main accelerator for the SPring-8 Compact SASE Source project. In order to confirm the performance of the C-band accelerator for the 8 GeV XFEL machine, the same accelerating structure and RF system have been installed in the SCSS prototype accelerator. A high power test of all the accelerator components has been performed. A 35 MV/m accelerating field was achieved during the beam test.

INTRODUCTION

The X-ray free electron laser (XFEL) is one of the next generation light source. In Japan, SPring-8 has a single-pass XFEL project, the SPring-8 Compact SASE Source (SCSS). This project uses a 8 GeV linac to generate 1 $\mathring{A}$ coherent intense X-ray laser. The construction will start in 2007: 128 C-band accelerating tubes and 64 klystrons will be installed as the main accelerator.

Since the C-band accelerator generates a higher accelerating gradient than the traditional S-band accelerator, the machine is more compact and the cost is lower. However, the C-band accelerator is a new technology for an electron linac. In order to check the performance of the developed hardware components and to prove SASE amplification, the prototype accelerator for the XFEL was constructed. After the beam commissioning, the first SASE amplification was observed at 49 nm in June 2006 [1].

In the prototype accelerator, four 1.8 m long C-band accelerating structures are used to accelerate electrons from 45 MeV to 250 MeV. Normal operation, the accelerating gradient of the C-band accelerator is 28 MV/m with the klystron output power of 27 MW.

On the other hand, the C-band accelerator for the 8 GeV linac is designed to operate with the field gradient of 35 MV/m. Therefore, the accelerating filed measurement has been performed after the high power test at the prototype machine.

SCSS C-BAND ACCELERATOR

The C-band accelerator consists of two units; each unit has one 50 MW klystron, pulse compressor and two accelerating structures. A schematic diagram of the C-band accelerator is shown in Fig. 1.

[#]kshira@spring8.or.jp

Figure 2 shows the photograph of the C-band accelerator of the SCSS prototype machine. As shown in Fig. 1 and Fig 2, the stable support stands made from a low thermal expansion material, cordierite ceramic, are used for the accelerating structure [2]. Cordierite ceramic has a thermal expansion coefficient ten times lower than that of iron.

Klystron and HV Power Supply

The C-band klystron (Toshiba E3746A) [3] generates a maximum power of 50 MW with a pulse width of 2.5 μsec and a repetition rate of 60 Hz. In order to provide pulsed high voltage for the klystron, the inverter type high voltage power supply and the compact oil-filled modulator are used. [4]. The inverter type high voltage power supply charges the pulse forming network (PFN) circuit of the modulator. The charging voltage is 50 kV. A 1:16 step-up transformer is inserted between the PFN circuit and the klystron. Consequently, a pulsed high voltage of -350 kV is provided for the klystron.

C-band Choke-Mode Type Accelerating Structure

The first C-band choke-mode type accelerating structure was developed in 1998 for the linear collider project [5, 6]. A 1.8 m long structure was developed in 2002 for this project. The main parameters are listed in Table 1. The structure consists of 89 regular-cells with damping slots and input/output coupler-cells. In order to get enough space for the choke, the $3\pi/4$ mode was used. In this mode, the space which can be used for the choke is longer than in the conventional $2\pi/3$ mode by about 2mm. Therefore, this structure shows quite effective damping of HOMs over a wide frequency range. It makes possible to accelerate the multi-bunched beam with no wakefield instability [7].

Pulse Compressor

At the SCSS prototype machine, two types of pulse compressors, SKIP or SLED, has been adapted for research and development. The SKIP was developed by the KEK injector group [8]. On the other hand, the SLED was originally designed for linear collider [9]. Three-cavity design was introduced to improve energy efficiency. To make simple the system, the traditional SLED design (single cavity) has been chosen for the SCSS project. Parameters for each pulse compressors are listed in Table 2. The quality factor was measured with low level RF. The SKIP is installed on

POSITRON INJECTOR ACCELERATOR AND RF SYSTEM FOR THE ILC*

J. W. Wang[#], C. Adolphsen, V. Bharadwaj, G. Bowden, E. Jongewaard, Z. Li,
R. Miller, J.C. Sheppard
SLAC, Menlo Park, CA94025, U.S.A.

Abstract

Due to the extremely high energy deposition from positrons, electrons, photons and neutrons behind the positron target, and because a solenoid is required to focus the large emittance positron beam, the 1.3 GHz pre-accelerator has to use normal conducting structures up to energy of 400 MeV. There are many challenges in the design of the normal-conducting portion of the ILC positron injector system such as obtaining high positron yield with required emittance, achieving adequate cooling with the high RF and particle loss heating, and sustaining high accelerator gradients during millisecond-long pulses in a strong magnetic field. Considering issues of feasibility, reliability and cost savings for the ILC, the proposed design for the positron injector contains both standing-wave (SW) and traveling-wave (TW) L-band accelerator structures. A short version of the new type of the SW section is under fabrication and testing, an updated status report is given. This paper also covers the acceleration vs. deceleration for pre accelerator sections, SW vs.TW structures, as well as the longitudinal matching from target to linac and linac to damping ring.

INTRODUCTION

The positron source relies upon an intense source of high energy photons impinging upon a metal target. The photons must be of sufficient energy, typically of order 10 MeV, to generate electron-positron pairs that can escape from the target material and be captured and accelerated. The photons are generated by synchrotron radiation in a helical undulate through the interaction of relativistic electrons with a periodic, helical, magnetic field. The photon beam is incident on the rim of a rotating target of thickness 0.4 radiation lengths contained in a vacuum vessel. Approximately 24 kW of power from the photon beam is deposited in the target in a spot of ~ 1 mm rms. The resulting electron/positron particles emerging from the downstream side of the target are captured in a 0.09 m-rad transverse dynamic aperture. The energy of the beam coming out of the target is 2-10 MeV. The target is followed by the tapering magnetic field of an Optical Matching Device (OMD) which has a field which decays from 5-0.5 T over 20 cm. The OMD is used to match the beam phase space coming out of the target into the capture L-band RF. The capture RF is placed after the target and OMD and accelerates the beam to 125 MeV.

ACCELERATOR SYSTEM LAYOUT

The capture region is composed of two 1.27 m SW accelerator sections at 15 MV/m accelerating gradient and three 4.3 m TW accelerator sections at 8.5 MV/m accelerating gradient in order to capture and accelerate the electron beam to 125 MeV as shown in Figure 1.
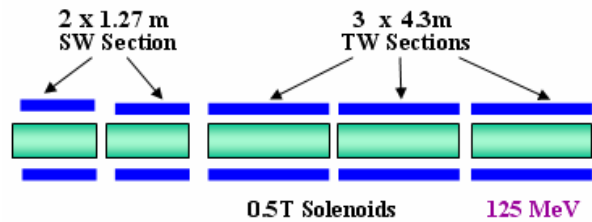
Figure 1: Schematic layout of the capture region.

The electrons are accelerated from 125 MeV to 400 MeV in a pre-accelerator region, which is composed of eight 4.3 m TW sections at 8.5 MV/m accelerating gradient. All accelerator sections are surrounded with 0.5 T solenoids as shown in Figure 2.
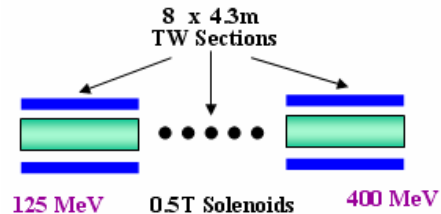
Figure 2: Schematic layout of the pre-accelerator region.

SW ACCELERATOR STRUCTURE FOR POSITRON CAPTURE

The high gradient (15 MV/m) positron capture sections have been designed to be simple π mode 11 cells SW type of accelerator structures. The advantages are a more effective cooling system, higher shunt impedance with larger aperture (60 mm), lower RF pulse heating, apparent simplicity and cost savings. The mode and amplitude stability under various cooling conditions for this type of structure have been theoretically verified. Figure 3 shows a cutoff view of the SW structure and Table 1 gives the important RF parameters.

DEVELOPMENT OF 100 KW RF AMPLIFIER FOR SUPERCONDUCTING CYCLOTRON AT VECC

S. Som[#], Saikat Pal, A.K. Mukherjee, D.S. Bhattacharyay, P. Gangopadhyay, J.S. Prasad, Mondal, S. Seth, P.R. Raj, S.K.Manna, M. Banerjee, K.V. Krishnaiah, M.S. Saha, S. Biswas, S. Saha.
Variable Energy Cyclotron Centre, 1/AF, Bidhannagar, Kolkata-700064

Abstract

High power rf amplifiers (3 nos.) have been developed at our centre for feeding power to three nos. of coaxial rf cavities of the k500 Superconducting Cyclotron. Each of this amplifier can supply output power of 100 kW (max.) at 50 ohm impedance within the frequency range of 9 MHz to 27 MHz. The amplifier, based on Eimac 4CW 150,000E water-cooled tetrode, is tuned by moving the sliding short of the coaxial cavity within the said frequency range[1]. An inductive coupling loop is inserted along one side of the coaxial cavity through the sliding short and is matching the output impedance of 50 ohm. The four identical Bridge-T networks in the grid of the final amplifier are driven with equal power levels of up to 150 watts. The amplifier is operated in Class-AB mode with power gain of 22 dB. Anode Power supply of 20 KV@7.5A, Screen Power supply of 1.5 KV@1A, Grid Power supply of -500V, and Filament power supply of 15.5V@215A are applied to the terminals of the aforesaid tetrode. A PC-based stepper motor controlled sliding short movement system have been developed. The movement of the 3 transmitter cavities for tuning at different frequencies can be done from a computer located in the main RF control room through LAN. This system has been used for movement of the sliding shorts of the 3 transmitter cavities for different measurements including Q, shunt impedances etc at different resonating frequency at different length of the cavity. Limit switches are connected at the cavity for upper limit and lower limit. These limits are decided according to required cavity length at 9MHz (lowest freq) and 27 MHz (highest freq).The frequency response of the input circuit of the amplifier has been measured using Vector Network Analyzer.

POWER AMPLIFIER

The high power rf amplifier (Cross-sectional view as shown in Fig.1.) is based on Eimac 4CW 150,000E water-cooled tetrode[2] and the output tank circuit of the amplifier consists of a $\lambda/4$ type variable length coaxial cavity. The short-circuited coaxial cavity is tuned by the precise movement (minimum 50 μm corresponding to tuning accuracy of 19.35 Hz at the lowest frequency and 1.135 kHz at the highest frequency) of the sliding short within the operating frequency range of 9 MHz to 27 MHz under unloaded condition.
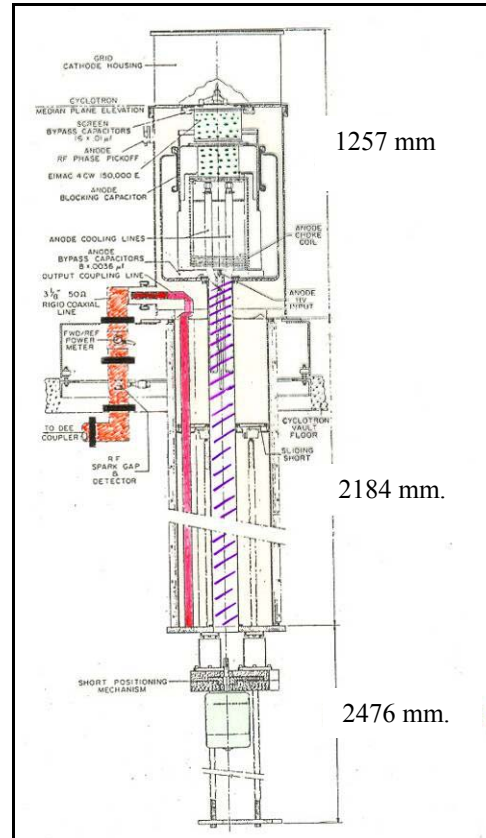
Figure 1: Cross-sectional view of high power rf amplifier.

The coaxial line is made of hexagonal outer conductor (with each side of hexagon 201.65±0.05 mm.) and circular inner conductor (with outer diameter 58.42±0.05 mm.). The sliding short plate is electrically connected to the outer and inner conductor of coaxial line by Be-Cu contact finger (as shown in Fig.2.) with sliver-graphite (99%Ag +1%C) contact ball at the tip. The sliding short contact must operate below the copper softening temperature (~460°k), since the softening could lead to fusion welding. The inner and outer conductors are aligned concentric preferably within ±0.25 mm., because large asymmetry may give rise to uneven stress on the contact finger. The contact resistance is of the order of 0.7mΩ per finger.

—————————————
[#] ssom@veccal.ernet.in

MECHANICAL ENGINEERING CHALLENGES IN THE DEVELOPMENT OF THE FEL AT RRCAT

Sanjay Chouksey[#], S. Krishnagopal, Vinit Kumar, Shankar Lal, K. K. Kumar Pant,
Vijendra Prasad; RRCAT, Indore (M.P.) 452013, India

Abstract

The Compact Ultrafast TErahertz Free-Electron Laser (CUTE-FEL) is being developed by BP&FEL Laboratory, RRCAT, which is designed to lase around 80 μm. Sub-systems like S-band high gradient accelerating structures, pre-buncher, buncher, pure permanent undulator etc. have already been developed and others are in advanced stage of fabrication/commissioning. In this paper we present the design, fabrication, measurements and status of various prototype developments of structures.

INTRODUCTION

The Compact Ultrafast TErahertz Free-Electron Laser (CUTE-FEL) is being developed by BP&FEL Laboratory, RRCAT for condensed matter research and chemistry applications. The FEL is designed to lase around 80 μm and will be driven by a 10 MeV Plane Wave Transformer (PWT) linac and will use planar, pure-permanent magnet (PPM) undulator with 5 cm period and 2.5 m length, developed in-house [1]. The major components needed
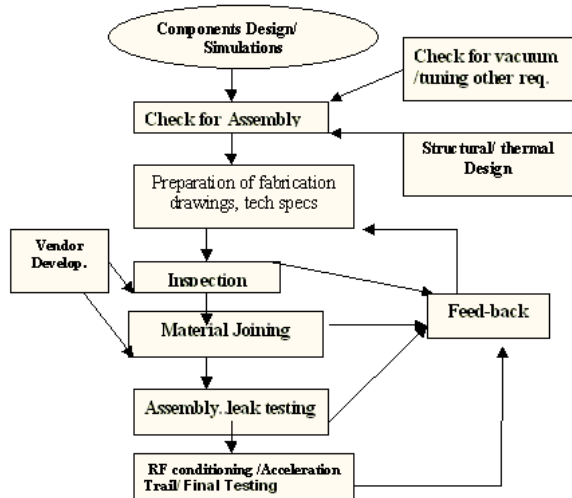
Fig.1 Process plan components development

for the development of the FEL are pre-buncher cavity, buncher, PWT linac and PPM Undulator. PWT linac and high brightness photo cathode guns are high gradient accelerating structures requiring an operational vacuum of better than 1×10^{-8} mbar. These devices require precise machining of components for accurate geometry on internal details with desired surface finish, and UHV

quality leak tight joining. Development of these structures from simulation to final testing commissioning/ RF trials involves various levels of prototyping. In this paper we present the design, fabrication, measurements and status of various prototype developments of structures. Fig.1 shows our process plan for component development.

In the next section, we will review their engineering considerations, various prototype developments, results achieved and future plan.

COMPONENT DEVELOPMENTS

Pre-buncher cavity

In order to bunch low energy electron beam coming from thermionic electron gun, a sub-harmonic buncher cavity (476 MHz) was designed. Mechanical design considerations are:

- Fabrication of nose cone geometry cavity cell in two asymmetric halves with surface profile tolerance better than 0.05 mm for 350mm inner diameter.
- Accurate assembly of cavity cell in two asymmetric halves with various orthogonal ports.
- Requirements of vacuum sealing & tuning
- Structural and thermal requirements

Fig 2   Aluminium prototype of pre-buncher cavity

Current Status & future plans:

First, a true-to-scale prototype was made out of aluminium alloy T6061 to perform the low power RF test as shown in Fig 2. Inspection results done on CMM showed a tolerance of better than 0.04mm on inner profile. Final structure design was suitably modified based on the feedback received from cold test results. Critical design feature includes water-cooling channels on both sides for heat removal, tuner plungers for RF tuning, spring metal Helicoflex seal of dia 400 mm for UHV

_____
[#]chouksey@cat.ernet.in

THERMAL SIMULATIONS OF A PHOTOCATHODE R.F. GUN

B. Biswas#, Shankar Lal, K. K. Pant, Arvind Kumar and S. Krishnagopal
Beam Physics and FEL, Laboratory, Raja Ramanna Centre for Advanced Technology,
Indore 452013, India

Abstract

We are developing a photocathode linac, which uses a 2856 MHz r.f. gun, with a copper cathode driven by a 102 MHz, 266 nm laser at inclined incidence. The laser photocathode r.f. gun is a 1.6 cell BNL/SLAC/UCLA type III r.f. gun. In this paper we present the dynamic thermal cooling simulations to calculate the structural deformations and consequent frequency drift of the gun. We have done a complete r.f.-thermal-structural-r.f finite-element analysis (FEA) of the gun in that order, using ANSYS/MULTIPHYSICS. We find that with the present coolant channel design the gun can operate at up to 2 Hz without any significant change in resonant frequency and field balance.

INTRODUCTION

There is a wide range of normal-conducting photocathode guns working or under development all around the world as injectors for x-ray free electron lasers and colliders [1-4]. Typically the S-band laser photocathode normal conducting guns deliver up to 150 MV/m peak accelerating electric field.

The S-band photocathode gun we are developing is a BNL type III gun [5, 6]. It has a simple longitudinal cooling arrangement unlike the circular cooling channels in higher r.f. pulse repetition rate guns. We have done the complete r.f.-thermal-structural-r.f finite element analysis (FEA) of the gun in that order. We found that it is necessary to model the gun with all its ports, to capture the high heat flux spots around these port discontinuities. We also found that the resonant frequency in the 1.6 cell photocathode gun is very sensitive to geometrical deformations. Hence we re-simulated the heated-deformed gun for its r.f. properties. As deformations are of the order of microns we morphed the r.f. region's FE mesh boundary to absorb the surface displacements by using the structural solution. This approach is different from regenerating the deformed structure in a CAD package and remeshing it for simulation – as the new mesh may not be similar to the original one and mesh-to-mesh differences will overshadow the desired detuning result. We show that we can go up to 2 Hz operation at maximum gradient with modest cooling parameters and no degradation in r.f. parameters. Higher repetition rates will need modification of the coolant channel design. However operation at lower gradients and higher repetition rates will still be possible.

#bbiswas@cat.ernet.in

THE ELECTROMAGNETIC SIMULATIONS

The RF parameters of the 1.6 cell BNL/SLAC/UCLA type photocathode gun, shown in Fig. 1, are given below in Table 1.

Table 1: Parameters of the photocathode gun.

Parameter	Value
Type	1.6 cell BNL/SLAC/UCLA type III
Frequency	2856 MHz
Bunch Charge	1nC
Field balance	~ 1.04
Peak accelerating field	147 MV/m
Rep. Rate	1 - 10 Hz
Laser pulse width	FWHM 12 ps
r.f. pulse width , power	4 μs , 8 –10 MW
Power dissipated at 10Hz, 4 μs r.f. pulse	0.5kW

We simulated the full model of the photocathode gun in FEA package ANSYS [7] to get the resonant π-mode at 2856.1 MHz and field balance of 1.042 as shown in Fig. 2. Copper and SS conductivity were applied at respective regions for calculation of heat loss/flux.

The average heat-flux obtained for an r.f. pulse of 4 μs and 2 Hz repetition rate obtained is shown in Fig. 3. The maximum heat flux, around the r.f./vacuum ports, is nearly three times the peak heat flux without ports (at full cell exit wall) when compared with SUPERFISH. The inner diameters of the two cells were fine tuned by up to 5 μm to get the required field balance. This is quite similar to the fabrication learning curve where final cuts of the order of 5-10 μm were taken on inner diameter of the two cells of prototype aluminium and then ETP copper gun.

THE THERMAL SIMULATIONS

The gun material comprises of OFE copper and some SS316L seal plates, beam and vacuum ports. For thermal (conduction) analysis all the metallic volumes were simulated. The o-ring was also modeled. The convection bulk temperature in the two channels for water flow is shown in Fig. 4 -for the 147 MV/m peak gradient at 4 μs r.f. pulse and 2 Hz repetition rate. For clarity only a one-fourth model is shown. The inlet water temperature is 30°C and the water flow is at 1.8 m/s. The ambient temperature is also 30°C.

07 Accelerator Technology
T06 - Room Temperature RF

CONTROL CHARACTERISTICS OF THE PEFP RF SYSTEM*

H. J. Kwon[#], Y. S. Cho, H. S. Kim, K. T. Seol, I. S. Hong, Y. G. Song
PEFP, KAERI, Daejeon 305-353, Korea

Abstract

A 20 MeV proton accelerator has been developed and tested at Proton Engineering Frontier Project (PEFP) as a front-end part of the 100 MeV accelerator. The initial test results showed that more stable RF operation was necessary to investigate the machine characteristics more comprehensively. A LLRF control system using commercially available digital board was newly developed and tested for this purpose. The goals of the RF control for 20 MeV accelerator are to achieve errors within 1% in amplitude and 1 degree in phase against external perturbations such as change of resonant frequency, fluctuation of klystron power supply voltage and also beam loading. In addition, the PEFP 20 MeV DTL has unique characteristics that single klystron drives four independent tanks simultaneously. In this paper, the initial test results of the RF system with digital controller are presented and its control characteristics are discussed.

INTRODUCTION

One of the missions of PEFP is to develop a 100 MeV proton linear accelerator. For this purpose, a 20 MeV accelerator was already fabricated and installed at KAERI test stand [1][2]. About two years later, the 20 MeV accelerator will be moved to be installed in Gyeongju city which was selected as an host city for PEFP 100 MeV accelerator. An initial test has been carried out at KAERI site to check the overall machine performance and tune the accelerator operating parameters. The test is being done with peak current of 1 mA at low duty, that is 50 μs beam pulse width and 0.1 Hz repetition rates, because of the improper radiation shielding for full beam power. The installed 20 MeV accelerator at KAERI site is shown in Figure 1. During the initial beam test, nearly 100 % beam acceleration was achieved through the four DTL tanks. But the pulse to pulse beam current fluctuation was observed. Moreover the beam current dependency on the tuning parameters such as RF power, RF phase, beam steering were not so obvious in the near 100 % beam transmission level. Therefore, more stable RF control system was necessary to investigate the machine performance more comprehensively. A digital control LLRF system was developed to satisfy the requirement [3]. Recently, the high power test using newly developed LLRF control system is being carried out to check the RF system characteristics and optimize the control parameters. In addition, the PEFP 20 MeV accelerator has unique characteristics, that is four independent tanks are driven by single klystron. Several methods were adopted to realize this scheme, and the DTL tank characteristics were investigated to obtain the basic parameters for the proper RF control.

Figure 1: 20 MeV proton accelerator installed at KAERI test stand.

20 MEV ACCELERATOR TEST STAND

The main accelerator facilities at KAERI test stand are 20 MeV accelerator itself, two sets of 1 MW, 350 MHz RF system, two sets of –100 kV, 20 A DC high voltage power supply for the klystron, two sets of 2 MW cooling system for the cavity and RF system.

The ambient condition at KAERI test stand is not stabilized. Therefore the RF cavities should be stabilized against changing ambient conditions – especially ambient temperature. For this purpose, heater and heat shield were installed around the RFQ and DTL cavities. A 1 kW heating power per RFQ and a DTL tank was used. The heater was controlled by PID mechanism of the SCR power unit. By using this method, the frequency could be stabilized within ± 1 kHz.

The design duty of the 20 MeV accelerator is 24 % and two sets of 1 MW, 350 MHz klystron are used to drive a 20 MeV accelerator, one is for RFQ and the other is for DTL. All the other ancillary facilities such as klystron power supply and cooling system were designed for 100 % duty operation. During the low duty operation at KAERI test stand, the RF system is operating such that the electron beam of the klystron is CW whereas only the input RF signal is modulated for the low duty pulse operation.

Two sets of klystron power supply are used to drive two sets of 1 MW klystron. As mentioned above, the design duty of 20 MeV accelerator is 24 %, therefore, not modulator, but DC high voltage power supply is used as a klystron power supply. During test, the klystron power supply is operating in CW mode.

Two sets of cooling system are operating, one is for RFQ, the other is for DTL. One set of the cooling system at KAERI test stand supplies cooling water both to the

DEVELOPMENT OF THE DIGITAL RF CONTROL SYSTEM FOR THE PEFP PROTON ACCELERATOR*

H. S. Kim[#], H. J. Kwon, K. T. Seol, I. S. Hong, Y. G. Song and Y. S. Cho
Korea Atomic Energy Research Institute, Daejeon 305-353, Korea

Abstract

The low level RF system is under development for the PEFP Proton Accelerator. The RF amplitude and phase stability requirements of the LLRF system are ±1% and ±1°, respectively. As a prototype of the LLRF, a simple digital PI control system based on commercial FPGA board is designed and tested. The main features are a sampling rate of 40 MHz which is four times higher than the down-converted cavity signal frequency, digital in-phase and quadrature detection, pulsed mode operation with the external trigger, and a simple proportional-integral feedback algorithm. The control logic is implemented in the Xilinx FPGA by using VHDL coding and the application program based on the VxWorks and VME platform is also developed. In this paper, the detailed design study and the test results of the prototype LLRF system are presented.

INTRODUCTION

In the 100 MeV proton linear accelerator for PEFP, the RF source will power an RFQ cavity and DTL tanks operated at a frequency of 350 MHz [1]. The low level RF(LLRF) system for 100 MeV proton linear accelerator provides field control including an RFQ and DTL tanks at 350 MHz. In our system, an accelerating field stability of ±1% in amplitude and ±1 deg. in phase is required for the RF system. The digital RF feedback control system using the FPGAs and PowerPC Embedded Processor is adopted in order to accomplish these requirements and flexibility of the feedback and feed-forward algorithm [2].

HARDWARE DESCRIPTIONS

The hardware components can be divided into the analogue parts and the digital parts. The analogue parts mainly deal with the signal mixing, IQ modulation and interlock system and the digital parts contain the control algorithm.

Analogue Components

The analogue parts consist of various components such as IQ modulator (Analog Devices AD8345), RF mixer, RF switch, RF amplitude detector, phase comparator and VSWR trip circuit along with many attenuators and power splitters. All of the analogue components are installed in the 19" subrack as shown in Figure 1. A 350 MHz cavity field pick-up signal is converted to 10 MHz IF signal in the analogue components subrack. The amplitude and phase of the cavity field can be measured

by RF detector and phase comparator, therefore it is possible to compare the RF amplitude and phase measured by analogue system with those measured by digital system. The VSWR trip circuit and interlock system protect the machine in the event of an arcing or an RF full reflection.

Figure 1: Analogue components subrack

Digital Components

The main hardware components of the digital RF feedback system are ADC for sampling of the RF signal, FPGA for the signal processing and DAC for driving the IQ modulator. A ICS-572B commercial board which is shown in Figure 2 is adopted for the ADC/DAC and FPGA board. ICS-572B is a PMC module with 2-channel 105 MHz ADC, 2-channel 200 MHz DAC and with 4 million gate onboard Xilinx FPGA.

The board uses two 14-bit ADCs (Analog Devices AD6645) with a maximum sampling rate of 105 MHz. The sampling clock can be either internally or externally generated. The minimum ADC sample rate is 30 MHz. However, the board includes a programmable ADC output decimator that can reduce the output data rate by a factor of up to 32. Both input channels are simultaneously sampled. The input signals are connected via two front panel SMA connectors. The full-scale signal is 5.5 dBm into 50 ohms. The inputs are transformer-coupled with turn rato of 4:1.

The outputs of the ADCs are connected to a Xilinx FPGA for direct processing of the ADC data. The ICS-572B includes a Xilinx Virtex-II FPGA (XC2V4000) that can be programmed by the user via a JTAG port or PCI communication. On the standard ICS-572B board, the FPGA contains firmware that provides switch and data formatting functionality to route ADC and/or DAC data to the buffers. The user FPGA is connected to 64 MB

DESIGN AND DEVELOPMENT OF 30 MEV, 3 KW RF ELECTRON LINAC

V.T.Nimje, D.Bhattacharjee, K.Dixit, D.Jayaprakash, K.C.Mittal and A. K. Ray
Accelerator & Pulse Power Division, BARC, Mumbai – 400 085.

Abstract

A 30 MeV, 3 kW on-axis coupled cavity RF electron linac is being designed, developed at BARC and will be installed at Vizag . It will be used as a neutron generator and will produce $\sim 10^{12}$-10^{13} n/sec. The design of the 94 cell RF structure, rf system, modulator for the electron gun and the Neutron generation target is in the advanced design stage . The design details of the linac are presented in this paper.

INTRODUCTION

Electron beams have played a key role in the field of basic sciences, applied sciences, medicine and agriculture. Over the last decade or so, the focus has shifted more towards industry. Depending upon the beam power and its energy, the electron beams have made tremendous impact in the area of food preservation, medicine, agriculture, biology, etc.[1]. Keeping in tune with the present and future scenario, the Accelerator and Pulse Power Division (APPD) of BARC has initiated the design and development of various types of electron accelerators. The project for Prototype Development of 30 MeV, 3 kW electron accelerator has been proposed based on the experience gained from 10 MeV RF Linac being commissioned at EBC, Kharghar, Navi Mumbai. This Accelerator can be used as a Prototype to study the Production of Medical Radioisotopes, Neutron rich Radioactive Nuclei, Energy Driver, Transmutation of Radioactive Waste, to study Electron beam based Nuclear physics including photonuclear reactions and target optimization for photoneutron production.
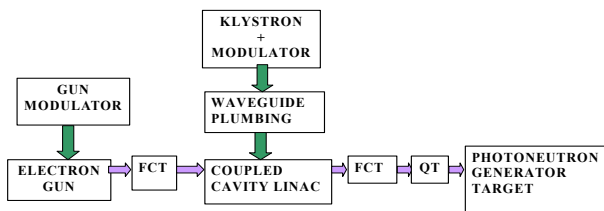
Figure 1: Schematic Diagram of 30 MeV, 3 kW Electron RF Linac System.

The linac is intended to deliver a beam with an average beam power of ~ 3 kW. It will be operated at a frequency of 2856 MHz. The duty cycle is chosen to be 0.1%, with a repetition rate (RR) of 100 Hz. The schematic of the linac is shown in Fig. 1. The electron gun (EG), will be directly coupled to the linac system, will inject a train of pulses into the linac at the rate of 100 pulses per sec, each having a pulse width of ~ 10 μsec. The beam will be accelerated to the required energy of ~ 30 MeV in the coupled cavity RF linac before being passed to the photoneutron generation target. The energy analysis will be done using the depth dose penetration method and the beam current will be monitored with the beam current transformer (ICT). A vacuum of ~ 4x10-7 torr will be maintained with the help of a turbo/sputter ion pump (TP/SIP) combination system. The RF power to the linac will be fed via a waveguide (WG) operated in the TE10 mode. The linac will have a horizontal configuration. The following sections give the brief details of the progress made in the design of various subsystems of the linac.

RF STRUCTURE

For the sake of simplicity of fabrication, constant impedance, on-axis coupled cavity linac configuration has been selected. It consists of two parts. Schematic of one of the part is shown in fig. 2. First part consists of 49 cells
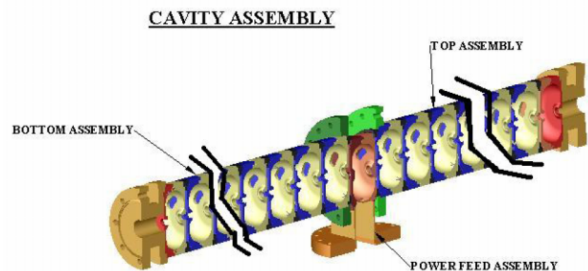
Figure 2: One part of On-Axis Coupled Cavity RF Linac

including 3 buncher cavities followed by 22 acceleration cavities and 24 coupling cavities. Second part consists of 45 cells, 23 acceleration cavities and 22 coupling cavities. These two parts will be separated by a drift space of ~ 15.7 cm. The length of the acceleration cavity is 52 mm, whereas the buncher cavities are 45, 48 and 50 mm respectively. A total length will be ~ 250 cm. An acceleration field gradient of 15 MV/m to 18 MV/m has been used for design considerations, leading to a Kilpatrick value of ~ 1.4, with a maximum field on the boundary as 62.712 MV/m. The corresponding maximum magnetic field is found to be 36.072 kA/m. The effective shunt impedance for the buncher cavities is ~ 80MΩ/m, while for the accelerating cavities, it is ~ 90MΩ /m. Some of the salient features of the two ½ accelerating cavity, sandwiching the coupling cavity, are shown in Fig. 3. The electric field distribution and profile are shown in Fig.4. The outer and inner nose radii have been optimised

COMPARATIVE ANALYSIS OF BLADE TUNER OPTIMIZATION OPTIONS FOR THE ILC

Carlo Pagani, Nicola Panzeri, INFN Milano, Italy

Abstract

Following the successful experience of the blade tuner concept for superconducting cavities, a full parametric analysis has been performed for ILC cost optimization. Different design details have been reconsidered and optimized on the basis of their impact on the ILC requirements and on production costs. Two different designs have been then developed for two options of fabrication material: titanium or stainless steel. The realization of two prototypes, one for each type, has been recently launched for the designs qualifications and comparison. In this paper we discuss the optimization rationales and the expected differences in cost and tuner integration and performances. Cold tests on cavities will be at the basis of the final choice for the ILC.

INTRODUCTION

For the ILC project more than 16000 coaxial tuner are required. The effort to optimize its design is widely justified by the subsequent enormous cost saving. Moreover the actual blade tuner version, although proved to fulfil the slow tuning requirements [1,2], it is far from being in the final design stage and some modifications are required in order to improve its reliability and reduce its total cost.

Two aspects have been considered in the optimization process here presented: first of all a whole design refinement of rings and blades has been performed. This has been obtained taking into account both the geometry and the material of the blade tuner, allowing to develop an unique geometrical solution that can be realized with the rings in titanium or stainless steel. This is very important in view of a possible future use of a steel helium tank when the technology will allow solving the problems in welding titanium to stainless steel. The second aspect considered concerns a major simplification of the driving mechanism and the moving of the motor from a central to a lateral position, thus freeing some space in correspondence of the invar rod of the ILC cryomodule.

The effectiveness of this solution has been proved by means of experimental tests and numerical simulations.

REVIEW OF THE TUNER DESIGN

The tuner review started from these considerations:
- the cost of materials (Ti) is steeply increasing;
- the cavity stability should have positive benefits from a lighter and more compact tuner design;
- the tuner strength and stiffness characteristics should be commensurate to the action on the helium tank and to the total stiffness of parts near the cavity.

By maintaining the original layout of the blade tuner [3-5] that assures a well symmetric behaviour, we optimized all the aspects, from the less relevant to the more important like the blades geometry and their distribution. The design of the optimized blade geometry has been driven by the following constraints:
- low cycle fatigue phenomena in the blades and a not reproducible tuner behaviour are unacceptable, therefore **no plasticity** has to occur in the blades in working conditions;
- the maximum **axial load** on the tuner occurs when the helium tank is under vacuum, and outside there is the atmospheric pressure. This compression force is equal to 4155 N;
- the reduction of the number of welds and machining steps leads to a total **cost reduction**.

Keeping in mind these constraints and the necessity to have at least the same tuning capabilities, different blade configurations have been analyzed: they have different materials and geometry, as reported in table 1 and table 2.

Table 1: Blade configurations taken into account

Combination	Geometry	Material
A	Original	TiGr5
B	Original	AISI 316
C	New	TiGr5
D	New	AISI 316
E	New thin	AISI 316
F	New	INCONEL 718

Table 2: different blade geometries considered
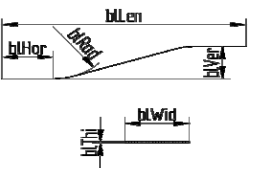
Geometry	blHor	blCla	blVer	blLen	blRad	blWid	blThi
Original	12	8	7.5	56	15	15	.5
New	12	8	10	66	15	16	.5
New thin	12	8	10	66	15	16	.2

PRELIMINARY DESIGN, ANALYSIS AND MANUFACTURING ASPECTS OF LOW BETA 350 MHZ REENTRANT SUPERCONDUCTING RF CAVITY

Deepak Mishra*, M.Prasad, V. Jain, M. Bagre, A M Puntambekar, G. Mundra, P. Shrivastava

Raja Ramanna Centre for Advanced Technology, PO: RRCAT, Indore, India

Abstract

A superconducting reentrant cavity for low beta, high intensity beam has been designed using SUPERFISH and MAFIA. The study has been done for cavity shape optimization. Further its structural design has been done and feasibility study of different manufacturing aspects has also been done. A full-scale mild steel model with copper coating has been fabricated. A twin arm mechanical tuner has been designed for slow tuning by elastic deformation. This was tested with low power RF to validate the design parameters and to check the tuning sensitivity. In this paper the design and development activity of the reentrant superconducting are discussed.

INTRODUCTION

It is proposed to build 100 MeV, high current H^+/H^- linac at RRCAT. The main components of linac are H^+/H^- ion source at 50 keV, low energy beam transport line, 4.5 MeV RFQ, MEBT, 100MeV injector linac. It is planed to use SFDTL structure after the RFQ from 4.5MeV to 100MeV. H^- linac will be used as an injector for 1Gev, 25Hz rapid cycling synchrotron, for the proposed Indian spallation neutron source (ISNS). Proton linac can be used as the low energy part of 1GeV linac, which will be used for accelerator driven subcritical systems (ADS).

As a technology development of superconducting cavity, we have started the work on reentrant low beta cavity. If we succeed in making the cavity to desired satisfaction, we will replace SFDTL structures with these re-entrant cavities.

CAVITY DESIGN CRITERIA

In designing the cavity, the criterion followed was to minimize the surface fields and maximize the R/Q. The cavity was optimized for beta equal to 0.20. All these issues are directly linked to shape of the cavity and the effects of the shape are different. The effects of shape on electric and magnetic fields compete and the optimization of the shape must be done wisely. Generally superconducting cavities are used to provide the high accelerating gradients (E_{acc}). But the linac beam dynamics design required relatively low energy gain per cavity in our case. The purpose of our design was not to achieve the maximum gradient but to operate it reliably and it must be capable of using the RF energy efficiently.

CAVITY SHAPE OPTIMIZATION

Fig.1 shows the quarter geometry and the cavity shape variables. The cavity optimization was done for frequency of 350MHz. The optimization was done step by step. The

* deepak@cat.ernet.in

first variable was the gap length g. The frequency was adjusted with the help of R_{eq}. The gap length was optimized for the maximum R/Q. Fig.2a, 2b shows the variation of R/Q and E_{max}/E_0 Vs. gap length respectively. The value for R/Q shows a maximum for gap value of 1.7408cm. At this value the curve of Emax/E0 changes its direction. The second variable was the radius r1.This parameter was optimized for the minimum surface electric and magnetic field. During the whole optimization process the frequency was adjusted with the help of R_{eq}. The details of the cavity optimization can be found in refrence [1] [2] [3].
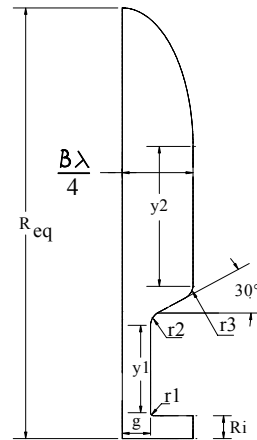
Fig.1 Cavity shape variables
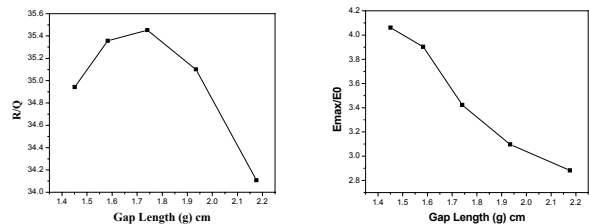
Fig2a R/Q Vs. Gap length   Fig.2b E_{max}/E_0 Vs. Gap length

Table-1 lists the basic parameter of the optimized cavity.

Table 1: Basic Shape Parameters of Reentrant cavity

Parameter	Value	Unit
g	1.7408	cm
Ri	1.5	cm
r1	5	mm
Y1	5.7564	cm
r2	2	mm
angle	30^0	degrees
r3	6	mm
Y2	10	Cm
R_{eq}	28.45	cm

SUPERCONDUCTING NIOBIUM RESONATOR FABRICATION AND TESTING AT IUAC

P.N. Prakash, S.S.K. Sonti, K.K. Mistri, J. Zacharias, D. Kanjilal, A. Roy
Inter-University Accelerator Centre, Aruna Asaf Ali Marg, New Delhi - 110067, India

Abstract

Inter-University Accelerator Centre is currently constructing fifteen niobium quarter wave resonators for the superconducting linear accelerator project. The production is presently nearing its completion. In addition to building resonators for the in-house programmes, a project to build 325 MHz single spoke resonators for the proton driver linac for Fermi National Laboratory will begin soon. This paper presents details of the current resonator production work and future plans at IUAC.

INTRODUCTION

The Superconducting Resonator Fabrication Facility (SuRFF) consisting of an electron beam welding machine, surface preparation lab and high vacuum furnace, for constructing niobium quarter wave resonators (fig. 1) for the linear accelerator [1], has been operational at Inter-University Accelerator Centre (IUAC) since July '2002 [2]. In the first phase a single quarter wave resonator (QWR) was successfully fabricated and tested [3]. It has been installed in the rebuncher cryostat of the linac and operated at 3.3 MV/m with 6 W RF input power [4]. In the second phase two more completely indigenous QWRs were fabricated. Figure 2 shows one of the resonators along with its niobium slow tuner bellows [5]. In cold test at 4.5 K the low field Q_0 on this resonator was measured to be $\sim 1.5 \times 10^9$, and with very little high power pulse conditioning it performed at 3.5 MV/m accelerating electric field with 3.5 W RF input power, exceeding the nominal design goal. Following the successful testing of the fully indigenously built resonators, production of fifteen more QWRs for the second and third linac modules began in July '2005 [6].

PRODUCTION OF QWRs

The resonator production is being done using both, the facilities setup at IUAC as well as commercial vendors. All the machining, forming, rolling and fitting of the niobium components and assemblies along with the fabrication of the outer stainless steel vessel are being done at a local vendor's site. Substantial amount of developmental work had been undertaken during the construction of the first two indigenous resonators to train the manpower in various machining and sheet metal works and in handling of the niobium material. This was done keeping the future resonator production and other projects in mind. All electron beam welding, electropolishing, heat treatment and testing are done using the SuRFF facilities setup at IUAC.
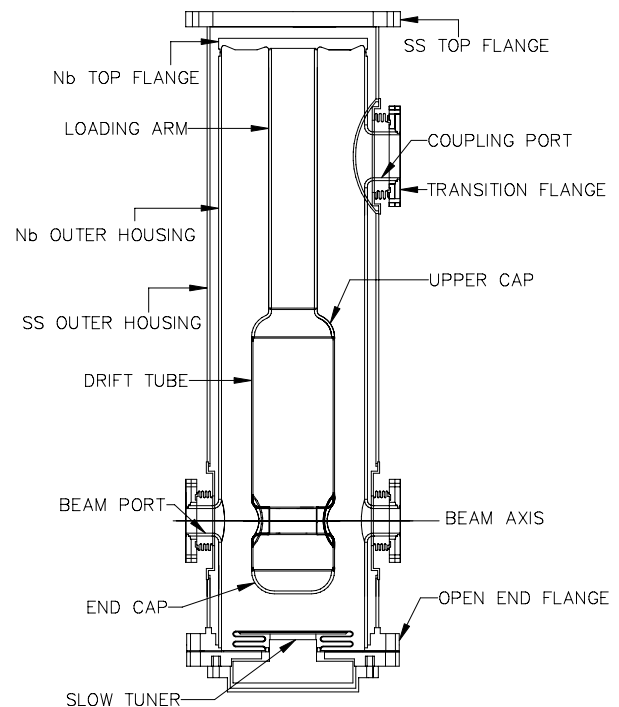
Figure 1: Schematic diagram of IUAC-QWR

Figure 2: One, of the two, fully indigenously built QWRs at IUAC along with its niobium slow tuner bellows.

07 Accelerator Technology
T07 - Superconducting RF

EVALUATION OF EXTERNAL Q USING KROLL-YU METHOD WITH MICROWAVE STUDIO

A.S.Dhavale and K.C.Mittal

Accelerator and Pulse Power Division

Bhabha Atomic Research Centre, Mumbai 400 085

Abstract

Design and development of a superconducting cavity has been taken up as a part of Accelerator Driven Subcritical project(ADSS). An input coupler is designed for the same using Kroll-Yu method[1]. The evaluation procedure is optimised and the method has been successfully implemented for the evaluation of high external Q [2]. The validity of the Kroll-Yu method is tested with the external Q calculations by P. Balleyguier method for the Benchmark cavtity which is a pillbox cavity of diameter ~200 mm, length ~150 mm with semi-rigid coaxial line[3]. It is found that the careful choice of data points provide accurate results over wide range.

INTRODUCTION

BARC is involved in the development of technology for the Accelerator Driven Sub-Critical System (ADSS) that will be mainly utilized for the transmutation of nuclear waste and enrichment of U^{233}. The application demands a proton beam (30mA, 1 GeV) that will be generated by various stages of accelerator structures. Up to 100 MeV proton beam will be generated by the normal conducting accelerator structures whereas from 100 MeV to 1 GeV superconducting structure will be more efficient. It will be a coupled cavity structure made up of niobium cavities of elliptical shape. As an initial step single elliptical cavities operating at 700 MHz and 1.056 GHz were designed. [4, 5]

A co-axial type of input coupler has been designed for the same cavity. The power will be transferred efficiently from the coupler to the cavity only when the impedance of the coupler matches with the cavity impedance i.e. the coupling factor between cavity and transmission line is unity. Coupling factor, β is defined as,

$$\beta = Q_0 / Q_{ext} \quad \text{--(1)}$$

where, Q_0 and Q_{ext} are the quality factors of the cavity and the transmission line respectively. Q_{ext} is the factor that depends solely on the geometry and can be evaluated by different computational methods with the help of 3-D electromagnetic codes.

COMPUTATION OF EXTERNAL Q

A number of computer programs viz., MAFIA, SUPERFISH, URMEL have been developed for the design of cavity resonators which give information about the field distribution, shunt impedance, Q-value but cannot calculate Q-value due to external coupling due to

waveguide/ co-axial line. Thus, Kroll-Yu in 1990 developed a procedure to calculate external Q by using these codes. As this method is based on the frequency resonance differences, it was thought that it is better suited for the computation of low Q_{ext}. In 1997, Pascal Balleyguier developed a method based on the field calculations for the computation of high external Q. [3,6]

This paper presents results of the external Q calculation using both the methods with the help of computer code Microwave Studio[7]. The results indicate that Kroll-Yu method is also suitable for the high external Q calculation provided the data points near the resonant frequency of the cavity are chosen.

Kroll-Yu Method

Kroll-Yu suggested a method [1] that is easy to implement. A (cavity + waveguide) system terminated in a short ($E_t=0$, E_t----tangential electric field component) can be treated as two coupled resonators, cavity and waveguide.

The formulation deals with frequency, ω, as a function of phase change, ψ along the guide length that is given by $2\pi D/\lambda_g$ where λ_g is the guide wavelength and D is the guide length. A quantity $G \equiv -(1/2) (d\psi/d\omega)$ plotted as a function of ω exhibits a typical resonance curve with peak at the resonant frequency of (cavity + waveguide) system feeding into the matched load. When multiplied by the resonant frequency, the height of the curve is equal to Q_{ext}. The eigen modes of this system are complex in nature viz, u + i v. Also,

$$G = (1/2) (v/(w-u)^2 + v^2) + (1/2) \chi'(u) \quad \text{---------(2)}$$

This is a resonant curve at frequency ω=u and $Q_{ext}=(1/2)(u/v) + (1/2)\chi'(u)$. The exact relation between ψ and ω is given by 4 – parameter formula,

$$\psi(\omega) = \tan^{-1}[v/(\omega-u)] - \chi(\omega) + n\pi \quad \text{--------(3)}$$

where , $\chi(\omega) \cong \chi(u) + \chi'(u) (\omega-u)$

By using simulation codes like MAFIA, Microwave Studio, HFSS one can obtain different ψ-ω pairs (data points) for different values of waveguide length, D. The essence of the method is to fit data points by 4 -parameter formula. The fitted values of u and v give information about the resonant frequency and external Q value.

Also it is observed that for $Q_{ext} > 20$, choice of $\chi'(u)$ equal to zero is excellent [1]. Thus, for determination of u and Q_{ext} just three points are sufficient (3-parameter fit).

The implementation formulae are given by ,

MECHANICAL ANALYSIS AND DESIGN OF THE PEFP LOW BETA CAVITY*

Sun An[#], Y. S. Cho and B. H. Choi
PEFP, KAERI, Daejeon 305-353, Korea

Abstract

The PEFP low beta superconducting RF cavity is the lowest beta elliptical cavity operating at pulse mode so far, the Lorentz force detuning control of the PEFP low beta cavity is a big challenge in cavity design. In this paper, a basic design consideration in the stiffening structure for Lorentz force detuning control has been presented. Based on this consideration, a new stiffening structure has been designed for the PEFP low beta cavity. The PEFP low beta cavity with this structure has low Lorentz force detuning coefficient K_L, reasonable cavity field flatness sensitivity, frequency sensitivity, tuning sensitivity and stable mechanical property.

INTRODUCTION

Superconducting RF (SRF) cavity is considered to accelerate a proton beam with repetition rate of 60 Hz at 700 MHz in the PEFP Linac being built at Gyeongju [1, 2]. The first section of the SRF linac is composed of 9 low beta cryomodules with three 5-cell elliptical cavities of β_g=0.42, and will accelerate a proton beam from 80 MeV to 178.6 MeV [3,4]. Table 1 lists the primary parameters of the PEFP Low beta cavity.

Table 1: Primary parameters of the PEFP Low beta cavity.

Parameters	Value
Frequency (MHz)	700
Geometrical beta β_g	0.42
E_{acc} (MV/m)	8.0
E_{pk}/E_{acc}	3.71
B_{pk}/E_{acc} [mT/(MV/m)]	7.47
R/Q (Ω)	102.30
Cell to cell coupling (%)	1.41
Geometrical Factor (Ω)	121.68

The cavity is deformed by the Lorentz radiation pressure, the tuner, the helium liquid pressure and the atmosphere pressure after pump-down. This deformation induces resonant frequency shift, field flatness change, ununiform stress distribution of the cavity. Therefore, mechanical stability of the SRF cavity is a fundamental consideration in the cavity design.

Generally, the lower beta cavities have stronger Lorentz force detuning than that of the higher beta cavities. For pulse SRF accelerators, the Lorentz force detuning is a more serious issue than that of CW accelerators. The

PEFP low beta cavity is the lowest beta elliptical cavity operating at pulse mode so far. Its Lorentz force detuning control is a big challenge in the cavity design. In order to control Lorentz force detuning, a optimized stiffening structure is installed on the cavity normally. In this paper, a basic consideration to optimize the stiffening structure is presented. The stiffening structure design of the PEFP low beta cavity is introduced.

STIFFENING STRUCTURE DESIGN

The function of the stiffening structure is to control Lorentz force detuning and protect cavity. A good stiffening structure should:

- Effectively control the Lorentz force detuning.
- Have low cavity field flatness sensitivity.
- Have low tuning sensitivity.
- Have low peak stress in the cavity.

The PEFP stiffening structure design follows above rule.

In the superconducting RF cavity, the RF power produces radiation pressures on the inside cavity wall [5]. The pressures deform the cavity wall, that produces the cavity resonant frequency shift. RF system needs to supply a surplus RF power to compensate the cavity frequency shift for keeping the cavity voltage constant. It can be demonstrated the cavity frequency shift is negative, and can be expressed as:

$$\Delta f = -K_L E_{acc}^2. \tag{1}$$

Here E_{acc} is the cavity accelerating gradient. K_L is the Lorentz force detuning coefficient, which strongly depends on the cavity shape and cavity wall's thickness. In order to reduce the RF system costs, usually a stiffening structure is used to control the Lorentz force detuning.

Stiffening structure design

The simulation method of combining Poisson Superfish with ANSYS is used to analyze PEFP cavity mechanical property [6]. The different stiffening structures have been simulated for PEFP low beta cavity, as shown in Fig. 1. Table 2 lists the Lorentz force detuning coefficient K_L with the cavity wall thickness of 4.3 mm for different stiffening structures at the best condition.

| -2622 | -307.473 | 2007 | 4322 | 6637 |
| -1465 | 849.877 | 3165 | 5479 | 7794 |
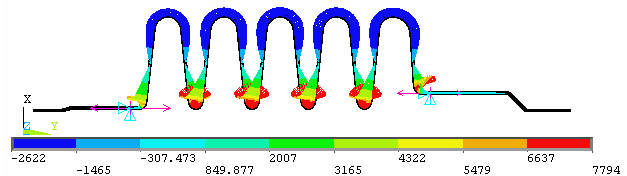
A. A PEFP low beta cavity without stiffening structure and the Lorentz pressure distribution on it.

DESIGN AND SIMULATION OF MULTIBEAM KLYSTRON CAVITY

Ashish Kumar Tiwari[#], Rajiv Kumar Arora, P. R. Hannurkar
Raja Ramanna Centre for Advanced Technology, Indore, India.

Abstract

The design and simulation of a multibeam re-entrant type cavity with four beams is presented for a 350 MHz, 250 kW CW klystron. The simulation is carried out using electromagnetic code CST Microwave Studio. This klystron will be used for 100 MeV proton Linac for Spallation Neutron source (SNS). Important Simulation results are presented.

INTRODUCTION

Klystrons have the inherent capability to provide maximum gain per unit length among the conventional electron beam devices. With the practical limits on increasing the number of cavities for a higher gain, increasing the output power level in conventional klystrons means increasing either operating voltage or the beam current. For increase in current the perveance of the gun is to be increased which results in increased space charge forces and the reduced efficiency of the device. Further high magnetic field is required to keep the beam focused throughout the drift length. Increase in anode voltage is limited by thermal and voltage breakdown considerations. A number of klystrons may be paralleled to get more power output and increased redundancy but phase matching at output remains a troublesome part of any such arrangement. Further any such arrangement is bulky and requires room.
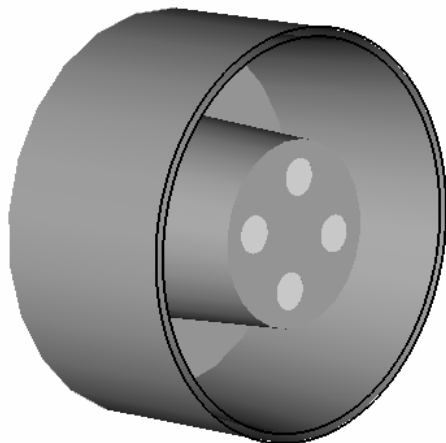
Figure 1: Cross-section of a multibeam cavity with four beamlets.

Another option is to parallel a number of beams within the same interaction structure. Since all the beams are accelerated through a common voltage and interaction takes place in a common structure namely multibeam

[#]atiwari@cat.ernet.in

cavity so the problem of phase matching no longer exists. This type of device is called the Multi-Beam Klystron (MBK). After the first experimentation in 1940's these klystrons have been developed and manufactured especially in Russia for past few decades. The multibeam klystrons are being looked into with renewed interest worldwide for their large scale application in accelerators. RRCAT has taken up the development of 350 MHz 250 kW CW klystrons for the accelerator applications. This paper presents the design and simulation of a multibeam cavity to be used as an interaction structure for the multibeam klystron.

DESIGN OF RE-ENTRANT CAVITY WITH MULTI-BEAM CHANNEL

Analytical methods can be used for the estimation of parameters of the cavity having simple shapes but for the more complex shapes experimentation or computer simulation are the only resorts. Analytical methods are still required for initial estimation of input geometrical parameters in computer models to be further analyzed and optimized numerically. The parameters were determined from the coaxial line analogy and parallel resonant circuit. Figure 1 shows the cavity shape. The RF interaction circuit for MBK is re-entrant cavity operating in TM_{010} mode. The diameter of gap channel is much larger than that of single beam klystron cavity in order to hold more beam channels. Therefore the RF electric field in inner layer beam channels is stronger as compared to outer layer beam channels. It is found that the electric field is not constant and slightly asymmetrical over the cross section of four beams for slightest disparity in interaction gap and field is more at the central beam if it exists. Therefore the radial dimension of the cavities must be chosen in order to minimize the disparities between the interaction gaps.

Suitable choice of the diameter of the gap projection is important for MBK design as it will influence the beam wave interaction and hence the efficiency. The following relation between cavity diameter and the diameter of gap projection is to be satisfied according to calculation and experience [1]

$$\frac{D_p}{D} < \frac{3}{4} \tag{1}$$

$$\frac{D}{\lambda} < \frac{3}{4} \tag{2}$$

where D_p = Diameter of gap projection
D = Diameter of cavity
λ = Operating wavelength

DEVELOPMENT OF HIGH-POWER MICROWAVE DEVICES IN TOSHIBA

Kenichi Hayashi, Masao Irikura, Yoshika Mitsunaka, Setsuo Miyake, Yoshihisa Ookubo
Mitsunori Sakamoto, Hiroyuki Taoka, Katsuhiko Tetsuka, Hiroto Urakata
Toshiba Electron Tubes & Devices Co., Ltd.
1385, Shimoishigami, Otawara-Shi, Tochigi 324-8550, Japan

Vacuum microwave devices continue to be essential for high-power RF accelerator systems and plasma heating or current drive systems for fusion experimental devices. Klystrons are suitable for use in amplification at the frequency ranges from 300 MHz to X band, while gyrotrons are mainly utilized in the millimeter wave range. Input couplers also play an important role in the building of acceleration cavity systems. TETD (Toshiba Electron Tubes & Devices Co., LTD.) has been developing these vacuum microwave devices in collaboration with some Japanese research institutes.

Two kinds of long-pulse klystron for the J-PARC project were developed in collaboration with KEK and JAEA, which each have their operation frequencies, 324 MHz and 972 MHz as listed in Table 1. Both tubes output 3 MW with a pulse duration of 0.62 ms at a repetition frequency of 50 pps. They have a triode-type electron gun and the same beam parameters and operate with an anode-modulating mode to reduce the cost of the power supply system. The tubes have a different output structure optimized for the operating frequency.

The 324-MHz tube, E3740A is horizontally oriented as shown in Fig. 1. Its weight was trimmed by 35% compared with the same size klystron by unifying it with the focusing solenoids. The maximum power of 3.03 MW was achieved with an efficiency of 57% for a beam voltage of 110 KV after some problems such as oscillation caused by reflected electrons from the collector and instability probably due to the magnetic field distribution like mirror field were solved. Twenty of the tubes were already installed in the J-PARC linac system and successfully completed acceptance testing.
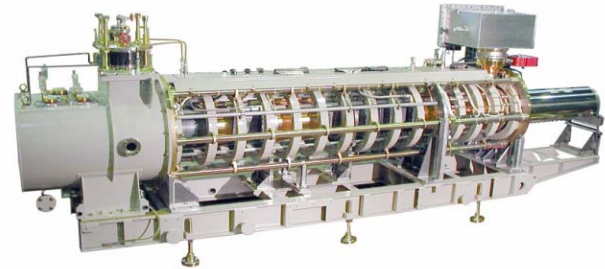
Figure 1: 324-MHz, 3-MW klystron E3740A

Figure 2 shows the 972-MHz tube, E3766. The second cavity incorporated in the first two prototypes had a relatively wide gap to meet a bandwidth of 10 MHz, and in addition, its RF electric field in the gap was symmetric with respect to the gap center, leading to TM011 and TM021-mode monotron oscillations. The 3-MW stable operation was obtained in the third tube with a new RF structure aimed at mass production.

TETD has been developing 1.3-GHz, 10-MW MBKs (multi-beam klystrons) for the Euro XFEL project in collaboration with KEK. A vertically-oriented MBK, E3736, the external view of which is shown in Fig. 3, already completed acceptance testing at DESY. Its design parameters are listed in Table 2. The MBK has six low-perveance beams operated at a relatively low voltage

Table 1: Design parameters of klystrons for J-PARC

	E3740A	E3766
Frequency (MHz)	324	972
Output Power (MW)	3	
Efficiency (%)	50	
Gain (dB)	55	
RF Pulse Length (ms)	0.62	
Beam Pulse Length (ms)	0.7	
Repetition Rate (Hz)	50	
Beam Voltage (kV)	110	
Anode Voltage (kV)	94	
Beam Perveance (I/V$^{1.5}$)	1.37×10^{-6}	
No. of cavities	5	6
Window	Coaxial	Pillbox
Output Flange	WR-2300	WR-975
Tube Length (m)	4.55	2.93

Figure 2: 972-MHz, 3-MW klystron E3766

Figure 3: 1.3-GHz, 10-MW, MBK E3736

DEVELOPMENT OF C-BAND MULTI BEAM SUB-BOOSTER KLYSTRON

M. Yoshida[#], S. Fukuda, KEK, Ibaraki, Japan
V. E. Teryaev, BINP SB RAS, Novosibirsk, Russia

Abstract

A C-band small multi beam klystron (MBK) has been under development. It is designed for the sub-booster klystron which is required to drive multiple 50 MW C-band klystrons for the SuperKEKB injector upgrade plan. The designed output power is 150 kW in case of the applied voltage of 25 kV which is suitable for the existing pulse modulator for the S-band sub-booster klystron. At this operating condition, the designed micro-perveances of the total and the each beamlet are 2.0 and 0.25 respectively. The design overview will be presented.

MOTIVATION

KEKB attained the highest luminosity of 1.7×10^{34} cm^{-2} s^{-1} in the world. KEKB consists of an 8 GeV electron ring (HER) and a 3.5 GeV positron ring (LER). The KEKB Injector linac [1] has provided 8 GeV electrons and 3.5 GeV positrons to inject those rings directly.

To aim for a ten-times higher luminosity, the SuperKEKB project [2] is under consideration as an upgrade of KEKB. In the SuperKEKB project, energy exchange of beams has an important role to escape the influence of electron clouds for the positron ring (LER). To exchange the beam energy of the LER and the HER, the energy of a positron beam has to be raised from 3.5 GeV to 8 GeV. However the acceleration length after generating positrons is restricted because a positron is a secondary particle. One of solutions is to double an acceleration field. Thus the C-band (5712 MHz) accelerating unit [3] has been developed to obtain the higher acceleration field over 40 MV/m.

A C-band accelerating unit consists of one 50 MW klystron and four accelerating structures. In the present KEKB Injector linac, eight S-band klystrons, which is called as a sector, are driven by one 80 kW sub-booster klystron and its low RF power circuits. In case of the C-band acceleration, one sector consists of 16 accelerating units because a C-band accelerating unit has only half length compared with the present S-band accelerating unit. Thus the C-band sub-booster klystron has to drive 16 high power klystrons. The required output power of the sub-booster klystron becomes 150 kW considering the power loss of the waveguide.

DESIGN OUTLINE

Assuming the lower expected efficiency of 0.8 - 0.2 μP which is obtained from the general experience, the relation between the applied high voltage and the RF output power satisfies the following equation.

$$\mu P\left(0.8 - 0.2\mu P\right) = Pout/\text{Vk}^{2.5} \times 10^{6} \qquad (1)$$

Figure 1 shows the micro perveance (μP) and the expected efficiency versus the applied high voltage in case of the required RF output power (Pout) of 150 kW.
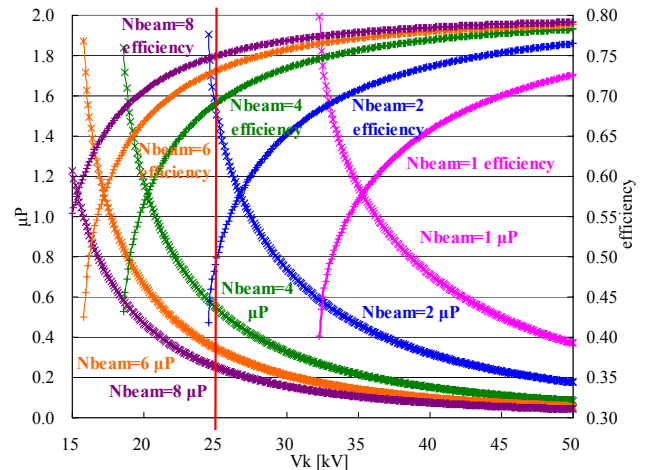
Figure 1: Micro perveance (μP) and Expected efficiency versus the applied high voltage in case of the required RF output power (Pout) of 150 kW.

The existing pulse modulator for the S-band sub-booster klystron is planned to use for the newly developed C-band sub-booster klystron. The operating high voltage (Vk) of the pulse modulator is 25 kV. From figure 1, more than 4 beamlets are required to obtain the RF output power of 150 kW.

Table 1 shows the klystron parameters corresponding to the number of beamlets.

The difficulty to construct the multi-beam klystron is the insertion of some iron plates to make the magnetic field parallel, even though the convergent electron gun is used. To avoid this difficulty, the immersed flow electron gun is chosen. Thus 8 beamlets are chosen for this C-band sub-booster klystron to make the cathode within the limited cathode beam loading (6 A/cm^2).

_____
[#]mitsuhiro.yoshida@kek.jp

COMMISSIONING AND OPERATIONAL EXPERIENCE WITH INDUS-2 RF SYSTEMS

M R Lad[#], M K Badapanda, Pritam Singh Bagduwal, Ashish Bohrey, R.K.Deo, P R Hannurkar, Akhilesh Jain, M K Jain, Narendra Kumar, Ramesh Kumar, Moonuku Prasad, Vikas Rajput D.Sharma, Nitesh Tiwari, R.Tyagi,

Raja Ramanna Centre for Advanced Technology (RRCAT), Indore-452013, India

Abstract

Indus-2 is a 2.5GeV/300mA third generation Synchrotron Radiation Source being commissioned at Raja Ramanna Centre For Advanced Technology, Indore. RF system provides sufficient voltage for boosting electron energy from 550 MeV to 2.5 GeV in addition to compensate for Synchrotron Radiation losses. 505.8 MHz Indus-2 RF systems is in operational state since April 2005. The beam injection into Indus 2 from Booster Synchrotron started in Aug. 2005.First beam accumulation was achieved on Dec.1st, 2005 with injected beam of 450 MeV.The injection energy was subsequently increased to 550 MeV. After achieving beam accumulation at the injection energy, the beam energy was ramped to 2 GeV. So far 38 mA of beam current has been stored at the injection energy and accelerated to 2 GeV at 26 mA.

During First commissioning phase of Indus 2 the RF system was switched on with one RF cavity and then for 2 GeV operation two RF cavities were energized. Modular RF system has been operating satisfactorily during machine operation. The low-level control system has been completely installed with optimization of phase & amplitude loop to the desired stability in progress; the tuning loop was installed in the beginning phase. For the stored beam of 38 mA.at 550 MeV no dangerous HOM frequencies were observed.

INTRODUCTION

Full description of Indus-2 RF system can be found in [1], but briefly it is composed of four numbers of bell shaped elliptical cavities (Fig.1) to generate 1500 kV accelerating RF voltage. 64 kW RF amplifier system powers each RF cavity. Each power plant can run independently of others. The power from Klystron amplifier is transmitted to RF cavity through 6 1/8" co-axial line. Two racks of low level & control electronics are installed for each plant. The RF module comprises of 64 kW klystron amplifier, 20 kV/5A HV power supply, 10 W solid-state driver amplifier, and low-level control. For fine regulation & stabilization of the cavity fields frequency, amplitude and phase loops are installed on each RF station. High precision cavity temperature control system is incorporated to control HOM. Protective equipment's interlock unit act directly to the RF switch, which cuts driving power to RF amplifier chain. The RF system is completely remote controlled from both RF & main control rooms

[#] ladm@cat.ernet.in

Figure 1

OPERATIONAL ASPECTS

RF cavity gap voltage requirement is 75 kV for injection and 375 kV at 2.5 GeV; correspondingly the wasted power on the cavity surfaces is 900 watts and 22 kW respectively. The power transferred to the beam is of the order of 50 kW per cavity at full beam current. Table1 shows the main parameters of Indus-2 RF system.

Initially with injection energy of 450 MeV few thousand turns were achieved without RF.Then the RF system was switched on by the end of Nov.2005.On 1st Dec 2005 first time SR was observed with **RF ON**. Only one RF cavity (Station 4) was switched on at 60 kV gap voltage. Later on injection energy was increased to 550 MeV & beam accumulation was observed in Feb 2006 with only one RF cavity at 60 kV gap voltage. Phase of RF signal was optimized for proper injection. With low beam currents stored the ramping trials were carried out. On 18th may 2006 the beam was ramped to 1.9 GeV at very low currents with only one RF cavity at around 350 KV of gap voltage. At 1.9 GeV the losses to restore were only ones due to bending magnets (no ID used at present) which are 210 keV, the beam power was very low. For these 3 months the machine was operated with RF cavity no.4 only. The cavity resonant frequency was set to 1.5 kHz below the generator frequency to avoid Robinson instability where as the remaining 3 cavities were detuned 100 kHz or more in order to avoid harmful interaction with the beam. The vacuum trip level was set at 10^{-7} mbar. The injection was tried at different gap voltages; at higher gap voltage injection rate was slightly lower.

HIGH-POWER, LOW-LOSS, RADIAL RF POWER DIVIDERS/COMBINERS

Akhilesh Jain, Deepak Kumar Sharma, Alok Kumar Gupta, P. R. Hannurkar
RRCAT, Indore INDIA

Abstract

Development of a 20 kW Solid State Power Amplifier (SSPA), at 352 MHz, is in progress at RRCAT. This design uses radial dividing and combining architecture. As a part of this system, two high power (4 kW) combiners have been designed and developed. First one is 8 way with output ports in opposite but parallel direction to input port. Second one is 16 way with radial output ports. This paper describes design and measured performance of these two structures. Predicted results are in good agreement with those measured results.

INTRODUCTION

With growing interest in high power solid state RF source for particle accelerator [1] [2], design of high Power Divider/Combiner (PDC) structures has received enormous attention. Among different combining approaches, radial combiners proved to be efficient for summing N (>2) amplifiers. The tree structures have simpler design, but they have disadvantage of using multitude of transmission line segments, which add losses. This significantly degrades overall performance, especially for higher N. Radial combiners on other hand, can lead to power combining efficiency over 90% and insertion loss less than 0.5dB. Being in phase structures, their phase and amplitude stability depends upon symmetry, which in turn can be achieved easily with good mechanical design. In this paper, using simplified design methodology, two type of PDCs (8 way and 16 way) have been designed with central feed (1-5/8" rigid line) and peripheral collecting ports (N type connector) structure. With these structures, combined RF power of the order of up to 4 kW can be achieved. Necessary vector and scalar measurements were carried out for testing these designs.

DESIGN

Radial power combiner offers low loss, excellent amplitude and phase balance, with high power handling capability [3]. Unlike corporate combining structures, radial structure permits placement of a large number of ports very close to central feed port, thus minimising combining path and losses. A careful optimisation of physical structure is essential to obtain low insertion loss and good isolation over desired bandwidth. Project design specifications, include 8 way and 16 way PDC with combining efficiency > 90%, 1 dB bandwidth of ± 5 MHz, at center frequency of 352 MHz. As total output power is within 5kW, 1-5/8" EIA flange at output port, has been selected. Similarly at combining port expecting maximum power of 300-400W, N type connectors were selected for these design. Overall design should have insertion loss (other than coupling) less than 0.5 dB between desired coupled ports.

Combiner/Divider model

Proposed combiner/divider structure consists of three parts: the launcher, combining path and N way peripheral ports (Fig. 1). The launcher is coaxial line, feeding radial transmission line. The combining path (the radial line) is a low loss parallel plate stripline type transmission structure, with a central point excitation. From central excitation, energy spreads uniformly outward in the dominant E mode with an axial electric field component. It is important to maintain mechanical stability in feeding power symmetrical in order to prevent propagation of higher order modes. Feed symmetry governs insertion loss and phase imbalance. Last part is N way peripheral port (usually 50 ohm) section, connected to circular combing path. Design methodology of complete structure is stated step by step in terms of these three parts.
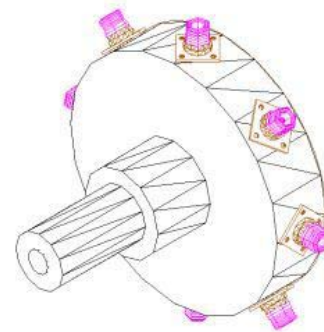
Figure 1: Radial combiner/divider structure

Designing Feed section

A 50 ohm input coaxial feed line is connected to radial line. In between these two lines, comes impedance matching section, realised in the form of coaxial lines having different characteristic impedance. Characteristic impedance of radial line is similar in nature to that of a TEM transmission line [4]. Hence, at feed point each dividing port can be thought as parallel connection of transformed impedance of port termination values. Transformation ratio can be deduced from formula for characteristic impedance of radial line. Problem is significantly complicated by the existence of complex characteristic impedance with spatial dependence, as well Bessel function arguments associated with radial line parameters. However, to simplify design, impedance of radial line at feed point can be assumed that of equivalent resistance of N port connected in parallel.

Using this formula we get approximate real value of radial line impedance, terminated by matched boundary at discrete ports. Coaxial impedance matching sections can be designed with this value for matching it to 50 ohms feed port. This initial step gives us idea for the design of coaxial sections. To improve this approximation and to

HIGH POWER MICROWAVE GENERATION FROM COAXIAL VIRTUAL CATHODE OSCILLATOR

A. Roy, J.Mondal, R. Menon, S. Mitra, D. D. P. Kumar, A. Sharma, K. C. Mittal
Accelerator and Pulse Power Division, BARC, Mumbai, INDIA

Abstract

A coaxial virtual cathode oscillator (VIRCATOR) has been designed to generate Relativistic Electron Beams and High Power Microwaves. Coaxial virtual cathode oscillators are known for better efficiency compared to the axial virtual cathode oscillators. This Coaxial VIRCATOR has been designed for the KALI-5000 (*1MeV, 60kA, 100 ns*) pulse power system. Provision for a large anode cathode gap has been kept to avoid the prepulse effect during the electron beam generation from the KALI-5000 system. Experimental studies are carried out to generate and characterize Relativistic Electron Beams and High Power Microwaves. Relativistic Electron Beams are generated by the Coaxial Explosively emitted graphite cathodes. Electron beam voltage has been measured by a copper sulphate voltage divider and beam current by a B-dot probe. High Power Microwaves are detected by the glow of neon lamps placed closed to the output window.

INTRODUCTION

Virtual Cathode Oscillators [1, 2] consist of an electron-beam diode and a waveguide. The electron beam is accelerated in the axial or coaxial direction and is injected into the waveguide. Electron beam is accelerated in the diode gap where pulsed high voltage is applied between the anode and the cathode. The beam passes through the anode, which is usually a thin foil or a mesh, and is injected into the area on the other side of the anode.

In the Vircator device the beam front forms a virtual cathode at a distance equal to the Anode Cathode (AK) gap if the injected current is greater than the space charge limiting current, I_l given by (for axial vircator)

$$I_l = \frac{4\pi\varepsilon_o m_o c^3 (\gamma^{2/3} - 1)^{3/2}}{e[1 + 2\ln(R/r_b)]}$$ (1)

Where r_b is the beam radius and R is the drift column radius, (γ is the relativistic factor, and e and m_o are electron charge and rest mass respectively.

The virtual cathode reflects the electrons that follow the beam front. Thus electrons oscillate between the cathode and virtual cathode and cause microwave emission. The reflexing frequency is given by [3, 4]

$$f_r = \frac{v}{4d}$$ (2)

where v is the velocity of the electrons.

The virtual cathode also emits radiation around the beam plasma frequency. The frequency at which maximum power emitted is given by [3, 4]

$$f_{vc} = 10.0 \left(\frac{J}{\beta\gamma}\right)^{1/2}$$ (3)

where J is the current density expressed in kA/cm^2. Schematic of Coaxial Vircator is shown in Figure 1, it has a coaxial pair of cathode and anode that injects the electron beam radially into the circular waveguide. The interaction is between the electron beam current and the radial electric field of the waveguide mode.

COAXIAL DIODE DESIGN

Space charge limited current in a coaxial diode is given by [5],

$$j = \frac{4 \in_o}{9} \left(\frac{2e}{m_e}\right)^{1/2} \frac{V^{3/2}}{d^{1/2} r_c^{3/2}} \left[\frac{1}{\ln\left(\frac{r_c}{r_a}\right)}\right]^{3/2}$$ (4)

Coaxial diode impedance is given by

$$Z_d = \frac{68307}{V^{1/2}} \frac{(dr_c)^{1/2}}{h} \left[\ln\left(\frac{r_c}{r_a}\right)\right]^{3/2} \Omega$$ (5)
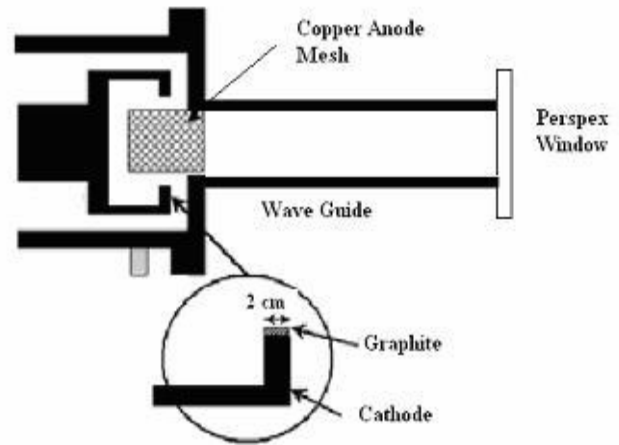
Figure 1: Schematic of Coaxial Vircator.

DEVELOPMENT OF 35 KW POWER AMPLIFIER AT 350 MHZ FOR RFQ BASED NEUTRON GENERATOR

Manjiri Pande, Atul Soni, Niranjan Patel, K.R.shinde, M.K.V.Rao, V.K.Handu
Vacuum Physics and Instrumentation Division,
Bhabha Atomic Research Centre, Mumbai-400085, India

INTRODUCTION

A 400 KeV, 1 mA (deuterium ion) radio frequency quadrupole (RFQ) based 14 MeV Neutron generator [1] is being developed in BARC to study physics of coupled neutron sources, sub-critical assembly and radio frequency (RF) coupling to accelerator. RFQ will accelerate the deuterium ion beam from 50 KeV to 400 KeV which will impinge upon a tritium target inside a sub-critical assembly to generate 14 MeV neutrons. Two RF systems of power around 35 KW each, are under development to feed the RF power at two ports of the RFQ. This paper describes the system design aspects, operating conditions and current status of the RF power system.

RF SYSTEM DESCRIPTION

Each 35 kW amplifier is a three-stage amplifier chain, comprising of a 100 W solid-state driver, a triode based intermediate power amplifier (IPA) of 1.5 kW and a tetrode based high power amplifier (HPA). Auxiliary power supplies, forced air/water cooling circuits and circulators are part of the associated electronics.

Driver

The solid-state driver [2] requires a maximum input of 20 dBm and provides up to 100W of power. It is coupled to Intermediate Power Amplifier (IPA) via a Y-junction circulator. The IPA uses EIMAC 8938 coaxial base triode. It is configured in cathode driven i.e. in grounded grid mode. Its input matching circuit uses 'L' type circuit using lumped components, output matching circuit uses a single ended half wave-length strip line (Fig. 1), capacitively loaded by the tuning capacitor at one end and by the tube output capacitance at the other end. This plate line is a short transmission line with characteristic impedance of 53 Ω. The triode is operated at an anode dc voltage between 1.5 kV to 3 kV by means of a variable 4 kV power supply.

Table 1: Test results of IPA at various frequencies.

Frequency (MHz)	Output power (W)	Efficiency (%)	Gain (dB)
343	500	25	8.3
350	200	12	4.0
368.8	740	34.3	10.2
368.8	420	60	7.25

A 47-Ω/50 W series resistance is inserted between the power supply and anode to dissipate energy in case of internal tube arc. Operating bias is established using 15 V zener. The test results of IPA are summarized in table 1. Efforts are being made to increase the rated output with better efficiency. Simultaneously a coaxial cavity based configuration for 8938 is being tried. Its design and simulation work is in progress.
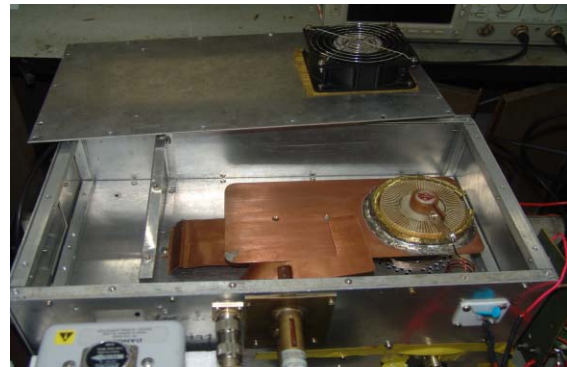
Figure 1: Intermediate Power Amplifier (IPA).

THE HIGH POWER AMPLIFIER (HPA)

DC Power Supplies

The HPA is powered by a variable 12 kV/10 A EHT supply (Fig. 2) and associated control grid and screen grid power supplies. EHT uses a 3 Phase, 6 Pulse thyristor based ac regulator on the primary low voltage (LV) side. The controlled output voltage is stepped up and rectified in a transformer unit. Suitable L-C filter is incorporated to keep output ripple within the desired limit of 1%. The power supply has been installed and tested at full load for a voltage regulation of 1%. Various protection circuits like over-voltage, over current, under voltage, phase failure, thermal overload, oil temperature sensor and its protection, spark/arc protection have been incorporated in this power supply. Various fault conditions were simulated in this power supply and all above-mentioned protection features were checked. Many LED indication features are provided in the front panel for quick detection and rectification of any fault condition. These include phase failure/phase reversal; fuse fail trip, thermal overload, oil temperature indicator, under voltage trip, over-volt trip, SCR over-volt, etc. A well regulated dc supply for screen grid (800 V / 500 mA) and control grid (-300 V/500 mA) has been bench tested and installed.

LINEAR ACCELERATOR DESIGNS FOR THE UPGRADE OF THE CERN PROTON INJECTOR COMPLEX (LINAC4, SPL)

M. Vretenar, G. Bellodi, R. Garoby, F. Gerigk, K. Hanke, A. M. Lombardi, S. Maury, M. Pasini, C. Rossi, E.Z. Sargsyan, CERN, Geneva, Switzerland

Abstract

Looking beyond the commissioning of the LHC, which is expected to start at the end of 2007, CERN is setting up its scientific plan for the years to come. The concerns about the reliability of the old LHC injectors and the need to progressively remove the technical bottlenecks towards higher luminosity in the LHC have initiated a reflection on the design of the main elements of the LHC injection chain.

A plan under consideration foresees in the years 2007-2010 the construction of a 160 MeV H$^-$ linear accelerator, Linac4, injecting into the old 1.4 GeV PS Booster (PSB). In a second stage, the PSB could be replaced by a superconducting linac, the SPL, at an energy between 3.5 and 5 GeV. The Proton Synchrotron (PS) would be in turn replaced by a new PS2 reaching a higher energy of 50 GeV. Linac4 and SPL can operate at a higher duty cycle than needed for LHC injection, allowing functioning as a high-intensity facility for neutrino or radioactive ion physics at a later stage.

This paper describes the design of the two linear accelerators involved in this upgrade strategy, Linac4 and SPL, and outlines some results of the R&D programme aimed at preparing the construction of Linac4.

INTRODUCTION

The present LHC injection chain (Fig. 1) consists of a 50 MeV proton linear accelerator (Linac2), followed by the 1.4 GeV PS Booster (PSB), the 26 GeV Proton Synchrotron (PS), and finally by the 450 GeV Super Proton Synchrotron (SPS), which injects into the LHC. While Linac2, PSB and SPS have been commissioned between 1972 and 1978, the first PS beam dates back to 1959.

The injection chain has been upgraded and partly modified in the years 1995-2000 [1] in preparation for the LHC. Beam tests following this upgrade have demonstrated that the nominal LHC beam can be provided at injection in the LHC. However, it is now clear that attaining and possibly exceeding the LHC ultimate luminosity of 2.3×10^{34} cm^{-2}s^{-1} will require higher beam brightness (intensity/emittance) from the injector chain, which can only be obtained after a major upgrade of the injectors. Moreover, all of the scenarios that are currently being detailed for possible LHC upgrades [2] rest on the renovation of the present injection chain.
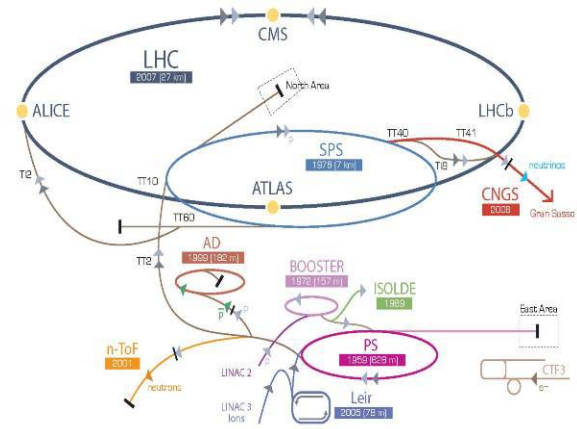
Figure 1: Scheme of the CERN Accelerator Complex

Another motivation for the reconstruction of the injectors concerns operational reliability of the present machines. The correct functioning of all the elements in the injection chain is essential for achieving the required LHC integrated luminosity. However, the past few years have shown recurrent reliability problems: radiation damage on the PS magnets, water leaks in the SPS magnets, failures of the PS main power supply, vacuum problems in the Linac2 tanks. An urgent consolidation programme has been launched, aimed at solving the most immediate problems to ensure a correct start-up and operation of LHC during its first years, but it is clear that some of the foreseen repairs are only temporary fixes and that more problems can be expected in the future.

A third argument for reconsidering the CERN injectors concerns possible future requirements for higher beam intensity from the CERN machines. For some of the presently planned experiments requiring intense secondary beams, ISOLDE for radioactive ion beam (RIB) physics and CNGS for neutrino physics, proton flux from the CERN machines is already at its limits, while both the neutrino and radioactive ion communities have presented ambitious long-term plans [3,4], which if approved would require significantly higher intensities from the CERN machines. Considering the relatively low beam energies required by these applications (~1 GeV for RIB, 5 to 10 GeV for neutrino production from pion decay), it appears attractive a scheme where the low energy accelerators in the new LHC injection chain are capable of a higher average beam current than what needed for the LHC, compatibly with the requirements of other physics experiments.

CONSTRUCTION AND COMMISSIONING OF THE HIRFL-CSR*

J.W. Xia[#], W.L. Zhan, Y.J. Yuan, Y. Liu, X.D. Yang, Y. He, J. C. Yang and CSR group
Institute of Modern Physics (IMP), Chinese Academy of Sciences (CAS)
P.O. Box 31, Lanzhou, 730000, P.R. China

Abstract

CSR is a new ion cooler-storage-ring system in China IMP, it consists of a main ring (CSRm) and an experimental ring (CSRe). The two existing cyclotrons SFC (K=69) and SSC (K=450) of the Heavy Ion Research Facility in Lanzhou (HIRFL) will be used as its injector system. The heavy ion beams from HIRFL will be first injected into CSRm, accompanying with the accumulation, e-cooling and acceleration, finally extracted to CSRe for many internal-target experiments. In 2005 the main construction of the CSR project was finished, and from that the preliminary commissioning of CSRm was started, including the first turn commissioning as a beam line, the stripping injection, and the zero-bumping orbit test, fixed-bumping orbit test with four in-dipole coils, bumping orbit test, C-beam accumulation and the investigation of the closed orbit with BPM. And now the correction of closed orbit, e-cooling and ramping test are just on going.

INTRODUCTION

From 1996 to 1998, a new ion accelerator plan was proposed [1] to upgrade the HIRFL with a multi-functional Cooling Storage Ring (CSR) forming an HIRFL-CSR accelerator system shown in Fig. 1. This will greatly enhance the performances of IMP for those researches by using Radioactive Ion Beams (RIB) and high-Z heavy ion beams in the fields of nuclear physics and atomic physics. In July of 1998 the Chinese center government approved this proposal, and at December 10 of 1999 the CSR project was started. The period from the beginning of 2000 to the summer of 2001 was the stage of the building construction, design optimization and prototype experiments. The machine fabrication was from 2001 to 2003, and the past two years of 2004 and 2005 were used for the machine installation and subsystem tests. The period from 2006 to 2007 will be the initial commissioning stage.

PROJECT DESCRIPTIONS

Outline

CSR is a double cooling-storage-ring system with a main ring (CSRm), an experimental ring (CSRe), and a radioactive beam line (RIBLL2) to connect the two rings, shown in Fig.1. The heavy ion beams with the energy range of 7~25 MeV/u from the cyclotron SFC or the cyclotron complex SFC+SSC will be accumulated, cooled and accelerated to the high-energy range of

100~500 MeV/u in the main ring CSRm, and then extracted fast to produce radioactive ion beams (RIBs) or highly charged heavy ions (high-Z beams). Those secondary beams will be accepted and stored or decelerated by the experimental ring CSRe for many internal-target experiments or high precision spectroscopy with beam cooling. On the other hand, the beams with the energy range of 100~1000MeV/u will also be extracted from CSRm by using slow extraction or fast extraction for many external-target experiments, and for the future development, the possibility of internal-target mode in CSRm was reserved for those high-energy proton experiments with the energy range of 2~2.8GeV.

Two electron coolers located in the long straight sections of CSRm and CSRe, respectively, will be used for beam accumulation and cooling.

The beam parameters and the major machine parameters of CSR are listed in table 1.
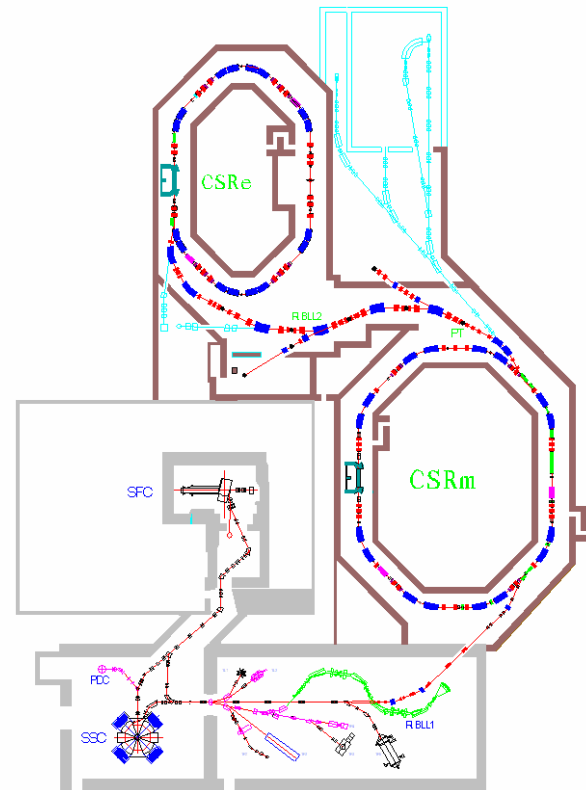
Figure 1: Overall layout of HIRFL-CSR.

Normal Operation Mode

CSR is a double ring system. The accumulation duration of CSRm is about 10s. Considering the ramping rate of magnetic field in the dipole magnets to be

---

KICKERS FOR INJECTION AND EXTRACTION IN DAMPING, COMBINER AND STORAGE RINGS

F. Marcellini, LNF-INFN, Frascati, Italy

Abstract

Injection and extraction kickers play a fundamental role in all the projects of new major accelerators at present under study. The feasibility of these accelerators depends also on the possibility to realize kickers based on unconventional design and new technologies. This paper describes the R&D carried out at LNF on two different types of deflecting devices. The first are the kickers for the Damping Ring (DR) of the International Linear Collider (ILC) and the Storage Rings (SR) of colliders like DAFNE. They require very low impedance, good field uniformity in a wide region around the beam axis and very short pulse duration for limiting the length and consequently the cost of the DR and for reducing the perturbation of the stored bunches in SRs. The tests made on stripline prototypes, fast high voltage pulsers and vacuum feedthroughs are presented. The second are the RF kickers for the CLIC Test Facility 3 (CTF3) for which an original SW structure has been designed and realized for the Delay Loop (DL) while a more conventional TW deflector allows the multiplication of bunch current and frequency in the Combiner Ring (CR). Results of their performances are described.

INTRODUCTION

An activity concerning the study, the design and the realization of devices for deflecting the trajectory of beams that must be extracted and/or injected in circular machines has been recently carried out at LNF.

The devices developed are different for typology and application and the motivations of the different choices are described in the following sections.

RF deflectors has been chosen in the two rings used for the bunch frequency multiplication in CTF3 [1][2]. In particular the RF deflector of the CR is a 10+2 cells TW structure operating in the TM_{11}, $2/3\pi$ mode [3][4], while the deflector for the DL is a system composed of a hybrid junction (HJ) coupler and two SW cavities which resonate in the TM_{110} deflecting mode [5][6]. The main differences between TW and SW RF deflectors are reported in Table I. All this characteristics are consequence of the different bandwidth between the two types of devices.

The possibility of using TW RF deflectors also for the DR of the ILC [7] has been investigated [8][9]. To get significant factors of bunch recombination in the DR, which means significant reduction of the DR circumference, groups of deflectors powered in multi-frequency mode are necessary.

However, an alternative solution looks now possible thanks to recent developments of new technologies in the field of high voltage (HV) pulse generators. The characteristics of the pulse (amplitude up to tens of kV, rise time from 100 ps to 1ns, pulse width from 5 ns to 50ns and repetition frequency up to hundreds of kHz) seem promising for the use of these fast pulsers to feed the kickers in the DR, where the bunch spacing must be strongly reduced.

Table 1: Comparison between TW and SW RF deflectors

main features	SW	TW
efficiency per unit length (deflection vs RF power)	high	low
filling time	proportional to the quality factor: generally slow.	~ to the group velocity and structure length: generally fast
deflecting field vs. n (# of cells)	scales as $\sqrt{n}$	scales as $n\left(1 - e^{-\alpha n}\right)$ with α=attenuation
maximum number of cells	the maximum number of cells is limited because of mode overlapping	in principle there are no limitations to the number of cells.
temperature sensitivity	automatic tuning system or precise temperature stabilization	less temperature sensitivity.

People from several different laboratories are working on the design of stripline electrode kickers or on development of fast HV pulsers [10].

At LNF we have studied this solution for the upgrade of the DAFNE injection system. A special stripline kicker has been designed and its realization is in progress[11]. This activity is also a valid R&D of the injection and extraction kicker for the ILC Damping Ring.

THE CTF3 DELAY LOOP DEFLECTOR

The RF deflector allows the bunch frequency doubling process that takes place in the DL. Referring to the scheme illustrated in Fig. 1, the beam coming from linac is composed of an alternate sequence of so called even
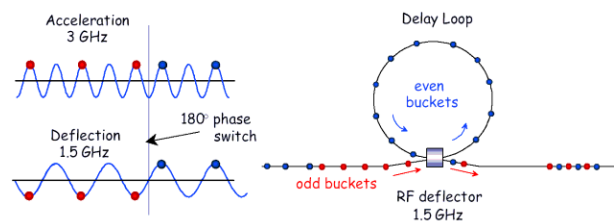
Figure 1: The bunch frequency multiplication scheme in the CTF3 Delay Loop.

and odd trains, which differ for a 180° phase jump between each other. This sequence of 140ns long sub-trains is realized by a pre-bunching system. The RF deflector gives kicks of the same amplitude but opposite

PROGRESS IN UNDERSTANDING THE HIGH-GRADIENT LIMITATIONS OF ACCELERATING STRUCTURES

W. Wuensch, CERN, Geneva, Switzerland.

Abstract

CLIC main linac accelerating structures have an extremely demanding high-gradient requirement and an intensive research and development program to raise the achievable gradient is under way. The current understanding of the effects which both limit the ultimate accelerating gradient and fix the practical operating gradient is presented.

INTRODUCTION

One of the main objectives of the CLIC study is to demonstrate that an accelerating gradient of 100 MV/m or higher is feasible using realistic accelerating structures under practical operating conditions. There are two main effects which limit achievable accelerating gradient: rf breakdown and fatigue cracking due to pulsed surface heating. This report considers mainly the limit due to rf breakdown which is currently the most severe. Dark current capture may also become a limitation in a high-gradient accelerator.

There are a number of issues which define 'realistic' which are quite specific to accelerating structures for linear colliders. One issue is that the structures must produce an rf to accelerated-beam efficiency as high as possible since this is one of the key efficiencies which define the overall efficiency of a linear collider complex and the power capacity which must installed. Another issue is that the beam aperture be sufficiently large so that the beam emittance growth driven by short-range wakefields be limited to acceptable values. Yet another is that the accelerating structures must contain features which suppress long-range wakefields so that bunch-to-bunch driven instabilities do not create relative offsets which give a train emittance growth. These efficiencies and emittance growths can all be determined from the geometry of the accelerating structures through electromagnetic and beam dynamic simulations. On the other hand, the achievable gradient is strongly affected by the geometry and this dependence is only approximately known. This creates one of the principle complications in optimizing and demonstrating the feasibility of a linear collider design.

One of the most important aspects of the 'practical' operating conditions is that the breakdown probability of the individual accelerating structures must be of the order of 10^{-6} to 10^{-7}. Breakdowns in the accelerating structures induce random kicks on the beam which can lead to either emittance growth or even loss of the beam if the kick is large enough. The acceptable breakdown probability is a function of the emittance loss caused by an individual kick, the number of structures in the linear collider (in the range of tens of thousands) and the acceptable emittance loss budgeted for this effect. After conditioning to certain gradient, accelerating structures become more stable as the gradient is reduced. The breakdown probability falls exponentially with gradient but many tens of percent are typically required to make the structures sufficiently stable. The cause of the breakdown rate and its dependence on field is not well understood, but initial ideas are presented below. Other aspects of practical operating conditions include: sufficiently fast rf (surface and heat treatments during production are being studied to reduce this time to a minimum or even to eliminate it) conditioning, acceptable surface modification caused by the conditioning process and the accumulated number of breakdowns over the lifetime of the linear collider and a vacuum level inside the structure during the rf pulse which is sufficiently low. All of these conditions depend on the length of the rf pulse and a longer pulse is worse for all of them. However the rf pulse length also influences the rf to beam efficiency mentioned in the previous paragraph where for this the longer pulse is better,

This objective of this report is to elaborate on the some of the effects which have been mentioned in this introduction to give the reader an idea, and the motivation, of the areas which are being pursued by the CLIC accelerating structure development program.

THE EFFECT OF SRUCTURE GEOMETRY

Very generally it has been observed that different accelerating structure designs result in a different accelerating gradient potential, all other parameters such as material, preparation and conditioning strategy being equal – although there are statistical variations between structures. The aspects of the structure design which appear to be relevant for the high gradient performance include the transition region between the input (and output) waveguide and the periodic part of the structure, the periodic part of the structure itself and its profile and the geometry of damping features. With modern three-dimensional electromagnetic field solving programs, the complete fields patterns and functions of the fields, including electric and magnetic fields, local power flow group velocity, energy density, of the structures can be determined.

What is less clear, however, is exactly how the gradient depends on these quantities, or indeed if the gradient can even be determined from the field pattern calculated without considering the fields perturbed by the currents and plasmas that are known to form during a breakdown. In fact, it appears that a fairly accurate prediction of gradient can be determined from the unperturbed fields.

The accelerating gradient limit for traveling-wave accelerating structures has been observed to depend on

COMMISSIONING EXPERIENCE OF SUPERCONDUCTING RADIO FREQUENCY SYSTEMS FOR THE TAIWAN LIGHT SOURCE

Ch. Wang[#], L.H. Chang, M.C. Lin, M.S. Yeh, F. Z. Hsiao, F.T. Chung, T.T. Yang, S.S. Chang, M.H. Tsai, M.H. Chang, Y.H. Lin

National Synchrotron Radiation Research Centre, Hsinchu 30076, Taiwan

Abstract

An industrially manufactured SRF module of CESR type has been routinely operated at the Taiwan Light Source (TLS) in the National Synchrotron Radiation Research Centre (NSRRC) since 2005 early March. The original goals of doubling the electron beam current to increase the intensity of synchrotron light and to eliminate the instability caused by the interaction of electron beams with higher-order modes of the cavity have been successfully demonstrated. We report here our operational experience over the past two years of the SRF module at TLS at a large beam current toward a maximum beam current 400 mA (300 mA in routine operation) in top-up mode from originally 200 mA in decay mode. Together with digital feedback systems, fluctuations of the synchrotron light intensity (I_0) are less than 0.1 % for more than 95 % of user beam time on the average. We emphasize the diagnostic analysis of SRF trip events and the continuous improvements of the operational analogue low-level RF system against instability caused by heavy beam loading. The greatest challenge to the operational reliability, which is the brevity of the mean time between failures (MTBF), has been successfully overcome; a mean time between failures of the complete RF system of the TLS storage ring more than 200 hr has been demonstrated.

SRF PROJECT AT NSRRC

Since the successful commissioning of the TLS storage ring in 1993, the electron beam has suffered from strong coupled-bunch instabilities caused mainly by two existing room-temperature RF cavities designed in the 1970s. To improve significantly the electron beam stability, many attempts have been made, including the improvement of the cavity cooling water system, replacement of the cavity's damping antenna with a higher-order mode (HOM) tuner, and the application of an RF modulation technique. Various efforts to increase the photon flux and brightness have also been undertaken, but only a limited improvement was achieved. In 1999, a major accelerator upgrade project [1] was initiated with the objectives to double the TLS photon flux by increasing the electron beam current to 500 mA and to improve substantially the stability of the electron beam by replacing the two existing room-temperature cavities with one SRF module most recently developed of CESR-III design. Figure 1 shows the schematic drawing of the SRF module. The

#rfwang@nsrrc.org.tw
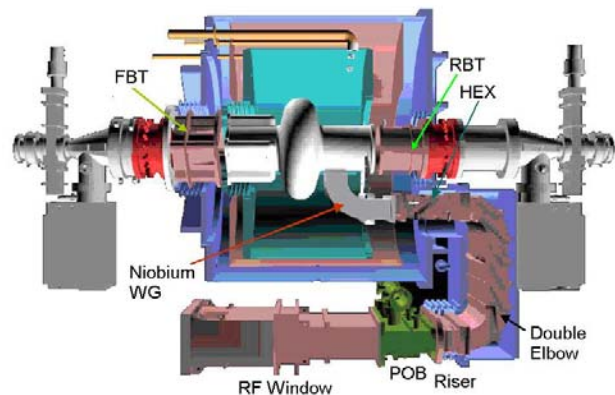
Figure 1: A schematic plot of the SRF module at TLS/NSRRC.

fabrication of the SRF modules was contracted to ACCEL after NSRRC arranged a technical transfer from Cornell University. Various difficulties were encountered during the production. Major faults were the buckling of the niobium waveguide during a warm high-pressure cryogenic safety test and the cracking of the RF ceramic window during high-power RF processing. The delivery of the repaired SRF module (named as S2) was again interrupted by an unexpected quenching at an extremely small field gradient due to indium contamination. An acceptable field gradient was radically achieved after an indium piece was removed from the cavity bottom.

A cryogenic plant has been built and installed by Air Liquide to support the operation of the SRF, according to NSRRC specifications and configurations. The final performance fulfils most design objectives and requirements for SRF operation at synchrotron light sources. These include (a) the capability of long-term continuous operation using a turbine cold box instead of a piston cold box, (b) isolating mechanical vibrations from the helium compressor by locating it remotely from the storage ring, (c) minimizing the two-phase mixture of the liquid helium supply and the diminution of return pressure drop of helium on locating the cold box near the SRF module, (d) convenience of operation on exploiting fully automatic control, (e) a large redundancy of helium cooling capacity by a safety factor 1.5, (f) a large redundancy of inventory of helium gas capable of sustaining once the loss of all helium in the SRF module, (g) capability of rapid cooling with the aid of a 2000-L main dewar, and (h) cryogenic load matching with a frequency driver in various operational modes to save electric power.

DEVELOPMENT OF QUARTER WAVE RESONATORS

Amit Roy

Inter University Accelerator Centre, Aruna Asaf Ali Marg

P.O.Box 10502, New Delhi - 110 067, India

Abstract

The accelerating structure for the superconducting linac booster for the 15 UD Pelletron at IUAC is a Nb QWR cavity, designed and fabricated as a joint collaboration between IUAC and ANL, USA.   Initial cavities required for the first linac module were fabricated at ANL. For fabrication of cavities required for future modules a Superconducting Resonator Fabrication Facility has been set up at IUAC. Three quarter wave resonator (QWR) cavities have been fabricated and fifteen more resonators for the second and third linac modules are in advanced stage of completion. This facility has allowed us to undertake repairs on some of the resonators which sprung leaks. First experiment with the accelerated Si beam through the first linac module having eight resonators along with a superconducting solenoid have been conducted recently.

INTRODUCTION

The Pelletron accelerator at IUAC is capable of accelerating ions having mass up to 40 amu above Coulomb barrier. To augment the beam energy above Coulomb barrier for mass up to 100 amu, a booster Superconducting Linear Accelerator structure is being installed[1]. The first Linac module consisting of eight Niobium Quarter Wave Resonators (QWR) optimized for IUAC Pelletron and a solenoid as focussing device, has been installed at IUAC. The QWR was designed and fabricated as a joint collaboration between IUAC and Argonne National Laboratory (ANL), USA[2]. The other elements of the Linac which have been installed are a superbuncher (SB) cryostat consisting of a single QWR and a rebuncher cryostat consisting of two QWRs.

A Multiharmonic Buncher has been installed and tested as the pre-buncher before the Pelletron. The bunch width delivered by this buncher is ~ 1-2 ns[3]. One superconducting QWR cavity has been installed after the Pelletron and operated as the Superbuncher delivering <150 ps pulsed beams for injection into one Linac module with eight resonators. Cryogenics facilities consisting of a 600 W liquid helium plant, LN2 plant, several large cryostats to house the cavities are fully functional and the cryogen distribution lines have been installed to supply cryogen to superbuncher and superconducting linear accelerator modules[4]. The cavity resonators for the 2nd and 3rd modules are being fabricated in house and a full fledged superconducting resonator fabrication facility has been established consisting of Electron Beam Welding machine, High Vacuum furnace and a Surface Preparation Laboratory. Major effort has been expended also in areas of beam transport and rf electronics required to operate this linac. Most of the required hardware has been built indigenously.

QUARTER WAVE CAVITY RESONATOR

The Quarter Wave resonator is a coaxial structure operating in the TEM mode with beam accelerating gaps in a direction perpendicular to the symmetry axis. The central conductor is shaped with two different diameters to reduce the effective length of the cavity by capacitive loading. This helps in reducing the frequency jitter and thus in the control of the cavity. The resonator is formed entirely of niobium and is closely jacketed in a vessel of stainless steel which contains the liquid helium. A small amount of niobium-stainless steel bonded composite material is used to provide welding transitions where beam and coupling ports penetrate the stainless steel jacket. A novel pneumatic slow tuner in the form of a niobium bellow provides a tuning range of approximately 100 kHz, substantially larger than in any working quarter wave resonators. A picture of completed QWR along with the Nb slow tuner bellows is given in figure 1.

Figure 1: Indigenously built niobium quarter wave resonator with slow tuner bellows at IUAC.

The pnematic drive for the slow tuner bellows has been further modified with the experience of running the cavities in the linac cryostat.

The prototype QWR and twelve more resonators were fabricated in ANL and out of these, 8 resonators are used in the first linac module. In the off-line tests, all the resonators have exceeded the minimum design goal of 3 MV/m with 4 watts of input power. The best performance achieved was 5.0 MV/m at 4 watts of input power. In the on-line tests the performance has been slightly worse compared to the off-line tests, but the field levels exceeded 3 MV/m at 4 W.

In order to fabricate the resonators in house, a Superconducting Resonator Fabrication Facility (SuRFF)

LOW-LEVEL RF CONTROL SYSTEM DESIGN AND ARCHITECTURE*

Lawrence Doolittle†, LBNL, Berkeley, California

Abstract

Low-level RF (LLRF) control hardware and its embedded programming plays a pivotal role in the performance of an accelerator. Modern designs implement most of the signal processing in the digital domain. This reduces the size and cost of the hardware, but places the burden of proper operation on the programming. FPGAs (field programmable gate arrays) and communications-grade ADCs and DACs enable sub-microsecond delay for the LLRF controller feedback signal. Ancient concepts of the virtue of simplicity are easy to apply to the hardware, but more of a challenge in the context of programming. Digital signal processing, combined with dedicated hardware, can control and maintain cavity phase (relative to an absolute reference) unaffected by drift or $1/f$ noise of any long cables or active components. Developing and testing that programming is a very real challenge. This paper discusses approaches and techniques to make LLRF systems meet their goals in upcoming accelerators.

INTRODUCTION AND THEORY
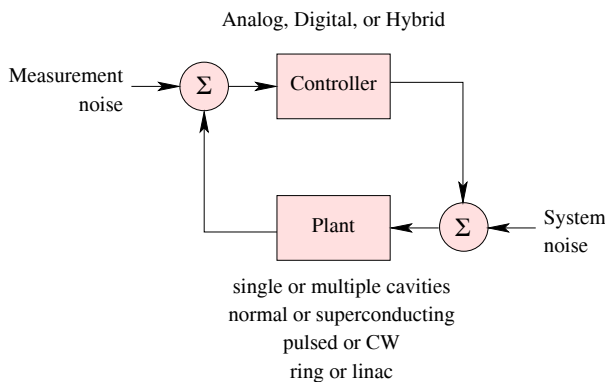
Figure 1: Textbook feedback topology.

At their simplest, modern LLRF control systems can be considered a combination op-amp and digital storage oscilloscope, with some additional built-in computational ability. An understanding of basic control theory, as diagrammed in figure 1, forms the starting point for a discussion of the signal processing needed to control cavity fields.

The feedback system is best understood in the rotating frame of the cavity resonance, so all signals are complex numbers. Cavity bandwidths can vary from 50 Hz to 1 MHz, although direct the direct feedback described here is only useful for cavity bandwidths up to 50 kHz.

While any pulsed machine can use pulse to pulse feedback (also known as adaptive feedback), the shortest pulse machines (e.g., SLAC-style linacs) only permit pulse-to-pulse feedback. These are the machines with cavity bandwidths greater than 50 kHz.

The dominant limitation on feedback gain is the delay around the feedback loop, usually dominated by the controller, cables, and waveguides. 1 μs delay limits the gain-bandwidth product to about 100 kHz. A zero in the control system gain can cancel the cavity pole, giving a pure integrator (plus delay) feedback system response.

Narrow band (e.g., superconducting) cavities could sustain a broadband (up to 5 MHz) gain of up to 70 dB within that plan, but that is not practical: too much noise would be sent to Klystron. Figure 2 shows a set of plausible controller gain curves that limit the noise output of the controller, keeping proper phase margins and the basic pole-zero cancellation response.

Figure 2: Frequency domain strategy for closing feedback loop.

For any given application, this control loop has to be thoroughly analyzed and/or simulated to understand its behavior under the stresses of

- beam loading
- ring dynamics
- microphonics
- ponderomotive tuning
- klystron nonlinearity

DESIGN OF THE PEFP LOW BETA CRYOMODULE*

Sun An[#], Y. S. Cho and B. H. Choi
PEFP, KAERI, Daejeon 305-353, Korea

Abstract

A low beta elliptical superconducting RF cavity has been designed for the linac of Proton Engineering Frontier Project (PEFP). A double stiffening-ring structure is used to reduce Lorentz force detuning of the low beta cavity. Higher order mode (HOM) analysis has shown, for the low beta cavities, the HOM coupler's Q_{ext} needs to be lower than 3×10^5 for reducing the influence of the dangerous modes on the beam instabilities and HOM-induced power. A coaxial coupler is designed for PEFP cryomodules. The cooling system and the magnetic shielding structures shaped by two coaxial cylinders for the low beta cryomodules are described.

INTRODUCTION

Superconducting RF (SRF) cavity is considered to accelerate a proton beam with repetition rate of 60 Hz at 700 MHz in the PEFP Linac being built at Gyeongju in Korea [1, 2]. The first section of the SRF linac is composed of the low beta cryomodules with three 5-cell elliptical cavities of β_g=0.42, and will accelerate a proton beam from 80 MeV to 178.6 MeV [3].

Generally, the low beta cavities have stronger Lorentz force detuning than the high beta cavities. For pulse SRF accelerators, the Lorentz force detuning is a more serious issue than that for CW accelerators. The PEFP low beta SRF cavity is the lowest beta elliptical cavity operating at pulse mode so far. The Lorentz force detuning control of the PEFP low beta cavity is a big challenge in the cavity design [4].

Although the TTF HOM coupler has been used on many cavities successfully, there are two faults: notch frequency shift and feed-through tip melting of the capacitive coupling, which have been found during SNS cavity VTA, cryomodule testing at JLab and the SNS commissioning at ORNL. In order to satisfy PEFP HOM damping requirements, easily control the notch frequency shift and avoid the feed-through tip melting, a new HOM coupler is needed to design.

In this paper, the low beta cavity design, the HOM analysis of the PEFP low beta linac, the HOM coupler design, the cooling system and magnetic shielding of the PEFP low beta cryomodule have been introduced.

RF CAVITY DESIGN

Cavity design

Considering the cavity field sensitivity and the cavity production difficulty, we chose 5 as the PEFP low beta cavity's cell number, 6 degree as the wall angle α of

internal cell, and 4220 as the field sensitivity that corresponds to the cell-to-cell coupling factor of 1.41%.

Based on the present SRF technology at KAERI, our choice was a reduction in the ratio of E_{pk}/E_{acc}, and a realization of the higher R/Q in the PEFP low beta cavity optimization.

After optimization design of the cavity shape in RF properties, a multipacting simulation code FishPact developed by Genfa Wu [4] is used to estimate the multipacting risk for the whole cavity. The calculations indicate the occurrence of the multipacting is unlikely, because the electrons can not gain sufficient energy to generate secondary electrons when impacting on the cavity surface. Table 1 lists the RF parameters of the PEFP low beta cavity.

Table 1: Primary parameters of the PEFP Low beta cavity.

Parameters	Value
Frequency (MHz)	700
Geometrical beta β_g	0.42
E_{acc} (MV/m)	8.0
E_{pk}/E_{acc}	3.71
B_{pk}/E_{acc} [mT/(MV/m)]	7.47
R/Q (Ω)	102.30
Cell to cell coupling (%)	1.41
Geometrical Factor (Ω)	121.68

Stiffening-ring structure design for reducing Lorentz force detuning

After optimization design of the stiffening structure regarding to the Lorentz force detuning control, cavity field flatness sensitivity, frequency sensitivity, tuning sensitivity and stability of the cavity mechanical property, a stiffening structure composed of double stiffening ring between inner cells and between Field Probe end cell and end dish, and single stiffening ring between FPC end cell and end dish has been designed for the low beta cavity. This structure can reduce Lorentz force detuning factor to -1.1 Hz/(MV/m)^2 for a wall thickness of 4.3 mm. Frequency sensitivity of the low beta cavity is 187.8 KHz/mm; the field flatness sensitivity of the cavity is 49.1%/MHz; and the tuning sensitivity is 4498 N/mm, and the maximum Von Mises stressin the cavity is 12.6 MPa [5]. Fig. 1 shows the stiffening structure and a PEFP low beta cavity with this structure.

HOM analysis [3]

Two main HOM related issues of the superconducting RF linac are the beam instabilities and the HOM-induced power. In order to understand the HOM issues regarding to beam stabilities and induced power in the PEFP low beta SRF linac, we have analyzed a normalized HOM-induced voltage, an induced power and a time-averaged

EXPERIENCES WITH THE MANUFACTURING, TESTING AND QUALITY CONTROL OF LARGE NUMBER OF SUPERCONDUCTING MAGNETS

A. Puntambekar, M. Bagre, Vikas Jain, Prashant Khare, M.G. Karmarkar, S. Kotaiah

Raja Ramanna Centre for advanced Technology, Indore, INDIA

R. Wolf, Guiseppe Mugnai, CERN, Geneva, Switzerland

Abstract

Raja Ramanna Centre for Advanced Technology has successfully completed the supply of nearly 1800 nos. Superconducting Corrector (SC) Magnets for the LHC project at CERN. Under the DAE-CERN collaboration agreement India through RRCAT, Indore was entrusted to manufacture, test & supply half of the total Sextupole Corrector (MCS) 1232 nos. and Decapole Octupole Corrector (MCDO) 616 nos. required for the LHC main dipole, while rest half were made in Europe. In this paper we describe the experience gained during technology development, prototyping and technology transfer to industry.

INTRODUCTION

The MCS & MCDO spool correctors consists of a coil assembly, glass fibre slit tube, steel laminations & aluminium shrinking cylinder for pre compression of coils, end plates for coil connection, parallel resistor for magnet protection (in case of MCS) and a magnetic shield also acting as a support. The coils have been wound using CERN supplied Nb-Ti SC wire in copper matrix.

Table 1: Main parameters of spool correctors

Parameters	MCS	MCD	MCO
Nominal strength	1970 T/m^2	1.2 X 10^6 T/m^4	8200 T/m^3
Length (mm)	160	110	
Aperture (mm)	58	63.6	58
Nom. current (A)	550	550	100
Working temp. (K)	1.9		
Turns per coil	2 x 13	2 x 20	1 x 43
Self ind. (mH)	0.8	0.4	
Quench current at 1.9K/4.2K (A)	1300/950	1250/915	297/195
Peak field (T)	1.9	2.4	2
Mass (Kg.)	~5.5	~5.0	

These corrector magnets require precision components and coils, accurate assembly procedure, elaborate testing plan and stringent quality control required for repeatable performance.

DEVELOPMENT CYCLE

Looking to the complexities and total quantum of work a two-fold strategy was adopted. All the technology was developed in-house at RRCAT in collaboration with CERN. The same was proved by way of making prototypes and elaborately testing them at 4.2 K at RRCAT & further at 1.9 K at CERN. Their large-scale production was planned at industries to make use of their infrastructure, expertise and efficiency under strict quality control from RRCAT.

Prototype Development

Prototype phase comprised of development of various critical components, tooling, coil winding & magnet assembly process and manual coil-winding machine. The coil former was CNC machined out of G-11 tubes. AISI M-45 grades Si steel laminations were punched using 0.5 mm thick sheet. Shrinking cylinder, its anodising treatment and different precision tooling for coil winding, magnet assembly & shrink fit tooling were developed at fabrication facility of RRCAT. Special bandage tooling was also developed for the application of B-stage semi cured glass epoxy tape over coil assembly, which was a messy affair. There were some troubles during assembly of hot shrinking cylinder over stacked laminations as it was getting stuck halfway. The inter coil connections were made using standard soldering. The individual modules were tested at 4.2 K in existing φ 200 mm bore cryostat & warm magnetic measurement (WMM) at 300 K was done at RRCAT on specially developed rotating coil vertical shaft bench. The 1.8 K training & also field quality test on these prototypes were done at CERN. The acceptance of prototype proved the tooling & process and gave confidence to proceed further [1].

Figure 1: MCS fitted at one end of LHC Dipole.

Various Developments

The zero period due to design modifications was utilised in development of components & special machine requiring long development cycle time. Compression moulding for the Central island & end spacers were tried. The dimensional accuracies were achieved however the strength was not consistent due to variation in resin and glass content from batch to batch. Different concepts were

DESIGN OF L-BAND SUPERCONDUCTING CAVITY FOR THE ENERGY RECOVERY LINACS

K. Umemori*, T. Furuya, S. Sakanaka, T. Suwada, T. Takahashi, KEK, Ibaraki, Japan

H. Sakai, K. Shinoe, ISSP/SRL, Chiba, Japan

M. Sawamura, JAEA/ERL, Ibaraki, Japan

Abstract

For the energy recovery linacs (ERLs), strong higher-order-mode (HOM) damping is indispensable to achieve high current operations. For this aim, we have designed L-band superconducting cavity which is optimized for the ERL operations. New cavity cell shape is designed. The HOMs are damped with microwave absorbers mounted on large beampipes. A new idea of eccentric fluted beampipe is proposed. Design concepts and estimated HOM characteristics are described in this paper.

INTRODUCTION

The ERLs are considered as promising future light sources which can provide excellent synchrotron radiation lights. The ERL project in Japan has been started with the cooperation of KEK, JAEA, ISSP and other SR institutes, with an aim to realize 5 GeV class ERLs [1]. For this aim, we have started to develop superconducting accelerating cavities for the main linacs, which are key components of the ERLs.

Accelerating gradient of $15 \sim 20$ MV/m is required to achieve high energy electron beams. For this purpose, multi-cell cavity is inevitable. A most challenging issue, which comes from a requirement of high current CW beams, is a strong suppression of HOMs excited in accelerating cavities. Dipole HOMs can cause current limitation due to the beam-breakup (BBU) instabilities. Even quadrupole HOMs can be problematic and lead to the quadrupole BBU instabilities. Typical simulation results, calculated by the Cornell university, show that the dipole and quadrupole HOMs should be damped to $(R/Q)Q/f < 1.4 \times 10^5$ $(\Omega \text{cm}^{-2} \text{GHz}^{-1})$ and $(R/Q)Q/f < 4 \times 10^6$ $(\Omega \text{cm}^{-4} \text{GHz}^{-1})$ respectively, for 100 mA operation [2], where f is the resonant frequency, Q is the quality factor, and R/Q is the ratio of the impedance and the quality factor. Monopole HOMs are also harmful. They are damped by HOM absorbers and could become significant heat load on cryo-modules. The frequencies of monopole HOMs should not be around multiples of 2.6 GHz to avoid resonant excitation.

The TESLA cavity is known as a representative L-band superconducting cavity. However, it is not adequate for the ERLs, because its HOM damping ability is not enough for high current operations. Furthermore, it is known that the loop-type HOM couplers, which are adopted for the TESLA cavity, have a heating problem for the CW operations [3]. Therefore, we decided to develop 1.3GHz su-

perconducting cavity which is optimized for the ERL operations, especially for HOM damping. We have designed new cavity cell shapes, applied large beampipes on which microwave absorbers are mounted, and adopted a new idea of an eccentric fluted beampipe. Details of the design concepts and its HOM characteristics are discussed below.

HOM SUPPRESSION BASED ON TESLA SHAPE CAVITY

At first, we start discussion based on the TESLA shape cavity. Subjects are concentrated on the effectiveness of the large beampipes and a number of cells

Large Beampipe

In order to investigate the HOM damping capability of the large beampipes with microwave absorbers, we designed the KEK-ERL model-1 cavity. In this model, cavity cell shapes are basically the same as the TESLA cavity, but one side of beampipe diameter is enlarged from 78 mm to 108 mm. All monopole and dipole modes, except TM010, propagate through the beampipe and are damped by the absorbers. From simulation results, it was found that the large beampipe damper is from several to ten times more effective than the loop-type HOM couplers, as shown later in Figure 4. Here, HOM impedances of the TESLA cavity are quoted from the data shown in [4, 5] and those of the KEK-ERL model-1 cavity are calculated using MAFIA. External Q (Q_{ext}) of the beampipe is estimated and used for the plot. For the KEK-ERL model-1 cavity, the value of $(R_t/Q)Q_{ext}/f$ is just below the 100mA threshold. Considering the fact that loaded Qs of absorber could be somewhat larger than the estimated Q_{ext}, further suppression of dipole HOMs is required.

Number of cells

One method to decrease the HOM impedances is to reduce number of cells per one cavity [6]. We attempted a seven-cell cavity with the KEK-ERL model-1 strategy. The HOM impedances are lowered around half, but the effect is not so drastic. The shunt impedance (R_{sh}) of the accelerating mode is also lowered more than 20 %. From this result, we decided to keep nine cells.

DESIGN OF THE KEK-ERL CAVITY

With the aim of strong HOM damping, we have designed a new cavity cell shapes which have larger iris diameter. As

* kensei.umemori@kek.jp

STATUS OF THE SOLEIL PROJECT

L. Nadolski, J.C. Besson, P. Brunelle, A. Buteau, L. Cassinari, M.E. Couprie, J.C. Denard, J.M. Filhol, C. Herbeaux, J.F. Lamarre, P. Lebasque, V. Le Roux, A. Lestrade, M.P. Level, A. Loulergue, A. Madur, P. Marchand, A. Nadji, R. Nagaoka, B. Pottin, J.B. Pruvost, F. Ribeiro, M.A. Tordeux, Synchrotron SOLEIL, Gif-sur-Yvette, France

Abstract

SOLEIL, the 2.75 GeV new French Synchrotron Radiation Facility, located near Paris, is under commissioning. Here are reported the main results obtained especially on the storage ring. The beam dynamics characterisation of the 3.7 nm.rad optics is presented, as well as the first measurements of the instability thresholds. Furthermore comparison is made with expectations of the linear optics model and instability calculations. First experience with innovative devices and technologies is also presented: TANGO control system, BPM system, extensive use of NEG coated vacuum vessels, unconventional RF system (Solid state amplifiers and superconducting cavities). Seven insertion devices accommodating a wide energy range from 5 eV to 30 keV (in-vacuum, Apple II, large period electromagnetic types) are now installed on the machine and some of them are producing the first photon beams which are delivered to the beamlines. Finally a roadmap towards beam delivery to users will be presented.

INTRODUCTION

SOLEIL is designed as a 2.75 GeV third generation light source with 21 out of 24 straight sections (SS) dedicated for installing insertion devices (IDs). This very large ratio of straight sections (43% of the 354 m long circumference, with 29% for magnetic structures) is shared between 4x12 m long SS, suitable for accommodating long period IDs, 12x7 m medium SS, and 8x3.8 m short SS to accommodate in-vacuum undulators. With a small emittance and a target 500 mA beam intensity, the average brilliance will range from 10^{16} to 10^{20} ph/s/0.1%bw/mm^2/mrad^2 for respectively bending magnet and ID based beamlines. Table 1 sums up the main storage ring parameters.

A total of 24 beamlines have been approved by the SOLEIL council. The spectral range is equally shared above and below the energy of 1.3 keV, with a distribution of 6 beamlines on bending magnets (BM) and 18 on ID beamlines, plus 2 IR beamlines.

Here are reported the commissioning results from the Linac to the beamlines with a focus on the storage ring (SR) and the performances reached by the end of 2006.

INJECTOR COMMISSIONING

The injector is composed of two parts, a 100 MeV Linac and a full energy Booster, that were both commissioned in 2005.

The Linac HELIOS is a turn-key system provided by THALES whereas the transfer line from Linac to Booster was constructed by SOLEIL. The performances are better than specifications and have been reported extensively before [1]. In the long pulse mode, the Linac produces a 300 ns train of pulses with a total charge up to 9.3 nC with an energy spread below ± 0.5 % and normalized (4 $\gamma\varepsilon_{rms}$) emittances of 47 (± 10) and 52 (± 10) π mm.mrad respectively in horizontal and vertical planes. For temporal structure a short pulse mode provides 1 to 4 pulses of 1.3 ns with an energy spread of ± 0.6 % for 1 pulse and ± 0.8 % for 4 pulses.

The 3 Hz 157 m long Booster ring provides a 140-150 nm.rad beam emittance at 2.75 GeV. The tracking of the SLS-type digitally control power supplies (dipole and quadrupoles) of ± 0.2 % keeps the tunes within ± 0.05 giving an injection efficiency of 90-95% without further losses during the energy ramping up for different filling patterns. Beam extraction and guiding from Booster to SR transfer line occurred smoothly on May 8th 2006. Further details are given in references [2,3].

Parameter	Value
Energy (GeV)	2.75
Circumference (m)	354.097
Revolution period (µs)	1.18
Betatron tunes H/V	18.2/ 10.3
Energy spread	$1.016 \ 10^{-3}$
H-Emittance (nm.rad), 1% coupling	3.7
Bunch length @ 4 MV (ps)	14
Damping times H/V/L (ms)	6.56/6.56/3.27
RF frequency (MHz)	352.2

Table 1: Storage ring main design parameters.

STORAGE RING COMMISSIONING

Challenges

Before injecting the first electrons, the storage ring was incorporating new technologies and challenges which potentially, could have jeopardized the commissioning schedule. Final 10 mm vertical aperture 5 m long ID vacuum chambers were installed from day one on the 10 medium straight sections. Moreover the ring was equipped with NEG coated aluminium chambers over 56 % of the circumference, with a SOLEIL designed super conducting cryomodule containing 2 HOM free SC RF cavities, new BPM digital electronics, and 4 insertion devices (1 Apple II type, 1 in-vacuum and 2 electro-

STATUS OF THE AUSTRALIAN SYNCHROTRON PROJECT

G. LeBlanc, Australian Synchrotron Project

Abstract

The Australian Synchrotron, a synchrotron light facility based on a 3-GeV electron storage ring, is currently being commissioned at a site in the Metropolitan District of Melbourne. On July 14, 2006 less than three years after earth moving machines started to prepare the site, beam was captured, accumulated and stored in the storage ring. Storage ring commissioning, and beamline installation and commissioning will continue through March 2007, after which the facility will become operational. In this paper we give a brief overview of the facility and its beamlines, followed by the latest results from accelerator commissioning activities.

FACILITY OVERVIEW

The Australian Synchrotron is located adjacent to Monash University in Clayton, Victoria. It has been built by a project team from Major Projects Victoria (MPV), a part of the Victorian State Government. The funding for the building and accelerators has been provided by the Victorian State Government. The beamlines are being funded by a group of interested parties, including universities, research organisations, other state governments, and New Zealand.

Staffing

The Australian synchrotron is being delivered with a relatively small staff of only 54 people, plus specialist contractors and consultants. Due to the relatively small number of staff, much of the responsibility for the design and project management has been placed on suppliers, with turn-key contracts. Contracts for the following systems included all design, engineering, project management, installation and commissioning:

- Injection system
- Storage ring RF system
- Storage ring vacuum vessels
- Beamline photon delivery systems
- Storage ring girders
- Front ends

Schedule

The original schedule milestones can be seen in Table 1. The project is currently on schedule and transition from the project stage to the start of operations will be in April 2007. All of the major schedule milestones have been achieved within days of the target dates, including the start of accelerator installation in April 2005, the completion of installation in May 2006 and first turns in the storage ring in June 2006.

Table 1: Schedule Milestones.

Design announced.	January 2003
Building contract placed	July 2003
Building complete	February 2005
Staff move into building	March 2005
Installation begins	April 2005
Injection system commissioning begins	October 2005
Storage ring installation complete	May 2006
Storage ring commissioning begins	June 2006
First turns in the storage ring	June 2006
Beamline installation begins	September 2006
Beamline commissioning begins	February 2007
Transition to operations	April 2007

ACCELERATOR SYSTEMS

The Australian Synchrotron accelerator systems are comprised of a 100 MeV linear accelerator, a 3 GeV booster synchrotron, and a 3 GeV storage ring. The entire injection system, from the electron source to the injection septa in the storage ring, was a single, turn-key contract. The storage ring equipment was provided by several different contractors and assembled using the local labour force with supervision from the different component contractors. A schematic of the layout of the accelerator systems is shown in Figure 1.
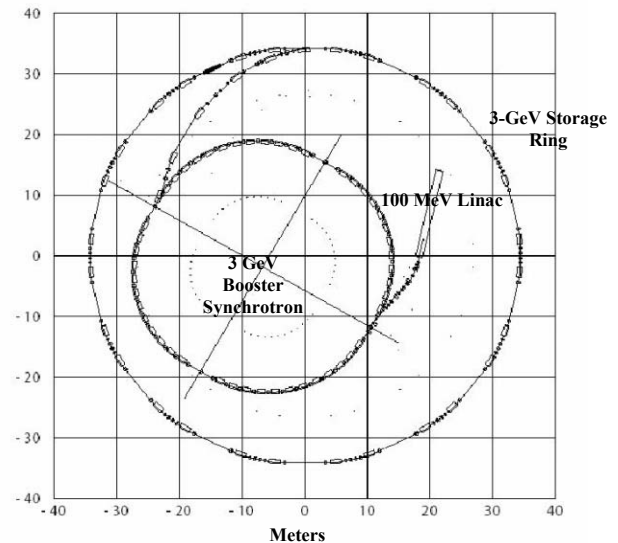
Figure 1: Layout of the accelerator systems.

The Linac

The electron source is a 90 keV thermionic gun that can run in both short pulse mode and long pulse mode. The operating frequency is 3 GHz. The short pulse mode is designed to deliver a single bunch into the 500 MHz

CONSTRUCTION OF SHANGHAI SYNCHROTRON RADIATION FACILITY

Z. T. Zhao, H. J. Xu, H. Ding for the SSRF Project Team
Shanghai Institute of Applied Physics, Shanghai 201800, P. R. China

Abstract

The Shanghai Synchrotron Radiation Facility (SSRF), a third generation light source based on a 3.5GeV storage ring, is under construction at Zhang-Jiang Hi-Tech Park in Shanghai. The SSRF groundbreaking was made in December 2004 and the construction of the SSRF main and auxiliary buildings was basically completed in November 2006. The construction and installation of the SSRF accelerator components are under going with the target schedule of starting storage ring commissioning in April 2008 and the user operation in April 2009. This paper reports the construction progress of the Shanghai Synchrotron Radiation Facility.

INTRODUCTION

The SSRF complex in phase one consists of a 150MeV electron linac, a full energy booster, a 3.5GeV storage ring with a circumference of 432m and seven beamlines and experimental stations [1].

The SSRF project was fully approved by the central government in December 2004, and its groundbreaking was made a few days later on December 25. Since then the SSRF construction has been in progressing towards the target schedule of starting user operation from April 2009 [1, 2]. Constructions of SSRF buildings, including the main building housing accelerator tunnels and the experimental hall, two utility buildings, a technical building, an office building, a cafeteria and a guesthouse, have been basically completed, and they have been fully opened for utilization, such as utility installation and commissioning, machine pre-assembly and installation. Figure 1 shows the SSRF main building in January 2007.

Figure 1: The SSRF main building, January 2007.

The SSRF utilities, including electric power stations water cooling systems, air cooling systems, compressed air system and etc., have been installed and partly commissioned. The main power station has been in operation since October 2006. The piping and cabling from the main stations to the substations of the utility systems have been finished, and the engineering work in the main building is still going on. The commissioning of the SSRF utility systems is progressed on schedule, which is able to meet the requirements of various accelerator equipment testing and commissioning.

At this writing, most of SSRF accelerator components are under manufactures in domestic and foreign industries. At the same time, the machine installations, including linac, the booster RF power transmitter, a storage ring mechanical and electrical sector C10 and etc. are under way. The engineering design of the seven beamlines and experimental stations is in the final stage, and beamline components procurements are under going. The contracts of seven front-ends, four mono-chromators and etc. have been awarded.

STORAGE RING

The SSRF storage ring has 20 double bend lattice cells with four-fold symmetry, which incorporate four 12m long and sixteen 6.5m straight sections to accommodate injection magnets, SRF cavity modules and various insertion devices. With the finite dispersions leaking into the straight section, the storage ring natural emittance can be optimized to less than 4 nm·rad. Table 1 shows the main parameters of the SSRF storage ring.

Table 1: Main Parameters of the SSRF Storage Ring.

Energy (GeV)	3.5
Circumference (m)	432
Harmonic Number	720
Number of cells/Super-periods	20/4
Nature Emittance (nm·rad)	3.9
Beam Current, Multi-Bunch (mA)	200~300
Single-Bunch (mA)	>5
Straight Lengths (m)	4×12.0, 16×6.5
Betatron tunes, Q_x/Q_y	22.22/11.32,
$\beta_x/\beta_y/D_x$ @12m straight (m)	10.0/6.0/0.15
$\beta_x/\beta_y/D_x$ @6.5m straight (m)	3.5/2.5/0.10
Momentum Compaction	4.2×10^{-4}
Relative Energy Spread	9.7×10^{-4}
RF Frequency (MHz)	499.65
Dipole Radiation per Turn (MeV)	1.448
Damping Times $\tau_x/\tau_y/\tau_s$(ms)	6.97/6.97/3.49
Bunch Length (mm)	4.0

Magnets and girders [3]

A total of 40 dipole magnets, 200 quadrupoles and 140 sextupoles, are being built for the SSRF storage ring. The dipole and quadrupole magnets are under fabrication at IHEP workshop, Beijing, and the magnetic measurements of the magnets for the first cell are completed. The first 10 dipoles achieved 3×10^{-4} variation in the integrated field across ±27mm, and their magnet to magnet integrated

STATUS AND FUTURE OF TAIWAN LIGHT SOURCE

Keng S. Liang, C.C. Kuo, J.R. Chen, D.J. Wang, G.H. Luo, and Y.W. Yang
National Synchrotron Radiation Research Center, No. 101, Hsin-Ann Road, Hsinchu, Taiwan

Abstract

The Taiwan Light Source of National Synchrotron Radiation Research Center (NSRRC) has reached a very stable operation condition and productive scientific outputs. The copper Doris RF cavities were replaced with a niobium Superconducting (SC) RF cavity in order to eliminate higher-order-modes and deliver higher beam current. Superconducting wigglers were installed to provide higher flux at higher photon energy. The storage ring is now operated at 300 mA top-up mode with better than 97 % of beam availability during users shifts. The original layout of the magnets has been greatly modified to accommodate one SC wavelength shifter at the injection section, one SC wiggler at the RF cavity section, and three SC wigglers in achromatic sections in addition to the original design of one wiggler and three undulators. In view of the future scientific demands, the NSRRC is proposing to construct a new synchrotron storage ring of 3.0~3.3 GeV and ultra low emittance, the Taiwan Photon Source (TPS). The TPS will provide brilliant X-rays at 10^{21} photons/s/0.1%BW /mm^2/mr^2 by SC undulator upon its completion, making it the brightest synchrotron light with the finest performance in the world.

TOP-UP INJECTION

Several major upgrades are integrated into routine operation in Taiwan Light Source (TLS) in recently years. Top-up injection mode was achieved after series upgraded of injector, transfer line and injection components. The operation current of Top-up injection reached 300 mA during users shift. The commissioning [1] of the first and second Superconducting RF cavities (SRF) was very smooth and exceeded the specification in several measures. The first In-Archromat-Superconducting-Wiggler (IASW) was installed and commissioned successfully. The associated beamlines will be commissioned in the first quarter of 2007.

To reach the ultimate goal of third generation light source, TLS prepared all the necessary steps to provide top-up operation to the users. To improve the thermal relaxing problem of dipole magnets and cure the orbit drift during the energy ramping era at TLS, the injector was upgraded to have the capability of full energy injection to the storage ring. This provided an essential tool to evaluate the feasibility of top-up injection at TLS.

The top-up mode [2, 3, 4, 5] provides the best solution to the thermal variation of beamlines' optical components and locks the launching condition of the synchrotron light to end-stations. This greatly benefits those superconducting wiggler x-ray beamlines which have large thermal load on the optical components and take relatively long time to reach thermal equilibrium. In addition, these beamlines generally have high demands on the photon energy stability after the monochromator, and top-up mode offers the best solution to the short beam lifetime of a storage ring. Top-up injection also opens new opportunities in probing better operation conditions, for example, the lower emittance, the lower gap of insertion device, and the increase of bunch current without the need to worry the impact of beam lifetime.

Figure 1 shows the stored beam current in user's shifts with top-up injection mode. The maximum stored current sets to 302 mA. The zoom-in to one-hour period of stored beam current is shown on top of Fig. 1. The intensity variation of the stored current can be maintained within ±0.25%. During users' shifts, the injection time interval was set to 60 seconds due to low lifetime, around 250 minutes, of stored current.
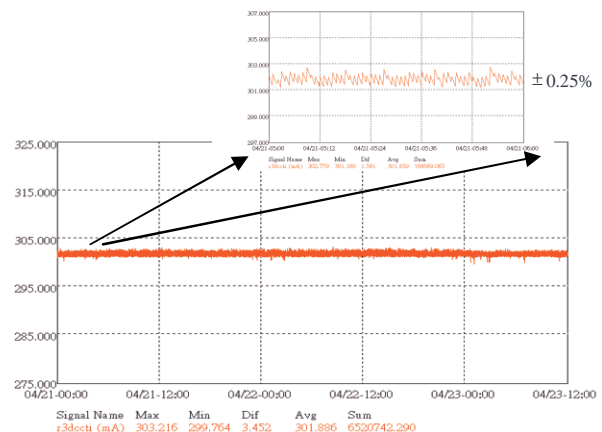
Figure 1: The standard operation of top-up injection and the zoom-in of current variation, ±0.25%.

To increase the transverse acceptance of the ring and have acceptable injection efficiency, the chromaticity is corrected to slight positive. Further help from the digital transverse feedback system, the transverse instability can be suppressed to the most minuscule range without scarifying the transverse acceptance and injection efficiency.

To ensure the radiation safety before switching to top-up operation, a series of radiation safety analyses including calculations and measurements were performed. Additional interlock logic has been integrated into the existing interlock system to prevent dipole failure, injection difficulty as well as excessive radiation exposure.

Six accumulation type dose meters were placed close to the shielding wall at straight sections, which tend to be the hot spots around the ring. The interlock system will be activated when the accumulated dose exceeds the threshold value, 4 μSv within 4 hours. All the

02 Synchrotron Light Sources and FELs
A05 - Synchrotron Radiation Facilities

REVIEW OF HADRON MACHINES FOR CANCER THERAPY

M. Kanazawa

National Institute of Radiological Sciences, 4-9-1 Aanagawa, Inage, Chiba, Japan 263-8555

Abstract

Particle cancer therapies with proton and light ion have been considered as excellent treatment for deep-seated tumors, which are due to excellent dose distributions with Bragg peak. To realize these therapies, dedicated accelerator facilities were constructed. With good clinical results in these frontiers, many plans of dedicated facility have been started in the both case of proton and light ion treatment facilities. In this paper, important types of accelerator facilities will be presented.

INTRODUCTION

Though radiotherapy of cancer patient is important treatment method, X-ray will be mainly used. This situation is from the low cost and compactness of the required hardware. If we can use charged particle beam like proton and light ion for deep seated tumor, depth dose distribution can be improved to concentrate the dose. This advantage is pointed out first by R.R Willson[1] in 1946. This comes from the existence of Bragg peak in the case of charged particle beam. We can adjust the depth position of Bragg peak at tumor to obtain high concentration of the particle dose.
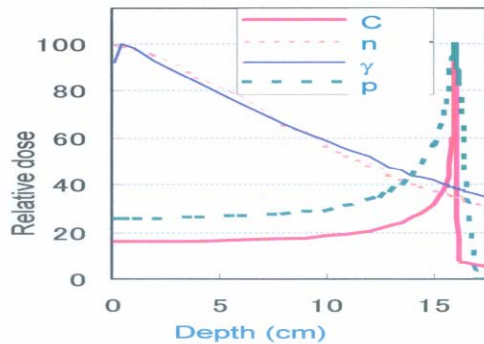
Figure 1: Depth dose distribution of X-ray, neutron, proton, and carbon ion.

In the actual treatment with charged particle, Bragg peak with different energies must be superimposed to fit on the tumor thickness. In Fig.2, calculated depth dose distributions[2] of several ions are compared with a SOBP (Spread Out Bragg Peak) width of 6cm. In these calculations, nuclear interactions of the incident beam with water and RBE (Relative Biological Effectiveness) are included. As seen from these calculations, entrance dose is less than 70% of the dose value at SOBP, which make the entrance dose on normal tissue low. In the cases of X-ray and neutron, the dose values are decrease

gradually in the patient body, and this nature is demerit in the treatment of a deep seated tumor.
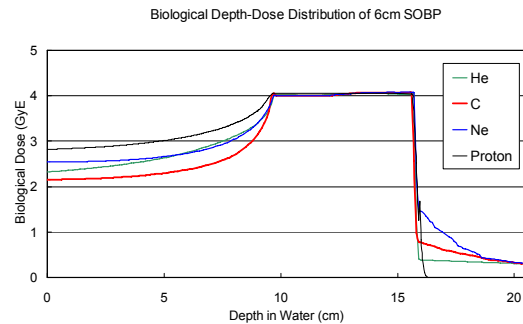
Figure 2: Calculated depth dose distributions of proton, helium, carbon, and neon beams with SOBP of 6xm.

In the case of light ion, there is another merit concerning biological effect. If we see the RBE as a function of a LET (Linear Energy Transfer), the RBE is maximum around 200keV/μ as shown in Fig.3. In the case of carbon, the RBE value at entrance is low with small LET value, and the value at SOBP region is high. This makes desired characteristic point that kill tumor effectively with light side effect on the normal tissue. With low OER (Oxygen Enhancement Ratio), carbon beam can well control the tumor of hypoxic cell that is considered as radio-resistant.
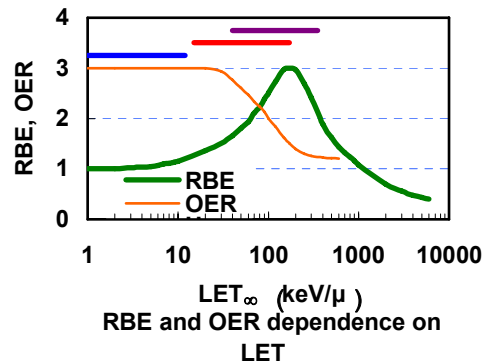
Figure 3: RBE and OER as a function of LET.

USE OF MICROBEAM AT JAEA TAKASAKI

M. Fukuda[#], K. Hatanaka, T. Yorita, RCNP, Osaka University, Osaka 567-0047, Japan
T. Kamiya, M. Oikawa, T. Satoh, T. Sakai, S. Kurashima, N. Miyawaki, S. Okumura, H. Kashiwagi,
W. Yokota, Department of Advanced Radiation Technology, JAEA, Takasaki, Gunma 370-1292,
Japan

Abstract

The TIARA facilities of JAEA in Takasaki is equipped with a several-MeV light-ion and a several-dozen-MeV heavy-ion microbeam formation systems of focusing type, and a several-hundred-MeV heavy-ion microbeam formation system of collimating type. The microbeams with a spot size of 1 μm or less in diameter are extensively utilized for the research in materials science and biotechnology. An in-air micro-PIXE analysis system using a 2 MeV proton microbeam is quite useful for medical science and dentistry to visualize two-dimensional distribution of very small quantities of elements in a microscopic area like cells with very high sensitivity. A single-ion hit system using a several-hundred-MeV heavy-ion microbeam is available for medical and biological applications such as elucidations of cellular radiation response. Highly stable ion beams with energy spread less than 0.02 % are required for the microbeam production. Improvements of accelerator performance are indispensable to realize the ion beams of high quality. A flattop acceleration system and a magnetic field stabilization system have been developed for the JAEA AVF cyclotron. These accelerator technologies are also required for very precise spectroscopic studies in nuclear physics. Ultrahigh energy resolution of 0.005 % has been achieved at the RCNP cyclotron facility of Osaka University.
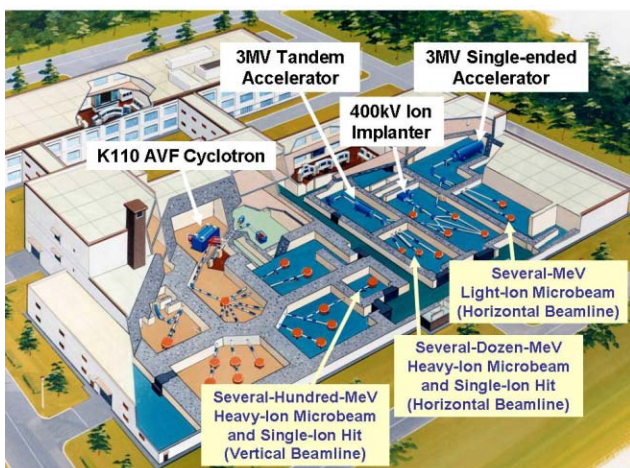
Figure 1: Bird view of the TIARA facility, equipped with four accelerators and three microbeam formation systems.

[#] mhfukuda@rcnp.osaka-u.ac.jp

INTRODUCTION

The ion beam irradiation research facility, TIARA (Takasaki Ion accelerators for Advanced Radiation Applications), was completed in 1993 at the Takasaki Radiation Chemistry Research Establishment of Japan Atomic Energy Research Institute(JAERI), the predecessor of the present Takasaki Advanced Radiation Research Institute of Japan Atomic Energy Agency (JAEA) [1]. Ion beam applications to the research and development in materials science and biotechnology have been fairly progressing after the full-scale operation of the ion accelerator complex facility. The bird view of the TIARA facility is shown in Fig. 1. A variety of ion beams are provided by a K110 AVF cyclotron, a 3 MV tandem accelerator, a 3 MV single-ended accelerator and a 400 kV ion implanter. The wide energy range from 20 keV through 1 GeV is covered by the accelerator complex.

Three kinds of light- and heavy-ion microbeams with a beam spot size of 1 μm or less in diameter are available at the TIARA facility. Use of the ion microbeam has greatly enhanced spatial and targeting resolutions of the ion irradiation in a finite area.

The micro-PIXE analysis has become widespread in various fields. Proton or helium ion beam with energies from 2 to 3 MeV is produced by the single-ended accelerator with acceleration voltage stability of the order of 10^{-5}. The helium ion microbeam with a spot size of 0.25μm has been produced using the high quality ion beam. The in-air micro-PIXE technique, first developed at TIARA, enables elemental analysis in cells without drastic change of the living cell condition by placing the frozen cell sample in atmosphere.

The tandem accelerator is equipped with a several-dozen-MeV heavy-ion microbeam formation system. The heavy-ion microbeam is useful for material processing and elucidation of radiation effects such as single-event upset of semiconductor devices used in space, caused by high LET(Linear Energy Transfer) irradiation. As the integration level of the semiconductor devices increases, higher spatial- and targeting-resolutions are required for the investigation of the radiation effects.

The LET range from 10 to 1000 keV/μm in water equivalent is covered by several-hundred-MeV heavy ions accelerated by the AVF cyclotron. The deposit energy is transferred in a localized area along the ion track. In case of the cell irradiation, the heavy ion causes high dose localization within the cell. A heavy-ion microbeam formation system of collimating type has been installed in a vertical beam line of the AVF cyclotron for

08 Applications of Accelerators, Technology Transfer and Industrial Relations

U02 - Materials Analysis and Modification

THE PROGRESS OF ACCELERATOR MASS SPECTROMETRY AND THEIR APPLICATIONS IN CHINA

Chen Jia-er, Guo Zhiyu, Liu Kexin, Institute of Heavy Ion Physics, Peking University and Key
Laboratory of Heavy Ion Physics, Ministry of Education, Beijing 100871, China
Wu Xiaohong, Yuan Sixun, School of Archaeology and Museology, Peking University,
Jiang Shan,China Institute of Atomic Energy
Zhou Weijian, Xi'an AMS Centre

Abstract

The facilities and technologies developed for AMS at Peking University, China Institute of Atomic Energy and Xi'an AMS Centre are presented. Interesting results about Chronology frame of Xia-Shang-Zhou dynasties based on radiocarbon dating with PKU-AMS on serial samples from various sites like Tianma-Qucun, Xinzha sites etc and oracle bones from Yinxu site, are given as examples of the AMS application in the field of Archaeology. Applications in the fields of earth sciences, biomedical sciences are introduced as well.

INTRODUCTION

As a result of substantial development for more than a quarter of a century, the accelerator mass spectrometry (AMS) has become a leading technique for the detection of long-lived radio nuclides such as ^{10}Be, ^{14}C, ^{26}Al, ^{36}Cl and ^{129}I at isotopic ratios between 10^{-10} and 10^{-15} and has been applied extensively in the fields of archaeology, earth sciences, environmental sciences, biomedical sciences, nuclear safeguards, nuclear physics and astrophysics.

Comparing with the conventional mass spectrometers and radio decay measurement, the AMS has following merits:

- Ultra high sensitivity. For a number of radioactive nuclides, the measuring background of isotopic ratios could be reduced down to 10^{-15} or even less, which is much lower than traditional mass spectrometer.
- Small sample size. The sample amount of AMS measurement is usually in the order of mg elements, which are three orders lower than that needed for decay counting method. In the case of meteorite measurement even 10 μg carbon sample is still workable.
- High throughput. The time of direct atom counting is much shorter than that of decay counting for the same precision.

However, to carry out a precise abundance measurement of rare nuclides is really a challenging issue. Careful precautions have to be made to eliminate various interferences in the whole process starting from sample collection and preparation, beam generation, beam handling and acceleration, gas stripping and finally to the data acquisition and processing. Precautions have to be made to ensure AMS facilities operating under conditions with extremely low machine background, low isotopic fractionation, high beam transmission efficiency, and high resolution beam analysis as well as with high performance stability.

There are about 60 AMS facilities around the world and more new facilities are to be developed or constructed. In China, AMS technology has been developed at the China Institute of Atomic Energy and Peking University since 1980's. There are now 5 AMS facilities working. In the following paragraphs, only tandem based AMS facilities in China and their features will be presented followed by some discussion on typical applications.

AMS FACILITIES IN CHINA

The HI-13 Tandem at China Institute of Atomic Energy (CIAE) was the first facility in China that used for AMS measurements of mid or heavy nuclei like ^{10}Be, ^{26}Al, ^{36}Cl, ^{41}Ca and ^{129}I etc.[1] and the applications has been concentrated on geosciences, biomedical sciences, nuclear physics and astrophysics. The layout of the facility is shown on fig. 1.

1; ION SOURCE
2; TRIM LENS
3; DEFLECTING MAGNET
4; APERTURE
5; PRE-ACCELERATION TUBE
6; 1X.1Y STEERER
7; MATCHING LENS
8; 1X.1Y STEERER
9; APERTURE
10; L.E CUP
11; 2X.2YSTEERER
12; GRIDED LENS
13; ACCELERATION TUBE
14; GAS OR FOIL STRIPPER
15; ELECTROSTATIC QUADRUPOLE TRIPLET
16; SECOND STRIPPER
17; H.E ACCELERATION TUBE
18; H.E 1X.1Y STEERER
19; H.E CUP
20; H.E MAGNETIC QUADRUPOLE DOUBLET
21; H.E 2X.2Y STEERER
22; OBJECT SLIT
23; OBJECT CUP
24; ANALYZING MAGNET
25; OFF-SET CUP
26; IMAGE SLIT
27; IMAGE CUP
28; MAGNETIC QUADRUPOLE DOUBLET
29; SWITCHER MAGNET
30; SLIT
31; 1X.1Y MAGNETIC STEERER
32; QUADRUPOLE DOUBLET
33; CUP
34; SLIT
35; ELECTROSTATIC DEFLECTOR
36; MICROCHANNEL PLATE DETECTOR
37; AMS TARGET CHAMBER
38; DETECTOR

Figure 1: The layout of CIAE's HI-13 AMS system.

It consists of mainly a HI-13 Tandem accelerator, sputtering ion source, injection section with low energy beam analysis, post acceleration beam analyzing magnet and electrostatic deflector, as well as AMS target chamber and micro-channel plate detector. Typical parameters of the CIAE AMS used for measurements of ^{10}Be, ^{26}Al, ^{36}Cl, ^{41}Ca nuclides are listed in Table 1.

Various methods have been developed along with ΔE-E ionization chamber for the detection of rare nuclides and the elimination of their isotope and isobar interferences, as indicated in the Table 1. For instance to measure ^{10}Be, an absorber of 15.3mg/cm^2 Ni is added in front of the ΔE-E ionization chamber, and for the measurement of ^{129}I, TOF technique is adopted for isotope identification while for

APPLICATION OF SYNCHROTRON RADIATION AMP; NEUTRON BEAMS TO THE STUDY OF NANOMATERIALS AND BIOMATERIALS

S.K. Sinha, UCSD, La Jolla, California

Abstract

The development of high-brilliance synchrotron radiation sources and high intensity neutron sources have provided powerful new methods for probing the structure and dynamics of nanostructured materials. We shall review some of the recent applications of these techniques to the study of nanomaterials and biomaterials. These include both scattering and real-space imaging methods and the use of coherent X-ray beams for studying nanostructures, the use of neutron scattering and resonant magnetic X-ray scattering to study magnetic nanostructures, and the use of inelastic neutron scattering and X-ray photon correlation spectroscopy to study their dynamics. Examples will be given of application of such techniques to the study of magnetic dot and hole arrays, structure of confined nanofluids, films exhibiting exchange bias and spin valve effects, spin injection into semiconductors, and biomembranes.

PAPER NOT YET RECEIVED

OPERATION AND RECENT DEVELOPMENTS AT THE SIAM PHOTON SOURCE

P. Klysubun[#], S. Rugmai, S. Rujirawat, S. Cheedket, C. Kwankasem, G. Hoyes, and M. Oyamada, NSRC, Nakhon Ratchasima, Thailand

Abstract

The Siam Photon Source (SPS) is a dedicated synchrotron radiation facility located in Nakhon Ratchasima, Thailand. After successful commissioning and recent energy upgrade from 1.0 GeV to 1.2 GeV, the Siam Photon Source is currently well into user mode of operation. The light source is now providing routinely synchrotron radiation in the vacuum ultraviolet and soft x-ray spectral ranges to both internal and external researchers. In this report we describe the overview of the current machine performance including user availability, the progresses made recently, and the planned machine improvements, which emphasizes on improving beam stability and machine reliability. Plan to install two insertion devices, a permanent magnet planar undulator and a superconducting magnet wavelength shifter, is also discussed.

INTRODUCTION

The Siam Photon Source (SPS) is a synchrotron light source operated by the National Synchrotron Research Center (NSRC), and is located in Nakhon Ratchasima, Thailand. The accelerator complex consists of two 20-MeV injector linacs, a 1.0-GeV booster synchrotron, and an electron storage ring. The storage ring was originally designed to operate at 1.0 GeV and was later upgraded for 1.2-GeV operation in 2005 [1]. The lattice of the storage ring is a double bend achromat (DBA) lattice with four superperiods for a total of eight bending magnets. The ring is equipped with four straight sections for insertion devices. Currently the beam is injected to the storage ring at 1.0 GeV and then ramped up to 1.2 GeV. It is planned that the energy of the booster synchrotron will also be upgraded to 1.2 GeV for full energy injection and subsequently top-up mode of operation of the storage ring. Machine specifications of the SPS can be summarized as listed in Table 1. At present there are three photon beamlines in operation: a photoelectron spectroscopy (PES) beamline (BL-4) operated in the vacuum ultraviolet (VUV) spectral range, an x-ray lithography (XRL) beamline (BL-6), and an x-ray absorption fine-structure spectroscopy (XAFS) beamline (BL-8). All three are bending magnet beamlines.

Table 1: Summary of SPS machine specifications

Electron beam energy [GeV]	1.2
Beam current [mA]	120
Lattice	DBA
Superperiod	4

Horizontal emittance [nm·rad]	41
Coupling [%]	0.8
Circumference [m]	81.3
Number of straight sections	4 (7 m)
Betatron tunes ν_x, ν_y	4.75, 2.82
Synchrotron tune ν_s	2.33×10^{-3}
Natural chromaticities ξ_x, ξ_y	-9.40, -6.61
Momentum compaction	0.0170
RF frequency [MHz]	118
Harmonic number	32
RF voltage [kV]	120
RF power [kW]	14
Number of RF cavity	1
Energy loss per turn [keV]	65.94
Injection beam energy [GeV]	1.0
Number of beamlines	3

OPERATION AND MACHINE PERFORMANCE

In the year 2006 the SPS has been operated in user mode of operation, providing routinely synchrotron radiation in the VUV and soft x-ray spectral ranges to users. The weekly operation schedule has been such that Monday morning was reserved for weekly preventive maintenance, while Monday afternoon and every other Tuesday were designated for machine study. The rest of the week until 2 PM Friday was scheduled for user experiments. Since the beam lifetime in the storage ring was still comparatively short, the beam was injected four times a day. The time it took for beam injection and energy ramping was approximately one hour for each round of injection. At the beginning of the year the beam lifetime was around 2.5 hours at 100 mA beam current. As time passed vacuum condition in the ring was improved by continual photodesorption, which in turn increased the beam lifetime. At the end of the year the beam lifetime increased to around 4 hours at 100 mA stored current, and was still increasing.

Table 2 shows the comparison between the scheduled beamtime and the beamtime actually delivered to the users in 2006. In total 1865 hours of user beamtime were scheduled and 1571 hours were actually delivered, resulting in the user beam availability of 84.25%. There were several machine problems which contributed to unscheduled downtime in 2006. It has been found that the main cause of the machine downtime was the electrical instability of the 22-kV electrical line supplying the SPS which led to numerous machine trips. This was even more prevalent during the rainy season. The problem is being addressed with the construction of a new electrical

SESAME STATUS

G. Vignola, A. Amro, M. Attal, H. Azizi, A. Kaftoosian, F. Makahleh, M. Shehab, H. Tarawneh, S. Varnasseri. SESAME, c/o UNESCO Amman Office, P.O. Box 2270, Amman 11181, Jordan

Abstract

An update of the status of SESAME[*] is presented. SESAME is a third generation light source facility, with an e-beam energy of 2.5 GeV, located in Allan, Jordan. The emittance is 26 nm.rad and 12 straights are available for insertion devices. The injector consists of a 22.5 MeV microtron and 800 MeV booster synchrotron, with a repetition rate of 1 Hz. The conceptual design of the accelerator complex has been frozen, and the engineering design is well advanced. The Phase I scientific program for SESAME has also been finalized, and it foresees 6 beam lines, including 2 IR ports. The construction of the SESAME building is in progress, and the beneficial occupancy is expected by late spring of 2007. The completion of the accelerators complex construction is scheduled for 2010.

INTRODUCTION

The technical evolution of SESAME is described in [1, 2]. The Building that will house SESAME is under construction with funds and site provided by Jordan (see Fig. 1), under the supervision of R. Al Sarraf, from Al-Balqa University. Its completion, including a 6.0 MVA dedicated Electrical Power Station, is scheduled by the first half of 2007.

Figure 1: A panoramic view of SESAME building during construction (Nov. 2006).

Fig. 2 shows the layout of the accelerator complex and beamlines in the experimental hall. The injector complex (800 MeV booster synchrotron and 22.5 MeV Microtron) is the one already used in Bessy I [3], with new power

---

supplies and vacuum pumps. The 2.5 GeV Main Storage Ring is completely new.
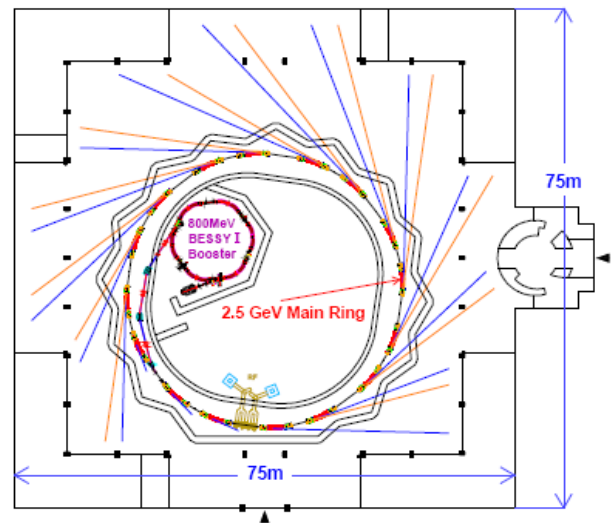
Figure 2: SESAME layout in the experimental hall.

THE MAIN STORAGE RING

The main storage ring parameters are given in Tab. 1. The storage ring is composed of 8 super periods with 16

Table 1: SESAME design parameters.

Energy (GeV)	2.5
Circumference (m)	133.12
N. of Periods	8
Dipole field (T)	1.455
Dipole field index	11
Q_x - Q_z	7.23 – 6.19
Mom. Compaction	0.00829
N. Emitt.(nm.rad)	26.0
U_0 (keV/turn)	589.7
τ_ε, τ_x, τ_z (ms)	2.80, 2.28, 3.77
RF freq. (MHz)	499.564
Harmonic Number	222
Peak Voltage(MV)	2.4
Synch. Freq. (kHz)	37.18
σ_L (cm)	1.15
Current (mA)	400
N. of bunches	200
1/e Lifetime(hrs)	16.9

---

[*]Synchrotron-light for Experimental Science and Applications in the Middle East is a cooperative venture by the scientists and governments of the region with founding members Bahrain, Egypt, Israel, Jordan, Pakistan, Palestine Authority, Cyprus and Turkey. Iran is in the process of finalizing its formal membership.

NSLS-II DESIGN: A NOVEL APPROACH TO LIGHT SOURCE DESIGN *

S.L. Kramer, J. Bengtsson, S. Krinsky, V.N. Litvinenko, and S. Ozaki for NSLS-II Design Team[#]
BNL/NSLS, Upton, NY 11973, U.S.A.

Abstract

The NSLS-II storage ring will be a replacement for the existing two NSLS light sources, which although innovative when proposed, have been exceeded by modern light source designs. NSLS-II design takes a new approach toward providing users with the very bright beams after commissioning and a strategy of evolving to higher brightness beams as more ID devices are installed during its operations. This is achieved not by pushing the basic lattice to lower emittance, an approach that hits severe limits in the control of the dynamic aperture of an ever increasing non-linear lattice. Our approach is rather to reduce the natural emittance using damping wigglers, in addition to damping from the user undulator's. Details on the lattice design are presented.

INTRODUCTION

NSLS-II is the proposed replacement of the NSLS light sources that have been operating for more that 23 years. The storage ring requirements of the lattice are:

Ultra-low horizontal emittance ε_x <1.0nm (achromatic),
Diffraction limited vertical emittance at 12KeV,
$I_o \geq$ 500mA, Top-off injection, and
More than 24 ID straight section $\geq$5m, for IDs,

After several years of study a DBA lattice with 30 cells has been selected.   This lattice while not reaching the emittance goal by itself has been designed to achieve this goal using damping wigglers (DWs) rather than the lattice functions. This avoids the difficulty in dealing with high chromaticity and low dynamic aperture (DA) that limits ultra-low emittance lattice designs. The DA impact of the DWs and undulators must be handled for any lattice and have less impact on the DA than the strong sextupole of alternate lattice designs. Also the number of cells provides for sufficient beam ports for our current VUV and Xray ring users, when those ring are decommissioned.

LINEAR LATTICE CHOICE

The basic light source lattices that can be used are: double bend (DBA) and triple bend (TBA) achromatic lattices. For *M* cells the theoretical minimum emittance is given by [2]:

$$\varepsilon_{MEDBA} = \frac{\gamma^2}{M^3}(0.77 \; pm-radians) \qquad (1)$$

$$\varepsilon_{METBA} = \frac{\gamma^2}{M^3}(0.151 \; pm-radians) \qquad (2)$$

where γ is the relativistic energy and the horizontal partition factor J_x is assumed unity. For low emittance, the lowest possible energy is preferred, this is possible due to the advances with in-vacuum, small gap and short-period

undulators pioneered at the NSLS [3]. The Xray energy range of 2-20 keV can now be achieved with ~3 GeV beam energy, lowering the RF power and shielding cost for either ring.

A 24-cell TBA, with a potentially factor of five lower emittance per cell, was initially preferred. Due to difficulties in achieving large DA, the emittance goal had to be relaxed [4]. At that time a bold suggestion was made by S. Krinsky [1], to provide the initial emittance with a DBA lattice and use the extra straight sections for DWs to lower the emittance. Although this was a novel approach for new 3rd generation light sources, this idea has been used in colliders [5,6] and previously proposed for light sources [7,8]. This is the approach taken for NSLS-II, using a 30 cell DBA lattice with alternating long and short ID straight sections, one cell is shown in Figure (1).
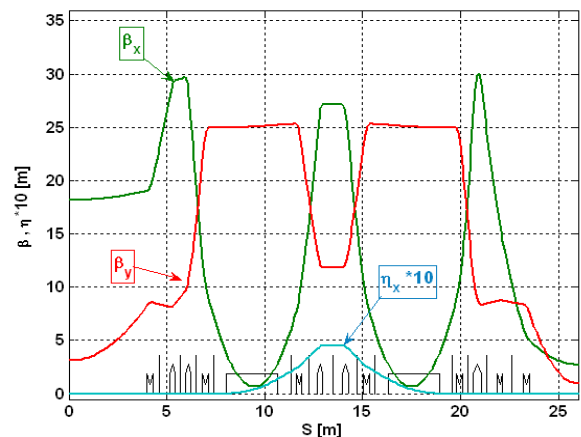
Figure (1) Twiss parameters for one cell of the DBA(15x2) lattice, with 8 and 5m ID lengths.
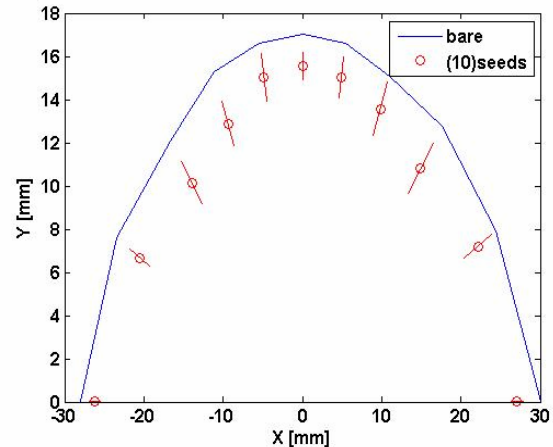
Figure (2) DA for the lattice with alignment tolerances (no field errors) and synchrotron oscillations (δ=0). Orbit distortions are corrected with beam based aligned BPMs.

This lattice was optimized for efficient use of the DWs for reducing the emittance, using weak dipole magnets

STATUS OF THE NOVOSIBIRSK HIGH POWER TERAHERTZ FEL*

S.V. Miginsky[#], N.A. Vinokurov, D.A. Kayran, B.A. Knyazev, E.I. Kolobanov, V. V. Kotenkov, V.V. Kubarev, G.N. Kulipanov, A.V. Kuzmin, A.S. Lakhtychkin, A.N. Matveenko, L.E. Medvedev, L.A. Mironenko, A.D. Oreshkov, V.K. Ovchar, V.M. Popik, T.V. Salikova, S.S. Serednyakov, A.N. Skrinsky, O.A. Shevchenko, M.A. Scheglov, Budker INP, Novosibirsk, Russia.

Abstract

The first stage of Novosibirsk high power free electron laser (FEL) has been commissioned in 2003. It is based on the normal conducting CW energy recovery linac (ERL). Now the FEL provides electromagnetic radiation in the wavelength range 120 - 230 micron. The maximum average power is 400 W. The minimum measured linewidth is 0.3%, which is close to the Fourier-transform limit. Four user stations are in operation now. Manufacturing of the second stage of the FEL based on a four-track energy recovery accelerator is in progress.

INTRODUCTION

A new source of terahertz radiation was commissioned a few years ago in Novosibirsk [1]. It is a CW FEL based on a ERL. Its differences from other ERL-based FELs [2, 3] are: a low frequency non-superconducting RF system and longer wavelength operation range. A full-scale Novosibirsk FEL will be based on the four-track 40 MeV energy recovery accelerator (see Fig. 1). It will generate radiation in the range from 5 micrometer to 0.24 mm [4, 5] together with the first-stage FEL.
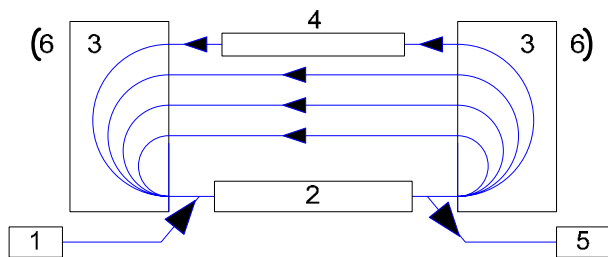
Figure 1: Scheme of an energy recovery accelerator based FEL. 1 - injector, 2 - accelerating RF structure, 3 - 180-degree bends, 4 – undulator, 5 – beam dump, 6 – mirrors of the optical resonator.

ACCELERATOR-RECUPERATOR

The first stage machine contains a full-scale RF system, but has only one track. The scheme of the ERL is shown in Fig. 2. A 2 MeV electron beam from an injector passes through the accelerating structure, gains 12 MeV energy there, and comes to an FEL, installed in the straight section. After interaction with radiation in the FEL the beam passes once more through the accelerating structure, returns the power, and comes to a beam dump at the injection energy. Main parameters of the accelerator are listed in Table 1. The electron source is a 300 keV DC gun with a gridded cathode. Maximum charge per bunch is 1.7 nC.

Table 1: Accelerator parameters (first stage)

RF frequency, MHz	180
Number of RF cavities	16
Amplitude of accelerating voltage at one cavity, MV	0.7
Injection energy, MeV	2
Final electron energy, MeV	12
Maximum bunch repetition rate, MHz	22.5
Maximum average current, mA	20
Beam emitance, mm·mrad	2
Final electron energy spread, FWHM, %	0.2
Final electron bunch length, ns	0.1
Final peak electron current, A	10

FEL

The FEL is installed in a long straight section of the backward track of the ERL. It consists of two undulators, a magnetic buncher, and an optical resonator. Both electromagnetic planar undulators are identical: the length is 4 m, the period is 120 mm, the gap is 80 mm, and the deflection parameter K is up to 1.2. The buncher is a three-pole electromagnetic wiggler. It is necessary to optimize the relative phasing of undulators and is used now at low longitudinal dispersion $N_d < 1$.

Both laser resonator mirrors are spherical, of 15 m curvature radius, made of gold-plated copper, and water-cooled [6]. There is a hole in the centre of each mirror. It is intended for mirror alignment (using the He-Ne laser beam) and output of small amount of radiation. The distance between the mirrors is 26.6 m. The forward mirror has the hole of the diameter 3.5 mm, while the rear one of 8 mm (see Fig.3). The calculated transparency of the 8-mm hole mirror is 1.5% at the wavelength 150 μm. The measured round-trip loss is near 7% at this wavelength. The output radiation passes through two windows which separate the FEL vacuum system from the atmosphere. An additional iris and a normal-incidence quartz window are installed after the forward mirror. A diamond window tilted at the Brewster angle is used for outcoupling behind the rear mirror.

BUNCH COMPRESSION USING THE TRANSPORT LINE AND SHORT BUNCH REVOLVING IN NEWSUBARU

S. Suzuki*, T. Asaka , JASRI/SPring-8, 679-5198, Japan

T. Matsubara[#], T. Mitsui, Y. Hisaoka, Y. Shoji, LASTI, University of Hyogo, 678-1205 Japan

Abstract

The electron bunches was compressed to a few pico-seconds rms by the transport line from SPring-8 linac to NewSUBARU storage ring (NewSUBARU). And the compressed bunch was circurated for some tens of turns after injection while maintaining the short bunch length in the NewSUBARU. The NewSUBARU was set to a quasi-isochronous condition. Bunch length in the NewSUBARU was measured the streak camera and maicrowave detector. There data was not accord by the deformation of the bunch structure.

INTRODUCTION

The production of short bunches is an important technique, since bunches on a millimeter scale are necessary for time-resolved experiments and for stable production of coherent synchrotron radiation (CSR). Some methods have been proposed for producing a short electron bunch in a storage ring, like the laser-slicing method [1] and the quasi-isochronous (QI) operation of a storage ring [2]. The ring stores electron bunches as short as a few pico-seconds in a stationary state. These two methods produce more stable radiation than that produced by a linac. However, the beam charge in a short bunch is much smaller than in a bunch produced by a linac.

This paper reports a demonstration of another method, which is based on a combination of a linac and a storage ring. A short, high-current bunch is produced with a linac and a bunch compression system. The short bunch is injected into an isochronous ring, and circulates for many turns. The bunch length becomes longer even in an ideal isochronous ring because of the longitudinal radiation excitation, but this takes many turns [3]. This method has several merits: (1) a bunch with higher charge is possible in a storage ring than with the existing two methods; (2) one short bunch produced by the linac is reused at every turn of the ring that it makes; (3) the repetition rate of the radiation pulse can be very stable in an isochronous ring; (4) pulsed light is obtained in every beam line of the storage ring; (5) a few pico-seconds long pulse is possible with no special expense; and (6) future improvements of the linac beam quality would give better performance of this method.

The aims of this report are (a) to demonstrate the method, (b) to investigate the problems associated with it, and (c) to clarify the limitations of the present hardware, the SPring-8 linac, and the NewSUBARU. The results of our experiment provide suggestions for future light source

projects with an energy recovery linac and a more sophisticated short-bunch circulator [4].

EXPERIMENTS AND MEASUREMENTS

Bunch Compression of Linac Beam

Figure 1 shows the layout of the SPring-8 linac [5], the energy compression system (ECS) [6], the booster synchrotron, and the NewSUBARU [7]. Tables 1 and 2 show the main parameters of the linac and the NewSUBARU. In normal operation, the typical bunch length of the linac bunch was about 20 ps (full width), and the energy spread was 0.7% (full width) at 1 GeV. However, in this experiment, the chicane of the ECS was bypassed and the acceleration cavities of the ECS were used to compress the bunch as it passed through the transport line to the NewSUBARU. Figure 2 shows the simulation of the bunch length from the ECS to the injection point of the time profile and η-function.
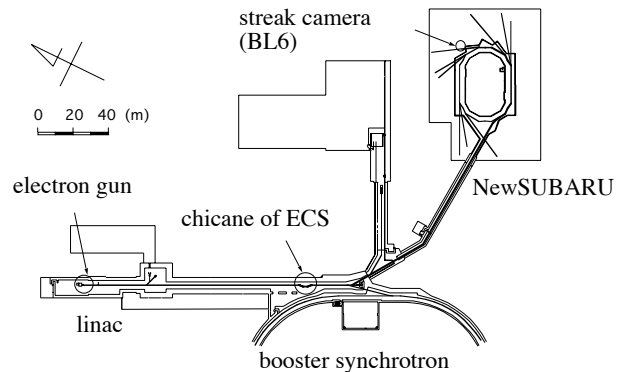
Figure 1: Layout of the SPring-8 linear accelerator, the energy compression system (ECS), the booster synchrotron, and the NewSUBARU. The streak camera is placed in beamline 6 (BL6) of NewSUBARU.
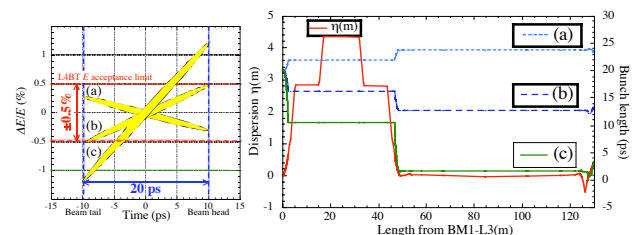
Figure 2: Simulation of the bunch length from the ECS to the injection point. Each line corresponds a difference of phase space of a left-hand figure.

Figure 3 shows the bunch length measured by a streak camera in beamline 6 (BL6) [8]. Stronger compression was in principle possible but the transport line would not

* shin@spring8.or.jp

Present address: Sumitomo Heavy Industries Ltd.

STATUS OF THE INDUSTRIAL RF-ACCELERATORS IN BINP

D. Artamonov, V. Auslender, V. Bezuglov, A. Bryazgin, V. Gorbunov, V. Cheskidov, I. Gornakov, B. Faktorovich, V. Nekhaev, V. Podobaev, A. Panfilov, A. Sidorov, E. Shtarklev, V. Tkachenko, A. Tuvik, L. Voronin,

BINP, Novosibirsk, Russia

Abstract

The report describes ILU type industrial electron accelerators. It describes their main parameters, design, principle of action, electron beam extraction devices, wide set of auxiliary equipment for various technological processes and ways of their usage.

INTRODUCTION

The pulse nature of the generated electron beam (their main difference from the widely used high voltage accelerators generating continuous electron beam) permits to adapt ILU machines easily to technological processes requiring formation of an irradiation zone with a complex configuration. The most bright example of such process is the irradiation of polymer insulation of cables and thermoshrinkable tubes. In this case the usage of 4-sided irradiation permits sharply to raise the productive rate of process, to improve quality of production and to expand the nomenclature of treated products without increase of electron energy. The ILU machines designed and produced in the Institute cover the energy range from 0.6 MeV to 5 MeV, and the maximum beam power is 50 kW.

The main activity field of ILU Laboratory of BINP is the development, manufacturing and supply of the ILU accelerators for industry. Up till now more than 50 machines are installed, about 30 of them are installed worldwide. The ILU machines are successfully working in the industrial lines in Korea, China, India, Italy, Poland, and other countries.

Table 1: Main parameters of the ILU accelerators.

PARAMETERS	ILU-6	ILU-8	ILU-10	ILU-12 Proj.
Energy of electrons, MeV	1.2-2.5	0.6-1.0	2.5-5.0	4.0-5.0
Average beam power (max), kW	20	25	50	300
Average beam current (max), mA	20	30	15	60
Power consumption, kW	100	80	150	700
Accelerator weight, tons	2.2	0.6	2.9	5

- Single-resonator ILU type accelerators have simple design, hence they are reliable, have low cost, and is easy to maintain. The used generator scheme with self excitation and pre-excitation allowed us to provide the absolute stability of the RF system.
- Placing the electron gun directly into the accelerating gap with using the adjustable cathode voltage shift allows us to adjust the beam pulse current and so the average power within the wide range of values.
- In ILU 10 the additional RF voltage of the operating frequency with the phase shift relative to the accelerating voltage is applied to the cathode-grid gap, that allowed us to greatly decrease the accelerated beam energy spread.

ACCELERATOR ILU-6.

The base model of the family is ILU-6. This machine has rather high parameters at modest dimensions and can be used for wide spectrum of technological processes. A principle of high-voltage acceleration is used in majority of modern accelerators, i.e., the energy of electrons corresponds to the voltage generated by the rectifier. The industrial accelerators type ILU are the exception of this rule. A principle of acceleration of electrons in the gap of HF resonator is used in the ILU machines. Such accelerator does not contain details, potentials of which with respect to the ground is comparable to accelerating voltage. So the complex high-voltage units (accelerating tubes, sections of rectifiers and etc.) which are damaged by the occasional discharges are not used in ILU machines. And so there is also no necessity to use insulating gas and high-pressure vessels. Use of a principle of high-frequency acceleration has allowed to create rather simple design of the machine having modest dimensions and weight. As a result the machine can be placed inside the hall of the smaller dimensions compared to the halls for high-voltage accelerators having the same parameters. Figure 1 represents the accelerating system of the accelerator ILU-6 for explanation of a principle of action of the ILU machines. The accelerating system consists of copper toroidal resonator 1 placed inside the vacuum tank 2. The resonator consists of top and bottom halves, on the internal protrusions of which the electrodes forming an accelerating gap are installed. The top electrode has a built-in control grid. The cathode unit is mounted on this electrode on the insulator, and together with the grid it forms an electron injector (gun). The bottom electrode and the injector together form the accelerating system. The current of a beam of accelerated electrons is controlled by varying the value of positive bias on cathode concerning the grid. To suppress the high-frequency resonance discharge in resonator the bottom half of it is installed on insulators and the bias

PRACTICAL CONSIDERATIONS IN THE DESIGN OF A HIGH CURRENT COMMERCIAL H-MINUS CYCLOTRON

M. Dehnel, T. Stewart, M. Roeder, J. Theroux, P. Jackle, Dehnel – Particle Accelerator Components & Engineering, Inc., P.O. Box 201, Nelson, B.C., Canada V1L 5P9

Abstract

High current H$^-$ cyclotrons (>1000 μA) are being developed and implemented for radioisotope production, radioactive therapeutic implants and other applications. The beam dynamics and general physics design of these cyclotron systems must be well done. However, to not compromise an elegant and effective physics design, engineering practicalities must be carefully considered and then implemented. Based on our experience in the design, upgrading, and maintenance of commercial H$^-$ cyclotron systems, we offer practical issues and solutions to be considered in the engineering design and implementation of such high current systems.

INTRODUCTION

Of the modern commercial 30 MeV H$^-$ cyclotrons utilizing axial injection, over thirty Cyclone30s, and about a half-dozen TRIUMF technology TR30s are installed.

Given the large number of Cyclone30s, this paper uses the Cyclone30 design circa the late 1990s and earlier as a baseline reference, and discusses practical engineering improvements to be made to this cyclotron to enable reliable and consistent operation at high current. This would increase radioisotope production yields, and operational cost-effectiveness.

ION SOURCE & INJECTION SYSTEM

The Cyclone30 ISIS is mounted on the moveable upper half of the cyclotron on a cantilevered support. Beam injection is downwards as shown in the left hand side (LHS) of Figure 1. This is problematic because the ISIS is moved each "lid-up" maintenance, and with a springy cantilevered support structure the ISIS frequently becomes misaligned and requires correction as shown in the right hand side (RHS) of Figure 1. The solution is to use a permanently aligned ISIS mounted to the lower fixed half of the cyclotron with a sturdy support structure.

The ISIS vacuum is provided by a diffusion pump system (Figure 2 LHS), which introduces hydro-carbon molecules into the ion source chamber [1,2]. The hydro-carbons interfere with H$^-$ production, reduce filament life-time to ~80 hours within months, and over this time scale deposits 2 to 3 mm of material on the chamber walls. With the ion source emitting the beam downwards, debris from the deposits falls onto the grounded plasma electrode as shown in Figure 2 RHS. Some of this debris falls through the lens aperture into the injection line buncher wires, and onto the inflector electrodes. Cleaning a thick coating with a blunt instrument requires

a great deal of force risking micro-cracking of the source chamber and concomitant water leaks.

An ion source mounted on the lower fixed side of the cyclotron stops debris falling into the cyclotron. Thick deposition and debris can effectively be eliminated by the use of the TRIUMF source [3]. The TRIUMF source utilizes Cryo/Turbo pumping for a clean environment, and only a very thin deposition layer must occasionally be cleaned using fine grit sandpaper.
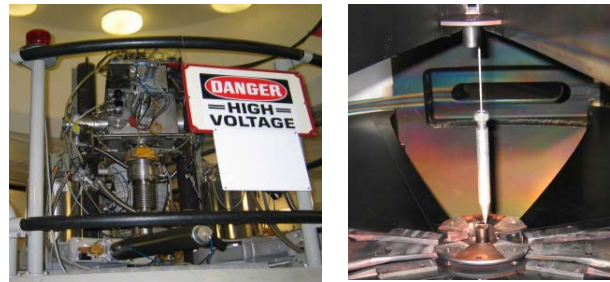
Figure 1: LHS shows ISIS on top of Cyclone30, and RHS shows ISIS out of alignment after several tank openings.

Figure 2: LHS shows Cyclone30 ISIS diffusion pump. RHS shows ion source with hydro-carbon debris.

Figure 3 LHS shows a hairpin tungsten filament with eroded supports due to exposure to the plasma, and RHS shows the backplate with two cusp magnet rows. The TRIUMF source utilizes tantalum ring filaments, recessed support posts, and four backplate cusp magnet rows for improved H$^-$ performance. The absence of a filament induced magnetic field in the TRIUMF ion source centre contributes to a quiescent plasma [4].

The plasma lens (Figure 2 RHS) is at the same electric potential as the source body, whereas in the TRIUMF case it is electrically biased for optimized H$^-$ production and a three-fold reduction in extracted electrons [1]. In addition, the TRIUMF puller lens utilizes a double-dipole magnetic electron filter with ($\int$Bdl = 0), whereas the Cyclone30 typically utilizes a single dipole magnetic field

THE COMPACT INDUCTION CIRCULAR ACCELERATOR FOR RADIATION TECHNOLOGIES

G.V. Dolbilov[#], Joint Institute for Nuclear Research, Dubna, 141980, Russia.

Abstract

The variant of the circular accelerator of electrons with energy up to 10 MeV is discussed. Acceleration is carried out by an induction electric field on a constant equilibrium orbit of radius about 50 cm. For reduction of reactive power of the accelerator the alternating magnetic fields are concentrated in small volume near to the equilibrium orbit. Use of high-frequency magnetic fields (tens or hundreds кHz) allows to increase power of the accelerated electron beam up to some tens kW or some hundreds kW.

INTRODUCTION

The wide range of possible parameters of a electron beam allows to use these accelerator for a wide spectrum of applications: protection of an environment (for example: clearing flue gases of the industrial enterprises from harmful impurity NOx, SOx, etc.), updating and reception of the new materials, new technologies without application of harmful chemicals (polymerization of various materials, etc.), sterilization of medical tools, disinfection of medical and other waste products. Researches have shown, that methods of radiating processing of foodstuff (radurisation) in many cases successfully solve the problem long storage of products without infringement of their flavouring and nutritious qualities. Small dimensions and low cost of the accelerator, will allow to use it on fishing seiners for sterilization of fish products.Manuscripts

For many radiation technologies electron beams with energy 0.5 – 10 Mev with average energy of a beam from $\sim 10^3$ to $\sim 10^5$ W are required. As to energy such beams can be received by acceleration of electrons in the circular induction accelerator – betatron. Essential feature of the betatron work consists in the fact that speed of change of the average magnitude of a magnetic field induction B_{aver} should exceed twice speed of change of an induction in an equilibrium orbit B_0. It is well-known a betatron condition «B_{aver}: $B_0 = 2:1$» when the radius of an electron orbit remains to constants in a magnetic field growing in time.

Betatron rate «2:1» limit an average power of an accelerated electron beam because magnetic flux inside an equilibrium orbit and magnetic energy are very high. The number of particles, accelerated in one cycle of acceleration, is limited to instability of an electron beam, and the increase of a repetition rate demands increase in average power of accelerator power supplies which has a limit too.

The radius of an equilibrium orbit can remain to constants at increase in a magnetic induction in an orbit at

B_{aver}: $B_0 << 1$ if special ratio between amplitude-time characteristics of a magnetic induction in an orbit and an induced accelerating voltage are carried out. At $B_{aver}<<B_0$ magnetic energy of the accelerator decreases and so both frequency of accelerating cycles and average capacity of the accelerated beam can be essentially increased. And use of rigid focusing by magnetic field B_0 with the high radial gradient (the module /n/>> 1) allows to increase number of electrons in the orbit and to reduce dimensions of magnetic system.

MAGNETIC SYSTEM

The magnetic field in an equilibrium orbit is formed by C-shaped electromagnets with the high parameter of the field $n_1 >> 1$ (Figure 1(a)) and $n_2 << -1$ (Figure 1(b)). The combination of such magnets allows to realize rigid focusing of electrons. Electromagnets are fed by a rectangular wave of a voltage V_0 (Figure 2(a)) and form the magnetic B_0 induction which form is shown on Figure 2(b). For reduction of energy losses at magnetic reversal of electromagnet cores the magnitude of induction chooses much less induction of saturation of a core material .
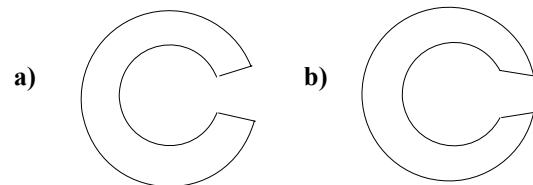
Figure 1: C-shaped cores of electromagnets: a) n >> 1, b) n <<-1.
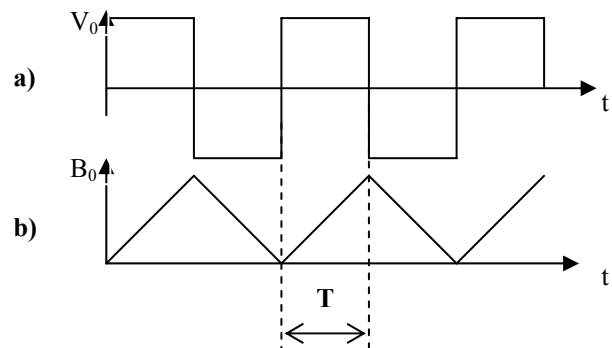
Figure 2: a) Square wave of Power System, produced by transistor converter, b) Form of magnetic induction B_0.

ACCELERATING SYSTEM

Electrons are accelerated by the electric field induced by O-shaped ferromagnetic cores which are located on

RF AMPLIFIERS AND STRUCTURES FOR ISAC/TRIUMF

A.K. Mitra, Z. T. Ang, Y. Bylinski, K. Fong, R.E. Laxdal , J. Lu, R. Poirier,
V. Zvyagintsev, TRIUMF, Vancouver, Canada

Abstract

   The ISAC-I accelerator is comprised of two room temperature linacs; a 35MHz RFQ and a 106MHz separated function drift tube linac producing an accelerating voltage up to 4.5MV and 8.1MV respectively. In addition a pre-buncher, chopper and several re-bunchers are used in the accelerator chain to manipulate the longitudinal phase space. A heavy ion superconducting linac is being installed at ISAC/TRIUMF to increase the energy of ISAC-I from 1.5 MeV/u to 6.5 MeV/u for ISAC-II. A first stage, now in commissioning, consists of twenty medium beta cavities driven by twenty, 106MHz, tube amplifiers. In the second stage of ISAC-II, 20 high beta quarter wave superconducting cavities will be installed operating at 141 MHz. A transfer line connecting ISAC-I and ISAC-II has a room temperature buncher cavity at 35 MHz. This report will summarize rf amplifiers employed in ISAC facility and discuss the choice of amplifiers for the second stage of ISAC-II. Some of the re-furbishing and improvements that are done to ISA-I rf system will also be discussed.

INTRODUCTION

   A heavy ion superconducting linac with a total accelerating voltage of 20 MV is being installed as a first stage of the ISAC-II upgrade as an addition to the existing room temperature linac ISAC-I. ISAC–I has the capability of maximum energy of 1.8 MeV/u for ions with A/q ≤ 6 [1]. For ISAC-II a beam of 1.5MeV/u is delivered from the exit of IH-DTL5 of ISAC-I to the entrance of the medium β section of the SC linac via a 25m transfer line. In the second stage of the ISAC-II upgrade, an additional 20 superconducting high beta cavities will be added in the same accelerating vault to produce an accelerating voltage of 20 MV for masses up to 150, with A/q ≤ 7. The medium beta cavities employ 106 MHz tube amplifiers whereas the rf amplifiers for the high beta cavities operating at 141 MHz will be decided soon.

ISAC

ISAC-I

   The ISAC–I heavy ion linac is composed of room temperature rf structures operating at various rf frequencies [2]. Figure 1 shows the layout of the accelerator as well as the S-bend transfer line joining ISAC-I and ISAC-II. Table 1 shows the list of room temperature rf structures and rf amplifiers with power requirements for the accelerating voltages. ISAC-I has been operational since 2000 with excellent performance [3]. Some of the re-furbishing and improvements that were carried out are mentioned here. The RFQ which was operational since 1999 was opened in 2006 spring

shutdown since the vacuum deteriorated to 2×10^{-6} from 5×10^{-7} Torr. Water leaks in two of the split ring resonators of the RFQ and cooling line brazing joints were the major cause for poor vacuum. They were replaced with two identical rings and joints were repaired.
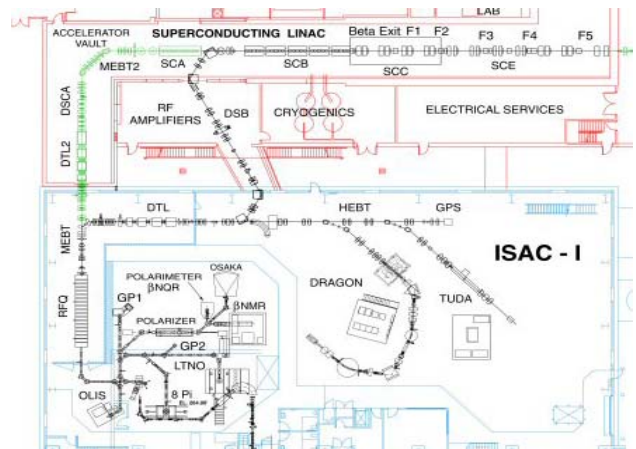
Figure 1: Layout of ISAC linear accelerator

Table 1: ISAC-I Room Temperature RF Structures

RF Device	RF Structure Type	Frequency	Electrode Voltage	Nominal Power
		MHz	V	P
Prebuncher	Parallel Plates	11, 23, 35	400 V	500 W
RFQ	Split Ring 4 Rod	35.36	74 kV	80 kW
Bunch Rotator	Split Ring	106.08	35.5 kV	3.5 kW
Chopper	Coil + Parallel Plates	5.89	5.5 kV	45 W
Chopper	Coil + Parallel Plates	11.78	7.4 kV	140 W
Rebuncher	Spiral	35.36	30 kV	1 kW
DTL Tank1	IH	106.08	47 kV	3.9 kW
Buncher 1	Split Ring	106.08	55 kV	8 kW
DTL Tank2	IH	106.08	69 kV	10 kW
Buncher 2	Split Ring	106.08	74 kV	10.2 kW
DTL Tank3	IH	106.08	97 kV	16 kW
Buncher 3	Split Ring	106.08	91 kV	11.6 kW
DTL Tank4	IH	106.08	109 kV	19 kW
DTL Tank5	Split Ring	106.08	116 kV	20.3 kW
Low Beta Buncher	Coil + Drift Tube	11.78	30 kV	1.5 kW
High Beta Buncher	Spiral	35.36	170 kV	12.6 kW
S-bend buncher	Spiral	35.36	170 kV	12.6 kW

The most probable cause is due the use of very aggressive flux which was applied for soldering of copper and

SCSS RF CONTROL TOWARD 5712 MHz PHASE ACCURACY OF ONE DEGREE

Yuji Otake, Hirokazu Maesaka , Masanobu Kitamura , Tumoru Shintake, RIKEN, Harima Institute
1-1-1 Kouto, Sayo-tyou, Sayo-gun, Hyogo, 679-5148, Japan
Takashi Ohshima, Naoyasu Hosoda, Toru Fukui, Toru Ohata, Japan Synchrotron Radiation
Research Institute (JASRI/SPring-8), Kouto, Sayo-tyou, Sayo-gun, Hyogo, 679-5198, Japan

Abstract

A 250 MeV prototype accelerator was built. Its low-level rf system, which mainly controls a 5712 MHz pulsed rf signal, was built to achieve very tight requirements: phase stability and a setting resolution of less than 1 deg.. These requirements correspond to a beam energy variation of 10^{-4} at the crest acceleration for the 5712 MHz rf. To realize the requirements, IQ-modulators/demodulators and arbitrary wave form generators/digitizers of VME modules (D/A, A/D) to handle an IQ-function were developed. The PID control method was employed to compensate for any time drift, such as an rf phase. We finally achieved phase setting and a detecting resolution of the IQ-modulators/demodulator of +/- 0.5 deg. at 5712 MHz. Decreasing the phase drift with in +/- 0.5 deg. was also achieved by a PID control program. By this control performance, a beam energy variation of 0.06% was achieved.

INTRODUCTION

To check the feasibility of X-FEL(SCSS),[1] the 250 MeV prototype accelerator was constructed at SPring-8 [2]. The construction was started from October, 2004, and finished in December, 2005. After construction, we confirmed 49 nm SASE light by the prototype accelerator with 250 MeV, 0.2 nC electron beams, and 10 Hz reputation [2,3]. This 60 m long accelerator comprises a 500 kV CeB6 mono-crystal thermionic electron gun with a beam deflector for making a 1ns (FWHM) beam pulse width, a 238MHz pre-buncher cavity and a 476 MHz booster cavity for bunching and accelerating beams, a 2856 MHz APS cavity and a 2856 MHz/2m long accelerator guide to obtain 50 MeV beams, four 1.8 m

long/5712 MHz accelerator guides to make the beam energy up to 250 MeV, and two 3 mm gap in-vacuum undulators to generate 49 nm laser light. In the case of the prototype accelerator, the pulse width of the beams should be compressed to 1 ps by a magnetic bunch compressor to obtain about a 1 kA peak current for generating SASE [3]. Therefore, a low-level RF system of the accelerator was built to achieve very tight requirements, which were 5712 MHz phase stability and a resolution of less than +/-0.5 deg., as well as 5712 MHz amplitude stability and a resolution of less than 10^{-4} [4]. These requirements correspond to a beam energy variation of less than 10^{-4} at a crest acceleration of a 5712 MHz rf. This phase value corresponds to time stability and a resolution of less than 500 fs. Such stability and a resolution are necessary to achieve 100 μm pointing stability of electron beams and to generate laser light for the undulator section of about 10 m long [5]. This paper gives a summary and describes the performance of the low-level rf system and its key components, such as an IQ-demodulator and an IQ-modulator as well as the PID control method to obtain long-term phase and amplitude stability.

RF SYSTEM

The low level rf system of the prototype accelerator was built as shown in Fig. 1 [6]. CW signals of 238 MHz, 476 MHz, 2856 MHz, and 5712 MHz for acceleration are provided with a signal source having a very low noise level, which causes an rf phase jitter. These signals are transmitted to rf components through phase-stabilized coaxial cables having a temperature coefficient corresponding to an electrical length of 10 ppm/^{O}k.
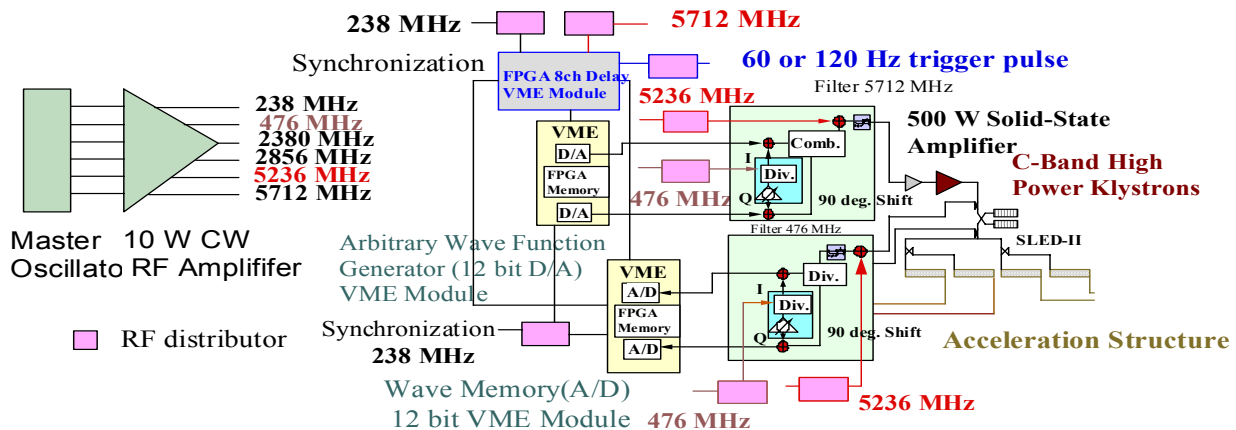
Figure 1: SCSS rf system. The system mainly comprise a very low-noise signal source, IQ-modulators/demodulators, A/Ds and D/As to control IQ- instruments, and 600 w solid state klystron driver amplifiers.

FIELD MEASUREMENT RESULTS OF THE QUADRUPOLE MAGNETS FOR ATF2

M.Masuzawa, R.Sugahara and Y.Suetsugu, KEK, Tsukuba, Japan

Abstract

ATF2 will be built at KEK as a test facility for the final focus system for the ILC. The specifications for the final focus system require transverse focusing of the electron beam to nearly 40 nm. The quadrupole magnets for the ATF2 magnets have to meet strict specifications on the multipole components, especially the sextupole components, in order to achieve the required small beam size. Preliminary measurement results of these magnets using a harmonic coil system will be reported in this paper.

INTRODUCTION

The Accelerator Test Facility (ATF) at KEK was built for R&D work for a future electron-positron linear collider [1]. The main goals of the ATF project are to produce, measure and control a very low emittance beam. The ATF is composed of an electron gun, a 1.5 GeV electron linac, a 1.5 GeV damping ring of 138 m circumference and an extraction line for beam diagnostics. The ATF2 project will extend the existing ATF extraction line with an ILC-type final focus system [2]. Most of the tolerances, such as the tolerances on magnetic field, jitter vibration and power supply stability, are common between the ATF2 and the ILC. ATF2 will be a very good model for the ILC final focus system and a successful commissioning of the ATF2 project will assist in the design of the ILC. The ATF2 beam line is shown in Fig. 1. The quadrupole magnets for the ATF2 extraction line are called the QEA magnets. The QEA magnets have been manufactured at IHEP in China. The basic mechanical and magnetic parameters are summarized in Table 1. Field error tolerances for the extraction quadrupole magnets are summarized in Chapter 3 in the ATF2 proposal [2]. Tolerances on the normalized sextupole amplitude to the quadrupole amplitude (B3/B2) for some of the quadrupole magnets are as tight as 0.04 % at r = 10 mm. The tolerance on the tilt is on the order of 0.1 mrad.
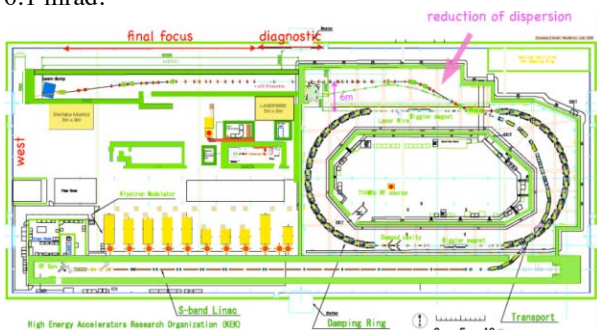
Fig.1. ATF and ATF2 layout.

Table 1

Bore diameter (mm)	32
Core length (mm)	180
# of turns per pole	48
Max. current (A)	150 or 50
Field gradient @115A (T/m)	54

MEASUREMENT SYSTEM

General

A harmonic coil system was used to measure the QEA magnets. The rod of the measurement coil, shown in Fig. 2, is made of ceramic (Alumina 99.5 %). The main and the additional bucking coils are mounted on the same frame made of Macor. Air bearings are used for smoother rotation. The number of turns and locations of the main and bucking coils are determined so that the dipole and quadrupole components are cancelled when two coils are connected in a certain configuration (bucking coil configuration). Polyurethane coated copper wire with a diameter of 0.1 mm is used for both coils. The field strength, magnetic center and the main quadrupole phase are measured by the main coil, without connecting the bucking coil (the main coil configuration). The sextupole component is evaluated by the bucking coil configuration. A coupling structure, shown in Fig. 3, is introduced in order to guarantee the relation between the coil and the encoder. When placing the magnet on the measurement system, the coil rod has to be removed from the encoder. With the coupling structure, the relative position of the coil to the encoder is expected to give good reproducibility.
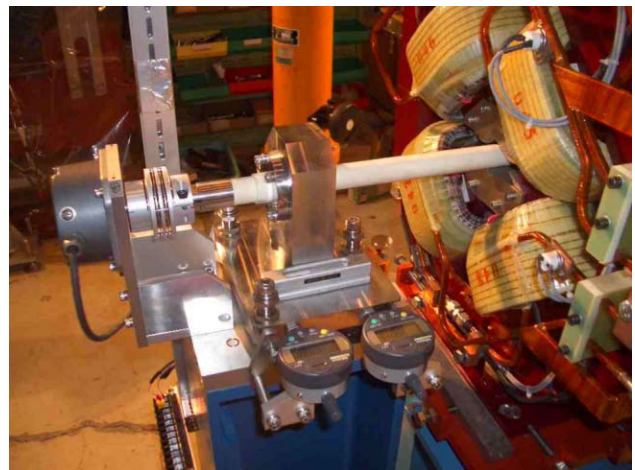
Fig.2. Harmonic coil system.

STRUCTURES OF QUADRUPOLE MAGNET CORE

Nanyang Li, SLAC, USA , M/S18,2575 Sand Hill Rd., Menlo Park, CA 94025

Abstract

In general, there are two different quadrupole core designs: two pieces (up half and low half cores) and four pieces (four quarter halves). Both structures work on those quadrupole magnets in different accelerators around the world. There is no certain standard about which design is good for what machine, it is most likely defends on the engineer's preference and the coil size. There are advantages and disadvantages with both structures. However, the disadvantage of four pieces design is rather visible. It is the goal of this paper to study those advantages and disadvantages of two types of core structure from manufacturer's point of view and the perturbations of the magnet field.

RIGIDITY COMPARISON OF TWO STRUCTURES

Figure 1 below is the prototype of LEB, SSC quadrupole magnet which was built at LBL. Its core was built by four quarter cores and the quarter core was stacked and glued by laminations. In addition to gluing laminations together and tightening the pole by a bolt in a stacking fixture under the pressure, a tight bar was welded on the back of the core. This prototype was checked at LBL and then shipped to SSC by air. After the shipment, the gaps between the poles and the diameter of the aperture were all shifted and were out of the tolerances.

Figure 2 below is a quadrupole magnet of SPEAR3, SLAC. Its core was built by two half cores. The half core was glued by laminations as well. Rather than a tight bar, laminations were tightened by four bolts in addition to gluing laminations together and tight bolt at pole. The quadrupole magnets were built at IHEP, China and inspected and measured there and then shipped to SLAC by boat. Some of those magnets were re-measured at SLAC. The results were correspondent with what IHEP people obtained, which indicated that the quadrupole rigidity is very good and the structure of the core experienced all sorts of impact during the shipment.

These two examples mentioned above demonstrated that a two piece core is more rigid than a four piece core.

But one may notice that the coil dimension of LEB SSC quadrupole made it impossible to be installed into a two piece half core. An engineer must examine the size and the shape of the coil carefully and make sure it will be installed into the half core without trouble should a two piece core structure is selected.

Figure 1: SSC, LEB Quadrupole
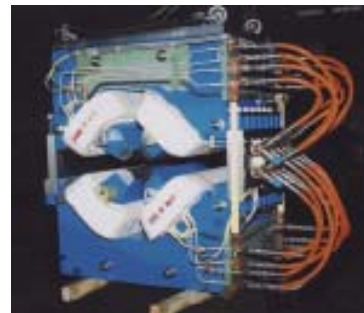
Figure 2: SLAC, SPEAR3 Quadrupole

COMPARISON OF GLUED CORE AND WELDED CORE

Figure 3 below is a half core of SPEAR3 quadrupole magnet. It was glued by laminations. Figure 4 below is a half core of LER, PEPII quadrupole, it was laminated as well, but was welded as one piece by angle plate instead of gluing.

Glued Core

The first problem with a glued core is an environment issue. The workers smell epoxy directly which is different from the case of coil impregnation. The later one is processed under the vacuum. In most case, the workers do not feel comfortable to work under a strong smell working place. The second problem with a glued core is that the cleaning work after core curing is a quite involvement. The cleaning work actually can be limited when the thickness of the epoxy layer is adjusted very carefully. But it is not an easy task, if the gluing machine is old and the roller of it is not built with very tight tolerance. The third problem with a glued core is that it leaves almost no room for re-adjusting after curing if the dimension(s) shifted during the curing by some reason(s). The advantage of gluing procedure is that it will avoid from deformation caused by welding, especially for a

EFFECT OF EDDY CURRENT IN MAGNETIC LAMINATIONS ON PULSED SEPTUM MAGNET RESPONSE

R.S. Shinde[#], R.K. Mishra, P. Pareek, M.M. Pandey, Vinod Gaud, S. Senthil Kumar, S. Kotaiah
Raja Ramanna Centre for Advanced Technology, Indore, Madhya Pradesh, India

Abstract

Pulsed Septum magnets have been developed for injection of 500 – 600 MeV, e beam into 2.5 GeV Storage ring (Indus-2). A Pulsed magnet system consists of a thin & thick passive type Septum magnets kept inside Vacuum Chamber & Kicker Magnets. Thin & thick septum magnets were excited using 50 µs & 100 µs half sine wave pulse respectively. A magnetic field homogeneity ($\Delta B/B$) of the order of 10^{-3} & integrated stray fields ($\int B_{stray}.\, dl$) of nearly 0.7 Gm has been achieved.

This paper focuses on Pulse magnetization of Ni-Fe laminations; engineering challenges for septum magnets, Eddy current in lamination & their effects on pulse response of magnets.

INTRODUCTION

Injection of e beam into the Storage ring in the horizontal plane is carried out by combination of Thin & Thick Septum magnets & four kicker magnets. The Septa are used to deflect a beam coming from the transfer line-2 (TL-2) into a direction, which is parallel to that of the beam circulating in the Storage ring [1].

This method provides a smooth & continuous injection. Injection efficiency is the main requirements of the Pulsed Septum magnets. To this end we rely on the field produced by the magnet to have a maximum relative error ($\Delta B/B$), below 10^{-3} in the useful aperture & time interval. There are several constraints on the development of these Septum magnets (Table-1). These are due to the accelerator geometry, the injection scheme and the materials used.

Table 1: Constraints on parameters of the Septum magnet

Parameters	Thin	Thick
Max. Septum Thickness (mm)	3.0	3.5
Deflection angle, degree	2	19
Magnet aperture (W X H), mm	28.5 x 10	26.5 x 10
Max. Stray magnetic field	< 2 G-m	--

In addition to the objectives & constraints, technology for development of the magnets taken into account the needs of low cost, HV insulations, Out gassing rates & easy maintenance.

[#]shinde@cat.ernet.in

MAGNET SYSTEM

Injection system of Indus-2 consisting of two Pulsed Septum magnets – thin & thick and Four Kicker magnets. In the injection scheme, a compensated bump (16 mm) produced by four Kicker magnets & the e beam is injected through two septum magnets. In order to minimize the thickness of septum magnets launching the e beam, thin & thick septum magnet combination has been adapted. Septum magnets are required to provide necessary deflection to the incoming beam to match the angle of the beam transfer line to the accelerator orbit. The design of such a system has to meet many requirements in order to achieve a high reliability injection operation, some of them are [2]:

(i)   Septum sheet as thin as possible in order to enhance injection efficiency as septa isolates injected beam & circulating beam
(ii) High magnetic field (due to geometrical limitation)
(iii) Pulse magnetization of Ni-Fe lamination – high Pulse Permeability for stability & homogeneity of field greater than 100 ppm, high frequency response upto 100 KHz
(iv) Low out gassing rate, as magnets are to be placed in UHV environment
(v)   Very low Stray fields (due to beam optics)

The magnet configuration, high pulse permeability & high Bknee on first magnetization curve of laminated yoke and Pulse power supply combinely determine the high performance of Septum magnet system

The main design criteria for the Pulsed Septum magnet are to produce Pulse magnetic field waveform with amplitude of ~ 1 T & pulse length ~ 50 µs & 100 µs. The requirement of magnetic field pulse shape for injection is half sine wave with field stability on top is of the order of ($\Delta B/B$) ~ 1 X 10-3. As magnets have to keep inside vacuum, there are severe engineering challenges both in space & fabrications are involved [2].

PULSE MAGNETIZATION

Pulsed Septum magnets are to be operated at high field strengths, the magnetization rates (dB/dt) are involved are up to about ~ 1 T / µs & magnetization reverses in the order of µs. Also magnet performance greatly depending on magnetization of laminations. Therefore, it is necessary to know the behaviour of soft magnetic materials when its magnetization reverses in the order of µs.

The response of the magnetic field due to the time varying current in the septum coil is influenced by the

MECHANICAL STABILITY OF OPEN-TYPE QUADRUPOLE MAGNETS FOR A 2.5 GeV SRS (INDUS-2)*

K.Sreeramulu[#], S. Das, Kailash Ruwali, M.G. Karmarkar, S.Kotaiah, P.K.Kulshreshta,
Raja Ramanna Centre for Advanced Technology, Indore, India
M.K.Ghosh, Banaras Hindu University, Varanasi, India

Abstract

The open type Quadrupole magnets (max. gradient: 16 T/m) for 2.5 GeV Indus-2 are made in C-configuration in which both of outer vertical sections of the steel are removed to take out the emerging synchrotron beam (SR) lines, in the region immediately adjacent to main dipole magnets of the ring. This induces engineering complexity relating to mechanical stability that critically controls the deviations in magnetic centre and field quality. To meet the stringent field quality requirements, the mechanical structure, which is precisely holding the magnet poles, is designed for minimum deflection at maximum gradient. The magnet is simulated with coupled magneto-structural analysis, using ANSYS. The measurement of deformation in prototype magnet assemblies with maximum excitation current is carried out and found within the acceptable limit. Measured magnetic centre shift with excitation is within 0.02mm. The magnetic measurement results show that the higher order multipoles are low and not changing with excitation current. The optimised open-type Quadrupole magnet design is implemented in series production of all 32 magnets for Indus-2. The mechanical assembly accuracies and stability of magnets with measurement results are discussed in this paper.

INTRODUCTION

The quadrupole magnets for Indus-2 are slowly ramped magnets (from 3.84 T/m to 16 T/m in 300 seconds). The main magnet design parameters are shown in Table 1. There are five families (Figure 1) in which Q1, Q2, Q5 families are of close type and Q3 (defocusing), Q4 (focusing) are of open type. The physical design of Indus-2 open-type quadrupole magnet is done using 2D POISSON group of magnet design codes [1]. Figure 2 shows $1/4^{th}$ cross-section of the open type quadrupole

Quadrupole magnets

Figure 1: Half unit cell of Indus-2.

magnet. The design of Q4 magnet is a non-conventional 'open-sided' design, with upper and lower pole pairs not connected magnetically to take-out the emerging SR beam lines, which are located in the main dipole magnets of the ring and also to maintain symmetry. The design of

Figure.2: Magnet lamination $(1/4^{th})$.

Q3 magnet is also kept same except supports at RHS (figures 4) to have symmetry in ring.

Table 1: Magnet Design Parameters.

Description	Unit	Values
Pole aperture diameter	mm	85
Steel & magnetic lengths	mm	362.50&400
Ampere turns/pole	AT	13,000
Good field region	mm	X=± 32, Z= ±17
Good field region field errors	$\Delta k/k$	$\pm 1 \times 10^{-4}$
Allowed centre shift	mm	$\delta X = \delta Y \leq 0.03$
Allowed gradient errors over good field region		
c_1l/c_2l	c_3l/c_2l	c_4l/c_2l	c_5l/c_2l	c_6l/c_2l	c_7l/c_2l
2.35E-4	8.59E-4	1.33E-3	5.34 E-4	5.07 E-4	1.65 E-3

Where $c_n = \sqrt{(a_n^2 + b_n^2)}$ and a_n, b_n are skew and normal components for 2n-pole fields.

MECHANICAL DESIGN OF MAGNET

The magnet is an assembly of four laminated stacks in order to accommodate the required number of excitation coil turns in each pole. The design of mechanical assembly structure for holding four laminated poles is done after estimating the amount of magnetic forces from

PERFORMANCE OF 6MW PEAK, 25 KW AVERAGE POWER MICROWAVE SYSTEM FOR 10MEV, 10KW ELECTRON LINAC

Purushottam Shrivastava[#], Jaikishan Mulchandani, Y. Wahnmode, P. Mohania
Pulsed High Power Microwave Section, Raja Ramanna Centre for Advanced Technology, RRCAT, Indore, India

Abstract

An S-Band microwave system with peak power capability of 6MW and average power capability of 25 kW was designed, constructed and commissioned at RRCAT. The in-house development of various microwave technologies and pulse modulator technologies was successfully achieved and the microwave system was interfaced to the 10MeV, 10kW electron LINAC. The electron LINAC could be tested to full rated energy and power using the present microwave system. The present paper highlights the details of the performance results.

INTRODUCTION

The microwave system for 10MeV, 10kW average beam power LINAC was designed and developed indigenously.
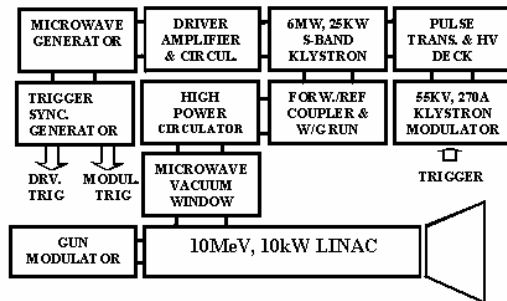
Figure 1: Schematic of 6MW S-band microwave system.

Table (1) shows the specifications of the Microwave system. The klystron needs 50-55kV, 270-300Amp beam voltage pulse to achieve the rated output power. The klystron modulator has been designed to give output pulse voltage of 15 microsec duration see fig 2.The specifications of the klystron modulator are listed in table (2). The klystron modulator and pulse transformer are designed to supply also the gun voltage up to 50kV. Challenging work on the technologies like droop compensation hyperboloidal tuneable pulse forming network, fast rise time   long pulse high average power pulse transformer, pulse voltage and current measurement systems, short circuit protection, optically triggered command charging system, solid state trigger drives for thyratron, high voltage power supplies with fault protection systems which were developed in-house have performed to expectations.

_____

[#]purushri@cat.ernet.in

Table 1: Microwave System Specifications Achieved

Peak o/p power	MW	6
Average o/p power	kW	25
Operating frequency	MHz	2856
Pulse duration	microsec	13/7
Pulse repetition rate	Hz	1-300
Pulse rise time	microsec	<2
Pulse top variation	%	<1
Pulse-pulse stability	%	<1
Frequency stability	/day	1×10^{-8}
	/ °C	1×10^{-8}

Table 2: Modulator Specifications Achieved

Pulse output power	MW	15
Pulse voltage output	kV	50
Output impedance	Ω	180
Pulse duration	microsec	15
Rise time	microsec	~2
Fall time	microsec	<2
Flat top variation	%	< ±1
Mean output power	kW	70

SYSTEM DETAILS

The microwave system consists of a stabilized signal generator, circulator, 200W solid state microwave amplifier driver, circulator, directional coupler, 6MW klystron amplifier and waveguide system. The power from the signal generator is amplified up to 200W by the driver amplifier, which in turn is fed to a 6MW klystron. The power from the klystron is fed to the accelerator by means of a dual directional coupler, flexible waveguide, waveguide pressurizing system, circulator, dual directional coupler and vacuum ceramic window see fig. (1). The klystron modulator is line type construction see fig. 2. A high voltage regulated dc power supply rated for 16kV, 6 amp continuous duty with regulation better than 0.5% has been built for charging the pulse-forming network. An air core charging inductor with RC damping for high frequency ringing, occurring due to parasitic components, has been used. A command charging thyratron placed on a floating deck is triggered by an optical isolated triggering system. The necessary power to the trigger supplies, filament and reservoir is supplied by means of a high voltage isolation transformer. Pulse forming line consists of 16 sections Gullemin E type network in which the number of cells can be selected for desired pulse width from the modulator.

A shunt diode fault circuit protects the components from mismatched loads or load short circuit/arcing. The pulse-forming network is discharged through a high voltage high power thyratron, which is triggered by

MEDIAN PLANE MAGNETIC FIELD MAPPING FOR SUPER CONDUCTING CYCLOTRON (SCC) IN VECC

Anindya Roy[#], Tanushyam Bhattacharjee, N. Chaddha, R. B. Bhole, M. K. Dey, J. Debnath, U. Bhunia, J. Pradhan, S. Paul, A. Dutta, Z.A. Naser, C. Nandi, G. Pal, C. Mallik, Sarbajit Pal

Variable Energy Cyclotron Centre, DAE, 1/AF Bidhannagar, Kolkata 700 064,

Abstract

The magnetic field at median plane of SCC Magnet (Peak field 5.8T) is measured over its operating range and upto 29 inch radius. The magnetic field is mapped at radial interval of 0.1 inch and angular interval of 1 degree. The complete map of 360 degree comprised of about 100K field points is obtained in less than 100 minutes. The field mapping system (MFM) is designed to minimise mapping time and human intervention. The control & data acquisition (DAQ) software (s/w) is developed to work as PC based TCP Client-Server mode to reduce the design complexity, system overload and debugging effort. The Server program is developed as windows console in 'C' and the Client is developed using LabView to provide a user friendly operation console along with online preliminary display and analysis of field data. This architecture provides a reliable and easily modifiable control s/w. The correctness of the magnet assembly is calculated from the acquired data, which in-turn represents the correctness of measurement system. A detailed study of the magnet characteristic is done. The first harmonics of the fields at different radii are obtained at all magnet excitation and corrected by coil-centering and shims placement. This paper also describes the major activities made during field mapping.

INTRODUCTION

The Magnetic Field Mapping (MFM) system comprises of a hardware system and a control & data acquisition software [1]. A search coil and Digital integrator combination are used to measure the difference in field between the center and any other point of the magnet [2]. The schematic diagram of the system is shown in Fig 1.

MFM DAQ HARDWARE

The hardware system consists of MFM jig, NMR Gauss meter, Digital integrator, DAQ Server PC and Client GUI PC. The MFM jig comprises of a centrally supported search-coil carrying arm, two Animatics smart motors, an angular encoder and a linear encoder. The schematic diagram of the jig is shown in Fig 2.

The radial movement range of the search coil is 29inch. An optical encoder system of 360 LPI was used to measure the search coil position. The angular position of the search coil carrying arm is measured by absolute rotary Inductosyn encoder (256/2 pole, 128/1 speed, 8.15 inch stator O.D.) associated with two dual channel preamplifier (219200) and AWICS converter board
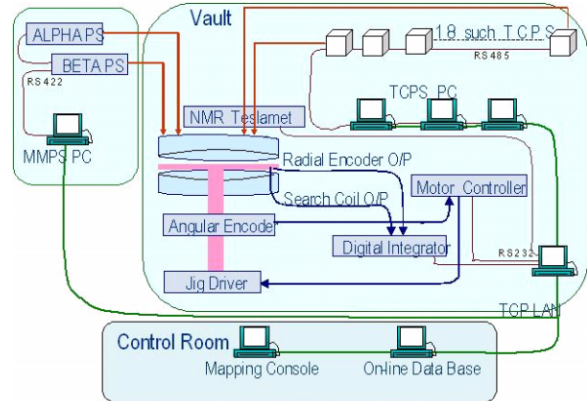
Fig 1: The schematic diagram of the system

(220500). A microcontroller based interface module was developed in house to read the angular position from the AWICS board online. The accuracy of the system was 1.7arc Sec.

The Measurement PC is placed at vault near the main magnet and connected by serial links with digital integrator, NMR Gauss meter, angular encoder and two smart motors. The Console PC is placed at the main control room. Both PCs are connected to the dedicated
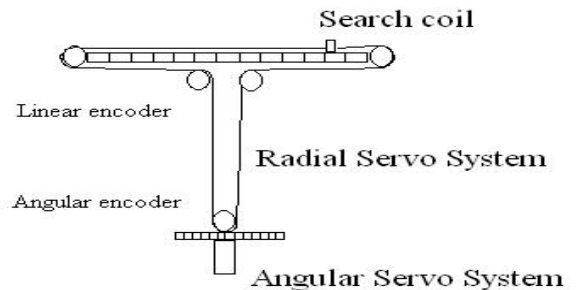
Fig 2: The schematic diagram of the jig

control LAN commissioned at Super-conducting cyclotron (SCC) building.

MFM DAQ SOFTWARE

The control & data acquisition software is designed in two independent modules i.e. Server Controller (SC) module and Client Graphical User Interface (GUI) module, to achieve distributed architecture, reduce system overhead, development and debugging effort. These two software modules incorporate the following features to satisfy the auto/manual mode of operation, minimum

---

[#]r_ani@veccal.ernet.in

MATHEMATICAL MODEL FOR FAST AND SLOW DUMPING OF K-500 SUPERCONDUCTING CYLOTRON MAGNET

Anirban De, S.K. Thakur, S. Saha, VECC, 1/AF, Bidhan Nagar, Kolkata 700064, INDIA

Abstract

A superconducting cyclotron (K-500) is under construction at Variable Energy Cyclotron Centre. Two superconducting coils – named 'Alpha' and 'Beta' – generates the main magnetic field of the cyclotron. Subsequent to the in-house fabrication of the two coils, it was assembled into the cryostat and the magnet assembly completed. Immediately after the cool down, the superconducting coils were energized. Two dump resistors – slow and fast – serve to dissipate the energy stored in the coils externally depending upon the situation.

Various sets of data were collected during dumping and based on these an approximate mathematical model was constructed to simulate the dumping characteristics. This model took into account the lead drops, the cable and the joint resistances along with the dump resistor values and the self- and mutual- inductances (that varied with current) of the coil.

INTRODUCTION

The two coils are powered by M/S Danfysik make two power supplies rated 20V, 1000A, 10ppm stability class. Along with this, each of the magnet coils are always connected with two dump resistors, viz., fast dump and slow dump as shown in Figure 1.
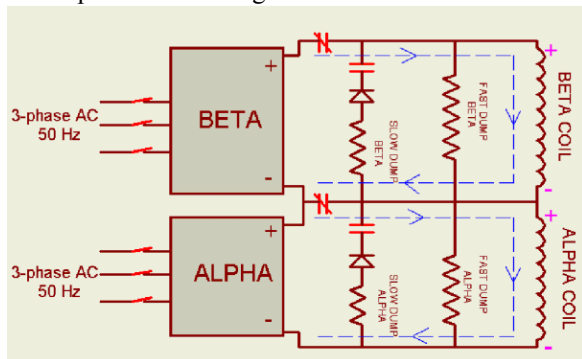
Figure 1: Schematic of Power Supplies with Superconducting Coils and Dump Resistors

The two dump resistors – slow and fast – serve to dissipate the energy stored in the coils externally depending upon the situation. For example, during power failure, the energy stored in the coils is slowly dissipated through the slow dump resistors. Slow dumping is also automatically triggered for the following conditions viz, He level in upper part of cryostat falling below 95%, He pressure rising to more than 306mbar, horizontal support link forces not within permissible range (1000lbs – 10000lbs), panic button operated manually, power supply tripped due to internal interlock failure. For a potentially catastrophic situation (like quench, lead voltage drop

increasing above 160mV, He pressure in coil exceeding 680mbar, cryostat vacuum exceeding 10^{-1}mbar, He level sensor in upper half of cryostat reading less than 80%) the energy is quickly dumped through the fast dump resistors.

MATHEMATICAL MODEL

Theoretical Model

During dumping, the 3φ supply is withdrawn and the series contact gets automatically opened and the system shown in Figure 1 reduces to the circuit as shown in Figure 2.
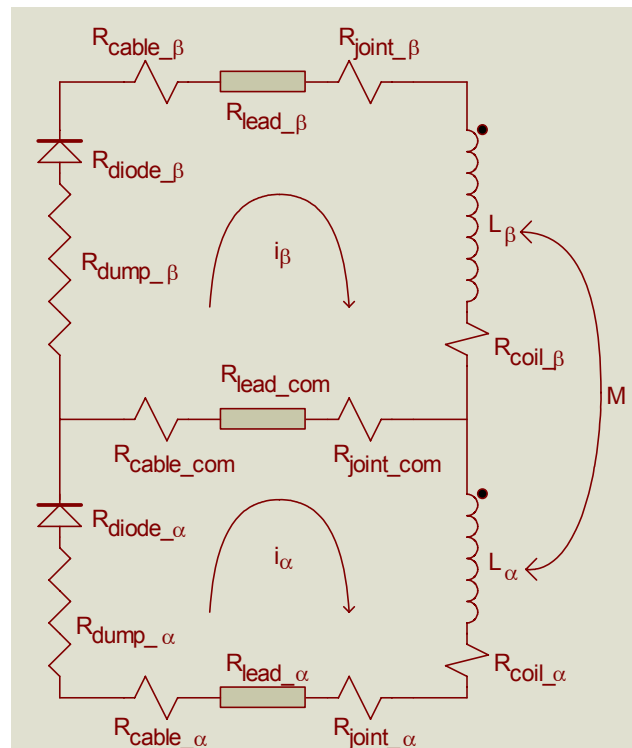
Figure 2: The dumping scheme

The governing differential equations for the model:

$$L_\beta \frac{di_\beta}{dt} + M \frac{di_\alpha}{dt} + R_\beta i_\beta + R_{com} (i_\beta - i_\alpha) = 0 \qquad (1a)$$

$$L_\alpha \frac{di_\alpha}{dt} + M \frac{di_\beta}{dt} + R_\alpha i_\alpha + R_{com} (i_\alpha - i_\beta) = 0 \qquad (1b)$$

where,
$M = k\sqrt{(L_\beta L_\alpha)}$
$R_\beta = R_{dump\_\beta} + R_{diode\_\beta} + R_{cable\_\beta} + R_{lead\_\beta} + R_{joint\_\beta} + R_{coil\_\beta}$
$R_{com} = R_{cable\_com} + R_{lead\_com} + R_{joint\_com}$
$R_\alpha = R_{dump\_\alpha} + R_{diode\_\alpha} + R_{cable\_\alpha} + R_{lead\_\alpha} + R_{joint\_\alpha} + R_{coil\_\alpha}$

IDEAL COIL-SHAPE FOR PERFECT FIELD IN SUPERCONDUCTING SEXTUPOLE MAGNETS

P. R. Sarma

VECC, 1-AF, Bidhannagar, Kolkata-700 064

email: sarma@veccal.ernet.in

Abstract

Superconducting magnets have become very essential components in high energy accelerators. The field in coil-dominated superconducting magnets depend mostly on the shape of the current-carrying coil. A coil shape generated by two overlapping ellipses produces the perfect dipole magnetic field. Similarly, a perfect quadrupole field can be produced with a coil shape generated by two perpendicular and concentric intersecting ellipses. For a sextupole, however, there is no mention of such coil shape in the literature. We have given here a coil shape for generating the perfect sextupolar magnetic field.

INTRODUCTION

In high energy accelerators like LHC at CERN [1,2], VEPP at Novosibirsk [3] etc. superconducting sextupole magnets are used as correctors of second order beam aberrations.

In these magnets the field quality depends on the coil shape. A $\cos\theta$ azimuthal current distribution on a cylindrical surface produces a perfect dipole magnetic field inside. Similarly, a $\cos(3\theta)$ azimuthal current distribution produces a perfect sextupole field. This, however, is not a practical way as one has to use a large number of power supplies for achieving the required current distribution. The practical way is to have a constant current pass through a coil winding whose number of turns varies azimuthally.

Figure 1. Coil cross-section and current direction.

It is well-known that a constant current flowing through a coil, whose shape is generated by two displaced overlapping ellipses, produces the perfect dipole field. Similarly, two perpendicularly intersecting and concentric ellipses produces a coil shape which generates the perfect quadrupole field [4-9]. However, for a superconducting sextupole no such ideal coil shape is available in the literature. In this work, we have worked out such an ideal coil shape for generating the perfect sextupolar field.

FIELD DUE TO LONG COIL

For a current I flowing along the z-direction through a point (x,y) in a thin strand of conductor of infinite length, the field B at a point (x_0,y_0) whose distance is r from the conductor, is given by the Biot-Savart law as

$$B(x_0,y_0) = \frac{\mu_0 I}{2\pi r} \qquad (1)$$

where μ_0 is the permeability in air.   The field B is perpendicular to both the radius vector r and the conductor. The field component in the y-direction is

$$B_y(x_0,y_0) = \frac{\mu_0 I}{2\pi} \frac{(x-x_0)}{(x-x_0)^2 + (y-y_0)^2} \qquad (2)$$

For a coil of extended dimension the field is calculated by integrating the above over the cross-section of the coil. For a uniform current density J flowing along the length (z-direction) of the coil, i.e., perpendicular to the cross-section of the coil (Fig. 1), the field $B_y(x_0,y_0)$ is

$$B_y(x_0,y_0) = \frac{\mu_0 J}{2\pi} \iint_{y\,x} \frac{(x-x_0)}{(x-x_0)^2 + (y-y_0)^2} dx dy$$

$$= \frac{\mu_0 J}{4\pi} \oint \ln\left[(x(y)-x_0)^2 + (y-y_0)^2\right] dy \qquad (3)$$

where $x(y)$ defines the boundary of the coil as a function of y, and integration is done for the closed path along the coil boundary. The x-component of the field is similarly

$$B_x(x_0,y_0) = \frac{\mu_0 J}{4\pi} \oint \ln\left[(x-x_0)^2 + (y(x)-y_0)^2\right] dy \qquad (4)$$

The coil profile $x(y)$ (or conversely $y(x)$) defines the field type and its quality. For an elliptic shape with semi-axes a and b, and defined by the parametric equations

$$x(\varphi) = a\cos\phi, \qquad y(\varphi) = b\sin(\varphi) \qquad (5)$$

eqs.(3) and (4) reduce to

DESIGN OF THE PROPOSED 250 MEV SUPERCONDUCTING CYCLOTRON MAGNET

M. K. Dey[#], A. Dutta Gupta, U. Bhunia, S. Saha, A. Dutta, J. Pradhan, S. Sur, S. Murali,
J. Chaudhuri, C. Mallik and R.K. Bhandari
Variable Energy Cyclotron Centre, Kolkata

Abstract

VECC has proposed a project for the design and development of a 250 MeV superconducting proton cyclotron, which may be used in therapy. In this paper we describe the preliminary design calculations for the superconducting cyclotron magnet. Hard-edge approximation method has been adopted for finding the poletip geometry to meet the basic focusing requirements of the beam. The uniform-magnetization method has been applied to calculate the 3D magnetic field distribution due to saturated iron poletips, to verify the beam dynamical issues and optimize the poletip geometry. GM type closed cycle cryo-cooler technology is being considered for steady state liquefaction of evaporated helium gas from magnet cryostat.

INTRODUCTION

Basic design parameters are decided by the requirements for medical application of the cyclotron, i.e., for the treatment of deep seated cancerous tumors. Proton energy of 250 MeV corresponds to approximately 40 cm penetration range in water. The cyclotron is targeted to be designed for delivering a few hundreds of nano-amperes beam current.

The design of the cyclotron magnet is an iterative process. Approximate hard-edge formulas are used to determine the basic dimensions and geometry of the poletip sectors [1, 2]. The 3D software TOSCA has been used to calculate median plane magnetic field distribution (fig 1). Since the superconducting magnet is operated in high field level (peak hill field at median plane ~3.6T), the pole-tip iron is fully saturated. So the uniform-magnetization method is adopted to simulate the azimuthal variation of the field due to spiral hill-valley structure of the magnet [3]. This makes the iterative optimization of the poletip geometry faster. Orbit tracking codes are used to calculate the equilibrium orbit properties.

The cryogenic system primarily consists of helium reservoir, GM type cryo-cooler, magnet cryostat with multilayer insulation and 80 K radiation shield inside, conduction cooled current leads, etc. The cold mass can be slowly cooled down from room temperature to reach liquid helium temperature either by directly coupling the cryostat with helium refrigerator or initially by liquid nitrogen and then by liquid helium. The evaporated helium gas from the cryostat will be reliquefied by condensing it through the cold head of the multistage GM type cryo-cooler. This is a very new and economic technology compared with the conventional technique of

[#]malay@veccal.ernet.in

coupling with liquid helium plant (as used in VECC K500 superconducting cyclotron magnet).
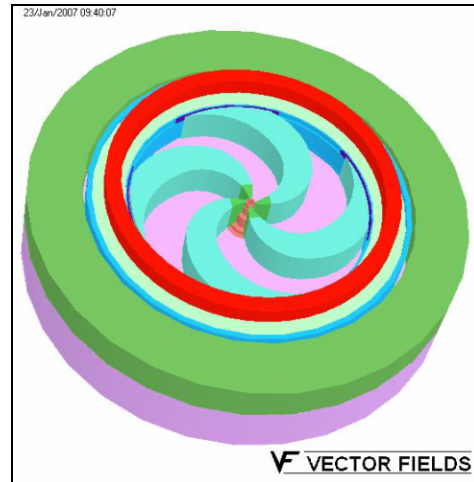
Figure1:TOSCA model of upper half of cyclotron magnet.
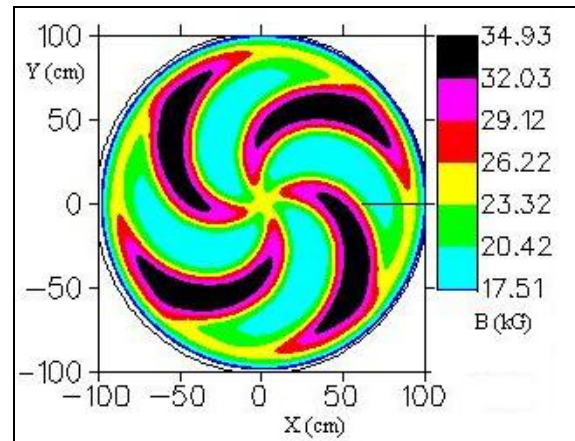
Figure 2: Contour plot of median plane magnetic field .

SECTOR GEOMETRY

To minimize the size and cost of the cyclotron it is desirable to operate at maximum possible magnetic field strength. But with stronger magnetic field, higher electric field is required at the deflector system to extract the beam, so making the extraction process very difficult and unstable. Moreover, since the fractional azimuthal variation of the field (flutter) decreases with increasing average field, stronger spiralling of the sector is required to compensate for the decrease in vertical focusing, causing manufacturing challenge. So an optimum value of

CONSTRUCTION OF SSRF MAGNET POWER SUPPLY SYSTEM

T.J. Shen, D.M. Li, R. Li, C.L. Guo, S.L. Lu, S.M. Zhu, H.G. Chen, R.N. Xu,
Z.M. Hu, D.X. Wang, W.F. Wu, H. Liu
Shanghai Institute of Applied Physics, Shanghai 201800, China.

Abstract

The Shanghai Synchrotron Radiation Facility (SSRF) is a third-generation synchrotron radiation light source under construction. In SSRF, there are 520 sets of magnet power supplies for the storage ring and 163 sets for injector. All of the power supplies are in PWM switched mode with IGBT. A high precision stable output power supply for 40 dipoles rated at 840A/800V with the stability of ±2E-5/8hrs will be used for storage ring. 200 sets of chopper type power supply will be used for exciting main winding of quadrupoles respectively. In booster ring, two sets of dynamic power supply for dipoles and two sets for quadrupoles will run at the biased 2Hz sinusoidal wave. All above power supplies will work with digital power supply controllers designed by PSI. All power supplies are being manufactured at professional power supply companies in China.

POWER SUPPLY CONTROLLER

A control solution of full digital control as Swiss Light Source(SLS) is adopted in large power supplies for dipoles of storage ring and booster. A pair of PSI controller (See Fig.1) are put inside the power supply cabinet as a master to control several analog slaves, to regulate the output current. There is a 60MHz DSP with 32/40 Bit floating point ALU, 8x16 bit electrically isolated AD converters (50ksps), 11 free memory units for 16,384 data points [2]. It can communicate with IOC through a pair of 5MB optical fibers. The main advantage of the full digital control is much better in stability, repeatability, and flexibility. At present, the long term stability for a sample power supply is up to 10ppm.

Figure 1: PSI power supply controllers

Additionally, in order to reduce the cost we have managed to develop a home-made power supply controller product. So far the stability is achieved 20ppm and this controller is expected to use in middle and small power supplies in SSRF linac after authentication.

Figure 2: Home-made power supply controllers

LINAC POWER SUPPLY

SSRF is mainly composed of three parts: the 150MeV linac, the 3.5GeV booster and the full energy storage ring. In linac, unipolar power supplies adopted the circuit of chopper, full bridge (or half bridge), and bipolar power supplies adopted the circuit of H-bridge. The medial power supplies above 1kW adopted the full 19" width structure which put inside a standard 3U case. Other small power supplies shared the full 19" width by 2 to 3 units and used the common input DC module [3].

A LEM as a current sensor is adopted for those stability requirement larger than 1000ppm, a DCCT for those stability better than 100ppm, and a resistor for the bipolar power supplies, such as corrector power supplies.

IMPLEMENTATION OF HIGH PRECISION MAGNET POWER SUPPLY USING THE DSP*

K. H. Park [#] , S. H. Jeong, D. E. Kim, J. H. Choi and C. W. Chung
Pohang Accelerator Laborator, POSTECH, Pohang, Kyungpook 790-784, Korea
B. K. Kang
Department of Electrical Engineering, POSTECH , Pohang, Kyungpook 790-784 Korea

Abstract

This paper presents an implementation of a precision magnet power supply (MPS) for the Pohang Light Source using the digitally controlled pulse width modulation method. The maximum output current of the power supply was 600 A at a precision of ~60 ppm. The digital control circuit of the power supply was implemented using two high speed 16-bit analog-to-digital converters and the TMS320F2808 digital signal processor. Three IGBTs are used at MPS with phase shifted parallel operation to increase the power rating and operating frequency. The duty ratio for IGBT control was determined using the PI control method. To reduce the output current ripple, the damped L-C filter was fabricated at both the DC link and output sides. Various experimental results, such as stability, drift, and controllability, are given to verify the characteristics of the DSP based magnet power supply.

INTRODUCTION

Many IGBT switching mode power supplies were implemented using a pulse width modulation controller such as UC1825 from Texas Instrument Co. This type of power supply can be a high precision MPS if the resolution and stability of the digital-to-analog converter, which generates an analog reference signal, is high. However, it requires many hardware components to implement the controller, and its output current is susceptible to variation of operating conditions.

A fully digital-controlled MPS has many advantages over the analog one. Its output characteristics are less sensitive to noise and less susceptible to parameter variations from thermal and aging effects. Also, it has a flexible and re-configurable control system [1]. We implemented and tested a fully digital-controlled MPS for the Pohang Light Source. The MPS used the phase shifted parallel operation [2] of three IGBTs to increase the power rating and operating frequency. The IGBTs were operated at a same duty ratio but 120° interleaved control phases. Because of this, the system operating frequency increased to three times higher than the one for a normal switching mode MPS, and the ripple content in output current could be reduced easily. The output of each IGBT was connected to a small separate inductor to reduce the size of inductor in the filter circuit. Digital control for MPS system was built on the DSP TMS320F2808 from

TI Co. In this paper, we present the design details and measured results of the fully digital-controlled high precision MPS for the Pohang Light Source.

AVERAGE CURRENT MODE CONTROL

The control of a switching mode power supply can be analysed using either the average current or peak current mode operations. For the peak current mode control, the instantaneous peak current of the inductor, which regulates the output current, is sensed and used to determine the duty ratio of the PWM. The duty ratio determined from the measured instantaneous peak current is quite fluctuating, and the peak current mode control is not suitable for a precision MPS for accelerator. For the average current mode (ACM) control [3], the load current is sensed and averaged for a given control loop duration, compared with the reference value to obtain the current error, and the current error is fed into the compensator in the control loop. Because the load current is averaged over the control loop duration, the noise immunity of the control loop is very high. A schematic diagram of buck mode MPS using the ACM control is shown in Fig.1. Here, D is the steady state duty ratio of the IGBT control signal, $H(s)$ is the gain of current sensor, and $G_c(s)$ is the proportional and integral (PI) compensator for load current regulation.
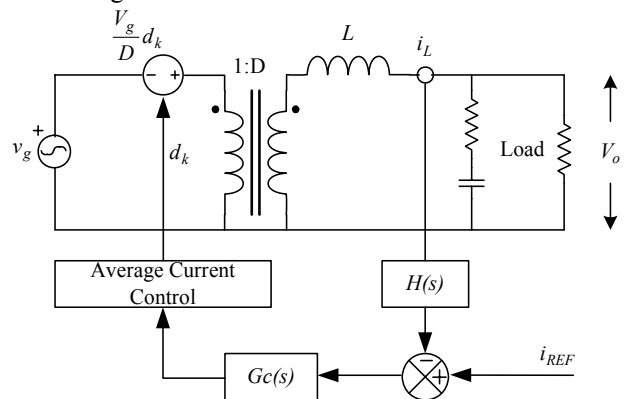
Figure 1: A schematic diagram of bucked mode MPS using the ACM control.

For an analysis of the MPS, we assume that the current through the filter capacitor is much smaller than the load current, and the converter operated at a continuous conduction mode. Then the inductor current is given by the following equations:

07 Accelerator Technology
T11 - Power Supplies

REGULATION SCHEME FOR PRECISION MAGNET POWER SUPPLY

Samit Bandyopadhyay, Manoranjan Das

Variable Energy Cyclotron Centre, 1/AF Bidhannagar, Kolkata – 700064, India

Abstract

Accelerators require extremely precise high-current magnet power supplies to drive its magneto-optic devices for proper beam dynamics. The dc precision of the power supply, which generally defines the absolute tolerance of its current, can be split up into three distinct parts - ripple, short-term and long-term stability. To ensure that the output current is within an error-band of 10ppm or less, a three-loop regulation topology has been developed and implemented in a high current magnet power supply (750A/12V) that uses transistor bank as the series pass element.

INTRODUCTION

The component of the dc precision, which also defines the stability of the magnet power supply, is divided into three major parts- a. Long-term stability, b. Short-term stability and c. Output ripple. The major components /modules of the magnet power supply that needs to function simultaneously to meet its required stability components by taking necessary action in terms of power supply output is shown in Figure 1.
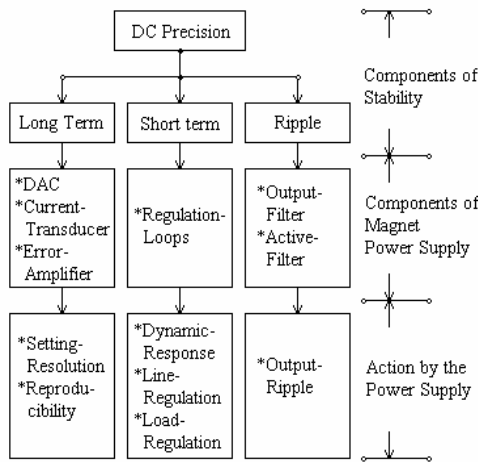
Figure 1: Components of stability of Magnet Power Supply

The factors that are responsible to affect the power supply stability are:

a. The input three-phase ac utility line, which may change in ramp or step.
b. The 12-pulse rectification of the ac signal gives an unregulated voltage, which contains an ac component of 600Hz and its harmonics.
c. Temperature, which affects semiconductor devices the most.
d. Load variation (Resistance of the load) with respect to temperature - a slow process.

REGULATION SCHEME

The implementations of close regulation highly stable low ripple magnet current require a special regulation scheme / topology [1]. The regulation scheme adopted for a high current 750A/12V, 10ppm magnet power supply using a series pass transistor bank is shown in Figure2.

gm = Transconductance of the series pass as seen from the base
gv = Transconductance of the series pass as seen from the collector
Zo = Output Impedence. (r+1/sC) || (R+sL)
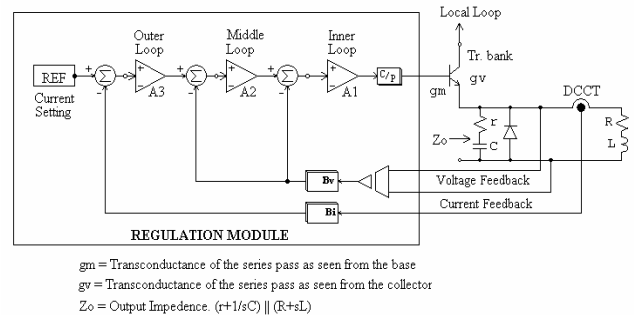
Figure 2: Regulation Scheme

The equivalent model of the designed regulation module along with the transfer function is shown in Figure 3.
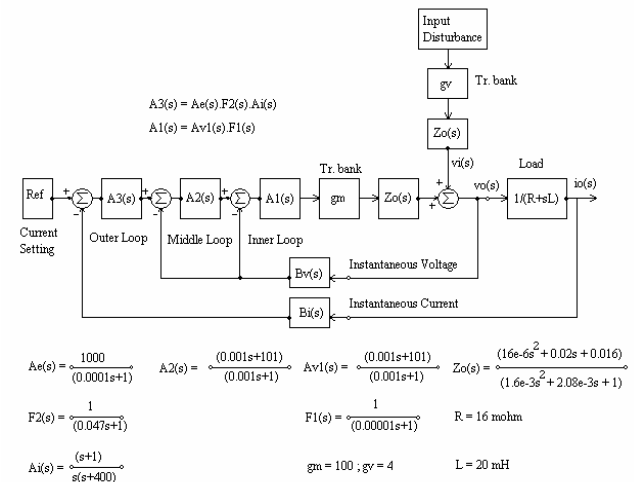
Figure 3 Equivalent model with transfer function

The underlying facts about this regulation topology are:
a. Precision low noise voltage reference source of very low drift and long-term stability for current setting.
b. Highly precise operational amplifiers with low offset voltage, exceptionally low TCV$_{os}$, high CMRR and PSRR used in the regulation module, increases the system accuracy over temperature.
c. Ultra-stable current sensor in the feedback loop. The current sensing for current regulation loop is done using DCCT [2] based on the zero flux principle. The

ACTIVE FILTER FOR HARMONIC MITIGATION FOR MAGNET POWER SUPPLIES OF INDUS-II

Yash Pal Singh[#], A.C.Thakurta, S.Kotaiah
Raja Ramanna Centre For Advanced Technology, Indore

Abstract

Power supplies used for powering of magnets in INDUS-I and INDUS-II use different type of power converters including SMPS and thyristorised power converters. Though considerations are given to keep the harmonic loading on a.c. mains low while designing these power supplies and selecting a suitable power converter for the required power, still they give a significant amount of harmonic loading on a.c. mains. In all the high power d.c. power supplies, wide variation in operating point leads to a considerable amount of reactive power generation and harmonic loading on ac mains.

In this work a study has been performed to know the variation of reactive power with time on some of the d.c. power supplies of INDUS-II. Various options to improve the power factor has been studied and their advantages & limitations for accelerator magnet power supplies have been highlighted. A combined system of a shunt passive and small rated series active filter has been proposed. The compensation principle is described and filtering characteristics are discussed in detail. A scaled down prototype of proposed series active filter has been developed in lab and experimental results produced.

INTRODUCTION

Harmonic interference problems generated by bulk thyristor converters become increasingly serious as they are widely used in industrial applications in general and accelerator power supplies in particular. So far shunt passive filters have been widely used to tackle this problem. However shunt passive filters have many problems to discourage their application. [6] Filtering characteristics of a shunt passive filter are determined by the impedance ratio of source and shunt passive filter. Fig 1 below shows the equivalent circuit of a shunt passive filter.
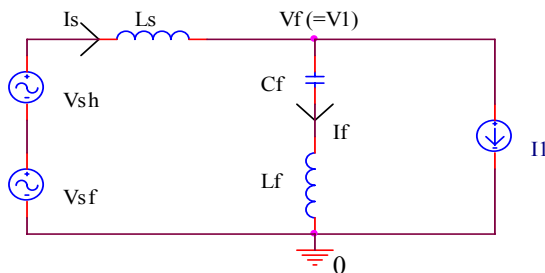
Figure 1: Basic principle of shunt passive filter

[#]ysp@cat.ernet.in

Therefore shunt passive filters have following problems.
(i) The source impedance, which is not accurately known and varies with the system configuration, strongly influences filtering characteristics of the shunt passive filter.
(ii) Shunt passive filter may fall in series resonance with source impedance for harmonic voltages in source voltage.
(iii) There is a possibility of parallel resonance between source impedance and shunt passive filter at a specific frequency at which even harmonic amplification may take place.

To solve the preceding problems of shunt passive filters, shunt active filters using PWM inverters have been used in recent years. A shunt active filter is controlled in such a way so as to actively shape the source current into sinusoid by injecting the compensating current. Fig 2 below shows the working principle of a shunt active filter.
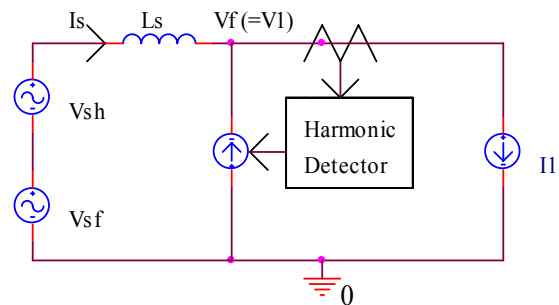
Figure 2 : Basic principle of shunt active filter

Difficulty in realising a large rated PWM current source inverter, high initial cost & low efficiency as compared to shunt passive filters and possibility of importing harmonics from other harmonic producing loads are the serious practical problems with the use of shunt active filters [5].

PROPOSED SCHEME

Conventional shunt passive and active filters have the aforementioned problems, which make their practical application difficult. As is already pointed out, filtering characteristics of a shunt passive filter partially depend on the source impedance which is not accurately known and is predominantly inductive. The impedance of the shunt passive filter should be lower than the source impedance at a tuned frequency to provide the attenuation required. Source impedance can be increased and thereby filtering characteristics of a shunt passive filter can be improved

DIGITAL POWER SUPPLY DEVELOPMENT AT THE PLS*

K.M Ha[#], S.C Kim, J.H Kim, J.Y Huang, H.S Kang, J Choi and I.S Ko
Pohang Accelerator Laboratory, Pohang 790-784, KOREA

Abstract

Digital power supply controller using the Digital Signal Processor (DSP) and Field Programmable Gate Array (FPGA) has been developed over the year at the Pohang Light Source (PLS). Recently, full digital buck type bi-phase PS development completed and tested using as the PSI card. A new digital controller is designed as 3 U euro-standard sizes and provides overall performance of the power supplies stability better than $\pm$ 5 ppm short-term stability (< 1 min) and $\pm$ 25 ppm long-term stability (< 12 hours). It is made use of the digital PI current controller which has one-pole digital filter and feed-forward voltage ripple compensation control algorithms. This paper presents the hardware and software structure of the developed digital controller and experimental results of digital power supply.

INTRODUCTION

Accelerator complex power supply application were increased to choose the based on digital technology [1],[3]. At 1999, the PSI developed the new digital control cards used DSP, FPGA and high precision AD. It was very successfully implemented to beam operation [2]. At 2005, PLS has been successfully replaced over 70 vertical correction PS sets same as PSI digital type, it has good performance and reliability for orbit feedback operation. At 2006, DLS facility commissioned digital type PS for BOOSTER, LINAC and even storage ring [3]. And SSRF in China also trying to develop digital controlled PS for the BOOSTER. PLS has the working experience of the digital PS since 2005 and had satisfactory experimental results. We choose the same type of digital controller for FIR solenoid PS. It is required single quadrant, 200 A, 25 ppm stability. The main topology has a phase shifted parallel operation mode. Practically bi-phase methods are complicated to have current balancing to each lags. But digital controller is capable of the fast cross-over frequency and 20 μs control loops for single feedback loops. This paper descries the implementation of the 20 V / 200 A bi-phase buck converters used full digital controller.

POWER SUPPLY SPECIFICATION

Hardware specification

Switch-mode power supply more advantages than linear type power supply. Switch-mode a buck type PS is common topology for single quadrant operation. The digital cards are simply provides single quadrant mode PWM for a buck converter driving. Fig. 1 shows the

proposed bi-phase type buck converter. The maximum output current is 300 A, so we chosen bi-phase method implement more high current rating capability. IGBT device is twins 400 A Ic for parallel operation. Two independent switches were derived by 180 degrees phase shifted (delay) PWMs which makes them two-phase operation.

The FIR solenoid PS hardware specification is shown in table 1.

Table 1: The Specifications of the FIR solenoid PS

Parameters	Specifications
Output voltage/current	20 V / 200 A
Load resistance	0.1 Ohm
Operating quadrant	1 Q
Stability (0 sec to 60 sec)	$\pm$ 5 ppm
Stability (> 12 hours)	$\pm$ 25 ppm
Resolution of output current	> 17 bit
Reproducibility	$\pm$ 10 ppm
Switching frequency	25 kHz bi-phase
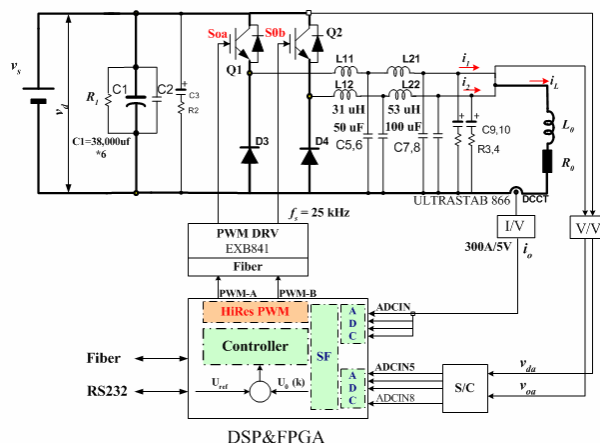
Figure 1: Hardware block diagram of the proposed switched-mode power supply

Controller description

Fig. 2 shows 3U size DSP and AD/DA cards for implementation of digital control power supplies. The core processor is Analog Device SHARC ADSP-21065L 66 MIPS floating-point capabilities with 66 MHz clock. FPGA are used for PWM generation and communication with 5 Mbps fibre channels and 115.2 Kbps serial as well

HIGH POWER MODULATOR FOR KLYSTRON OF PROTON ACCELERATOR

J.H. Jeon, B.H. Chung, Dankook University, Seoul;
K.-H. Chung, KAPRA, Cheorwon;
J.S. Hong, Dankook University, Seoul;
S.K. Ko, University of Ulsan, Ulsan;
S.J. Noh, Dankook University, Seoul

Abstract

KAPRA is under the processing of 700MHz 1MW Klystron development project for PEFP. We have already developed a modulator of high voltage power source to conduct a basic performance test of klystron. This power source of -95kV and 16.5A for 2ms pulses is designed to meet the drop within about 5%. The system is composed of the DC electric charging power supply, the high energy capacitor, the pulse switching unit, the cathode heating transformer, the discharging unit and the pulse controller. Recently, both the high voltage conditioning test and the cathode heating experiment for the klystron have been completed successfully. The beam conditioning and the RF conditioning was performed at -95kV and the peak current generated was measured to be 16A.

PAPER NOT YET RECEIVED

UTILIZING MULTIPLIER STACK'S REFLECTED PARASITIC CAPACITANCE TO ACHIEVE ZVS OPERATION OF RESONANT INVERTER FOR 750 keV DC ACCELERATOR

A. Kasliwal[#], R. Banwari, S. Kotaiah, T.G. Pandit, A. Upadhyay

Raja Ramanna Centre for Advanced Technology, Indore 452 013, India

Abstract

This paper presents the analysis and design of a high order LCLC resonant inverter that uses the reflected capacitance of the Cockcroft-Walton based multiplier stack as its tank circuit component. The inverter is being used for energizing the HV generator of the 750 keV dc accelerator developed at RRCAT, Indore. High frequency resonant inverters are replacing the conventional PWM counterparts due to high efficiency, reduced size, weight and cost. The operating characteristics and analysis of series resonant (SRC), parallel resonant (PRC) and series parallel (SPRC) resonant converters have been reported for fixed frequency operation. It has been shown that SPRC takes the advantage of both SRC and PRC curtailing their disadvantages. The inverter described feeds a high frequency, high voltage (HV) transformer isolation and utilizes the otherwise unwanted parasitic components to its advantage.

INTRODUCTION

Hard switching PWM inverters for high voltage application need to feed a very high voltage transformer. The HV transformer requires a relatively large spacing between the primary and secondary windings, which leads to a relatively large leakage inductance. In this case, it is generally difficult to employ a PWM type inverter due to output voltage lost during the reversal of current in the large leakage inductance of a high voltage transformer. On the other hand, an operating frequency higher than 30 KHZ is generally desired to avoid voltage drop across the capacitive column of the high voltage multiplier stack and to avoid any audio frequency noise that may be generated. This in turn improves the load regulation of the system. But it also enhances the effect of parasitic components. A sinusoidal voltage is desired as high frequency harmonics in the square wave voltage impose high dv/dt stress. For lower switching losses, high power density, better EMI characteristics and sinusoidal voltage and currents, resonant inverters have proved to be a better proposition. A series resonant inverter has the disadvantage of high circulating currents that increases the switching device ratings. Furthermore, a series resonant inverter cannot actually be developed due to the large parasitic capacitance generally existing in a high voltage transformer. Hence a series parallel LCLC combination has been used as it gives the advantage of low device currents and a better load regulation. The converter utilizes the leakage inductance and the inter-winding capacitance of the high voltage transformer it

[#]apollo@cat.ernet.in

feeds to and the parasitic capacitance of the multiplier stack, for its resonant operation. This LCLC resonant tank functions to position zero voltage across the switching device prior to turn on, eliminating any power loss due to the simultaneous overlap of switch current and voltage at each transition.

The multiplier stack basically consists of several similar circuits containing diodes and capacitors, which are connected in series to achieve voltage multiplication. The high voltage rating demands the placement of components to be fairly apart to achieve required voltage isolation. The circuit is fed with a 40 kHz sine wave to achieve better regulation and minimum ripple at the DC output. Combined together, all these results in higher parasitic components. These capacitances are mostly contributed by parasitic capacitance between DC and AC columns of multiplier stack, diode capacitance etc. Moreover the stack is fed from a 45 kV-0-45 kV high voltage transformer with a very high step-up ratio, which is 150 in our case. The transformer secondary itself imposes high distributed capacitance
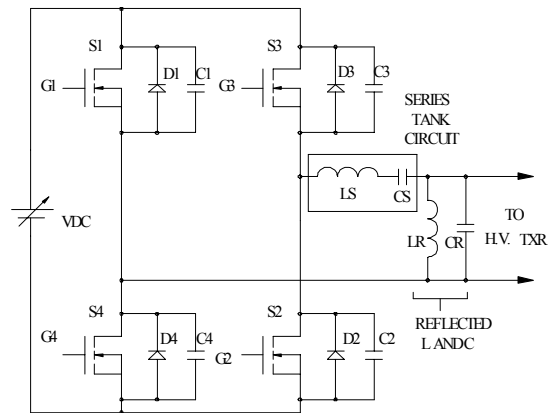
Figure 1: High frequency inverter.

OPERATION

When measured at the primary of the HV Transformer with the multiplier stack connected at its secondary, the reflected load at inverter output was found to be purely capacitive with a value of 4.1 µF. This could have been compensated by a parallel inductance on the primary side but it would have then resulted in high circulating currents in the transformer winding. Referred to the secondary side of the transformer, this capacitive reflection effectively comes out to be 0.177 nF.

300 KV, 6 KW POWER SUPPLY SYSTEM FOR SELF-SHIELDED LOW ENERGY DC ACCELERATOR AT RRCAT INDORE

R. Banwari*, A. Kasliwal, Ajay Kumar, A. Upadhyay, P. R. Nath, S. Kotaiah and T. G. Pandit
Raja Ramanna Centre for Advanced Technology, Indore

Abstract

A compact, low energy, self-shielded dc accelerator for industrial applications requiring beam energy in the range of 100 to 300 keV is under development at RRCAT, Indore. The power supply and control system for this accelerator is discussed here in this paper. The high voltage source is a series fed cascade generator driven by a 30 kHz sine wave inverter. Two asymmetrical cascade generators are run in parallel to enhance the current capacity of the generator. A 15-0-15 kV, 30 kHz ferrite core transformer interfaces the cascade generators with IGBT based H-bridge inverter. A buck chopper controls the dc bus voltage of the inverter so as to control the terminal voltage of the high voltage generator. A low power high frequency inverter generates the filament power supply floating at terminal voltage of the accelerator through a capacitive isolation column. Control of the filament power supply is achieved by sensing the accelerator beam current and controlling the low power inverter in a closed loop. A PC based control system designed with Lab-View 7.0 software and ADuC812 Micro-converter cards monitors and displays the various parameters of the power supply and accelerator.

INTRODUCTION

Electron beam curing is an energy efficient process, which creates unique products and improves the existing ones. It occupies less space as compared to thermal ovens and cures all the colours equally with complete removal of solvents. Radiation curable inks and coatings can be employed essentially to any substrate imaginable including paper, wood, metal, leather, vinyl, plastic, glass and magnetic tape etc. Being radiant energy the electron beam directly converts reactive liquids into solids and do not have to rely on energy-intensive evaporation system to remove solvents or water.

Electron beams are currently being used in industries for the curing and cross-linking of coatings, inks and adhesives. An energy in the range of 100 to 300 keV is useful in many applications like heat shrinkable foils and tubes, hardening of coatings, wrinkle free textiles by graft polymerisation, surface sterilization of food materials and surface hardening of plastics. Keeping these applications in focus a compact, **S**elf-shielded, **L**ow **E**nergy dc **A**ccelerator (SLEA) is being developed at RRCAT. The operating energy of the accelerator is chosen as 100 to 300 keV with maximum beam power of 6 kW. The accelerator assembly is compact and light enough to be transported and installed at the site of demonstration or application. Design features and developmental aspects of the high voltage generator, filament power supply and control system for this accelerator is described in following sections.

HIGH VOLTAGE GENERATOR

The required accelerating voltage for this accelerator is generated using high frequency multi doubler circuits driven in parallel as shown in block schematic of Fig 1. A 30 kHz, 10 kW driver inverter feeds the power to the multiplier column through a centre-tap ferrite core high voltage transformer. A resistive voltage divider is used for measurement and control of the accelerator terminal voltage. A fast acting stabilization circuit operates the high voltage power supply either in a constant voltage or constant current mode. Both these functions can be controlled and monitored remotely through a PC that also displays the beam parameters.

For safety considerations the multiplier stack is designed for minimum stored energy. At the same time the ripple in the output voltage is kept low by selecting the high frequency operation. The power supply is short circuit protected by use of damping resistor and trip features of the chopper and inverter units. The filament power supply is generated through a capacitive isolation column, which is fed from a low power inverter. The beam current is stabilized by controlling this inverter in a closed loop with respect to emission current. The high voltage terminal of the multiplier stack is provided with a hemispherical dome and individual decks are fitted with equipotential rings so as to give electrostatic shielding to multiplier components and to control the external electric fields.

The multiplier stack embedded with high voltage divider and capacitive isolation column is fully contained in a SF_6 filled tank, which provides excellent insulation. The design aspect and constructional features of various subsystems of the high voltage generator are briefly described in following subsections.

Rectifier and Chopper Unit

The three-phase AC mains is rectified and filtered by an uncontrolled bridge rectifier and resultant DC voltage is fed to a buck-chopper, which regulates the inverter DC bus voltage in a closed loop. A half bridge IGBT module is chosen for this application where the first device is used as a chopping element and second one, with its gate-source shorted, serves as the freewheeling diode for the output stage thus reducing the size. The feedback signal for the chopper unit is derived from the terminal voltage of the HV generator through a resistive voltage divider. This means, controlling the chopper output voltage finally controls the beam energy of the accelerator.

*banwari@cat.ernet.in

DEVELOPMENT OF 3 MeV, 30 kW DC ELECTRON ACCELERATOR AT EBC, KHARGHAR

K.C.Mittal, K.Nanu, A.Jain, K.V.Nagesh, S.Acharya, G.P.Puthran, R.I.Bakhtsingh, P.C.Saroj, D.K.Sharma, R.N.Rajan, Mukesh Kumar, S.K.Srivastava, A.S.Chawla, A.R.Chindarkar, S.R.Ghodke, D.Jayaprakash, Mahendra Kumar, Rajesh Barnwal, R.L.Mishra, Vijay Sharma, S.Dewangan, S.R.Barje, R.M Agarwal, M.K.Pandey, S.R.Raul, D.P.Chakravarthy and A.K.Ray

Electron Beam Centre, Accelerator and Pulse Power Division, Bhabha Atomic Research Center, Kharghar, Navi Mumbai, India

Abstract

A 3 MeV, 30 kW DC industrial electron accelerator has been designed and is in advanced stage of development at Electron Beam Center, Kharghar, Navi Mumbai. Electron beam at 5 keV is generated in electron gun with LaB_6 cathode and is injected into accelerating column at a vacuum of 10^{-7} torr. After acceleration, the beam is scanned and taken out in air through a 100 cm X 7 cm titanium window for radiation processing applications. The DC high voltage accelerating power supply is based on a capacitive coupled parallel fed voltage multiplier scheme operating at 120 kHz. The electron gun, accelerating column and high voltage multiplier are housed in accelerator tank filled with SF_6 gas insulation at 6 kg/cm^2. This paper describes about the design details and current status of the accelerator and its various subsystems.

INTRODUCTION

Electron beam accelerators are finding wide ranging applications like surface curing of coatings, cross-linking polymeric materials, sterilization of medical products, coloration of diamonds, disinfection and preservation of food products, purification of industrial and biological waste etc. Electron beam energy and dose rate for different application differs widely depending upon the type of product and the desired modification. The beam energy and dose rate requirement for these types of applications ranges between 0.15 MeV to 10 MeV and few kilowatt to hundreds of kilowatts. In view of the growing needs we have taken up indigenous development of industrial accelerators at APPD, BARC. A machine rated for 3 MeV, 30 kW beam power is now under development [1] which being commissioned at Electon Beam Centre, Kharghar, Navi-Mumbai. The 3 MV DC supply for this based on a parallel fed voltage multiplier scheme considering power efficiency, energy stability and reliability [2]. The accelerator is designed to operate with beam energies from 1 MeV to 3 MeV with beam current of 0 -10 mA.

ACCELERATOR DESIGN

Schematic of the accelerator is shown in Fig. 1. The accelerator and its high voltage power supply are housed in a pressure vessel filled with SF_6 gas as the insulation at 6 kg/cm^2. The accelerator is a vertical assembly housed in a concrete building where the accelerator is located in the upper cell and the product irradiation facilities in the lower cell. A triode electron gun using LaB_6 cathode generates the electron beam and injects into the accelerating column at 5 keV. This beam is accelerated through a 3.5 m long accelerating column assembly consisting of 10 numbers high gradient metal-ceramic diffusion bonded tubes made by NEC, USA. Potential grading of the accelerating column is accomplished by a resistive divider chain. Electron beam after acceleration is transported through a beam line, scanned and brought out to atmosphere through titanium window for radiation processing applications.
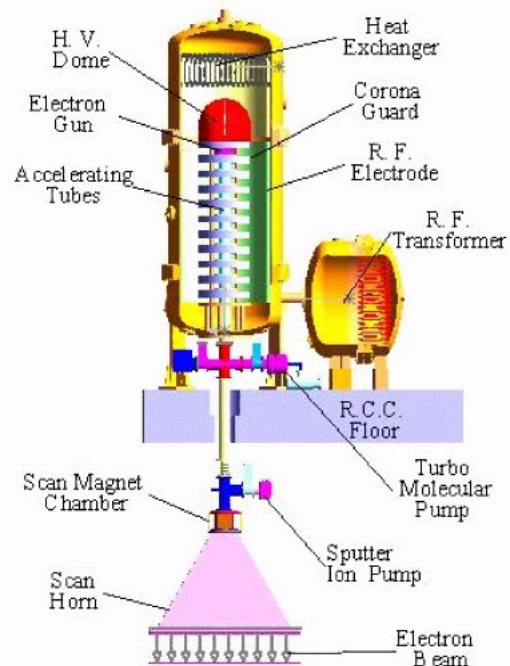
Figure 1: Schematic of 3MeV, 30kW Accelerator

High Voltage Supply System

The 3 MV, 10 mA DC supply for the accelerator is based on a 68 stage, capacitive coupled parallel fed voltage multiplier scheme operating at 120 kHz. The input to the voltage multiplier is 150 kV - 0 -150 kV (peak), 120 kHz which is fed to a pair of semi-

ANALYSIS AND DESIGN OF A PARALLEL RESONANT NETWORK POWER SUPPLY FOR A RAPID CYCLING SYNCHROTRON

Sunil Tiwari[#], Mangesh Borage and Swarna Kotaiah
Raja Ramanna Centre for Advanced Technology, Indore 452 013, India

Abstract

Rapid Cycling Synchrotron (RCS) requires dc biased sinusoidal excitation for electromagnets. Power supplies based on resonant schemes are best suited for such applications, as only the losses of the resonant network are drawn from the mains and the magnets are energized by resonating its inductance with external energy storage elements. In this paper study of various options for powering the magnets and its excitation source is carried out. Optimization of network elements for parallel resonant network with respect to the operating and investment cost is carried out. Tolerance analysis of a high-*Q* resonant network with respect to variation in component values and its effect on amplitude and phase of magnet current, and the ac component reflected in the magnet current due to presence of ac and dc input source ripple is documented. Design of a parallel, continuous ac excited resonant network for the QF2 magnet for the proposed 1 GeV RCS is presented.

INTRODUCTION

A spallation neutron source which is an important tool for research in material science, life science, chemistry, fundamental and nuclear physics, earth and environment science is proposed at RRCAT. It mainly consists of a 1 GeV, 25 Hz RCS for production of high energy protons and a target which is bombarded with these protons to produce neutrons. This paper describes the analysis and design of a powering scheme for a family of quadrupole magnets of the proposed RCS. The requirements of a power supply for these electromagnets are quite different from conventional dc power supplies [1]. A method where the energy of the magnets, which is needed only for a short time during each period, can be stored is preferred. Therefore oscillatory circuits are used where the energy is stored in the capacitors and only the losses of the resonant network are drawn from the mains. A string of magnets energized with a single source develops a very high voltage with respect to ground. To overcome
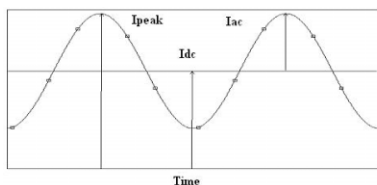
Figure 1: A dc biased sinusoidal current wave for excitation of RCS magnets.

[#]sunil@cat.ernet.in

this problem, the circuit elements are connected in a configuration called White circuit [2]. The objective of this paper is to present a systematic approach for selection of circuit topology, to carry out tolerance analysis of the resonant network and finally to recommend a powering scheme for QF2 magnets.

SCHEMES

General specifications of the QF2 magnet are summarized in Table 1. The excitation frequency is 25 Hz and the peak current is 1230 A. Typical waveform of a dc biased sinusoidal current is shown in Fig. 1. I_{ac} is the peak current of the ac component and I_{dc} is the average current in the magnet. Parallel and series resonance circuits (PRC and SRC, respectively) are best suited for such applications. The PRC and SRC schemes are shown in Fig. 2. The comparison between PRC and SRC is as follows:

Table 1: Specifications of QF2 Magnet

Total Numbers	:8
I_{dc}	:1230 A
$I_{ac\ Peak}$	:730 A
I_{pk}	:1960 A
Inductance/magnet	:11 mH
Peak energy/magnet	:11kJ
DC resistance/Magnet	:2 mΩ
Resonant Frequency	:25 Hz

(a)

(b)
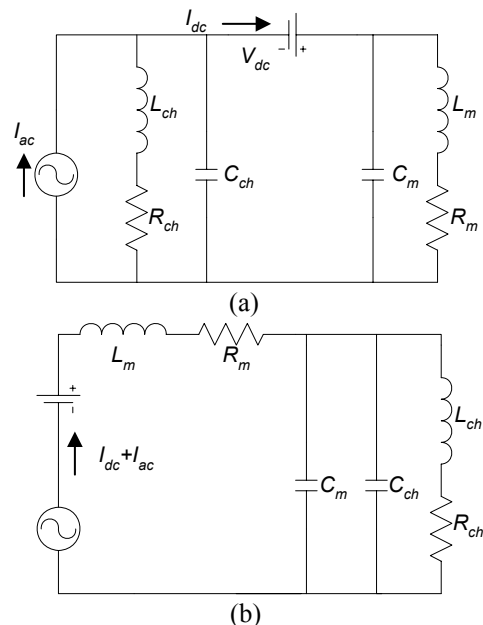
Figure 2: Resonant excitation schemes: (a) PRC (b) SRC.

STUDY AND COMPARISON OF REACTIVE POWER COMPENSATION SCHEMES FOR AIR-CORE TRANSFORMER IN ELV-TYPE DC ACCELERATORS

Mangesh Borage[#], Sunil Tiwari and Swarna Kotaiah
Raja Ramanna Centre for Advanced Technology, Indore 452 013, India

Abstract

The ELV-type accelerators use air-core, multi-secondary step-up transformer to generate the high voltage. The transformer has large leakage inductance and small magnetizing inductance. Suitable compensation scheme is required to minimize the reactive power loading on the source feeding the primary winding. The results of studies done to investigate suitability of various compensation networks are presented in this paper. Characteristics are studied and compared using simulation software PSpice, wherein normalized results suitable for comparison are directly obtained.

INTRODUCTION

The high-power ELV-type electron accelerators are widely used in industrial and research applications. The scheme for generating high voltage in these machines is based on air-core, multi-secondary step-up transformer. Each secondary has voltage doubler rectifier and filter, the outputs of which are connected in series to generate the high voltage. As opposed to the conventional transformer, the air-core transformer has large leakage inductance (L_s) and small magnetizing inductance (L_m). Moreover, the values of L_s and L_m are nearly the same [1]. A simplified equivalent circuit is shown in figure 1. The air-core transformer has poor regulation and draws a large reactive power from the source feeding the primary winding. Suitable compensation scheme must therefore be employed to minimize these undesirable effects. The compensation network (CN) should offer following benefits: (1) Near-unity power factor operation under all loading conditions. (2) Nearly load independent output voltage. (3) Minimum additional reactive components. (4) If possible, no additional compensating inductor.

The conventional compensation scheme [1] however can either achieve good voltage regulation or minimum reactive power depending on the operating frequency. Besides, the network uses an additional bulky inductor.
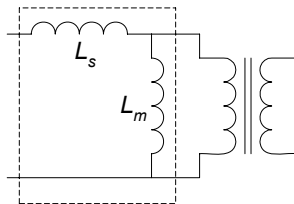
Figure 1: Simplified equivalent circuit of air-co re transformer in ELV-type accelerators.

[#]mbb@cat.ernet.in

Therefore, the possibility of using various other CNs is examined. In this paper, the results of studies done to investigate suitability of various CNs are presented. Characteristics of the CNs are studied and compared using PSpice [2].

COMPENSATION NETWORKS

The CNs considered for study and comparison are shown in Fig. 2. In the networks N1, N2 and N3, the inductive components of air-core transformer are compensated using one or more capacitors. The network N4 uses additional inductor (L_a) and is the conventional CN [1]. PSpice is used for analysis of these CNs. However, a method described in [3] is followed to obtain the normalized results for comparison directly from the simulation. Amplitude of input source V_{in} is assumed to be unity. The values of L_s and L_m are assumed to be the same [1]. Resonant frequency (f_o), characteristic impedance (Z_n) and circuit Q are defined as:

$$f_o = \frac{1}{2\pi\sqrt{(L_s+L_m)C}} , Z_n = \sqrt{\frac{(L_s+L_m)}{C}} , Q = \frac{R_{ac}}{Z_n} \quad (1)$$

where C is the compensating capacitor and R_{ac} is the resistive equivalent of secondary-side doubler-rectifier and load reflected on the primary side. Table 1 give the values of L_s, L_m and C making f_o and Z_n unity.
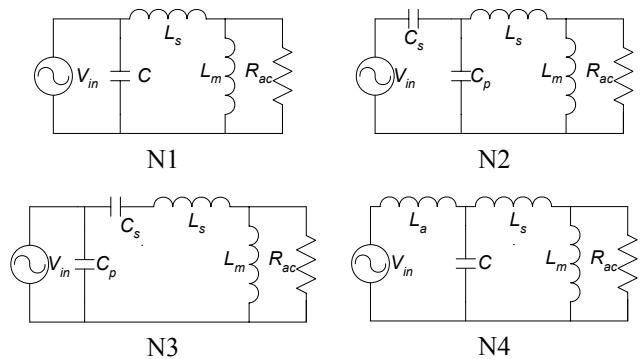
Figure 2: Compensation networks.

Table 1: Values of L_s, L_m and C used in simulation.

Component	Compensation Network			
	N1	N2	N3	N4
$L_s = L_m$	$\dfrac{\left(\frac{1}{2\pi}\right)}{2}$			
C	$\left(\frac{1}{2\pi}\right)$	—	—	$\left(\frac{1}{2\pi}\right)$
$C_s = C_p$	—	$\left(\frac{1}{2\pi}\right)=C$	$2\left(\frac{1}{2\pi}\right)=2C$	—

07 Accelerator Technology
T11 - Power Supplies

STAIR CURRENT OUTPUT POWER SUPPLY FOR SWITCHING MAGNET*

Seong-Hun Jeong [#] , Ki-Hyeon Park, Heung-Sik Kang, Dong-Eun Kim, Jin-Hyuk Choi,
PAL, Pohang, 790-784, Korea

Abstract

The switching magnet for beam distribution is served with Digital Signal Processor (DSP) controlled PWM switching-mode power supply (SMPS). This SMPS is employed phase-shifted parallel (PSP) operation of IGBTs. This technique allows ± 350 A, 2.5 Hz stair output, and ± 350 A at bipolar mode operation. Current feedback and input voltage feed-forward control schemes are applied to improve the output current stability. Experimental results showed that the implemented converter achieved a useful versatile power supply.

INTRODUCTION

High current sources are needed in accelerators to bend and focus of electron beam. For these application, the power supply demands several types of output. In some cases, high stability current source for stringent specification of load was required.

The DSP had been developed primarily for application in various high speed digital signal processing. Due to its fast computational speed nowadays, the DSP has replaced much of the complex control hardware. The applications of high-performance DSP in complicated power electronic systems have found great potential in synthesis of sophisticated control algorithms and PWM switching schemes [1].

In order to achieve requirements of accelerator current source, DSP based current-controlled PWM bipolar SMPS using the TMS320F2808 from the Texas Instrument was developed for universal purposes. This SMPS is possible to operate in two modes by program. The one mode is arbitrary waveform current source and the other is bipolar current source. Each mode use phase-shifted parallel operation of IGBTs, so, it is possible to increase power rating and operating frequency by a factor of 2 [2].

Conventionally, the regulation circuits of a SMPS are realized using analog circuit technique. Analog controller is easy to implementation and good for simple circuits. With a good DAC and the other fine circuits, a high stability SMPS can be archived. But, analog control technique also has its demits in complex circuit design, low reliability, non-flexibility, and higher manufacturing cost.

This paper describes the development of a programmable power supply (PPS) using a DSP-controlled phase-shifted parallel SMPS for accelerator magnet.

SYSTEM DESCRIPTION

The simple diagram of the power supply with LC output filter and magnet load were shown in Figure 1. The SMPS scheme consists of two full bridge rectifiers followed by each full bridge inverter. Two DC-links of full bridge rectifiers are connected to each other to maintain same voltage. The topology is full bridge parallel inverter, which can be a dc-to-ac inverter. The basic concept of operation mode is phase-shifted parallel operation of IGBTs modules, where each IGBT has shared equal average current that is inherent in the PSP operation mode. This power supply has two operation modes. First mode is arbitrary current waveform generator and second is bipolar SMPS.
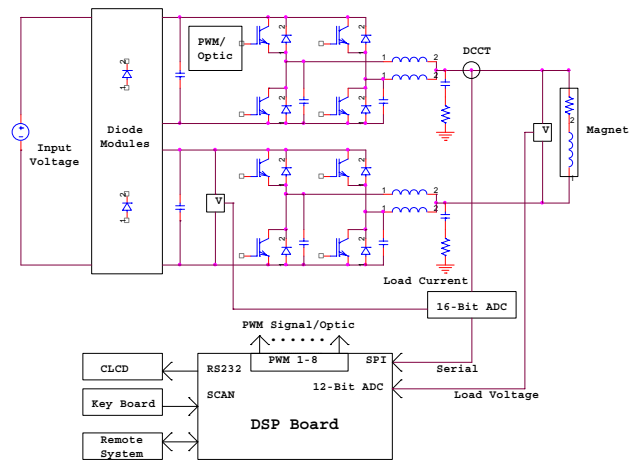
Figure 1: System Schematic Diagram.

Figure 1 shows control signal flow between the IGBT modules and the DSP and external devices.

This PPS was configured as a parallel full bridge type for driving higher load current, where each full bridge can drive 200A at 10 KHz switching frequency.

Owing to the PSP, the system operating frequency is doubled to 20 kHz and each IGBT current burden is one half of total current. Another advantage of PSP is one that the inductance value for output filter was reduced to one half comparing to the single full bridge type.

Current feedback and input voltage feed-forward control schemes are applied to improve the output current stability. The switching device is four dual packages of IGBT FF400R12KF4 from Eupec. The fiber optic connector HFBR series from Agilent Co. is used to interface from DSP to driver board for IGBT to improve system noise susceptibility and ground isolation. Two

STUDY OF VACUUM RELATED PROBLEMS DURING THE ENERGIZATION OF K-500 SUPERCONDUCTING CYCLOTRON

Md. Z.A.Naser[#], U.Bhunia, J. Pradhan, J Debnath, S. Paul, M.Dutta, A. Pole, D.L.Bandopadhaya, A. Sur, C. Mallik and R.K.Bhandari

Variable Energy Cyclotron Centre, 1/AF Bidhan Nagar, Kolkata-700 064, INDIA

Abstract

The K500 superconducting cyclotron main magnet has been commissioned successfully in VECC, Kolkata. During the process of energization, it has been observed that there is vacuum deterioration in the cryostat outer vacuum chamber (OVC). Detail studies have been carried out to examine the occurrence of such a situation. The electro-magnetic stress due to Lorentz force increases with current, and is more pronounced in the median plane region of cryostat having maximum number of welded joints. This could be the possible reason for the OVC vacuum degradation. The paper reports various observations on vacuum deterioration during energization. An extensive study has been carried out to understand and explain the situation.

INTRODUCTION

The K-500 Superconducting Cyclotron (SCC) main magnet consists of two superconducting coils (alpha coil and beta coil), which has been energized to different current levels for extensive magnetic field measurement. The superconducting coil inside the liquid helium chamber is suspended by nine number of support links; of which, three pulling up, three pulling down and three pulling radially out. This support system carries the whole weight of the coil and cryostat. An annular vacuum chamber, made of magnetic steel, referred as cryostat OVC, surrounds the stainless steel cryostat bobbin. Prior to cool-down of the cryostat, the force experienced on the support links is estimated theoretically, which is reported elsewhere [1] and compared with measured values. This is very crucial for the health of the support links, which is attached to the outer wall of the OVC. During higher excitations of superconducting coil, it is observed that the OVC vacuum degrades gradually. The mass spectrograph for helium leak detection (MSLD) is carried out and multiple leaks in the order of 10^{-4} mbar-lt/sec are found. Occurrence of such a situation is analysed in this paper. One of the basic reasons may be, that, during excitation a huge magnetic force develops on the OVC wall (coil tank) made of magnetic steel. This leads to a localised magnetic stress on coil tank, which is having several welded joints around the median plane. There is a possibility of mechanical failure on the defective welded joints (if any) of the coil tank at higher excitation. Another reason of failure may be due to the radial force experienced by the bobbin if the coil is off-centred with

[#]zamal@veccal.ernet.in

respect to surrounding iron yoke. This force propagates to the coil tank through support links.

ANALYSIS

Experimental Observations

During cool-down of the superconducting coil a huge thermal force is developed as shown in figure 1 by the shrinkage of the cold mass and support links. Though the experimentally observed link force profile during cool-down matches with calculated value, there is mismatch between calculated and experimentally observed values. This is may be due to the differences of material property used during the calculation.
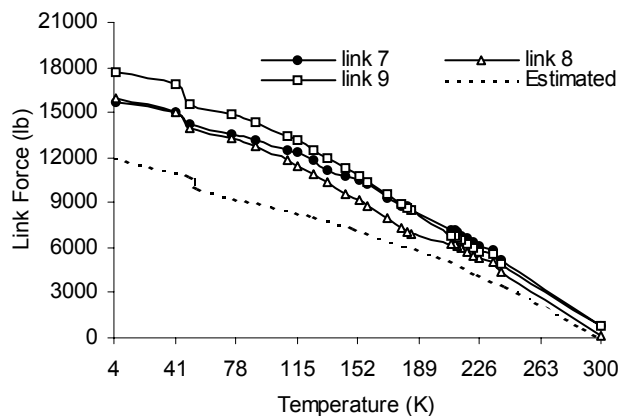
Figure 1: Support link force variation during cool-down of the superconducting coil.
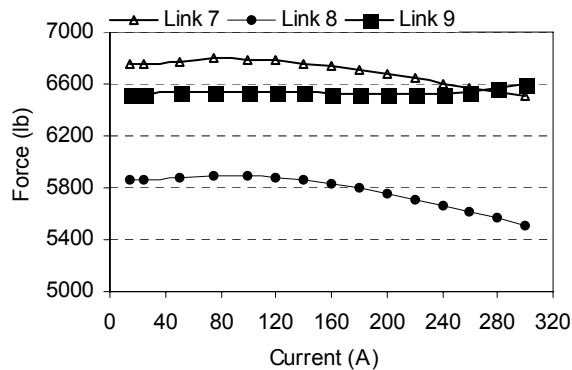
Figure 2: Support link force variation during energization of superconducting coil.

PERFORMANCE OF CRYOMODULE AND CRYOGENIC NETWORK SYSTEM FOR THE SUPERCONDUCTING LINAC AT IUAC. DELHI.

T. S. Datta, J. Antony, S. Babu, J. Chacko, A. Choudhury, S. Kar, M. Kumar
R..S. Meena & A. Roy.
Inter- University Accelerator Centre. Aruna Asaf Ali Marg. New Delhi- 110067. India.

Abstract

The Superconducting Linear Accelerator as a booster of existing 15 UD Pelletron Accelerator is under construction at IUAC. The heart of superconducting linac is three cryomodules, each one housing eight quarter wave niobium cavities. In recent past two online tests with one linac module have been carried out and the beam ($28 Si^{+10}$) energy has been enhanced approximately from 130 MeV to 150 MeV with five effective cavities. The present paper highlights the operational experience of the cryogenic network system and its accessories during present run. Analysis of measured heat load at 4. 5 K from first Linac cryomodule is also presented

INTRODUCTION

To augment energy of heavy ion from 15 UD pelletron and to widen the mass range up to 80 to have energy above coulomb barrier, the Superconducting Linear Accelerator [1] is under development at IUAC, Delhi. Acceleration is achieved by using Superconducting quarter wave bulk niobium cavities operating at 97 MHz. The heart of linac is three cryomodules, each one is housed with eight cavities and one solenoid magnet. At present the first linac module along with superbuncher and rebuncher cryostats are installed in beam line and are integrated with helium and nitrogen refrigerator through indigenously developed cryogen distribution line. Except the portion of field joints connecting the cryomodules, the entire helium transfer line [2] is liquid nitrogen shielded, multilayer insulated and enclosed in a vacuum jacketed pipe of 8inches diameter. The Central VME based Cryogenics Data Acquisition System is developed to monitor and control operating parameters of cryostat, refrigerator and distribution system. Static and dynamic loads at 4. 2 K from all the cryomodules along with distribution line is met by a CCI make helium refrigerator of capacity 600 W at 4.2 K. The total load at 4.2 K on complete system as well as break up load in each cryomodule has been measured. Measured data with respect to vacuum, helium pressure, temperature of linac cryomodule related to the performance of cavities are analyzed and presented in this paper.

LINAC CRYOMODULE & COOLING METHODOLOGY

This is a rectangular cryostat [3] of dimension 3.0m x 1.2m x 1.9 m to house eight cavities and one solenoid magnet. A rectangular copper shield at 80- 100K is used to reduce the radiation load. Eight cavities and solenoid magnet are supported on two solid rectangular aluminum

bar, which is supported from top plate with two SS sheet. Each cavity can be individually aligned in X – Y - Z
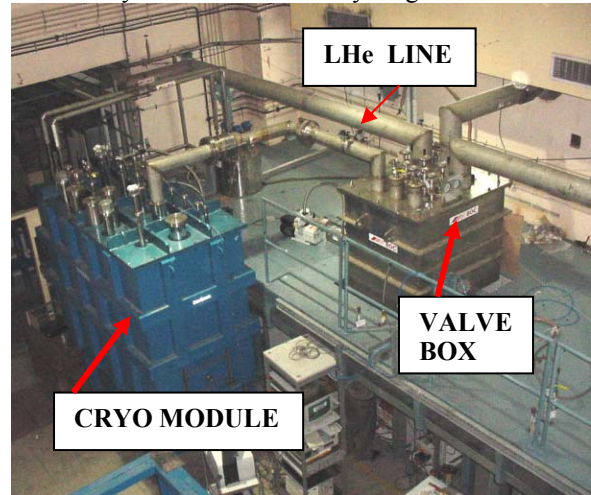
Figure 1 : Linac cryomodule with valve box

direction. Total cold mass in one linac module is estimated to be ~ 600 kg. All RF accessories like drive coupler, slow tuner, liquid nitrogen cooled RF cable are assembled from top plate of cryostat.
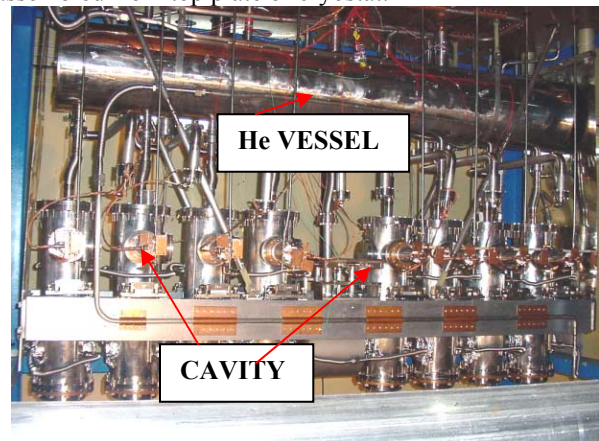
Figure 2 : Inside view of Linac cryomodule

Cool down of linac cavities [4] from 330 K to 4.2K is achieved in three steps, viz. inverse radiation cooling (330-220K) from shield, LN2 precooling (220- 140 K) and liquid Helium cooling (140 – 4.2 K). In-spite of slow cool down rate (15 K/ hr) in the critical zone, Q disease has not been reported. Minimum human interference is achieved by reducing final JT pressure with moderate liquid helium flow rate of 40 litres/hr. A complete cool down profile of linac module over three days is shown in figure 3.

CURE OF TEMPERATURE FLUCTUATIONS ON THE NITROGEN-COOLED SECTIONS OF A CESR-TYPE SRF MODULE

M. C. Lin[#], Ch. Wang, M. H. Tsai, M. S. Yeh, F. T. Chung, T. T. Yang, M. H. Chang, L. H. Chang
TLS, NSRRC, Hsinchu 30076, Taiwan

Abstract

A strong correlation between tuner motion of the SRF module and the pressure fluctuation of the shielding liquid nitrogen flow is observed. The double elbow waveguide section with nitrogen cooling channels is one of the possible fluctuation sources. Thus it is tested along to investigate the mechanism of pressure and temerature fluctuations, whereas a phase separator with pressure regulation function is used to stabilize the supply pressure of liquid nitrogen. Also it is tried to stabilize the pressure fluctuation by optimizing and regulating the vent flow rate. System setup and primary test results are presented herein.

INTRODUCTION

As a major accelerator upgrade to increase the stored beam current and to eliminate the beam instability caused by higher-order modes of the cavity [1], an industrially manufactured superconducting radio-frequency module was installed into the storage ring at the Taiwan Light Source (TLS), in late 2004. The CESR-type SRF module[2], developed in the Newman Laboratory of Nuclear Studies, Cornell University, USA, was chosen for this project. During normal operation of the SRF module in 2005 and 2006, it is observed the cavity tuner motion has a strong correlation with the temperature variations of the thermal transition beam tubes of the SRF module [3].

The thermal transition beam tubes are located in between the room-temperature end plates and the nitrogen-cooled sections. Thus its temperature fluctuation must come from the temperature variation of liquid nitrogen shielding flow. As shown in Fig. 1, when the
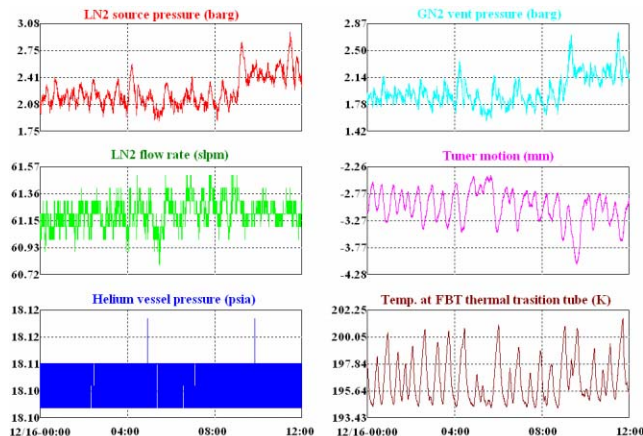
Figure 1: Tuner motion is correlated with the temperature of thermal transition tube and the nitrogen pressure, when the helium vessel pressure has a small variation.

[#]chyuan@nsrrc.org.tw

variation of helium vessel pressure is controlled within +/- 0.01 psia, correlations between the tuner motion, nitrogen supply pressure, nitrogen vent pressure, and the temperature at the thermal transition tube are observed.

For the CESR type SRF module, liquid nitrogen cools not only the thermal shielding layers and the thermal transition tubes, but also a double elbow waveguide section. The double elbow waveguide section has much bigger cooling channels than the 1/2" copper pipes for thermal shielding. Thus it is highly suspected to be the source of pressure fluctuation. A spare double elbow waveguide section is used to study the fluctuation mechanism herein. With the help of a phase separator as liquid nitrogen supply source and a bypass flow control valve, the test results shows the cure of temperature and pressure fluctuations is promising.

EXPERIMENT SETUP

Layout

The layout of experimental setup is shown in Fig. 2. A phase separator with pressure regulation supplies liquid nitrogen to the double elbow waveguide through the inlet valve and a vacuum-jacketed flexible line. The double elbow waveguide section is wrapped with super-insulation layers and then installed into a vacuum sealed vessel. Its lower end section is connected to the vacuum vessel through a dummy waveguide section. Temperatures at 3 locations are monitored: T_u at upper end near the inlet cooling channel, T_{out} on the surface of cooling channel outlet, and T_b on the bottom end near thermal transition section. The vent nitrogen is warmed up to room temperature by a passive warmer.
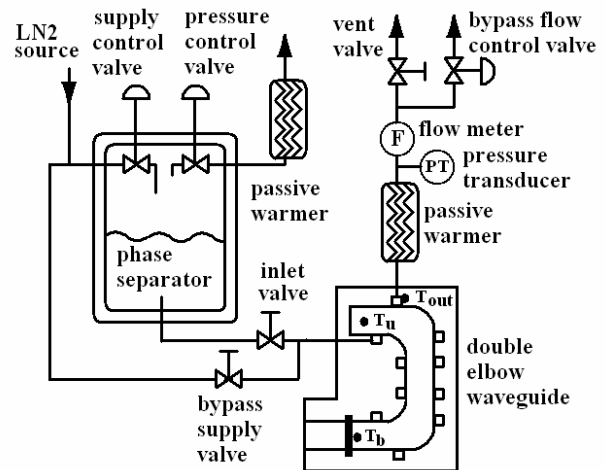
Figure 2: Layout of test setup, with a phase separator for supply pressure regulation.

DESIGN OF THE TPS BENDING CHAMBER

C. K. Chan, G. Y. Hsiung, C. C. Chang, Y. B. Chen, C. Y. Yang, C. L. Chen, H. P. Hsueh,
S. N. Hsu, Y. H. Liu, NSRRC, Hsinchu, Taiwan.
Ivan Liu, NTHU, Hsinchu, Taiwan.
J. R. Chen, NSRRC, Hsinchu; NTHU, Hsinchu, Taiwan.

Abstract

This article describes the design, manufacture and treatment of the bending vacuum chamber (B-chamber) of the 3-GeV Taiwan Photon Source (TPS). The B-chamber is a aluminium-alloy chamber ~5 m long with an antechamber on the near side of the beam duct. The design of the B-chamber is aimed to diminish the power density and the photon-stimulated desorption (PSD) induced by synchrotron radiation. Simulations, by finite-element analysis, of the B-chamber deformation due to evacuation and pressure profiles of the vacuum systems of a unit cell by a Monte-Carlo method are also described.

INTRODUCTION

The TPS is a continuing project to construct a third-generation synchrotron source at the National Synchrotron Radiation Research Center (NSRRC) in Taiwan. The TPS storage ring, a 6-fold super-period of DBA structure with 24 unit cells, has an electron beam energy 3 GeV and a beam current 400 mA. Aluminium alloy is chosen as the B-chamber material because of its properties well known for the construction of accelerators, including large thermal conductivity, absence of magnetism, small rate of thermal outgassing, small residual radioactivity, and ease of machining. Because the latest lattice design alters the circumference of the storage ring from 518.4 m to 486 m, the design of the vacuum systems must be amended. The following sections update the design of the TPS B-chamber.

BENDING CHAMBER

Figure 1 shows the drawing of the TPS B-chamber, which consists of two pieces of aluminium plate (lower and upper halves); each has thickness 50 mm. The TPS B-chamber is designed to have the following features: (1) a large triangular aluminium chamber (~5 m) to confine almost outgassing sources induced by the PSD inside the B-chamber; (2) absorbers located as far from the beam source as possible to decrease the heat load on absorbers; (3) vacuum pumps arranged on the antechamber and near the outgassing sources to increase the effective pumping speed and to decrease the beam impedance generated by the pumping orifices.

Although many advantages can be gained, the compromise requires more complicated interfaces between the B-chambers and the magnets. Fig. 2(a) and 3(b) depict the cross-sectional views of the B-chamber combined with the quadrupole (Q-) and sextupole (S-) magnets, respectively. To attain a criterion of deformation < 0.1 mm in the beam duct, the outer profiles of the aluminium plates are machined according to the shape of the poles and coils of the Q-magnets and S-magnets. The clearance is generally maintained at 3 mm. The spaces with a clearance < 3 mm will be tested in the engineering with care taken during assembly. The channel between the beam duct and the antechamber has a height 10 mm. Figure 3 shows, by finite-element analysis, the deformation of half of the B-chamber due to evacuation. The result shows the maximum deformation at the coil of Q-magnet to be 0.13 mm, and the deformation in the beam duct is controllable within 0.1 mm.
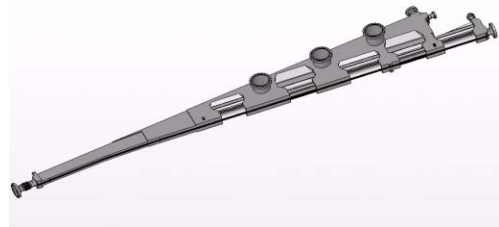
Figure 1: Assembly drawing of a TPS bending chamber 5 m long.
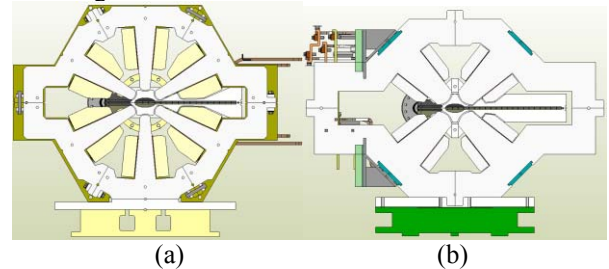
Figure 2: Cross-sectional views of a B-chamber combined with a Q-magnet (a), and a S-magnet (b).

TREATMENTS

Some research reveals that ozone is effective to remove carbon on the surface and in the sputter-profiled passivation layer of aluminium alloys [1-3]. Treatments of three kinds, proposed to machining and to clean materials of the aluminium-alloy vacuum chambers for the TPS project, are listed below and evaluated by the techniques of thermal outgassing and PSD.

(A) Oil machining
     -chemical cleaning with strong alkaline etching [4].
(B) Ethanol machining
     - cleaning with ozonized water with a flow rate 5 L/h and a concentration 6.7~6.9 ppm at 24 ^{0}C for 30 min.
     - drying with pure nitrogen gas (99.9999 %).
(C) Ethanol machining only

CYCLOTRON R.F. STRUCTURE'S LEAKS, CAUSES AND REPAIR

Deba Prasad Hajra, Debabrata Adak, Bidhan Chandra Mondal, Jayanta Chaudhuri,

Rakesh Kumar Bhandari,

VECC, DAE, 1/AF Bidhan Nagar, Kolkata-700064, India

SYSTEM DESCRIPTION

The room-temperature cyclotron (K-130) at VECC, Kolkata is delivering beam since June 16, 1977.The R.F. power of the cyclotron 'D' is passed through a cantilever type D-stem structure of 2750 mm long & 1350 wide. This structure has been fabricated by thin OFE grade copper sheet inside which has been reinforced by a structure made of light SS sections. The skin of the structure has been fabricated in a corrugated fashion to increase both surface areas for R.F skin current and mechanical strength (section modulus). A pair of moving panel has been assembled on both top and bottom side of the D-stem for frequency tuning of R. F. The whole system is functioning inside a big resonator tank of 3.1mx 2.4m x 2.1m which is under high vacuum of 10^{-7} m bar. LCW at pressure of 12.5kg/cm^2 flowing through 10mm OD and 1.1mm thick OFE copper tubes to remove the heat generated by the R.F. skin current. These tubes are brazed on the inner surface of corrugated copper sheets.

FABRICATION

Brazing in a vacuum furnace could provide uniform heating, no thermal distortion, uniform filler distribution, no oxidation and clean joint but it was not done because arge size facility was not available at that time. 10mm O.D copper tube to tube was joined by lap joint. Tube to copper strip of 25 mm wide and 1.6 mm thick of different lengths were brazed first. Then 25 mm strips were brazed with 2mm thick sheet of corrugated copper panel. This type of design has created some air gap (between strip and sheet) due to thermal distortion and this prevents efficient heat-transfer. Also it created a small under cut on the thin wall of the cooling tubes along the brazing line.

OBSERVATION OF LEAKS

Round the clock cyclotron operation for last 30 years, brazing joints of the cooling tubes and undercut of tube wall develops water leaks inside the resonator tank working under high vacuum. It is observe that the leaks are more near the 'D' region possibly due to the phenomenon like ion induced desorption, image current, nuclear scattering and high energy scattered beams. It also observe occurrence of leaks increases whenever the RF panels are kept open in atmosphere for considerable period of time. It is also noticed that after repair and during hydraulic testing at 15kg/cm^2 pressure numbers of new leak open-up. This indicates the existence of many other corroded weak points inside the tubes. As the

dhajra@veccal.ernet.in

cooling tubes are brazed inner surface of the structure and it is not easily accessible without dismantling. Repair of leak requires shut down of the cyclotron and takes a considerable loss of beam time.

CAUSES OF LEAKS

The water leaks appear from the under-cut of thin walled of tubes. Because silver brazed alloys has very good compatibility with copper and forms continuous solid solution with copper at lower temperature of eutectic composition. Surface erosion occurred due to large mutual solubility resulting an undercut on the thin walled tubes. Brazing joints leaks of tube-to-tube, tube-to-sheet, SS couplings, bimetallic joint appear mainly due to electro chemical corrosion created over a time span of 30 years. The electrolyte for corrosion forms due to the following reasons.

1. Corrosion caused by spurious free chlorine ions from the irradiated halogen containing products like cable insulation, tapes.

2. Residue of brazing flux, trapped cleaning agents like tricholorethyline, carbon tetra chloride etc forms hydrochloric acid and highly toxic gases in contact with the brazing flame.

3. More than 60% relative humidity in vault atmosphere (when panels & R.T. is in air) is one of the causes of corrosion. The relative humidity is considerably higher close to the cooling tubes outer surface than the remaining vault areas this accelerates corrosion.

4. Presence of radioactivity enhances corrosion due to formation of free radical in the air, ozen, nitrogen oxide and subsequently form acids with surface moisture films.

5. Nitrogen oxide can also be formed by spurious discharge of high electric field.

6. Corrosion occurs in bimetal joints of aluminum &copper tubes in trimmer capacitator cooling tubes due to different electro-chemical potentials.

7. Corrosion also enhance by the speed of the cooling water and its residual impurities

8. Porosity will develop in the joint filler due to presence of low vapor pressure (less than 10^{-3} m bar) elements like zinc, cadmium, phosphorus in the filler alloy during brazing at high temperature. Micro-pores may appear under prolong high vacuum (10^{-7} m bar) and high

07 Accelerator Technology
T14 - Vacuum Technology

THE VACUUM SYSTEM FOR THE SSRF STORAGE RING

D.K.Jiang, Y.L.Chen, L.P.Chen, W.Li, Y.Lu, Y.Y.Liu
Shanghai Institute of Applied Physics, Chinese Academy of Sciences,
P.O.Box 800-204, Shanghai 201800, P. R. China

Abstract

SSRF is the first third generation light source in China. The storage ring vacuum system adopts SS316LN chambers with antechamber structure and discrete absorbers. Several chamber models using SS316L material were developed to confirm the fabrication technology. There are three types of absorber in the ring. TSP and SIP+NEG combined pumps are used for the system. The vacuum chambers with accessory components will be pre-baked before installation. RF shielded bellows with single finger structure have been designed and tested.

INTRODUCTION

The Shanghai Synchrotron Radiation Facility (SSRF) is the first third generation light source in China. The main part of the facility is a 3.5GeV, 300mA storage ring with a circumference of 432m. There are about 60 beam lines can be set to the ring and 7 beam lines are constructed at the first stage [1].

SYSTEM DESIGN

The main performance requirements for the storage ring vacuum system are as follows: (1) To keep the average pressure $<1\times10^{-7}$Pa for more than 10Hrs beam lifetime. (2) To design a reliable chamber with low impedance. (3) To extract the required SR beams and to absorb the rest part of the SR safely. (4) To enhance the mechanical stability for the chambers. The general design for the vacuum system was done under the detail consideration for all the above items. All the SR is stopped on discrete photon absorbers except to the beam lines. The photons will not irradiate the chamber inside wall directly. Large pumping speed pumps are located near the absorbers. There are 6 short section chambers in one cell. They are connected to 3 longer sections through 3 pairs of rectangular flanges with knife edge sealing structure. The 3 long chamber sections are connected by 2 DN150 RF shielded bellows. The location and structure of the absorbers are optimized to make the chamber narrow. The centre of the flange is designed offset to the centre of the beam channel in order to reduce the whole size of the bellows and valves. A standard cell vacuum chamber arrangement is shown in Fig.1.

Figure 1: Layout of a standard cell

CHAMBER

The vacuum system for the storage ring adopts stainless steel chambers with antechamber structure. Stainless steel, aluminum and copper are all suitable materials for the medium energy storage ring. Stainless steel chambers are cheaper compared with the one made of aluminum alloys or copper. Stainless steel 316LN is used for the cell chambers in SSRF due to its higher yield strength and very low magnetic permeability after forming and welding. The beam position monitor blocks are used to connect short chamber sections by welding. The chamber pieces are formed by a deep-drawing die and cut by laser or wire cutting methods along the contour. TIG welding is used for the chamber. A section chamber is shown in Fig.2. There is no cooling channel design for the straight section of the chamber in quadruple and sextupole magnets region because of the space limited. The OFHC shielding bar inside of the chamber in dipole region, the absorbers, and the RF shielded bellows are designed with cooling water channel. All the chambers must withstand the power of synchrotron radiation emitted from dipole magnets up to 5mA without interlock operation.

To keep the BPM position stable is a key point for the support design. A stiff support is set to the BPM block as a fixed point for each chamber while other parts are supported on flexible SS plates. In order to avoid the chamber vibration generated by cooling water, smooth water channel and suitable valves are adopted and the flow velocity is limited below 2m/s in design.
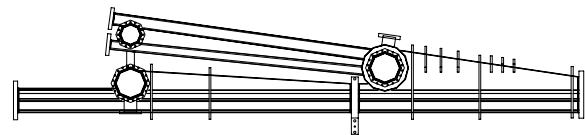
Figure 2: The section chamber structure

PUMPING SYSTEM

The required pressure in the storage ring is 1×10^{-7}Pa or less to get a beam lifetime of 10hrs or more. Assuming that the photon stimulated desorption coefficient $\eta=2\sim3\times10^{-6}$mol./ph. after 100Ah operation, the estimated total gas load is $Q=1.3\times10^{-2}$Pa.l/s. The required nominal pumping speed is about $2\sim3\times10^{5}$l/s in the ring. A sputter ion pump combined with NEG can increase the pumping speed at low pressure and the ratio of pumping speed to pump volume. Titanium sublimation pumps are used near absorbers for large gas load. The model for the combined pump has been tested and shown in Fig.3.Larger pumping speed is also necessary for the place where β_y is larger.

NUMERICAL STUDY OF FIELD ERRORS DUE TO MECHANICAL TOLERANCES IN SUPERCONDUCTING MINIUNDULATORS

C.Z. Diao, H.O. Moser, Singapore Synchrotron Light Source, National University of Singapore, 5 Research Link, Singapore 117603

Abstract

Using a wire model, analytical formulae are derived to describe the spatial distribution of the magnetic field of a superconducting miniundulator (supramini) as determined by the errors in positioning the wires. Semi-analytical numerical simulations are performed to estimate the tolerances of various errors required for a satisfactory function of the supramini, including the effects of systematic errors such as pitch, yaw and roll of a whole supramini coil, and random errors of the wire positions. These results can be used to help assess the minimal required mechanical tolerances.

INTRODUCTION

Superconducting miniundulators (supraminis) are believed to be a key component of 4th generation sources including FELs and Energy Recovery Linacs (ERL). Furthermore, they are expected to play an important role in the upgrading of 3rd generation sources [1-4].

In this paper, we evaluate the influence of the different potential mechanical errors on the quality of the magnetic field and specify acceptable tolerances. Based on a wire model introduced earlier [5], we derive analytical formulae to calculate the magnetic field including the mechanical errors. The effects of systematic errors are treated analytically, random errors are simulated numerically. The effects of these errors on the quality of the field are then graphically analyzed.

MODEL AND PROCEDURE

According to [5], the magnetic field that is produced by an array of wire pairs (wp) and that includes the effect of compensation coils can be written as

$$B_y(x,y,z) = B_y^u(x,y,z) + B_y^l(x,y,z) + B_y^c(x,y,z) \quad (1)$$

where B_y^u is the magnetic field produced by the upper part of coil, B_y^l is the magnetic field produced by the lower part of coil, and B_y^c is the magnetic field produced by the compensation coils. Explicit expressions for the first field contribution will be derived in the following while the other two will be taken from [5].

In our analysis of the mechanical errors of the supramini, we include systematic as well as random errors. To define coordinates, we call (x,y,z) the space frame where the (x,z)-plane is the midplane of the supramini without positional errors and z the direction of the electron beam. Coordinates (X,Y,Z) represent the body frame of the upper coil in which the (X,Z)-plane contains the wire axis and the current flow, X runs either along the axis of the central wire in the case of an odd

number of wire pairs or along the equivalent straight line at half-distance between the two central wires in the case of an even number of wire pairs, Y is normal to the (X, Z)-plane through the center of the wire arrangement which is the origin of the coordinate frame as well.

Starting from the ideal position of the upper and lower coils, we construct the displaced error-causing position by translating and rotating the upper coil only while keeping the lower one in its ideal position. This is no restriction of the general validity. Translations are carried out along the space axes (x,y,z) and rotations according to the Euler angles as defined in fig. 1. We define, as shown in fig. 1,

-   the pitch error when the upper coil is rotated by an angle θ about the x' axis,
-   the yaw error when the upper coil is rotated by an angle α about the y_1 axis, and
-   the roll error when the upper coil is rotated by an angle φ about the z_2 axis.

All rotations are in a counter-clockwise sense, i.e., right-handed in the mathematically positive sense. The transition from the space frame (x,y,z) to the body frame of the upper coil (X,Y,Z) is achieved by an initial translation along y by the distance from a wire centre to the midplane, three subsequent translations along x, y, z, and three rotations as defined in fig.1 where we adopted a convention as given in [6].
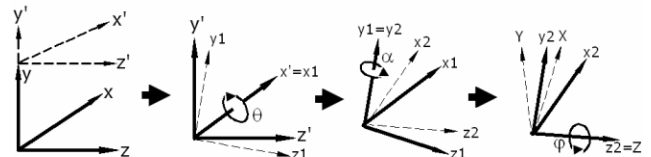
Figure 1: Coordinate transformations leading from the space frame to the body frame of the upper coil with positional errors. Translations of the (x',y',z') frame are not shown.

All error rotation angles θ, α, φ and translational errors $\bar{x}, \bar{y}, \bar{z}$ are supposed to be <<1 and <<g which is the gap, respectively. The magnetic field components produced by the upper coil in the coordinates X, Y and Z are written as $B_X^u(X,Y,Z)$, $B_Y^u(X,Y,Z)$ and $B_Z^u(X,Y,Z)$.

Assuming $B_X^u(X,Y,Z) = 0$, we obtain the magnetic field of the upper coil in the coordinates x, y, and z as

$$B_y^u(x,y,z) = B_Y^u(X,Y,Z)(\cos\varphi\cos\theta - \sin\theta\sin\alpha\sin\varphi) - B_Z^u(X,Y,Z)\cos\alpha\sin\theta$$

with

$$\begin{bmatrix} X \\ Y \\ Z \end{bmatrix} = \begin{bmatrix} \cos\varphi & \sin\varphi & 0 \\ -\sin\varphi & \cos\varphi & 0 \\ 0 & 0 & 1 \end{bmatrix} \begin{bmatrix} \cos\alpha & 0 & -\sin\alpha \\ 0 & 1 & 0 \\ \sin\alpha & 0 & \cos\alpha \end{bmatrix} \begin{bmatrix} 1 & 0 & 0 \\ 0 & \cos\theta & \sin\theta \\ 0 & -\sin\theta & \cos\theta \end{bmatrix} \begin{bmatrix} x-\bar{x} \\ y-\bar{G}-\bar{y} \\ z-\bar{z} \end{bmatrix}$$

AN APPLE-II TYPE HELICAL UNDULATOR FOR SSRF

Q.G. Zhou, M. Zhang, Y. Li, Z.M. Qian, J.D. Zhang
Shanghai Institute of Applied Physics, Shanghai 201800, P.R. China

Abstract

Shanghai Synchrotron Radiation Facility (SSRF) is an intermediate energy (3.5GeV) light source under construction. Specially designed insertion devices will be required to realize the high brightness photon beams made possible by the low emittance of electron beam. The first insertion device being designed is a 4.2m long, 10 cm period, APPLE-II type helical undulator, EPU10.0. This device will use a pure permanent magnetic configuration corresponding to four standard Halbach-type magnet rows which consist of two pairs of planar permanent magnet rows above and below the electron orbit plane. The C-frame support structure is selected. The complete design for EPU10.0, including the magnetic structure, the backing beams, the support structure and the drive systems, is described.

INTRODUCTION

As the third generation of dedicated synchrotron light source, Shanghai Synchrotron Radiation Facility (SSRF) with 3.5GeV energy is scheduled for completion in 2009 [1]. Based on input from the user community, we are designing a set of insertion devices (IDs) and associated beam lines.

Table 1: Main Parameters of the EPU10.0

Magnetic structure	APPLE-II
Period length	100mm
Period number	42
Available gap range	30~85mm
Available phase shift range	-55~+55mm
Speed of gap motion	4mm/s
Speed of phase shift	1mm/s
Peak field for horizontal polarization	0.6 T
Peak field for vertical polarization	0.3 T
Peak field for circular polarization	0.3 T

An elliptically polarizing undulator for the SSRF has been designed and will be under construction recently. The EPU10.0 can generate a linearly (horizontal or vertical plane), an elliptically or a circularly polarized radiation by providing the phase position shifts to the magnet rows of the undulator. The EPU10.0 will produce very bright photon beams in the spectral range of 70eV to 2000eV. The magnetic design is a moveable quadrant pure permanent magnet structure featuring adjustable magnets to correct phase errors and on-axis field integrals. The support structure, backing beam, and positioning system are all designed to function comfortably with a maximum magnetic load of 2,100kg. Main parameters of the EPU10.0 are shown in Table 1.

MAGNETIC STRUCTURE

The four magnetic quadrants [2] [3] [4] are attached to separate backing beams which allow a and d to translate axially relative to b and c, which are fixed. The structure of the four magnetic quadrants is shown in Figure 1. Each quadrant has a magnetic structure length of 4.3m, including 42 full magnetic periods, the ends for achieving a gap-independent steering and displacement free entrance and exit, and magnetic trim sections for correction of integrated multipoles.
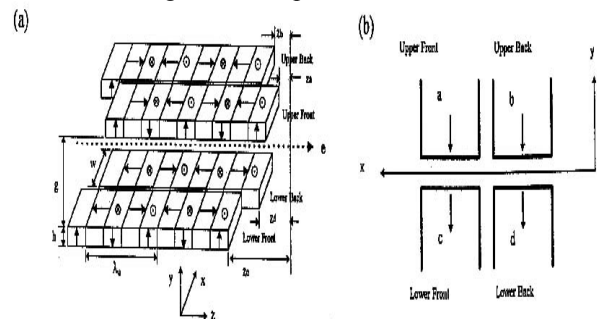
Figure 1: Four quadrants schematic of EPU10.0

Within each quadrant, the basic assembly unit is a 3, 5, or 7 blocks module. Each block within the module is bonded to an aluminium keeper which is mounted to the dove tail connector. Figure 2 shows the scheme of basic module with 5 blocks. Each magnet array consists of 173 blocks of NdFeB including six end blocks. The thickness of the end blocks are designed so as not only to make the first and the second integrals of fields (horizontal and vertical) along the axis of the undulator be zero but also to give no offset of oscillation axis from the axis of the undulator. The same dimensions of the width and the height (35mm × 35mm) of all blocks will give more freedom in the magnet sorting procedure. The magnet holder can be adjusted within ±0.25mm in horizontal and vertical positions by using different thickness shims for the magnetic field tuning. The clearance of 3.7mm between two magnet arrays provides the space for the magnet holder adjustment in horizontal direction.

The magnetic fields were calculated using the analysis formulae for each magnet then linearly superposed for all the magnets. Figure 3 and Figure 4 show the magnet fields on the axis of the undulator and the trajectories of the central electron in the horizontal linear polarization mode and the circular polarization mode with the permanent field of the magnet being 1.2 Tesla and the gap 32mm.

ENERGY STABILIZATION OF 2.5 GeV LINAC USING DEQING

S. H. Kim, S. S. Park, Y. J. Han, J. Y. Huang, S. H. Nam, S. C. Kim

Pohang Accelerator Laboratory, POSTECH, San 31 Hyoja-dong, Pohang, Kyeongbuk, 790-784, Korea

Abstract

The 2.5 GeV electron linac of Pohang Accelerator Laboratory (PAL) employs 80 MW klystrons with matching 200 MW modulators as RF sources. Beam voltage stability of the klystron is directly related to a PFN (pulse forming network) charging voltage of the modulator. Therefore, a good regulation of a PFN charging voltage is essential in the modulator. The regulation of the klystron pulse voltage amplitude is made by controlling the PFN charging voltage. In a conventional resonant charging pulse modulator, the regulation is usually achieved by using a deQing circuit. The required beam voltage regulation of less than +/- 0.5 %, without deQing circuit, has been achieved by using a SCR phase controller with a voltage regulator. For further improvement of the beam voltage stability for the PAL XFEL (x-ray free electron laser) linac, PAL is studying a deQing circuit aiming at the stabilization of less than 0.02%. A prototype deQing controller has been developed with a compensation function which can reduce a charge voltage fluctuation by about several times. The design concept and performance of the deQing circuit will be discussed.

INTRODUCTION

Without a deQing circuit, the beam voltage regulation of about 0.5% has been achieved by using a SCR phase controller with a DC feedback circuit. However, we have to study a deQing circuit aiming at the stabilization of about 0.02% due to getting further improvement of the beam voltage stability for the PAL XFEL linac.

A deQing system is a conventional method of regulating the PFN charging voltage [1]. The klystron beam voltage stability depends on the PFN charging voltage of the modulator. To keep a good regulation of PFN charging voltage in the modulator a deQing circuit is employed, and it can accomplish the required regulation. Finally the deQing unit controls the stability of PFN voltage. When the PFN charging voltage reaches desired level, the deQing SCR is triggered to remove energy remained in a charging inductor. The deQing unit consists of a deQing controller and deQing SCR switch assembly. The deQing should satisfy the following two most important conditions: (1) the peak voltage across primary of charging inductor during a period of deQing should be smaller than the PFN charging voltage. (2) The energy in the charging inductor should be removed by the deQing action before starting next charging cycle.

The prototype deQing controller has been tested in a test linac modulator that has a 150 MW peak power, and a HV divider is installed near the PFN inside of the modulator to use it for PFN charged voltage measurement. A signal coming from the divider will be compared with a DC reference voltage in the deQing controller, and according to the compared result, when the desired level of PFN voltage exceeds the DC reference voltage the comparator in the deQing controller generates an output pulse to trigger the SCR. The prototype deQing controller has a compensation function which can reduce E_{PEN} jitter and a charge voltage fluctuation of dV/dt.

POWER CONTROL SECTION

There are some voltage fluctuations in the input AC line. Since the AC line stability is not good and its amplitude is unstable, that makes fluctuated dV/dt. The dc power supply of the modulator is a conventional, three-phase full-wave bridge dc supply with choke input filter. In stead of using an induction voltage regulator (IVR), a phase-control system with six SCRs is used because the phase controller is more effective than IVR in terms of cost, space, and controllability. A SCR AC-AC voltage regulator controls primary 3-phase 480V AC power. The voltage regulator receives feedback signals from the primary AC voltage and the high voltage DC (HVDC) detector. The closed loop control of the AC-AC voltage regulator ensures stable HVDC output. Therefore, the phase control charging scheme has been used for control of full three phase primary power. Using a SCR phase controller with active feedbacks in a high voltage dc power supply can help us to get a stabilization of PFN charging voltage. We stabilized a high voltage charging power supply within 1% by a phase controlled SCR voltage regulator with AC feedback. We get about 0.5% variation of the PFN charging voltage by employing dc feedback circuit in the phase controller.

DEQING CRICUIT DESCRIPTION

The deQing SCR switch assembly is shown in Fig. 1. The amplitude of the PFN voltage is controlled by the deQing unit connected in parallel to a charging choke. The charging choke has a secondary winding to match the relatively low voltage components of the deQing unit to a high voltage charging circuit in the primary winding. When the desired PFN voltage exceeds the dc reference voltage coming from the prototype deQing controller, the comparator in the deQing controller generates an output pulse to trigger the SCR. The energy left in the charging chock at that time is dissipated in the secondary load resistors. The deQing circuit is normally adjusted to dissipate a few percent (about 3 ~ 5%) of the charge in each cycle. It can regulate the PFN voltage to 0.1% or more low levels.

DEVELOPMENT OF A 200KEV LINEAR INDUCTION ACCELERATOR

K.V.Nagesh, Archana Sharma, S.Acharya, Rehim N.Rajan, D.K.Sharma, P.C.Saroj, S.Mitra, D.P.P.Kumar, Senthil K, A.Roy, Ritu Agrawal, S.Raul, K.C.Mittal and D.P. Chakravarthy, Accelerator and Pulse Power Division, Bhabha Atomic Research Centre, Mumbai-400085, India.

Abstract

Electron Linear Induction Accelerator (LIA) are for applications in high power microwaves (HPM), high gradient accelerators, flash X-rays radiography (FXR), flue gas clean-up, detoxification of chemicals, cross-linking of polymers, sterilization of food and medical waste/devices etc. The LIA-200 is being developed at APPD,BARC consists of mainly (i) solid state pulse modulator based on semiconductor devices, (ii) pulse compression and voltage amplifications stages, steps up to 200kV, 5μs and compresses these pulses to 75kV,10kA,50ns (FWHM) in five stage and (iii) three stage induction cavities in ADDER mode for relativistic electron beam generation, with matched load of 5Ω. Metglas cores have been used in transformers, switches and induction cavities. Deminearlised water capacitors and water pulse forming line have been used for low impedance energy storage and compactness. The complete system has been assembled and ready for commissioning. LIA-200 will be operated from a PLC based control system which is under testing.

INTRODUCTION

The principle of magnetic induction has often been applied to the acceleration of high-current beams in a variety of induction accelerators. The induction linac (IL) consists of a simple non resonant structure where the drive voltage is applied to an axially symmetric gap that encloses a toroidal ferromagnetic material. The change in flux in the magnetic core induces an axial electric field that provides particle acceleration. This simple non resonant (low-Q) structure acts as a single-turn transformer that can accelerate beams of hundreds of amperes to tens of kilo amperes, limited only by the drive impedance. The IL is typically a low-gradient structure that can provide acceleration fields of varying shapes and time durations from tens of nanoseconds to seve ral microseconds. The acceleration voltage available is simply given by the expression $V = A*(dB/dt)$ Hence, for a given cross sectional area A of material, the beam pulse duration influences the energy gain. Following is th e details of LIA-200 configuration.

CIRCUIT DESCRIPTION

Fig.1 shows the photograph of the Linear Induction Accelerator and Fig.2 shows the simulated electrical equivalent circuit diagram in Orcad. Capacitor C1 is charged to 2.5kV with a constant current power supply. This is a Phase Shift Pulse Width Modulated (PS-PWM) power supply operating at 30 kHz. This topology has the capability to eliminate turn on losses and minimizes turn

off losses of IGBTs present in the inverter. A Thyristor (X1) is placed to initiate the command resonance charging. T1 is a pulse transformer of 2.5kV / 20kV. L1 is the equivalent leakage inductance of the transformer T1. Diode D2 is placed to block the reverse pulses from the forward stages. Capacitor C2 gets charged to 20kV after the gate pulse to the Thyristor X1 is given. S1 is a magnetic switch to compress the pulse duration from 20μs to 5μs. Pulse transformer T2 steps up the voltage pulse of 20kV to 200kV. C3 and C4 are water capacitors of value 10nF. Magnetic switch S2 compresses the pulse from 5μs to 1μs and S3 from 1μs to 250ns. Deminaralized water Pulse Forming Line (PFL), is required to get a flat topped pulse of 50ns duration at the output. Magnetic switch S4 holds the output pulse from PFL for 250ns. It gives output pulse of 50ns with sharp rise time and is applied to an induction adder cavity. Each induction cell acts as a single turn 1:1 pulse transformer in co-axial configuration.

Pulse Transformers

Amorphous core toroids based pulse transformers are designed and developed with final parameters are tabulated in table-1. Each core has outer diameter, inner diameter and hight as 240mm, 160mm and 25mm respectively. Each transformer is kept in degassed transformer oil chamber for cooling and insulation. Teflon covered wires are used for winding with kepton tape and mylar as insulating layers. Perspex flanges were used to hold the full assembly.
Chokes are designed for DC resetting of cores at 20kV and 200kV side separately.

Table 1 : Parameters of pulse transformer 1 and 2

Main Parameters	Pulse Transformer-1	Pulse Transformer-2
Turns Np/Ns	22/176, parallel 6-cores (6P)	35 x 8P/50-on all 8-cores
Voltage Vp/Vs	2.5kV/20kV, 20μs	20kV/200kV,5μs
Current Ip/Is	15kA/1.8kA	8kA/800A
Leakage L	0.55 μH	3.5μH

OPERATION OF LIA

Magnetic pulse compression is the key in achieving the output of 200kV, 50ns pulse. The operation of Induction Linac is based on series magnetic pulse compressor as reported by D.Birx [1]. Three induction cells in parallel are driven by this output pulse from PFL. It is estimated that final output pulse to cavities will be of >75kV, 5kA, 100ns FWHM [2].

THEORETICAL ANALYSIS OF THE RECOVERY TIMES IN LOW PRESSURE SPARKGAPS - POSITIVE ION DIFFUSION METHOD

K.V.Nagesh, Accelerator and Pulse Power Division, Bhabha Atomic Research Centre, Trombay, Mumbai, 400085, India.

Abstract

Presently there are no methods ideally suitable for the calculation of recovery times of low pressure sparkgaps. However an attempt has been made to calculate and analyze the recovery times of low pressure sparkgaps based on diffusion of positive ions here. The recovery times are calculated based on the reported data of plasma diffusion rates. The spherical ambipolar and free diffusion recovery times are generally in good agreement with the experimental recovery times at higher pressures. The cylindrical ambipolar and free diffusion recovery times are an order of magnitude lower than spherical diffusion recovery times. The recovery times are not in good agreement for positive polarity experimental recovery times. The theoretical calculation of recovery times, comparison of calculated & experimental recovery times and discussions are presented in this paper.

INTRODUCTION

The electrical breakdown and pre-breakdown characteristics of gases at atmospheric pressure and above, and at low pressures are widely investigated and there is reasonable agreement on the mechanism of growth of the current in the breakdown. But the recovery processes after the sparkgap breakdown are not studied extensively at low pressures. These are due to short duration {~100ns FWHM} of the present experimental voltage pulses leading to the lower plasma densities. The cross-sectional view of experimental setup and photograph of the system used for these studies are shown in Fig.1 and Fig.2 respectively. The recovery experiments are conducted at 10mm gap for argon gas, 10 and 2.5mm gaps for hydrogen gas and 2.5mm gap for deuterium gas with gap pressure varying from 1.1Pa to 34Pa at room temperature 295K [1, 2].
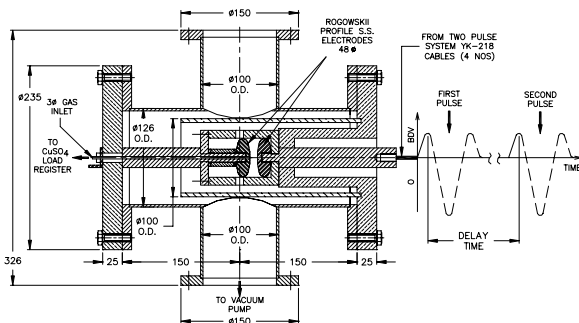
Figure 1. Cross-sectional view of experimental setup of Low Pressure Sparkgap

Figure 2. Photograph of the experimental setup of Low Pressure Sparkgap

The ratio of λ_e/d varies approximately from 40 for gap pressure of 1.5Pa to 1 at 23Pa and lower at higher pressures. Whenever the ratio λ_e/d is very much higher than 1, it indicates that the breakdown mechanism is initiated, developed and sustained by electrode mechanism. Here the recovery process mainly depends upon the anode temperature decay. Whenever the ratio λ_e/d is closer to 1 and lower, it indicates that the breakdown mechanism is initiated by electrode mechanism and developed and sustained by gas mechanism. Here the recovery process mainly depends upon the positive ion diffusion. Whenever the ratio λ_e/d is between these two extremes, the breakdown is initiated by electrode mechanism and sustained by gas discharge. Here the recovery process is a combination of anode temperature decay and positive ion diffusion with anode temperature decay being predominate at higher ratios and vice-versa. The recovery of the gap mainly depends upon diffusion of positive ions under the conditions of low gap current {<2.5kA}. The positive ion diffusion may be either spherical or cylindrical depending upon the discharge initiation. If the discharge is from a point then the diffusion is spherical. If it is diffuse discharge over a large surface area, then the diffusion is cylindrical. The spherical diffusion takes place when the discharge is due to pulses having risetimes in the microsecond range and above. The cylindrical diffusion is possible with applied pulses having rise times of 10 to 100ns. The positive ion diffusion may be classified as ambipolar or free diffusion, depending upon the Debye length of the plasma in the discharge. If the Debye length is less than characteristic diffusion length, then the diffusion is ambipolar and in other cases, it is free diffusion. Generally the diffusion is

THEORETICAL ANALYSIS OF THE RECOVERY TIMES IN LOW PRESSURE SPARKGAPS – ANODE TEMPERATURE DECAY METHOD

K.V.Nagesh, Accelerator and Pulse Power Division,
Bhabha Atomic Research Centre, Trombay, Mumbai, 400085, India

Abstract

The recovery characteristics of the low-pressure sparkgaps in the time interval of 300μs to 50ms, with stainless steel electrodes, in the pressure range of 1 to 40Pa, for gap spacings of 2.5mm & 10mm, have been determined experimentally for hydrogen, argon and deuterium gases. An attempt has been made to analyze the recovery times of low pressure sparkgaps by anode temperature rise and decay method based on liquid & solid vapour phases here. The liquid & solid phase recovery times, theoretical calculation of recovery times, comparison of calculated & experimental recovery times and discussions are presented in this paper.

INTRODUCTION

The recovery processes after the sparkgap breakdown are not studied extensively at low pressures with short duration pulses {~100ns FWHM} which do not allow sufficient time for the metal surface to melt. The cross-sectional view and photograph of the experimental setup are shown in Fig.1 and Fig.2 [1, 2]. The typical effects of electrodes after experiments, is shown in Fig.3.
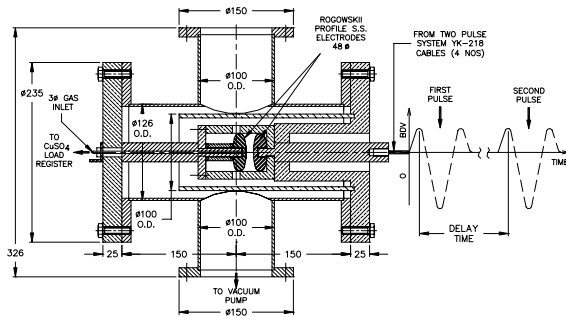
Figure 1. Cross-sectional view of experimental setup of Low Pressure Sparkgap.

Presently there are only three papers on calculation of recovery times of sparkgaps [3, 4, 5]. The experimental arc discharge times of Frind et. al. [3] are 300μs and 4500μs and currents in the range of 250A to 12kA. Since the discharges are in vacuum (1.3 x 10^{-4}Pa - 1.3x10^{-5} Pa) having longer pulse durations with higher currents, the anode spot has been observed in this case. The ionization potential (7.5V) is assumed to be equal to the anode drop with full recovery is assumed to be at 10^{-2} Torr with anode spot temperature decaying to 1200^{0}C for copper electrodes. However there is an order

of magnitude difference between theoretical and experimental recovery times. Rich & Farrall [4] has assumed that recovery pressure is equal to twice the gap spacings as mean free path in the recovery of vacuum circuit breakers. There is good agreement in some cases and large difference in others. Tsuruta & Ebara [5] has calculated the recovery of air gaps based on gas temperature decay with the assumption as the gas temperature reduces to 300K at full recovery from peak discharge temperatures of 2000-5000K. There is good agreement at gap spacing of 3mm but the calculated recovery time is lower for 1mm and higher for 7mm than the experimental value.

Figure 2. Photograph of the experimental setup of Low Pressure Sparkgap

Figure 3. Photograph of the typical effects of electrodes after experiments.

The recovery experiments of the present studies [1, 2] have been conducted for gases of hydrogen, deuterium and argon gases. The energy per pulse varies from 0.4 to 8J, which gives the peak power densities are of the order of 2×10^{11}W/m^2 which is lower than the critical power densities for melt zone. Presently there are no methods ideally suitable for calculation of recovery times of low pressure sparkgaps, however an attempt has been made to analyze the recovery times here by anode temperature rise and decay method based on Frind's work [3].

Recovery Time Calculation by Anode Temperature Rise and Decay Method

The rise in anode temperature for can be calculated using the following equation of Frind et. al. [3]

$$T = \frac{0.239.S. \Delta t}{\rho.C \quad \{\alpha. \pi .t\}^{0.5}} \ e^{-\{x^2 /(4.\alpha.t)\}} + 273 \quad (1)$$

Where T = Temperature in K.

STABILITY ANALYSIS OF A KLYSTRON-MODULATOR FOR PAL XFEL

J. S. Oh, S. D. Jang, S. J. Kwon, Y. G. Son, J. H. Suh, C. W. Chung, I. S. Ko, and W. Namkung
PAL/POSTECH, Pohang 790-784, Korea

Abstract

The PAL (Pohang Accelerator Laboratory) is persuading to construct a SASE-XFEL facility (PAL XFEL). The stable electron beam is essential for the single-pass free electron laser facility. The beam stability requirement for XFEL linac is determined from XFEL physics analysis. We need to find correlation between the beam parameters and related sub-system parameters to define the stability criteria of each sub-system. The beam stability is governed by an accelerating RF field, of which fluctuation is mainly caused by the modulation of a klystron voltage pulse. Therefore, it is directly determined by the charging stability of a modulator. This paper shows the detail analysis of the stability dependency of a klystron-modulator on the related parameters.

INTRODUCTION

PAL XFEL is a 4th generation light source that is a coherent X-ray free electron laser by utilizing an existing 2.5-GeV linac [1]. In order to provide reasonably stable SASE output, the RF stability of 0.02% rms is required for both RF phase and amplitude [2]. This is a technologically challenging issue for PAL XFEL.

The beam stability is given by the fluctuation of both RF power and phase driven by a klystron voltage pulse that is directly determined by the PFN (pulse forming network) charging voltage of a modulator. Therefore, it is useful to define the stability by using a sensitivity of the system parameters such as klystron voltage, RF phase and RF power by its relative stabilities to the one of a charging voltage. This paper analyzes the sensitivities of RF parameters and beam energy related to the PAL XFEL, in which Toshiba E3712 klystron (S-band, peak power of 80 MW) is to be used as main klystrons driving a XFEL linac [3].

MODULATOR SENSITIVITY

From the Ohm's law for a modulator and a klystron, $V_O = V_K + Z_{PFN} \times I_K$ and the klystron beam current, $I_K = k\, V_K^{1.5}$ with given klystron perveance k, we can define the sensitivity of a klystron voltage by

$$s_V = \left(\frac{dV_K}{V_K}\right) \Big/ \left(\frac{dV_O}{V_O}\right) = \left(1 + \frac{Z_{PFN}}{Z_K}\right) \Big/ \left(1 + 1.5\frac{Z_{PFN}}{Z_K}\right) \qquad (1)$$

$$= \left(1 + \sqrt{\frac{V_K}{V_{K,nom}}}\right) \Big/ \left(1 + 1.5\sqrt{\frac{V_K}{V_{K,nom}}}\right)$$

where V_o is a PFN charging voltage, V_K is a klystron

voltage, $V_{K,nom}$ is a nominal klystron voltage where the impedance is designed to be matched, Z_{PFN} is PFN impedance, Z_k is klystron impedance. Figure 1 shows the equation (1) with measured data of E3712 klystron for PAL XFEL. At the klystron voltage where the impedance is matched, the sensitivity of a klystron voltage is 0.8 and it is slowly varying over wide range of beam voltage.
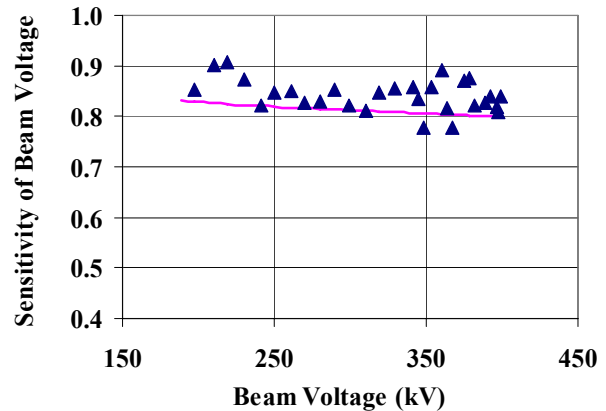
Figure 1: Sensitivity of klystron beam voltage (line: equation (1), triangle: measured data of E3712 klystron).

The sensitivity of a klystron beam current in the Figure 2 is given by

$$S_I = \left(\frac{dI_K}{I_K}\right)\left(\frac{dV_O}{V_O}\right) = \left(\frac{V_O}{I_K}\right)\left(\frac{dV_O}{dI_K}\right) = \left(1 + \frac{Z_{PFN}}{Z_K}\right)\left(2/3 + \frac{Z_{PFN}}{Z_K}\right)$$

$$= \left(1 + \sqrt{\frac{V_K}{V_{K,mon}}}\right)\Big/\left(2/3 + \sqrt{\frac{V_K}{V_{K,mon}}}\right) \qquad (2)$$
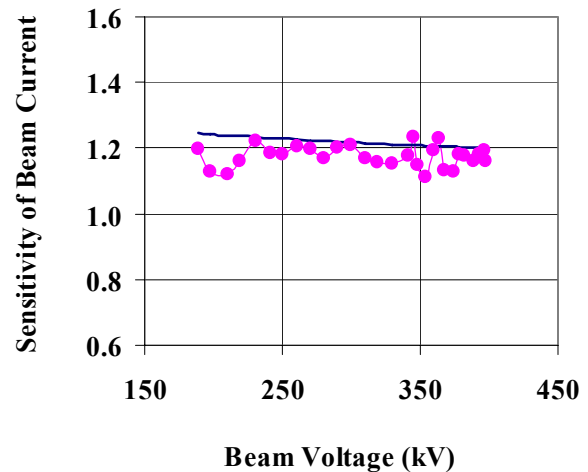
Figure 2: Sensitivity of klystron beam current (line: equation (2), circle: measured data of E3712 klystron).

CHARACTERIZATION OF AMORPHOUS MAGNETIC MATERIAL WITH MULTIPLE PULSE EXCITATION

Archana Sharma, S. Acharya and K.V.Nagesh,
Accelerator and Pulse Power Division,Bhabha Atomic Research Centre, Mumbai - 400085
Uday Kumar and G.R. Nagabhushana,
High Voltage Engineering Department, Indian Institute of Science, Bangalore -560 012

Abstract

The magnetic characteristics of an amorphous magnetic material have been studied by applying multiple square voltage pulses to an inductor containing the magnetic material. The pulser is a 20 kV, 200 ns, 20 Ω source which drives the core of dimension 160/240/25 mm. Effect of the number of turns and the magnitude of the exciting voltage pulse on the saturation behaviour of the material are presented.

INTRODUCTION

The use of amorphous magnetic material in magnetic switches and induction cells has received widespread attention in the development of pulse power systems of high average power and high repetition rate. The physical dimension of these devices depend on the flux swing offered by the material when driven from remanence to saturation. [1,2]. It is well-known that the magnetic properties of amorphous material are influenced by several factors such as annealing, heat treatment, surface coating, rate of flux change dB/dt, toroidal radius and applied input power etc [3,4]. We are using the material 30 KCP obtained from Russia in the development of a 200 keV, 5 kA, 100 pps Induction Linac. Therefore, we studied the magnetic properties of cores available in standard sizes in the intended frequency regime of operation before designing the switches and induction cells

To emphasize the need for our investigation, we cite here a few problems which one may encounter while using a magnetic core as a switch. For example, when the input capacitor of a magnetic switch is getting charged, the magnetic switch is supposed to have practically infinite impedance. However, there is always a leakage current due to finite impedance, which charges the output capacitor to some extent. A crude design based upon only the flux swing data ignores this fact and one may start worrying why the input capacitor did not get charged to the estimated value.

Similarly the transition from high impedance to low impedance is not an instantaneous affair as one would like to have. Complete saturation means that the relative permeability of the material approaches the value in air. Depending on the material, this approach, say from $\mu_r = 10$ to $\mu_r = 1$ can be slow or fast. The charging time of the output capacitor of a switch is generally calculated by using $\mu = 1$ in the saturated state of the switch. It is likely that the switch remains in the quasi-saturated state for quite sometime. Unless one knows this charging time, it will be difficult to design the switch for the next compression stage.

 Besides this, the magnetic data provided by the manufacturers are obtained by experimenting with continuous sinusoidal power sources. The characteristics of the magnetic material differ considerably from the above situation when they are used as core material in switches and induction cavities. It is imperative to know the pulse characteristics of the material while designing these devices.

Thus, more insight into these limitations are needed for almost perfect designs of pulse transformers, magnetic pulse compression chain and induction cavities in Linear Induction Accelerators.

EXPERIMENTAL SET-UP

The amorphous core material used in our experiment was supplied to us by   M/S Tukson Inc., Moscow, Russia, under the trade name 30KCP[5]. The chemical composition of the material is Fe(63.95%), Co(30%), Cr(3%), B(3%) and C(0.05%). The core is made from 25 μm thick tapes with SiO_2 insulation between layers and annealed in longitudinal field. The magnetic characteristics, provided by the manufacturer at 50 Hz, indicates that the core material has a flux swing around 3T (-B_{max} to -B_{max}) and coercive field of 12A/m. The toroidal test core is taken to be of the same size as that to be used in the actual system i.e. inner diameter 160 mm, outer diameter 240 mm and height 25 mm.. Before using the core, it was cleaned with alcohol and then two layers of 2 mil semi-cured kapton tape were wound on it to prevent incursion of outside dirt and any damage during handling the material.

STUDY OF INSULATION COORDINATION IN THE PRESENCE OF MULTIPLE DIELECTRIC MATERIALS

S. Mitra, D. Durga Praveen Kumar, Archana Sharma,
K. V. Nagesh and D.P. Chakravarty
Accelerators and Pulse Power Division, Bhabha Atomic Research Centre, Mumbai-400085.

Abstract

Use of various dielectric materials for insulation is inevitable in high voltage systems. Choosing a particular insulating material (solid, liquid, and gas) depends on various factors like the nature of the system, insulation level required, dielectric strength and thermal & mechanical stress handling capability of the material. Besides the surface break down strength of two material interfaces plays important role in the high voltage design considerations of the system. This paper critically analyses the field stress in high voltage points in presence of multiple dielectric media, in particular on the existing system of Kilo Ampere Linear Injector (KALI – 5000) system.

In this paper, local field enhancement phenomenon due to presence of different solid and liquid dielectrics is evaluated. Mathematical derivations of the percentage increment of field, at the critical point, due to presence of hybrid dielectric materials, are calculated for planar, spherical and cylindrical geometry of the high voltage elements. 2-d simulations of the same to support the mathematical calculations are done using MAXWELL SV software.

INTRODUCTION

This paper is all about local field enhancement of high voltage system due to lack of proper co-ordination of multiple dielectric materials instead of a single dielectric material. the work is inspired by some chronic corrosion leading to damage of a Perspex sheet inside MARX generator of KALI-5000 system. During investigation of the problem it has been found that use of multiple dielectric materials to avoid breakdown may lead to local field enhancement of any high voltage object of a high voltage system. The object can initiate to some other high voltage problems like corona discharge, higher leakage current, local heating etc. for the ease of analysis, some standard geometrical structures resembling to the practical situation is analyzed and simulated. Mathematical derivation is done to find out the range of enhancement of electric field stress at any particular point. The variation of per unit enhancement is also plotted against permittivity ratio of the multiple dielectric, their thickness and position. Simulation of similar structures is also done to support the mathematically derived results. Entire comparative and analytical study is reported in this paper.

THEORETICAL DERIVATIONS AND ANALYSIS

A mathematical approach to find out local field enhancement is attempted in this section. Let us assume that two points having high potential differences between them is separated by a dielectric of relative permitivity of ε_{r1}. Now, another dielectric material of higher relative permitivity value ε_{r2} is inserted in between the high voltage points without increasing the space between them. This is one of the very common practices for the high voltage engineers to avoid the bulk breakdown through the dielectric media. But, in this case, the metal boundary in contact with the lower relative permitivity value, experiences higher electric field stress than previous condition of single dielectric separation.

As far as bulk breakdown through the dielectric is concerned this method helps sometimes if the breakdown strength of the second dielectric is much higher than the previous one. The increased breakdown limit takes care of the added increment in field stress. But, if corona and all other high voltage unwanted phenomena are concerned then this method creates problem by local field enhancement. The above discussion is simplified considering two dielectric materials of different relative permitivity values. But the same inference is true for any number of dielectric materials used (two or more) two separate high voltage points. Below, it has been given, the mathematical explanation of the above mentioned conclusion in a generalized fashion.

Let us consider one object of voltage V is separated from the ground plane using a dielectric material of relative permitivity ε_r. The field experienced by the dielectric material at the metal dielectric juncture is E. Now, n number of dielectric materials of relative permitivity ε_{rn} and thickness t_n is inserted in between. Now the field at the same point of concern has changed to EM. For the ease of calculation let us replace the ground plane with the mirror reflection of the object and the dielectrics about the ground plane. The reflected object will be assigned a voltage of –V. Now, let us consider, the perpendicular distance between object and the ground plane is R and any point P is present on the line joining the object and its mirror image (same as the line perpendicular on the ground plane from the object) at a distance r. hence field strength at P can be defined as

ARTIFICIAL NEURAL NETWORK CALCULATES BACKWARD WAVE OSCILLATOR PARAMETERS RELIABLY FOR PULSED ACCELERATORS

Arti Gokhale, Archana Sharma and B. P. Dubey

Accelerator and Pulse Power Division Reactor Control Division, BARC, Mumbai-40085, INDIA

email:arti5_99@yahoo.com

Abstract

Backward wave oscillator (BWO) is a high power microwave-generating device, which is harmful for people and capable of damaging electronic equipments. It is mandatory to shield the critical control systems and instrumentation especially of strategic importance against such High Power Microwaves (HPM). To know the effects of HPM on human being and electronics, BWO is an efficient device, driven by pulsed accelerator electron beam of high power in Giga-Watt (GW) regime. These intense power electron beam pulses are obtained by an impulse generator followed by a pulse forming line and coupled to a field emission diode. Thereafter the electron beam interacts with electromagnetic modes of the wave-guide and produces microwaves in the frequency range of 1-20 GHz. Resultant frequency depends upon the wave-guide parameters, beam current, beam geometry etc. With analytical techniques, design optimization is cumbersome and slow. Every time the simulation program is run, it takes nearly 6 to 8 hours to generate a single result.Artificial Neural Networks (ANNs) have been used successfully in various applicatioins. A trained ANN generates its output in a fraction of a second. In this study ANN was used to calculate BWO frequency. The training of the ANN takes about half an hour. Once trained, the ANN takes plasma density, wave number and ripple amplitude as inputs and calculates the BWO frequency in a fraction of second. The frequencies calculated by ANN and that by simulation program differ at the most by about 2%. This shows that ANN is a reliable substitute for repeated run of simulation program.

INTRODUCTION

Accelerator driven Relativistic backward wave oscillators (BWO) are promising candidate as source of High Power Microwave (HPM) radiation. They were studied extensively in the last two decades and detailed overview of this research is presented in [1]. Microwave radiation in a relativistic BWO is produced by interaction between a pulsed accelerator relativistic electron beam and an electromagnetic field of a slow wave structure. Usually, the beam is generated by a field emission gun and guided by a strong homogeneous magnetic field. Metallic periodic structures are widely used as slow wave structure. In the construction of such device it is necessary to examine coupling coefficients of the electron beam with the fields of the slow wave structure (SWS), the solution of mode competition, and determination of the electrical strength of the SWS. The most complete analysis of theses problems is possible only for the dispersion description of the SWS.In the last two decades, significant research effort was directed in increasing output power and operating frequency. In most research and studies different wave-guide and beam parameters were assumed. In order to meet the requirement of maximum peak power, it is essential to explore accurate but fast technique of the dispersion relation's calculation for different wave-guide and beam parameters. This paper extends on our previous work and establishes a dispersion relation for a pulsed sheet beam driven backward wave oscillator in which a rectangular rippled wall wave-guide is used as SWS.

The generally believed superior cognitive capabilities of an Artificial Neutral Network (ANN) are being utilized these days for various event characterizations /classifications exercise in a wide range of fields. ANN had been used for estimating channel power distribution of a 220 MWe Pressurised Heavy Water Reactor [9]. An interesting and novel application of ANN is demonstrated in this work. It has been found that a properly trained ANN can be employed to reliably estimate the generating frequency of a BWO, depending upon the different wave-guide and pulsed accelerator beam parameters. A comparison of the results obtained by the ANN and the simulation program is presented at the end of this paper.

DISPERSION RELATION

Consider the interaction between pulsed accelerator sheet electron beam of density N_b in axially rippled infinitely long rectangular wave guide as considered in ref. [8]. The whole geometry of the slow wave structure (SWS) along with the sheet beam is immersed in a strong longitudinal magnetic field ideally having infinite magnitude.
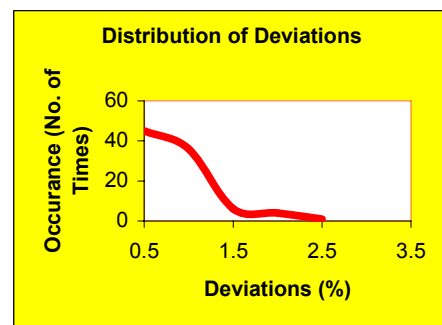
Figure 1: Deviations of the ANN calculated frequencies from the desired ones

OPERATIONAL ANALYSIS OF KLYSTRON-MODULATOR SYSTEM FOR PLS 2.5-GEV ELECTRON LINAC *

S. S. Park, S. H. Kim, S.C. Kim, J. Y. Huang,
Pohang Accelerator Laboratory/POSTECH, Pohang, Kyungbuk 790-784 S. Korea,
S. W. Park, K. T. Lee, Modulator & Klystron Technology Co., Ltd.
San 31, Hyoja-dong, Nam-ku, Pohang, Kyungbuk 790-784 S. KOREA

Abstract

The klystron-modulator(K&M) system of the Pohang Light Source (PLS) generates high power microwaves for the acceleration of 2.5 GeV electron beams. There are 12 modules of K&M system to accelerate electron beams up to 2.5 GeV nominal beam energy. One module of the K&M system consists of a 200 MW modulator and an 80 MW S-band (2856 MHZ) klystron tube. The total accumulated high-voltage run-time of the oldest unit among the 12 K&M systems has reached nearly 95,000 hours as of Dec. 2006. The overall system availability is well over 95%. In this paper, we review overall system performance of the high-power K&M system and the operational status of the klystrons and thyratron lifetimes, and overall system's availability will be analyzed for the period of 1994 to Dec. 2006.

INTRODUCTION

The Pohang Light Source is a third-generation synchrotron radiation facility composed of an injector Linac and a storage ring. The klystron-modulator(K&M) system of PLS Linac had been supplying high power microwaves for the acceleration of 2 GeV electron beams from 1994 to 2002. A 2.5 GeV full energy electron injection has been launched since on October 2002. The 2.5 GeV full energy electron beam from the linac is transported through a beam transfer line (BTL) to the storage ring. Total 12 units of high power klystron-modulator (K&M) systems are under continuous operation in the PAL linac. The peak powers of the modulator and the klystron are 200 MW and 80 MW, respectively. The klystron output frequency is 2856 MHz. Each klystron output is compressed with a SLED and supplied to four of three-meter long accelerating columns. The linac has been operated as a full energy injector for the PAL since December 1994. Annual operation hour of the K&M system is about 7,000 hours.

KLYSTRON AND MODULATOR

To satisfy PAL linac design requirements for peak power and maintainability, E3712 S-band klystron tube has been selected as a main microwave source. The tube is manufactured by Toshiba in Japan and SLAC in USA. A SLAC 5045 (65 MW peak) klystron is used for the pre-injection module and the following eleven klystrons are Toshiba E3712. The 200 MW modulator for the klystron

tube is designed and manufactured inhouse by Pohang Accelerator Laboratory(PAL).

Klystron

Operational parameters of the Toshiba E3712 and SLAC 5045 klystron tube are listed in Table 1. The klystrons have two output ceramic windows to accommodate 80 MW and 60 MW peak power, respectively. The two outputs are combined after the window by a power combiner. The microwave power is compressed with a SLED to enhance accelerating field in the accelerating columns. Maximum accelerating field gradient of linac is 17 MV/m [2].

Table 1: Parameter of klystrons

Parameter	Toshiba E3712	SLAC 5045
Frequency	2,856 MHz	2,856 MHz
Pulse Width	4 µs	3.5 µs
Repetition Rate	60 Hz	180 Hz
Beam Voltage	400 kV	350 kV
Beam Current	500 A	420 A
µ-perveance	2.0	2.0
RF Output Power	84 MW	60 MW
Drive Power	500 W	600 W
Gain	53 dB	49 dB
Efficiency	42 %	40 %

Modulator

The specifications of the modulator are listed in Table 2. Maximum repetition rate of the modulator is 180 Hz as given in Table 1. However, the normal operating rate is 30 Hz. The injection rate of the electron beam to the PAL storage ring is further reduced 10 Hz. Fig. 1 shows a simplified modulator circuit. The modulator can be divided into four major sections: a charging section, a discharging section, a pulse transformer tank, and a klystron load. In the charging section, a SCR AC-AC voltage regulator controls primary 3-phase 480 V AC power. The voltage regulator receives feedback signals from the primary AC voltage and the high voltage DC (HVDC) detector as shown in Fig. 1.

DEVELOPMENT OF THE KLYSTRON MODULATOR USING A HIGH-VOLTAGE INVERTER POWER SUPPLY*

Y. G. Son[#], S. J. Kwon, J. S. Oh, D. E. Kim, and C. W. Chung
Pohang Accelerator Laboratory

Abstract

The existing klystron modulator in the Linac use a 60 Hz high voltage power supply and adopt traditional L-C resonant charging scheme with De-Qing circuit. The stability of the output high voltage is not satisfactory especially when the AC line voltage fluctuations. If an inverter power supply is used as a HV generator, it will just meet the demands A high frequency inverter switching makes the overall system size small. The command-charging feature can guarantee the high reliability of switching function. In order to increase the stability, operating reliability and comply with the PLC (programming logic controller) and touch screen control system of PLS, an upgrading works is now in progress. This paper will discuss some inverter power supply design considerations and show the test results.

INTRODUCTION

The existing modulators of PLS 150 MW test lab began operation form 1991. The main component of high voltage charging power consists of a motorized 3-phase variable phase control (SCR), a high voltage step-up transformer, a rectifier assembly and charging inductance as show in Figure 1. After more than ten years' operation, some components are no longer in good condition and circuit failure occurred often. The stability of the output high voltage is not satisfactory especially

when the AC line voltage fluctuations. The control of the modulators is based on manual method and therefore can not meet the requirement of new control system of PLS. Development of inverter power device was begun since 1996. In 2005, the modulator upgrade program using inverter power supply started. The upgrading includes two major parts. One is the replacing old HV powers with four 50 kV constant-current charging powers (Dong-A Hitec). The other is the addition of PLC in modulator as local machine controller. In the new control system, PLC achieves command control, status-monitor, safety interlock and real-time communication with the IOC.

SYSTEM DESCRIPTION

Klystron

The klystron currently used in the PAL linac is the Toshiba model E-3712, which was originally rated at 80 megawatts and 4 microseconds and 16 kilowatts average RF power. This tube is a pulsed cathode design with an oxide cathode. However, this new klystron station is designed to be easily adaptable to the other klystron tubes in the event it becomes necessary to change over. The nominal parameters of the klystron station are listed in Table 1.
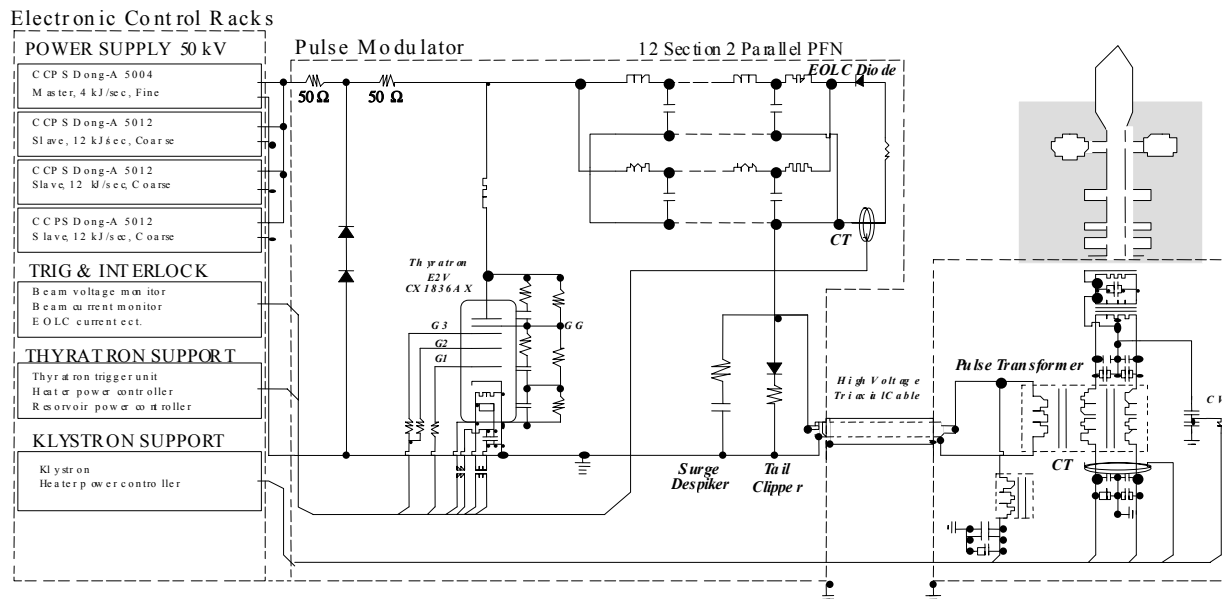
Figure 1: Simplified circuit diagram of line-type modulator for klystron station.

WIDEBAND CURRENT TRANSFORMERS FOR THE SURVEILLANCE OF THE BEAM EXTRACTION KICKER SYSTEM OF THE LARGE HADRON COLLIDER

C. Defrance, J. Bergoz, Bergoz Instrumentation, 01630 Saint-Genis-Pouilly, France
L. Ducimetière, E. Vossenberg, CERN, Geneva, Switzerland.

Abstract

The LHC beam dumping system must protect the LHC machine from damage by reliably and safely extracting and absorbing the circulating beams when requested. Two sets of 15 extraction kicker magnets form the main active part of this system. A separate high voltage pulse generator powers each magnet. Because of the high beam energy and the consequences which could result from significant beam loss due to a malfunctioning of the dump system the magnets and generators are continuously surveyed in order to generate a beam abort as soon as an internal fault is detected. Amongst these surveillance systems, wideband current transformers have been designed to detect any erratic start in one of the generators. Output power should be enough to directly re-trigger all the power trigger units of the remaining 14 generators.

The current transformers were developed in collaboration with industry. To minimize losses, high-resistivity cobalt alloy was chosen for the cores. The annealing techniques originally developed for LEP beam current measurement in collaboration between CERN and industry allowed to extend the frequency response beyond that of traditional core materials.

The paper shows the results obtained, exposes the problems encountered with shielding, conductor position sensitivity, load resistor technology and their solutions.

The know-how acquired during the collaboration was further applied by the industrial partner to cover a wider range of sensitivity, size and frequency.

INTRODUCTION

The LHC beam dump system is a safety system that must protect LHC machine components from damage due to excessive beam losses, or personnel from radiation hazards. Failing to respond to dump requests has severe consequences. The functional operation and the required reliability of functioning are described in the LHC design study [2]. An important ingredient in terms of reliability and safety is the dual branch generator with two parallel 30 kV semiconductor power switches. For a correct dump action the 15 generators are all fired at the same time and are synchronised with the 3 µs abort gap in the beam.

In case of an accidental un-triggered discharge of one of the generators beam would be deflected into the collider vacuum tube and cause severe damage to machine components. Therefore, in this event the other 14 generators are triggered automatically within 700 ns to deflect the beam into the extraction channel and dump it safely on the absorber block.

BEAM EXTRACTION KICKER SYSTEM

The circuitry of the dual branch generator is shown in Fig. 1.
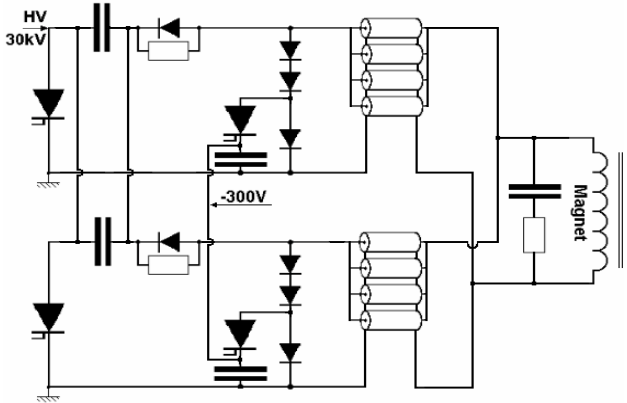
Figure 1: Dual branch generator circuit layout.

It consists basically of a discharge capacitor in series with a 30 kV semiconductor solid state switch, that produces in combination with a free-wheel diode stack parallel to the magnet a current pulse of 2.7 µs rise time and about 2 ms fall time, of which only 95 µs are used to empty the machine. After the magnet current has reached its peak amplitude the polarity of the generator inverses and the freewheel diode stacks start to conduct the magnet current. Simultaneously the 2.5 kV current droop compensation switch, which is connected in series with a 3.25 mF, -300 V capacitor, is closed and the current in the fast recovery diode is commutated. The 3.25 mF capacitor is then connected in series with the magnet inductance and oscillates with a superimposed half-sine wave, which compensates for the resistive losses of the magnet current freewheel circuit.

The generator capacitor voltages are tracked with the beam energy between 2.2 kV at 450 GeV and 30 kV at 7 TeV. The main parameters are listed in Table 1.

Table 1. Main generator parameters.

Voltage range	2.2-30	kV
Peak magnet current (7 TeV)	18.5	kA
Peak magnet current (450 GeV)	1.29	kA
Magnet current flat top 100-105%	95	µs
Current rise time 0-100%	2.7	µs
Repetition time, minimum	30	s

PRECISE POSITIONING OF MAGNETIC FIELD CENTERS OF QUADRUPOLE MAGNETS ON THE GIRDER

Liren Tsai, Duan Jen Wang, Shen Yaw Perng, and Tai-Ching Fan

NSRRC, HsinChu, Taiwan

Abstract

Conventional alignment of quadrupole magnets on one girder was mainly based on the measurement from theodolite and fiducial. Most of the measurement errors came from human-eye resolution and fiducial precision. The resultant cumulative error could be in the order of 100μm. In this paper, vibrating wire method is proposed to align a group of quadrupole magnets concentrically on one girder to precision about 30μm. A short wire was adopted to reduce the sag. A laser PSD system was used to identify the position of the wire. Descriptions of the setup and test results are presented.

INTRODUCTION

The alignment of quadrupole magnets directly affects the closed orbit of electron beams in synchrotron light source. In past years, many efforts have been performed to accurately locate the magnetic center of quadrupole magnets, which include Hall probe measurement, pulsed wire technique, vibrating wire field measuring technique, moving wire technique, moving probe technique, and rotating coil technique, etc [1]. Through these techniques, individual quadrupole magnetic center could be identified with less than 50μm error. However, when aligning two or three quadrupole magnets on girder, the error generated from using fiducial and theodolite could be cumulative. Rotating coil can exam quadrupoles in detail, nevertheless it is extremely difficult to be used on nominal girders. Pulsed wire method has good resolution in narrow areas [2]; however it does not provide the information of quadrupole pitch and yaw. Moving wire method would be more effective in measuring high magnetic fields like superconducting quadrupoles [3]. In order to precisely align quadrupoles on girder, a new alignment system is developed in National Synchrotron Radiation Research Center, Taiwan. This technique adopted the advantages from both vibrating wire method and position sensitive detectors (PSD).

Vibrating Wire Method (VWM)

The vibrating wire method (VWM) is composed of a stretched wire in a magnetic field. By sending a sinusoidal current through the wire, the vibration of the wire induced by the Lorentz Force is observed [4] and the magnitude and orientation of this magnetic field can be determined. To precisely align quadrupoles on a girder, VWM has some clear advantages over other methods: (a) It can be fairly easily operated on a girder; (b) It requires no more than 10cm operating space beside a quadrupole; (c) It requires less operation time, however is as accurate as other techniques.

PSD Alignment System

The position sensitive detector (PSD) has been widely used in many engineering areas to precisely align multiple targets. It is composed of large area photodiodes to detect and record the position of an incident light beam. In this research, two PSDs were attached to the ends of the vibrating wire, as shown in Figure 1. When the laser position is fixed, one can literally "extend" the magnetic center of quadrupole Q1 to quadrupole Q2 by precisely reposition the wire using PSDs. Experiment setup and operation procedures were detailed in next section.
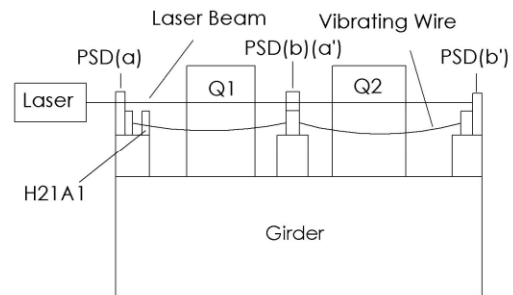
Figure 1: Experiment setup for vibrating wire method plus PSD system.

EXPERIMENT SETUP

Figure 1 shows the experiment setup of the vibrating wire and PSD systems. Two quadrupole magnets were pre-aligned on the girder using the traditional fiducial and theodolite method. The experiments took place in the following orders:

(1) The vibrating wire was tensioned around the ideal centerline of the first quadrupole magnet (Q1). The wire used in the experiment was 650mm length and 125μm diameter Be-Cu wire from GoodFellow[TM]. In order to increase the repeatability of VWM, 100A constant current was applied to the testing quadrupole magnets while supplying the magnet coils with cooling water to keep their temperature at 20±0.5℃.

(2) HP 33120A function generator was connected to the wire to provide AC sine current. The frequency of the input current was carefully adjusted to match the fundamental mode frequency of the Be-Cu wire in order to maximize the vibration amplitude.

THE MAGNET ALIGNMENT METHOD FOR THE J-PARC MAIN RING

M. J. Shirakata, K. Ishii, K. Niki, K. Okamura, T. Oogoe, E. Yanaoka and M. Yoshioka
KEK, Tsukuba, Japan

Abstract

In the J-PARC site, the infrastructure for the whole site measurement is planned for the global alignment of the accelerator components. For the neutrino experiments, the J-PARC main ring must be directed to the SUPER-KAMIOKANDE exactly. The global measurements from the Kamioka site to the J-PARC site are carried out by using GPS system on the ground level. Several measurement through-holes, in order to transport the coordinates from the ground level into the accelerator floor level directly, are prepared around the J-PARC accelerator complex. The beam-line definition and the magnet alignment method for the J-PARC main ring are reported with the present alignment status.

INTRODUCTION

The J-PARC accelerator complex [1] consists of a LINAC, RCS (Rapid Cycling Synchrotron) and MR (Main Ring). In the early stage of the J-PARC project, the through holes, which transfer the coordinates of GPS measurement on the ground level into the accelerator tunnel, were proposed on the MR construction plan because the MR has to be aligned precisely to have a direction to the SUPER-KAMIOKANDE which is 300 km away from the J-PARC site. Finally, this idea is adopted all over the site because it is convenient to grasp the relative positions of accelerator components. The whole site measurements is carried out every winter including these through holes in order to check the arrangement of accelerators.

The MR is composed of three straight lines (named as: INS-A, INS-B and INS-C) and three arcs (ARC-A, ARC-B and ARC-C). A schematic view of the J-PARC MR tunnel is shown in Fig 1. Six through holes are prepared MR_01 to MR_06. The 136 level target are distributed for the floor level measurement. Moreover, L-type and washer-type targets are placed on both walls among the level targets for the beam-line definition and magnet alignment.

BEAM-LINE DEFINITION AND MAGNET INSTALLATION

In usual, the beam-line is defined based on the whole ring measurement after the completion of the construction work. Unfortunately, we had to define the beam-line even the MR tunnel was under construction. The beam-line was defined in these four periods:

- The first stage: August 2005, (all 50BTHs, MHR01 to MHR56)

- The second stage: March 2006, (MHR57 to MHR74)

- The third stage: September 2006, (MHR75 to MHR103)

- The last stage: December 2006, (MHR104 to MHR124)

The parentheses indicate the corresponding areas. The on-wall targets (L-type and washer-type) are measured by laser-tracker (LT) system in the local coordinates. The LT measures the relative positions of the on-wall targets in the area of radius of 20 m at a time. By moving its location along the MR tunnel, the on-wall targets figure out the shape of MR tunnel. Measured position data of the on-wall targets are transformed to the KEK_J-PARC coordinates using GPS global measurement. The KEK_J-PARC coordinates are the right-hand system whose origin is set to the center of RCS ring and whose x-axis is parallel to the INS-C. The beam-line and central points of the magnet bases were drawn and marked on the floor by using the on-wall target coordinates. The magnets were installed on them.

Fig. 2 shows the floor levels of the MR tunnel. The vertical displacement is about ± 10 mm except for one section. At the MHR10, the 3NBT beam line which transfers the RCS beam to the neutron experimental hall is crossing above the MR tunnel. There is a largest vertical displacement of about 40 mm. The magnets were placed on high plane of 2.1 below the sea level considering the future subsidence. The magnets in the descended area were installed with spacers under their bases as shown in Fig 3 in order to compensate the floor subsidence.
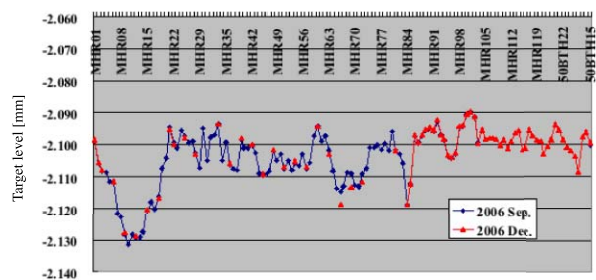
Figure 2: Measured target level of the MR tunnel from the sea level. The floor level is -13 mm from the target level. The floor level displacement is about -40 mm at the maximum.

A MECHANICAL INSTALLATION PROTOTYPE FOR THE SSRF STORAGE RING

L.X. Yin, H.W. Du, D.K. Jiang, Q.G. Zhou, Z.B. Yan, C.H. Yu, X. Wang
Shanghai Institute of Applied Physics, Shanghai 201800, P.R. China

Abstract

The engineering design of the mechanical system for SSRF storage ring was finished. The first group components in each system, such as the magnets, vacuum chambers, BPMs, girders and other hardware, were fabricated and tested, respectively. In order to check the overall design and the installation procedure, a lattice cell prototype was installed by using these components. Based on it, the related utility system was installed and checked. The dynamic properties of the girder-magnet assembly were also tested in this prototype. Most of the design was confirmed during the installation, but still some problems were found. The modification for the overall design and some components design has been made before their mass production. The detail design and installation of the cell prototype and the test results are described in this paper.

INTRODUCTION

The Shanghai Synchrotron Radiation Facility (SSRF) is a 3.5GeV, 300mA light source currently under construction [1]. The engineering design for the mechanical system was finished and the fabrication for the first group of components in each system, such as the magnets, vacuum chambers, BPMs, girders and others, was completed. The mass production for the components will be started. In order to check the overall design and the installation procedure, a lattice sector prototype was installed by using the first group of components in the tunnel.

MECHANICAL STRUCTURES FOR THE STORAGE RING

The physical study in the storage ring led to an optical design composed of four super-periods, each divided into five sectors. Each of the twenty sectors contains 10 quadrupoles, 7 sextupoles, 4 static correctors and 3 dynamic correctors distributed on three girders, as well as 2 dipoles isolated from the girders by its own supports. The structure of a typical sector in the storage ring is shown in figure 1.
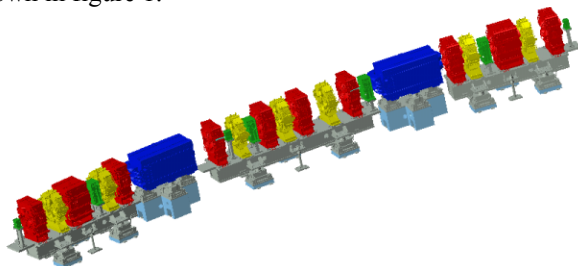
Figure 1: A typical sector in SSRF storage ring.

The support system for quadrupoles and sextupoles is composed of three parts, the girder, the adjuster unit and the concrete pedestal. Each girder is supported by three adjuster units on the pedestals. The girder is a box-structure welded from Q235A steel plates. Each adjuster unit contains a spherical bearing mounted on a wedge block adjuster, shown as figure 2. The bearing with flange is attached to the bottom of the leg in the girder. The flange can rotate 7 degrees maximum in any direction. The range of adjustment for the wedge block is ±7mm. There are two base plates under the adjuster unit to adjust the position in horizontal plane by blots. Self-lubricating plate is used in friction couple to reduce the force between slip surfaces. A concrete pedestal with damping effect is set on bottom of the adjuster unit. The pedestal can be set on the same height by adjusting the space to the floor. It is fixed on the floor tightly using the anchor bolts and a kind of non-shrinking concrete. For the dipole, the steel girder is eliminated and the magnet is supported on a higher concrete pedestal by the same adjuster unit.
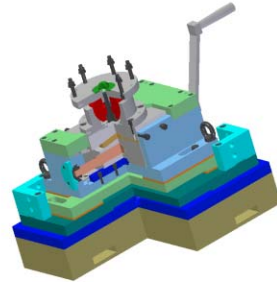
Figure 2: Girder adjuster.

The magnets are fixed on the girder by bolts. The precise position of the magnets on the girder is aligned by shimming in vertical direction and by bolt screw in horizontal direction.

There are three pieces of stainless steel vacuum chambers connected by two RF shielded bellows in one sector. The 6m bending chamber is supported on the first and the second girders, and the 5m bending chamber is on the second and the third girders. Only the 3m straight chamber is supported on the middle girder itself. Figure 3 shows the relation between chambers and girders. Each chamber is fixed on a stiff support near the downstream
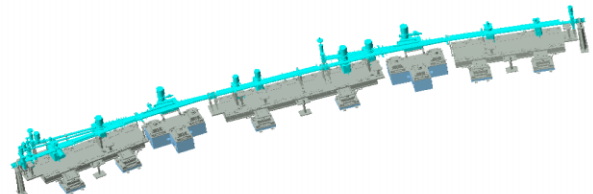
Figure 3: Vacuum chambers on girder.

MECHANICAL COUPLING BETWEEN THE LHC CRYOGENIC DISTRIBUTION LINE AND THE SHORT STRAIGHT SECTION HOUSING THE SUPERCONDUCTING QUADRUPOLE - THEORETICAL ANALYSIS AND EXPERIMENTAL VALIDATION

Subhajit Dutta[#], Jishnu Dwivedi, Abhay Kumar, RS Sandha, HC Soni, SC Bapna and S Kotaiah

Raja Rammana Centre for Advanced Technology, Indore, India,

Alain Poncet , Blazej Skoczen and Cedric Garion, CERN, Geneva, Switzerland

Abstract

Liquid and Gaseous Helium are supplied to the superconducting magnets of the Large Hadron Collider (LHC), presently being assembled at CERN, by a cryogenic distribution line (QRL). The cryogenic module of the twin-quadrupole Short Straight Section (SSS) is supplied with these cryogens through a jumper connection linking the service module of the QRL and the SSS. The internal as well as external features of the jumper construction allow for relative displacements between the QRL and SSS with sufficient flexibility to reduce the reaction forces responsible for elastic deformations when the SSS is moved for alignment. The SSS is composed of a cold mass and of a vacuum vessel equipped with fiducials posted on the external vacuum vessel reinforcement rings allowing the precise alignment of the machine when the cryostat is finally closed. A deformation of the structure linking the cold mass and the external vacuum vessel resulting from reaction forces induced by relative displacements of the SSS and the QRL, if unpredictable, would result in an unacceptable misalignment of the quadrupole magnetic axis. A unified FE model was generated at RRCAT to study the elastic behavior of the SSS under the conditions of alignment. This model was validated using a 40 meter long dedicated test setup at CERN. Correlations in the matrix form were generated so that all displacements of the cold mass can be related to the corresponding movements done for alignment. This transfer function, linking the action on the SSS external alignment jacks and the position of the cold mass will be used to properly align the machine in operation.

INTRODUCTION

The SSS can be structurally divided into two main parts: the external cryostat and the internal cold mass of the magnet. The cryostat is an 8 mm thick cylindrical vessel made of carbon steel with a diameter of 1025 mm and a length of 6480 m. Large Sleeves having length of 840 mm and diameter of 1077 mm connect the cryostats of adjacent magnets. Two 'Glass Fibre Reinforced Epoxy (GFRE)' composite support posts, separated by 2.57 m, support the cold mass of the magnet. One of the composite supports is free to move in the longitudinal direction and is also free to move upwards. The other support is bolted to the cryostat. The three-ply magnet-to-

#subhajit@cat.ernet.in

magnet interconnection bellows carrying the superconducting bus bars are welded to the cold mass. The service module of the SSS is connected to the distribution line through a "jumper connection". The jumper connection consists of seven (for the Arc) helium carrying internal pipes enveloped by an external vacuum jacket. Each pipeline has one vertical and one horizontal metal hose. The vacuum jacket has one vertical double gimbal universal joint and one horizontal gimbal assembly.

The Short Straight Section (SSS) of the Large Hadron Collider (LHC) may undergo relative displacements between the cold mass and the cryostat for the following two reasons:

- Manufacturing tolerances of in situ welding
- Global smoothing after pre-alignment
- Ground motion in a sector of the LHC tunnel

The forces responsible for such displacements stem from finite stiffness of interconnect bellows & metal hoses of the internal piping of the jumper connection and from relatively flexible composite supports of the cold mass. In addition, the vacuum jacket of the jumper connection and the large sleeves attached to both ends of SSS produce elastic deformations of the cryostat vessel. The cold mass also deforms when subjected to forces. The magnets after being transported to the tunnel are placed in their theoretical position. The welding of the interconnect bellows and the mounting of jumper and large sleeves are done at this stage. The interconnection bellows may be transversely deformed due to their deviation from the theoretical position in vertical or radial directions thus producing a relative displacement between the cold mass and vacuum vessel. Another reason for relative displacement is the fine alignment (global smoothening) done after initial cool down to 77 K, which may cause magnet movements up to ± 2 mm. Some areas of the tunnel are prone to ground motion up to 1 mm per year. This displacement is the third reason for relative displacement between the cold mass and the cryostat. The knowledge of the absolute position of the cold mass for each jack movement in radial and vertical directions is essential. The maximum relative displacement for satisfactory machine operation is 0.1 mm.

FINITE ELEMENT MODEL

The major components that contribute to the analysis of the structural behaviour are: Cold Mass, Cryostat,

PRECISE SURVEY AND ALIGNMENT OF SYNCHROTRON RADIATION SOURCE INDUS-2

Vijendra Prasad[#], R.K.Sahu, Dinesh Barapatre, M. Jagannath, K. P. Sharma & Gurnam Singh
Accelerator Programme, RRCAT, Indore-452013, India

Abstract

The 2.5GeV third generation synchrotron light source Indus-2 at RRCAT, which is in advance stage of commissioning, demanded a high precision of survey and alignment of all its components. In particular, we had to control the transverse and azimuthal positions of all quadrupoles and dipoles within a relative accuracy of 0.1 mm and overall circumference within 2.5 mm. This required a tight control over all the sources of errors starting from fiducializations, survey of networks, final alignment and smoothing. We have successfully accomplished this task by adopting the triangulation-trilateration technique of survey and alignment along with indigenously developed software for online survey data collection, least square adjustment of redundant measurements and error analysis. The accuracy of alignment was reflected from the successful circulation and storage of electron beam in the machine with a very small closed orbit distortion. This paper, in brief, presents the methodology adopted for survey and alignment and final accuracies achieved.

INTRODUCTION

Indus-2 with a circumference of 172.4743 meters consists of 16 dipole magnets, 72 quadrupoles, 32 sextupoles, 48 steering magnets, 56 beam position monitors and some special components like injection septums, kickers and RF cavities. The relative tolerances for alignment of magnets are given in table-1. These are the total error budgets in the placement of components including ambiguities in knowledge of the magnetic axis and errors in fixation of fiducials etc.

Table 1: Alignment tolerances.

Object name	δS mm	δX mm	δZ mm	θs mrad	θx mrad	θs mrad
Dipole	0.1	0.2	0.1	0.2	0.5	0.5
Quadrupole	0.1	0.1	0.1	0.2	0.5	0.5
Sextupole	0.5	0.1	0.1	0.2	1.0	1.0
Steering Magnet	1.0	1.0	1.0	2.0	2.0	2.0

Figure-1 shows the general layout of accelerators at RRCAT. The already existing Booster Synchrotron acts as injector for Indus-2. Hence before start of construction of building for Indus-2, it was necessary to mark the centre of building and fix the central monument with respect to Booster synchrotron.

[#]vijen@cat.ernet.in

During building construction the embedded plates for mounting girder jacks, embedded pipes for synchrotron beam lines, primary control network monuments etc. were fixed at their designed positions/orientations and elevations with in a fair accuracy. Since Indus-2 is housed in a narrow over-ground tunnel of 5.2meter width, the visibility of machine is limited to a very small zone. So we decided to adopt a network approach of alignment for controlling the overall shape and size of the machine and at the same time to align all components within specified tolerances [1]. For this we established three control networks, namely Primary Control Network, Secondary Control Network and Elevation Control Network.
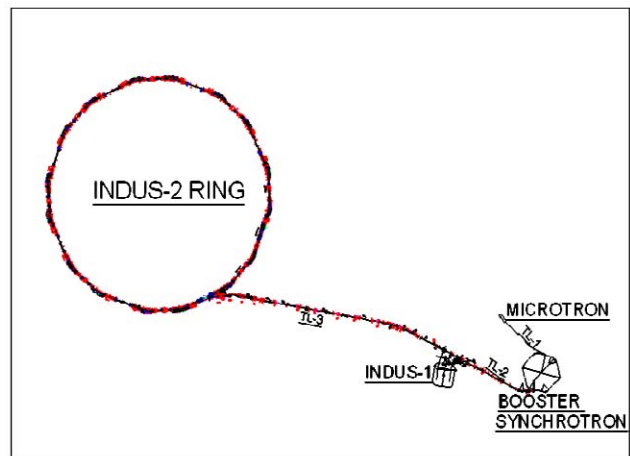
Figure 1: Layout of Accelerators at RRCAT.

SURVEY CONTROL NETWORKS AND FIDUCIALIZATION

Primary Control Network

The primary control networks are in the form of 400 mm diameter concrete pillars (monuments) with forced centering sockets over them for mounting survey instruments and optical targets [Figure 2]. Out of 11 monuments, the locations of 4, that lie in the tunnel, were decided in such a way that the whole machine is divided into four approximately equal parts. Holes have been provided in the inner wall of the tunnel, to facilitate direct measurements of distances and directions between them. The primary control network defines the coordinate system of Indus-2 and acts as a reference for the secondary control network. The coordinates of these monuments have been determined by least square adjustment of repetitive redundant distance and direction

PROTOTYPE BEAM DUMP FOR 10 kW LINAC

R.S. Sandha[#], Jishnu Dwivedi, S.C. Bapna, V.C. Petwal, H.C. Soni
Raja Ramanna Centre for Advanced Technology, Indore (INDIA).

Abstract

A 10 MeV, 10 kW electron beam accelerator (Linac) has been developed at RRCAT, Indore for developing applications in the area of radiation processing of agricultural products and medical sterilization. This paper presents the functional requirements, design and manufacture of beam dump for this LINAC. Activation of beam dump, conversion of electron energy into primary bremsstrahlung and radiation damage are important parameters for selection of material. Other parameters considered are thermal conductivity, corrosion in ozone environment, manufacturability and mechanical strength. Thermal, hydraulic, structural and engineering design was done. FEM based analysis was performed for calculating temperature rise and stresses. The maximum temperature in beam dump is estimated to be about 325 K. A prototype beam dump was manufactured and installed and it is being tested in actual operating conditions.

INTRODUCTION

Beam dump is installed in front of scan horn after the product as shown in Figure 1. The pulsed electron beam obtained from Linac has a diameter of 30 mm. It is scanned in scan horn mounted at the end of beam transport line. The scanning system comprises of a scanning electromagnet that provides 600 mm wide radiation field at the product surface in its path. The electron beam will be dumped on beam dump in the absence of product. The scanned electron beam field has approximate size of 100 mm x 900 mm at the location of beam dump. Considering this, size of beam dump is kept as 120 mm by 1000 mm. The beam dump shall stop most of the electrons so that the electrons transmitted in nearby structure are minimised. Maximum power incident on beam dump will be 14 kW. Specifications of Linac are given in Table 1 [1].

Table 1: Specifications of Linac

Nominal energy of accelerated electrons	MeV	10
Maximum beam power	kW	14
Pulse current of accelerated electrons in nominal mode	A	0.33
Duration of beam current pulse	µs	14
Pulse repetition frequency	1/s	300

DESIGN FEATURES

Activation of beam dump and conversion of electron energy into primary bremsstrahlung are important parameters for selection of material. Radioactivity may be induced in beam dump irradiated by electron beam or bremsstrahlung beam due to γ-n reaction. The activity

#rssandha@cat.ernet.in

induced in beam dump depends on energy and power of incident beam. The threshold energy for γ-n reaction in copper, stainless steel and aluminium is 9.9 MeV, 10.57 MeV and 13 MeV respectively. Copper and stainless steel are susceptible to activation at 10 MeV energy while aluminium is insusceptible [2]. Keeping this in view, aluminium was selected. Other parameters are thermal conductivity, corrosion in ozone environment, manufacturability and mechanical strength. The thermal fatigue behaviour of the material is also an important consideration, which will be taken care of in design of regular beam dump. Practical range of 10 MeV electron beam in aluminium is 20 mm, hence beam dump thickness (including water) was kept as 30 mm.
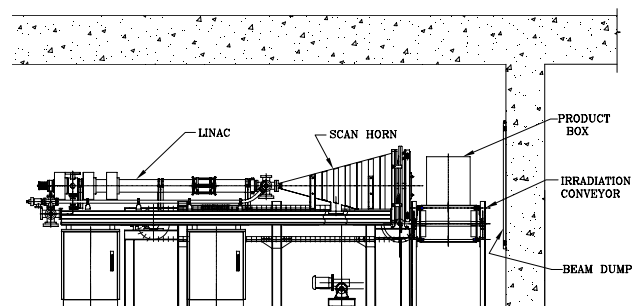
Figure 1: Location of beam dump

THERMAL AND STRUCTURAL ANALYSIS

Dittus-Boelter correlation [3] has been used for calculation of average heat transfer coefficient in the turbulent region over the cooling channels:

$$h= 0.023 \ (k/d) \ (Re)^{0.8} \ (Pr)^{0.3}$$

Where h is average heat transfer coefficient, k is thermal conductivity of fluid, d is hydraulic diameter and Re is Reynolds number, Pr is Prandtl number.

Reference temperature was taken as 303K. Flow rate of 30 Litre/minute results in turbulent flow with water velocity of 3 m/s. Reynolds number of 40,000 and heat transfer coefficient of 8000 W/m^2.K is achieved with this flow. The pressure drop in entire circuit is about 0.1 MPa. The beam dump cooling circuit can take a maximum pressure of 0.5 MPa, hence a separate coolant supply with low circuit pressure will be provided for beam dump. The normal cooling circuit in the building operates at a pressure of 1 MPa.

Finite element code ANSYS [4] was used for analysis. Second order quadrilateral element Plane77 were used to model the structure and obtain temperature rise in beam dump. Sequential coupled field analyses were performed to calculate thermal displacements and stresses.

07 Accelerator Technology
T18 - Radiation Monitoring and Safety

BREMSSTRAHLUNG CONVERTER FOR HIGH POWER EB RADIATION PROCESSING FACILITY

V.C.Petwal[#], S.C.Bapna, R.S.Sandha, Swarna Kotaiah, K.V.Subbaiah[1]

IMA Section RRCAT, Indore. [1]SRI, IGCAR. Kalpakkam, Tamilnadu

Abstract

A radiation processing facility based on 10 kW Linac is being set up at RRCAT for radiation processing of food products and sterilization of medical items. The facility is planned to operate in electron (10 MeV) and X-ray (5 & 7.5 MeV) mode. The required X-rays will be generated by bombarding an optimized target with 5 or 7.5 MeV electron beam. The composite target is made of Ta, water & SS. Monte Carlo simulation with MCNP has been performed to optimize the design of the target for maximizing the X-ray output. Characteristics of the emerging X-ray field e.g. photon energy spectrum, angular distribution, radial dose and depth dose distribution in unit density material have been simulated & compared for 5 & 7.5 MeV. Our simulation results show that for optimized design, the fraction of the energy transmitted and useful for radiation processing at 5 & 7.5 MeV is 9.3% & 14.2 % respectively. The most probable energy of the photons is 0.3 MeV for both 5 and 7.5 MeV electrons and the average energy is 0.84 MeV & 1.24 MeV respectively. Large fraction of electron beam power is dissipated as heat in the targets. Necessary data has been generated to carry out thermal design.

INTRODUCTION

Four types of ionizing energy have been approved by regulatory authorities for radiation processing of food products. These are gamma rays from Co-60 and Cs-137, electrons with energy up to 10 MeV and X-rays with energies up to 5 MeV. FDA has recently approved use of X-rays generated by 7.5 MeV electron beam for food processing (*Federal Register 2004)*. The selection of the energy source for a particular application is usually based on practical considerations like product shape, size, density, average dose requirement, dose uniformity ratio, processing rate and cost. Treatment with direct electron beam provides the highest processing rate and the lowest unit cost but electron has relatively short range. X-rays have higher penetration quality and hence permits the treatment of dense objects in large packages.

TARGET MATERIAL

X-rays are produced when energetic electrons strike any target material. The intensity and efficiency of X-ray conversion increase with the energy of incident electron and the atomic no of the target material. In order to maximize the X-ray output, Ta, W, Au are the suitable choice for the target material. Tungsten has high brittleness, hence difficult for machining and fabrication,

#vikash@cat.ernet.in

while Au is not cost effective, so both are not considered for target material. Tantalum is the suitable choice as a compromise between photon yield, residual radioactivity, physical properties, mechanical properties and fabrication simplicity for commercial environment. At 5 MeV no activation will arise from the Ta target as the threshold energy level for two common isotopes of tantalum (Ta-180 and Ta –181) are 6.6 and 7.6 MeV respectively. When operated at 7.5 MeV i.e. above the threshold for γ-n reaction in target material, two radio nuclide Ta^{180} and Ta^{182} are formed respectively by (γ-n) and (n-γ) reaction on naturally abundant Ta^{181}. The former has half-life of 8.1 h mostly β emitter, and the latter has half-life of 114 days emitting γ of 1.2 MeV. Also, the order of saturation dose rate (due to the induced activity) measured immediately after the shut down of the accelerator is reported about 1 mGy/h for Ta target at 7.5 MeV (*J. Mckeeown et.al, 1998*). Extensive study have been performed to investigate the induced activity in the irradiated product and concluded that the amount of induced activity created by 7.5 MeV X-rays in food product is negligible small. The IAEA report *(IAEA-TECDOC-1287*) says that the possible radiation exposure from induced radioactivity to human, consuming 40 kg/yr of beef irradiated by 7.5 MeV beam on Ta target for a dose of 30 kGy (a dose more than 6 times the maximum permitted dose level of 4.5 kGy) is 300 times less than the yearly dose due to the natural activity present in the food. Keeping these points in view Ta is suitable & acceptable for X-ray converter at 7.5 MeV. In order to make cooling channel SS is suitable as the threshold energy for γ-n reaction in Fe, Ni the major constuient of SS is more than 10 MeV.

TARGET GEOMETRY

To obtain the basic data for the study, multi-layered composite target geometry is considered (see Figure 1). The shape of target for simplicity is cylindrical (radius 5 cm) and is made of three layers, tantalum, water, and stainless steel. Tantalum is used to generate the bremsstrahlung radiation from incident electron beam, while water is used to remove the heat deposited on the tantalum. The SS is used to make the water channel and stop the unwanted electron contamination coming out with the bremsstrahlung radiation. The thickness of tantalum is varied in the range 0-20 mm while the thickness of water channel and SS; each, is taken judiciously 2 mm (for both 5 MeV and 7.5 MeV). A water phantom of size   40 cm x 40 cm x 40 cm, placed 10 cm away from target, is simulate to study the dose profile in unit density material.

STUDIES OF METALLIC ION BEAMS USING ECRIS

P. Kumar, G. Rodrigues, P.S. Lakshmy and D. Kanjilal
Inter University Accelerator Centre, New Delhi 110067, INDIA

Abstract

Low energy (from a few keV to a few MeV) metallic ion beams have wide applications in various research fields especially in materials science, atomic and molecular physics. Several metallic ion beams have been developed successfully using all permanent magnet 10 GHz electron cyclotron resonance (ECR) ion source based low energy ion beam facility (LEIBF) at Inter University Accelerator Centre (IUAC), New Delhi. For the development of these metallic ion beams, different methods e.g. oven, sputtering, insertion and metal ions using volatile compounds (MIVOC) have been utilized. The charge state distribution (CSD) studies of two metallic ion beams are presented.

INTRODUCTION

To get the operational experience of ECR ion source [1] on high voltage platform and to provide the low energy ion beams from gaseous and solid species, the LEIBF [2] has been set up at IUAC. The most important feature of the facility (LEIBF) is that the ECR ion source and all its peripheral components including electronics (power supplies and RF power amplifier) and vacuum systems are on a high voltage (300 kV) platform. The various parameters of the source are controlled through fiber optics communications at 300 kV isolation. The regular operation of this facility provided us experience and expertise to design and build the world's first High Temperature Super-conducting ECR Ion Source (PKDELIS) [3] for use on a high voltage (400 kV) platform. The ion source has been tuned to get optimum intensities of metallic ion beams which are being used for research in emerging fields like nano science and spintronics. The high intensities of low energy metallic ion beams are suitable to engineer the optical, electrical and structural properties of materials via ion implantation and ion irradiation.

METALLIC ECR PLASMA PRODUCTION

The ions, inside the source, are produced by the impact of resonant electrons and are confined axially and radially by using permanent magnets (NdFeB). The desired vapors of materials are introduced into the source for ionization using micro-oven, sputtering system and MIVOC [4] method. A micro-oven, compact in size, is used for the heating of metallic elements in a temperature range of 100^0 - 1200^0 C. The heating is done using a 36 V, 4 A power supply. For micro-oven, a typical voltage of 14 volt is required in order to achieve a oven temperature of about 1000^0 C. A small cylindrical crucible (ceramic) filled with a few mg quantity of desired metallic element in powder or rod form is placed into the micro-oven. The micro-oven along with crucible, placed on a mounting system is injected into the plasma chamber from the injection side of the source. In order to have a continuous operation of the source to complete the experiments, the operational temperature is kept well below the melting point of the materials.

In the process of plasma sputtering, the sputtering target (high melting point > 1000^0C) in the form of a disc, wire or pellet is exposed to a background plasma. In regular operation of the source, the background plasma is developed using noble or inert gases. The ions lost from the plasma strike the sputtering target and the vapors of desired metallic species are released for the process of ionization. In MIVOC method, the vapors of volatile compounds are allowed to diffuse into the plasma chamber using a pressure control valve. The metal atoms in the structure of volatile compounds are released in the plasma. The ionization of these metal atoms then takes place by the impact of resonant electron.

ION EXTRACTION AND ANALYSIS

The extraction system consists of an extraction aperture (at high voltage (30 kV max.)) of 3 mm in diameter, puller electrode El1 in conical shape (at ground potential), a focus electrode El2 (at high voltage (15 kV max.)) and another electrode El3 at ground potential. The puller electrode, focus electrode and the last grounded electrode form two gaps (decelerating and accelerating gap) for the extraction and strong focusing of the ion beams. A rough sketch of the structure (plasma chamber and extraction) is shown in figure 1.
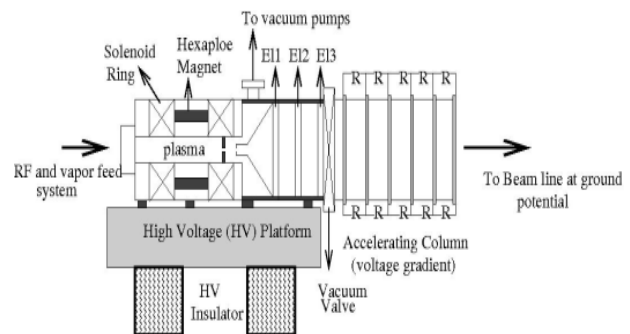
Figure 1: Schematic of source and extraction system

AIR TEMPERATURE ANALYSIS AND CONTROL IMPROVEMENT FOR THE INJECTION AREA AT TLS

Jui-Chi Chang[#], Zong-Da Tsai, Yung-Hui Liu,
National Synchrotron Radiation Research Center, Hsinchu, Taiwan

Abstract

This paper presents the air temperature analysis and control improvement for the injection area at the Taiwan Light Source (TLS). The injector consists of a 50-MeV LINAC and a 1.5-GeV booster synchrotron. Because of insufficient cooling capacity, the air temperature was too high (> 27 ^{o}C) and the temporal temperature variation was more than 2 ^{o}C in one day. The air relative humidity was often higher than 60%. The problem of insufficient cooling capacity became more serious after the top-up mode operation. To cope with the above-mentioned thermal problem, the cooling capacity was increased and the PID parameter of the temperature control was also optimized. Totally 27 temperature sensors were distributed in this area to on-line record the air temperature history. The temperature control was improved to suppress temporal temperature variation within ± 0.1^{o}C. The air humidity was also much improved than ever.

INTRODUCTION

We had studied the utility effects on beam quality [1] [2] to verify those effects on the stability of the electron beam orbit at TLS. According to those studies, thermal effect is one of the most critical mechanical factors affecting the beam stability. Accordingly, we had conducted a series of air conditioning (A/C) system improvements of the storage ring and applied the numerical simulation to analyze the flow field and temperature distribution. Those A/C improvements and analyses had been respectively conducted on the experimental hall [3], the storage ring tunnel [4] and the core area of technical equipment [5]. However, the cooling capacity of the injection area was insufficient to keep air temperature low and steady enough three years ago. This thermal problem would become worse after the project of the top-up injection mode was launched because waste heat generated by the top-up injection mode is steadier but much higher than that generated by the decay mode.

Figure 1 shows the 3D schematic drawing of the injection area, which includes the booster area and the transport line area. There are a 50-MeV LINAC and a 1.5-GeV booster synchrotron installed in the booster area. The booster synchrotron is mainly consisted of magnet system, rf system, and vacuum chambers. The transport line is not shown in this figure. Blue ducts and green ducts shown in Figure 1 are supply air ducts and return air

_____
[#]jcchang@nsrrc.org.tw

ducts, respectively. Air exits and air exhausts are respectively distributed on the ceiling and side walls of the booster area. All air exits and air exhausts are distributed in the ceiling on the transport area.

Figure 1: Schematic drawing of the injection area.

COOLING CAPACITY ENHANCEMENT FOR THE TOP-UP INJECTION MODE

As abovementioned, the cooling capacity of the injection area became insufficient while its A/C system was still kept as its original design of 13 years ago. The injection system had been upgraded from its original 1.3-GeV to 1.5-GeV and added some new air-cooled equipment in past decade. The air temperature was usually higher than 27 ^{o}C and the temporal temperature variation was more than 2 ^{o}C in one day even the valve of the cold water was fully opened. The air relative humidity was also often higher than 60% three year ago.

A new AHU was installed to replace the old one in 2004 accordingly. Specifications of both the old and new AHUs are list in the Table 1. The cooling capacity of the new AHU is about double that of the old one, as list in the table.

Table 1: Specifications of the old and new AHUs for the injection area.

AHU Specification		Old	New
Air Flow (CFM)		16900	30000
Fan	Total Static Pressure (in-WG)	3.5	3.5
	RPM	1485	914
	Motor (HP)	20	30
Cooling Coil	Enter air temp(^{o}C DB)	24.8	24.8
	Enter air temp(^{o}C WB)	18.3	18.3
	Face Area (FT^2)	40.4	71.9
	Energy (RT)	40	80

VIBRATION EVALUATION FOR UTILITY INSTRUMENTS AND WATER PIPING SYSTEM IN TLS*

Yung-Hui Liu[#], Duan-Jen Wang, Jui-Chi Chang, June-Rong Chen,
NSRRC, 101Hsin-Ann Road, Hsinchu Science Park, Hsinchu
30076, Taiwan.

Abstract

The purpose of this paper is to estimate the vibration source from water systems and the piping system in utility system. Analysis the vibration path from piping system is the first step. Then, propose the feasible proposals to eliminate the vibration source and reduce vibration propagation. The construction standards for water systems will be established before design. The test is based on TLS operating systems. Besides, the distance and path between utility building and storage ring is another factor for vibration propagation. Elimination the vibration source and propagation path in TLS will be the next step. The experimental results will be the guidline of TPS construction in the future.

INTRODUCTION

In order to design the new synchrotron light source in NSRRC, the vibration issue is more restrict. Vibration source from utility systems is one factor of instability. In 2004, ANL[1] studied the mechanical vibration control systems and the specifications for all rotational facilities. TLS has also investigated on water induced vibration[2] and ground vibration. In order to find out the vibration propagation from the utility systems, the dynamic signal analyzer also need to be studied.

LAYOUT AND PIPING SYSTEM IN UTILITY

The utility systems in 1st utility building (UT-1) are shown in Fig.1. There are air conditioning systems and de-ionized water (DIW) systems in the 1st utility building. The DIW systems and air conditioning systems are the two major cooling systems in the TLS. The DIW systems consist of three subsystems, the copper system, the aluminium system and the RF system.

The copper DIW system supplies DIW to magnets and magnet power supplies. The aluminium and RF DIW systems supply DIW to vacuum chambers and to RF transmitters and cavities, respectively. In each DIW loop, there are two heat exchangers in order to adjust the DIW flow temperature. After the heat exchangers, the DIW flow to the storage ring by the water pumps with variable frequency drive. The DIW piping is cross through the trench to the core area and was divided into 12 loops. Each DIW loop flows to half of the section in order to cool the half section. The inlet and outlet DIW were divided into subsystems here.
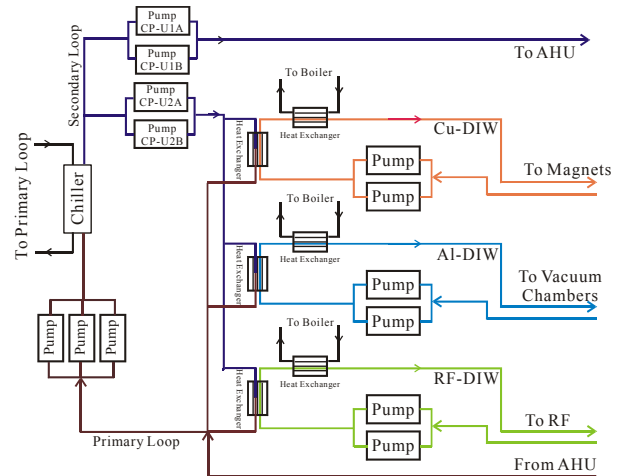
Figure 1: Layout of UT-1.

THE EXPERIMENTAL SETUP

The vibrations were measured by the portable spectrum analyzer COMMTEST VB2000 and piezoelectric type accelerometer IMI 603M56. The spectrum range is from 4 Hz to 200 Hz, and the resolution is 800 lines. The experiments were average for four times and recorded in displacement or accelerometer by the spectrum analyzer.

THE CHILLER VIBRATIONS

The chilled water is produced by three centrifugal chillers (YORK) in UT-1. Each capacity is 320 RT. The vibration on the top side of the chiller is much higher than the base of the chiller, which the significant frequency is ~60 Hz produced by the compressor. The cooling water side of chiller is connected to the cooling tower and the power for these 4 motors is 75 HP with fixed 1800 rpm. On the base of chillers, the rubber pad is located between the chiller and the ground. The experimental results show that the vibrations from 4 Hz to 200 Hz reduce for 2.1 to 4.5 times by using the rubber pad depends on the vibration amplitude.

VIBRATION PROPAGATION FOR DIW SYSTEMS

There are three DIW subsystems in UT-1, the copper system, the aluminium system and the RF system. Because of the DIW is delivered direct to the magnets and vacuum chambers, the vibration propagation is very important to the beam stability. The vibration propagation for the Al and Cu DIW systems are tested as follow.

07 Accelerator Technology
T20 - Infrastructures

SF₆ GAS HANDLING SYSTEM FOR 3 MeV, 30 kW ELECTRON BEAM ACCELERATOR AT EBC, KHARGHAR, NAVI MUMBAI

Shyam Rao Ghodke, Rajesh Barnwal, Mahendra Kumar, D. Jayaprakash, Barje Supriya, Radhelal Mishra, Nagesh Lawangare, K. Nanu, G. Puthran, Vinod Sopan Veer, K. K. Abdullah, Kailash Chandra Mittal, Devi Pada Chakravarthy and Asish Kumar Ray (BARC, Mumbai), India.

Abstract

The 3 MeV Accelerator Project involves designing, fabrication, installation and commissioning of a 3 MeV, 30 kW Industrial Electron Beam Accelerator with a terminal voltage of 3 MV and is housed inside the Electron Beam Centre building at Kharghar, Navi Mumbai. The Accelerator has capability of delivering electron beam of 3 MeV energy for radiation processing applications. For ecological and economical reasons, the SF_6 gas is reincorporated into a closed cycle because gas should not be released into the atmosphere. The aim of the SF_6 gas handling system is to introduce the gas at high pressure to the accelerator tank after evacuation and to bring back into the storage tanks with minimum loss. The gas handling system also provides purification of gas, prevention from mixing with air or any other substances, which may contaminate and thus bring down the high voltage insulation characteristics of the gas. A heat load of 12 kW is coming due to high frequency transformer, electron gun, power supplies, motor alternator system, fan motor and blower etc. A radiator type heat exchanger with high-pressure blower and finned tube has been used for cooling the gas.

This paper discusses about mechanical design, fabrication, testing and safety of different components of SF_6 gas handling system such as gas piping, non lubricating compressor, dryer, vacuum pump, dust & oil filters, storage tanks etc. It also discusses about mechanical and thermal design of heat exchanger, which includes calculations of heat transfer coefficient, surface area, pressure drop, design and selection of high-pressure blower, 5-ton chiller unit, insulation and cooling tower.

INTRODUCTION

3 MeV Accelerator is an electrostatic accelerator in which terminal is floating at a voltage of 3 MV and the accelerator tank is at ground potential. As shown in the fig. 1, from voltage gradient point of view there is two geometries, coaxial cylindrical and spherical geometry. Design calculations show that SF_6 is the most suitable medium for insulation and cooling purpose. Apart from excellent electrical properties, SF_6 has good chemical stability, thermal properties and nontoxic. SF_6 Gas Handling System of 3 MeV project mainly covers SF_6 gas **transfer** system and SF_6 gas **cooling** system. The Accelerator Pressure vessel [1] is the main body of the 3 MeV Accelerator, which will house high voltage multiplier columns, RF electrodes, corona shields, high voltage terminals, electron gun, accelerating tubes, motor

generator set, heat exchangers, RF transformer etc. All of these components require SF_6 gas insulation and efficient cooling. Hence there is a need of SF_6 gas and its handling system. Normal operating pressure inside the accelerator is 6 kg/cm². The accelerator tank has to be evacuated to vacuum of 10^{-1} torr before filling the gas.

Detail design [1] and fabrication [2] of the accelerator pressure vessel using ASME B&PV SEC-VIII, DIV-1 Code was carried out and reported earlier.
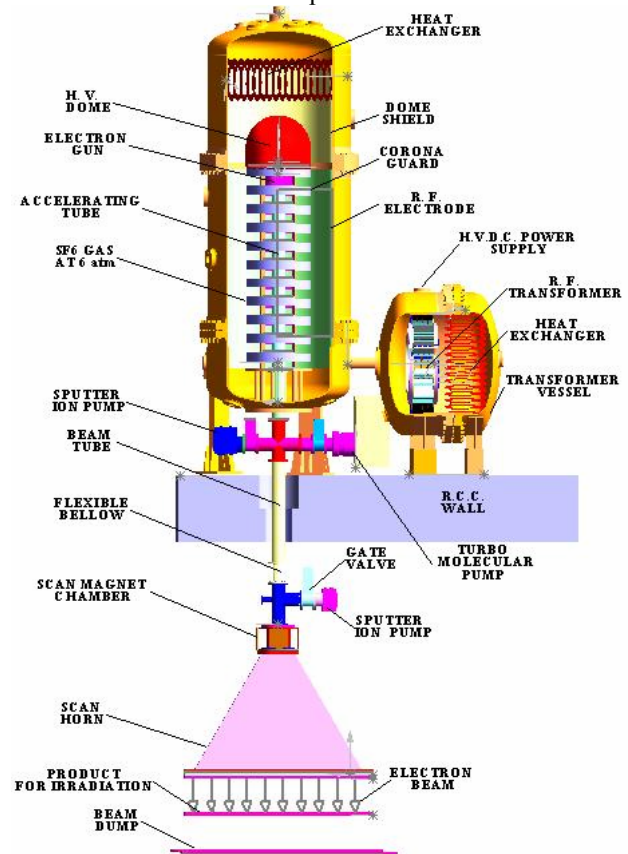
Figure 1: 3D Schematic of 3 MeV Electron Beam Accelerator

SF₆ GAS TRANSFER SYSTEM

The main objectives of SF_6 gas handling system is:
► Transfer of SF_6 gas from SF_6 cylinders to SF6 storage tank for storage.
►Transfer of SF_6 gas from Storage tank to accelerator tank while starting the accelerator
► Transfer of SF_6 gas from accelerator tank to storage tank for maintenance
► Recirculation of SF_6 gas during accelerator operation for removal of moisture and secondary products.

INSTALLATION AND INTEGRATION OF INDUS-2

Sanjay Chouksey[#], S. Kotaiah, S. S. Prabhu, Sridhar R, Vijendra Prasad,
S. K. Shukla, D. P. Yadav: R. R. C.A.T., Indore 452013, India

Abstract

The Synchrotron Radiation Sources consists of a large number of components of varying nature. Some components are light but highly delicate whereas some are big and heavy. However all components need a careful handling during their installation. Unit-cell mock-up assembly and virtual simulation of the installation process using software tools contributed significantly in visualizing various handling schemes, checking interferences and defining the assembly sequences. We have recently completed the installation and integration of 2.5 GeV Synchrotron Radiation Source, Indus-2, by adopting a set procedures of installation and pre-defined sequences. This paper presents an overview of procedures, sequences of assembly, equipments and toolings used for material handling and safety precautions taken during the whole task of installation and assembly.

INTRODUCTION

Indus-2 is a 2.5 GeV, 300mA electron storage ring designed for production of hard x-rays. It consists of 8 unit cells (or super periods) with a total circumference of 172.474 meter Each unit cell has two 22.5° bending magnets, a triplet of quadrupoles in the achromat section, two quadrupole in the long straight sections and four sextupoles in the achromat section..

Table 1: Components details for installation

Components	Approx. size (meter), Weight (kg)	
Dipole (16 Nos.)	2.2x1.35x0.88, 10000 kg	
Dipole vacuum chamber (16 Nos)	3.57x0.65x0.1, 300 kg	
Support Girders	Short straight section (8 Nos.)	6.5x0.92x0.37, 1500 kg
	Long straight section (16 Nos.)	3.25x0.92x0.37 1000 kg
	Dipole girder (16 Nos.)	1.83x0.84x0.47 1500 kg
	TL-3 Support (20 Nos)	3.0x0.58x0.8, 1000 kg
Quadrupole (72 Nos.)	0.56x0.86x0.8, 1500 kg	
Sextupole (32 Nos.)	0.78x0.3x0.75, 1000 kg	
Septum Magnets	1.3x0.6x0.6, ~1000 kg	

A total 27 number of beam lines are planned to tap the

[#]chouksey@cat.ernet.in

synchrotron radiation from Indus-2 for various purposes. (Ref.1). The electron beam from booster synchrotron is injected into Indus-2 through 65 meter long Transport line-3, which consists of 3 dipoles, 18 quadrupoles and 24 independent steering magnets (12 horizontal + 12 vertical). Major components for installation in Indus-2 with their critical features are given in Table 1.

The task of Installation of Indus-2 was much more complex due to narrow circular ring tunnel and severe restrictions on availability of space. The installation work started after the construction of the civil building (12000 Sq m) and was accomplished in stages (fig 3).

SEQUENCE OF INSTALLATION

Machine Component Installation

Installation of Indus-2 and Transport line-3 components can be broadly divided in two groups i.e. magnet and vacuum components. R.C.C. foundation is specially designed and constructed for this purpose with passive isolation of sensitive magnetic lattice from rest of the floor by using a sand blanket. Embedded Plate (MS) of 250 mm X 250 mm are provided in the ring floor to bear the large static loads of magnets and other components. After completion of the construction work, concrete floor adjacent to EPs was leveled to ensure uniform load distribution.

Installation of Support Girders & Alignment jacks

Threaded holes were drilled on the Floor Embedded plates (120 Nos.) for fixing the dipole girders and straight sections girder-jacks to make the machine foundation ready for installation. The positions of these holes were controlled by a combination of specially made template and theodolite equipped with distance meter. Afterward all dipole girders and straight section jacks were installed and anchored with these holes. Subsequently the straight section girders were installed on their jacks. References for drilling holes, for fixing of Transport line–3 support structures (20 nos.), were taken from the footprint marked as per designed location of TL-3. All support structures were first anchored to TL-3 RCC foundation.

Installation of Magnetic Components

Dipole magnets were the heaviest component for installation in the tunnel ring (fig 1). These magnets were transported by a truck in the Indus-2 building and there unloaded by 10 MT fixed hoist over a suitably designed transit trolley, used for transporting the magnets inside tunnel area. In the tunnel area they were transported to their designed locations by 10 MT EOT crane. A special fixture for handling and storing of multipoles was

MULTIPACTING STUDY OF LINAC PREBUNCHER AT CAMD*

Y. Wang[#], CAMD, Baton Rouge, LA 70806, USA.

Abstract

   Multipacting currents can absorb RF energy and produce breakdown in the prebuncher cavity of CAMD linac. This phenomenon starts when the magnetic field to focus the electron beam is applied [1]. The multipacting has been studied in different magnetic field and RF electric field, and can be eliminated by RF processing. In the paper, the theoretical and experimental results of multipacting study will be presented; moreover, the operability of the system will be analyzed.

INTRODUCTION

   A 500 MHz pillbox cavity in the linac [1] acts as the prebuncher, which is excited to a TM_{010} mode to produce an accelerating field. It can remove the unused electrons for the storage ring [2-3]. The cavity main specifications in operation are listed in Table 1.

Table 1: Prebuncher Specifications

Electron energy	50keV
Frequency	499.7MHz
Peak field	100kV
Cavity gap	9cm
Pulsed power	4.75kW
β	1
Q	4360
Filling time	5.6uS

EXPERIMENT SETUP

   The prebuncher RF system in the linac is shown in Figure 1. In order to produce proper RF power for the cavity, there are a 500MHz, 54 dB, 250 W, pulsed amplifier and a 500MHz, 16 dB, 5 kW, pulsed amplifier to amplify the 500MHz, 0 dBm, CW signal coupled from storage ring master signal generator.

0dBm
IN
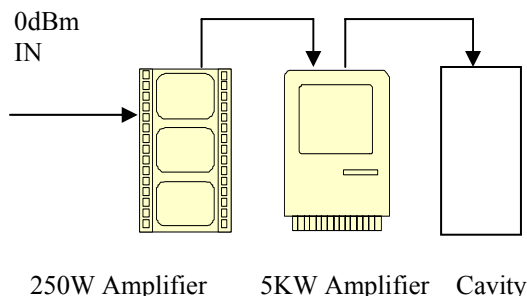
250W Amplifier   5KW Amplifier   Cavity
Figure 1: Diagram of the experiment.

   The RF output waveforms from the two amplifiers are

shown in Figure 2. The top one is the RF output of the 500MHz, 54 dB, 250 W, pulsed amplifier, and the bottom one is the RF output of the 500MHz, 16 dB, 5 kW, pulsed amplifier. The 30 μS pulse length is required by the cavity filling time in Table 1.
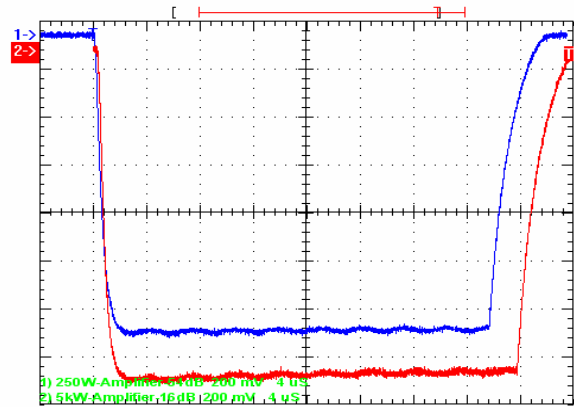
Figure 2: The RF output.

PRELIMINARY EXPERIMENT RESULTS

   The RF system of prebuncher was tested and cavity was conditioned by RF power during recommissioning prebuncher. But when attending to operate the prebuncher work, multipacting in the cavity started when the power supplies for the focusing coils which generate magnetic field perpendicular to cavity surfaces in the buncher were turned on. In Figure 3, the signal is gotten by a coupler in the prebuncher cavity, the bottom waveform is without power supplies on, and the top one is with the power supplies on.
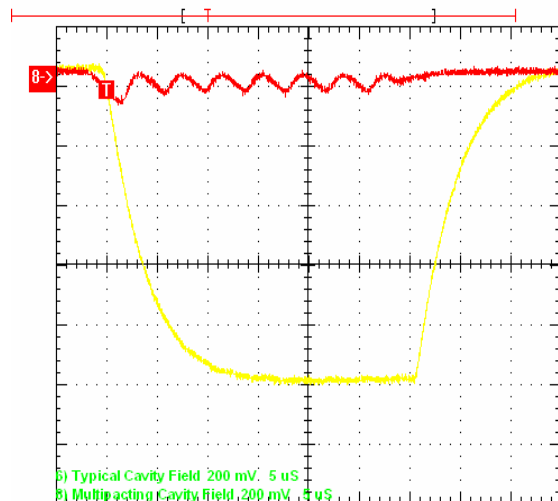
Figure 3: Cavity field.

   In order to condition the cavity, the multipacting has been studied in RF power vs. magnetic field as shown in

THE PROTON AND ION LINEAR ACCELERATOR ILU-9

V.G. Abdulmanov, V.L. Auslender, A.A. Bryazgin, F.A. Emanov, E.S. Konstantinov,
A.D.Panfilov, V.S. Podobaev, B.L. Faktorovich, V.G. Cheskidov
BINP, Novosibirsk, Russia

Abstract

The pulse RF ion linear accelerator of ILU-9-type is described. The accelerator is intended to use for various radiation-technological processes and investigations. The parameters of the accelerator and the ion beam measured during the tuning are given.

INTRODUCTION

The proton and ion linear accelerator ILU-9 was designed basing on experience gained in BINP SB RAS, Novosibirsk, during development, production and operation of single-resonator pulse radio frequency linear accelerators of ILU series. This machine is purposed for work as an injector for accelerating complexes for research, technological and medical application. The pulse duration required for synchrotron injection is 5 mks, energy – more than 2 MeV.

Figure 1: View of the vacuum tank and resonator inside it, RF generator is removed

Views of the ILU-9 vacuum tank and resonator inside it and RF generator with power input loop are shown in Fig.1 and Fig.2. Distinctive features of this machine are simplicity of design, convenience of operation and reliability at long work. The machine is designed to accelerate ion beams with Z/A = ½ up to energy 5.8 MeV per charge unit in the main channel, the other options are the possibility of proton beams acceleration up to energy 2.9 MэB and ion beams with Z/A = 1/3 acceleration up to energy 8,7 MeV per charge unit at injection energy of 70 keV. After passage of magnetic turning system and acceleration in the additional channel the particles energy makes: 9.8 MeV per charge unit for ions with Z/A = ½, 14.7 MeV per charge unit for ions with Z/A = 1/3 and 4.9 MeV for protons.

Figure 2: RF generator with power input loop

ACCELERATING STRUCTURE

The design of the accelerator is shown in Fig.3. The machine is based on radio frequency (RF) resonator performed as an antiphase excited quarter wave asymmetrical shielded pair line. The upper sides of the double lines 1 are shortened by a disk 5, the other ends of the lines are loaded by capacity of drift tube 2. The main accelerating channel contains eight accelerating gaps and six drift tubes having the lengths determined by acceleration rate.

Lengths of accelerating gaps in the initial part of acceleration path are calculated so that the first gap transit angle is close to π at the given electric field tension. The drift tubes' lengths are growing along the beam line due to increase in particles' speed as passing the accelerating gaps with the acceleration period of $\beta\lambda/2$ (β=v/c, λ – length of a wave of the resonator) so the accelerating rate is decreasing. To keep the constant accelerating rate with the same accelerating electric field tension in all accelerating gaps it is necessary to increase the voltage on the last accelerating gaps by increasing their length. This problem is solved by a proper choice of double line design values.

08 Applications of Accelerators, Technology Transfer and Industrial Relations

T24 - Industrial Collaboration

RF ACTIVITIES OF ACCEL INSTRUMENTS IN ASIA-PACIFIC

M. Pekeler, K. Dunkel, M. Peiniger, C. Piel, H. Vogel, P. vom Stein
ACCEL Instruments GmbH, D-51429 Bergisch Gladbach, Germany

Abstract

Since the foundation of ACCEL Instruments, Asia-Pacific has been an important market for RF, magnet and x-ray beam line devices. For the RF activities, pioneering work was done for JAERI, where complete superconducting RF modules where designed, built, tested and delivered. An important step for industrialization of superconducting RF modules was done, when NSRRC decided in 2000 as the first Light Source, to contract turn key superconducting 500 MHz modules of the Cornell design to ACCEL. Similar modules have been delivered in the meantime to CLS, Cornell and DLS and three more will be delivered to SSRF in Shanghai next year. Peking University is planning to use a Rossendorf design superconducting RF module housing two 1.3 GHz TESLA cavities for the operation of their FEL project. On the normal conducting RF systems, a complete 3 GHz 100 MeV linac has been delivered to ASP together with the 500 MHz booster cavities and the LLRF system. Booster cavities and LLRF system will be also delivered for SSRF. For SOREQ in Israel, ACCEL is developing a complete superconducting 40 MeV proton/deuteron linac. The first stage of this linac is currently under delivery and installation.

SUPERCONDUCTING 500 MHZ MODULES FOR JAERI

In the Asia-Pacific region, ACCEL is so far mostly supplying complete accelerator systems rather then single accelerator components like cavities or couplers. A good example already from the early 90's is the supply of turn key superconducting accelerator modules for JAERI.

Figure 1: Superconducting accelerator module housing one 5-cell 500 MHz module completely assembled and tested prior shipment to JAERI site.

JAERI decided in 1991 to order 4 superconducting 500 MHz modules, two modules housing a single cell cavity and two modules housing a 5 cell cavity. The complete design of the module was done in industry. As the modules are operated at a very low duty cycle of maximum 3 %, the RF losses are below 1 W and the modules were designed for as low as possible static losses. Two thermal shields at 20 K and 70 K were designed and each module is able to be cooled by a power of 4 W cryocooler at 4.5 K.

All modules were RF tested in house prior delivery and then shipped to JAERI site in 1993. The modules are still in operation at an operating gradient of 5 MV/m with Q values above 10^9. A RF coupler with external Q tunable from 10^5 to 10^9 was developed. Fig 1 shows one module prior delivery to JAERI site.

SUPERCONDUCTING 500 MHZ MODULES FOR LIGHT SOURCES IN TAIWAN AND SHANGHAI

In 2000 NSRRC decided as the first Light Source to take benefit of superconducting cavities. The decision finally was made to order two superconducting 500 MHz modules of the Cornell type design. ACCEL had agreed with Cornell University on a technology transfer and was thus able to produce those modules as a turn key system including the SRF electronics and the cryogenic valve boxes needed for helium bath pressure and level control In the same year also the Canadian Light Source and Cornell University itself ordered two more modules each. Diamond Light Source ordered three more modules in 2003 and Shanghai Light Source three more in 2005.

All modules are delivered with guaranteed values of about 2 MV accelerating voltage and can provide more than 250 kW of RF power to the beam. The cryogenic loss (static loss plus RF dissipation) is specified to be below 100 W. All modules for NSRRC, CLS, Cornell and Diamond are delivered; the first module for Shanghai Light Source will be shipped in the middle of 2007.

The cavities and the windows of the SRF module are tested separately prior assembly and have passed the acceptance test already. Figure 2 shows one of the NSRRC module prior shipment to Taiwan and during installation into the NSRRC storage ring.

During the last 6 years, the Cornell type module has developed into a product and the SRF electronic has been further improved and upgraded with state of the art data logging (S7) and interlock application. The installation, integration with helium plant and klystron and taking into operation of a module can be done within a time period of 4-6 weeks.

STATUS OF BINP AMS FACILITY

M.V. Petrichenkov, A.D. Goncharov, V.F. Klyuev, S.G. Konstantinov, A.V. Kozhemyakin,
A.M. Kryuchkov, V. V. Parkhomchuk, S.A. Rastigeev, V.B. Reva, BINP, Novosibirsk, Russia

Abstract

Present status of the accelerator mass spectrometer (AMS) facility at BINP is described. The AMS facility is dedicated for precise measurements of isotopes ratios. The scheme of the facility includes negative ion source, electrostatic tandem accelerator with accelerating voltage up to 2 MV and magnesium vapors stripper and also includes the high-energy and low-energy beam lines with analyzers. There is an additional beam separator (180°bend) with crossed electric and magnetic fields in high voltage terminal of tandem accelerator. The results of experiments on ion beams acceleration, stripping and selection are given.

INTRODUCTION

The accelerator mass spectrometry is a powerful method of isotopic analysis for archaeology, environment science, biomedical applications and etc.

The specialized building for AMS center is being prepared now. The accelerator will be placed in the underground room for radiation shielding. It will allow operation with accelerating voltage 0.5 MV and higher after May 2007.

The AMS is based on the electrostatic tandem accelerator. The AMS system consists of the negative ion source, low energy beam line, tandem accelerator and high-energy beam line. The low energy beam line is used for initial isotope selection. The tandem accelerator is used for molecular ions removal and, of course to obtain the required beam energy for the final detector.

The negative ion beam is horizontally extracted from the ion source. Then the beam is analyzed in low-energy beam line by 90° double-focusing magnet and injected vertically into the first accelerating tube. After acceleration negative ions are stripped into plus charge state in magnesium vapors stripper. The ions of 3+ charge state will be used for isotope analysis of Carbon–14. It requires 1.5-2 MV terminal voltage for necessary C^{3+} yield. Then they pass through the middle energy separator (180° combined bend with crossed fields) and are accelerated again in the second accelerating tube. The accelerated ions are analyzed in high-energy beam line by 90° double-focusing magnet and putted horizontally to the final detector.

The most distinguishing features of BINP AMS facility are the use of the middle energy separator (180° beam bend with crossed fields in HV terminal) of ion beams and the magnesium vapors target as a stripper. The aim of these innovations was described earlier [1].

LOW ENERGY BEAM LINE

Some modifications of low energy beam-line are to be made very soon. The gate valve will be installed just after the ion source to provide quick replacement of ion sources for their cleaning and samples change. Now the gate valve is located only at the exit of the bending magnet and vacuum conditions can be obtained during three-hour period after attachment of the ion source by 250 l/s turbo pump. In addition, the low-energy line will be equipped with a differential pumping system to decrease the gas flow from ion source to the beam line. The RGA system is installed after bending magnet for residual gas analysis in injection channel. At present time, the vacuum in the injection channel is $\sim 10^{-6}$ Torr with sputter ion source.

TANDEM ACCELERATOR

The AMS tandem accelerator is a folded type vertical machine with 180° bending system in the high voltage terminal where the beam is pre-selected at medium energy in crossed electric and magnetic fields. It consists of electrostatic 180° bending system with 40 cm orbit radius. The cylindrical electrostatic plates with 2.5 cm width and 1 cm pole gap are placed into vacuum chamber. The operation at required 30 kV/cm field of bending system has been demonstrated. The 180° dipole magnet with up to ~600 Gs field surrounds the vacuum chamber with electrostatic plates.

The magnesium vapors stripper has worked more than 600 hours in the BINP AMS facility under 450°C average temperature without refilling the magnesium. The precise system for magnesium target positioning developed in 2006 works well. The transverse position of the target is adjusted by the beam transmission. For this purpose, the bellows are placed at the entrance and exit of the magnesium target. The stripper channel has the inner diameter of 3 mm and puts the main limitation on the beam transfer.

The 500W gaseous turbine generates the power used in the terminal. The circuits of four electrostatic dipoles, 180° bend and three ion pumps are supplied by this turbine. Special unit for magnesium stripper temperature stabilization has been developed and tested. It allows to decrease significantly the pulse load on turbine and its circuits. The control and management of this electronics is realized through optical link by ADAM modules. The 15 l/s ion pump is installed just after 180° bend. The vacuum in tandem accelerator is kept better than 10^{-6} Torr. The gas pressure is measured by ion pump currents. The gate valve is placed after 180° bend. The

08 Applications of Accelerators, Technology Transfer and Industrial Relations
U02 - Materials Analysis and Modification

TARGET ASSEMBLY AND NEUTRONICS DESIGN STUDY FOR THE INDIAN SPALLATION NEUTRON SOURCE USING NMTC/JAM CODE*

V.K. Senecha[1#] and Masayoshi Kawai[2], [1]Power Supply Division, RRCAT, Indore, India;
[2]Institute of Material Structure Science, KEK, Ibaraki, Japan

Abstract

Target-moderator-reflector assembly (TMRA) design studies for the best neutronics performance of the proposed Indian Spallation Neutron Source (ISNS) have been carried out using high energy particle transport code NMTC/JAM. The issues relevant for TMRA design like selection of target material, effect of target shape and dimensions and placement of moderator, suitable material for reflector its size have been addressed using the code calculations. Code calculations have shown that the neutron yield per proton for thick Pb target and for varying target lengths are in good agreement within the error limit with the results reported by the experimental group and matching with the results of JAERI code calculations (JAERI –Data/code 2001-07). Different geometrical configurations for TMRA were attempted and resulted tallies for track-length, surface crossing, nuclide yield, heat deposition, and time for the neutrons have been calculated. It has been observed that wing type structure of moderator position with respect to the target is suitable for optimum neutron yield in the pulsed mode.

INTRODUCTION

Raja Ramanna Centre for Advanced Technology (RRCAT) is planning to establish a 1 GeV proton beam rapid cycling synchrotron (RCS) accelerator facility at Indore. The proton beam from the RCS will be directed towards the spallation target station which will produce intense pulsed neutrons as a complementary probing tool compared to x-rays from the synchrotron radiation source. Internationally, few such facilities are operational and efforts are being made towards development of advanced neutron sources that will revolutionize the future prospects in the basic science, material science, biology and new technologies. As next generation neutron sources are under advanced stages of construction at ORNL and JPARC which will exceed the neutron intensity level in the pulsed mode by nearly 1-2 orders of magnitude higher than the highest intensity available till date by the high flux nuclear power reactors (ILL). The neutron scattering experiments will be carried out at much higher resolution and efficiency level and in the wider range of wavelength and momentum to cover applications in almost all branches of science be it chemistry, physics, biology or material science. In the present study related to design of Indian Spallation Neutron Source (ISNS) the high energy proton beam interaction with the high atomic number solid targets have been performed using the

NMTC/JAM code developed by the JAERI [1]. The TMRA design study involves evaluating best neutronics performance by selecting suitable target material its dimensions, position of moderators, reflector material its size and thermal energy deposition and related parameters that will be suitable for ISNS.

PROPOSED ISNS PARAMETERS

The conceptual design of the spallation neutron source is based on the 1 GeV proton beam extracted out of the RCS. Typical parameters of the system are as below:

RFQ Injection Energy (keV)	50 keV
DTL Injection	4.5 MeV
RCS Injection Energy (MeV)	100 MeV
Beam Energy on Target	1.0 GeV
RCS Repetition Rate	25 Hz
Average Beam Current	100 µA

NMTC/JAM CODE CALCULATIONS

NMTC/JAM can simulate transport of nucleons, mesons, baryons, leptons as well as their anti-particles through a given medium using Monte Carlo technique. It allows any target nucleus to be used for the material in the medium except the light ions like He^3 and α and heavy ions.

Maximum energy of the particle transporting in a medium is limited to 200 GeV for all transport particles, while the minimum energy is restricted to 20 MeV for neutrons and 0.1 MeV for other particles. The cut-off neutrons below the limit of nuclear models can be stored along with phase space information data of each such neutrons can be stored in a file for subsequent transport calculations using the MCNP4A code. A user supplied source routine is required to read the phase information data of individual cut off neutrons and photons in the MCNP4A code.

In order to check the validity and accuracy of various models used in the NMTC/JAM code, we have performed the simulations of a proton beam (12 GeV energy) interactions with the cylindrical lead target with 20 and 10 cm diameter and 60 cm length. These parameters were chosen so that it can be compared with the experimental results obtained at KEK using the Mn-bath moderation method. Neutron yields data are derived experimentally by changing the target length in steps of 10 cm. First we

ACTIVITIES ON THE NUCLEAR DATA MEASUREMENT AT THE POHANG NEUTRON FACILITY BASED ON ELECTRON LINAC [*]

G.N. Kim[#], A.K.M.M.H. Meaze, and M.U. Khandaker

Department of Physics, Kyungpook National University, Taegu 702-701, Korea

Y.D. Oh, H.S. Kang, M.H. Cho, I.S. Ko, and W. Namkung

Pohang Accelerator Laboratory, POSTECH, Pohang 790-784, Korea

Abstract

We report the present status of the Pohang Neutron Facility which consists of an electron linear accelerator, a water-cooled Ta target, and a 12-m time-of-flight path. We measured the neutron total cross-sections in the neutron energy range from 0.1 eV to few hundreds eV by using the neutron time-of-flight method. A ^{6}LiZnS(Ag) glass scintillator was used as a neutron detector. The neutron flight path from the water-cooled Ta target to the neutron detector was 12.1 m. The background level was determined by using notch-filters of Co, In, Ta, and Cd sheets. In order to reduce the gamma rays from bremsstrahlung and those from neutron capture, we employed a neutron-gamma separation system based on their different pulse shapes. The present measurements of Ta, Hf, Ag, and Mo samples are in general agreement with the evaluated data in ENDF/B-VI.

INTRODUCTION

The Pohang Neutron Facility (PNF) was proposed in 1997 and constructed at the Pohang Accelerator Laboratory on December 1998 [1]. It consists of a 65-MeV electron linac, water-cooled Ta neutron producing target, and a 12-m-long evacuated vertical flight tube leading to the detector location. The electron linac consists of a thermionic RF-gun, an alpha magnet, four quadrupole magnets, two SLAC-type accelerating sections, a quadrupole triplet, and a beam-analyzing magnet. The overall length of the linac is about 15 m. As a photoneutron target, we choose a tantalum, which has advantages of high density (16.6 g/cm^3), high melting point (3,017^{o}C), and high resistant against the corrosion by cooling water. The characteristics of PNF are described elsewhere [2].

We report the measured neutron total cross-sections of natural Ta, Hf, Ag, and Mo in the neutron energy range between 0.1 eV and 100 eV by using the neutron time-of-flight (TOF) method at the PNF. The results were compared with other measurements and the evaluated data in ENDF/B-VI.

POHANG NEUTRON FACILITY

The Pohang Neutron Facility (PNF) consists of an electron linac, a water-cooled Ta target, and an 11 m long TOF path. The electron linac consists of standard subsystems: a thermionic RF-gun, an alpha magnet, four quadrupole magnets, two SLAC-type accelerating sections, a quadrupole triplet, and a beam-analyzing magnet. The overall length of the linac is about 15 m. The RF-gun is one cell cavity with a dispenser cathode of 6 mm diameter. The RF-gun produces electron beams of 1 MeV, 300 mA, and 1.5 µs [3]. The alpha magnet is used to match the longitudinal acceptance from the RF-gun to the first accelerating section. Electrons move along an alpha-shaped trajectory in the alpha magnet with the bend angle of 278.6^o. Four quadrupole magnets are used to focus the electron beam in the beam transport line from the thermionic RF-gun to the first accelerating section. The quadrupole triplet installed between the first and the second accelerating sections is used to focus the electron beam during the transport to the experimental beam line at the end of the linac.

A water-cooled Ta target was designed by the Electron Gamma Shower simulation code, EGS4 [4]. The Ta target was composed of ten Ta sheets, 49 mm in diameter and 74 mm in total length [5]. There was 1.5 mm water gap between Ta sheets in order to cool the target effectively. The target housing was made of 0.5 mm thick titanium. The calculated conversion ratio from a 100 MeV electron to neutrons was 0.032 obtained by using the EGS4. According to this result, the neutron yield per kW beam power for the electron energy above 40 MeV at the target was 2.0×10^{12} n/sec, which was about 2.5% lower than the calculated value based on the Swanson's formula, 1.21×10^{11} $Z^{0.66}$, where Z is the atomic number of the target material and the electron energy is above 40 MeV [6].

Since we have to utilize space and infrastructure at PAL, an 12 m long TOF path and a detector room were constructed vertically to the electron linac. The TOF tubes were made by stainless steel with two different diameters of 15 and 20 cm.

08 Applications of Accelerators, Technology Transfer and Industrial Relations

U04 - Other applications

PRESENT STATUS OF THE FFAG ACCELERATORS IN KURRI FOR ADS STUDY

M. Tanigaki*, Y. Mori, M. Inoue, K. Mishima, S. Shiroya
RRI, Kyoto University, Kumatori, Osaka 590-0494, Japan
Y. Ishi, S. Fukumoto, Mitsubishi Electric Corporation , Kobe, 652-8555, Japan
S. Machida, CCLRC/RAL, Chilton, Didcot, Oxon, OX11 0QX. UK

Abstract

KART (Kumatori Accelerator driven Reactor Test) project has started at Kyoto University Research Reactor Institute (KURRI) from the fiscal year of 2002. The purpose of this project is to demonstrate the basic feasibility of ADS, studying the effect of incident neutron energy on the effective multiplication factor of the subcritical nuclear fuel system. A proton FFAG accelerator complex as the neutron production driver for this project is now in the final stage of the test operation.

INTRODUCTION

As a substitute for the 5 MW reactor at Kyoto University (KUR), a neutron source based on the Accelerator Driven Sub-critical Reactor system (ADSR) concept has been proposed in 1996[1]. The conceptual design study on ADSR using the MCNPX code clarified the lack of reliable effective multiplication factor k_{eff} in the proton energy region between 20 MeV and 150 MeV. Since our current experimental studies are limited to those with a 300 keV Cockcroft-Walton accelerator[2, 3], a proton beam source which covers between 20 MeV and 150 MeV is required to extend our study on ADSR system.

A Fixed Field Altenating Gradient (FFAG) accelerator orignally proposed by Ohkawa 40 years ago[4] has a lot of advantages compared to synchrotrons such as a large acceptance, a possible fast repetition rate because of no active feed back in the acceleration. In ADS system, the stability of beam acceleration is directly connected to the stability of reactor itself. In such meaning, FFAG accelerators can be a good candidate for the neutron source driver in ADS system.

While an FFAG has a potential to a neutron source driver, there are still technical difficulties in FFAG accelerators, such as the lack of wide band high voltage RF cavity or the short straight section insufficient for beam injection and extraction. Mori has demonstrated that these difficulties can be overcome by recent developments [5], [6] with the successes of a 500 keV PoP FFAG and an 150 MeV FFAG with RF.

On such basis of our study and the technical developments on FFAG, KART project has been approved and started from the fiscal year of 2002. In this project, a practical proton FFAG accelerator complex of $E_p = 20 \sim 150$

* tanigaki@rri.kyoto-u.ac.jp

MeV as a proton driver for ADSR is constructed in KURRI and the basic feasibility of ADSR system and the multiplication factor k_{eff} in the energy region of $E_p = 20 \sim 150$ MeV will be studied.

FFAG ACCELERATOR COMPLEX

The FFAG accelerator complex for KART project consists of one FFAG with an induction acceleration as the injector and two FFAG with RF as the booster and main accelerators, respectively. Basic specifications for this FFAG complex are summarized in Table 1. The layout of these FFAG accelerators in the accelerator room is shown in Fig. 1. All of these accelerators will be in pulse operation up to the repetition rate of 120 Hz. The beam energy of the current FFAG complex can be varied between $20 \sim 150$ MeV by the change of beam energy from the injector.
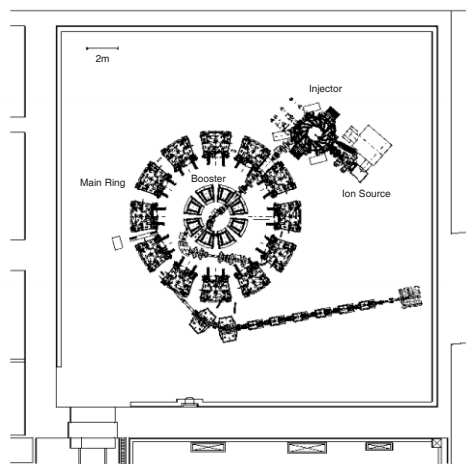
Figure 1: FFAG complex at KURRI.

Ion source and injector FFAG with induction acceleration

H^+ ions are extracted from the typical multi-cusp type ion source and accelerated to 100 keV, then transported to the injector. Since all of the FFAG complex are operated in the pulse mode, the ion source itself is also operated in the pulse mode for less power consumption. The arc voltage is pulsed at the duty of $\sim 10\%$, then the pulsed beam is

DESIGN AND FABRICATION OF ARUPS U6 UNDULATOR AT PLS

H.G.Lee, H.S.Suh, H.S.Han, Y.G.Jung, W.W.Lee, K.H.Park, D.E.Kim, C.W.Chung
Pohang Accelerator Laboratory, POSTECH, KOREA

Abstract

Pohang Accelerator Laboratory(PAL) had developed and installed U6 undulator recently to utilize brilliant undulator radiation for ARUPS (Angle Resolved Ultraviolet Photoemission Spectroscopy) beamline at Pohang Light Source (PLS). The U6 is a hybrid type device with period of 6 cm, minimum gap of 18 mm, maximum flux density of 0.902 Tesla and total magnetic structure length of 1830 mm. The support locations and structure of an insertion device are optimized to achieve a minimum deflection due to the magnetic loads. A Finite Element Analysis (FEA) is performed to find out the amount of maximum deflection and optimal support positions on the backing beam. The optimized maximum deflection is estimated to be about 11.6 μm, while the deflection before any optimization is 48.8 μm. In this report, all the mechanical design, fabrication and assembly details of the PLS U6 undulator are described.

INTRODUCTION

Pohang Light Source (PLS) is a 2.5GeV 3rd generation synchrotron light source [1]. The critical photon energy of the synchrotron radiation from bending magnet is about 5.48 keV at 2.5 GeV electron energy. U6 is designed for research on the electronic structure of solid surfaces and low dimensional nanostructures on surfaces. Using one sagittal focusing mirror and a specially designed chamber where a tube is passing through, brilliant UV and soft x-rays from two undulators can be efficiently delivered to the ARUPS system. The total energy resolution is about 10 meV at 20 eV photon energy.

The U6 consists of a magnetic structure, a support structure, and a drive and control system. Magnetic gap is adjusted by the drive system and the support structure, which includes the L-frame to support the magnetic structure. The L-frame structure is designed to allow for easy installation of the vacuum chamber and for easy magnetic field measurement. The U6 shown in figure 1 was designed with very rigid moment of inertia to length ratio resulting in minimum deflection. To reduce the deformation further, we designed and successfully implemented a Belleville washer springs system that counteracted the magnetic loads[2]. The compensation spring system will reduce the system friction, which gives better positional response from the drive system, reduced structure compression and no motor holding torque required at any magnetic gap. The drive system

provides the gap adjustment mechanism to align the magnetic structure from gap 1.0 to 20.0 cm. The drive system includes two independent drive system in a standard structure. Each drive system is composed of step motor, gear reducer and absolutely rotary encoder. The positional accuracy is determined by two encoders attached on both ends of a ball screw. The measured gap repeatability is less than 7 μm. Five types of insertion device (U7, EPU6, U10, MPW14 and ARUPS U6) had been installed in the electron storage ring. The U6 described in this report is similar to other types of insertion device and built on the successful mechanical design concept, fabrication and assembly procedure

MAGNETIC STRUCTURE

The hybrid magnetic configuration consists of permanent magnets and ferromagnetic poles (vanadium permendur) to concentrate the magnetic flux to the poles. This hybrid scheme gives a higher peak field compared to pure permanent magnet structures. Using Radia developed in ESRF, magnetic geometry analysis have been carried out to study the optimal magnetic geometry. In the final design, the maximum magnetic field is 0.902 Tesla. Multiple trim magnets at the ends of the undulator will be installed to decrease the transverse multipole components and to correct the field integrals. The main parameters of U6 are listed in Table 1, and the schematic geometry configuration of half period is shown in figure 2.

The basic block of the magnetic structure is a half-period pole assembly which consists of an aluminium keeper, a Vanadium Permendur pole and six Nd-Fe-B magnetized blocks.

Table 1: Main parameters of the U6 based on 2.5GeV beam energy and 250mA beam current

Parameters	Value
Period length	6 cm
Number of full field poles	57
Peak field	0.902 Tesla
Total power	1.452 kW
Device length	1.83 m
Min. gap of magnetic structure	18 mm
Max. gap speed	10 mm/sec
Nominal gap speed	5 mm/sec
Max. magnetic load	2.4 Tons
Encoder type	Absolute rotating encoder
Encoder resolution	1.3 μm
Step motor	2-phase stepper motor
Motor resolution	< 1 μm/step

08 Applications of Accelerators, Technology Transfer and Industrial Relations

U04 - Other applications

ELECTRON ACCELERATOR OF ELV-TYPE AND THEIR WORLDWIDE APPLICATION

Yu.I. Golubenko, N.K. Kuksanov, P.I. Nemytov, R.A. Salimov,
S.N. Fadeev, M.E. Veis, V.V. Prudnikov
Budker Institute of Nuclear Physics SB RAS Lavrentyev av. 11, Novosibirsk, 630090, Russia

Abstract

Beginning from 1971, the Budker Institute of Nuclear Physics Siberian Branch of Russian Academy of Science started its activity in the development and manufacturing of electron accelerators of the ELV-type for their use in the industrial and research radiation-technological installations. The ELV-type accelerators were designed with use of the unified systems and units enabling thus to adapt them to the specific requirements of the customer by the main parameters such as the energy range, beam power, length of extraction window, etc.. INP proposes a series of electron accelerators of the ELV-type covering the energy range from 0.3 to 2.5 MeV with a beam of accelerated electrons of up to 450 mA and maximum power of up to 400 kW. The design and schematic solutions provide the long term and round-the -clock operation of accelerators under the conditions of industrial production processes. The ELV accelerators are most popular accelerators not only in Russia, but in China, Korea, and etc.

INTRODUCTION

The main features of ELV-accelerators are as follows:

1. High power of electron beam in wide energy range, it means high productivity of EB processing;
2. High efficiency of conversation of electricity power to electron beam power. The efficiency is limited by frequency converter and in case of transistors frequency converter efficiency is increased up to 85-92%;
3. Simple procedure of accelerator control by operator due to control system based on IBM compatible computer. It allows operating accelerator in on-line mode.
4. Accelerator control system comprises a set of software and hardware covering all the accelerator units required an operative control and diagnostics.
5. Accelerator itself has simple design and high reliability. If some troubles appear our customers repair accelerator by themselves with our consulting by phone, as a rule.
6. After warranty service. It means we delivery spare parts or parts with limited lifetime or make any accelerator service after warranty period by separate contracts with the low price.
7. A set of additional equipment (such as transportation line, ring or double side irradiation system, 4-side irradiation system) increases the accelerator possibility.

8. ELV accelerators are stable in operation. The energy and beam current instabilities practically do not exceed +/-2%.

Basic parameters of the ELV-type accelerators are given below at the Table1. and ELV-4 is sown at Fig1.

Table1

	Energy range, MeV	Beam power, kW	Max. beam current, mA
ELV-0.5	0.4 - 0.7	25	50
ELV-1	0.4 - 0.8	25	50
ELV-2	0.8 - 1.5	20	25
ELV-3	0.5 - 0.7	50	100
ELV-4	1.0 - 1.5	50	50
ELV-6	0.8 - 1.2	100	100
ELV-8	1.0 - 2.5	90	50
ELV-6M	0.75 - 0.95	160	200
ELV-12	0.6 - 0.9	400	500

By now, over 100 accelerators had been delivered inside of Russia and abroad.

50 accelerators were delivered inside of former USSR
33 accelerators were delivered in China
12 were delivered in Korea
2 accelerators were delivered in Japan
2 accelerators were delivered in Poland
1 accelerators was delivered in Germany
1 accelerators was delivered in Chech Republic
1 accelerators was delivered in Bulgaria,
2 accelerators are delivering in India, and etc..

On international market we have strong competition with other firms producing accelerators. But number of delivered ELV accelerator during last 5 years is more than any others delivered accelerators. Many firms prefer to buy new ELV accelerator. So there are many plants where ELV accelerators are operating at same place and conditions with NHV and RDI accelerators.

ACCELERATOR BASED APPLICATIONS AT BARC-TIFR PELLETRON ACCELERATOR FACILITY

P.V.Bhagwat, P.Surendran, A.K.Gupta, J.P.Nair, S.C.Sharma, A.Shrivastava, N.G. Ninawe,
M.L.Yadav, A. Shanbhag[†], R.M.Kale*, S.K.Sarkar*, J.A. Gore, S. G. Kulkarni, N. Mehrotra,
Ramlal, Q.N. Ansari, U.V. Matkar, Ramjilal, , R.N Lokare, M. Ekambaram, Hillary Sparrow,
N.T.Jadhav, S.B.Salvi, M.B.Kurup*, R.K.Choudhury, S.Kailas and V.C.Sahni
Nuclear Physics Division,
[†]Radiation Safety Systems Division
Bhabha Atomic Research Centre, Mumbai-400 085.
*Tata Institue of Fundamental Research, Mumbai-400 005.

Abstract

The 14 UD Pelletron Accelerator, set up as a collaborative effort between Bhabha Atomic Research Centre and Tata Institute of Fundamental Research, has been operational since it's inception in 1989. Apart from basic research, various accelerator based programmes including accelerator mass spectrometry, production of track-etch membranes, production of radio isotopes, irradiation damage studies are being pursued. This contribution will describe the details of currently ongoing programmes.

ACCELERATOR MASS SPECTROMETRY

Accelerator mass spectrometry (AMS) is an ultra sensitive method of counting individual atoms having sufficiently long half life and available in low abundance. The medium energy tandem accelerator of this kind is an ideal machine to carry out AMS studies with heavy species like ^{36}Cl, ^{129}I etc. Cosmogenic radio isotope ^{36}Cl is widely being detected using AMS as it has got applications in ground water research, radioactive waste management, atmospheric ^{36}Cl transport mechanism studies of Arctic Alpine ice core etc [1]. As the interfering isobar in the ^{36}Cl detection is ^{36}S, a split anode ionization chamber, being the most suited one, was developed indigenously [2]. The detector was calibrated using very low yields of ^{35}Cl and ^{37}Cl (keeping source parameters low) from the natural sample. The source parameters were optimised and Mass 36 was injected and transported through the machine up to the detector. Background ^{36}S (coming from the ion source as an impurity or memory effect) is identified in the detector. Recently, a beam chopper required for this measurement has also been developed.

^{36}Cl was produced by irradiating sodium chloride (NaCl) with thermal neutrons at Apsara reactor, BARC by the nuclear reaction $^{35}Cl(n, \gamma)^{36}Cl$. The irradiated sample was used to prepare the ion source sample.

The distinct peaks of ^{36}Cl and ^{36}S can be seen in the signals from anode 2 and Silicon detector (Fig.1). The yield of ^{36}Cl in the detector and the ^{35}Cl beam intensity in the Faraday cup located in close to the detector was measured. The ratio ^{36}Cl / ^{35}Cl in the sample is found to be ~ $1.5*10^{-10}$.
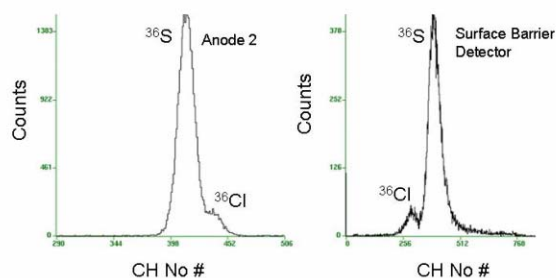
Figure 1: Spectra from Anode 2 and Silicon Detector.

PRODUCTION OF TRACK-ETCH MEMBRANES

Microporous membranes with features such as well defined and uniform pore size and pore density, uniform thickness, high tensile strength, inertness to toxic environments are in good demand for growing number of scientific and technological applications. Track Etch Membranes (TEMs) made by irradiating polymer films with heavy ions using accelerators are well known. Heavy ion accelerators provide greater flexibility to produce TEMs of a wide range as they can provide heavy ions of different atomic number (Z), kinetic energy (E) and particle flux. The damage size created by the heavy ions is of the order of $50 – 80$ A^o. Chemical etching is essential to enlarge the pore size to micron range. Pore densities of the order of 10^6 to 10^8 pores/cm^2 and pore size of the order of 0.2 to 1.0 micron are required for many applications. Large scale industrial application needs membranes of large area and in bulk quantity.

The polymer films of 25 micron thickness were used. A magnet [3] was used to scan the heavy ions from the accelerator in horizontal direction and the polymer film was moved in vertical direction using a roller mechanism. The scanner magnet gives a peak magnetic field of 1.35 KGuass. To get larger deflection, higher charge states of

ANALYSIS AND EVALUATION OF GAMMA AND NEUTRON DOSIMETRY FROM 48MeV 7Li ON NATURAL Cu AND ITS DOSE SIMULATION WITH MCNP

R. G. Sonkawade, Birender Singh, Pankaj. Kumar, S.P. Lochab, Inter University Accelerator Centre, Aruna Asaf Ali Marg, New Delhi-110 067, India

R. V. Kolekar, Radiation Safety System Division, Bhabha Atomic Research Centre, Mumbai-400 085, India

Abstract

Neutron and gamma radiation dose as a function of angle was measured from 48MeV, $^7Li^{3+}$ ion beam incident on thick natural copper target. The experiment is simulated keeping in view the health physics importance for monitoring the radiation environment in charged particle accelerator. The neutron dose observed in the forward direction is slightly higher compared to the lateral direction. Gamma energy of the same reaction is also monitored in the experimental setup with the HPGe-detector. The experimental results are compared with the calculated dose from empirical formulations. From the observed gamma spectrum, and PACE calculation, possible reactions were identified and correlated with the observed spectrum.

INTRODUCTION

In an accelerator, prompt secondary radiations such as gamma and neutrons are produced during the acceleration of ions, due to the interaction of the projectiles with the beam line materials. In a medium energy heavy ion accelerator, neutrons are the dominant prompt radiation. There are a number of low to medium energy accelerators utilized for research in various fields. In a heavy ion accelerator facility, neutron emission from thick targets are important, as they constitute the major component of prompt radiation environment owing to beam loss during normal operations or accidental situations. In this connection, energy and angular distribution of neutron and gamma dose distribution from thick targets are important for radiation protection point of view. The neutron dose in any direction is a function of the energy and angular distribution of neutrons, which in an accelerator environment vary depending upon the projectile, target and incident energy. Such measurements have been reported in the literature for protons and alpha particles but in the case of heavy ions, the experimental data are very few [1-5]. Moreover, most of the neutron yield data from heavy ion projectiles are in the energy region of 20MeV amu^{-1} and above. There are only few experimental measurements in the region of 10MeV amu^{-1} and below [6-7].

EXPERIMENTAL ARRANGEMENT

The experiment was performed at 15 UD Pelletron Accelerator Facility at the Inter University Accelerator Center (IUAC), New Delhi. The neutron energy spectrum and the radiation dosimetry were measured for $^7Li^{3+}$ ion beam accelerated through the Pelletron accelerator to 48MeV energy, stopped on thick Cu target of 1mm. Projectile ^7Li of 48MeV, has a range of 0.1026mm in Cu as calculated by SRIM [8]. The experiment is performed in the General Purpose Scattering Chamber (GPSC), which has the specially designed flanges of very small wall thickness to allow neutrons to emerge without much energy degradation . Spherical NDE meters are kept around 1.0m distance from the target at 0, 30, 60 and 90 degrees with respect to the beam direction. The neutron survey meter of make "Meridian" model 5085 is also used for monitoring the neutron dose level around the chamber. The gamma dose measurement is done with the gamma survey meter at one location at an angle of 90^0. The calibrated CR-39 sheet of thickness 500um procured from Pershore Moulding Ltd., UK and Lithium Borate radiators (Kodak, CA80-15 type B) of thickness 9.4mgcm^{-2} were used in the experiment. CR-39 with 1mm polyethylene radiator and with Lithium Borate external radiator are used for discrimination of fast and thermal neutrons respectively. PACE is used to cross check the possible formation of compound nuclei from this reaction and to correlate with the observed gamma spectrum. MCNP simulation code is used for the simulation of gamma and neutron dose in the experiment. The high purity germanium detector from M/S EG&G, ORTEC, Oak Ridge, USA, Model MPX20P4 is used for gamma spectrum analysis from the Li projectile on Cu target. The detector has a resolution of 2.0 KeV at 1332 KeV and relative efficiency of 20%. A BC501 liquid scintillation detector of 5cm(ϕ)x5cm (thick) was kept at distance of 1.0m from the target at 30^0 with respect to the beam. Time of Flight set up is used for the discrimination of neutron and gamma. This detector is shielded with the 9cm wax to minimize the contribution of the scattered neutrons during the experiment.

UNCERTAINTIES IN THE MEASUREMENT

Error or uncertainties in the measurement arises due to different factors including the uncertainty in overall beam current normalization which is estimated ~2%. For rem meters major contribution to error is from the pulsed nature of radiation fields, pile up (a random overlapping of pulses due to multiple events within a spill) can lead to large systematic errors [9]. The overall effect is due to possible underestimation of dose. Another source of error is due to pick up of radiofrequency (RF) pulses generated in accelerator. This is likely to add spurious

BEAM OPTICS DESIGN FOR DC HIGH-VOLTAGE ACCELERATOR OF MW LEVEL

WANG Han-bin, XU Zhou, LI Ming, JIN Xiao, LIU Xi-san
Institute of Applied Electronics CAEP, P.O.Box 919-1014, Mianyang 621900, China.

Abstract

Here, we report on the working group ''beam optics design'' of MW levels dc high-voltage accelerator, that will be used in radiation technologies in large-scale industrial production (flue gas treatment, metallurgy, waste water treatment, etc.). This workshop also had working groups on ''Electron Guns Designs and Beam control device'', ''MW level high-voltage power supply designs and fabrication'', and ''Beam scanning and extraction devices designs and fabrication''. Comparing with existent high-voltage accelerators, our facility have higher average power of >500mA dc, which resulting in some technological challenges on beam production, power supply, and beam extraction. Here, we are concerned with several proposals that other laboratories have been working on. Subjects of concern are optics, accelerator design and modeling, stability requirements that connects the conventional DC high-voltage accelerators for round-the-clock operation. We describe the design, the projected performance and the status of our facility.

INTRODUCTION

We developed a series of RF accelerator whose electron beam is small in size, and they have been the driver of high energy industrial CT. To satisfy the requirement of radiation technologies in large-scale industrial production (flue gas treatment, metallurgy, waste water treatment, etc.), we have started the developmental program of MW level's dc high-voltage accelerator.

This accelerator is designed with unified systems and units enabling them to be adapted to the specific requirements by varying the main parameters such as energy range, beam power, etc. The design is suitable to transmit high intensity current and realize the cathode of long lifetime, and can provide long term and round-the-clock operation of accelerators under the conditions of industrial production processes.

ACCELERATING TUBE STRUCTURE CHARACTERISTICS

A picture of the accelerating tube is shown in Fig 1. The cathode is single crystal LaB_6 and its best operating vacuum is less than 10^{-4}Pa. The channel aperture is 120 mm. This provides good vacuum conditions in the cathode region and consequently long time. The outer diameter of the insulator is 150 mm, its inner diameter is 130mm. A distance between the electrodes is 14mm. The ratio of the electrode's thickness to the insulator's height

is 1/7. The 95 Al_2O_3 ceramic rings are connected to the 1Cr18Ni9Ti electrodes by thermodiffusion welding.

An accelerating tube is made up of seven sections, and a section includes ten electrodes, eleven insulators and two mounting flanges. Its rated voltage is 1.2 MeV, and the mean operation gradient in the tube is 11.13kV/cm. Operating experience indicates the tube can be safely running as high gradient as 20kV/cm in a steady state.

DESIGN OF POTENTIAL DISTRIBUTION

We introduce the paraxial movement track equation in electrostatic field:

$$r'' + \frac{V'(z)}{2V(z)}r' + \frac{1}{4V(z)}(V''(z) - \frac{I}{\pi\varepsilon_0 r_b^2 v})r = 0 \quad (1)$$

the quantity V the generalized potential of charged particles, v equals to $\sqrt{\frac{2eV}{m}}$, r is the radial position of charged particle, and the prime symbol denotes a derivative taken with respect to z. The third term on the left hand side of Eq.1 represents the electrostatic focusing and defocusing progress of space charge force. Apparently, if want to have a beam form requisite, we must acquire some field gradient to counterbalance space charge force. Therefore ,we have to adjust the potential difference between adjacent electrodes. Now, for 0.5 ampere beam size of $\phi6$, the required field gradient varies with generalized potential can be displayed in table 1.

Table 1: V & V'' for 0.5 ampere beam size of $\phi6$

V (kV)	5	10	15	20	25
V''(kV/cm^2)	4.77	3.37	2.75	2.38	2.13

Cathode immerses in electrostatic field of accelerating tube. The beam current value is controlled by the cathode temperature, i.e. the gun is operated in a regime of full emission current take-off. Hence, the field on the cathode must be sufficiently strong, or it maybe in a space-charge-limited flow region. Considering the feasibility of beam current control, the quantity of field should be more than 7kV/cm on the surface of a $\phi6$ cathode for 0.5 ampere. Table 2 lists the corresponding field for different current intensity of different size cathode.

DEVELOPMENT OF L-BAND ELECTRON ACCELERATOR FOR IRRADIATION SOURCE*

S. H. Kim#, S. I. Moon, B. Park, H. R. Yang, S. D. Jang, Y. G. Son,
S. J. Park, J. S. Oh, M.H. Cho, and W. Namkung

POSTECH, Pohang 790-784, Korea

Abstract

An intense L-band electron accelerator is under development for irradiation applications. It is capable of producing 10-MeV electron beams of 30 kW with the fully beam-loaded condition. The accelerator is powered by a pulsed klystron of 1.3 GHz and 25 MW with the 60-kW average power. The accelerating column, a traveling-wave structure, is operated with the $2\pi/3$ mode and is installed vertically with other beam-line components. With the beam dynamics simulation, the beam transmission efficiency is over 90% and the beam size is enough to clear the apertures. Design details and the status of installation are presented for the L-band electron accelerator.

INTRODUCTION

Recently, the interests are increased in industrial applications of the electron linear accelerators [1]. The electron beam energy is limited by about 10 MeV due mainly to neutron production. For the clinical X-ray systems, low current and low repetition rate are required. The X-ray source for the container inspection requires 5-10 MeV with a few kilowatts of the average beam power [2]. On the other hand, the food or waste sterilization system requires relatively high average beam power since the process speed is proportional to it [3].

We are developing a high average-power electron accelerator for the grain sterilizing application by the institutional collaboration between the Korea Accelerator and Plasma Research Association (KAPRA) and Pohang Accelerator Laboratory (PAL) at POSTECH. The accelerator is required to provide an average beam power of 30 kW at the beam energy of 10 MeV. In order to achieve the beam power, we use a single L-band klystron with a matched pulse power supply. For an accelerating structure, the travelling-wave structure with $2\pi/3$ mode is adopted in which the bunching section is included for compactness. Each component of the accelerator system is described in the next section. The design detail of the accelerating column follows.

SYSTEM OVERVIEW

The Thales TV2022D klystron generates the pulsed 25-MW and average 60-kW RF power at 1.3 GHz. It is transmitted to the accelerating column through the L-band

waveguide network. These waveguides are filled with SF_6 gas. Since the column is a travelling-wave structure, the extra RF power is exhausted in the high-power load as shown in Figure 1. For the pre-buncher cavity, the RF power is bypassed in the cross-coupled directional coupler and transmitted through the coaxial cable with the adjusted power and phase. The pulse modulator developed at PAL supplies 264-kV and 230-A pulse power to the klystron with the pulse length of 7 us and the repetition rate of 350 Hz. Due to the high average power requirement, 8 units of 30-kW high-voltage inverter stack connected in parallel are used for the PFN charging. E-gun high-voltage pulser supplies the 80-kV and 1.6-A pulse power between the cathode and the anode of the E-gun.

Table 1: Accelerator parameters.

RF Parameters	
Operating Frequency	1.3 GHz
Pulsed RF Power	25 MW
Pulse Length	7 μs
Repetition Rate	350 Hz
Averaged RF Power	60 kW
E-gun Parameters	
High Voltage	80 kV
Pulsed Beam Current	1.6 A
Pulse Length	6 μs
Repetition Rate	350 Hz
Beam Parameters	
Beam Energy	10 MeV
Pulsed Beam Current	1.45 A
Beam Transmission Rate	91%
Averaged Beam Power	30 kW
Accelerating Structure Parameters	
Type of Structure	Constant-impedance
Shape of Cell	Disk-loaded
Operating Mode	$2\pi/3$ mode
RF Filling Time	0.8 μs
Operating Temperature	40°C ± 1°C
Averaged Accelerating Gradients	4.2 MV/m
Beam Loading Factor	- 4.7 MeV/A
Temperature Shift Factor	- 2.3 MeV/1°C

HIGH POWER INDUSTRIAL ELECTRON ACCELERATOR

S. C. Bapna, R. Banwari, M. Borage, A. Kasliwal, S. Kotaiah, Ajay Kumar, Pankaj Kumar,
R. Promod, Sunil Tiwari, S. V. Venkateswaran
RRCAT, Indore M.P.

Abstract

At RRCAT, we have a program of development of accelerators for Industrial applications. Under this, a 750 keV, 20 kW DC accelerator developed [1], is in operation since Nov. 2002. A 10 MeV, 10 kW electron linac is commissioned and is undergoing characterization. A 300 keV, 6 kW low energy accelerator is in advanced stage of development for curing applications. We have taken up development of a 2.5 MeV, 100 kW high power accelerator in collaboration with Budker institute of Nuclear Physics, Russia. In this paper we describe design details of the high power industrial accelerator

INTRODUCTION

The development of 2.5 MeV/ 100 kW air-core transformer type Industrial Accelerator is in progress in collaboration with Budkar Institute of Nuclear physics, Russia. Energy of the accelerator can be varied from 1 to 2.5 MeV with electron beam current up to 50 mA and maximum beam power up to 100 kW. The specifications are given in table 1. It is to be used for long term, round the clock continuous operation under industrial condition.

Table 1: Specifications of HPIA.

Operating Voltage	1 - 2.5 MeV
Max. beam Current	50 mA@ 2.0 MeV
Max. Beam Power	100 kW
Energy Dispersion	0.5 % at 2.0 MeV
Electron Gun	Indirectly heated triode electron gun with LaB_6 as emitter.
Maximum heater power	60 W
Accelerating Tube	PVA glued Accelerating tubes from BINP
HV Scheme	Air core transformer at frequency of 400-1000 Hz
Beam Scanning width	50 cm – 150 cms
Scanning frequency	50 Hz along the window and 1kHz in transverse direction.

DESCRIPTION

Figure 1 is a schematic of such an accelerator. The vessel is filled with an electrically insulating gas SF_6 and contains the primary winding, a high-voltage rectifier decks, electron gun, accelerating tube, a high- voltage electrode, and injector control unit. The elements of the vacuum unit with the output device are attached to the bottom of the vessel. The electron beam emitted by the cathode attached to the upper end of the accelerating tube is accelerated to the high voltage Uo and are transported through the beam line having vacuum pumps to the beam extraction window and is extracted into the atmosphere. The beam is scanned on the foil by X and Y scanning in order to increase the radiation field and also to distribute evenly the heat dissipated on to the foil. The irradiated material is conveyed under the beam exit window using a conveyor system.

Figure 1: 2.5 MeV High Power Industrial Accelerator.

High-voltage rectifier

The HV scheme is based on Air Core Transformer (ACT), which has a water-cooled primary winding, and an epoxy molded multi-section secondary winding. Each section of the secondary winding is connected with a voltage doubler circuit and then they are stacked one upon another to build the complete high voltage column. The secondary modules are known as decks and their number in the system depends on the power supply voltage rating. Each deck generates a high voltage of 40 kilovolts and thus 64 number of such decks will be stacked in series for a total built up of 2.5 MV accelerating voltage.

The magnetic circuit consists of a tape wound yoke that surrounds the primary and secondary windings from the

INTRODUCTION OF EPICS IN VEC & SCC CONTROL SYSTEM

Tanushyam Bhattacharjee[#], Anindya Roy, Biswajit Sarkar, R. B. Bhole, Samit Bandopahdyay,
Anirban De, Jaydeep Mishra, Niraj Chaddha, K. Kundu, Sarbajit Pal
Variable Energy Cyclotron Centre, 1/AF Bidhannagar, Kolkata – 700064, India

Abstract

As a part of computerization of the VEC and SCC Control System, using a standard open-source software tool for designing distributed control system named as EPICS (Experimental Physics and Industrial Control System), several IOCs (Input Output Controller) are developed to control and monitor the Main Magnet Power Supply (MPS), Beam line MPS, Deflector Power Supply, Beam line instruments and LCW (Low Conductivity Water) system. The device layer of IOC, responsible for communication with MPS distributed over several multi-drop networks (RS485) ensures reliable and fast response while setting several MPS simultaneously. Process parameters e.g. water level, temperature and conductivity in different subsystems are measured using standard industrial sensors. An IOC is developed for acquiring process data form sensors using Modbus-TCP based distributed DAQ modules on Windows platform. An IOC is developed for affecting the necessary control for conditioning of the electrostatic deflector with facility for supervisory intervention. Application of EPICS in sub-systems will lead towards unified distributed control architecture for auto beam tuning of the machines.

INTRODUCTION

The subsystems like MPS, LCW, Cryogenic control, Beam line control, beam diagnostics etc for VEC/SCC are interdependent and most of the control subsystem often require handling of control/monitoring parameters from other subsystems. The control/monitoring parameters handling among the subsystems become difficult as different proprietary software solutions are used by each group responsible for designing and maintaining their subsystems. The unified open source accelerator control system s/w tools of EPICS provide rugged distributed architecture and implementation of it helps to overcome the control data sharing difficulties. Many developed open source drivers to control various devices are already available for EPICS and these drivers are extremely useful for the system designer to reuse by modifying and rebuilding as per the specific system requirements.

The portability of EPICS in different platform/processor [1] provides the advantage of distributing EPICS applications without changing existing OS/processor architecture. Several EPICS device drivers, OPIs (Operator Interface) and input output controllers are developed recently and integrated with the existing system. Input Output Controllers are also developed to run on arm based embedded systems and operator interface is developed for Windows and Linux on x-86 processor.

[#]btanu@veccal.ernet.in
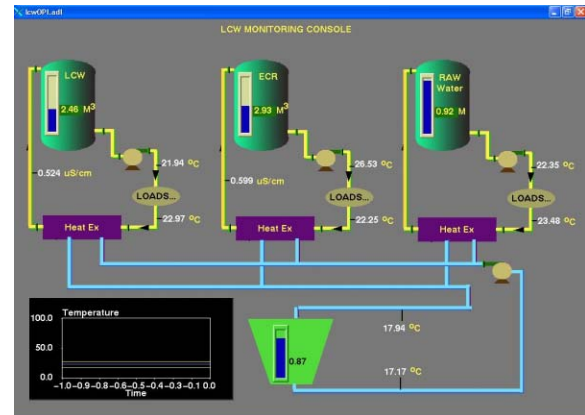
Figure 1: LCW OPI

CHANGE-OVER TO EPICS

Upgradation of LCW Monitoring for VEC

The web enabled modules with TCP connectivity are used for monitoring of plant parameters of Main LCW, ECR Cooling Water and Raw Water Systems. The gauge pressure type smart level transmitters are chosen to measure water levels in Raw-water storage tank, Main LCW Storage tank, ECR LCW Storage tank and Cooling-tower sump. The capacitance type level switches are also selected to provide HI & LOW level indications to initiate alarms. The temperatures at inlet and outlet headers of each subsystem by RTD and conductivities at different points are measured. EPICS asyn device support is used to develop the driver for DAQ modules having MODBUS-TCP connectivity.

The IOC uses the driver to communicate with the device and sends the channel data as Process Variables (PVs) to the client by Channel Access (CA) protocol. The LCW IOC loads the memory resident database which comprises of records contains several fields (variables). The bundled attributes of each record like scan rate, alarm limits etc. are defined according to the system requirements. The user interface as shown in Figure 1 is designed by MEDM (Motif Editor and Display Manager).Both the IOC and OPI is developed and running on win-x86 environment.

Upgradation of MPS system

The device driver for the commercially available magnet power supply (MPS) is developed using EPICS asyn device support routines. The device layer of IOC is responsible for communication with the Main Magnet and beam line power supplies having serial multidrop connectivity with ASCII protocol.

INDIAN PARTICIPATION IN LHC, SPL AND CTF-3 PROJECTS AT CERN, SWITZERLAND

V. Bhanage, J. Dwivedi, A.K. Jain, P. Khare, S. Kotaiah, P.K. Kush, Abhay Kumar, S.S. Prabhu, A.M. Puntambekar, A. Rawat, V.C. Sahni[#], A. Sharma, R. Shridhar, Purushottam Shrivastava, G. Singh, Raja Ramanna Centre for Advanced Technology, Indore, India, R.K. Sadhu, Bhabha Atomic Research Centre, Mumbai, India

Abstract

India has contributed to the construction and commissioning of CERN's most ambitious particle accelerator project the "Large Hadron Collider" (LHC) and is now engaged in other activities, namely, CTF 3 and LINAC-4. The contributions to LHC span from hardware, software, expert manpower support for evaluation of some of the LHC sub-systems and commissioning support of various subsystems of LHC. India has developed and supplied a total of 7080 Precision Magnet Positioning Systems (PMPS) Jacks for supporting Cryo-dipole magnets of LHC, 1146 Superconducting Corrector Magnets (MCS), 616 Superconducting octupole-decapole correcting magnets (MCDO), 5500 Quench Heater Power Supplies(QHPS), 1435 Local Protection Units (LPUs) etc., for LHC.   With the background of these contributions to CERN's satisfaction, India was invited to participate in CERN's upcoming Advanced Accelerator Projects, like, Superconducting Proton LINAC, SPL and Compact Linear Collider Test Facility, CTF 3. The present paper describes the highlights of the past, ongoing and future collaboration activities.

INTRODUCTION

CERN has started commissioning world's biggest particle accelerator the Large Hadron Collider (LHC) located over the Swiss-French border about 100m below ground. It would be colliding protons, each with 7 TeV energy during end 2007-2008 and will later collide lead nuclei, each of 1150 TeV energy. Indian involvement in LHC began in 1996. Earlier, after informally working for many decades with CERN, India formally signed a cooperation agreement in 1991 which was then followed by a protocol (signed in 1996) that led to Department of Atomic Energy's various laboratories to participate in the construction and utilization of LHC. The protocol provided a framework to deliver hardware and expert manpower envisaging an 'in kind' Indian contribution valued at 34 million Swiss Francs (i.e. US $25 million at 1994 rates). This was later raised to 60 MCHF under an agreement signed between DAE and CERN. Half of the value of this 'in kind' contribution is treated as India's contribution to LHC and other half is credited to 'Indian Fund' which was created to provide support to our scientists for their stay at CERN and also to meet essential expenses in foreign exchange required for some of the contributions. The lead DAE lab for this

collaboration is RRCAT, Indore. After successful completion of LHC related contributions, CERN invited India to join in its Advanced Accelerator Projects like Super Conducting Proton LINAC (SPL) and Compact Linear Collider Test Facility CTF-3. For this an additional protocol has been signed between Prof. Robert Aymer, Director General, CERN and Dr. Anil Kakodkar, Chairman AEC, India. This envisages additional contributions up to 5 MCHF on similar lines as done before for LHC contributions.

CONTRIBUTIONS TO LHC

The in-kind contributions that DAE committed is described in detail elsewhere [1][2] and a summary of some of these is given in Table 1. All the equipments, components and devices have been designed, developed, tested and supplied to CERN and accepted.

Table 1: Major Contributions to LHC

Sr.	Details of Indian Contributions	Qty.
1	50000 litres Liquid Nitrogen tanks.	2
2	Superconducting corrector magnets i) Sextpole (MCS) ii) Decapole and Octupole (MCDO)	1146 616
3	Precision Magnet Positioning System (PMPS) Jacks	7080
4	Quench Heater Protection Systems (QHPS)	5500
5	Integration of QHPS units into racks	6200
6	Control electronics for circuit breakers of energy extraction system	70
7	Local protection units (LPU)	1435
8	SC Dipole magnet tests/measurements, expert support in Man years	100
9	LHC Hardware Commissioning of Cryogenics, Power converters, Protection systems, Controls. Man years	20
10	Data management software upgrade, Data analysis software/documentation projects	41 Man years eq.
11	Development of JMT-II software	
12	Software development-slow control of Industrial Systems of LHC	
13	Design and calculations for Vacuum system for beam dump line	
14	Analysis of cryo-line jumper and magnet connections	

The items listed in table 1 were pursued with the help from different units of DAE with RRCAT acting as nodal

_____

[#]vcsahni@cat.ernet.in, vcsahni@magnum.barc.ernet.in

PROGRESS OF THE LASER-PLASMA ACCELERATION RESEARCH AT KERI

H. Suk[#], M.S. Hur, H.J. Jang, J. Kim, and S.H. Yoo
Center for Advanced Accelerators, KERI, Changwon, Republic of Korea

Abstract

An intense laser pulse can produce a plasma wake wave, which has an extremely strong electric field. This electric field can be used for electron acceleration with a ultrastrong high acceleration gradient (100 times or more compared with RF-based conventional accelerators). We have an experimental program on the laser-plasma acceleration research at KERI (Korea Electrotechnolgy Research Institute), where a 2 TW (700 fs in pulse duration) Nd:glass/Ti:sapphire lasser system and a 20 TW (30 fs in pulse duration) Ti:sapphire laser system (located at GIST-APRI) are used. In this paper, we present an overview of the experimental results for the laser-plasma acceleration research.

INTRODUCTION

RF-basedd conventional accelerators have a limited accelerating electric field of $\sim$ 100 MV/m. Compared with this field, a focused laser beam has a much stronger electric field. For example, if the intensity is I=1018 W/cm2, which can be nowadays easily achieved with a table-top terawatt laser system, the field strength is E=3 TV/m. However, the laser electric field can not be directly used for particle acceleration because the electric field is transverse. This problem can be solved if the laser beam is sent into a plasma, so the laser field is converted into a strong longitudinal plasma wake field that is almost in the same order of magnitude as the laser field itself [1]. There are several ways to excite a strong laser-plasma wake wave. One way is to send a rather long (longer than the plasma wavelength) laser pulse, so the plasma wave can be resonantly excited by a pulse train from the Raman scattering instability. This is called the self-modulated laser wakefield acceleration (SM-LWFA). Another way is to send a short laser pulse (pulse duration $\sim$ plasma wavelength) and this can excite the plasma wake wave almost resonantly as well. We have an experimental program on the SM-LWFA and resonant LWFA at KERI in collaboration with GIST-APRI (Gwangju Institute of Science and Technology-Advanced Photonics research Institute). In this paper, we show some experimental results from the SM-LWFA and LFWA research.

EXPERIMENTAL RESULT ON THE SELF-MODULATED LASER WAKEFIELD ACCELERATION

For the self-modulated laser wakefield acceleration experiment, we used the 2 TW (1.4J/700 fs) Nd:glass/Ti:sapphire hybrid type laser system at KERI. The experimental schematic is shown in Fig. 1. The 2 TW laser beam with a diameter of 5 cm is focused to a small spot ($\sim$ 10 μ m in diameter) by the gold-coated parabolic mirror in the He supersonic gas jet (backing pressure $\sim$ tens of bars, gas jet diameter=0.8 mm), so the He gas is ionized to a plasma by the strong electric field of the laser beam. Due to the interaction of the plasma and the laser beam, a self-modulated laser wakefield is generated and some background plasma electrons are randomly injected into the acceleration phase. The injected electrons are accelerated and the produced beam passes through the dipole magnet. And then it arrives at the LANEX film (a kind of phosphor film). This measurement gives an energy and energy spread of the generated electron beam. The beam charge is measured with an ICT (integrating current transformer) that is located after the thin LANEX film (made by KODAK). In this experiment, the generated electron beam has a continuous energy spectrum because plasma electrons are randomly injected into the acceleration phase. Hence, we used a very small pinhole-like collimator with a diameter of 1 mm to select only high energy electrons that are distributed mainly along the axis.
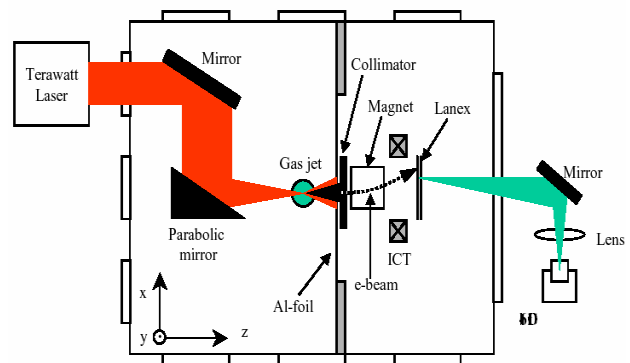
Figure 1: Schematic for the SM-LWFA experiment.

_____
[#] hysuk@keri.re.kr

03 Linear Colliders, Lepton Accelerators and New Acceleration Techniques
A13 - New Acceleration Techniques

ADVANCES IN ERLS AND MICROWAVE SUPERCONDUCTIVITY FOR LEPTON ACCELERATORS, COLLIDERS AND LIGHT SOURCES

J.R. Delayen, S. Chattopadhyay, Jefferson Lab, Newport News, Virginia

Abstract

Recent progress in efficient use and recovery of microwave energy in high current and high energy CW superconducting recirculating electron linacs such as the Continuous Electron Beam Accelerator Facility and the Free Electron Laser at Jefferson Lab are presented. Simultaneous with operational success of the ERL, progress in achievable gradients and performance of single crystal and large grain niobium superconducting cavities (including various processing techniques such as electropolishing), at the fundamental limit of RF superconductivity, will also be presented. The promising future direction in lepton accelerators, colliders and light source development using ERL and SCRF will be pointed out.

PAPER NOT YET RECEIVED

ACHIEVEMENT OF ATF AND ITS FUTURE PLANS *

Junji Urakawa for the ATF International Collaboration

High Energy Accelerator Research Organization(KEK), 1-1 Oho, Tsukuba-shi, Ibaraki, Japan

Abstract

The ATF (Accelerator Test Facility at KEK) International collaboration has been launched formally under the MoU (Memorandum of Understanding) from August 1, 2005, so as to maximally contribute to the world design and development efforts in the areas of particle sources, damping rings, beam focusing and beam instrumentation towards the International Linear Collider (ILC) project. I will give a talk on the achievement at ATF and its future plans, especially ATF2 project.

OUTLINE OF ATF AT KEK

The Accelerator Test Facility (ATF) at KEK comprises a multibunch-capable RF gun (with up to 20 bunches, spaced by 2.8ns, per pulse), an 1.3GeV S-band injector linac, a damping ring, and a beam diagnostic section(EXT)[1]. Each part directly contributes to the development of technologies relevant to high luminosity linear colliders. ATF at KEK is a research center for studies of issues concerning the injector, damping ring and beam delivery systems for ILC. Fig.1 shows a schematic plan view of ATF[2, 3, 4]. The multibunch scheme is essential to boost the rf-to-beam transfer power efficiency in the accelerator.

ATF generates, accelates, damps, and extracts a train of 20 bunches with $1x10^{10}$ electrons/bunch and 2.8ns spacing. The achievable normalized emittance is $3.8\mu m$ horizontally and $0.0125\mu m$ vertically, and an energy spread 0.08% and the bunch length 8mm for the multibunch beam. The small emittance from the damping ring has been achieved by special design of a strong focusing lattice with precise alignment of components and beam orbit control. The nonlinear behavior of the beam has to be well understood to provide enough dynamic aperture under such strong focusing conditions.

After the technology choice for ILC Main Linac, we proposed ATF2 project as a test beam line using very flat beam from the ATF damping ring to realize 37nm vertical beam size at the final focus point stably. Then, we have established an International Collaboration of ATF (including ATF2 project) with many institutes and it was launched on Aug. 1st 2005. Now several other institutes were added to join into this collaboration.

The International Collaboration of ATF is based on the Memorandum of Understanding (MoU) which defines the organization of the international collaboration to carry out the research programs at ATF and its extension ATF2, so as to maximally contribute to the world design and development efforts in the areas of particle sources, damping rings, beam focusing and beam instrumentation towards the ILC project. We are adding the MoU, the

chart of the organization and related material into new ATF Web Site (http://atf.kek.jp/).

As evidence from this MoU, the construction and operation of ATF2 will be executed in the framework of the International Collaboration of ATF. The management of activities of ATF2 will be carried out under the supervising bodies as described in the later section.

I described the simplified explanation of the ATF MoU in the following sub-sections. Also, I explain the achievement of ATF and the plan of ATF2[5].
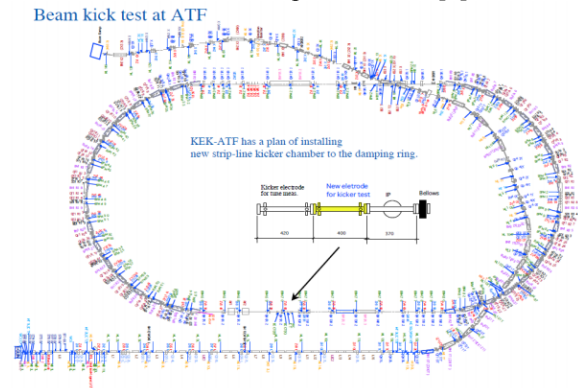
Figure 1: Schematic plan view of ATF.

MISSION OF ATF/ATF2

ATF is to establish the technologies associated with producing the electron beams with the quality required for ILC and to provide such beams to ATF2 in a stable and reliable manner.

ATF2 is effectively to use the beams extracted from ATF at a test final focus beamline which is similar to what is envisaged at ILC. The goal is to demonstrate the beam focusing technologies that are consistent with ILC requirements. For this purpose, ATF2 aims to focus the beam down to a few tens of nm (rms) with a beam centroid stability within a few nm for a prolonged period of time.

Both ATF and ATF2 is to serve the mission of providing the young scientists and engineers with training opportunities of participating in R&D programs for advanced accelerator technologies.

ORGANIZATION OF ATF/ATF2

To execute the scientific programs at ATF/ATF2, the following bodies were instituted:
- International Collaboration Board (ICB)
- Technical Board (TB)
- Spokesperson (SP) with his/her Deputies
- System/Group Coordinators (SGCs)

International Collaboration Board (ICB)

The International Collaboration Board (ICB) is the decision making body for executive matters related to the

EXPERIENCE WITH THE HERA LEPTON-PROTON COLLIDER

F. Willeke, DESY, Hamburg, Germany

Abstract

A review of the experience of operating the HERA lepton proton collider with a high luminosity of up to $5 \cdot 10^{31} \text{cm}^{-2}\text{s}^{-1}$, a discussion of the important accelerator physics issues and a summary of the most important physics results of the lepton-hadron (ep) collider HERA is presented.

INTRODUCTION

Collisions of high energy leptons with hadrons reveal the structure and dynamics and the nature of the forces between the constituents of hadrons. Electron scattering experiments on protons were performed already fifty years ago when R. Hofstadter and co-workers measured the nuclear form factor by analysis of (200-600) MeV electrons scattered on protons [1]. As leptons with energies of several GeV became available, a series of lepton nucleon scattering experiment revealed an inner structure of the proton with point-like constituents [2, 3]. This discovery was followed by many experiments yielding a better understanding of the proton structure. The experiments E49-89 at SLAC [4] observed that the cross section for small x[†] remained constant in the range of x ≈ 1/3-0.01. This result (among others) suggested that additional quarks-antiquark pairs are produced inside the proton by the strong force between the valence quarks and the gluons. A lepton-hadron collider with large centre of mass energy (E_{cm}) was expected to provide the ultimate experimental evidence for this model because it would provide access to small x with sufficient spatial resolution or high Q^2. At that time, the HERA ep collider with E_{cm} = 318 GeV was proposed [5]. HERA was expected to provide precision measurements of the proton dynamic structure function F_2, of electro-weak and strong interactions, and to provide experimental evidence of lepton quark resonances. HERA was approved in 1984 and the physics program was started in 1992.

HERA OVERVIEW

HERA consists of two 6.4 km long storage rings, one with 5T superconducting magnets for the 920 GeV protons and another with normal conducting magnets for the 27.5GeV electrons or positrons. The beams collide at two collision points (IP) denoted by North and South, where the detectors H1 and ZEUS are located. The interaction

[†]The parameter x is the fractional momentum of the interacting proton-constituent. It is related to the transfer of energy ν = E-E' and the transfer of 4-momentum $Q^2 = (k-k')^2$ from the projectile to the target by basic kinematics (neglecting terms with the proton rest mass M) by $x = Q^2 \cdot (2M\nu)^{-1}$ and is thus determined from the directly measured quantities Q^2 and ν. While Q^2 constitutes the parameter which controls the spatial resolution, x controls the dynamics of the proton structure.

regions (IR) were upgraded for a high luminosity of L > $5 \cdot 10^{31} \text{cm}^{-2}\text{s}^{-1}$ in 2001 [6]. The HERA lepton beam is spin polarized by the Sokolov-Ternov [7] effect. Three pairs of ppin rotator magnets [8] around each of the three experiments provide longitudinally polarized leptons for collisions with protons.

HERA ACCELERATOR PHYSICS ISSUES

The HERA injection energy for protons is only 40 GeV, 0.043 times the operation energy of 920 GeV. The corresponding large persistent current field errors of the superconducting magnets at injection [9] are the cause for a small dynamic aperture of only 3.8 RMS times the beam sizes $\sigma_{x,y}$ [10]. This serious issue is solved by strictly controlling the beam parameters. Emittance dilution at injection is avoided by correcting injection errors to < 1mm transversely and to < $4 \cdot 10^{-4}$ in relative energy at each proton injection. The tunes during injection and the first part of acceleration must be kept to within a small window of $\Delta Q_{x,y} \leq 0.002$. They are controlled by a software-based feedback [11] with a non-destructive tune measurement [12]. Persistent and eddy current sextupole components of the guide fields must be suppressed dynamically to a level of 0.3% which is accomplished by a combination of continuous monitoring and correction via a reference magnet system, by look-up tables for correction of systematic errors and by manual fine tuning the chromaticity on analysis of the tune spectra. As a result, the chromaticities $\xi_{xy} = \Delta Q_{xy} (^{\Delta p}/_p)^{-1}$ are controlled to about one unit. The betatron-oscillations must be decoupled to levels of < 0.005 in the coupling strength. Failure to meet these requirements leads either to beam loss > 1% due to poor dynamic aperture, or multi-mode head tail instabilities. The head tail instability is driven by a conspiracy of coupling and small values of chromaticity [13]. Attempts to control the instabilities during acceleration by broadband dampers [14] have been abandoned because of significant emittance growth due to feedback noise and the then required PLL-type tune measurement, and, more importantly, due to the loss of information necessary to fine-tune the chromaticities based on analysis of the tune spectra for maintaining good lifetime. This part of HERA experience may be relevant for the LHC. High precision, non-destructive tune and chromaticity measurements in conjunction with low-noise damper systems are deemed necessary for the LHC.

The lepton beam tune working space is limited by strong 2nd and 3rd order synchro-betatron resonances. In the vicinity of these resonances the emittance of the leptons growth dramatically and the lifetime becomes very poor. These resonances are excited by accumulative effects around the long circumference of HERA. The widths of

TOWARDS A MULTI TEV LINEAR COLLIDER; DRIVE BEAM GENERATION WITH CTF3

H.H. Braun, CERN, Geneva, Switzerland for the CLIC team

Abstract

The 3 TeV compact linear collider, CLIC, foresees an RF source based on a high current drive beam running parallel with the main linac. To generate this drive beam of very high instantaneous power a sophisticated complex consisting of a fully beam-loaded linac and several stages of beam compression is used. Although this scheme is very promising in terms of cost and power efficiency, it needs demonstration in a scaled version before construction of CLIC can be envisaged. This is the aim of the CLIC Test Facility CTF3, built by an international collaboration. CTF3 is constructed and exploited in several phases. Here we report present status, experimental achievements and future plans for CTF3.

INTRODUCTION

The CLIC study develops the technology for a linear electron-positron collider with a centre of mass energy reach of $E_{CMS} = 3$ TeV [1]. This energy is chosen to complement the discovery potential of LHC Hadron collider with a Lepton collider capable to perform crucial precision measurements in the whole energy range accessible by LHC [2]. The luminosity requirement for these measurements is $L_1 > 3 \cdot 10^{34}$ cm^{-2} s^{-1}, where L_1 denotes the luminosity available in a 1% energy bin. To reach 3 TeV in a reasonable length high accelerating gradients are essential. These gradients are in excess of the fundamental limitations for superconducting RF at about 50 MV/m. Therefore normal conducting, high frequency RF is the technology of choice for CLIC. As a consequence of the high gradient, high peak RF power is required to feed the accelerating structures. This power is extracted from a second beam of high intensity and low energy, running parallel with the main beams. Such a two beam scheme provides the required RF peak power with good efficiency. Since the drive beam is produced in a central area no active high power components are required along the linacs and a single tunnel scheme with an inner diameter of 4.5 m as shown in fig. 1 can be used [3].

Recently combined results from RF structure testing [4], an overall optimisation of parameters [5] and the introduction of a scalable cost estimate in the optimisation lead to a major parameter revision for CLIC. The main modification are the reduction of the main linac RF frequency from the former value of 30 GHz to now 12 GHz and the reduction of accelerating gradient from 150 MV/m to 100 MV/m. This leads to an overall length including beam delivery system of 47 km for 3 TeV CLIC.
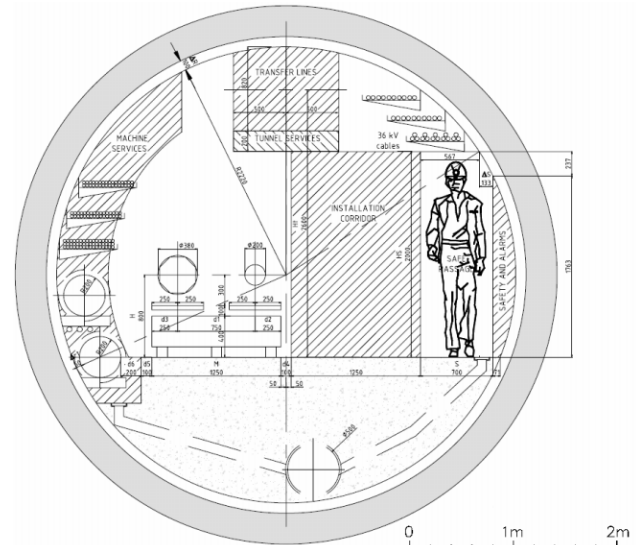
Figure 1: CLIC tunnel layout.

CLIC TEST FACILITY CTF3

The two beam scheme has been successfully demonstrated in the former CLIC test facility CTF II achieving accelerating fields of almost 200 MV/m [6]. However, in CTF II the drive beam was not produced in a manner representative for CLIC. In consequence the RF pulse length was limited to 16ns and the power efficiency of drive beam acceleration was poor.

The present CLIC test facility CTF3 aims to demonstrate the nominal CLIC drive beam production scheme [7] together with most other technical feasibility issues [8] as raised by the International Linear Collider Technical Review Committee ILC-TRC in 2003 [9]. CTF3 is build by a collaboration of institutes (table 1), with an organisation structure similar to large particle physics experiments.

The ILC-TRC issues addressed in CTF3 are:

a) *Demonstration of the CLIC accelerating structure at design gradient and pulse length*. CTF3 is already used as RF power source for 30 GHz testing. The 30 GHz CLIC accelerating structures are being tested in a well instrumented test stand. A vigorous development programme of accelerating structures is under way.

b) *Demonstration of the Drive Beam scheme*. The main issue here is the generation of the Drive Beam, i.e. acceleration of a long bunch train with conventional klystrons and subsequent bunch manipulations in order to increase the bunch repetition frequency, together with an increase in electron current in short, compressed bunch

THE ACCELERATOR ACTIVITIES OF THE
EUROTRANS PROGRAMME*

Paolo Pierini[†], INFN Sezione di Milano, LASA

Abstract

The objective of the EC Integrated Project EUROTRANS is the design and feasibility assessment of an industrial accelerator driven system prototype dedicated to the transmutation of high level waste from nuclear power plants. A part of the program is dedicated to the further development of the high power proton accelerator needed for both the short term experimental demonstrator systems and the long term large scale industrial realizations. In particular the accelerator program addresses the issues of the qualification of the beam reliability with respect to the spallation target requirements, the development of the beam transport line to the subcritical reactor, and the demonstration of the key prototypical components of the proposed linear accelerator. This communication will present an overview and status of the accelerator activities carried out by the partners of the EUROTRANS project.

INTRODUCTION

The European Research Programme for the Transmutation of High Level Nuclear Waste in an Accelerator Driven System is a research program funded by the European Commission in the 6th Framework Programme, involving 31 partners between research agencies and nuclear industries and with the contribution of 16 universities. EUROTRANS is a 4 year program extending previous activities (PDS-XADS, Preliminary Design Study for an eXperimental Accelerator Driven System) and paving the road towards the construction of an eXperimental facility demonstrating the technical feasibility of Transmutation in an Accelerator Driven System (XT-ADS) in the next EC framework programmes.

The main objective of EUROTRANS is to work towards a European Transmutation Demonstration (ETD) in a step-wise manner:

- to provide an advanced design of all components of an XT-ADS system at significant power levels of the subcritical assembly (50 to 100 MWth), driven by conventional MOX fuel, in order to allow its realization in a short-term (~10 years),
- to provide a generic conceptual design of modular European Facility for Industrial Transmutation (EFIT), with power levels exceeding several 100 MWth and operated with new fuel loaded with reprocessed waste. The EFIT is the long-term objective of the program.

TRANSMUTATION IN AN ADS

Transmutation in an Accelerator Driven System (ADS) intends to address the problem of the long term disposal of the nuclear waste. In particular its objective are to reduce the radiotoxicity of the waste, to minimize the volume and the heat load of the nuclear waste sent to the deep geological storage in underground repositories.

The EU has (2001 data [1]) 145 reactors, providing more than 125 GW of electrical power, with an 850 TWh yearly production (covering 35% of the total), and producing an yearly amount of 2500 tons of spent fuel, among which 25 are Pu.

The strategy aimed at solving this problem relies on partitioning and transmutation, i.e. to separate chemically the waste fuel - that is, isolate Pu, the Minor Actinides (MA) and the Long Lived Fission Fragments (LLFF) – and to recombine the chemically pure elements obtained in this way in proper assemblies that could fuel dedicated transmuter systems, aimed at disposing of them in times much shorter than the natural decay times.

In order to deploy a solution for the waste disposal problem, two main technological ingredients are needed for a transmutation system:

- a **subcritical reactor** (with a criticality factor k substantially smaller than 1) where the fission chain reaction is not self-sustained, and operating with U-free fuel, in order to avoid nuclear proliferation problems
- an **intense neutron spallation source** (i.e. a high proton flux on a liquid lead target) that provides the "missing" neutrons that are needed to keep the reaction going. The neutrons produced by a high energy proton beam by spallation have also the broad energy spectrum which is needed to "burn" the MA components, that are otherways accumulated in conventional critical reactors operating with a thermal neutron spectrum.

The radiotoxicity of the spent fuel decreases to the level of the starting raw uranium ore used to produce the fuel elements only after a period greater than a million years. In order not to release these toxic elements in the biosphere it is thus necessary to dispose of the waste in deep and stable geological repositories, ensuring proper containment and surveillance for this extremely long period. The Partioning and Transmutation (P&T) goal is, via chemical separation and irradiation in a fast and intense neutron flux, to reduce this time to 700-1000 years (See Figure 1).

PARTICLE COLLIDERS AND THE QUEST FOR REVEALING THE HIDDEN NATURE OF SPACE AND TIME

N. Lockyer, University of Pennsylvania, Philadelphia, Pennsylvania

Abstract

Particle Physics is thought to be on the verge of a revolution. This viewpoint was affirmed in the recent Report of the National Aacdemies "Revealing the Hidden Nature of Space and Time", Charting the Course for Elementary Particle Physics. The report, its physics, and some of its conclusions will be discussed with emphasis on collider physics from the Tevatron, LHC and International Linear Collider.

PAPER NOT YET RECEIVED